



EM 1110-2-6051
22 December 2003

US Army Corps
of Engineers®

ENGINEERING AND DESIGN

Time-History Dynamic Analysis of Concrete Hydraulic Structures

ENGINEER MANUAL

AVAILABILITY

Electronic copies of this and other U.S. Army Corps of Engineers (USACE) publications are available on the Internet at <http://www.usace.army.mil/inet/usace-docs/>. This site is the only repository for all official USACE engineer regulations, circulars, manuals, and other documents originating from HQUSACE. Publications are provided in portable document format (PDF).

DEPARTMENT OF THE ARMY
U.S. Army Corps of Engineers
Washington, DC 20314-1000

EM 1110-2-6051

CECW-EW

Manual
No. 1110-2-6051

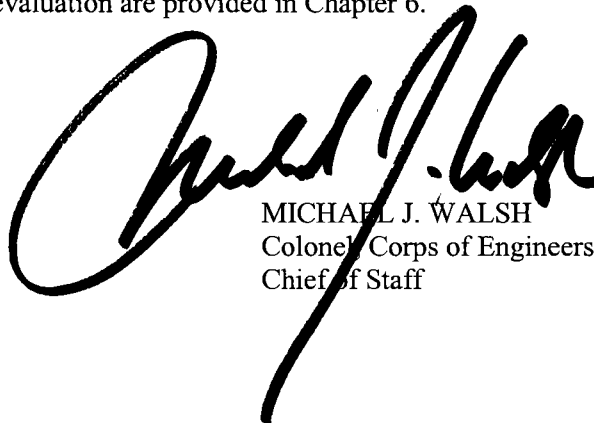
22 December 2003

Engineering and Design
TIME-HISTORY DYNAMIC ANALYSIS
OF CONCRETE HYDRAULIC STRUCTURES

- 1. Purpose.** This manual describes procedures for the linear-elastic time-history dynamic analysis and development of acceleration time-history dynamic analysis for seismic design and evaluation of concrete hydraulic structures (CHS). The manual also provides guidance on the formulation and performance of the linear-elastic time-history dynamic analyses and how the earthquake input time-history are developed and applied.
- 2. Applicability.** This manual applies to all USACE commands having responsibility for civil works projects.
- 3. Distribution.** Approved for public release; distribution is unlimited.
- 4. Discussion.** Chapter 1 provides an overview of the seismic assessment process for CHS and the responsibilities of the project team involved in the process. In Chapter 2, methodology for analytical modeling of concrete hydraulic structures is discussed, including types of CHS, analytical modeling procedures, fluid-structure interaction, and foundation-structure interaction. Chapter 3 describes time-history numerical solution techniques. Chapter 4 describes methodology for structural performance and damage criteria. Chapter 5 describes methodology for developing of acceleration time-histories. Examples of earthquake response evaluation are provided in Chapter 6.

FOR THE COMMANDER:

6 Appendices
(See Table of Contents)



MICHAEL J. WALSH
Colonel, Corps of Engineers
Chief of Staff

CECW-EW

Circular
No. 1110-2-6051

22 December 2003

**Engineering and Design
TIME-HISTORY DYNAMIC ANALYSIS
OF CONCRETE HYDRAULIC STRUCTURES**

Table of Contents

Subject	Paragraph	Page
Chapter 1		
Introduction		
Purpose.....	1-1	1-1
Applicability	1-2	1-1
Scope.....	1-3	1-1
References.....	1-4	1-1
Explanation of Symbols and Acronyms.....	1-5	1-1
Responsibilities of Project Team	1-6	1-2
Overview of Seismic Design and Evaluation Procedure	1-7	1-2
Chapter 2		
Analytical Modeling of Concrete Hydraulic Structures		
General.....	2-1	2-1
Types of Concrete Hydraulic Structures	2-2	2-1
Concrete Gravity Dams.....	2-3	2-1
Concrete Arch Dams.....	2-4	2-3
Intake-Outlet Towers	2-5	2-3
U-frame and W-frame Navigation Locks	2-6	2-4
Massive Concrete Lock Walls	2-7	2-4
Massive Concrete Guide Walls.....	2-8	2-4
Analytical Modeling Procedures	2-9	2-5
Substructure Method.....	2-10	2-5
Standard Finite Element Method	2-11	2-8
Concrete Gravity Dams.....	2-12	2-9
Concrete Arch Dams.....	2-13	2-10
Intake-Outlet Towers	2-14	2-13
U-frame and W-frame Navigation Locks	2-15	2-18
Massive Concrete Lock Walls	2-16	2-22
Massive Concrete Guide Walls.....	2-17	2-23
Subject		
Paragraph		
Page		
Fluid-Structure Interaction.....	2-18	2-25

Simplified Added Hydrodynamic Mass Model	2-19	2-25
Finite Element Added Hydrodynamic Mass Model.....	2-20	2-30
Compressible Water with Absorptive Boundary Model.....	2-21	2-35
Reservoir Boundary Absorption	2-22	2-36
Foundation-Structure Interaction	2-23	2-37
Rock Foundations	2-24	2-37
Soil and Pile Foundations	2-25	2-38

Chapter 3

Time-History Numerical Solution Techniques

Introduction.....	3-1	3-1
Equation of Motion	3-2	3-1
Direct Integration	3-3	3-2
Mode Superposition.....	3-4	3-4
Stability and Accuracy Considerations.....	3-5	3-5
Frequency Domain-Based Solutions	3-6	3-6
Transfer of Acceleration Time-History to the Frequency Domain.....	3-7	3-6
Frequency Response Functions.....	3-8	3-8
Frequency Response Functions.....	3-8	3-8
Computation of Structural response.....	3-9	3-10
Selection of Parameters for Frequency Domain Analysis	3-10	3-10

Chapter 4

Structural Performance and Damage Criteria

General.....	4-1	4-1
Basis for the Proposed Performance and Damage Criteria.....	4-2	4-1
Gravity Dams.....	4-3	4-5
Arch Dams	4-4	4-9
Navigation Locks.....	4-5	4-27
Free-Standing Intake Towers.....	4-6	4-35

Chapter 5

Development of Acceleration Time-Histories

Introduction.....	5-1	5-1
Overview of Approach for Time-History Development.....	5-2	5-1
Initial Selection of Time-Histories.....	5-3	5-3
Simple Scaling Approach to Final Development of Acceleration Time-Histories	5-4	5-10
Spectrum-Matching Approach to Final Development of Acceleration Time-Histories	5-5	5-12
Modifying Time-Histories for Site Response Effects.....	5-6	5-16

Subject	Paragraph	Page
Chapter 6		
Earthquake Response Evaluation of Concrete		
Folsom Dam Nonoverflow Monolith.....	6.1	6-1
Background.....	6.1-1	6-1
Purpose and Objectives.....	6.1-2	6-1
Scope.....	6.1-3	6-1
Earthquake Ground Motions.....	6.1-4	6-1
Finite Element Analysis.....	6.1-5	6-4
Material Properties.....	6.1-6	6-5
Dynamic Characteristics.....	6.1-7	6-5
Time-History Analysis.....	6.1-8	6-8
Conclusions.....	6.1-9	6-9
Portugues Arch Dam.....	6.2	6-18
Background.....	6.2-1	6-18
Purpose and Objectives.....	6.2-2	6-18
Scope.....	6.2-3	6-18
Earthquake Ground Motions.....	6.2-4	6-18
Selection of Analysis Procedures.....	6.2-5	6-23
Finite Element Models.....	6.2-6	6-23
Material Properties.....	6.2-7	6-25
Computation of Earthquake Response.....	6.2-8	6-25
Evaluation of Results.....	6.2-9	6-30
Conclusion and Recommendations.....	6.2-10	6-31
Olmsted Lock Chamber Monolith.....	6.3	6-47
Background.....	6.3-1	6-47
Purpose and Objectives.....	6.3-2	6-47
Scope.....	6.3-3	6-47
Selection of Analysis Procedures.....	6.3-4	6-49
Finite Element Modeling.....	6.3-5	6-50
Material Parameters.....	6.3-6	6-53
Loading Conditions.....	6.3-7	6-54
Presentation and Evaluation of Results.....	6.3-8	6-65
Conclusions.....	6.3-9	6-71
Unit Conversion.....	6.3-10	6-92
References.....	6.3-11	6-92
Seven Oaks Incline Intake Tower.....	6.4	6-93
Background.....	6.4-1	6-93
Subject	Paragraph	Page
Purpose and Scope.....	6.4-2	6-93
Description of Intake Tower.....	6.4-3	6-93
Earthquake Ground Motions.....	6.4-4	6-95
Structural Model.....	6.4-5	6-99
Computation of Earthquake Response.....	6.4-6	6-101

Appendix A
References

EM 1110-2-6051
22 Dec 03

Appendix B
Synthesizing a Suite of Simulated
Recorded Motions

Appendix C
Spectrum Matching

Appendix D
Effects of Spectrum Matching on
Characteristics of Earthquake
Ground Motion Time-Histories

Appendix E
Discrete Soil Models

Appendix F
Notations

Chapter 1 Introduction

1-1. Purpose

This manual describes procedures for the linear-elastic time-history dynamic analysis and development of acceleration time-histories for seismic design and evaluation of concrete hydraulic structures. The manual provides guidance on the formulation and performance of the linear-elastic time-history dynamic analyses and how the earthquake input time-histories are developed and applied. Time-history dynamic analysis is employed as the final design and evaluation procedure to compute the probable seismic behavior of a concrete hydraulic structure in accordance with the progressive method of analysis described in Engineer Regulation (ER) 1110-2-1806 and Engineer Manual (EM) 1110-2-6050.

1-2. Applicability

This manual applies to USACE Commands having responsibility for Civil Works projects.

1-3. Scope

This chapter provides an overview of the earthquake performance evaluation process for concrete hydraulic structures, and summarizes the methodologies for time-history dynamic analysis and development of acceleration time-histories described in following chapters. In Chapter 2, methodology for the time-history dynamic analysis of hydraulic structures is formulated, including a general description of structures, structural modeling, interaction with water and foundation rock, energy absorption at the reservoir boundaries, and the required earthquake input acceleration time-histories for each structure type. Chapter 3 describes computational methods and algorithms for solution of the equations of structural dynamics in the time and frequency domains. In Chapter 4, methodologies for performance evaluation and qualitative estimation of the probable level of damage are discussed. Chapter 5 presents methodologies and procedures for development of earthquake input acceleration time-histories and discusses important factors that should be considered in their selection and development. Chapter 6 provides examples of time-history evaluation for major concrete hydraulic structures including a gravity dam, a concrete arch dam, an inclined intake tower, and a W-frame lock structure. Concrete hydraulic structures are built from plain or lightly reinforced concrete that respond to earthquake in a less ductile manner than normal reinforced concrete building. Such behavior combined with complicated structure-foundation and structure-water interaction effects often requires special time-history analysis for the earthquake performance evaluation of major concrete hydraulic structures.

1-4. References

Required and related publications are listed in Appendix A.

1-5. Explanation of Symbols and Acronyms

Symbols and acronyms used in this manual are explained in the Notation (Appendix F).

1-6. Responsibilities of Project Team

a. Project team concept. Time-history dynamic analysis and selection or development of earthquake input acceleration time-histories for the design and evaluation of concrete hydraulic structures require the close collaboration of a project team that includes the principal design engineer, seismic structural analyst, materials engineer, and geotechnical specialists. The principal design engineer is the leader of the project team and has overall responsibility for the design or evaluation of the structure. The seismic structural analyst plans, executes, and evaluates the results of seismic analyses of the structure for earthquake ground motions for the design earthquakes. The materials engineer characterizes the material properties of the structure based on test data and appropriate assumptions. The geotechnical specialists conduct evaluations to define the design earthquakes and input ground motions and also characterize the properties of the soils or rock foundation for the structure. Any potential for seismically induced failure of the foundation is evaluated by the geotechnical specialists. The geotechnical evaluation team typically involves the participation of geologists, seismologists, and geotechnical engineers who closely work with the principal design engineer and the seismic structural analyst.

b. Consulting technical experts. Time-history evaluation of hydraulic structures is a highly complex field of earthquake engineering, which requires special expertise and substantial judgment to be effective. In many instances, the project team should augment the in-house staff with technical experts to ensure independent review of the methodology and results, to add credibility to the results, and to ensure public acceptance of the conclusions. Such experts should be selected and their responsibilities defined in accordance with ER 1110-2-1806.

1-7. Overview of Seismic Design and Evaluation Procedure

Seismic design and evaluation of hydraulic structures generally consist of the following steps:

- Selection of design/or evaluation earthquakes.
- Selection of method of analysis.
- Development of acceleration time-histories.
- Definition of load combinations.
- Development of structural models.
- Definition of material properties and damping.
- Selection of numerical analysis procedures.
- Determination of performance and probable level of damage, if any.

a. Design earthquake criteria. Design and safety evaluation earthquakes for concrete hydraulic structures are the operating basis earthquake (OBE) and the maximum design earthquake (MDE) as required by ER 1110-2-1806.

(1) Operating Basis Earthquake (OBE). The OBE is defined in ER 1110-2-1806 as an earthquake that can reasonably be expected to occur within the service life of the project, that is, with a 50 percent probability

of exceedance during the service life. This corresponds to a return period of 144 years for a project with a service life of 100 years. The associated performance requirement is that the project function with little or no damage, and without interruption of function. The purpose of the OBE is to protect against economic losses from damage or loss of service; therefore, alternative choices of return period for the OBE may be based on economic considerations. The OBE is determined by probabilistic seismic hazard analysis (PSHA). The response spectrum method of analysis described in 1-7b(2) is usually adequate for the OBE excitation, except for the severe OBE ground motions capable of inducing damage. In these situations, the time-history analysis described in this manual may be required.

(2) Maximum Design Earthquake (MDE). The MDE is defined in ER 1110-2-1806 as the maximum level of ground motion for which a structure is designed or evaluated. The associated performance requirement is that the project performs without catastrophic failure, such as uncontrolled release of a reservoir, although severe damage or economic loss may be tolerated.

(a) For critical structures ER 1110-2-1806 requires the MDE to be set equal to the maximum credible earthquake (MCE). Critical structures are defined as structures whose failure during or immediately following an earthquake could result in loss of life. The MCE is defined as the greatest earthquake that can reasonably be expected to be generated by a specific source on the basis of seismological and geological evidence (ER 1110-2-1806).

(b) For other than critical structures the MDE is selected as a less severe earthquake than the MCE, which provides for an economical design meeting specified safety standards. This less severe earthquake is chosen based upon an appropriate probability of exceedance of ground motions during the design life of the structure (ER 1110-2-1806). In these cases, the MDE is defined as that level of ground motion having as a minimum a 10 percent probability of exceedance in 100 years. This corresponds to a return period of 950 years for a project with a service life of 100 years.

(c) Design and evaluation of hydraulic structures for the MDE ground motion may require time-history analysis as described in 1-7b(3).

b. Method of analysis. Seismic analysis of concrete hydraulic structures, whenever possible, should start with simplified methods and progress to a more refined analysis as needed. A simplified analysis establishes a baseline for comparison with the refined analyses, as well as providing a practical method to determine if seismic loading controls the design, and thereby offers useful information for making decisions about how to allocate resources. In some cases, it may also provide a preliminary indication of the parameters significant to the structural response. The simplified methods for computation of stresses and section forces consist of the pseudo-static or single-mode response-spectrum analysis. The simplified method for sliding and rotational stability during earthquake excitation is usually based on the seismic coefficient method. The permanent sliding displacements may be computed using Newmark's rigid block model or its numerous variants. The response-spectrum mode superposition described in EM 1110-2-6050 is the next level in the progressive method of dynamic analysis. The response-spectrum mode superposition fully accounts for the multimode dynamic behavior of the structure, but it is limited to the linear-elastic range of behavior and provides only the maximum values of the response quantities. Finally, the time-history method of analysis is used to compute deformations, stresses, and section forces more accurately by considering the time-dependent nature of the dynamic response to earthquake ground motion. This method also better represents the foundation-structure and fluid-structure interaction effects.

(1) Simplified procedures.

(a) Simplified procedures are used for preliminary estimates of stresses and section forces and sliding and rotational stability due to earthquake loading. The traditional seismic coefficient is one such procedure employed primarily for the analysis of rigid or nearly rigid hydraulic structures. In this procedure the inertia forces of the structures and the added mass of water due to the earthquake shaking are represented by the equivalent static forces applied at the structure center of gravity and at the resultant location of the hydrodynamic pressures. The inertia forces are simply computed from the product of the structural mass or the added mass of water times an appropriate seismic coefficient in accordance with ER 1110-2-1806. The static equilibrium analysis of the resulting inertia forces together with the customary static forces will then provide an estimate of the stresses and section forces.

(b) The sliding stability is determined on the basis of the limit equilibrium analysis. The sliding factor of safety is computed from the ratio of the resisting to driving forces along a potential failure surface. The resisting forces are obtained from the cohesion and frictional forces and driving forces from the resultant of static and seismic forces in the tangential direction of the sliding surface. When the factor of safety against sliding is not attainable, the sliding may occur as the ground acceleration exceeds a critical acceleration a_c and diminish as the acceleration falls below a_c . If a hydraulic structure is treated as a rigid block, the critical acceleration a_c is estimated from the seismic inertia forces necessary to initiate sliding. The upper bound estimate of permanent sliding displacement may be obtained using Newmark's charts (Figure 2-11 of EM 1110-2-6050).

(2) Response-spectrum modal analysis. The maximum linear elastic response of concrete hydraulic structures can be estimated using the response-spectrum mode superposition method described in EM 1110-2-6050. The procedure is suitable for the design, but it can also be used for the evaluation of hydraulic structures subjected to low or moderate ground motions that are expected to produce linear elastic response. In response-spectrum analysis, the maximum values of displacements, stresses, and section forces are first computed separately for each individual mode and then combined for all significant modes and multicomponent earthquake input. The modal responses due to each component of ground motion are combined using either the square root of the sum of the squares (SRSS) or the complete quadratic combination (CQC) method. The SRSS combination method is adequate if the vibration modes are well separated. Otherwise the CQC method may be required to account for the correlation of the closely spaced modes. Finally the maximum response values for each component of ground motion are combined using the SRSS or percentage methods in order to obtain the maximum response values due to multicomponent earthquake excitation. The response-spectrum method of analysis, however, has certain limitations that should be considered in the evaluation of results. All computed maximum response values including displacements, stresses, forces, and moments are positive and generally nonconcurrent. Therefore, a plot of deformed shapes and static equilibrium checks cannot be performed to validate the results. For computation of section forces from element stresses, appropriate signs should be assigned to the stresses by careful examination of deflected shapes of the predominant response modes. Alternatively, section forces may be computed first for each individual mode and then combined for the selected modes and multicomponent earthquake input, a capability that may not exist in most finite-element computer programs. Other limitations of the response-spectrum method are that the structure-foundation and structure-water interaction effects can be represented only approximately and that the time-dependent characteristics of the ground motion and structural response are ignored.

(3) Time-history analysis. Time-history earthquake analysis is conducted to avoid many limitations of the response-spectrum method and to account for the time-dependent response of the structure and better

representation of the foundation-structure and fluid-structure interaction effects. The earthquake input for time-history analysis is usually in the form of acceleration time-histories that more accurately characterize many aspects of earthquake ground motion such as the duration, number of cycles, presence of high-energy pulse, and pulse sequencing. Time-history analysis is also the only appropriate method for estimation of the level of damage as described in 1-7h and Chapter 4. Response history is computed in the time domain using a step-by-step numerical integration or in the frequency domain by applying Fourier transformation described in 1-7g.

c. Development of acceleration time-history input motions. Chapter 5 describes the procedures for developing site-specific acceleration time-histories of ground motion for dynamic analysis of hydraulic structures. The overall objective is to develop a set (or sets) of time-histories that are representative of site ground motions that may be expected for the design earthquake(s) and that are appropriate for the types of analyses planned for specific structures. The following steps are included in this process:

(1) Initially selecting recorded time-histories that are reasonably consistent with the tectonic environment of the site; design earthquake (magnitude, source-to-site distance, type of faulting); local site conditions; and design ground motion characteristics (response spectral content, duration of strong shaking, and special characteristics, e.g. near-source characteristics). If sufficient recorded motions are not available, simulated recorded time-histories can be developed using ground motion modeling methods.

(2) Modifying time-histories selected in (1) above to develop the final set(s) to be used in dynamic analysis. Two approaches that can be used in this process are simple scaling of time-histories (by constant factors) so that a set of time-histories has spectral values that, on average, are at the approximate level of the design response spectrum; and spectrum matching, which involves modifying the frequency content of a given time-history so that its response spectrum is a close match to the design response spectrum.

(3) Further modifying the time-histories for site response effects, if the site is a soil site and the time-histories have been developed for outcropping rock conditions.

(4) Further modifying the time-histories for spatial variations of ground motion, if it is desired to incorporate effects of wave passage and incoherence in the ground motions that would arrive beneath a very large or long structure.

d. Load combinations. Concrete hydraulic structures should be designed and evaluated for three basic *usual*, *unusual*, and *extreme* loading combinations. In general, the usual loading combinations are formulated based on the effects of all applicable static loads that may exist during the normal operation of the structure such as the usual concrete temperatures and the most probable water level, with dead loads, tailwater, ice, uplift, and silt. The unusual static loading combinations refer to all applicable static loads at the floodwater pool elevation with the effects of mean concrete temperatures, dead loads, and silt. The unusual dynamic loading combination includes the OBE loading plus any of the usual loading combinations. Extreme loading combinations consist of the effects of the MDE loading plus any of the usual loading combinations.

(1) Combination with usual static loads. Time-history dynamic analysis is conducted mainly for the MDE loading conditions but also for the OBE if seismic demand is severe. At each time-step, results of such analyses should be combined with results of any of the usual loading combinations in order to obtain total displacements, stresses, and section forces needed for design or evaluation of structures.

(2) Combination for multicomponent earthquake input. Modeled as two- or three-dimensional (2-D or 3-D) structural systems, time-history analysis of concrete hydraulic structures should consider two or three orthogonal components of acceleration time-histories of earthquake ground motions. At each time-step,

response quantities of interest are first computed for each component of the earthquake input and then combined algebraically to obtain the total responses due to two or all three components. Only scalar and similarly oriented response quantities are combined algebraically. After the initial algebraic combination, the resulting displacements, shear forces, and moments in orthogonal directions need to be combined vectorially if the absolute maximum values of such response quantities are required.

(3) Combination for earthquake input direction (phase relation). Seismic waves of identical amplitudes, but traveling in two opposite directions, could lead to different structural response. The opposite of acceleration time-histories (i.e., all values multiplied by minus one) should also be considered as a simple way to account for some directional effects. In general, a complete permutation of all three components with positive and negative signs may be required to obtain the most critical directions that would cause the largest structural response.

e. Development of structural models. Meaningful time-history analysis of probable seismic behavior of a concrete hydraulic structure for design and evaluation requires thorough understanding of the system components, their interaction, and their material properties. Modeling of the structural system and its interaction with the foundation and water are summarized in this section. The required material properties for the analysis are specified in *f* below. In general, structural models for the time-history analysis should be developed to capture the main dynamic characteristics of the structure and represent the effects of fluid-structure interaction and foundation-structure interaction accurately. Depending on the geometry and mass and stiffness distributions, a particular hydraulic structure may be idealized using a simple beam, a 2-D finite element, or a 3-D finite element model. The structural model should provide an accurate representation of the mass and stiffness distributions, and in the case of existing structures it should account for the effects of any existing cracks, deteriorated concrete, or any deficiency that might affect the stiffness. The fluid-structure interaction effects may be adequately represented by simple added hydrodynamic mass coefficients, or may require a finite element (or boundary element) solution with or without the effects of water compressibility and boundary absorption. Modeling of the foundation-structure effects may range from a simplified massless finite element mesh to more elaborate formulations involving soil-structure or soil-pile-structure interaction analyses. For embedded structures, the effects of dynamic backfill pressures on the structure can also be significant and should be considered.

(1) Concrete gravity dams.

(a) Relatively long and straight concrete gravity dams built as independent monoliths separated by transverse joints may be idealized using a 2-D finite element model including the foundation rock and the impounded water. The 2-D dam-water-foundation model, usually of the tallest cross section, may be analyzed as three separate systems in the frequency domain using the substructure method (2-12a(1)) or as a single complete system in the time domain using the standard finite element procedures (2-12a(2)). The substructure method may be employed if the assumption of homogeneous material properties for the foundation region can be judged reasonable and a more rigorous formulation of the dam-water interaction including water compressibility and reservoir bottom absorption is desirable. Otherwise the standard finite element method with much simpler added-mass representation of the dam-water interaction should be used in order to account for variation of the foundation rock properties.

(b) Curved concrete gravity dams and those built in narrow canyons should be analyzed using 3-D finite element models similar to those described for arch dams in (2) below.

(2) Concrete arch dams. The complicated 3-D geometry of an arch dam requires a rather refined 3-D model of the dam, its foundation, and the impounded water for evaluation of its response to all three components of seismic input (2-13). The arch dam-water-foundation system may be formulated in the time

domain using the standard finite element procedures or in the frequency domain using the substructure method. The standard method employs a massless foundation rock included as part of the dam finite element model in conjunction with an incompressible liquid mesh representing the impounded water. Treating each system separately, the substructure method considers the same dam model as the standard method, but employs the flexibility as well as the damping and inertial effects of the foundation rock, with a reservoir water that accounts for the effects of water compressibility and the reservoir boundary absorption. In both methods the seismic input consists of three components of the free-field acceleration time-histories applied uniformly along the dam-foundation interface in the substructure method and at the fixed boundary of the massless foundation in the standard method. The standard method provides reasonable results for small dams and those built on a competent foundation rock having a deformation modulus at least equal that of the concrete and with impounded water whose fundamental resonance frequency is at least twice that of the arch dam. Otherwise, the more rigorous formulation of the dam-water and dam-foundation interaction effects offered by the substructure method might be required.

(3) Intake-outlet towers. Freestanding towers may be idealized using the substructure or standard finite element method of analysis. The available substructure method is restricted to towers having two axes of plan symmetry and supported on the horizontal ground surface of a foundation with homogeneous material properties (2-14a(2)). The substructures consist of the tower, surrounding water, contained water, and the foundation rock or soil system. The tower is modeled as an assemblage of beam elements. The hydrodynamic forces and moments due to pressures on the outside and inside surfaces of the tower are determined by the finite element and boundary integral procedures; and the foundation region is represented by the frequency-dependent stiffness or impedance functions. The seismic input for the tower-water-foundation system is defined by two horizontal components of the free-field acceleration time-histories applied at the base of the tower. The effects of vertical component of the ground motion are considered negligible and thus are ignored.

(a) The standard method is restricted neither to symmetric towers nor to homogeneous foundation material properties, but employs foundation models that only approximately account for the structure-foundation interaction (2-14a(1)(a)). Towers with regular cross-section geometry may adequately be represented by beam elements in conjunction with a foundation model idealized by equivalent linear springs attached to the base or to the embedded portion of the tower model. The water-structure interaction for such a model is approximated by the added hydrodynamic mass described in 2-19d. The earthquake input for the tower beam model is defined by two horizontal components of acceleration time-histories. The irregular freestanding towers may require finite-element idealization, in which case a finite element model should also be developed for an appropriate portion of the foundation region. The seismic input for such a model should include two horizontal components and possibly the vertical component of the free-field ground acceleration histories.

(b) The 3-D geometry of supported towers (combined with seismic input exciting the tower not only at the base but also at the abutment supports) requires a 3-D finite element treatment of the structure. Three-dimensional solid elements or a combination of 3-D solid and shell elements may model the tower. An appropriate portion of the foundation and the abutment support regions should be modeled as part of the finite element model of the tower. The effects of hydrodynamic pressures are represented by the equivalent added mass concept but should be computed using the finite element or boundary element procedures to accurately account for the tower geometry as well as topography of the surrounding foundation-abutment region. The seismic input for the analysis of a supported tower includes all three components of the ground acceleration time-histories applied at fixed exterior nodes of the foundation model.

(4) U-frame and W-frame navigation locks. Navigation locks constructed of separate monoliths are generally idealized using 2-D finite element procedures. The lock itself is modeled using the standard finite element method, but dynamic interactions with the soil-pile foundation, backfill soils, and the contained and

surrounding water require special considerations and must be represented accurately. The soil-pile-structure interaction (SPSI) effects can be incorporated in the analysis by two different approaches: direct method (2-15a) and substructure method (2-15b). In the direct method a complete model of the soil-pile-structure system is developed and subjected to the vertical and one horizontal component of the seismic input usually prescribed at the rock outcrop. In the substructure method, the lock structure and the foundation soil including the piles are treated separately. The lock structure is modeled by the standard finite element method, and the soil-pile foundation is represented either by impedance functions in the form of frequency-dependent springs and dashpots or by simple frequency-independent springs attached to the base of the structure. To obtain conservative values of forces and moments at pile heads and to model imperfect contact and possible separation along the structure-foundation interface, the finite element model should also incorporate a thin soft-soil layer beneath the base of the lock structure. The model is then subjected to a foundation-input motion developed on the basis of kinematic interaction analysis. In both methods, the water-structure interaction effects are adequately represented by the added hydrodynamic mass described in 2-15a(3).

(5) Massive concrete lock walls. Time-history analysis of lock walls founded on rock with no backfill soils is evaluated using the standard finite element method described for concrete gravity dams in 2-12a(2). Analysis of lock walls with backfill soils involves consideration of dynamic soil pressures induced by the ground shaking in addition to the interactions with the foundation rock and water. Depending on the expected movement of the backfill soil, it may be modeled as yielding backfill, nonyielding backfill, or an intermediate case in accordance with 2-16b. The yielding backfill, which may induce a limit or failure state, is analyzed based on the well-known Mononobe-Okabe method. The nonyielding backfill responding within the linear elastic range of deformations may be modeled using a constant-parameter single-degree-of-freedom (SDOF) model or a more elaborate frequency-independent multi-degree-of-freedom (MDOF) lumped-parameter system. The intermediate case is evaluated as an equivalent linear system using an SPSI model.

(6) Massive concrete guide walls. Fixed guide walls supported on cellular piles or drilled shafts are best represented by 3-D soil-structure-interaction models (2-17). The 3-D model may include only one cellular pile or drilled shaft, but whenever possible may take advantage of the structural symmetry to reduce the size of the problem. The overall model usually consists of various components including the cellular sheet pile, soil layers and soil within the sheet pile, concrete pier or block above the ground surface, precast concrete beams, and the hydrodynamic forces acting on the pile and the concrete block. The seismic input includes three components of acceleration time-histories usually prescribed at the rock outcrop.

f. Material properties. Concrete hydraulic structures are built using both plain and lightly reinforced forms of concrete construction and may be supported by rock, soil, or pile foundations. Concrete condition, function, age, and properties for existing structures and concrete mix and properties for new designs usually vary widely from structure to structure. These factors and geotechnical information of the subsurface conditions have potentially significant influence on the seismic performance of concrete hydraulic structures. It is essential that the time-history seismic evaluation effort conform to guidelines for determination of material properties and assessment of physical condition described in other references. The primary material properties relevant to time-history dynamic analysis are summarized in the following paragraphs.

(1) Concrete properties. The primary material properties of interest in a concrete structure are those that affect prediction of the structural response and those that are required for evaluation of the structural performance. The structural response is predicted on the basis of unit weight and elastic properties of the concrete including modulus of elasticity and Poisson's ratio. Many laboratory and field measurements have shown that modulus of elasticity is affected by the rate of loading and generally is higher for the dynamic than it is for the static loading. Under the sustained static loading conditions, the effects of creep on the mass concrete may be important and generally can be considered by determining a sustained modulus of elasticity taken as 60 to 70 percent of the laboratory value of the instantaneous modulus of elasticity. For seismic

analyses the measured or estimated dynamic modulus is more appropriate and should be used. In the absence of measured data, dynamic modulus of elasticity should be obtained by increasing the laboratory value of the instantaneous modulus by 20 to 30 percent. Compressive and tensile strengths of concrete are properties used to evaluate acceptability of new designs or seismic performance of the existing structures. Like modulus of elasticity, concrete strength parameters are also affected by the rate of loading. Seismic design and performance evaluation of concrete hydraulic structures should therefore be based on the measured or estimated dynamic strength of concrete. Other material properties such as shear strength of concrete, tensile and shear strengths of construction joints, yield strength and modulus of elasticity of reinforcing steel, and reinforcing steel bond strength and ductility may also be required. In general tensile strength across the deteriorated or poorly constructed joints could significantly be lower than that of the parent concrete. Determination of tensile and shear strengths across such joints may be warranted under severe earthquake loading.

(2) Foundation rock properties. Foundation rock properties for use in structural analyses include shear strength and rock mass modulus of deformation. Procedures for estimating shear strength and modulus of deformation are described in Chapter 10 of EM 1110-2-2201. Shear strength parameters provide a measure of shearing resistance to sliding at the structure-rock interface or within the foundation and abutments, when potential sliding wedges or planes of rock that could cause instability have been identified. The modulus of deformation is a measure of foundation deformations for the rock mass as a whole including the effects of its discontinuities. In contrast, modulus of elasticity is determined for an intact specimen of the rock.

(3) Foundation soil properties. Foundation soil properties for use in soil-structure or SPSI studies include low-strain shear wave velocity or shear modulus of soil layers, mass density, Poisson's ratio, material damping, and variation of shear modulus and damping with strain. The low-strain material parameters are estimated from the geotechnical data such as the blow counts, measured shear wave velocities, and soil borings. Many studies have concluded that shear modulus and damping characteristics of soils vary with level of strain and that the strain dependency is a function of soil type, stress history, density state, and other factors. In practice, a set of modulus reduction and damping curves suggested by Seed and Idriss (1970) is commonly used to account for variation of these parameters with strain.

(4) Reservoir bottom absorption. Studies of the dam-water interaction indicate that the earthquake response of concrete dams is sensitive to the water energy loss at the reservoir boundaries. If the reservoir boundary materials are relatively soft, an important fraction of the reservoir water energy can be absorbed, leading to a major reduction in the dynamic response of the dam. An earthquake-generated hydrodynamic pressure wave impinging on the reservoir boundary is partly reflected in the water, and partly refracted (absorbed) into the boundary materials. The energy loss or partial absorption at the reservoir boundary is approximately represented by a reflection coefficient α , which is the ratio of reflected to incident wave amplitudes (Hall and Chopra, 1980; Fenves and Chopra 1984b). The reflection coefficient α varies between 1 and -1, where $\alpha = 1$ corresponds to a total reflection (nonabsorptive or rigid boundary), $\alpha = 0$ represents a complete absorption or transmission into the boundary materials, and $\alpha = -1$ characterizes 100 percent reflection from a boundary with an attendant phase reversal. The in situ values of α for the seismic safety evaluation of concrete dams can be measured using three independent approaches developed and employed at several dams in the United States and abroad. These include the seismic reflection and refraction techniques (Ghanaat and Redpath 1995) and a technique based on the acoustic reverberation (Ghanaat et al. 1999).

(5) Damping.

(a) In practice, damping characteristics of typical structures are generally expressed in terms of equivalent viscous damping ratios. The velocity-proportional viscous damping is commonly used because it leads to convenient forms of equations of motion. The energy-loss mechanism for the viscous damping,

however, depends on the frequency of excitation, a phenomenon that has not been observed experimentally. As a result it is desirable to remove this frequency dependency by using the so-called *hysteretic* form of damping. The hysteretic damping is defined as a damping force proportional to the strain or deflection amplitudes but in phase with the velocity. The structural response provided by hysteretic damping can be made identical to that with viscous damping if the hysteretic damping factor is selected as

$$\zeta = 2\xi\beta \quad (1-1)$$

where

ζ = hysteretic damping factor

ξ = viscous damping ratio

β = ratio of the excitation frequency to the natural free-vibration frequency

To remove the frequency dependency term from Equation 1-1, the value of hysteretic damping ζ is computed at resonance by setting $\beta = 1$. The hysteretic damping computed in this manner provides identical response to that of the viscous damping at the resonance and nearly identical response at all other frequencies for $\xi < 0.2$.

(b) Viscous damping is commonly used in the time-domain solution, whereas the hysteretic damping factor taken as twice the viscous damping ratio is usually employed in the frequency domain solution. Linear time-history analysis of concrete hydraulic structures should employ a damping equivalent to a 5 percent viscous damping ratio. However, in situations where a moderate level of nonlinear behavior such as joint opening and cracking is predicted by a linear analysis, a higher damping ratio in the range of 7 to 10 percent could be used to account somewhat for the energy loss due to nonlinear behavior.

g. Numerical analysis procedures. Computation of earthquake response history for typical concrete hydraulic structures involves solution of coupled sets of equations of motion that include large numbers of equations or degrees of freedom. In linear response analyses the system equations of motion can be formulated either in the time domain or in the frequency domain. Only time domain formulation is suited to analysis of nonlinear response. These formulations and the corresponding response analysis procedures are described in Chapters 2 and 3, respectively. Following is a brief summary to provide a general idea of how these techniques are applied in the solution of the earthquake response behavior of concrete hydraulic structures.

(1) Analysis in the time domain. In practice, time-domain response analyses are generally based on some forms of step-by-step methods using numerical integration procedures to satisfy the equations of motion. In all the step-by-step methods the loading and the response history are divided into a sequence of time intervals or "steps." The response during each step is computed from the initial conditions (displacement and velocity) at the beginning of the step and from history of loading during the step. The structural properties within each step are assumed to remain constant, but could vary from one step to another (nonlinear behavior) or remain the same during all time-steps (linear behavior). The step-by-step methods may be classified as explicit or implicit. In an explicit method, the new response values calculated in each step depend only on the response quantities available at the beginning of the step. The analysis therefore proceeds directly from one step to the next. In an implicit method, on the other hand, the new response values for a given step include one or more values pertaining to the same step, so that trial values and successive iterations are necessary. The iteration within a step makes implicit formulations inconvenient and in some cases even prohibitive. Only explicit methods such as those described in Chapter 3 may be considered. The primary factors to be considered in

selecting a step-by-step method include efficiency, round-off and truncation errors, instability, phase shift or apparent change of frequency, and artificial damping in accordance with Chapter 3.

(a) Mode superposition method. In linear response analysis, the mode superposition techniques can be used to uncouple the system equations of motion, so that the dynamic response can be obtained separately for each mode of vibration and then superimposed for all significant modes to obtain the total response. This way the step-by-step integration discussed in (1) above is applied separately to a number of independent SDOF equations and then the resulting modal response histories are superimposed to compute the total response of the structure. The main effort in this method includes computation of eigenvalue problems followed by modal coordinate transformation to uncouple the MDOF dynamic analysis to the solution of a series of SDOF systems. It is important to note that the equations of motion will be uncoupled only if the damping can be represented by a mass proportional and stiffness proportional damping matrix known as Rayleigh damping. The Rayleigh damping is suitable when the damping mechanism is distributed rather uniformly throughout the structure.

(b) Direct step-by-step method. In this method, the step-by-step integration is applied directly to the original equations of motion with no need for modal coordinate transformation to uncouple them. Thus there is no need to obtain natural mode shapes and frequencies or to limit damping to the proportional type. The method can be used for both the linear and nonlinear response analyses.

(2) Analysis in the frequency domain. An alternative approach to solving the modal equations of motion for linear systems is to perform the analysis in the frequency domain. In particular, when the equation of motion contains frequency-dependent parameters such as foundation stiffness and damping, the frequency domain approach is much superior to the time domain approach. In simple terms the frequency domain solution involves expressing the ground motion in terms of its harmonic components; evaluating the response of the structure to each harmonic component; and superposing the harmonic responses to obtain total structural response. In this process, the harmonic amplitudes of the ground motion in the first step and superposition of harmonic responses in the third step are obtained using the Fast Fourier Transform (FFT) algorithm.

h. Structural performance and damage criteria. Chapter 4 describes methodologies and procedures for evaluation of earthquake performance and qualitative estimation of the probable level of damage using the results from linear time-history analyses. The overall process involves describing the results in terms of the demand-capacity ratios, cumulative inelastic duration of excessive stresses or forces, and spatial extent and distribution of high-stress or high-force regions, and then comparing them with a set of acceptance criteria set forth for each type of structure. Another important factor in the evaluation process is consideration of probable nonlinear mechanisms and modes of failure that might develop in a concrete hydraulic structure. The damage in a particular structure is considered to be minor and the linear time-history analysis will suffice if estimated level of damage meets the acceptance requirements established for that structure. Otherwise the damage is considered to be severe, in which case a nonlinear time-history analysis would be required to estimate damage more accurately.

(1) Gravity dams. The dam response to the MDE is considered to be within the linear elastic range of behavior if the computed stress demand-capacity ratios are less than or equal to 1.0. The level of nonlinear response or cracking is considered acceptable if demand-capacity ratios are less than 2, overstressed regions are limited to 15 percent of the dam surface area, and the cumulative duration of stress excursions beyond the tensile strength of the concrete falls below the performance curve shown in Figure 4-2.

(2) Arch dams. The dam response to the MDE is considered to be nearly within the linear elastic range if the computed stress demand-capacity ratios are less than or equal to 1.0. The dam is considered to exhibit

nonlinear response in the form of opening and closing of contraction joints and cracking of lift lines if the estimate demand-capacity ratios exceed 1.0. The amount of joint opening and cracking is considered acceptable if demand-capacity ratios are less than 2, overstressed regions are limited to 20 percent of the dam surface area, and the cumulative inelastic duration falls below the performance curve given in Figure 4-18.

(3) Navigation locks. If all computed demand-capacity ratios for piles and concrete sections are less than or equal to 1, then the lock structure and piles are expected to respond elastically with no damage. Demand-capacity ratios of greater than 1 show the structure will experience nonlinear behavior in the form of yielding of steel members and cracking or crushing and spalling of the concrete. On the basis of linear time-history analysis the level of damage or nonlinear response will be acceptable if the following performance conditions are met:

- Pile demand-capacity ratios remain below 1.5 and the percentage of piles yielding with the associated cumulative yield duration fall below the performance curves given in paragraph 4-5a (Figures 4-25 and 4-26). For example, for the “*Expected Yield*” case, the yielding should be limited to less than 10 percent of piles and the cumulative yield duration should not exceed one-tenth of a second.
- Demand-capacity ratios of concrete sections should not exceed 1.5 and those exceeding one be limited to less than 10 percent surface area of the lock.

(4) Free-standing intake towers. If the computed demand-capacity ratios are less than or equal to 1.0, the tower is considered to respond essentially within the linear elastic range with negligible or no damage. Demand-capacity ratios of greater than 1 indicate the tower would suffer some damage in the form of yielding of steel members and cracking or crushing and spalling of the concrete. In this situation, the damping ratio of 5 percent for the linear time-history analysis should be increased to 7 percent if demand-capacity ratios are approaching 2 and to 10 percent if they exceed 2. After adjustment for the damping, the damage is considered moderate and acceptable if the following conditions are met:

- Bending moment demand-capacity ratios computed on the basis of linear time-history analysis remain less than two.
- Cumulative duration of bending-moment excursions above demand-capacity ratios of 1 to 2 fall below the acceptance curve given in Figure 4-53.
- The extent of yielding along the height of tower (i.e., plastic hinge length for demand-capacity ratios of 1 to 2) is limited and falls below the acceptance curve.

Otherwise, the damage is considered to be severe and should be assessed using nonlinear analysis procedures.

Chapter 2 Analytical Modeling of Concrete Hydraulic Structures

2-1. General

Structural modeling procedures consistent with the time-history method of analysis are discussed in this chapter. First the massive concrete hydraulic structures are defined and their general dynamic characteristics described. Then modeling procedures applicable to each hydraulic structure and fluid-structure and foundation-structure interactions are discussed, followed by description and application of the earthquake input motions required in the analysis. In general, the structural models developed should consider the most important dynamic characteristics of each particular hydraulic structure, including the fluid-structure and foundation-structure interactions. The effects of dynamic backfill pressures on the navigation lock walls and the reservoir boundary absorption for concrete dams can also be significant and should be considered (1-7f(4)). The structural modeling of a particular hydraulic structure is generally accomplished using a beam and/or finite element idealization of the structure. However, modeling for the fluid-structure interaction, foundation rock-structure interaction, and SPSI is more involved and may include simple procedures as well as more elaborate formulations. Earthquake input motions are described, and the manner in which they are applied to the structure is also discussed.

2-2. Types of Concrete Hydraulic Structures

Hydraulic structures considered in this manual include massive concrete structures designed for impounding water, regulating the release of impounded water, or fulfilling navigation demands during the periods when the riverflows are inadequate. These massive concrete structures include gravity and arch dams, intake towers, U-frame and W-frame navigation locks, and their associated approach walls.

2-3. Concrete Gravity Dams

a. Gravity dams are massive concrete hydraulic structures that retain the impounded water by resisting the forces imposed on them mainly by their own weight (Figure 2-1a). They are designed so that every unit of length is stable independent of the adjacent units. Although a typical gravity dam is usually straight, the dams are sometimes curved in plan to accommodate site topography and to gain added stability through arch action. The construction materials for gravity dams have evolved from stone masonry of the historic dams to mass concrete. To reduce the construction costs in comparison with those of the earth-fill and rock-fill dams, more gravity dams are now being built using the roller-compacted concrete (RCC), which uses earth-fill construction techniques.

b. Traditionally, analysis of a gravity dam considered a very simple mathematical model of the structure. Such a method was based on the concept that the resistance to external forces was 2-D in nature, so only a unit slice of the dam taken in the upstream-downstream direction was analyzed. The earthquake forces were expressed as the product of a seismic coefficient and were treated simply as static forces. Only the effects of horizontal ground motion applied in the upstream-downstream direction were considered. However, to represent the resistance mechanism realistically, it now has become standard practice to use some form of

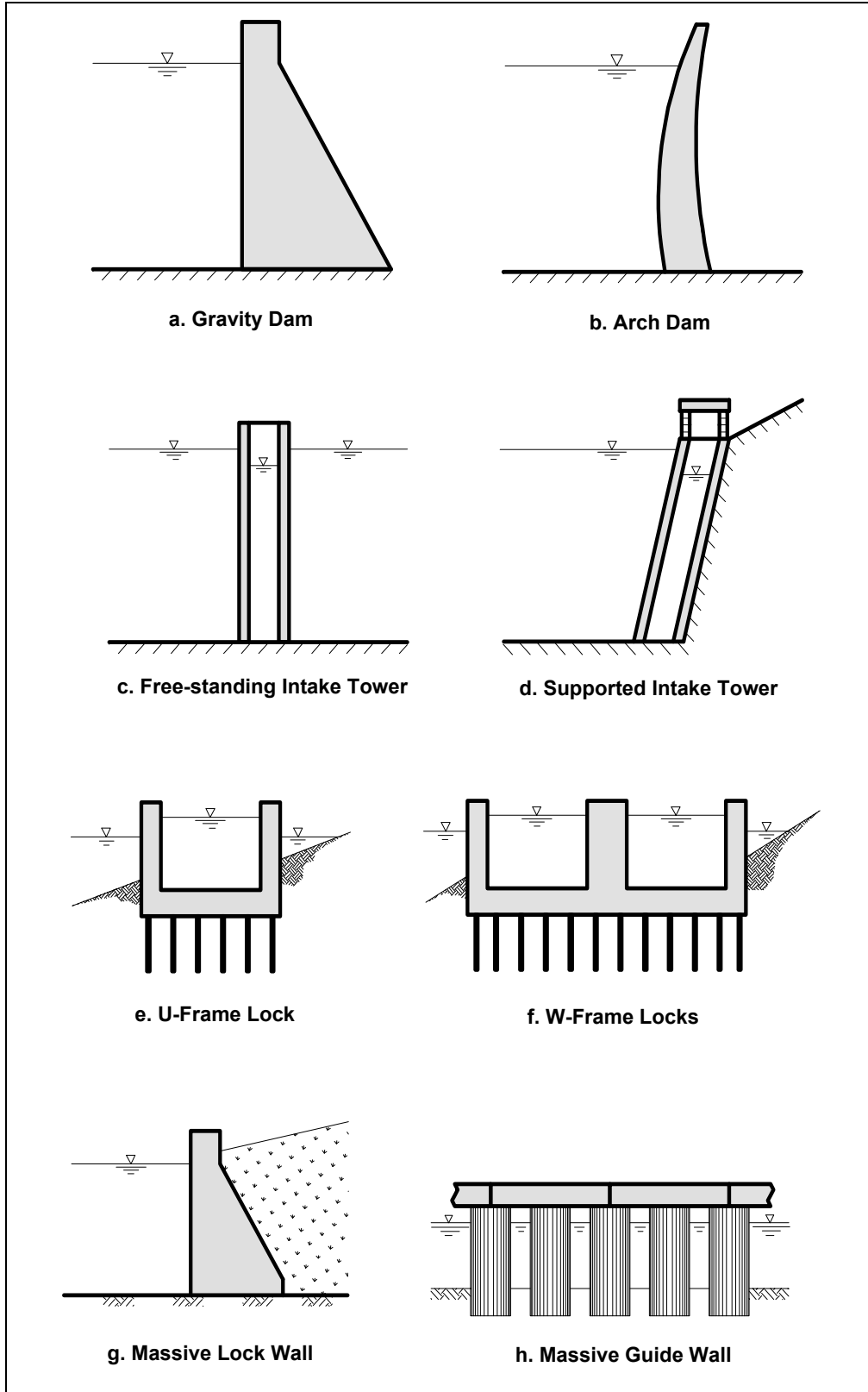


Figure 2-1. Types of concrete hydraulic structures

finite element model in the analysis of both the static and dynamic response of concrete gravity dams. The finite element method not only represents the resistance mechanism more realistically, but it also takes into account the dynamic characteristics of the dam-water-foundation system as well as the characteristics of earthquake ground motion. The inherent strength and stiffness of gravity dams in the cross-stream direction are so great that there usually is no concern about their response to earthquake excitation acting in that direction. However, it has been demonstrated (Chopra 1987) that the dynamic response of a gravity dam to the vertical component of the earthquake motions may be similar in amplitude to that induced by the horizontal ground motions and should be considered in the analysis.

2-4. Concrete Arch Dams

a. An arch dam (Figure 2-1b) is a solid concrete hydraulic structure curved in plan and possibly in elevation, which transmits a large portion of the water pressure and other loads by means of thrust (arch action) to the abutment, therefore utilizing the compressive strength of its material. Deriving their structural behavior from material strength rather than the sheer weight of the dam, arch dams are recognized for their structural competence and economical construction.

b. Arch dams are generally classified as thin, medium-thick, and thick arch dams. Their shapes have gradually changed from the early circular, horizontal, constant-thickness arches and vertical upstream faces to the more elaborate thin double-curvature arch dams with variable radii, variable thickness, and noticeable overhangs.

c. The response of an arch dam to ground shaking is similar to that of a gravity dam in the sense that both types are subject to dynamic response amplification in accordance with the relationships between the frequencies of the dam system and those of the earthquake motions. However, because of the complicated 3-D configuration of an arch dam, its response must be considered with regard to all three components of seismic input. Hence a rather refined 3-D model must be formulated of the dam and its foundation to calculate the vibration properties that control the dynamic amplification of the input accelerations. The inertial and damping effects of the reservoir water have an important effect on the vibration properties and response of an arch dam as they do for a gravity dam, and thus they must be included in the mathematical model as described in paragraph 2-13c.

2-5. Intake-outlet Towers

a. Intake-outlet towers form the entrance to reservoir outlet works. They are often equipped with gates for regulating the release of water, or for lowering the reservoir as a precautionary measure after a major earthquake event. The failure of an intake-outlet tower during an earthquake could possibly disrupt delivery of important public services and sometimes contributed to failure of a dam. It is therefore important that intake-outlet towers in seismically active regions be designed or evaluated to withstand earthquakes using rational analytical methods, which are based on a sound understanding of the dynamic behavior of the tower-water-foundation system.

b. Most intake-outlet towers are free-standing structures surrounded by water and founded on an enlarged base on the reservoir bottom or partially encased through bedrock or hard soil (Figure 2-1c). Some are embedded within embankment dams; others are structurally connected to the upstream of concrete dams. There are yet other intake towers that are inclined against the rock slopes and partially embedded into the bedrock formation (Figure 2-1d). The intake structures at Seven Oaks Dam in southern California and at Cerrillos Dam in Puerto Rico are two examples of inclined towers designed by USACE. The design of Seven

Oaks Dam intake tower also included anchoring it to the inclined slope rock to provide resistance for severe earthquake force demands of the southern California earthquakes.

c. Regardless of their types, intake towers are surrounded by water, sometimes to a significant height, and may contain internal water. Intake towers are therefore subjected to the fluid-structure interaction effects that can significantly influence their responses to earthquakes. The response of intake towers is also influenced by soil-structure interaction (embankment, rock, or soil foundation), and possibly by the access bridge, mass of the internal equipment, and response of the dam when the towers are tied to concrete dams. Depending on the complexity of the geometry of the tower, stick models with beam element and lumped masses or 3-D finite element mathematical models are required to adequately represent their vibration characteristics and their dynamic responses.

2-6. U-frame and W-frame Navigation Locks

Navigation locks are massive concrete hydraulic structures designed to provide navigable pass for towboats during the periods when the riverflows are inadequate. A U-frame (single chamber, Figure 2-1e) or W-frame (dual chamber, Figure 2-1f) lock consists of reinforced concrete walls constructed integrally with a reinforced floor slab founded on a pile foundation. On major navigable rivers, locks are usually built in conjunction with navigation dams, and may cover several hundreds to over one thousand feet in total length. A typical lock normally includes numerous monoliths of variable length and type separated by construction joints. The chamber monoliths make up the main portion of the lock, while the culvert intake, upper gate, culvert valve, culvert discharge, and lower gate monoliths serve as the special-purpose monoliths covering the remaining length of the structure. Lock structures contain water and are bounded by water on the river wall, which may reach a significant height. Thus they are subjected to fluid-structure interaction effects that can influence their response to earthquakes. The response of lock structures can also be affected significantly by the interactions with the soil-pile foundation and the backfill soil. Considering that the SPSI also affects the seismic input motion, SPSI analyses are required to adequately represent both the seismic input and the dynamic response of the pile-founded locks.

2-7. Massive Concrete Lock Walls

At locations where sound and durable rock is available, lock chambers and their extensions upstream and downstream may be constructed with separate massive walls founded on the foundation rock (Figure 2-1g). These gravity-type lock walls usually have a thin or nonexistent floor section. The land wall and river wall may therefore be treated as separate gravity sections subjected to all applicable loads discussed in paragraph 2-16.

2-8. Massive Concrete Guide Walls

a. Massive concrete guide walls control navigation conditions in the upper and lower approach areas of a lock structure. The purpose of the walls is to guide towboat traffic and other vessels into and out of the locks. Guide walls are designed as either a drilled shaft or cellular fixed wall or a floating pontoon wall. Fixed guide walls (Figure 2-1h) normally consist of cast-in-place concrete walls supported on circular sheet pile cells. The loads applied to the foundation from the fixed walls are usually high due to the large quantity of concrete resting on the cells. High seismic loads, large towboat impact loads, and the dead load from the fixed guide walls may require that the cells be founded on steel piles driven through the cells and into the competent rock formation.

b. The floating guide walls usually consist of a floating pontoon spanning pylons, one at each end. The wall may also include a nose pier at one end for protection against direct impacts. A single drilled shaft several feet in diameter may support the pylons while three or more drilled shafts may be required to support the nose piers. The drilled shafts normally consist of a steel pipe filled with reinforced concrete. Similar to the fixed walls, floating approach walls are also designed to resist a variety of loads including barge impact, wind, current forces, and seismic base motions. Both the fixed and floating walls are subjected to the fluid-structure interaction effects that can significantly influence their responses to earthquake and impact loading. The response of approach walls is also influenced by the SPSI effects and should be represented adequately in the analysis.

2-9. Analytical Modeling Procedure

Modeling procedures for time-history analysis of hydraulic structures including the effects of fluid-structure interaction and foundation-structure interaction can be classified into the standard finite element and the substructure methods. In the standard finite element method, the complete structure-water-foundation system is modeled as a single or composite unit. The substructure method consists of dividing the complete system into three substructures: the structure, the water, and the foundation, each of which can be partly analyzed independently of the others. The main difference between the two methods in terms of structural modeling is that the interaction effects of the water and foundation are more accurately represented by the substructure method.

2-10. Substructure Method

a. As stated previously, in the substructure method, the complete system is divided into three substructures: the structure, the water, and the foundation rock region (Figure 2-2). The structure is normally represented as a beam or 2-D or 3-D finite element system, which permits modeling of a general geometry and linear elastic material properties. The water domain may be idealized as a continuum or as a combination of a finite element and continuum system. Dynamic interaction between the structure and the water is expressed as frequency-dependent or frequency-independent hydrodynamic forces at the structure-water interface. The foundation region may also be idealized as a continuum (Dasgupta and Chopra 1979) or as a finite element system. The continuum idealization permits accurate modeling of the structure-foundation interaction when similar materials extend to large depths. For sites where soft rock or soil overlies harder rock at shallow depths, a finite element idealization of the foundation region is more appropriate. Dynamic interaction between the structure and the foundation is expressed by interacting forces at the structure-foundation interface (i.e., base nodes). These interacting forces are frequency-dependent and are related to the displacements through the dynamic stiffness (impedance) matrix for the foundation region.

b. The equations of motion for the structure including the effects of the structure-water interaction and the structure-foundation interaction most conveniently are expressed in the frequency domain, because the hydrodynamic forces and the impedance functions for the foundation region depend on the frequency of excitation. The general form of the frequency domain equations of motion for a structure-water-foundation system is given by

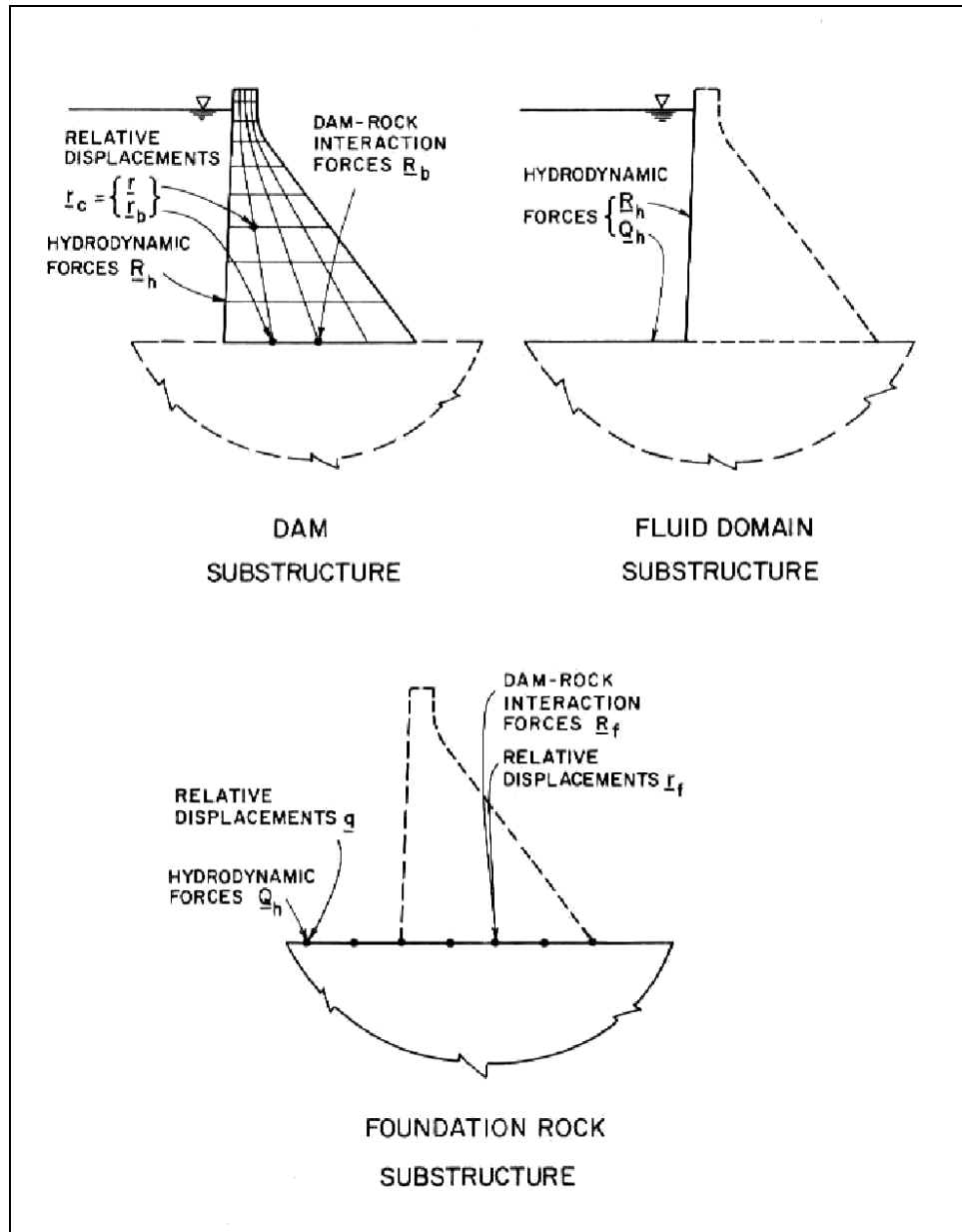


Figure 2-2. Substructure representation of dam-water-foundation system (from Fenves and Chopra 1984b)

$$\begin{aligned}
 & \left\{ -\omega^2 \begin{bmatrix} m & \underline{0} \\ \underline{0} & m_b \end{bmatrix} + (1 + i\eta_s) \begin{bmatrix} k & k_b \\ k_b^T & k_{bb} \end{bmatrix} + \begin{bmatrix} \underline{0} & \underline{0} \\ \underline{0} & \underline{S}_f(\omega) \end{bmatrix} \right\} \begin{Bmatrix} \bar{r}^l(\omega) \\ \bar{r}_b^l(\omega) \end{Bmatrix} = \\
 & - \begin{Bmatrix} m_b^l \\ m_b^l \end{Bmatrix} + \begin{Bmatrix} \bar{R}_h^l(\omega) \\ -\underline{S}_{rq} \underline{S}_{qq}^{-1} \bar{Q}_h(\omega) \end{Bmatrix} \quad (2-1)
 \end{aligned}$$

where

- ω = harmonic excitation frequency
- m = mass submatrix corresponding to nodal points above the base
- m_b = mass submatrix corresponding to nodal points at the base
- i = $\sqrt{-1}$
- η_s = constant hysteretic damping factor for the structure
- k = stiffness submatrix corresponding to nodal points above the base
- = stiffness submatrix corresponding to nodal points at the base
- k_{bb}
 - k_b = coupling stiffness submatrix relating nodal points above the base to nodal points at the base
 - k_b^T = transpose of k_b
- $S_f(\omega)$ = dynamic stiffness matrix of the foundation region defined with respect to nodal points at the base
- $\bar{\Gamma}^l(\omega)$ = frequency response functions for nodal displacements above the base ($l = x, y, \text{ or } z$)
(see Figure 2-2)
- $\bar{\Gamma}_b^l(\omega)$ = frequency response function for nodal displacements at the base (see Figure 2-2)
- $\underline{1}^l$ = subvector of 1's corresponding to nodal points above the base (see Figure 2-2)
- $\underline{1}_b^l$ = subvector of 1's corresponding to nodal points at the base
- $\bar{R}_h^l(\omega)$ = vector of frequency response functions for hydrodynamic forces corresponding to nodal points at the structure-water interface (see Figure 2-2)
- \underline{S}_{rq} = coupling submatrix of dynamic stiffness of foundation region relating nodal points at the foundation surface under the structure base to nodal points at the foundation surface beneath the water
- \underline{S}_{qq} = Submatrix of dynamic stiffness of foundation region defined with respect to nodal points at the foundation surface beneath the water
- $\bar{Q}_h(\omega)$ = vector of frequency response functions for hydrodynamic forces corresponding to nodal points at the foundation surface beneath the water (see Figure 2-2)

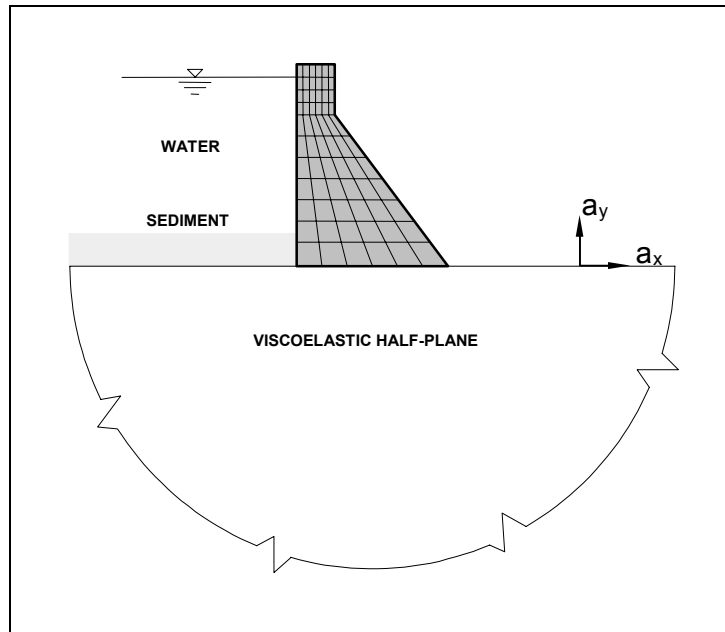
The foundation impedance matrix relates the interacting forces and displacements relative to the free-field ground motion in the l^{th} direction as given by

$$S_f(\omega)\bar{\Gamma}_f^l(\omega) = \bar{R}_f^l(\omega) \quad (2-2)$$

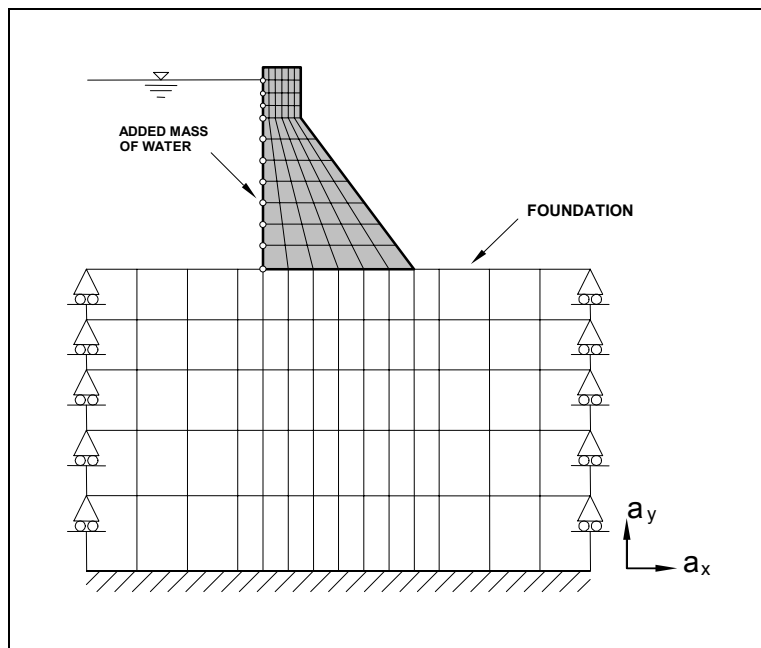
The hydrodynamic forces and the foundation impedance functions are obtained from the separate analysis of the fluid domain and the foundation rock substructures.

2-11. Standard Finite Element Method

In the standard finite element approach, the complete system consisting of the structure, the water, and the foundation region is modeled and analyzed as a single composite structural system. Similar to the substructure approach, the structure is modeled as an assemblage of beams or finite elements. The water and the foundation are generally represented by simplified models that only approximately account for their interactions with the structure. In most cases the water is modeled by an equivalent added hydrodynamic mass, and the foundation rock region is represented by a finite element system accounting for the flexibility of the foundation only. Based on these assumptions the equations of motion for the complete system become



a. Substructure model



b. Standard model

Figure 2-3. Finite element model of gravity dam

$$(m_s + m_a)\ddot{r} + c\dot{r} + kr = -(m_s + m_a)\int_S^x a_g^x(t) - (m_s + m_a)\int_S^y a_g^y(t) - (m_s + m_a)\int_S^z a_g^z(t) \quad (2-3)$$

where

- m_s = mass matrix of the structure
- m_a = added hydrodynamic mass matrix having nonzero terms only at the structure-water nodal points
- \dot{r}, \ddot{r} = velocity and acceleration vectors, respectively
- c = overall damping matrix for the entire system
- k = combined stiffness matrix for structure and foundation region
- r = vector of nodal point displacements for the complete system relative to the rigid base displacement
- $\underline{1}_s^x$ = vector of 1's corresponding to x-DOFs
- $a_g^x(t)$ = ground acceleration input in x-direction

The added hydrodynamic mass generally includes nonzero terms for x-, y- and z-DOFs, because they arise from the hydrodynamic pressures acting normal to the structure-water interface. For the structure-water interface with simple geometry, the added hydrodynamic mass terms associated with certain DOFs may be zero. For example, only the added hydrodynamic mass terms corresponding to the x-DOFs (horizontal direction) are nonzero for a gravity dam having vertical upstream face.

2-12. Concrete Gravity Dams

Conventional concrete gravity dams are constructed as monoliths (blocks) separated by transverse contraction joints. Oriented normal to the dam axis, these vertical joints extend from the foundation to the top of the dam and from the upstream face to the downstream face. For the amplitude of motion expected during strong earthquakes, the shear forces transmitted through the contraction joints are small compared with the inertia forces of the monoliths. For this condition, the monoliths in a long and straight gravity dam tend to vibrate independently, and their responses to earthquakes can be evaluated on the basis of a 2-D model. However, curved gravity dams and those built in narrow canyons need to be analyzed using a 3-D model.

a. 2-D gravity dam model. A 2-D model of a gravity dam for the time-history earthquake analysis consists of a monolith section supported on the flexible foundation rock and impounding a reservoir of water. The tallest monolith or dam cross section is usually selected and modeled using plane stress finite elements. The 2-D model of the selected monolith and the associated foundation rock and the impounded water may be developed as separate systems using the substructure method (Figure 2-3a), or as a complete structural system employing the standard finite element procedures (Figure 2-3b).

(1) Substructure method. In the substructure method the foundation is usually modeled as a viscoelastic half plane (paragraph 2-24b(1)). The interaction between the dam and foundation is represented by an impedance matrix (i.e., $S_f(\omega)$ in Equation 2-2), defined with respect to the nodal points at the dam-foundation rock interface. The impedance matrix for the viscoelastic half plane is obtained from a separate continuum solution of the foundation region (Dasgupta and Chopra 1979). Assuming that reservoir water can be modeled as a fluid domain with constant depth and infinite length in the upstream direction, the frequency-dependent hydrodynamic forces at the dam-water interface also are obtained from a separate continuum solution (paragraph 2-21). The seismic input includes the vertical and one horizontal component of the free-field acceleration time-histories applied at the dam-foundation and at the water-foundation interface regions. Since the foundation impedance matrix and hydrodynamic forces are frequency dependent, the dam response is first carried out in the frequency domain using a discrete Fourier transformation and then the results are presented in the time domain by the application of an inverse discrete Fourier transformation (Fenves and Chopra 1984b).

(2) Standard method. The viscoelastic half plane model discussed in (1) above is applicable to a homogeneous foundation where identical rock properties are assumed to exist for the entire unbounded foundation region. In general, foundation rock properties vary with depth and along the footprint of the dam. The effective modulus of the jointed rock within the shallow depths may significantly differ from that at greater depths. In these situations the viscoelastic half plane model is not appropriate and needs to be replaced by a finite element foundation model that can account for the variation of rock properties. The standard procedure is to develop a complete finite element model, which consists of the dam and an appropriate portion of the foundation region, as shown in Figure 2-3b. The foundation model, however, is assumed to be massless in order to simplify the application of the seismic input and avoid the use of large foundation models (paragraph 2-24a). The foundation mesh needs to be extended a distance at least equal to the dam height in the upstream, downstream, and downward directions. The nodal points at the base of the foundation mesh are fixed both in the vertical and horizontal directions. The side nodes, however, are attached to horizontal roller supports for the horizontal excitation and to vertical roller supports for the vertical excitation of the dam. The earthquake ground motions recorded at the ground surface are directly used as the seismic input and are applied at the base of the foundation model. The impounded water is also assumed to be incompressible so that the dam-water interaction effects can be represented by the equivalent added-mass concept. The added mass is obtained using either the simplified procedure developed by Fenves and Chopra (1986) or the generalized Westergaard method described in paragraph 2-19b.

b. 3-D gravity dam model. Sometimes monolith joints are keyed to interlock two adjacent blocks, or the dam is built in narrow canyons or is curved in plan to accommodate the site topography and to transfer part of the water load to the abutments. In these situations, the dam behaves as a 3-D structure and its response especially to earthquake loading should be evaluated using 3-D idealization similar to that described for arch dams in paragraph 2-13.

2-13. Concrete Arch Dams

Because concrete arch dams are 3-D structures, their responses to earthquake loading must be evaluated using a 3-D model. The 3-D model for an arch dam is developed using the finite element procedures and includes the concrete arch, the foundation rock, and the impounded water (Ghanaat 1993a, 1993b). The arch dam-water-foundation system may be analyzed using the substructure method or the standard finite element procedures. Both methods use the same mathematical model to represent the concrete arch, except that the substructure method permits more rigorous analysis of the dam-foundation and the dam-water interaction effects (Tan and Chopra 1995). The standard method employs a massless foundation rock with an incompressible finite element model for the impounded water (Ghanaat 1993a, 1993b). The substructure method considers not only the foundation flexibility but also the damping and inertial effects of the foundation rock, and also includes a reservoir water model that accounts for the effects of water compressibility and the reservoir boundary absorption.

a. Dam model. Concrete arch dams are usually idealized as an assemblage of finite elements, as shown in Figures 2-4 and 2-5. The finite element model of the dam should closely match the dam geometry and be suitable for application of the various loads and presentation of the stress results. To the extent possible, the finite element model of an arch dam should be developed using a regular mesh with elements being arranged on a grid of vertical and horizontal lines (Figure 2-4). This way the gravity loads can easily be applied to the individual cantilever units, and the stresses computed with respect to local axes of the element surfaces would directly relate to the familiar arch and cantilever stresses. The finite elements appropriate for modeling an arch dam include 3-D solid and shell elements available in the computer program GDAP (Ghanaat 1993a) or a general 3-D solid element with 8 to 21 nodes (Bathe and Wilson 1976). A thin or medium-thick arch dam can be modeled adequately using a single layer of shell elements through the dam thickness. A thick arch dam may

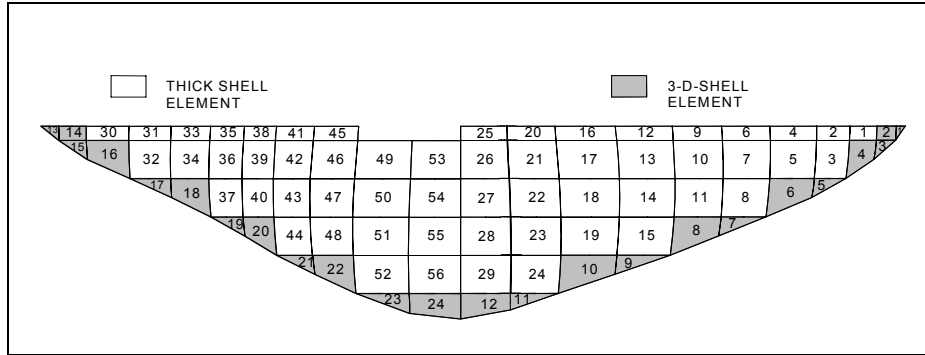


Figure 2-4. Finite element mesh of arch dam showing elements used in the dam

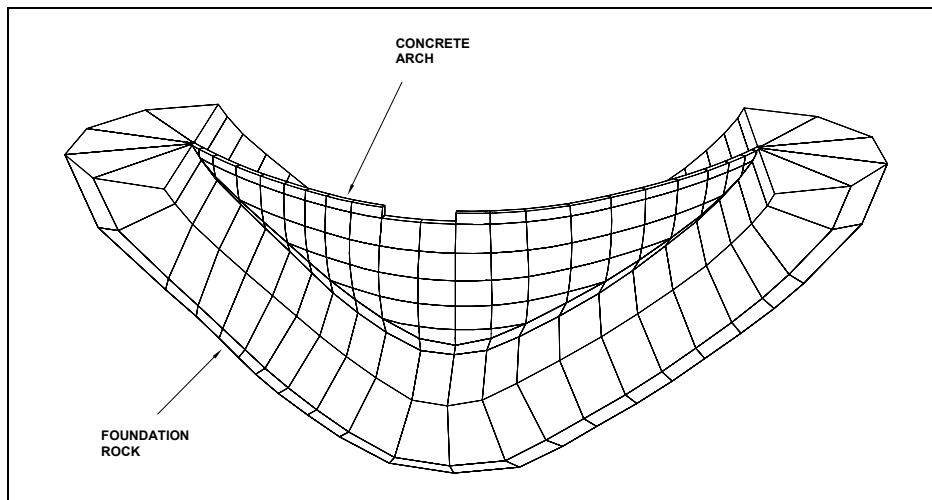


Figure 2-5. Perspective view of dam-foundation finite element model

require three or more layers of solid elements through the dam thickness to better represent its dynamic behavior. The level of finite element mesh refinement depends on the type of elements used. In general, a finite element mesh using the linear 8-node solid elements needs to be finer than that employing shell elements whose displacements and geometry are represented by quadratic functions.

b. Foundation model

(1) The standard foundation model for analysis of arch dams is the massless foundation discussed in paragraph 2-24a, in which only the effects of foundation flexibility are considered. Such a foundation model should extend to a distance beyond which its effects on deflections, stresses, and natural frequencies of the dam become negligible. The size of the foundation model should be determined based on the modulus ratio of the foundation to the concrete E_f/E_c . For a competent foundation rock with $E_f/E_c \geq 1$, a foundation mesh extending one dam height in the upstream, downstream, and downward directions is adequate. For a more flexible foundation rock with E_f/E_c in the range of 1/2 to 1/4, the foundation model should extend at least twice the dam height in all directions and include more elements. In general, the foundation model can be developed to match the natural topography of the foundation rock region. Such a refined model, however, is not usually required in practice. Instead, a prismatic model employed in the GDAP program (Ghanaat 1993a) and shown in Figure 2-5 may be used. The seismic input for the massless foundation model includes three-component ground acceleration time-histories applied at the fixed boundary nodes of the foundation mesh. Since no wave propagation takes place in the massless foundation model, the seismic input is obtained from

the earthquake motions recorded on the ground surface using scaling or spectrum-matching procedures described in Chapter 5.

(2) In the substructure method of arch dam analysis, the impedance matrix of the foundation rock region is employed to represent dam-foundation interaction effects (Tan and Chopra 1995). The impedance matrix (or frequency-dependent stiffness matrix) includes both the inertia and damping of the foundation rock region as well as its flexibility. This impedance matrix for arch dams is determined using a direct boundary element formulation applied to a uniform cross-section canyon cut in a homogeneous viscoelastic half space (Zhang and Chopra 1991). The assumption of a uniform cross-section canyon is to reduce the original 3-D boundary value problem into an infinite series of 2-D problems. The foundation model therefore is represented by the dam-foundation rock interface discretized into a set of boundary elements whose nodal points match the finite element idealization of the dam (Tan and Chopra 1995). The properties of the foundation rock are characterized by its Young's modulus, Poisson's ratio, and unit weight, which are assumed to be constant over the entire unbounded foundation region. Although this foundation model overcomes the limitations of the massless foundation, it overestimates damping for a foundation rock having relatively low modulus.

c. Reservoir water.

(1) The standard dam-water interaction analysis for arch dams is based on the finite element added hydrodynamic mass model described in paragraph 2-20a (Ghanaat 1993a). Assuming the water is incompressible, the hydrodynamic pressures acting on the dam-water interface are first obtained from the finite element solution of wave equation and then converted into equivalent added-mass terms. The resulting added-mass terms are subsequently combined with the mass of concrete nodal points on the dam-water interface. In most cases a prismatic finite element fluid mesh similar to that shown in Figure 2-22 (paragraph 2-20) is adequate for computation of the added hydrodynamic mass. However, for reservoirs with irregular topography and shape, a fluid mesh that matches the actual reservoir topography is recommended (Figure 2-6).

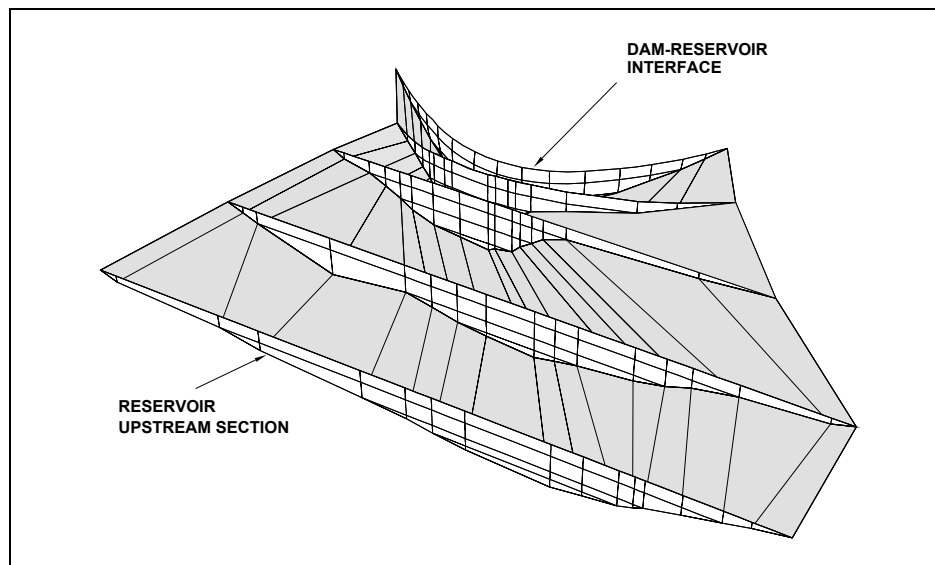


Figure 2-6. Finite element mesh for incompressible water developed to match reservoir bottom topography (shaded region)

(2) A rigorous analysis of the dam-water interaction may be required when the fundamental frequency of the reservoir water is relatively close to fundamental frequency of the dam. Such an analysis, which includes the effects of water compressibility and reservoir boundary absorption on the response of the dam, is performed as described in paragraph 2-21.

2-14. Intake-outlet Towers

Intake-outlet towers are designed in various structural configurations and geometric shapes. In terms of their structural configurations, they may be classified into two types: free-standing and supported towers. Free-standing towers are vertical structures typically founded on an enlarged base on the reservoir bottom or deeply embedded in bedrock or stiff soils. The elevation profile may be uniform or tapered, and the plan section may be rectangular, circular, or irregular. Supported towers are built against an abutment to provide increased structural stability and improved seismic performance. They may be designed as vertical or inclined towers supported in the lower portion or along the entire length. Like the free-standing towers, the supported towers are also designed in various geometric shapes, but they are subjected to earthquake excitation at the base as well as along the abutment supports. The following paragraphs discuss the modeling procedures for both types of towers.

a. Free-standing towers. Free-standing towers may be modeled using the substructure or standard finite element method of analysis. The available substructure method is restricted to a tower supported on the horizontal ground surface and has two axes of plan symmetry with homogeneous material properties for the unbounded foundation region (Goyal and Chopra 1989). The standard finite element model is not restricted to homogeneous material properties for the foundation but employs foundation models that account only approximately for the foundation-structure interaction. Each model is described in the following paragraphs.

(1) Standard finite element model.

(a) Free-standing towers with regular cross-section geometry, whose dimensions may remain constant or vary along the height of the tower, can be idealized adequately using beam elements as depicted in Figure 2-7. Slender towers exhibit primarily flexural behavior, and their responses may be approximated ignoring the shear deformations. The response of squat towers (i.e., towers with a height-to-width ratio less than 10), especially for higher modes, is affected by shear deformations and should be considered in the analysis by using beam elements that include shear deformation capabilities. The response of towers is also influenced by the water-structure interaction, foundation-structure interaction, mass of internal equipment, and possibly the access bridge. The water-structure interaction is approximated by the added hydrodynamic mass described in paragraph 2-19*d*. The added hydrodynamic mass and the mass of the structure are lumped at the element nodal points. The foundation-structure interaction effects are approximately represented by equivalent linear springs attached to the base or to the embedded part of the model. If permitted by the computer program selected for the analysis, a combination of springs and dashpots may be used to represent the unbounded foundation region (paragraph 2-25*a*). For towers accessed by a light footbridge, the effects of the bridge may be considered by simply lumping part or all of the mass of the bridge at the nearest nodal points. A massive reinforced concrete access bridge, however, may significantly influence the response of a flexible tower, and its effects should be accounted for by modeling the bridge as part of the tower structure, as shown in Figure 2-7. The effects of a flexible access bridge may be negligible on the response of a stiff tower because their fundamental frequencies are completely different, but the tower provides support and excitation to the bridge and its effects on the response of the bridge should be considered.

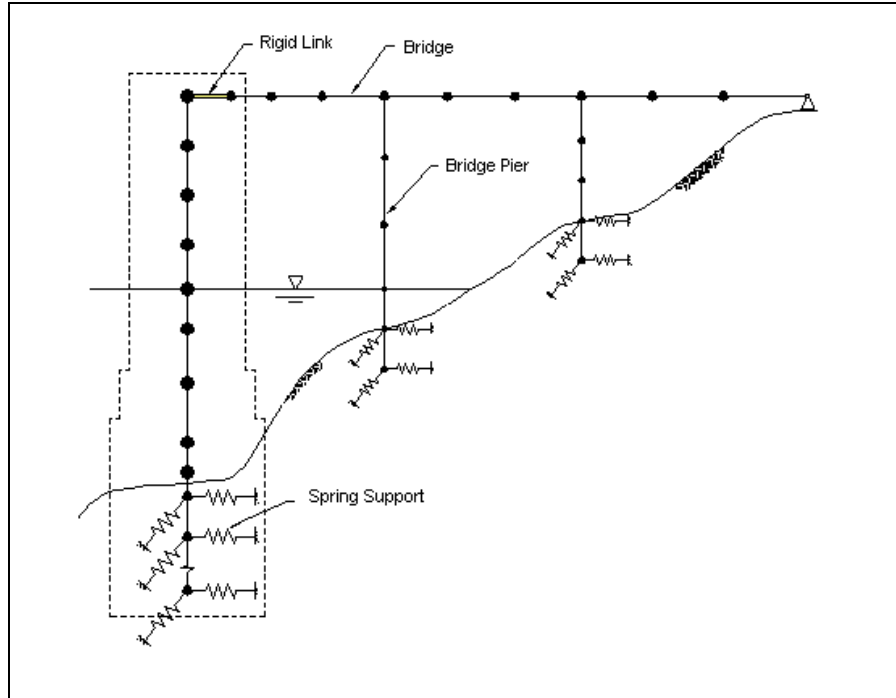


Figure 2-7. Finite element idealization of free-standing tower and access bridge

(b) The earthquake input for the tower beam model described in (a) above is defined by two horizontal components of the free-field ground acceleration time-histories. The effect of the vertical component of ground motion is expected to be negligible and is therefore not considered in the analysis. The ground motion is assumed to be identical at all support points.

(c) An irregular free-standing tower may require finite element discretization using solid elements as discussed in *b* below. In that case a finite element foundation model should also be developed. The earthquake excitation for such a model is defined by the vertical and two horizontal components of the free-field ground acceleration histories.

(2) Substructuring model.

(a) Free-standing towers supported on the horizontal surface of flexible rock or soil may be idealized as four separate substructures: the tower, the surrounding water domain, the inside water domain, and the foundation rock or soil system (Figure 2-8). The available substructuring procedure for intake-outlet towers assumes the tower to have arbitrary geometry, but it must have two axes of plan symmetry (Goyal and Chopra 1989). The tower is modeled as an assemblage of one-dimensional beam elements, including bending and shear deformations as well as rotatory inertia (Figure 2-9). Each beam element node has two degrees of freedom, translational and rotational displacements. The part of foundation block above the ground surface may be assumed rigid or represented by beam elements as part of the tower; the remaining part below the ground surface is treated as a rigid footing of negligible thickness supported by a homogeneous viscoelastic half space. The impedance functions (frequency-dependent stiffness) of the homogeneous viscoelastic halfspace are obtained from the analytical solution available for a circular foundation. For noncircular foundations, the impedance functions are determined approximately by using an equivalent circular foundation that has the same area and moment of inertia as the actual foundation.

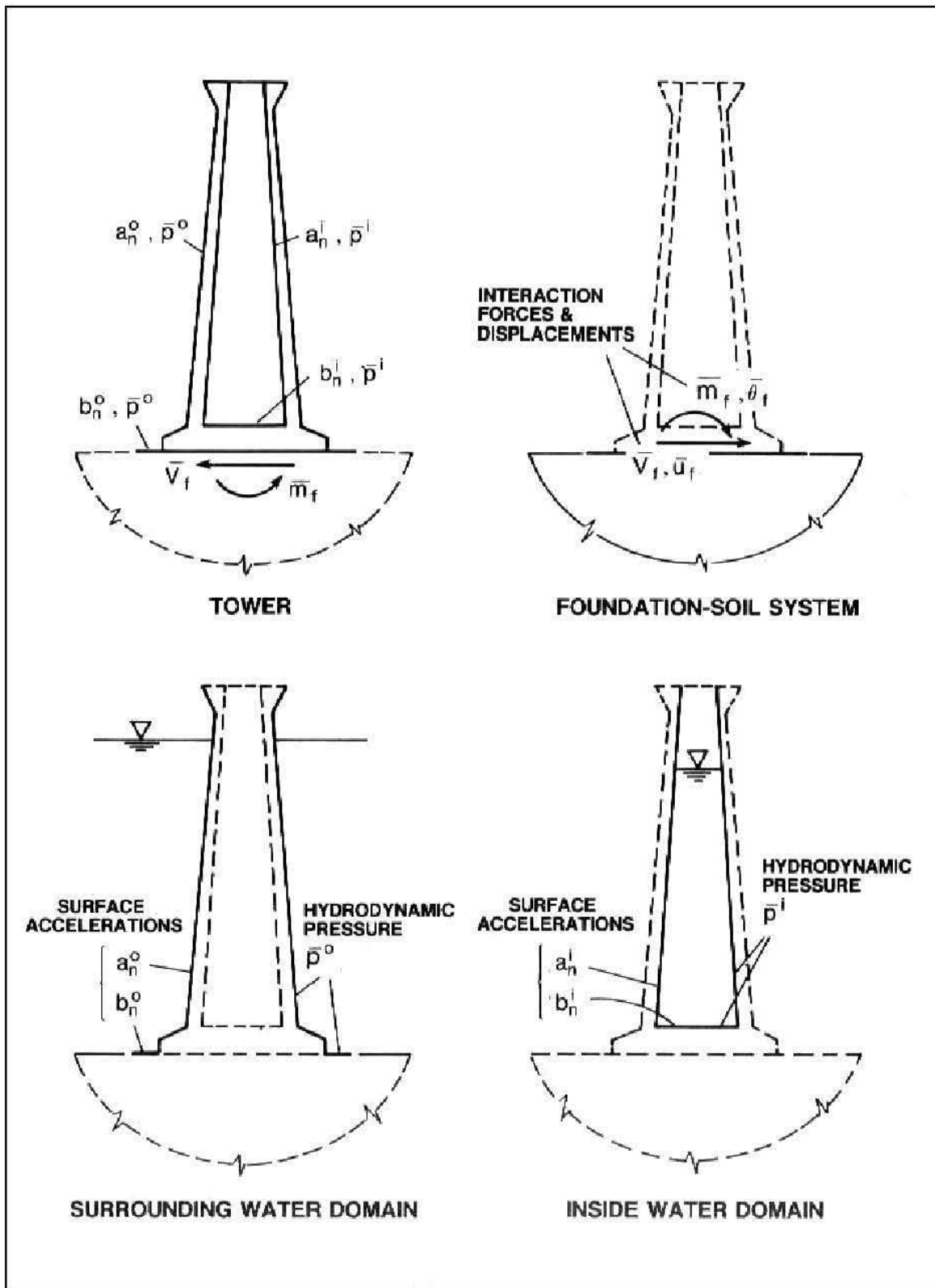


Figure 2-8. Substructure representation of tower-water-foundation soil system (from Goyal and Chopra 1989)

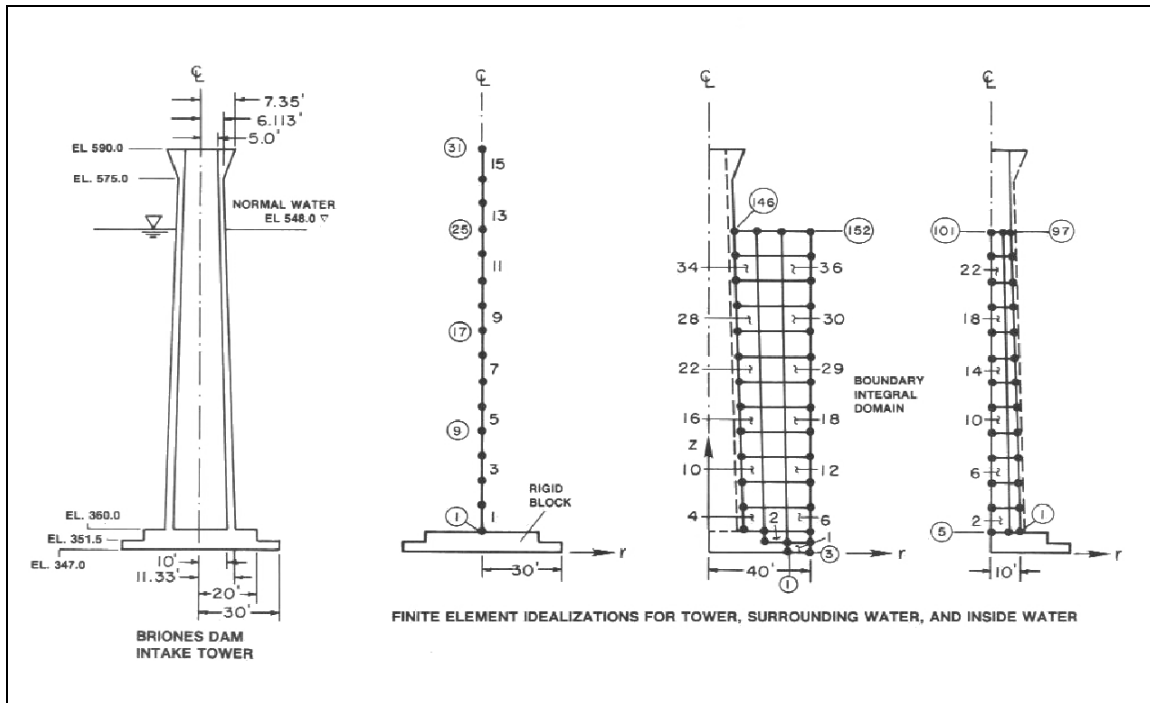


Figure 2-9. Finite element idealization of Briones Dam intake tower (from Goyal and Chopra 1989)

(b) The lateral hydrodynamic forces and external hydrodynamic moments due to pressures on the outside and inside surfaces of the tower are determined by the finite element coupled with the boundary integral procedure described in paragraph 2-20b. The fluid domain between the outside surface of the tower and a hypothetical cylindrical surface is discretized by finite elements, and the effects of the fluid domain beyond the hypothetical surface are treated by boundary integral procedures (Figure 2-9). The analysis of inside water for determining the lateral hydrodynamic forces and external moments acting on the inside face of the tower is carried out by the finite element discretization, as shown in Figure 2-9. The solution neglects the effects of surface wave and water compressibility, but has been shown to be valid for towers with a wide range of slenderness ratios and excitation frequencies (Liaw and Chopra 1973, 1974).

(c) The earthquake excitation for the tower-water-foundation system is defined by two horizontal components of the free-field ground acceleration. The vertical component of ground motion is expected to have little influence on the response of towers and is therefore not considered in the analysis. The ground motion is assumed to be identical at all points on the horizontal base of the tower. The dynamic response of the tower for each horizontal component of ground motion can be evaluated separately and the responses to the two components superimposed to determine the total response.

b. Supported towers

(1) For dams in regions of high seismicity where a free-standing tower may not be feasible, an intake structure supported against the abutment should be considered. Two examples of supported towers are the inclined intake structure for the Seven Oaks Dam by U.S. Army Engineer District, Los Angeles, and the vertical intake/outlet tower for the Eastside Reservoir Project by the Metropolitan Water District of Southern California. The Seven Oaks intake structure, shown in Figure 2-10, is a reinforced concrete intake tower inclined against the abutment and partially embedded into the rock formation. Located in southern California, the inclined tower was anchored to the rock slope to withstand the earthquake forces generated by OBE and MCE events.

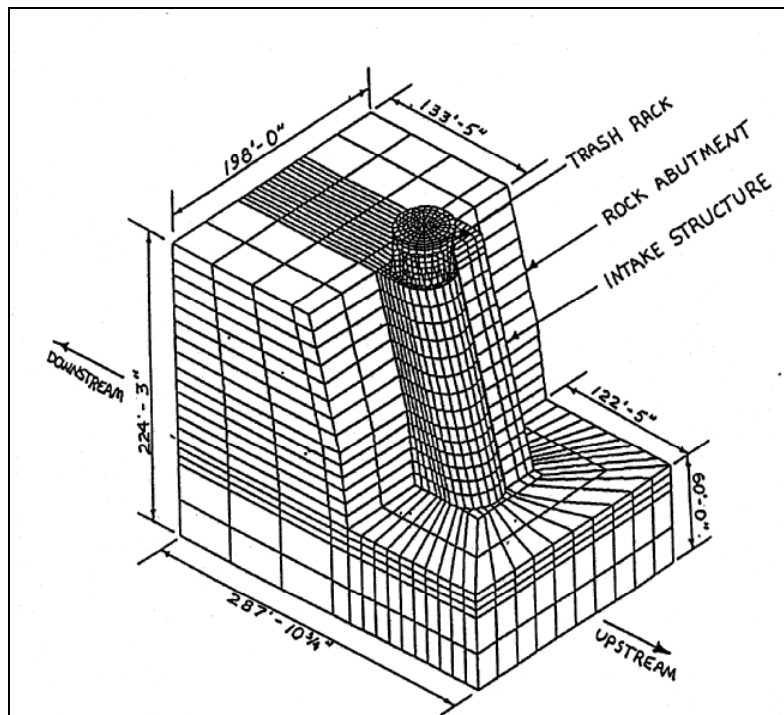
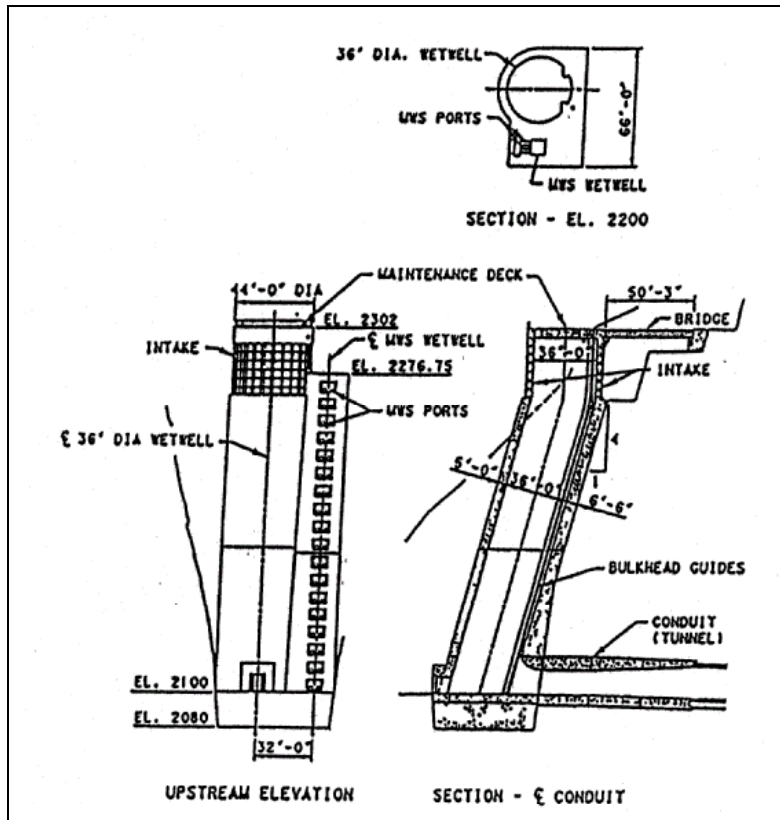


Figure 2-10. Seven Oaks Dam intake structure and associated finite element idealization (U.S. Army Engineer District, Los Angeles, 1992)

(2) The 3-D geometry of supported towers combined with severe seismic demand and substantial hydrodynamic forces influenced by the complicated site topography requires a 3-D finite element treatment of the structure. In addition, the nonuniform distribution of mass and stiffness and the irregular geometry of the tower cross section usually produce complicated bending and torsional behavior that can be captured only by a 3-D idealization of the structure. Generally, supported towers should be discretized using a combination of 3-D solid and shell elements or simply by 3-D solid elements. However, some components of the tower such as the trashrack may be modeled more appropriately using beam elements. The tower-foundation interaction may be considered by including an appropriate volume of the surrounding abutment-foundation rock region as part of the finite element model of the tower. The foundation model should be developed to have dimensions approximately equal to the height of the tower in all three directions. In practice, the massless foundation rock model discussed in paragraph 2-24a is usually adequate, while foundation soil models may be represented by equivalent springs or by a combination of springs and dashpots described in paragraph 2-25a. Figure 2-10b shows a finite element model of Seven Oaks intake structure constructed exclusively of 8-node solid elements, except that a combination of 3-D solid and beam elements was used in idealization of the trash rack. The seismic input for analysis of the supported towers includes three components of ground acceleration time-histories applied at the fixed exterior nodes of the foundation model.

(3) The effect of hydrodynamic pressures on supported towers is represented by the equivalent added-mass concept (paragraph 2-19). The added hydrodynamic mass for these towers, however, depends not only on the geometry of the tower but also on topography of the surrounding abutment-foundation region and should be computed using the finite element or boundary element procedures described in paragraph 2-20c. Figure 2-24 (paragraph 2-20c) is an example of the boundary element added-mass model applied to the analysis of Seven Oaks intake tower.

2-15. U-frame and W-frame Navigation Locks

The interactions with the soil-pile foundation, backfill soil, and the contained water can significantly affect dynamic response of lock structures. These effects should therefore be modeled with reasonable accuracy in the time-history analysis. In most cases water-structure interaction is adequately represented by the added hydrodynamic mass described in paragraph 2-15a(3). The SPSI effects can be incorporated in the analysis by two different approaches: direct method and substructure method. In the direct method, a complete model of the soil-pile-structure system is developed and subjected to a prescribed input motion. For lock structures whose monoliths are supported by several hundred piles, the 3-D direct method of SPSI analysis may not be feasible. In these situations, a series of 2-D approximations of the complete soil-pile-structure system is required in order to capture the 3-D effects. The 2-D approximation should be attempted for both the upstream-downstream and the cross-stream directions. In the substructure method, the lock structure and the foundation soil including the piles are treated separately. The structure is modeled using the standard finite element method. The soil-pile foundation is represented by impedance functions in the form of springs and dashpots attached to the base of the structure. The earthquake response of the structure is then computed by subjecting the soil-pile-structure system to a foundation-input motion.

a. Direct method. The 2-D direct method of SPSI analysis can be carried out using the computer program FLUSH (Lysmer et al. 1975). In this program, the response computation is carried out in the frequency domain and then the results are converted into time domain by the inverse Fourier transformation. The method of response computation in the frequency domain is described in Chapter 3.

(1) Lock model. A cross section of the lock monolith is idealized using primarily 2-D solid concrete elements. Rigid links and beam elements may be required for modeling the rigid connections and the beam-like components. Minor voids and stiffness irregularities present in the lock monolith may be represented by a *smear*d 2-D model in which the mass and stiffness of corresponding elements are adjusted (reduced) to

account for such effects. Major voids may still be smeared in 2-D elements, but upper and lower bound models consisting of solid and partially hollow sections may also be required. The model of a bridge monolith, which supports an access bridge, should include the bridge piers as part of the finite element model of the lock, as shown in Figure 2-11. The mass of the bridge deck, if significant, may simply be lumped at the top of the piers.

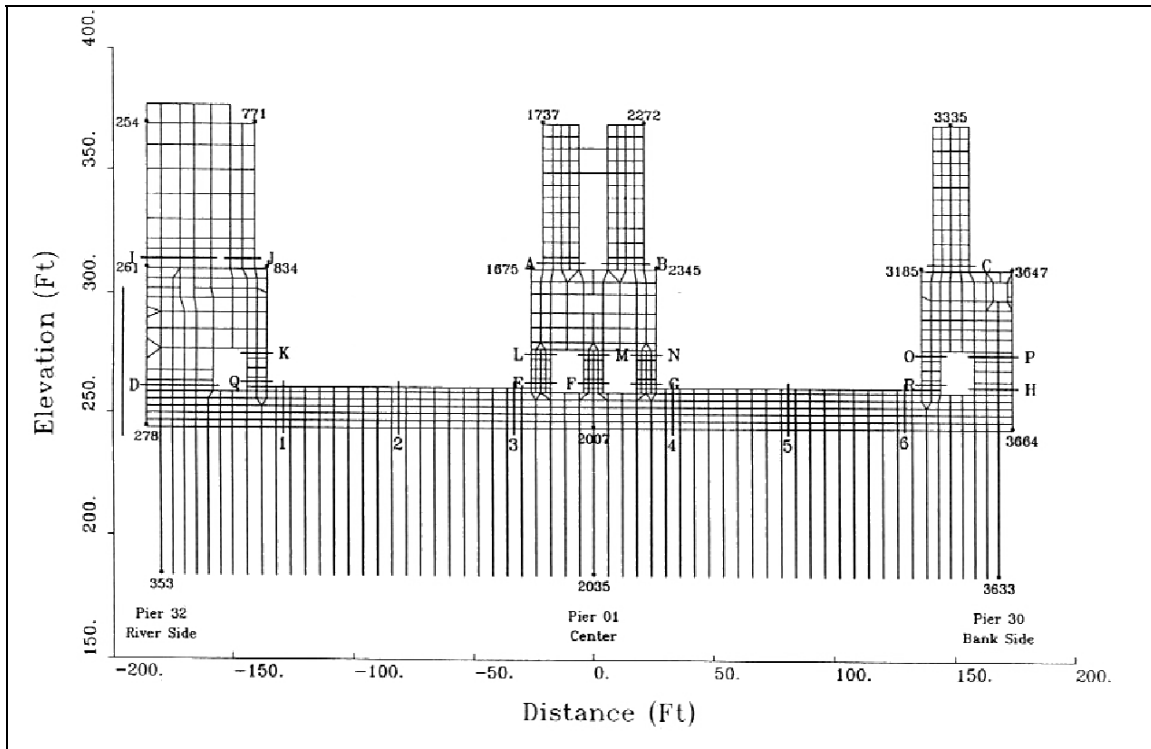


Figure 2-11. Finite element idealization of bridge pier monolith and associated H-piles for Olmsted Locks (U.S. Army Engineer District, Louisville, 1994a)

(2) Soil-pile foundation model

(a) For the SPSI analysis, each individual pile is modeled by a series of beam elements and the supporting soil is represented by plane-strain 2-D solid elements (Figure 2-12). To simulate the rigidity of the connection between the pile head and the basemat of the lock structure, the pile elements should be extended a minimum of 0.9 m (3 ft) into the basemat or special provisions adapted to ensure the moment transfer between the concrete solid elements and the pile beam elements. The vertical dimension of the soil elements should be selected carefully, because it controls the maximum frequency of the motion that can be retained in the analysis. As suggested by Lysmer et al. (1975) the vertical dimension of the soil elements should not be greater than 1/5 of the shortest wavelength of interest. The shortest wavelength of interest is defined as the ratio of the lowest shear wave velocity to the maximum frequency to be retained in the analysis. The horizontal dimension of soil elements can be selected several times the vertical dimension and may be governed by the pile spacing and other conditions.

(b) The soil model should also include a thin soft layer of about 76 mm (3 in.) beneath the lock structure in order to simulate the seismic loads being carried primarily by piles, as required by EM 1110-2-2906. Another reason for including a thin soft layer or gap beneath the lock is because complete fixity between the

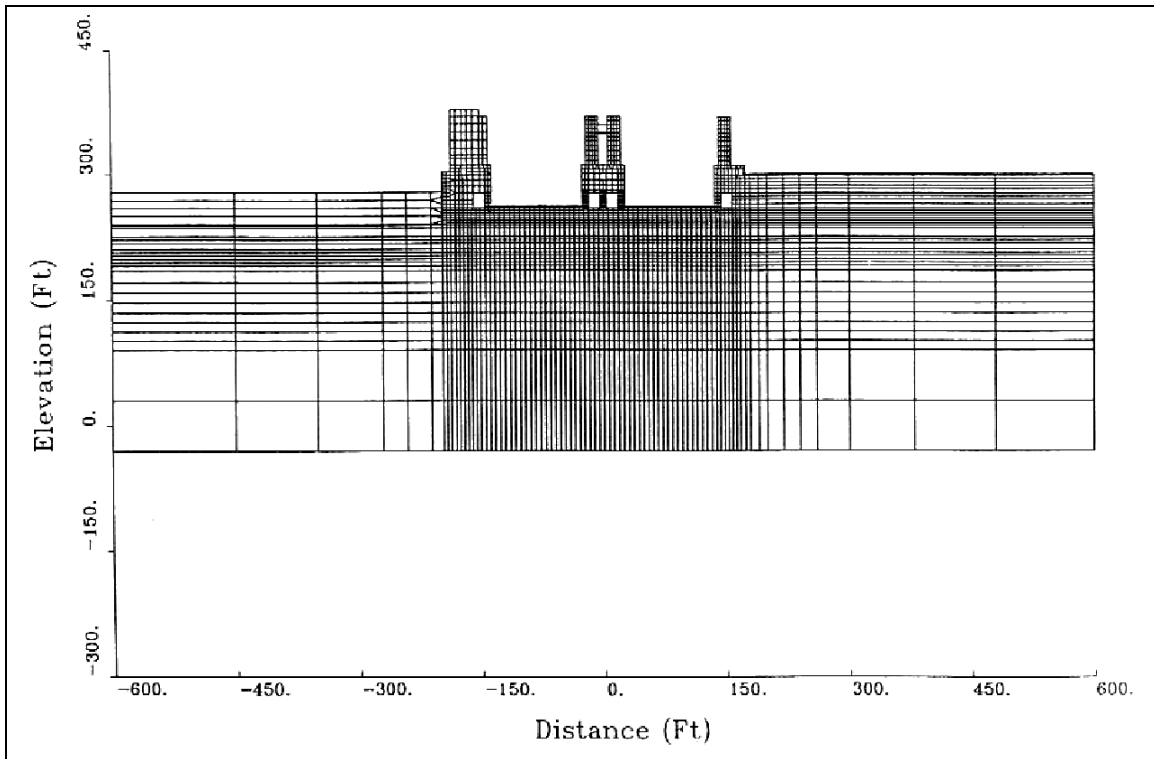


Figure 2-12. Finite element representation of bridge pier monolith, soil-pile foundation, and backfill soils for Olmsted Locks (U.S. Army Engineer District, Louisville, 1994)

lock and underlying soil either does not exist or is diminished during the ground shaking. It is therefore necessary to consider such a possibility to ensure a conservative design with sufficient numbers of piles.

(c) Another important aspect of the soil-pile foundation analysis is the appropriate characterization of the dynamic soil properties. Both the shear modulus and soil damping affect the foundation response and the soil-structure interaction. These parameters need to be defined in terms of both the low-strain shear modulus and damping and their variation with shearing strain. The large shear deformations that occur in soils during strong earthquakes introduce significant nonlinear behavior in the foundation soil region that must be accounted for in the analysis. In the frequency domain SPSI analysis, which is limited to the linear viscoelastic system, the nonlinear soil response is approximated by the equivalent linear method (Seed and Idriss 1969). According to this method a linear analysis can provide an approximate nonlinear solution if the stiffness and damping used in the analysis are compatible with the level of shear strains developed in the soil. Seed and Idriss (1970) provide data on variation of shear modulus and damping with shear strain for typical clays and sands.

(3) Water-structure interaction model.

(a) Earthquake ground motions generate two types of hydrodynamic pressures in a lock structure—impulsive and convective. The impulsive pressure represents the effects of that portion of the water that moves in unison with the lock; the convective pressure represents the effects of the sloshing action of the water. The impulsive pressures exerted on the lock walls during earthquake ground shaking are computed using the velocity potential method described in paragraph 2-19c. For the purpose of computing hydrodynamic pressures, and only for this purpose, the lock walls are assumed to be rigid. The pressure distribution obtained in this manner is converted into nodal lumped masses according to the tributary area

associated with each node. These hydrodynamic masses are then considered as additional nodal masses in the earthquake analysis of the lock. The added hydrodynamic mass should be computed for all lock walls subjected to the hydrodynamic pressures during earthquake excitation. For example, the added hydrodynamic mass for a w-frame lock (Figure 2-11) may be required for the inside surface of the land wall, both sides of the center wall, and the inside and outside surfaces of the river wall. Impulsive pressures are also exerted on the lock floor, but the added hydrodynamic masses associated with the floor pressures must be considered only in the vertical direction.

(b) Convective pressures associated with the water sloshing are evaluated as described in paragraph 2-19c(2). The fundamental period of water sloshing for a typical navigation lock is usually several seconds long. At such long periods the generated hydrodynamic pressures are probably as much as two orders of magnitude smaller than the impulsive hydrodynamic pressures. The effect of water sloshing on the response of navigation locks is therefore negligible and may be ignored.

b. Substructure method. In the substructure method of analysis the lock structure and the foundation soil including piles are treated separately. Similar to the direct method, the lock structure is idealized by the standard finite element method as described in *a(1)* above. The soil-pile foundation is represented either by impedance functions in the form of frequency-dependent springs and dashpots or by simple frequency-independent springs attached to the base of the structure as described in the following paragraphs.

(1) Impedance function (dynamic stiffness). The impedance functions are complex frequency-dependent coefficients whose real part can be visualized as a frequency-dependent spring coefficient and the imaginary part as a frequency-dependent damping coefficient. Also known as the dynamic stiffness, the impedance functions are computed by analytical or numerical solutions. The numerical solution of the dynamic stiffness of the soil-pile foundation may involve development of a model similar to that described in *a(2)* above. Usually the foundation mat is assumed to be rigid and the piles embedded in a layered soil medium. The properties of each soil layer and each pile are characterized by their corresponding modulus of elasticity, mass density, Poisson's ratio, and material damping. The solution is carried out in the frequency domain by applying unit harmonic loads at the structure-foundation interface nodes and obtaining the displacements or flexibility coefficients at the corresponding degrees of freedom. The dynamic stiffness is then computed by inverting the dynamic flexibility. Note that all the operations must be repeated for each frequency. Incorporation of the dynamic stiffness in the subsequent structural analysis depends on the capabilities of the computer program selected for the analysis. If the computer program selected for the subsequent structural analysis can perform response analysis in the frequency domain, the dynamic stiffness can be used directly as the input. Otherwise the impedance function needs to be approximated at or near the fundamental frequency of the system by frequency-independent stiffness, mass, and damping coefficients.

(2) Frequency-independent spring, mass, and damping. The impedance function may be approximated by frequency-independent stiffness, mass, and damping at or near the fundamental frequency of the system using regression or curve-fitting procedures. The real part of the impedance function represents mainly the stiffness and inertia of the foundation, and the imaginary component reflects the radiation and material damping. The real part Re may be approximated by:

$$Re[I(\omega)] = K - \omega^2 M \quad (2-4)$$

where

$I(\omega)$ = impedance function at frequency ω

K = stiffness coefficient

M = mass coefficient

The imaginary part of the impedance function Im is approximated by:

$$Im[I(\omega)] = i\omega C \quad (2-5)$$

where C is the damping coefficient. Using these approximate relationships the spring, mass, and damping coefficients corresponding to each structure-foundation interface DOFs are selected such that they would reproduce as closely as possible the actual impedance function. The procedure usually provides a good fit in the low and medium frequency ranges, but the inertia term leads to a significant error in the higher frequencies. Although this approximation provides frequency-independent lumped parameters, the structural analysis program should have capabilities for including dashpots at selected DOFs.

2-16. Massive Concrete Lock Walls

a. Massive walls with no backfill. The time-history dynamic response of a massive lock wall with no backfill soil can be evaluated using the standard finite element procedures described in paragraph 2-12a(2) for concrete gravity dams. A 2-D model of the wall section and the associated foundation rock is developed as described for gravity dams and illustrated in Figure 2-3b. The hydrodynamic pressures exerted on the lock wall are computed using the velocity potential method discussed in paragraph 2-19c. The resulting pressure distribution is then converted into equivalent nodal masses according to the tributary area associated with each node. Details of the finite element modeling of the wall section and the foundation rock and the application of seismic input should closely follow those of the gravity dams.

b. Massive walls with backfill. The time-history response evaluation of lock walls with backfill soil is more complicated because in addition to the interaction with the foundation rock and water, the wall is also subjected to the dynamic soil pressures induced by ground shaking. In this situation an accurate evaluation of the dynamic soil pressures is essential to the seismic analysis and design of the lock wall. The available methods of analysis of the backfill soil pressures fall into three categories according to the expected movement of the backfill and wall during seismic events.

(1) Yielding backfill. The relative motions of the wall and backfill material are sufficiently large to induce a limit or failure state in the soil. Representative of this approach is the well-known Mononobe-Okabe method (Mononobe and Matuo 1929; Okabe 1924) and its several variations, in which a wedge of soil bounded by the wall and an assumed failure plane are considered to move as a rigid body subjected to the same ground acceleration. The dynamic soil pressures using this approach are obtained as described in Ebeling and Morrison (1992). The resulting dynamic pressures expressed in terms of an equivalent force are then considered as an external load in the time-history analysis of the wall-foundation system as described in *a* above.

(2) Nonyielding backfill. For sufficiently low intensity ground motions the backfill material may be considered to respond within the linear elastic range of deformations. Under this condition the shear strength of the soil is not fully mobilized and the backfill is said to be nonyielding. The dynamic soil pressures and associated forces for a nonyielding backfill are computed on the basis of elastic response. The dynamic pressures of a backfill idealized as a semi-infinite uniform soil layer can be computed using a constant-parameter SDOF model (Veletsos and Younan 1994) or a more elaborate frequency-independent, lumped-parameter, MDOF system (Wolf 1995). The dynamic pressures for a more general backfill soil condition can be determined by the finite element method discussed in (3) below.

(3) Intermediate case. The intermediate case in which the backfill soil undergoes nonlinear deformations can be represented by the finite element procedures using a soil-structure-interaction computer program such as FLUSH (Lysmer et al. 1975). As illustrated in Figure 2-13, a SPSI model of the wall section should include interaction with the foundation rock, backfill soil, and the water. The wall section is idealized primarily using 2-D solid concrete elements. The foundation rock is represented by plane-strain 2-D solid elements with modulus, Poisson's ratio, and unit weight appropriate for the rock. Transmitting boundaries in the form of dashpots are introduced at the sides of the foundation rock to account for the radiation damping. The backfill soil is modeled using plane-strain 2-D soil elements. The model should account for the variation of soil properties with depth and the material nonlinear behavior of soil. The shear modulus and soil damping vary with level of shearing strain. The nonlinear behavior is usually approximated by the equivalent linear method. The unbounded boundary condition of the backfill soil may be represented by dashpots. The hydrodynamic pressures exerted on the lock wall are computed using the velocity potential method discussed in paragraph 2-19c.

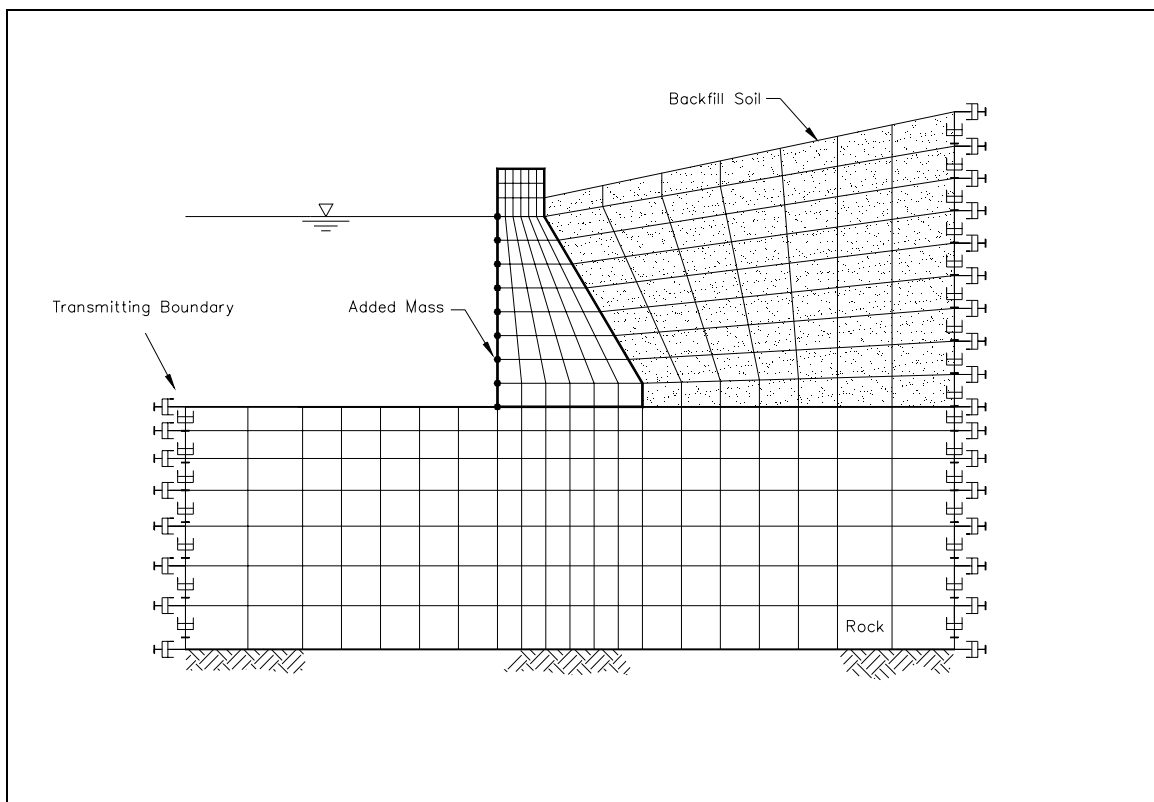


Figure 2-13. Finite element discretization of concrete lock wall, foundation rock, and backfill soil with transmitting boundaries

2-17. Massive Concrete Guide Walls

The time-history analysis of a fixed guide wall supported on cells or drilled shafts is best represented by a 3-D soil-structure-interaction (SSI) analysis. Such analysis can be performed using the computer program SASSI (Lysmer et al. 1981) or other programs and methods with similar capabilities. Since the precast concrete beams placed on the wall are not structurally connected to the wall, the 3-D model may include only one cellular pile or drilled shaft as shown in Figure 2-14. The model may be developed for analysis in the critical transverse direction (i.e., perpendicular to long axis). Whenever possible the model should take advantage of the structural symmetry to reduce the size of the problem and make the numerical solution more manageable.

The overall model usually consists of various components including the cellular sheet pile, soil layers and soil

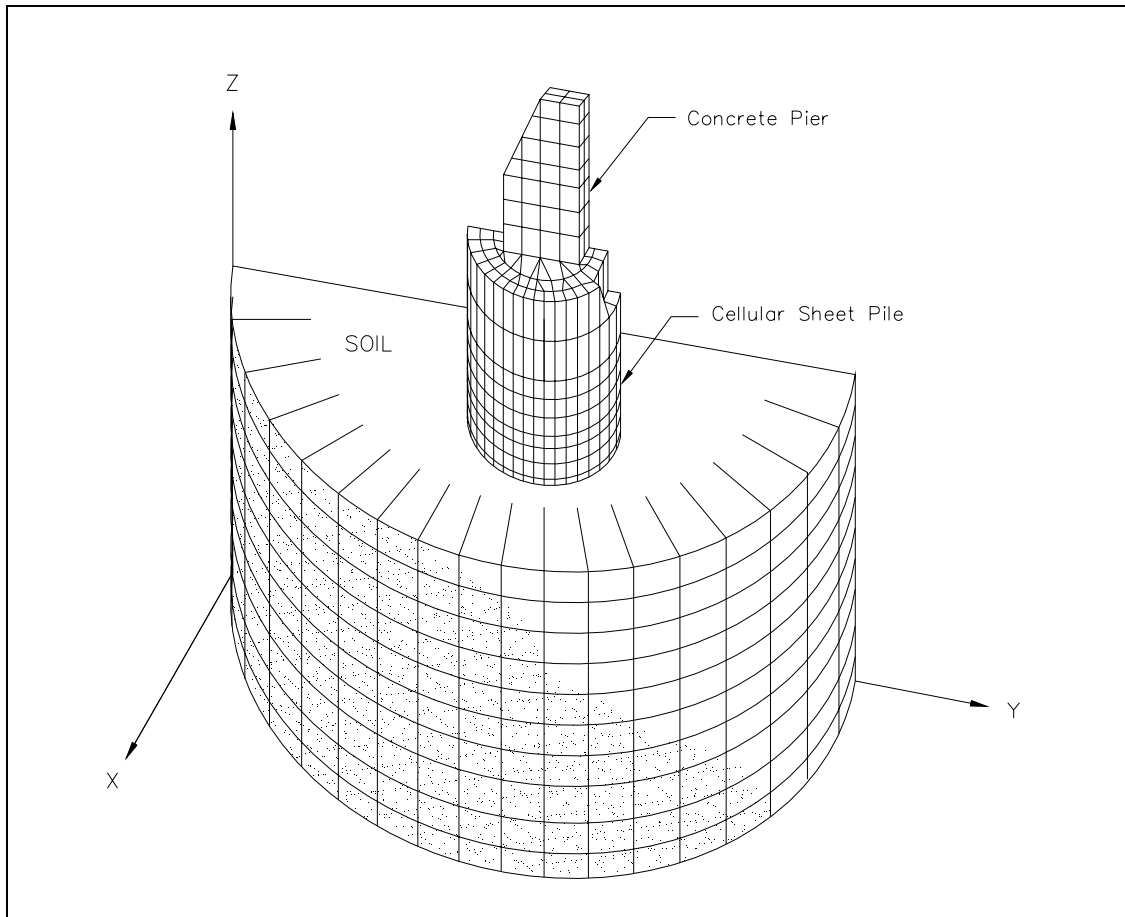


Figure 2-14. Three-dimensional finite element idealization of a fixed guide wall supported on cellular sheet pile

within the sheet pile, concrete pier or block above the ground surface, precast concrete beams, and the hydrodynamic forces acting on the pile and the concrete block.

a. Sheet piles. The cellular sheet piles are modeled using plate or shell elements. Each sheet pile is represented by a series of plate/shell elements connected horizontally and vertically to each other and at top to the concrete block. The elastic modulus of the plate/shell elements can be obtained from the work of Mosher (1992). Mosher has concluded that the field experimental data indicate that due to imperfect contact along the interlock between two adjacent sheet piles, the interlock initially undergoes significant movement but gradually stiffens after some movements, thus resulting in reduced subsequent lateral movements. The correlation studies by Mosher have also shown that the sheet piles modeled by plate/shell elements having a horizontal-to-vertical modulus ratio of 0.03 result in a good agreement between the computed and measured interlock forces. This research shows that orthotropic material properties are required for the plate/shell elements. Since SASSI and probably other SSI programs do not have orthotropic plate element capabilities, vertical beam elements can be used to compensate and represent the vertical stiffness of the sheet piles. That is, the low stiffness based on the modulus ratio of 0.03 is used for the plate/shell elements to simulate the interlock action along the horizontal planes, and vertical beam elements are employed to represent the vertical stiffness of the sheet piles. The mass and bending stiffness of the beam elements are set to zero, because only the axial stiffness of beam elements is needed.

b. Soil model. Both the soil surrounding the structural model shown in Figure 2-14 and that confined within the cellular sheet piles should be incorporated in the computer model. As shown in this figure, the structural model is embedded in the foundation soil. The free-field soil at the site may consist of several soil layers having different dynamic properties including the unit weight, shear modulus/shear wave velocity, Poisson's ratio/compression wave velocity, and the damping. The dynamic properties of the soil confined within the cell should be selected by giving due consideration to the effects of shaking on the strain-dependent nature of soil properties and the mechanism of load transfer from the sheet piles to the confined soil, whose properties depend on the confining pressure. For the soil confined inside the cell, it is reasonable to assume that the earthquake shaking will induce insignificant shear straining of the soil. Thus, the low-strain dynamic soil properties may be more representative for the inside soil. With regard to the effect of transfer of the sheet-pile load to the underlying soil, two cases may be analyzed. In one case the weight of sheet-pile cells is assumed to be carried directly by the soil within the cell, resulting in higher confining pressures than that due to the weight of overlying soils alone. In the second case the weight of sheet-pile cells is assumed to be carried by the sheet piles-soil interface, resulting in negligible increase in confining pressures of the inside soil. These two cases produce two different sets of dynamic soil properties that can be used in a parameter study to examine the effects of soil properties on the dynamic response of the guide wall.

c. Concrete block or pier. The structural concrete block or pier at the top of the sheet piles can be modeled using 8-node solid concrete elements. Since the precast beams are not structurally connected to the wall, only their masses may be considered and added to the mass of the concrete block or pier.

d. Hydrodynamic effects. The effects of hydrodynamic forces acting on both the cell and the precast concrete blocks are approximated by the added hydrodynamic mass concept. The hydrodynamic pressures on the circular cell can be computed based on the procedure described in paragraph 2-19*d*. The hydrodynamic pressures on the precast concrete blocks and beams are calculated by the generalized Westergaard method discussed in paragraph 2-19*b*.

Section III *Fluid-Structure Interaction*

2-18. General

A hydraulic structure and water interact through hydrodynamic pressures at the structure-water interface. In the case of concrete dams, the hydrodynamic pressures are affected by the energy loss at the reservoir boundary. Generated by the motions of the structure and the ground, hydrodynamic pressures affect deformations of the structure, which in turn influence the pressures. The complete formulation of the fluid-structure interaction produces frequency-dependent hydrodynamic pressures that can be interpreted as an added force, an added mass, and an added damping (Chopra 1987). The added hydrodynamic mass influences the structure response by lengthening the period of vibration, which in turn changes the response spectrum ordinate and thus the earthquake forces. The added hydrodynamic damping arises from the radiation of pressure waves and, for dams, also from the refraction or absorption of pressure waves at the reservoir bottom. The added damping reduces the amplitude of the structure response especially at the higher modes.

2-19. Simplified Added Hydrodynamic Mass Model

If the water is assumed to be incompressible, the fluid-structure interaction for a hydraulic structure can be represented by an equivalent added mass of water. This assumption is generally valid in cases where the fluid responses are at frequencies much greater than the fundamental frequency of the structure. Following sections

describe the simplified added-mass procedures including original and generalized Westergaard methods, velocity potential method for Housner's water sloshing model, and Chopra's procedure for intake-outlet towers and submerged piers and shafts.

a. *Westergaard added mass.* According to Westergaard (1933) the hydrodynamic forces exerted on a gravity dam due to earthquake ground motion are equivalent to inertia forces of a volume of water attached to the dam and moving back and forth with the dam while the rest of the reservoir water remains inactive. For analysis of gravity dams idealized as a 2-D rigid monolith with vertical upstream face, Westergaard proposed a parabolic shape for this body of water as shown in Figure 2-15. The added mass of water at location m_{ai} is therefore obtained by multiplying the mass density of water ρ_w by the volume of water tributary to point i :

$$m_{ai} = \frac{7}{8} \rho_w \sqrt{H(H - z_i)} A_i \quad (2-6)$$

where

H = depth of water

z_i = height above the base of the dam

A_i = tributary surface area at point i

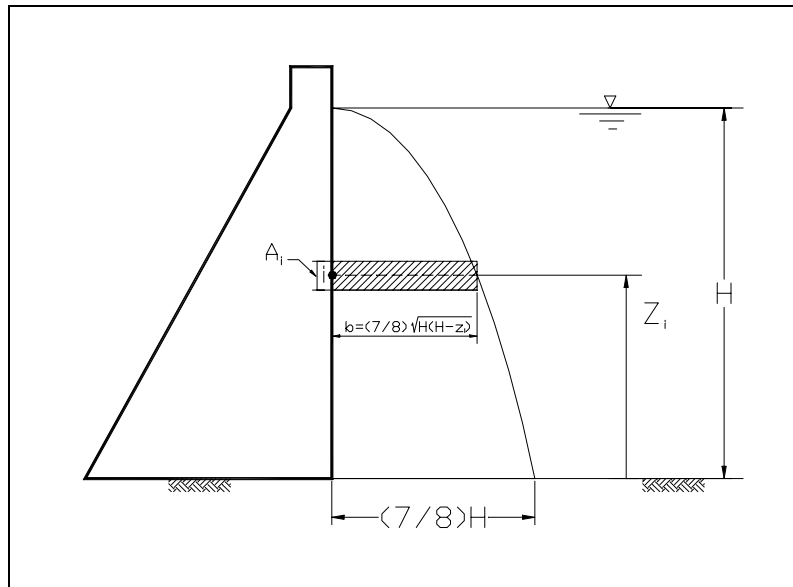


Figure 2-15. Westergaard added-mass representation

b. *Generalized Westergaard added mass.* Westergaard's original added-mass concept described in a above is directly applicable to the earthquake analysis of gravity dams and other hydraulic structures having a planar vertical contact surface with the water. For structures having sloped or curved contact surfaces, a generalized formulation of the added mass should be employed. The generalized formulation assumes that the pressure is still expressed by Westergaard's original parabolic shape, but the fact that the orientation of the pressure is normal to the face of the structure and its magnitude is proportional to the total normal acceleration at that point is recognized. In general, the orientation of pressures on a 3-D surface varies from point to point; and if expressed in Cartesian coordinate components, it would produce added-mass terms associated with all

three orthogonal axes. Following this description the generalized Westergaard added mass at any point i on the face of a 3-D structure is expressed (Kuo 1982) by

$$m_{ii} = \alpha_i A_i \lambda_i^T \lambda_i = \alpha_i A_i \begin{bmatrix} \lambda_x^2 & & \\ \lambda_y \lambda_x & \lambda_y^2 & \\ \lambda_z \lambda_x & \lambda_z \lambda_y & \lambda_z^2 \end{bmatrix}_i \quad \text{sym.} \quad (2-7)$$

where

A_i = tributary area associated with node i

$\lambda_i = \langle \lambda_x, \lambda_y, \lambda_z \rangle_i$ is the normal direction cosines (Figure 2-16)

α_i = Westergaard pressure coefficient given by

$$\alpha_i = \frac{7}{8} \rho_w \sqrt{H_i (H_i - z_i)} \quad (2-8)$$

For a 3-D surface such as an arch dam curved both in plan and elevation, the added-mass terms associated with a particular node form a 3×3 full matrix. However, matrices for various nodes are not coupled.

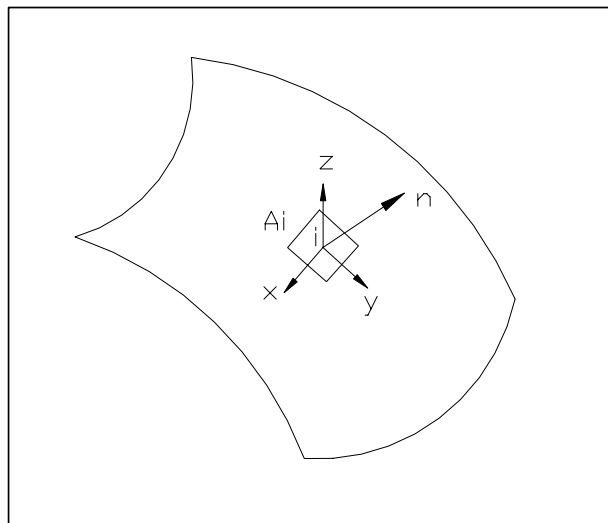


Figure 2-16. Normal and Cartesian directions of curvilinear surface

c. Velocity potential solution of added-mass navigation locks. The hydrodynamic pressures of contained water exerted on navigation lock walls due to earthquake excitation can be divided into impulsive and convective components (Housner 1957). The impulsive pressure represents the effects of the portion of the fluid that moves in unison with the lock (added mass); and the convective pressure represents the effects of the sloshing action of the fluid.

(1) The impulsive pressures due to a horizontal component of ground motion \ddot{u}_x can be obtained from a velocity potential function that satisfies the Laplace equation with appropriate boundary conditions (Haroun

1984). The hydrodynamic pressure solution for a navigation lock chamber with a cross-section width of $2L$ filled with water to a depth of H (Figure 2-17) is given by

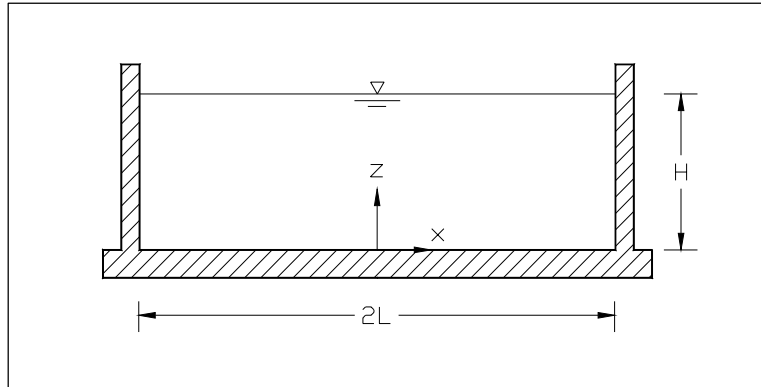


Figure 2-17. Lock chamber dimensions and coordinate system

$$P(L, y, z, t) = \frac{2\rho_w}{H} \sum_{i=1}^{\infty} \frac{(-1)^i}{\lambda_i^2} \tanh(\lambda_i L) \cos(\lambda_i z) \ddot{u}_x(t) \quad (2-9)$$

where $\lambda_i = (2i - 1)\pi / 2L$ and ρ_w is the mass density of water. It should be noted that the series in Equation 2-9 converges rapidly, and only one to three terms may be needed in practical applications. Figure 2-18 compares the pressure distributions given by this equation and the pressure distribution obtained from the Westergaard method. This comparison shows that the pressure distributions given by Westergaard and the velocity potential solution are quite different, and that the difference between the two distributions increases with the $H/2L$ ratio. Therefore, for analysis of lock structures the impulsive pressure distribution given by Equation 2-9 should be used for determination of the added hydrodynamic mass.

(2) Water sloshing in navigation locks. The liquid sloshing force exerted on navigation lock walls during the earthquake shaking can be obtained from Housner's mathematical model for water tanks (Housner 1957). According to Housner the sloshing force exerted on a tank wall would be the same as that exerted by a mass M_1 attached to the tank by a restraining spring K , as shown in Figure 2-19. The mass M_1 and spring constant K correspond to the fundamental mode of the oscillating fluid and are mounted at a height of h_1 to give the same moment as the fluid. The mass M_0 attached rigidly to the tank at height h_0 gives the force resultant associated with the impulsive pressure discussed previously. Formulas for these parameters initially derived by Housner (1957) and later presented by Epstein (1976) are as follows.

$$M_0 = \left[\frac{\alpha}{\sqrt{3}} \tanh\left(\frac{\sqrt{3}}{\alpha}\right) \right] M \quad (2-10)$$

$$M_1 = \left[\frac{0.527}{\alpha} \tanh(1.58\alpha) \right] M \quad (2-11)$$

$$h_0 = \frac{3}{8} h \quad (2-12)$$

$$h_1 = \left[1 - \frac{\cosh(1.58\alpha) - 1}{(1.58\alpha) \sinh(1.58\alpha)} \right] \quad (2-13)$$

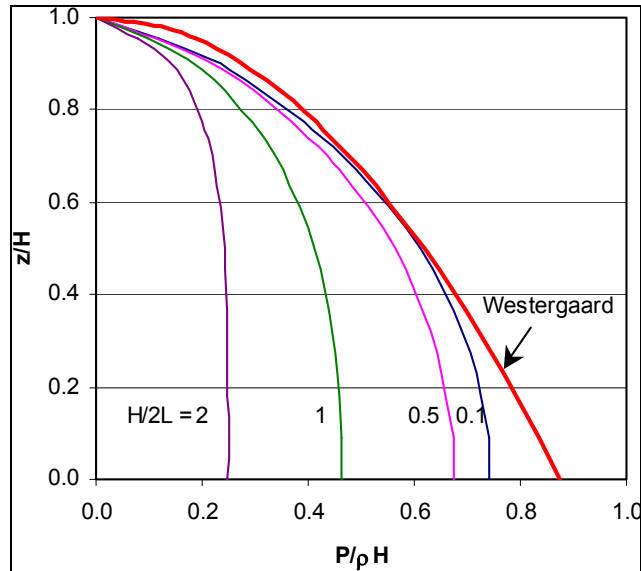


Figure 2-18. Comparison of hydrodynamic pressures for various section dimensions

where $\alpha = H/L$ and M is the total mass of water for a unit width section of the tank or lock. The period of fundamental mode of sloshing T is given by

$$T = 2\pi \left[\frac{L}{1.58g \tanh(1.58\alpha)} \right]^{1/2} \quad (2-14)$$

where g is the acceleration of gravity. Knowing the mass M_1 and period T , the sloshing force P_1 as a function of time t is obtained from

$$P_1 = M_1 S_a \sin \left(\frac{2\pi}{T} t \right) \quad (2-15)$$

where $M_1 S_a$ represents the maximum sloshing force and S_a is the spectral acceleration at period T obtained from the response spectra of earthquake ground motion. These equations are applicable for shallow tanks, i.e., $\alpha = H/L \neq 1.5$, which should be valid for most navigation locks. For the cases $\alpha > 1.5$, refer to Epstein (1976).

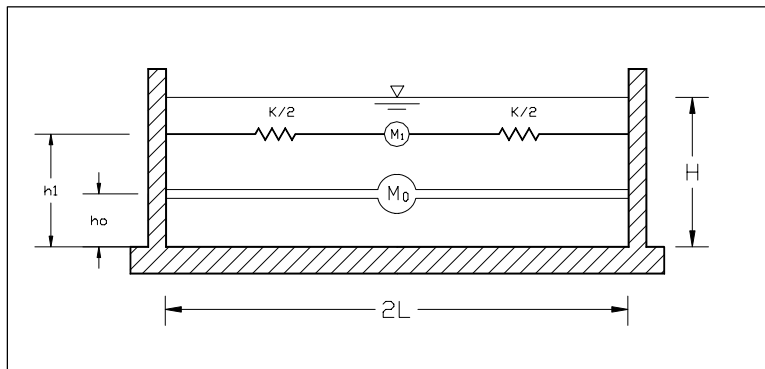


Figure 2-19. Housner's mathematical model for impulsive and convective (sloshing) hydrodynamic forces

d. Added mass for towers and supporting shafts.

(1) The hydrodynamic interaction effects of the surrounding water in the analysis of intake/outlet towers and submerged shafts and piers are approximated by an equivalent added mass of water. The procedure is based on the assumption of a rigid structure surrounded by incompressible water. The inertial effects of water, therefore, are represented by added-mass functions computed for unit horizontal ground acceleration. These added-mass functions are available only for circular cylindrical towers (Jacobson 1949; Liaw and Chopra 1973; and Rashed 1982) and for uniform elliptical towers (Kotsubo 1965). For towers and piers of arbitrary cross section having two axes of symmetry, the added mass is obtained from analysis of an “equivalent” circular tower in accordance with a simplified procedure developed by Goyal and Chopra (1989).

(2) The added mass for circular cylindrical towers or piers surrounded by water is obtained from an analytical solution of the Laplace equation, as presented in Figure 2-20 and various charts and tables by Goyal and Chopra (1989). The normalized added mass for a uniform tower of arbitrary cross section is obtained by converting the arbitrary section first into an equivalent elliptical and then into an equivalent circular section for which Goyal and Chopra’s chart and tables can be used (Goyal and Chopra 1989). The procedure is also extended to the added mass analysis of nonuniform towers, simply by applying these steps to various portions of the tower or pier that actually are, or assumed to be, uniform.

(3) The added hydrodynamic mass associated with the water inside a tower is also computed from the solution for an equivalent circular section in a manner similar to that described for the surrounding water. For the equivalent circular cylindrical towers the added mass of contained water is also obtained from an analytical solution of the Laplace equation, as presented in Figure 2-21 and various charts and tables by Goyal and Chopra (1989).

2-20. Finite Element Added Hydrodynamic Mass Model

The simplified added hydrodynamic mass concept described in paragraph 2-19 is generally not appropriate for refined analysis of hydraulic structures having complex geometry such as arch dams and irregular intake/outlet towers. For such structures a finite element idealization of the fluid domain permits a more realistic treatment of the complicated geometry of the structure-water interface as well as the reservoir bottom. Assuming water is incompressible, inviscid, and irrotational, the small-amplitude motion of water is governed by the wave equation

$$\frac{\partial^2 p}{\partial x^2} + \frac{\partial^2 p}{\partial y^2} + \frac{\partial^2 p}{\partial z^2} = 0 \tag{2-16}$$

where $p(x,y,z)$ is hydrodynamic pressure in excess of the static pressure generated by acceleration of the structure-water contact surface and acceleration of the reservoir bottom. The hydrodynamic pressures acting on the structure-water interface are obtained by solving Equation 2-16 using appropriate boundary conditions. Neglecting the effects of surface waves, which are known to be small, the boundary condition at the free surface is:

$$p(x, y, z) = 0 \tag{2-17}$$

On the structure-water contact surface, where the normal acceleration \ddot{u}_{nd} (Figure 2-22) is prescribed, the boundary condition becomes:

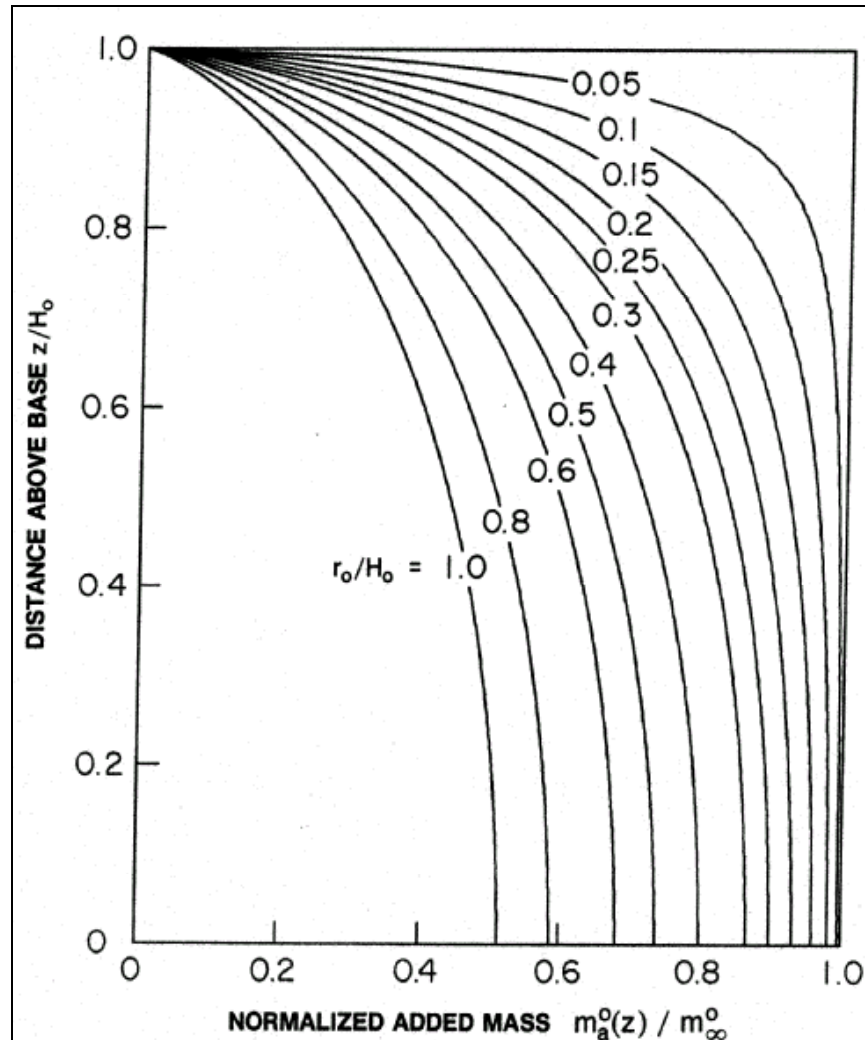


Figure 2-20. Normalized added hydrodynamic mass for circular cylindrical towers associated with surrounding water where z = distance above the base of the tower or pier, H_0 = depth of the surrounding water, r_0 = radius of the outside surface of the tower, $m_\infty^0 = \rho_w \pi r_0^2$ = the added mass per unit height of an infinitely long uniform tower of the same radius, and $m_a^0(z)$ = the added mass for circular tower or pier surrounded by water (from Goyal and Chopra 1989)

$$\frac{\partial p}{\partial n} = -\rho_w \ddot{u}_{nd} \quad (2-18)$$

where n represents the direction normal to the surface. A similar boundary condition may also be applied at the reservoir boundary

$$\frac{\partial p}{\partial n} = -\rho_w \ddot{u}_{nb} \quad (2-19)$$

where \ddot{u}_{nb} is the normal component of ground acceleration at the reservoir boundary (Figure 2-22). In addition to these boundary conditions, $p(x,y,z)$ should remain bounded in the far field of the unbounded fluid domain.

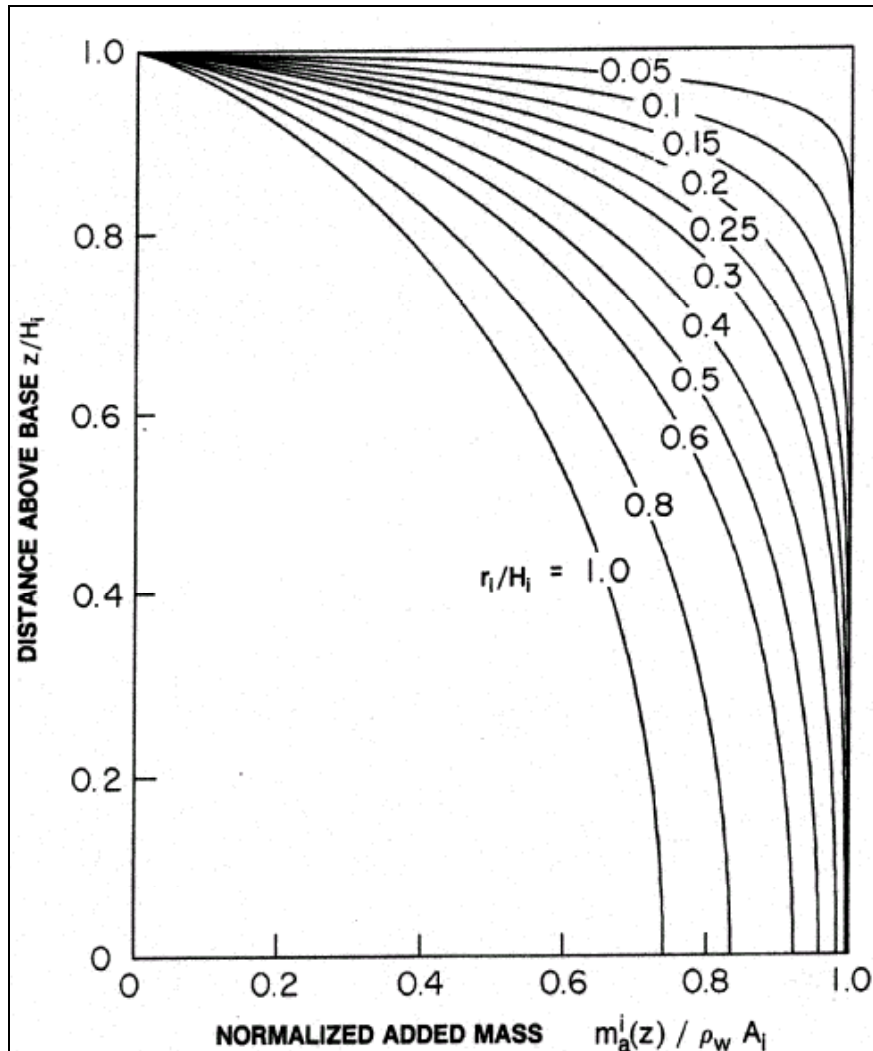


Figure 2-21. Normalized added hydrodynamic mass for circular cylindrical towers associated with inside water where z = distance above the base of the tower or pier, H_i = depth of the inside water, r_i = radius of the inside surface of the hollow tower, $m_\infty^i = \rho_w A_i = \rho_w \pi r_i^2$ = the mass of water contained within an infinitely long uniform tower with the radius of r_i , and $m_a^i(z)$ = the added mass of water contained within the circular tower (from Goyal and Chopra 1989)

a. *Arch dams.* For arch dams the solution of Equation 2-16 for hydrodynamic pressures is obtained numerically using the finite element method (Kuo 1982; Ghanaat 1993b), but the reservoir bottom and a truncating vertical plane at the upstream end are assumed to be rigid. This means that the ground motion \ddot{u}_g is not applied to the reservoir bottom (i.e., $\ddot{u}_{nb} = 0$ in Equation 2-19) and that the radiation damping due to propagation of pressure waves in the upstream direction is not considered. The analysis involves development of a finite element discretization of the fluid domain with the truncating upstream plane located a distance at least three times the water depth from the face of the dam. At such distance, parameter studies show that the acceleration at the truncated plane has a small effect on the hydrodynamic pressures at the face of the dam and,

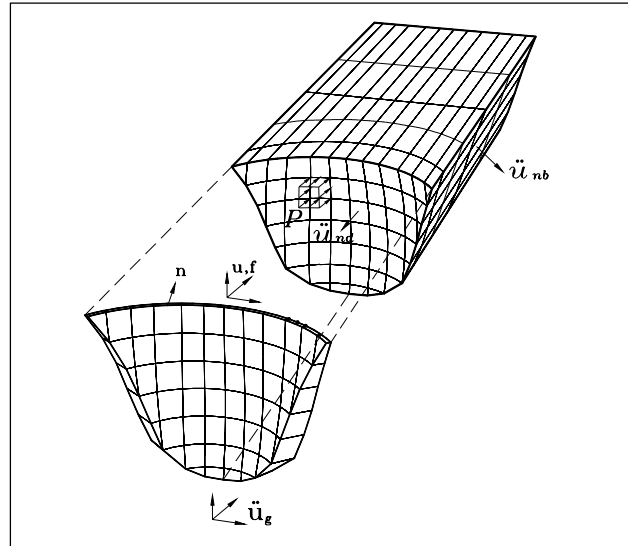


Figure 2-22. Finite element idealization of incompressible impounded water for arch dams (from Ghanaat 1993b)

thus, can be assumed zero in practical applications (Clough et al. 1984a, 1984b). In most cases a prismatic fluid mesh generated by translating the dam-water interface nodes in the upstream direction is adequate for practical purposes (Figure 2-22). However, if the actual reservoir topography is substantially different from a prismatic model, a fluid mesh that closely matches the reservoir topography may be required. In either case, the distance between the successive surfaces or planes arranged approximately parallel to the dam axis should be such that the fluid layers closer to the dam face contain finer elements. The finite element solution of Equation 2-16 results in nodal pressures on the upstream face of the dam, which after conversion into nodal forces gives the added hydrodynamic mass matrix for earthquake analysis of the dam. The resulting added-mass matrix is a full square matrix with a dimension equal to the number of degrees of freedom on the dam-water interface nodes.

b. Intake-outlet towers with two axes of symmetry. If the geometry of the tower is more complex or if the effects of the vertical acceleration of the reservoir bottom are to be considered, the simplified added mass computed on the basis of an “equivalent” circular tower may not properly represent the hydrodynamic forces acting on the tower. In such cases, the added mass for the surrounding water can be obtained from the finite element solution of Equation 2-16 together with appropriate boundary conditions at the tower-water interface, the reservoir bottom, and the free surface of water. For free-standing towers of arbitrary cross section but having two axes of symmetry, a semi-analytical procedure formulated by Goyal and Chopra (1989) may be employed. In this formulation, as illustrated in Figure 2-23, the surrounding water adjacent to the tower τ_A^o is represented by the finite element approximation, and the fluid domain beyond this immediate region τ_B^o is treated analytically using boundary integral procedures. Since the analytical solution of the boundary integral domain is evaluated for circular-cylindrical towers, the hypothetical surface Γ_c^o between the finite element and the infinite region is restricted to a circular-cylindrical surface. Note that the vertical ground motion is not included in this formulation; only the vertical acceleration on the surface Γ_c^o caused by the rotation of the foundation is considered. Similar to the surrounding water, the hydrodynamic pressures associated with the inside water are also obtained from the solution of Equation 2-16, except that boundary conditions now correspond to the tower-water interface and free surface of the inside water. This formulation has been implemented in the computer program TOWER3D (Goyal and Chopra 1989), but is restricted to 3-D response analysis of towers having two axes of symmetry in plan.

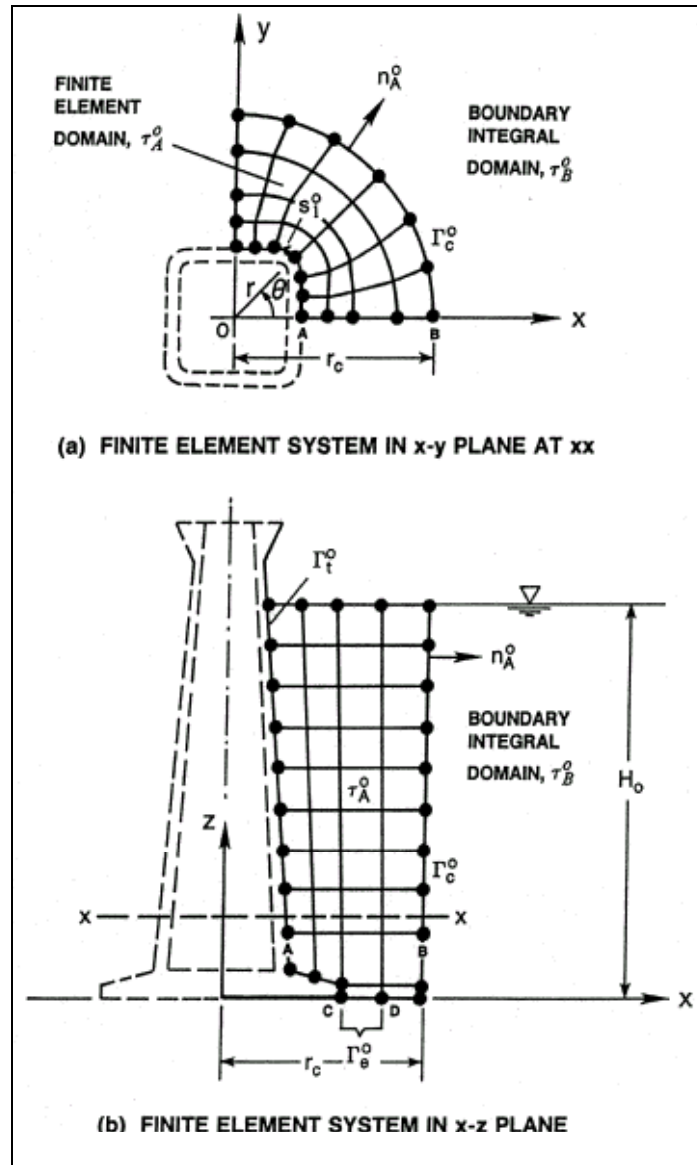


Figure 2-23. Three-dimensional finite element system for surrounding water domain (from Goyal and Chopra 1989)

c. *Irregular intake towers.* The added hydrodynamic mass for the analysis of irregular towers with no axis of symmetry can be obtained by the procedure described for arch dams using either the finite element or boundary element formulation. Figure 2-24 shows an example of the boundary element formulation applied to added-mass analysis of the Seven Oaks intake tower. In this approach the water partially surrounding the intake tower is represented by surface areas of the intake tower and the reservoir bottom and sides. The added-mass solution is obtained as if the entire space represented by these surface areas were filled with water. The water domain beyond the generated mesh can be assumed to extend to infinity, and the earthquake ground motion may be applied to the tower as well as to the reservoir bottom.

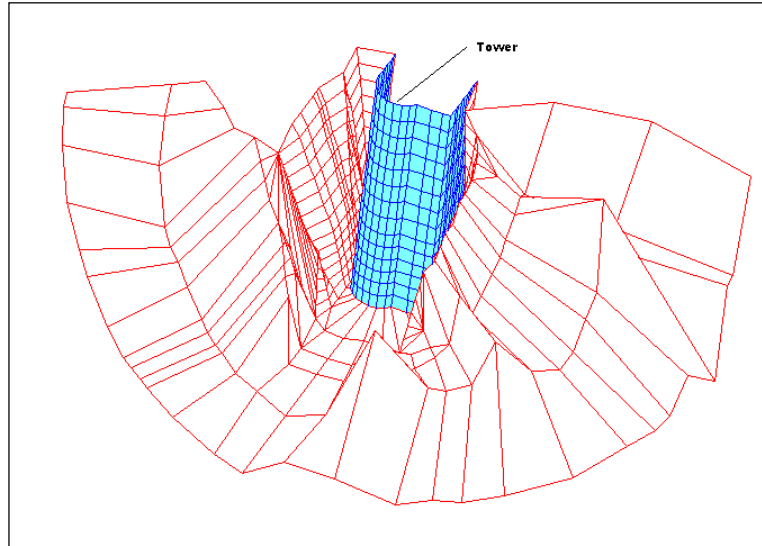


Figure 2-24. Boundary element added-mass model of Seven Oaks intake tower

2-21. Compressible Water with Absorptive Boundary Model

a. The added-mass representation of hydrodynamic pressure previously described ignores the effects of water compressibility and water-foundation interaction. Refined dam-water interaction analysis including these factors (Hall and Chopra 1980; Fenves and Chopra 1984b; Fok and Chopra 1985) indicates that water compressibility and the water-foundation interaction can significantly affect the hydrodynamic pressures and hence the response of concrete dams to earthquakes. The effects of water compressibility are generally significant when the fundamental frequency of the dam without the water is relatively close to the fundamental resonant frequency of the impounded water, $f_1' = C/(4H)$, where C is the velocity of sound in water and H is the water depth. The water compressibility and the water-foundation interaction effects can be considered by solving the wave equation for compressible water

$$\frac{\partial^2 p}{\partial x^2} + \frac{\partial^2 p}{\partial y^2} + \frac{\partial^2 p}{\partial z^2} = \frac{1}{C^2} \frac{\partial^2 p}{\partial t^2} \quad (2-20)$$

subjected to the boundary conditions given in Equations 2-17 to 2-19. The water-foundation interaction, as indicated by Equation 2-19, can be considered by using finite elements to represent the flexible foundation or modeling the foundation material as a viscoelastic half space. This effect has also been accounted for in an approximate manner by using a simplified boundary condition that models the energy dissipated at the water-foundation interface, as described in paragraph 2-22. The most extensive study of concrete dams with compressible reservoir water has been carried out by Chopra and his co-workers (Hall and Chopra 1980; Fenves and Chopra 1984b; Fok and Chopra 1985) using the substructure method of analysis. Assuming the reservoir water can be idealized as a fluid domain with constant depth and infinite length in the upstream direction, the hydrodynamic pressures for 2-D analysis of gravity dams is obtained from a continuum solution (Fenves and Chopra 1984b). For irregular reservoir boundaries, the fluid domain is usually assumed to consist of an irregular portion adjacent to the dam and a uniform section of infinite length in the upstream direction (Figure 2-25). The irregular portion is represented by a finite element discretization (Hall and Chopra 1980) or boundary element method (Humar and Jablonski 1988), whereas the uniform portion is analyzed by a continuum solution. The equal pressure conditions at the interface then enforce the coupling between the two

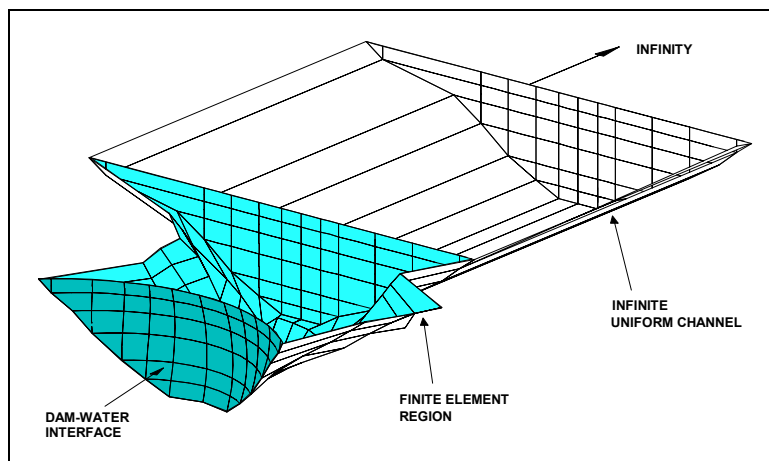


Figure 2-25. Finite element model of compressible water with absorptive boundary for Dongjiang Arch Dam, China (from Ghanaat et al. 1993)

regions. Such formulation of the hydrodynamic pressure results in frequency-dependent hydrodynamic terms that are best treated in the frequency domain. This procedure has been implemented in the computer program EACD-3D (Fok, Hall, and Chopra 1986) for the earthquake analysis of arch dams.

b. The hydrodynamic pressure in the reservoir, as given by Equation 2-20, is generated by the acceleration of the upstream face of the dam and vertical accelerations of the reservoir bottom. The solution in frequency domain produces the frequency response functions for the hydrodynamic pressures in the impounded water. The computed pressure frequency response functions at the face of the dam and at the reservoir bottom are then converted into statically equivalent nodal forces $\bar{R}'_h(\omega)$ and $\bar{Q}_h(\omega)$ and are substituted into the system equations of motion (Equation 2-1).

2-22. Reservoir Boundary Absorption

a. The energy loss capability of the reservoir bottom materials is approximately modeled by a boundary that partially absorbs (refracts) the incident pressure waves (Hall and Chopra 1980). In the boundary condition for the reservoir bottom, this energy loss is represented by the damping coefficient q , which is related to the wave reflection coefficient α by

$$\alpha = \frac{1 - qC}{1 + qC} = \frac{1 - \frac{\rho C}{\rho_s C_s}}{1 + \frac{\rho C}{\rho_s C_s}} \quad (2-21)$$

where ρ and C are the density and sound velocity for water, respectively, and ρ_s and C_s are the density and sound velocity for the bottom materials, respectively. The reflection coefficient α provides a measure of the level of absorption of the reservoir bottom materials. It is defined as the ratio of the amplitude of the reflected pressure wave to the amplitude of incident pressure wave impinging on the reservoir bottom. The values of α vary between 1 and -1 where $\alpha = 1$ represents a nonabsorptive rigid boundary with 100 percent reflection, $\alpha = 0$ corresponds to a complete absorption with no reflection, and $\alpha = -1$ characterizes 100 percent reflection from a free surface with an attendant phase reversal (water surface). Recent field investigations have

indicated that the average values of α for the reservoir bottom materials measured at several concrete damsites varied over a range from -0.55 to 0.66 (Ghanaat and Redpath 1995). Three of the measured values were negative and the largest (0.66) was much less than 1—the value corresponding to a rigid boundary. The results also showed that some sites had thick layers of soft and muddy sediments with propagation velocities less than that of water, thus leading to negative values of α , a situation never before considered analytically.

b. All hydrodynamic pressure terms (i.e., added mass, added damping, and added force) are affected by the reservoir bottom absorption. Previous studies (Hall and Chopra 1980; Fenves and Chopra 1984b; Fok and Chopra 1985) indicate that the reservoir bottom absorption increases the effective damping, hence reduces the dam response to earthquake loading. The reduction of dam response due to reservoir bottom absorption, however, is much larger for the response to vertical ground motion than to horizontal. Considering that the dam responses due to the vertical and horizontal components of the ground motion are not usually in phase, the effect of reservoir bottom absorption on the total response of the dam is less than that for the vertical ground motion.

2-23. Foundation-Structure Interaction

Foundation-structure interaction introduces flexibility at the base of the structure and provides additional damping mechanisms through material damping and radiation. The interaction with the flexible foundation affects the earthquake response of the structure by lengthening the period of vibration and increasing the effective damping of the system. The increase in the damping arises from the energy radiation and material damping in the foundation region. However, interaction with the flexible foundation also tends to reduce the structural damping that the structure would have had in the case of a rigid foundation (Novak and El Hifnawy 1983). For lightly damped hydraulic structures (less than 10 percent damping) the reduction in structural damping is usually more than compensated for by the added damping of the flexible foundation. Such interaction effects introduce frequency-dependent interacting forces at the structure-foundation interface, which are represented by the dynamic stiffness (or impedance) matrix for the foundation rock region, as described previously.

2-24. Rock Foundations

a. *Massless finite element foundation model.*

(1) The effects of dam-foundation interaction can most simply be represented by including, in the finite element idealization, foundation rock or soil region above a rigid horizontal boundary. The response to the earthquake excitation applied at the rigid base (bedrock) is then computed by the standard procedures. Such an approach, however, can lead to enormous foundation models where similar materials extend to large depths and there is no obvious "rigid" boundary to select as a fixed base. Although the size of foundation model can be reduced by employing viscous or transmitting boundaries to absorb the wave energy radiating away from the dam (Lysmer and Kuhlemeyer 1969), such viscous boundaries are not standard features of the general-purpose structural analysis programs.

(2) These difficulties can be overcome by employing a simplified massless foundation model, in which only the flexibility of the foundation rock is considered while its inertia and damping effects are neglected. The size of a massless foundation model need not be very large so long as it provides a reasonable estimate of the flexibility of the foundation rock region. A foundation model that extends one dam height in the upstream, downstream, and downward directions usually suffices in most cases. Unlike the homogeneous viscoelastic half plane model described previously, this approach permits different rock properties to be assigned to different elements, so that the variation of rock characteristics with depth can be considered. The massless

foundation model also permits the earthquake motions recorded on the ground surface to be applied directly at the fixed boundaries of the foundation model. This is because in the absence of wave propagation, the motions of the fixed boundaries are transmitted to the base of the dam without any changes.

b. Viscoelastic foundation rock model.

(1) The stiffness and damping characteristics of foundation-structure interaction in a viscoelastic half-plane (2-D) or half space (3-D) model are described by the impedance function. Mathematically, an impedance function is a matrix that relates the forces (i.e., shear, thrust, and moment) at the base of the structure to the displacements and rotations of the foundation relative to the free field. The terms in an impedance function are complex and frequency dependent with the real component representing the stiffness and inertia of the foundation and the imaginary component characterizing the radiation and material damping.

(2) Viscoelastic half plane model. For sites where essentially similar rocks extend to large depths, the foundation rock for 2D analyses may be idealized as a viscoelastic half plane. In other situations where soft or fractured rock overlies harder rock at shallow depth, a finite element idealization (*a* above) that permits for material nonhomogeneity and structural embedment would be more appropriate. In viscoelastic half plane idealization, foundation-structure interaction is represented by a complex valued impedance or dynamic stiffness matrix ($S_f(\omega)$ in Equation 2-2). Assuming that the structure is supported on a horizontal ground surface with homogeneous material properties, the dynamic stiffness matrix $S_f(\omega)$ is evaluated using the approach by Dasgupta and Chopra (1979) or other approaches that use boundary element and Green's functions to analyze the problem (Wolf and Darbre 1984; Alarcon, Dominguez, and Del Cano 1980).

(3) Viscoelastic half space model. The foundation rock for 3-D analyses of concrete hydraulic structures supported on essentially similar rocks with homogeneous material properties may be represented by viscoelastic half space. Employed in the substructure method of analysis, the half space model leads to an impedance matrix for the foundation rock region defined at the structure-foundation interface. A variety of boundary element methods using different Green's functions, finite element techniques in frequency domain using transmitting boundaries, finite element method in time domain, infinite elements, and hybrid methods are available to compute impedance matrices for surface and embedded foundations. Without certain simplifying assumptions, these techniques are computationally demanding and are usually unsuitable for practical applications. One such assumption applied to the analysis of arch dams is to assume that the dam is supported in an infinitely long canyon of arbitrary but uniform cross section and thus break down the problem into a series of two-dimensional boundary problems (Zhang and Chopra 1991). In situations where soft or fractured rock overlies harder rock at shallow depth, a finite element idealization accounting for the material nonhomogeneity should be used.

2-25. Soil and Pile Foundations

a. Discrete spring-mass-damper soil model. Time-history analysis of concrete hydraulic structures including soil-structure interaction effects can be performed in the time domain using a discrete model of the soil. Such a discrete model of the soil consists of frequency-independent springs, dampers, and masses. The simplest model that can be developed for each degree of freedom of a rigid basemat includes a spring and a damper connected to the basemat with a fictitious mass of the soil added to mass of the structure. The frequency-independent coefficients of this SDOF system are obtained by a curve-fitting procedure such that a good agreement between the dynamic stiffness of the SDOF model and that of the actual soil (computed using continuum solutions in *b* below) is achieved. However, the performance of the SDOF system in reproducing the actual response of the soil is limited. A better agreement can generally be achieved by introducing an additional mass connected to the basemat through a damper (Wolf 1988; Figure B-1 of Appendix B). Appendix B provides descriptions and tables of discrete model dimensionless coefficients for a disk supported

by a homogeneous half space, an embedded cylinder, an embedded prism, and a strip supported on the surface of a homogeneous half space.

b. Continuum model. In the substructure method of analysis in the frequency domain, the soil medium is analyzed separately to obtain the force-displacement relationship of the soil defined at the structure-soil interface. This frequency-dependent impedance function (dynamic stiffness) for the unbounded homogeneous surface foundation can be obtained using continuum solutions. The viscoelastic model described in paragraph 2-24b(2) is an example of such procedure, which is equally applicable to analysis of the soil medium.

c. Finite element model. The frequency-dependent impedance function (dynamic stiffness) for layered and nonhomogeneous soil medium is obtained using finite element procedures. The finite element analysis for development of impedance functions for 2-D and 3-D problems may be performed using FLUSH (Lysmer et al. 1975) and SASSI (Lysmer et al. 1981) computer programs, respectively. Using these codes, first the equations of motion for the foundation substructure are solved for unit harmonic loads applied at the boundary interface to calculate displacements at corresponding degrees of freedom (dynamic flexibility). The impedance functions are then obtained from the inverse of the dynamic flexibility matrix.

Chapter 3 Time History Numerical Solution Techniques

3-1. Introduction

a. Numerical solutions of equations of motion for structures are divided into two methods: direct integration and mode superposition. In direct integration the equations of motion are integrated directly using a numerical step-by-step procedure, without transforming the equations into a different form. In mode superposition method the equations of motion are first transformed into a more effective form (modal forms) before they are solved using either a step-by-step integration in the time domain or by application of the frequency-domain procedures. Only a brief description of these procedures as applied to the linear time-history analysis are presented in this chapter. A more detailed description of the methods can be found in Ebeling, Green, and French (1997) and other cited references. The chapter is divided into two sections: Section I and Section II. Section I begins with a general description of the equations of motion followed by presentation of several time-domain solution procedures commonly used in the earthquake engineering. Section II is devoted to solution of the equations of motion in the frequency domain. It begins with a preview and conversion of the seismic input into the frequency domain, followed by introduction of the frequency response functions, and finally computation of the structural response first in the frequency domain and then converting back to the time domain.

Section I Time Domain Solutions

3-2. Equations of Motion

a. The equations of motion for a hydraulic structure are formulated from the equilibrium of the effective forces associated with each of its degrees of freedom (Clough and Penzien, 1993). In a matrix form these equations may be expressed by

$$\mathbf{m} \ddot{\mathbf{u}}(t) + \mathbf{c} \dot{\mathbf{u}}(t) + \mathbf{k} \mathbf{u}(t) = \mathbf{p}(t) \quad (3-1)$$

where \mathbf{m} , \mathbf{c} , and \mathbf{k} are the mass, damping, and stiffness matrices, respectively; $\mathbf{u}(t)$, $\dot{\mathbf{u}}(t)$, and $\ddot{\mathbf{u}}(t)$ are respectively nodal displacement, velocity, and acceleration vectors; and $\mathbf{p}(t)$ is the effective load vector. For hydraulic structures the coefficient matrices and the effective load vector also include contributions from interaction with the water and the foundation rock. However, depending on the type of finite-element formulation used, the interaction effects are treated as described below.

b. In standard finite-element formulation (2-11) with massless foundation and incompressible water the mass matrix \mathbf{m} contains both the structure mass and the added mass of water. The matrix \mathbf{k} is the combined stiffness for the structure and the foundation. The effective load vector $\mathbf{p}(t)$ resulting from the earthquake ground shaking, includes inertia loads due to the mass of the structure and of the water.

c. In substructuring finite-element formulation (2-10), the interaction with water is generally represented by hydrodynamic forces that are included as part of the effective load vector. The damping and stiffness are represented in the form of dynamic stiffness or impedance matrix that also includes interacting forces with the foundation. Since foundation impedance and hydrodynamic forces are frequency dependent, the substructuring formulation is usually developed in the frequency domain and solved as described in Section II of this chapter.

3-3. Direct Integration

a. General. In direct integration the equations of motion in (3-1) are directly integrated using a step-by-step numerical procedure without prior transformation of the equations to a different form. The step-by-step integration procedures provide an approximate solution at n discrete time intervals $0, \Delta t, 2\Delta t, 3\Delta t, \dots, t, t+\Delta t, \dots, T$, where T is duration of the input motion or loading and $\Delta t = T/n$. Many numerical integration procedures have been developed. However, only a very brief summary of the most common methods are presented to show how they are applied in seismic analysis of hydraulic structures. Direct integration methods are generally classified as either *explicit* or *implicit*. In general, linear time-history analyses of hydraulic structures described in Chapter 2 are conducted using implicit methods. However, explicit methods are briefly discussed here because they are included in some commercial computer programs and the reader may use them in solution of certain problems.

b. Explicit Methods. The basic concept common to most explicit methods is to write the equations of motion for the beginning of the time step, approximate the initial velocity and acceleration terms by finite-difference expressions, and then solve for response at the end of time step. This way the response values calculated in each step depend only on quantities obtained in the preceding step. Therefore, the numerical process proceeds directly from one step to next. Explicit methods are very convenient, but they are only conditionally stable and will “blow up” if time step is not sufficiently small.

(1) The central Difference Method. The central difference method is a very simple explicit method that uses the following finite-difference expressions for approximation of the initial velocity and acceleration terms (Clough and Penzien 1993, Bathe and Wilson 1976).

$$\ddot{\mathbf{u}}_t = \frac{1}{\Delta t^2} [\mathbf{u}_{t-\Delta t} - 2\mathbf{u}_t + \mathbf{u}_{t+\Delta t}] \quad (3-2)$$

$$\dot{\mathbf{u}}_t = \frac{1}{2\Delta t} (-\mathbf{u}_{t-\Delta t} + \mathbf{u}_{t+\Delta t}) \quad (3-3)$$

The displacement solution for time step $t+\Delta t$ (i.e. $\mathbf{u}_{t+\Delta t}$) is obtained by considering the equations of motion (i.e. (3-1)) at time step t

$$\mathbf{m} \ddot{\mathbf{u}}_t + \mathbf{c} \dot{\mathbf{u}}_t + \mathbf{k} \mathbf{u}_t = \mathbf{p}_t \quad (3-4)$$

Substituting (3-2) and (3-3) into (3-4), leads to

$$\left(\frac{1}{\Delta t^2} \mathbf{m} + \frac{1}{2\Delta t} \mathbf{c} \right) \mathbf{u}_{t+\Delta t} = \mathbf{p}_t - \left(\mathbf{k} - \frac{2}{\Delta t^2} \mathbf{m} \right) \mathbf{u}_t - \left(\frac{1}{\Delta t^2} \mathbf{m} - \frac{1}{2\Delta t} \mathbf{c} \right) \mathbf{u}_{t-\Delta t} \quad (3-5)$$

This equation shows that the stiffness matrix does not appear in the coefficient of $\mathbf{u}_{t+\Delta t}$, and thus factorization of the (effective) stiffness matrix will not be required. If mass and damping matrices are diagonal, even the matrices need not be assembled. In that case the solution is obtained at the element level which allows solving very large structural systems without substantial computer resources. These advantages make the central difference method convenient and efficient. However, the method is only conditionally stable and its stability depends on the choice of time step Δt . To obtain a stable solution, Δt must be $< T_n/\pi$, where T_n is the shortest natural period of the structural system. If the central difference method is used with a $\Delta t > T_n/\pi$ the solution will increase exponentially. This may not be a limiting factor for a SDOF system, because more than π or 3

steps are needed to adequately define one vibration cycle. However, the size of time step would be an issue for the MDOF systems where very short-period modes of vibration (compared with time step of input loading) are essential to the dynamic response of the system. In these situations extremely small time step would make the explicit methods undesirable.

c. Implicit Methods. In an implicit method the expressions for new values at $t+\Delta t$ use equilibrium equations at $t+\Delta t$, and thus include one or more values pertaining to that same step. Examples of implicit integration methods are presented below.

(1) Newmark- β Method. The Newmark- β method is a general step-by-step procedure with the following integration equations for the displacement and velocity at time step $t+\Delta t$ (Clough and Penzien 1993, Bathe and Wilson 1976).

$$\mathbf{u}_{t+\Delta t} = \mathbf{u}_t + \Delta t \dot{\mathbf{u}}_t + \Delta t^2 \left[\left(\frac{1}{2} - \beta \right) \ddot{\mathbf{u}}_t + \beta \ddot{\mathbf{u}}_{t+\Delta t} \right] \quad (3-6)$$

$$\dot{\mathbf{u}}_{t+\Delta t} = \dot{\mathbf{u}}_t + \Delta t \left[(1 - \gamma) \ddot{\mathbf{u}}_t + \gamma \ddot{\mathbf{u}}_{t+\Delta t} \right] \quad (3-7)$$

where β and γ are weighting factors and can be chosen to obtain optimum stability and accuracy.

(a) If $\beta = 1/4$ and $\gamma = 1/2$ the Newmark- β method is unconditionally stable (i.e. regardless of the size of the time step). In this case the acceleration within the time step Δt is constant and is usually referred to as the Newmark's constant-average acceleration scheme.

(b) If $\beta = 1/6$ and $\gamma = 1/2$ the Newmark- β method is identical to the linear acceleration method, in which the acceleration varies linearly within each time step. The linear acceleration method, however, is only conditionally stable. The linear acceleration method will be unstable unless $\Delta t/T_n \leq \sqrt{3}/\pi = 0.55$. This restriction has no effect in the analysis of SDOF systems because a shorter time step than $\Delta t/T_n = 0.55$ is needed for satisfactory representation of the dynamic response and input, but may require extremely short time step for analysis of MDOF systems having short periods of vibration.

(c) In general assuming a linear acceleration within each time step gives a better approximation of the dynamic response and provides more accurate results than the constant acceleration method.

(2) Wilson θ Method. For a general type of structure the period of the highest mode is related to the properties of the individual elements. An element with relatively small mass results in a very short period of vibration, with the effect of requiring an extremely short time step of integration, as discussed above. Although the unconditionally-stable constant acceleration method can be used in this situation, for accuracy reasons an unconditionally-stable linear acceleration method such as the Wilson θ -method (Clough and Penzien 1993, Bathe and Wilson 1976) is more desirable. The Wilson θ -method is based on the assumption that the acceleration varies linearly over an extended computational interval $\tau = \theta \Delta t$, where $\theta \geq 1$. For $\theta = 1$, the method reverts to the standard linear acceleration method, but for $\theta > 1.37$ it becomes unconditionally stable. However, the Wilson θ -method tends to damp out the higher modes and could produce large errors when contributions of higher modes are significant. Therefore, the use of this method is no longer recommended. Instead the Hilbert, Hughes and Taylor α method, described next, is now being implemented in many computer programs in recent years.

(3) The Hilbert, Hughes and Taylor α Method. The HHT- α method (Hughes 1997) is a generalization of the Newmark- β method and reduces to the Newmark- β method for $\alpha = 0$. The finite-difference equations for the HHT- α method are identical to those of the Newmark- β method (i.e. (3-6) and (3-7)). The equations of motion are modified, however, using a parameter α .

$$\mathbf{m}\ddot{\mathbf{u}}_{t+\Delta t} + (1 + \alpha)\mathbf{c}\dot{\mathbf{u}}_{t+\Delta t} - \alpha\mathbf{c}\dot{\mathbf{u}}_t + (1 + \alpha)\mathbf{k}\mathbf{u}_{t+\Delta t} - \alpha\mathbf{k}\mathbf{u}_t = (1 + \alpha)\mathbf{f}_{t+\Delta t} - \alpha\mathbf{f}_t \quad (3-8)$$

With $\alpha = 0$ the HHT- α method reduces to the constant acceleration method. If $-1/3 \leq \alpha \leq 0$, $\beta = (1 - \alpha^2)/4$, and $\gamma = 1/2 - \alpha$, the HHT- α method is second-order accurate and unconditionally stable. The HHT- α method is useful in structural dynamics simulations incorporating many degrees of freedom, and in which it is desirable to numerically attenuate (or dampen-out) the response at high frequencies. Decreasing α (below zero) decreases the response at frequencies above $1/(2\Delta t)$, provided that β and γ are defined as above.

3-4. Mode Superposition

a. The number of operations in the direct integration method is proportional to the number of time steps used. In general the use of direct integration may be considered effective when the response is required only for a relatively short duration. However, if the integration must be carried out for many time steps, it may be more effective to transform the equations of motion into a form for which the step-by-step integration is less costly. For this purpose the equations of motion for linear analysis are usually transformed into the eigenvectors or normal-coordinate system. Applying the normal-coordinate transformation in accordance with Clough and Penzien (1993) to Equation (3-1) leads to the following decoupled equation of motion for individual modes

$$M_n \ddot{Y}_n(t) + C_n \dot{Y}_n(t) + K_n Y_n(t) = P_n(t) \quad (3-9)$$

where the modal coordinate mass, damping, stiffness, and load are defined as follows:

$$M_n = \phi_n^T \mathbf{m} \phi_n \quad (3-10a)$$

$$C_n = \phi_n^T \mathbf{c} \phi_n \quad (3-10b)$$

$$K_n = \phi_n^T \mathbf{k} \phi_n \quad (3-10c)$$

$$P_n = \phi_n^T \mathbf{p}(t) \quad (3-10d)$$

The modal Equation (3-9) may also be expressed in the following form

$$\ddot{Y}_n(t) + 2\xi_n \omega_n \dot{Y}_n(t) + \omega_n^2 Y_n(t) = \frac{P_n(t)}{M_n} \quad (3-11)$$

where ξ_n is the modal damping ratio, and ω_n is the undamped natural frequency. Now the time integration can be carried out individually for each decoupled modal equation (3-11). This can be accomplished using any of the above integration schemes or by numerical evaluation of the Duhamel integral (Clough and Penzien, 1993)

$$Y_n(t) = \frac{1}{M_n \omega_n} \int_0^t P_n(\tau) \exp[-\xi_n \omega_n (t - \tau)] \sin \omega_{Dn} (t - \tau) d\tau \quad (3-12)$$

where $\omega_{Dn} = \omega_n \sqrt{1 - \xi_n^2}$ is the damped natural frequency. Having obtained the response of each mode $Y_n(t)$ from Equation (3-12), the total displacement of the structure in the geometric coordinates can be computed using

$$\mathbf{u}(t) = \phi_1 Y_1(t) + \phi_2 Y_2(t) + \dots + \phi_N Y_N(t) \quad (3-13)$$

b. In summary, the response analysis by mode superposition requires: 1) the solution of the eigenvalues and eigenvectors for transformation of the problem to the modal coordinates, 2) solution of the decoupled modal equilibrium equations (3-11) by the Duhamel integral or other integration schemes, and 3) superposition of the modal responses as expressed in (3-13) to obtain the total response of the structure.

c. In the linear time-history analysis the choice between the direct method and mode superposition is decided by effectiveness of the methods and whether a few modes of vibration can provide accurate results or not. The solutions obtained using either method are identical with respect to errors inherent in the time integration schemes and round-off errors associated with computer analysis.

3.5 Stability and Accuracy Considerations

a. The aim of numerical integration of the equations of motion is to obtain stable and accurate approximation of the dynamic response with minimal computational effort. An integration method is unconditionally stable if solution for any initial conditions will not grow without bound for any time step Δt . The method is said to be only conditionally stable if the aforementioned stability condition holds when $\Delta t/T$ is smaller than a critical value. On this basis, it is clear that if a conditionally stable method such as the Newmark's linear acceleration method is employed, the time step Δt should be less than the value specified in 3-3c(1)(b). While an unconditionally stable method such as the Newmark's constant acceleration has no restriction on the size of the time step for stability consideration, the time step should still be small enough so that the method yields an accurate and effective solution. In general stability and accuracy of any method can be improved by reducing the size of the time step.

b. The main factor in selecting a step-by-step method is efficiency, which concerns with the computational effort needed to achieve desired level of accuracy. Accuracy alone is not a good criterion for method selection. This is because any desired level of accuracy can be achieved by any method if the time step is made adequately short. In any case the time step should be short enough to provide adequate definition of the loading and the response history. A high frequency load or response cannot be described by long time steps.

c. The integration time step should be selected based on the frequency content of the applied load and the highest significant frequency (shortest significant period) of vibration of the structure. If the load history is relatively simple, the choice of the time step will depend essentially on the shortest significant period of vibration. In general, using a time step $\Delta t \leq T_p/10$ will give reliable results. Here T_p is the lowest period of vibration that will contribute significantly to the dynamic response. Considering that an earthquake tends to excite mainly a few lower modes of vibration, T_p need not be very short. For example a $\Delta t = 0.01$ can adequately define an earthquake acceleration digitized at intervals of 0.01 sec and provide accurate results for periods of vibration up to 0.1 sec. Note that even though such an earthquake acceleration contains frequencies up to Nyquist frequency $f = 1/2\Delta t = 50$ Hz, the significant input energy is usually confined to frequencies less than about 10 Hz (0.1 sec). Thus selecting a short time step than 0.01 sec to account for higher modes may not change the response significantly, because the earthquake input energy to excite such higher modes is expected to be negligible. If there is any doubt about the accuracy of the results, a second analysis can be made with a time step reduced by one-half to ensure that the errors produced by numerical integration are acceptable.

Section II
Frequency Domain Solutions

3-6. Preview

An alternative approach to solving the modal equations of motion (3-9), instead of step-by-step integration in the time domain, is to make use of the frequency domain analysis procedures. The frequency domain analysis is especially convenient when the equation of motion contains frequency dependent stiffness and damping parameters, as in the case of structure-foundation and fluid-structure interaction problems (Clough and Penzien 1993). Only an outline of the frequency domain analysis is presented here. A frequency domain solution consists of three phases as described below and illustrated in Figure 3-1.

a. The first phase involves conversion of the applied loading from the time domain to the frequency domain by means of the Fourier transform procedure. This process replaces the loading amplitude values expressed at a sequence of time steps by complex values that express the harmonic load amplitudes at a specified sequence of frequencies. These complex values may be interpreted as the frequency-domain expression of the loading.

b. In the second phase the structure responses for a specified sequence of given frequencies are characterized by the complex frequency response functions, which express the harmonic response amplitudes of the structure due to unit harmonic loading. In other words, the frequency response function of a system is the ratio of response amplitude to input amplitude when the input is a complex exponential or sinusoid. When the complex frequency response functions are multiplied by the harmonic input amplitudes obtained in Step 1, the results give the frequency-domain expression of the structure response for the specified loading.

c. In the final phase of the analysis, the frequency domain response obtained in Step 2 is converted back to the time domain by means of the inverse Fourier transform procedure. Once the time-domain structure response of interest, usually displacements, have been determined in this manner, other response quantities such as stresses and section forces and moments are evaluated using the standard relationships between displacements and these quantities.

3-7. Transfer of Acceleration Time-History to the Frequency Domain

a. The first step in the frequency-domain response analysis is an understanding that an acceleration time-history $\ddot{x}_{ground}(t)$ can be represented by Fourier series using the discrete Fourier transform. Consider for example an $\ddot{x}_{ground}(t)$ digitized at a time-step $\Delta t = 0.01$ sec with a total duration $t_p = 40.96$ sec. The total number of points N , equally spaced in time, is 4096 ($N = t_p/\Delta t$). The trigonometric form of the Fourier series representation of the acceleration time-history is given by:

$$\ddot{x}_{ground}(t) = a_0 + \sum_{n=1}^{infinity} a_n \cos(\omega_n t) + b_n \sin(\omega_n t) \quad (3-14)$$

where a_0 , a_n , and b_n are *Fourier coefficients*. All Fourier coefficients a_0 , a_n , and b_n are constants for a given time-history. Note that the Fourier series is simply a summation of simple harmonic sine and cosine functions. The general trigonometric form of the Fourier series assumes a periodic function of period T_p , equal to duration t_p , and $\omega_n = 2\pi n/T_p$. These circular frequencies ω_n are not arbitrary but equally spaced at a circular frequency increment $\Delta\omega = 2\pi/T_p (=2\pi/t_p)$.

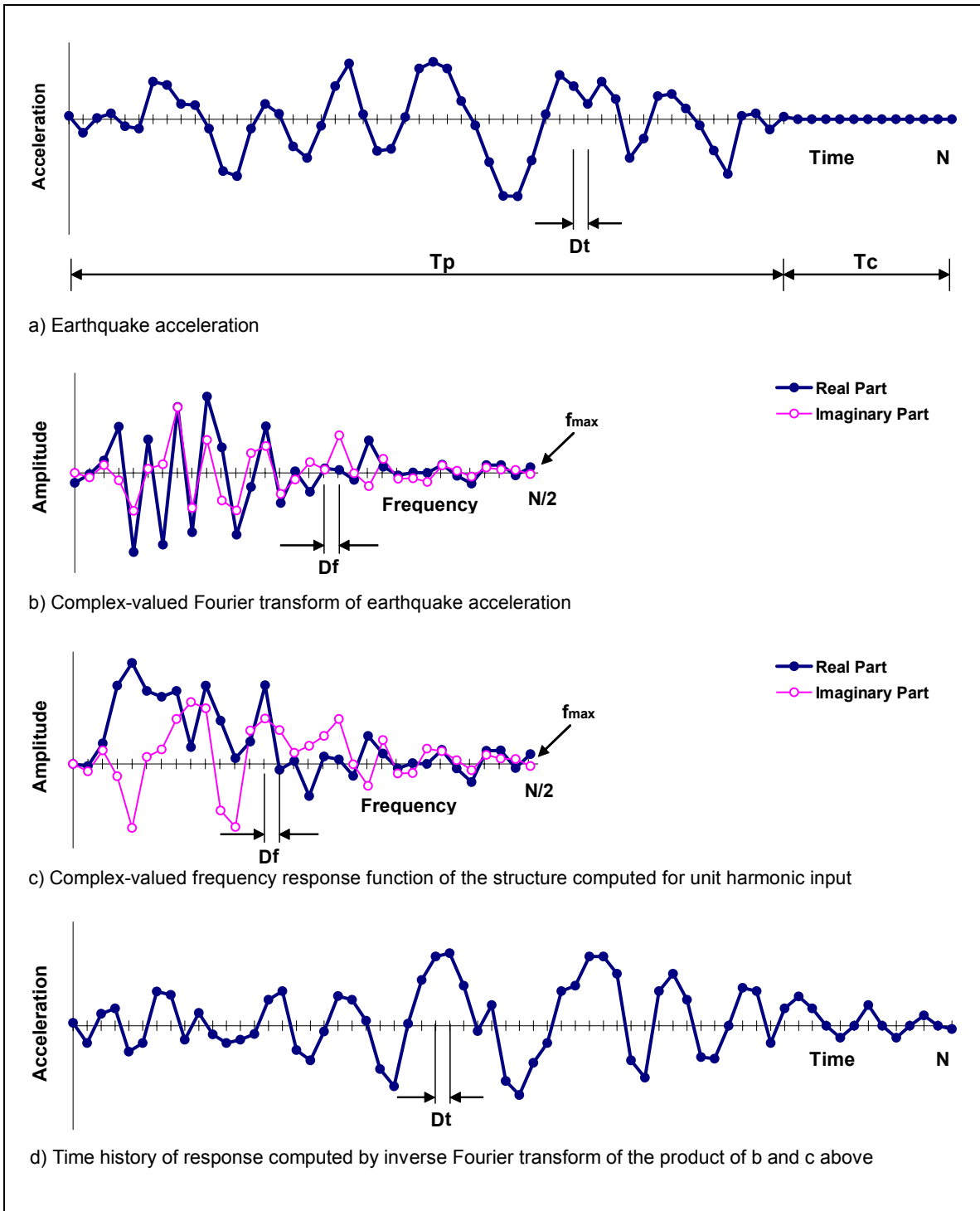


Figure 3-1. Phases of dynamic response computation in frequency domain and relationships between response parameters

b. In practice the Fourier series of $\ddot{x}_{ground}(t)$ is frequently expressed in complex exponential form and computed using the computerized Fast Fourier Transform (FFT):

$$\ddot{x}_{ground}(t) = Re \sum_{s=0}^{N/2} \ddot{X}_s \exp(i \omega_s t) \quad (3-15)$$

where Re designates the real component of the complex series and

$\ddot{X}_s = (N/2 + 1)$ complex Fourier amplitudes

ω_s = the circular frequency of each of $(N/2 + 1)$ harmonic

and

$$i = \sqrt{-1} \quad (3-16)$$

The circular frequency of each harmonic ω_s is given by:

$$\omega_s = \frac{2 \pi s}{T_p} = \frac{2 \pi s}{t_p} \quad \text{for } s = 0, 1, 2, \dots, N/2 \quad (3-17)$$

Note that for a given time-history each complex Fourier coefficient \ddot{X}_s is a constant value corresponding to each circular frequency ω_s and comprises of real and imaginary parts. Use of the FFT is based on letting $N = 2^j$ (e.g., $N = \dots, 512, 1024, \dots, 4096$, etc.), following the Cooley and Tukey (1965) algorithm for computers.

3-8. Frequency Response Functions

a. *Definition.* The frequency response function of a system is the ratio of response (output) amplitude to input amplitude when the input is a complex exponential or sinusoid. For the input force set to

$$p(t) = P e^{i \omega t} \quad (3-18)$$

where F is the input amplitude, the output displacement x will be in the form

$$x(t) = X e^{i \omega t} \quad (3-19)$$

In general, X and P may be complex numbers. The complex-valued frequency response function for the system is then given by

$$H(i \omega) = \frac{X}{P} \quad (3-20)$$

b. Frequency Response Function of a SDOF system. Consider an oscillator with mass m , spring k , and damper c , driven by movements of the ground supporting the mass. From the free body diagram the equation of motion in the time domain is

$$m\ddot{x} + c\dot{x} + kx = -m\ddot{y}_g = p(t) \quad (3-21)$$

Assuming $p(t) = Pe^{i\omega t}$, and taking Fourier transform of the above equation, results in the equation of motion in the frequency domain

$$(-m\omega^2 + ic\omega + k)X(\omega) = P(\omega) \quad (3-22)$$

By definition the complex-valued frequency response function for the SDOF system is given by

$$H(i\omega) = \frac{1}{(-m\omega^2 + ic\omega + k)} \quad (3-23)$$

or

$$H(i\omega) = \frac{1}{k(1 - \beta^2 + 2i\xi\beta)}$$

and

$$X(\omega) = H(i\omega)P(\omega) \quad (3-24)$$

b. Frequency Response Functions for MDOF Systems. The modal equations of motion for a MDOF system in the frequency domain is expressed by

$$[(\mathbf{K} - \omega^2\mathbf{M}) + i(\omega\mathbf{C})]\mathbf{Y}(i\omega) = \mathbf{P}(i\omega) \quad (3-25)$$

where $\mathbf{P}(i\omega)$ is the Fourier transform of the modal loading vector $\mathbf{P}(t)$, which contains modal components $P_1(t), P_2(t), \dots, P_n(t)$ as defined in 3-10d; $\mathbf{Y}(i\omega)$ is the Fourier transform of the normal coordinate vector $\mathbf{Y}(t)$ containing $Y_1(t), Y_2(t), \dots, Y_n(t)$; \mathbf{K} and \mathbf{M} are the diagonal modal stiffness and mass matrices containing elements in accordance with Equations (3-10b) and (3-10a); and \mathbf{C} is the normal modal damping having elements as given by Equation (3-10c). Note that Equation (3-25) may contain all N normal modal equations or only a smaller specified number of lower modes that provide reasonable accuracy. Making use of the impedance matrix $\mathbf{I}(i\omega)$ which is equal to the entire bracket matrix, Equation (3-25) can be written in the following compact form

$$\mathbf{Y}(i\omega) = \mathbf{I}(i\omega)^{-1}\mathbf{P}(i\omega) \quad (3-26)$$

From this equation it is obvious that the complex-frequency-response functions $\mathbf{H}(i\omega)$ is the same as inverse of impedance matrix. In practical computation the elements of complex-frequency response functions are obtained from inversion of the impedance matrix, but interpolation procedures are used to reduce the solution efforts. This way frequency response functions are computed at specified number of frequencies but interpolated at the intermediate closely spaced frequency increments.

3-9. Computation of Structural Response

After obtaining all frequency response functions $H_{ij}(i\omega)$ by inversion solution of the impedance matrix and the use of interpolation, the response vector $\mathbf{Y}(i\omega)$ is obtained by superposition using

$$\mathbf{Y}(i\omega) = \mathbf{H}(i\omega)\mathbf{P}(i\omega) \quad (3-27)$$

where $\mathbf{H}(i\omega)$ is the $N \times N$ complex-frequency-response matrix

$$\mathbf{H}(i\omega) = \begin{bmatrix} H_{11}(i\omega) & H_{12}(i\omega) & \cdots & H_{1N}(i\omega) \\ H_{21}(i\omega) & H_{22}(i\omega) & \cdots & H_{2N}(i\omega) \\ \vdots & \vdots & \vdots & \vdots \\ H_{N1}(i\omega) & H_{N2}(i\omega) & \cdots & H_{NN}(i\omega) \end{bmatrix} \quad (3-28)$$

determined for an appropriate range of excitation frequencies. Once the complex frequency response matrix has been determined the modal response of structure $\mathbf{Y}(i\omega)$ to any arbitrary loading can be obtained simply by Fourier transforming the load by the FFT procedure and multiplying the results by the complex-frequency-response matrix. Knowing the modal response vector $\mathbf{Y}(i\omega)$, the corresponding modal displacements $\mathbf{Y}(t)$ in the time domain can be obtained by the inverse FFT procedure, and other response quantities are then easily obtained using the standard time-domain procedure described previously.

3-10. Selection of Parameters for Frequency Domain Analysis

To ensure that frequency domain analysis leads to accurate dynamic response of a structure, the parameters that govern the response computation must be selected carefully, as described below.

a. Maximum Excitation Frequency. The maximum excitation frequency selected for the analysis should be greater than the frequencies of all significant harmonics in the input ground acceleration record. The maximum excitation frequencies should also be large enough to include the range of frequencies over which the structure has significant dynamic response.

b. Number of Generalized Coordinates or Vibration Modes. The number of vibration modes required to represent earthquake response of a hydraulic structure is much less than the number of degrees of freedom in the finite-element model. In general, all the modes that contribute significantly to the dynamic response should be included. A final check that enough modes have been considered is to investigate that the maximum stresses and section forces do not change if the number of modes is increased.

c. Number of Excitation Frequencies and Time Interval. As illustrated in Figure 3-1, the parameters used in an FFT analysis include T , Δt , N , f_{max} , and Δf . These are described below.

(1) $T = N \cdot \Delta t$ is the duration of response history. In Fourier analysis both the excitation and response are periodic; i.e. the values at times $\dots t-2T, t-T, t, t+T, t+2T \dots$ are the same. Considering that an acceleration record is generally thought to be non-periodic, the input signal should be augmented by several seconds of “trailing zeros” to satisfy this condition. It is expected that adequate zeros are added so that the structure response present at the end of the input record decays to a relatively small value.

(2) Δt is the time increment at which excitation and response values are defined.

(3) $N = T/\Delta t$ is the number of discrete time steps. The choice of N is made so that $N=2^j$ by selecting T as demonstrated in Figure 3-1:

$$T = T_p + T_h$$

where T_p is the duration of the earthquake signal, and T_h is the time required for the structure response to decay to negligible value at the end of earthquake signal.

(4) $f_{max} = 1/2\Delta t$ is the maximum frequency that is included in the analysis and is referred to as the *Nyquist* frequency, the largest frequency contain in the input acceleration record.

(5) $\Delta f = 1/T$ is the frequency increment in Hz. The frequencies included in the analysis are 0, Δf , $2 \Delta f$, $3 \Delta f$, ..., f_{max} – a total of $N/2+1$ frequencies.

Chapter 4 Structural Performance and Damage Criteria

4-1. General

a. The purpose of this chapter is to use linear time-history analysis to formulate a systematic and rational methodology for qualitative estimate of the level of damage. In linear time-history analysis, deformations, stresses, and section forces are computed in accordance with elastic stiffness characteristics of various members and components. Using acceleration time-histories as the seismic input, the linear time-history analysis computes both the magnitudes and time-varying characteristics of the seismic response. A systematic interpretation and evaluation of these results in terms of the demand-capacity ratios, cumulative inelastic duration, spatial extent of overstressed regions, and consideration of possible modes of failure form the basis for approximation and appraisal of probable level of damage. The damage in this manual refers to cracking of the concrete, opening of construction joints, and yielding of the reinforcing steel. If the estimated level of damage falls below the acceptance curve for a particular type of structure, the damage is considered to be low and the linear time-history analysis will suffice. Otherwise the damage is considered to be severe, in which case a nonlinear time-history analysis would be required to estimate damage more accurately. The methodologies and procedures for estimation of the probable level of damage in this chapter were adopted from Ghanaat (2002).

b. If the results of linear time-history analysis indicate only limited performance inadequacy, the use of a nonlinear procedure may demonstrate acceptable performance. This is because the nonlinear procedures provide more accurate estimates of demands than do linear procedures. Linear procedures are most applicable to structures that actually have sufficient strength to remain nearly elastic when subjected to the MDE demands and to structures with regular geometries and distributions of stiffness and mass. To the extent that concrete hydraulic structures analyzed by this method do not have such strength or regularities, the indications of inelastic ductility demands predicted by the elastic methods may be inaccurate. In recognition of the relative inaccuracy of the linear techniques in predicting nonlinear response, the acceptance criteria have intentionally been set conservatively to provide a reasonable level of confidence in the method. Although the methodology formulated in this chapter is considered to be conservative, estimation of damage by the linear time-history analysis should still be used with considerable caution and careful interpretation and evaluation of the results. Examples of a gravity dam, two arch dams, a pile-founded navigation lock, and a free-standing intake tower are provided to illustrate the methodology and discuss probable nonlinear response and failure mechanisms for each structure.

4-2. Basis for the Proposed Performance and Damage Criteria

a. Traditional Criteria. Seismic performance of concrete hydraulic structures is being assessed on the basis of simple stress (or section-force) checks obtained from the linear elastic analysis combined with engineering judgment. The acceptance criterion for compressive stresses is that they should be less than the compressive strength of the concrete by a factor of 1.5 for new designs (USACE, 1994) and 1.1 for existing dams (FERC, 1999). Generally tensile stresses should not exceed tensile strength of the concrete. However, in practice up to five stress excursions above the tensile strength of the concrete have been considered acceptable based on engineering judgment and other considerations. This criterion neither puts limit on the magnitudes of stresses exceeding the tensile strength of the concrete nor offers any provisions regarding the spatial extent of such stresses. Rather it is left to the analyst to judge how high the magnitudes of critical tensile stresses could reach and how large an area they could occupy.

b. Proposed Criteria. To overcome the above shortcomings, this manual proposes a systematic approach for assessment of the seismic performance and probable level of damage using linear-elastic time history analyses. The performance evaluation and assessment of level of damage is formulated based on magnitudes of demand-capacity ratios, cumulative duration of stress excursions beyond the tensile strength of the concrete, spatial extent of overstressed regions, and load combination cases defined below. The acceptable level of damage on the basis of linear-elastic analysis is presented by a performance curve, as shown in Figure 4-1 (c), bounded by a demand-capacity ratio of 2 and an inelastic cumulative duration that varies with the type of structure.

(1) Demand-Capacity Ratios

(a) The demand-capacity ratio (DCR) for plain concrete is defined as the ratio of computed tensile stress to tensile strength of the concrete. For gravity dams, DCR is computed using principal stress demands. In the case of arch dams, where high stresses are usually oriented in the arch and cantilever directions, DCR is evaluated using arch or cantilever stress demands. The tensile strength or capacity of the plain concrete used in computation of DCR is obtained from the uni-axial splitting tension tests or from the static tensile strength

$$f_t = 1.7 f_c'^{2/3}$$

proposed by Raphael (1984), in which f_c' is the compressive strength of the concrete. The maximum permitted DCR for linear analysis of dams is 2. This corresponds to a stress demand twice the tensile strength of the concrete. As illustrated in the stress-strain curve in Figure 4-1(d), the stress demand associated with a DCR of 2 corresponds to the so called "apparent" dynamic tensile strength of the concrete (i.e. $3.4 f_c'^{2/3}$, Raphael 1984), used for evaluation of the results of linear dynamic analysis.

(b) DCR for the reinforced concrete hydraulic structures such as locks and intake towers is defined as the ratio of the section force demand to section force capacity. The maximum DCR is taken equal to 2 for bending moments and 1 for shears.

(2) Cumulative Inelastic Duration. The main problem with the traditional stress criterion is that the number of stress cycles alone is not always a good indicative of the level of damage. For example, the stress history in Figure 4-2 with 2 energetic stress cycles poses much higher damage potential than the stress history in Figure 4-3 with more than five stress cycles exceeding the tensile strength of the concrete. Both magnitudes and duration of stress cycles in Figure 4-2 are greater than those of the Figure 4-3, two factors that the traditional stress criterion ignores. For this reason the proposed damage criterion employs the cumulative inelastic duration in conjunction with DCR to account for these factors in assessment of the probable level of damage. The cumulative inelastic duration refers to the total duration of stress excursions above the tensile strength of the concrete, which as a measure of energy is a better indicator of the damage than the number of stress cycles.

(a) The cumulative inelastic duration of stress excursions, as defined in Figure 4-1(a) and 4-1(b), refers to the total duration of stress excursions above the tensile strength of the concrete (a DCR of 1 or greater). Figure 4-1(a) shows a sinusoidal stress history with five stress cycles and Figure 4-1(b) with one cycle exceeding a DCR of 1. In both cases the peak values are twice the tensile strength (i.e. DCR = 2). For each sinusoidal cycle duration of the stress excursion above the tensile strength is equal to $T/3$, where T is the period of the sinusoid. Thus for the Figure 4-1(a) the total inelastic duration for all five stress excursions (shaded area) amounts to $5T/3$. Considering that the periods of signals in Figures 4-1(a) and 4-1(b) are respectively 0.24 and 1.2 sec, the cumulative inelastic duration of stress excursions above f_t for both signals is 0.4 sec. Similarly, the cumulative inelastic duration of stress magnitudes exceeding $1.5f_t$ is 0.2 sec and of those exceeding $2f_t$ is zero.

(b) The limit values set for the cumulative inelastic duration vary with the type of hydraulic structures. The cumulative-inelastic-duration is estimated based on the dynamic characteristics, load resisting mechanism, and

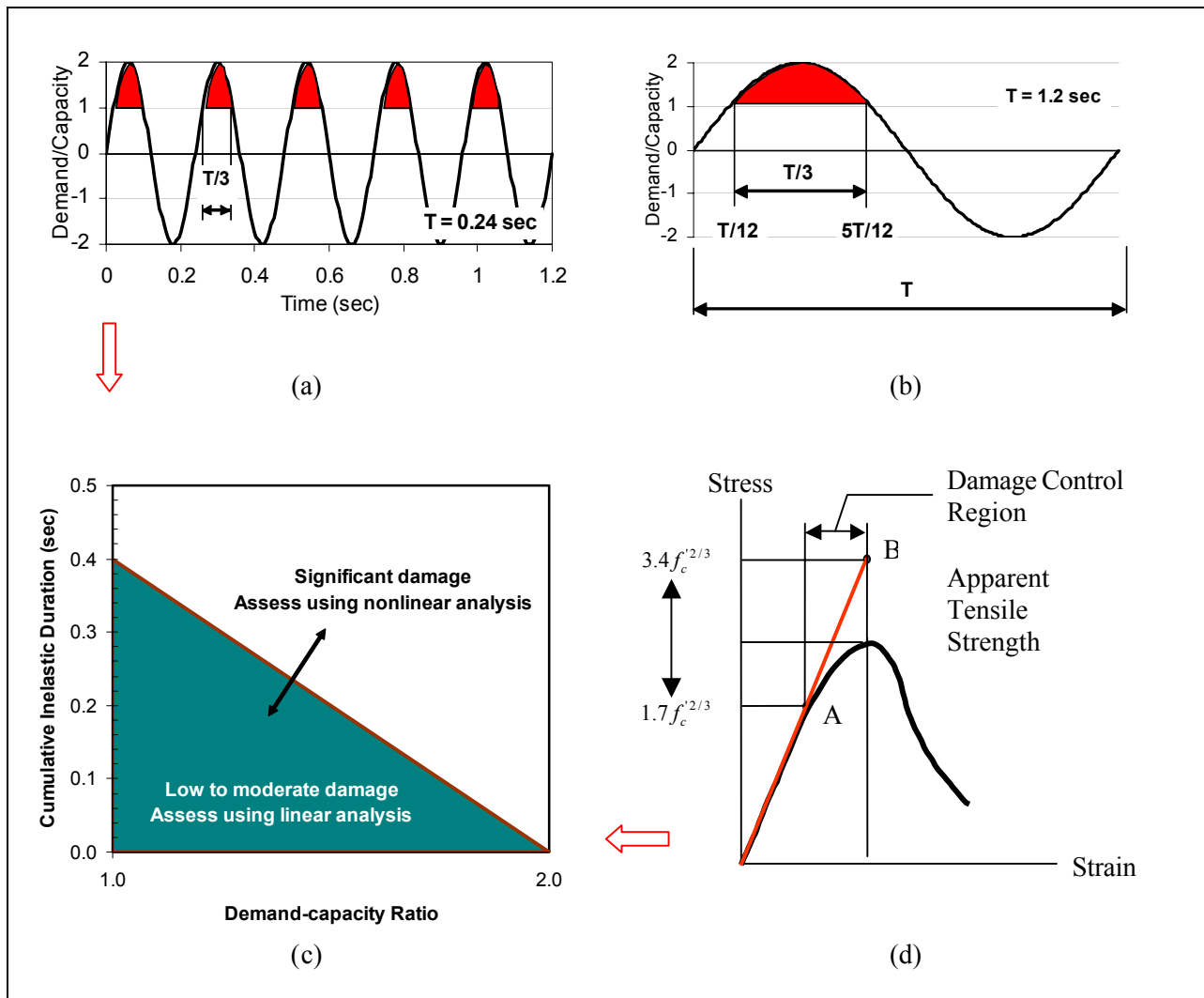


Figure 4-1. Basis for upper limit demand-capacity ratio and cumulative inelastic duration

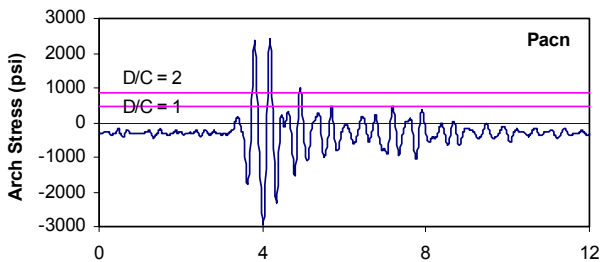


Figure 4-2. Fewer than five cycles exceed the capacity

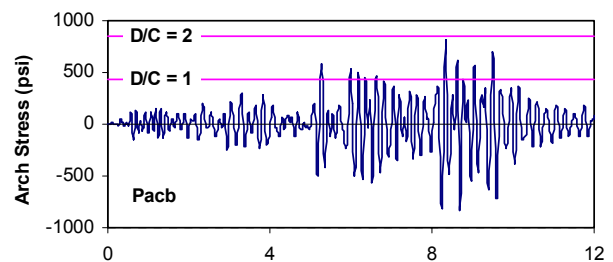


Figure 4-3. More than five cycles exceed the capacity

redundancy of the structure. For example arch dams that resist loads through both the arch and cantilever actions can sustain higher level of nonlinear deformation (or longer cumulative-inelastic-duration) than gravity dams that rely on cantilever mechanism alone to resist loads. Similarly, a reinforced concrete free-standing inlet/outlet tower exhibiting dominant flexural mode of behavior can tolerate even higher amount of nonlinear behavior. Another important factor in determining the cumulative inelastic duration is the frequency content of the earthquake input to ensure that the effects of most intense input pulses have been considered. Figure 4-4 shows that on the average the most intense earthquake pulses have frequencies roughly in the range of 0.8-to-4.4 Hz or periods in the range of 1.2-to-0.24 seconds. Making use of this, a single stress pulse with a period of 1.2 sec and the peak amplitude of $2f_i$ (Figure 4-1(b)) forms the basis for cumulative-inelastic-duration on the long-period end and five stress pulses with a period of 0.24 (Figure 4-1 (a)) on the short-period end of the intense shaking range. The cumulative inelastic durations for these signals are respectively $T/3$ and $5T/3$ or 0.4 seconds. This means a structure with a predominant period of 1.2 sec. can have only one stress cycle exceeding the tensile strength, while another with a period of 0.24 sec. can have up to five cycles. However, in either case the total cumulative inelastic duration remains at 0.4 seconds. In addition to these considerations, the selected cumulative-inelastic-duration for each type of structure was validated through numerous linear and nonlinear time history analyses and response evaluations, as discussed in 4-3 to 4-6 below.

(3) Extent of damage or nonlinear behavior. In addition to the foregoing performance curve (Figure 4-1(c)) the proposed damage criteria require the damage be confined to small regions, so that the evaluation on the basis of linear analysis is still valid. The spatial extent of damage or nonlinear response for each type of hydraulic structure is presented in the following paragraphs specific to that structure.

(4) Load Combination Cases. The performance and damage criteria discussed above require the use of three or more sets of earthquake acceleration time histories. For each set of two- (2D analysis) or three-component (3D analysis) ground motions the effects of static loads and earthquake ground motions components are combined by multiplying each earthquake component by +1 or -1 to account for the most unfavorable direction of earthquake attack.

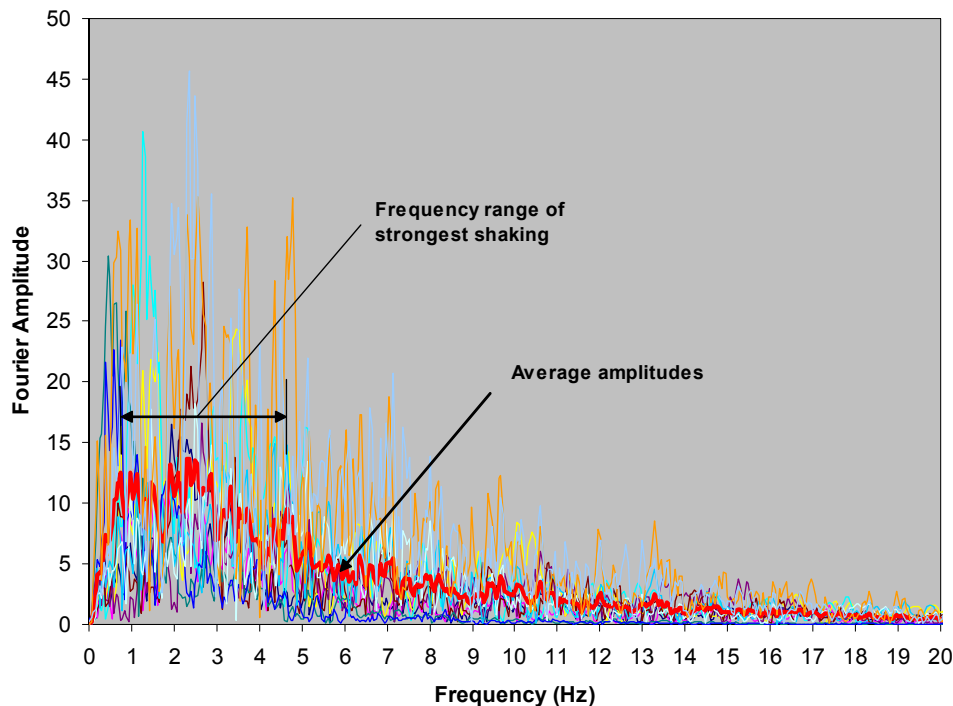


Figure 4-4. Fourier amplitudes of 12 earthquake recordings and their average

EM 1110-2-6051
22 Dec 03

used to determine frequency range of strongest shaking

4-3. Gravity Dams

Concrete gravity dams are modeled and analyzed in accordance with the linear dynamic analysis procedures outlined in Chapters 1 and 2. The results of such analyses include peak values and time-histories of displacements and stresses. Combined static and seismic stresses obtained for three or more sets of earthquake ground motions and load combination cases described in this paragraph form the basic parameters needed for evaluation of the dam. Other parameters include an understanding of nonlinear response of the dam in the form of probable cracking profiles and possible modes of failure and evaluation of demand-capacity ratios and cumulative duration of stress excursions beyond the tensile strength of the concrete. Types of probable damage, modes of failure, and influence of earthquake ground motion on the level of damage are described using the results from a nonlinear analysis of a typical gravity dam, followed by performance criteria and presentation and evaluation of results for the linear time-history analysis.

a. Nonlinear response and modes of failure. Figure 4-5 provides some examples of probable cracking profiles and possible modes of failure for a typical gravity dam analyzed using nonlinear fracture mechanics and various types of earthquake input motions (Leger and Leclerc 1996). Leger and Leclerc's results show that the cracking always initiates at the base of the dam, starting from the upstream face and propagating in the downstream direction. The cracks at the top of the dam generally initiate from the downstream face during an upstream swing of the dam and are either horizontal or sloping downward. A crack profile sloping downward from the downstream toward the upstream is considered more stable against a sliding failure than a crack with a reverse slope. This is because in the former case the water pressure is opposing the sliding whereas in the latter it is acting as a driving force. Any failure mode would likely involve sliding stability along the cracked surfaces with the water pressure as a driving force, acting both on the upstream face of the dam and in the crack. Should through cracks form near the crest of the dam, the consequences of failure may not be as critical as lower cracks, mainly because the failure of the upper portion of the dam might release only a small portion of the impounded water provided that the remaining section can resist overtopping.

b. Influence of earthquake ground motion. The results in Figure 4-5 clearly demonstrate that formation, location, extent, and orientation of tensile cracking are sensitive to characteristics of the earthquake ground motion. Three types of earthquake ground motions were considered: scaled recorded, spectrum-compatible recorded, and spectrum-compatible synthetic records. The top three graphs in this figure show dam responses to the horizontal components of scaled recorded signals from the 1989 Loma Prieta, 1988 Saguenay, and 1985 Nahanni earthquakes. The critical peak ground acceleration (CPGA) in this figure refers to a peak ground acceleration (PGA) value required to induce dynamic instability in the system. The Loma Prieta record containing significant energy near the fundamental period of the dam was scaled down from a recorded PGA of 0.44 g to a CPGA = 0.2 g, Saguenay was scaled up from 0.131 g to 0.65 g, and Nahanni from 0.545 g to 0.57 g. The middle three graphs are the crack profiles and required CPGA for the same natural records but with modified Fourier amplitude spectra compatible with a target response spectrum. The modified Loma Prieta record provided results comparable with the modified Saguenay and Nahanni records, as variation of the system energy was reduced as a result of spectrum compatibility. The modified records generally produced cracks at the same elevation as those estimated for the scaled natural records. The spectrum-compatible synthetic ground motion records produced somewhat similar cracks among themselves (lower graphs in Figure 4-5) but different from those obtained from the scaled and modified natural records. The cracks for the synthetic records formed and propagated at higher elevations than those for other records. Such sensitivity to characteristics of earthquake ground motion proves that damage should be estimated using a series of natural records scaled consistent with the design response spectra in the range of important structural periods.

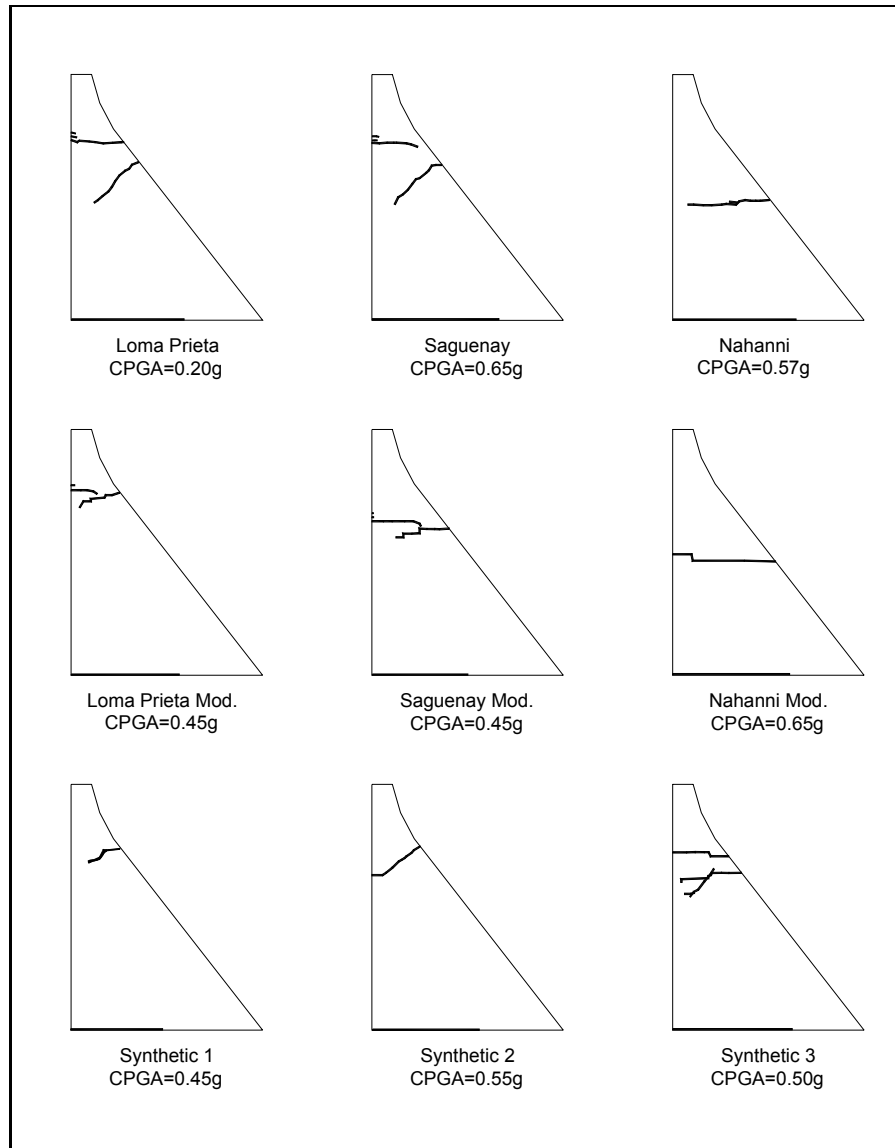


Figure 4-5. Probable cracking profiles of a typical gravity dam subjected to different types of earthquake ground motions (adapted from Leger and Leclerc 1996)

c. Performance criteria for linear analysis. The earthquake performance of gravity dams is evaluated on the basis of combined static and seismic stresses in accordance with the load combination cases in paragraph *d* below, demand-capacity ratios and the associated cumulative duration in *e* below, and presentation and interpretation of the results described in *f* below. The dam response to the MDE is considered to be within the linear elastic range of behavior with little or no possibility of damage if the computed demand-capacity ratios are less than or equal to 1.0. The dam will exhibit nonlinear response in the form of cracking of the concrete and/or opening of construction joints if the estimated demand-capacity ratios exceed 1.0. The level of nonlinear response or cracking is considered acceptable if demand-capacity ratios are less than 2.0 and limited to 15 percent of the dam cross-section surface area, and the cumulative duration of stress excursions beyond the tensile strength of the concrete falls below the performance curve given in Figure 4-6. Consideration should also be given to the relation between the fundamental period of the dam and peak of the earthquake response spectra. If lengthening of the periods of vibration due to nonlinear response behavior

causes the periods to move away from the peak of the spectra, then the nonlinear response would reduce seismic loads and improve the situation by reducing stresses below the values obtained from the linear time-history analysis. When these performance conditions are not met, or met only marginally with the nonlinear response increasing the seismic demand, then a nonlinear time-history analysis might be required to estimate the damage more accurately.

d. Load combination cases. Two-dimensional models of gravity dams should be evaluated for the vertical and one horizontal components of earthquake ground motion plus the effects of static loads. For each earthquake record, the static loads and earthquake components should be combined in accordance with Table 4-1. Three-dimensional models of gravity dams, when required, should be evaluated for three components of earthquake ground motion in accordance with Table 4-7.

e. Demand-capacity ratios. The demand-capacity ratios for gravity dams is defined as the ratio of the calculated principal stresses to tensile strength of the concrete. The tensile strength of plain concrete is obtained in accordance with 4-2b(1)(a). As discussed previously the demand-capacity ratio is limited to 2.0, thus permitting stresses up to twice the static or at the level of *dynamic apparent tensile strength* of the concrete.

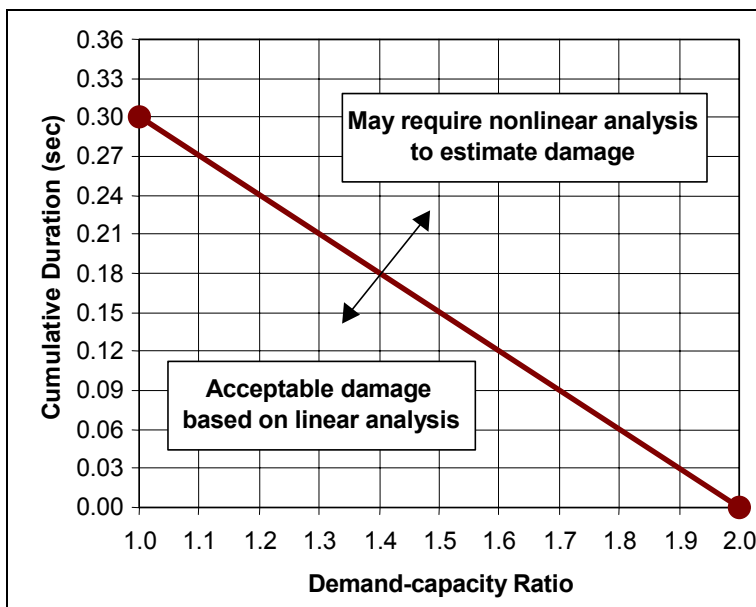


Figure 4-6. Performance curve for concrete gravity dams

Table 4-1 Load Combination Cases for Combining Static and Dynamic Stresses for 2-D Analysis			
Case	Seismic Loads		
	Vertical (V)	Stream Horizontal (H1)	Static Loads (Stress)
1 ¹	+	+	+
2	+	-	+
3	-	+	+
4	-	-	+

Note: The (+) and (-) signs indicate that the loads are multiplied by +1 or -1 to account for the most unfavorable earthquake direction.
¹ Case 1: Static + H1 + V

The cumulative duration in Figure 4-6 refers to the total duration of stress excursions beyond a certain level of demand-capacity ratio. For example, a cumulative duration of 0.21 sec at a demand-capacity ratio of 1.3 (Figure 4-6) indicates the total duration of stress excursions above the 1.3 times the tensile strength of the concrete. The cumulative duration beyond a certain level of demand-capacity ratio is obtained by multiplying number of stress values exceeding that level by the time-step used in the time-history analysis. As shown in Figure 4-6, the cumulative duration for gravity dams is set to 0.3 sec.

f. Presentation and performance evaluation. For performance evaluation of gravity dams described in *c* above, the following results from linear time-history analyses are required.

(1) Natural frequencies and mode shapes. Natural frequencies and natural modes of vibration provide important information on the dynamic characteristics of the dam, its degree of dynamic coupling or interaction with the impounded water, and its level of response to earthquake loading. A strong dynamic coupling with the impounded water indicates that more accurate representations of the dam-water interaction effects are required. Depending on whether the lower modes of the dam fall on the ascending or descending part of the earthquake response spectra, it can be inferred that nonlinear behavior would increase or decrease the seismic demand.

(2) Displacement histories. The magnitudes and time-histories of nodal displacements at critical locations such as the crest should be presented and evaluated. While displacement patterns provide a visual means of validating the results, displacement magnitudes are examined to ensure that they are small and that the overall stability of the dam is maintained.

(3) Maximum and minimum principal stresses. Maximum and minimum principal stresses due to static plus seismic loads should be determined and presented as contours or vector plots. In general vector plots are more useful than the contour plots because stress vectors provide both the magnitude and direction of principal stresses, thus can be used to predict probable direction of the tensile cracking. The maximum and minimum stress plots represent the largest tensile (positive) and the largest compressive (negative) stresses that occur in the dam generally at different times during the earthquake excitation.

(4) Demand-capacity ratios. The maximum principal stresses in (3) above could also be displayed as plots of the demand-capacity ratios by dividing the maximum stresses by the tensile strength and minimum stresses by the compressive strength of the concrete.

(5) Time-histories of critical principal stresses. Time-histories of the most critical maximum principal stresses identified in (3) above should be displayed and evaluated. Such time-histories are examined to determine the total duration of stress excursions beyond demand-capacity ratios of 1.0 to 2.0 for comparison with the performance curve in Figure 4-6. The total duration can simply be obtained by multiplying the number of stress values exceeding a stress level (or equivalent demand-capacity ratio) by the integration time-step used in the analysis. The magnitude of total duration indicates whether the peak stresses are merely spikes with little or no damage potential or they are of longer duration capable of producing significant damage.

(6) Concurrent principal stresses at the time of maximum stress. The maximum principal stresses in (3) above are not concurrent and generally occur at different time-steps during the earthquake excitation. They serve to identify the overstressed regions and locations of the critical principal stresses. From this information, time-steps at which the critical principal stresses reach their peak values are determined and used to obtain the corresponding concurrent or simultaneous principal stresses. The concurrent principal stresses should be displayed in the form of contours or vector plots and used to estimate the extent, location, and direction of probable tensile cracking following the general description provided in *a* above.

4-4. Arch Dams

Concrete arch dams are modeled and evaluated following the linear time-history analysis procedures outlined in Chapters 1 and 2. The results of analysis include peak values and time-histories of nodal displacements and element stresses. The analysis is repeated for three or more three-component sets of earthquake input acceleration time-histories. The results of each analysis are combined as described in this paragraph to account for the effects of static loads and phasing of the earthquake ground motion components. The magnitude, spatial extent, and spatial distribution of the combined stresses together with duration of stress excursions beyond the allowable values and an understanding of the possible nonlinear mechanism form the basis for earthquake performance evaluation of arch dams. In this paragraph probable nonlinear mechanism, modes of failure, and influence of earthquake ground motion characteristics on the level of damage are described first, followed by formulation of performance criteria and presentation and evaluation of results of linear time-history analysis.

a. Nonlinear behavior and modes of failure.

(1) Nonlinear behavior. Arch dams are generally built as cantilever monoliths separated by vertical contraction joints. Since contraction joints cannot transfer substantial tensile stresses in the arch direction, the joints can be expected to open and close repeatedly as the dam vibrates in response to severe earthquake ground motion. The contraction joint opening releases tensile arch stresses and transfers forces to the cantilevers. The increased cantilever stresses may exceed tensile strength of the lift lines (or horizontal joints), possibly resulting in crushing or horizontal cracking of the cantilevers. Potentially opened contraction joints and cracked lift joints may subdivide the monolithic arch structure into partially free cantilever blocks, capable of transmitting only compressive or frictional forces (Figure 4-7).

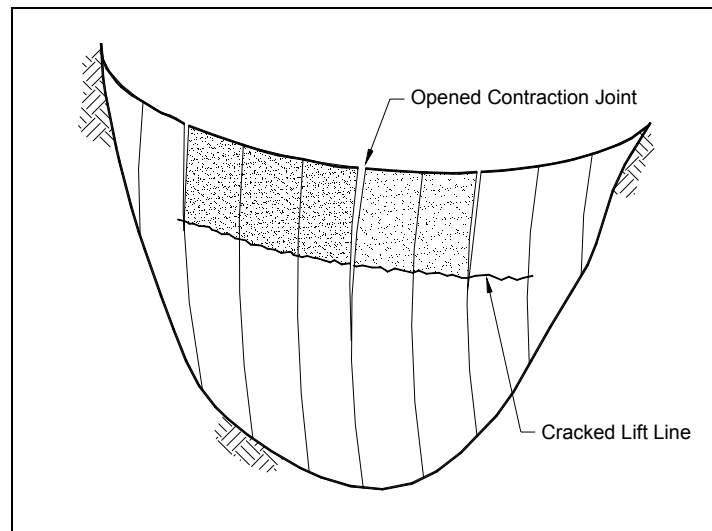


Figure 4-7. Contraction joint opening and lift line cracking in Arch dams

(2) Modes of failure. Any failure mode of the arch structure more likely would involve sliding stability of the partially free cantilevers. For small and moderate joint openings, the partially free cantilever blocks, bounded by opened joints, may remain stable through interlocking (wedging) with adjacent blocks. The extent of interlocking depends on the depth and type of shear keys and the amount of opening to be expected. Such concepts have similarities to Goodman and Shi's Block Theory (Goodman and Shi 1985) for the stability evaluation of rock masses: a continuous block, isolated by the intersection of discontinuities or free surfaces, can move only by sliding on one or two faces or by combined sliding and rotation. If potentially dangerous blocks can be shown to be incapable of moving because of friction, tapering, gravity, or orientation consideration, their stability is of no concern. A perfect shear key (i.e., rectangular shape) would permit only normal opening, but no sliding. Triangular or trapezoidal shear keys allow both opening and some sliding. Hence, the depth of the shear keys controls the maximum amount of joint opening for which adjacent blocks would remain interlocked; deeper shear keys permit larger joint openings. When the partially free cantilevers are treated as rigid blocks, the maximum joint opening with active interlocking can be estimated from rigid block geometry. Therefore, under nonlinear dynamic analysis, the magnitude of compressive stresses, the extent of joint opening or cracking, and the amplitude of non-recoverable movements of concrete blocks bounded by failed joints will control the overall stability of the dam, rather than the magnitude of calculated tensile stresses.

b. Influence of earthquake ground motion. The magnitude and characteristics of earthquake input motions and the way they are applied to the dam and foundation model have significant effects on the linear and especially nonlinear responses and must be evaluated carefully. For the linear elastic response analysis, the frequency content of the seismic input defined by the shape of the response spectrum plays a more significant role than any other parameter. For nonlinear analysis and linear analysis used for qualitative evaluation of damage, in addition to the frequency content, other ground motion characteristics such as duration, energy, and pulse sequencing become extremely important, and must be considered in selecting or developing acceleration histories. This paragraph illustrates the effects of ground motion characteristics on the response of two arch dams analyzed by the linear time-history method using six different sets of acceleration time-histories.

(1) Selected earthquake ground motions. For qualitative damage evaluation using linear time-history analysis, example arch dams were assumed to be located in the near field of a maximum earthquake event having a moment magnitude M_w of about 6-1/2. Five three-component sets of recorded acceleration time-histories from four recent earthquakes were selected. In addition, a three-component spectrum-compatible time-history derived using the 1971 Pacoima Dam record was also included. The smooth response spectra for the horizontal and vertical components of ground motion were constructed to be representative of median ground motions for an M_w 6-1/2 earthquake occurring at a distance of $R \approx 5$ km. The records considered are listed in Table 4-2 and the smooth response spectra are shown in Figure 4-8. The ground motions were scaled such that the sum of ordinates for the response spectra of each natural record would match the sum for the smooth response spectra in the period range of 0.1 to 0.4 sec. This period range was selected to contain the most significant modes of vibration for both example dams (i.e., all periods longer than 0.1 sec). The resulting scale factor for each record is listed in Table 4-2, and the response spectra for all records in the period range of 0.1 to 0.5 sec are compared in Figure 4-9. Time-histories of the larger horizontal component of the records are plotted in Figure 4-10. The figure clearly demonstrates the pulsive ("fling") type motions contained in the Pacoima Dam and Morgan Hill records.

Table 4-2
Near-Source Earthquake Records

Earthquake Record	Designated Name	Scale
Pacoima Dam, downstream record 1971 San Fernando earthquake, M_w 6.6, R = 2.8 km	Pacx	0.52
Spectrum-matched 1971 Pacoima Dam record	Pacb	1.00
Pacoima Dam, downstream record 1994 Northridge earthquake, M_w 6.7, R = 8 km	Pacn	1.13
Newhall, West Pico Canyon Boulevard 1994 Northridge earthquake, M_w 6.7, R = 7.1 km	U56	1.80
Coyote Lake Dam 1984 Morgan Hill earthquake, M_w 6.2, R = 0.1 km	Cld	0.64
Gilroy Array No. 1 1989 Loma Prieta earthquake, M_w 6.9, R = 11 km	Gly	0.81

(2) Description of arch dams. The geometry and finite element models of two arch dams, Dam-1 and Dam-2, analyzed for damage evaluation are given in Figure 4-11. The model of each dam includes three layers of solid elements through the dam thickness. The foundation models also use solid elements and are constructed on semicircles having a radius twice the dam height. The water level at Dam-1 is at 64 percent of the dam height and at Dam-2 is at the crest level. The dam-water interaction, therefore, is less significant for Dam-1 than it is for Dam-2. The lowest ten modes of Dam-1 have periods ranging from 0.23 to 0.09 sec and of Dam-2 from 0.34 to 0.10 sec.

(3) Earthquake response of Dam-1. This paragraph summarizes earthquake responses of Dam-1 to six sets of three-component earthquake ground motions discussed in (1) above. The computed natural periods for the 10 lowest modes of the dam are 0.233, 0.237, 0.161, 0.133, 0.128, 0.118, 0.110, 0.102, 0.096, and

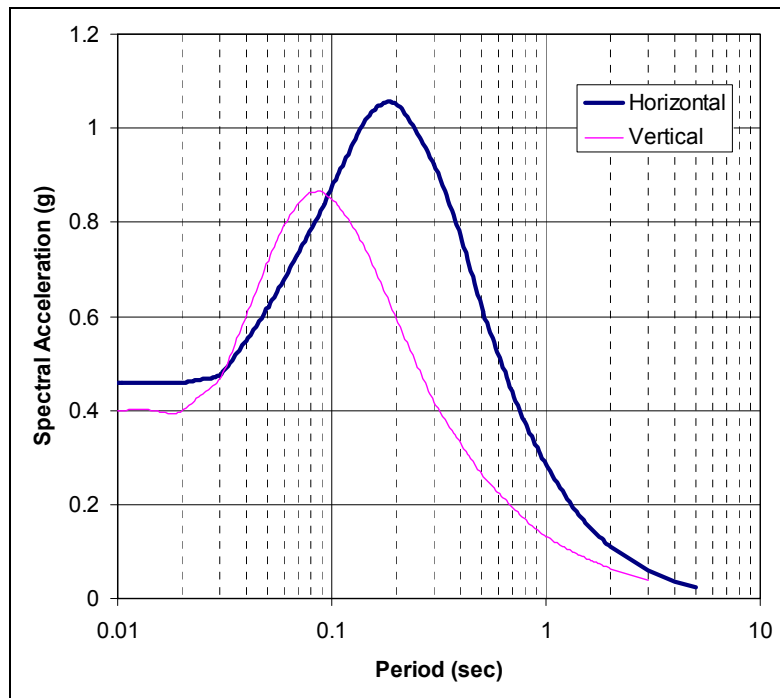


Figure 4-8. Horizontal and vertical smooth response spectra

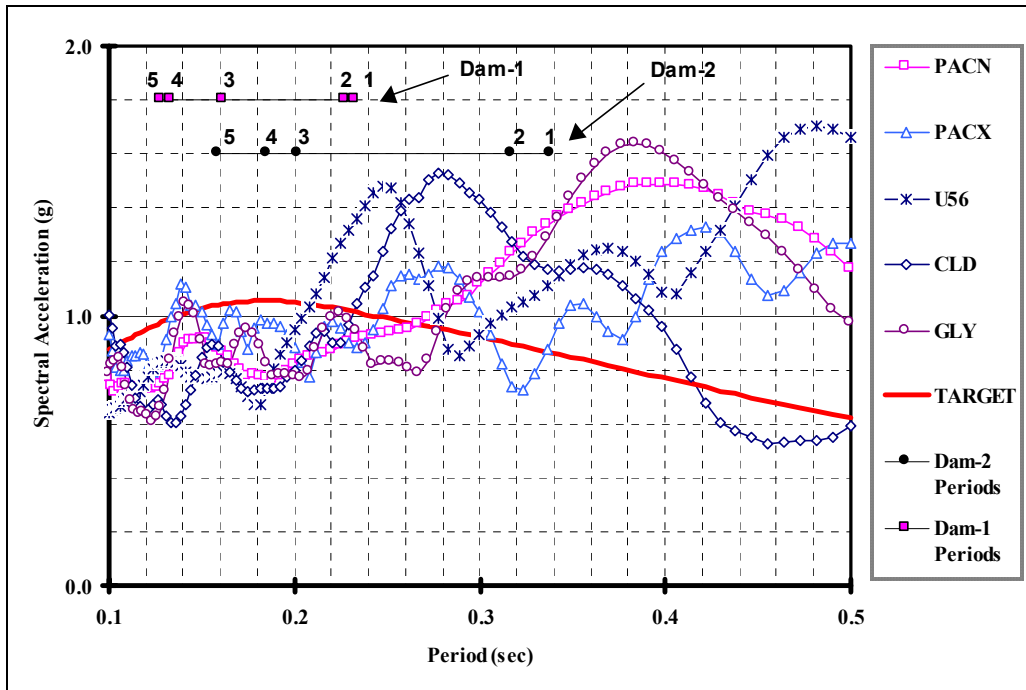


Figure 4-9. Response spectra of scaled records

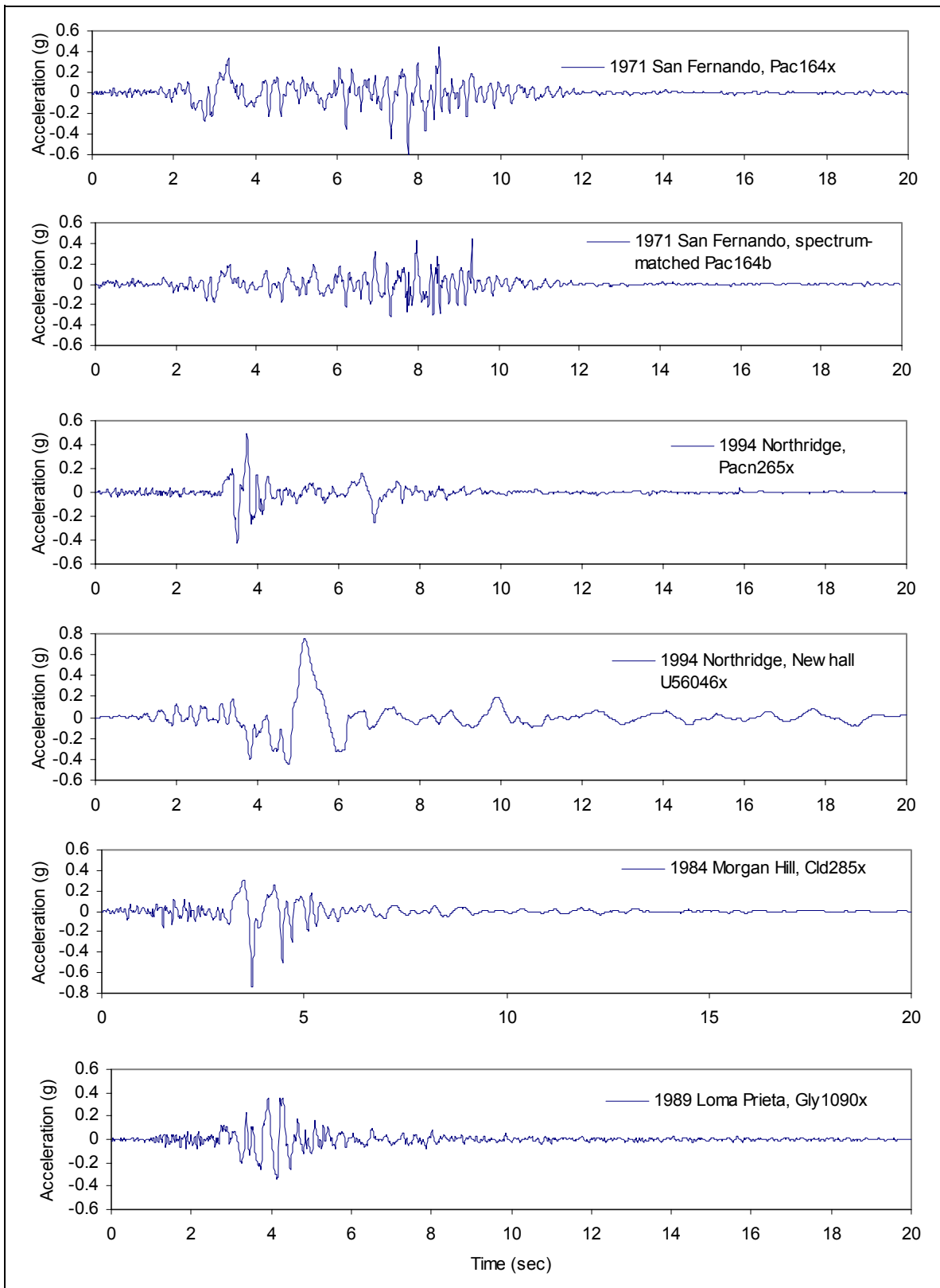


Figure 4-10. Scaled acceleration time-histories for near-source, $M_w \sim 6\text{-}1/2$ earthquake

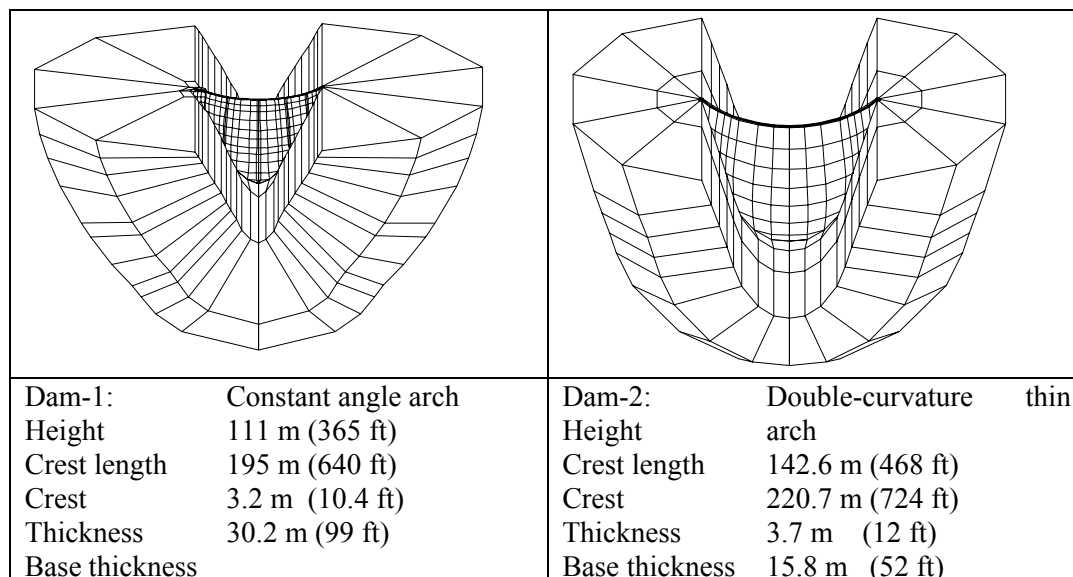


Figure 4-11. Finite element models and geometry data for example Dam-1 and Dam-2

0.088 sec, the first 5 of which are displayed in Figure 4-9 for comparison with response spectra of the earthquake input motions. Only spectral ordinates of U56 at the periods of Modes 1 and 2 exceed the values for the target and other spectra. The spectrum-compatible record (Pacb) induces the largest upstream-downstream displacements at the center and right 1/4 point of the crest. The 1994 Northridge Newhall record (U56) produces the largest vertical and cross-stream displacements at the right 1/4 point, center, and the left 1/4 point of the crest (Table 4-3). Time-histories of the midcrest displacements (Figure 4-12) for different records show significant differences, but the magnitude of peak displacements closely relates to the spectral ordinate values. None of the earthquake records produces both the arch and cantilever peak maximum stresses on both faces of the dam. Pacb produces the peak upstream arch and peak upstream cantilever stresses, Pacx induces the peak downstream arch stress, and U56 provides the peak downstream cantilever stress (Table 4-4). This is expected since several lower modes contribute to the dynamic stresses developed in the dam and the spectral ordinates of these modes are significantly different from one scaled record to another. The distributions of maximum stresses for all earthquake records are nearly the same and quite similar to that for Pacb shown in Figure 4-13. On the upstream face high tensile arch stresses occur in the upper central region of the dam, while on the downstream face they develop in the upper regions near 1/4-point locations. High tensile cantilever stresses occur in the upstream central region of the dam at about 1/4 of the dam height below the crest and on the downstream region toward the right abutment. The concurrent stress contours at the time of maximum arch stress (Figure 4-14) indicate that the simultaneous tensile arch stresses are essentially developed on the upstream central region and downstream 1/4-point locations of the dam. The corresponding concurrent cantilever stresses (right graphs in Figure 4-14) are mainly compressive on the upstream face with small tensile stresses on the upper part of the downstream face of the dam. The magnitude and concurrent stress distributions at the time of maximum arch stress suggest that joint opening, if any, would be minor, possibly involving the joints at the crown and 1/4-point locations. Time-histories of maximum stresses in Figures 4-15 and 4-16 show that time variation of stresses is quite different for each earthquake record and that the number of stress peaks beyond 500 psi is within 5 cycles for arch stresses and none for cantilever stresses. The cumulative duration of stress cycles beyond the tensile strength of the concrete discussed in *c* below generally meets the performance criteria for the linear elastic analysis.

Table 4-3
Dam-1 Maximum Displacements, inches

Ground Motion	Right ¼ Point			Center			Left ¼ Point		
	x	y	z	x	y	z	x	y	z
Pacx	0.58	1.15	0.17	0.33	1.80	0.20	0.57	1.20	0.19
Pacb	0.63	<u>1.52</u>	0.18	0.35	<u>2.05</u>	0.23	0.57	0.92	0.18
Pacn	0.46	<u>0.87</u>	0.10	0.28	<u>1.54</u>	0.13	0.53	1.10	0.12
U56	<u>0.66</u>	0.89	<u>0.27</u>	<u>0.46</u>	1.82	<u>0.35</u>	<u>0.80</u>	<u>1.28</u>	<u>0.23</u>
Cld	0.52	1.10	0.17	0.37	1.97	0.21	0.66	1.26	0.20
Gly	0.62	1.14	0.15	0.32	1.81	0.12	0.56	1.13	0.14

Note: Bold underlined values are the largest maximum displacements.

Table 4-4
Dam-1 Maximum Arch and Cantilever Stresses, psi

Earthquake Record	Arch		Cantilever	
	Upstream	Downstream	Upstream	Downstream
Pacx	698	<u>537</u>	406	238
Pacb	<u>784</u>	520	<u>440</u>	255
Pacn	558	392	222	134
U56	649	500	223	<u>274</u>
Cld	755	508	359	234
Gly	688	476	288	217

Note: Bold underlined values are the largest maximum stresses.

(4) Earthquake response of Dam-2. This paragraph describes earthquake responses of Dam-2 to six sets of three-component earthquake ground motions discussed in (1) above. The computed natural periods for the 10 lowest modes of the dam vary from 0.338 to 0.104 sec, the first 5 of which are displayed in Figure 4-9 for comparison with response spectra of the earthquake input motions. Compared to the target spectrum, all scaled records show higher spectral ordinates for Mode 1 and Mode 2 and lower for Modes 3 to 5, with the exception of Pacx whose spectral value for Mode-2 is lower. None of the earthquake records produces peak maximum values for all displacement components at all locations. The Gilroy record (Gly) induces the largest upstream-downstream displacement of 6.9 in. at the center of the crest, while other records produce peak vertical and cross-stream displacements, as highlighted in Table 4-5. Consistent with the input records, time-histories of the midcrest displacements vary significantly in terms of the wave forms (Figure 4-17). The magnitudes of peak radial displacements are about the same for all earthquake records, except for Gly, which is 60 to 70 percent higher due to the harmonic wave form of this record. None of the earthquake records produces both the arch and cantilever peak maximum stresses. While the Gilroy record produces the peak upstream and downstream arch stresses, the Northridge record (Pacn) produces the peak upstream and downstream cantilever stresses, as highlighted in Table 4-6. The distributions of maximum stresses are nearly the same for Pacx and Pacb but different for other records. This is expected since several lower modes contribute to the dynamic stresses developed in the dam and the spectral ordinates of these modes are significantly different from one scaled record to another. The maximum stress contours for Gly producing the largest arch stresses are shown in Figure 4-18. On the upstream face high-tensile arch stresses develop in the upper half of the central region of the dam, while on the downstream face they develop mostly in the 1/4-point locations but also in the upper central region. High-tensile cantilever stresses occur in the upstream middle region of the dam and in the upper abutment regions. The concurrent stress contours at the time of maximum arch stress (Figure 4-19) indicate that the simultaneous tensile arch stresses are developed on the upstream central region and downstream 1/4-point locations of the dam. The corresponding concurrent cantilever stresses (right graphs in Figure 4-19) are mostly compressive on both the upstream and downstream faces of the dam. The magnitude and concurrent stress distributions at the time of maximum arch stress suggest that joint opening would be significant. Figure 4-20 shows that the maximum arch stresses for all records are greater than 13.8 MPa (2,000 psi), indicating significant contraction joint opening. Time-histories of maximum cantilever stresses in Figure 4-21

Dam-1

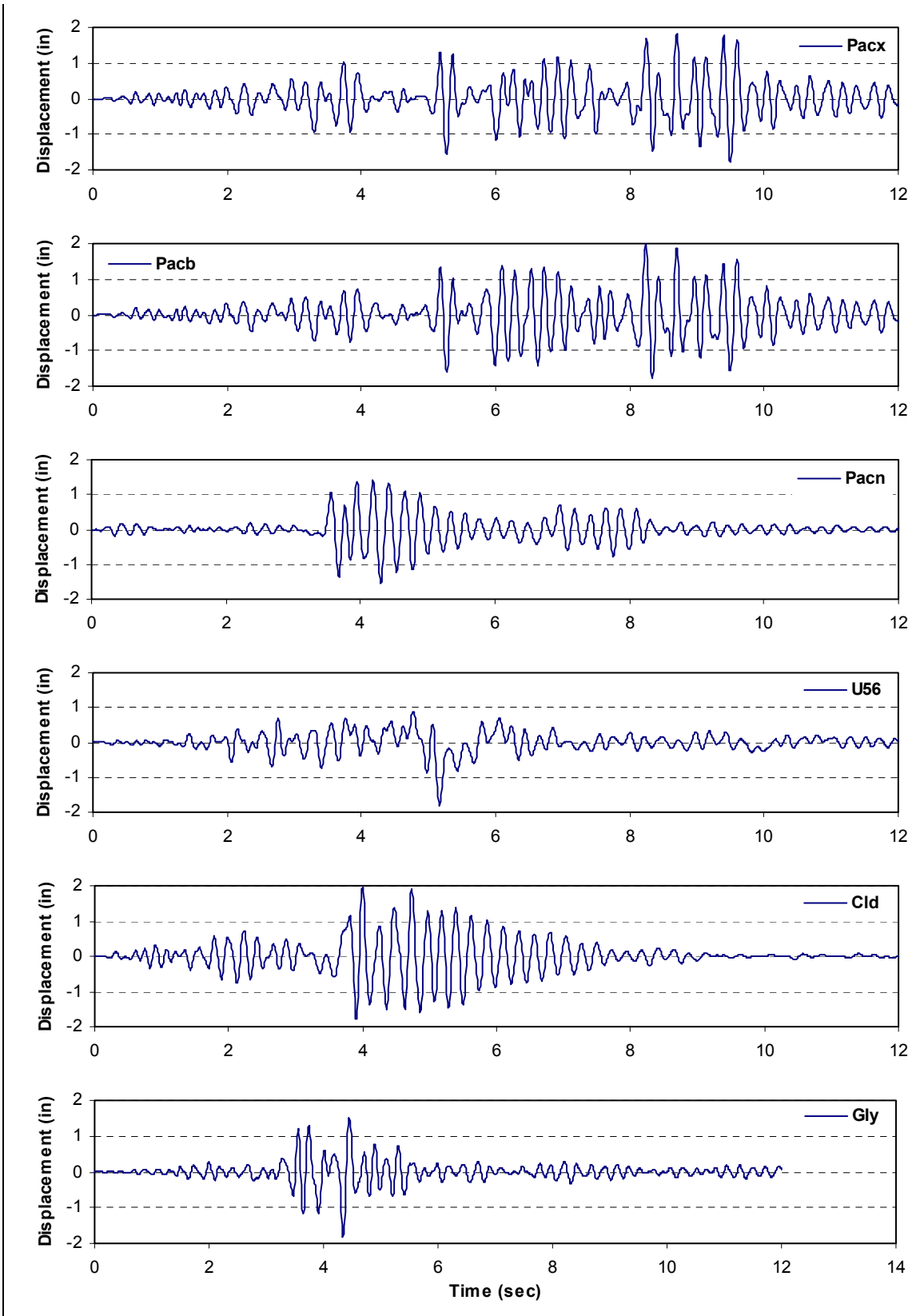


Figure 4-12. Time-histories of midcrest radial displacements for Dam-1

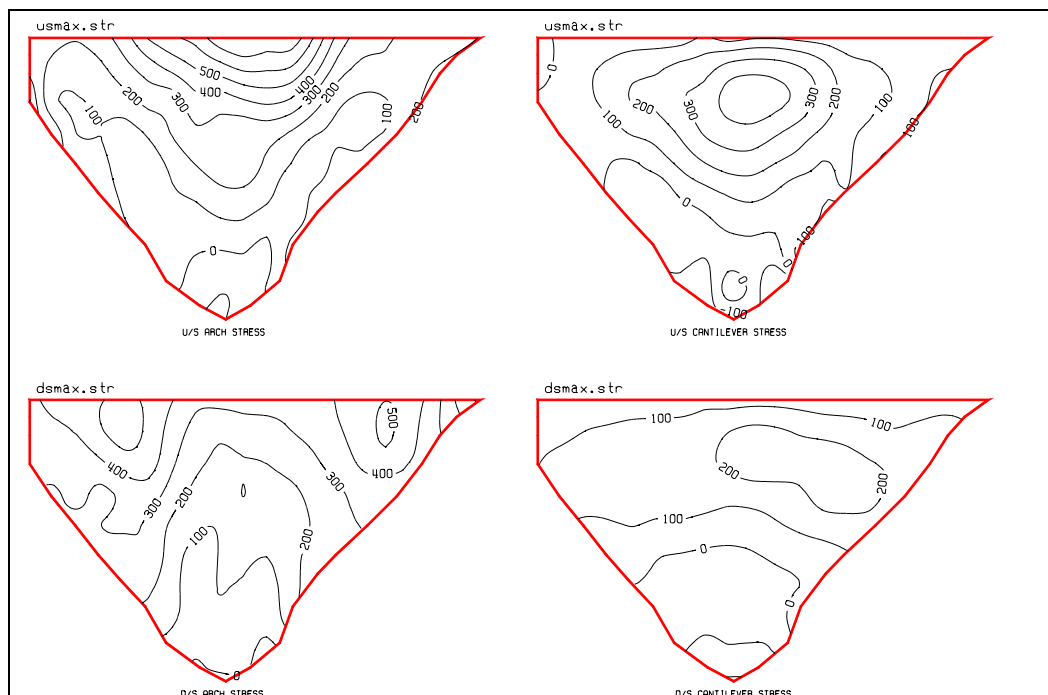


Figure 4-13. Envelope of maximum stresses due to spectrum-matched Pacb record (Dam-1)

Table 4-5
Dam-2 Maximum Displacements, inches

Ground Motion	Right ¼ Point			Center			Left ¼ Point		
	x	y	z	x	y	z	x	y	z
Pacx	1.19	1.25	0.25	0.56	4.03	0.31	1.08	2.16	0.25
Pacb	0.89	1.03	0.18	0.39	4.04	0.28	0.96	1.70	0.20
Pacn	1.51	1.49	0.11	0.61	4.38	0.17	0.78	1.96	0.21
U56	1.17	1.13	0.20	0.54	4.21	0.33	0.83	1.28	0.21
ClD	1.26	1.37	0.22	0.46	4.08	0.31	0.76	1.43	0.23
Gly	1.12	1.05	0.25	0.40	6.94	0.23	1.07	1.57	0.27

Table 4-6
Dam-2 Maximum Tensile Stresses, psi

Earthquake Record	Arch		Cantilever	
	Upstream	Downstream	Upstream	Downstream
Pacx	2,088	1,697	895	576
Pacb	2,099	1,415	650	461
Pacn	2,360	2,117	1,028	639
U56	2,019	1,891	741	424
CLD	2,315	1,890	975	504
GLY	2,917	2,508	748	636

are quite different for each earthquake record. The maximum cantilever stresses, even without further increase due to contraction joint opening, are about 6.9 MPa (1,000 psi). At such high stress levels it is expected that the cracking of the lift lines would also be significant. The cumulative duration of stress cycles beyond the tensile strength of the concrete discussed in *c* below markedly exceeds the performance criteria for the linear elastic analysis.

c. Performance criteria for linear analysis. The earthquake performance of arch dams is evaluated on the basis of combined static and seismic stresses in accordance with the load combination cases in *d* below,

demand-capacity ratios and the cumulative inelastic duration in *e* below, and presentation and interpretation of

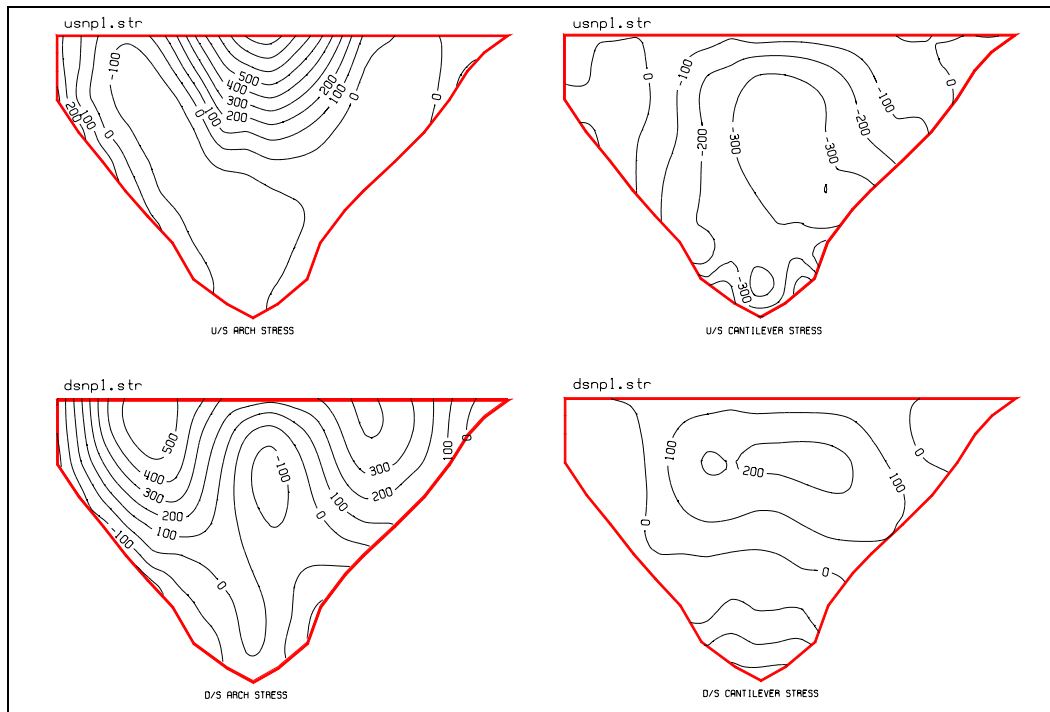


Figure 4-14. Concurrent stresses at the time of maximum arch stress due to spectrum-matched Pacb record (Dam-1)

results described in *f* below. The dam response to the MDE is considered to be within the linear elastic range of behavior with little or no possibility of damage if computed demand-capacity ratios are less than or equal to 1.0. Considering that the ability of contraction joints to resist tension is limited, the joints may still open even if demand-capacity ratios are less than or equal to 1.0. The amount of contraction joint opening at a demand capacity ratio ≤ 1 , however, is expected to be small with negligible or no effects on the overall stiffness of the dam. The dam is considered to exhibit nonlinear response in the form of opening and closing of contraction joints and cracking of the horizontal joints (lift lines) if the estimated demand-capacity ratios exceed 1.0. The level of nonlinear response or opening and cracking of joints is considered acceptable if the demand capacity ratio < 2 , overstressed region is limited to 20 percent of the dam surface area, and the cumulative inelastic duration falls below the performance curve given in Figure 4-22. The relation between the fundamental period of the dam and peak of the response spectra should also be considered to determine whether the nonlinear response behavior would increase or decrease the seismic demand. If these performance criteria are not met, or met marginally with increasing demand due to nonlinear behavior, then a nonlinear analysis would be required for more accurate estimate of the damage.

d. Load combination cases. Three-dimensional analysis of arch dams should be evaluated for three or more sets of three-component earthquake ground motions. For each set of three-component earthquake ground motions the static loads and earthquake ground motion components should be combined in accordance with Table 4-7.

e. Demand-capacity ratios. The demand-capacity ratio for arch dams is defined as the ratio of the calculated arch or cantilever stress to tensile strength of the concrete. The tensile strength of the concrete is measured by the uniaxial splitting in accordance with American Society for Testing and Materials (ASTM) C496. Although tensile strength of concrete is affected by the rate of seismic loading, the acceptance criteria in *c*

above employ the static tensile strength in computation of the demand-capacity ratios. The reason for this is to account for the lower strength of the lift lines and provide some level of conservatism in estimation of damage

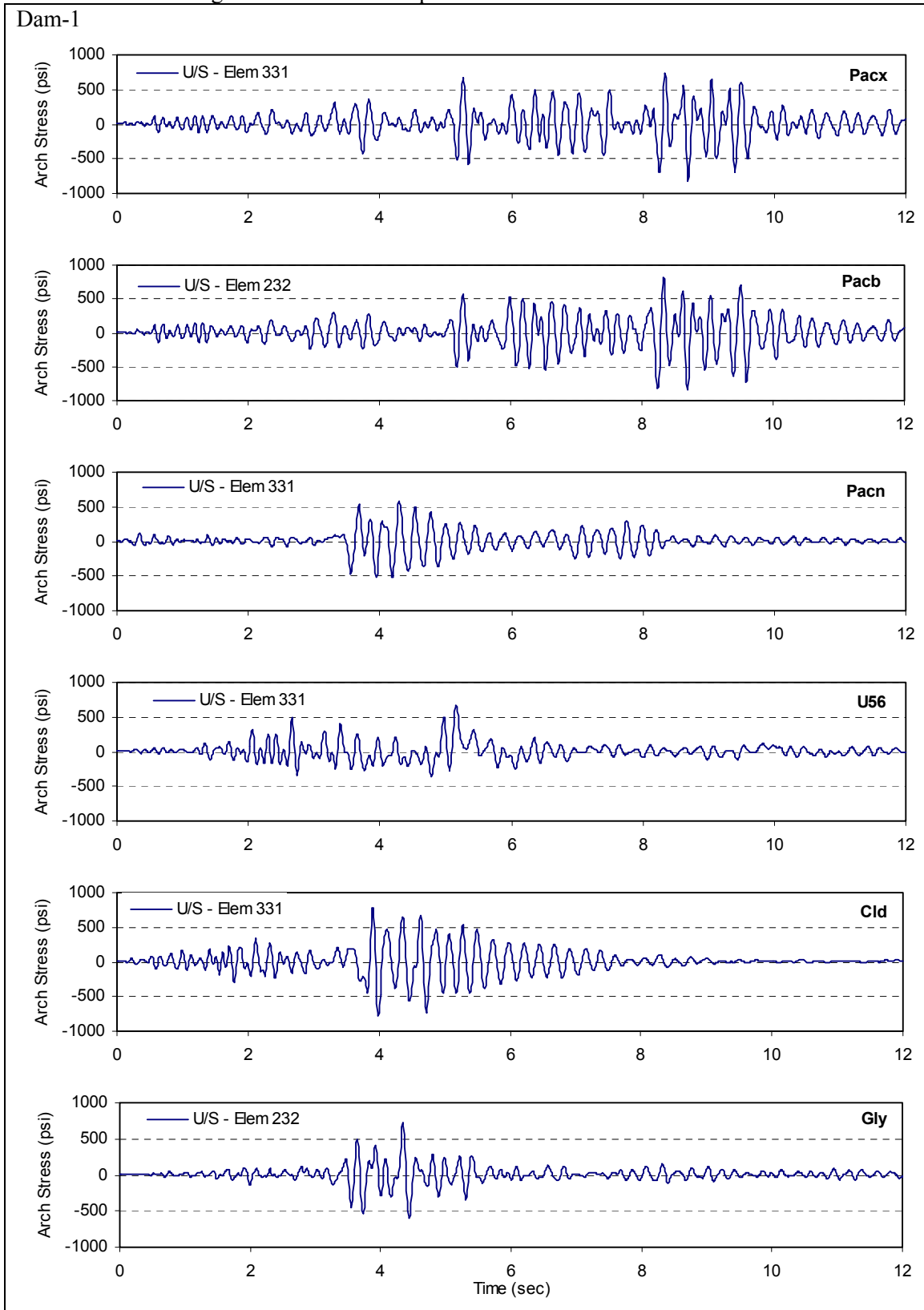


Figure 4-15. Time-history of maximum arch stresses for Dam-1

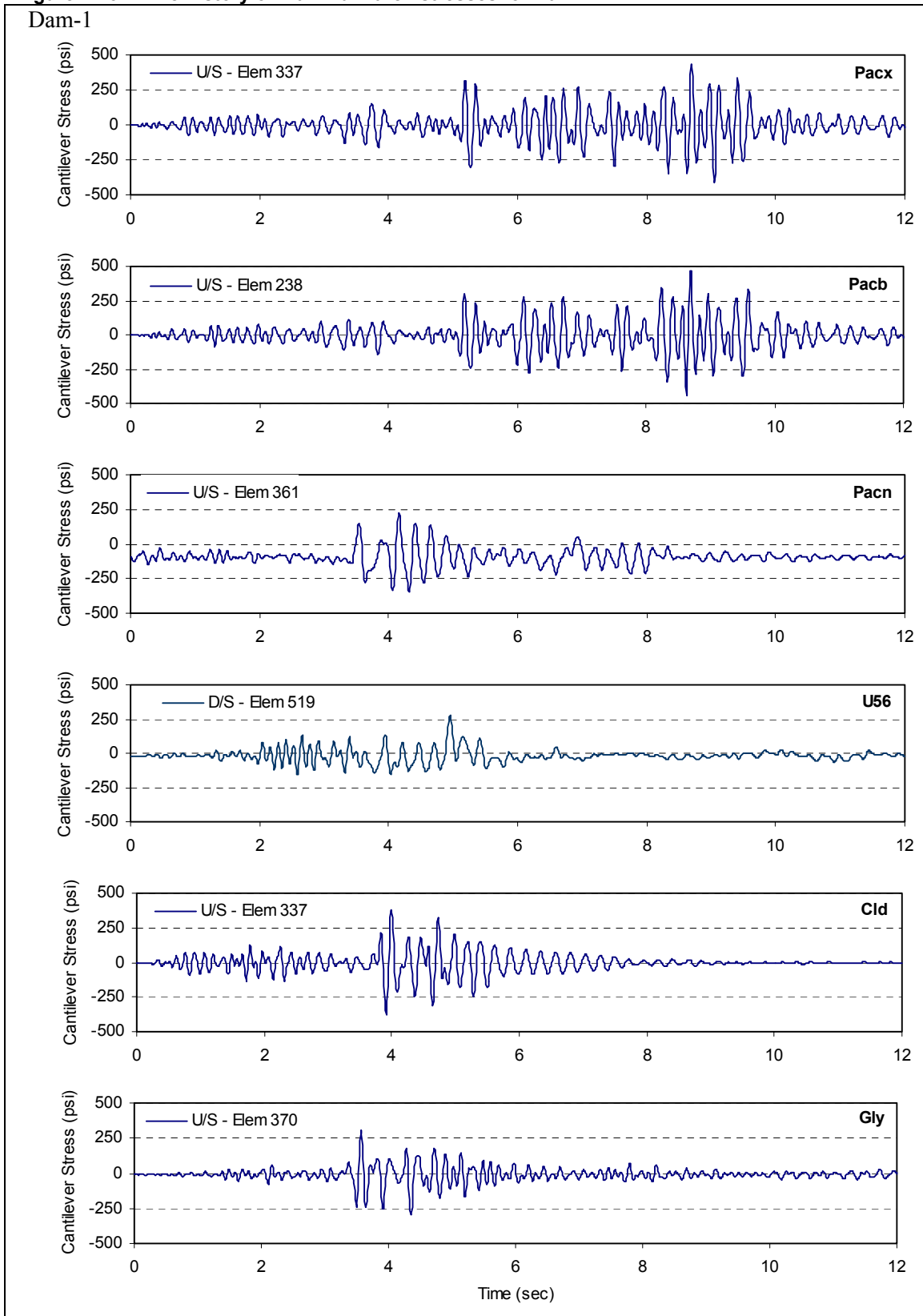


Figure 4-16. Time-histories of maximum cantilever stresses for Dam-1

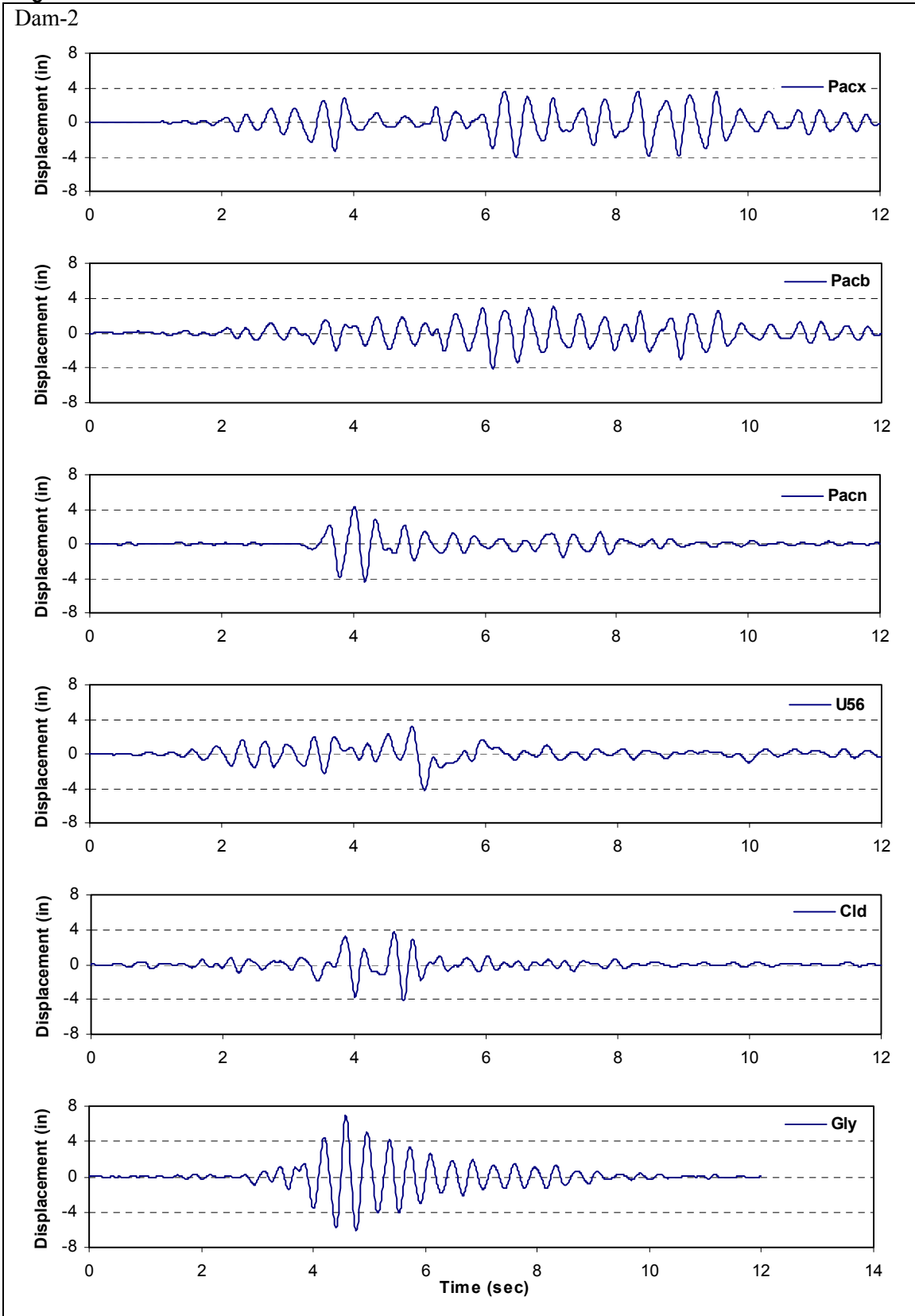


Figure 4-17. Time-histories of midcrest radial displacements for Dam-2

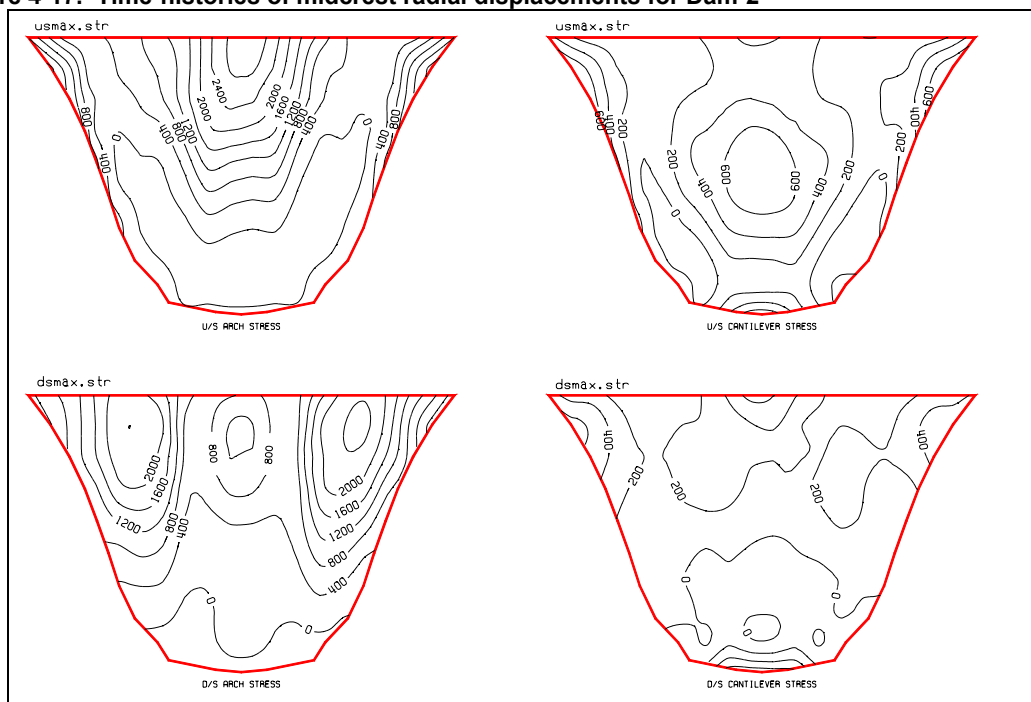


Figure 4-18. Envelope of maximum stresses due to Gilroy record (Dam-2)

using the results of linear elastic analysis. A demand-capacity ratio of 2 allows stresses up to twice the static tensile strength of the concrete or to the level of dynamic apparent tensile strength, as long as the overstressed region is less than 20 percent of the dam surface area. The cumulative duration beyond a certain level of demand-capacity ratio is obtained by multiplying number of stress values exceeding that level by the time-step of the time history analysis. The cumulative inelastic duration in Figure 4-22 refers to the total duration of all stress excursions beyond a certain level of demand-capacity ratio. The cumulative inelastic duration for the example Dam-1 and Dam-2 is presented in Figures 4-23 and 4-24, respectively. The results for Dam-1 show that demand-capacity ratios for all earthquake input records are less than 2 and that the cumulative inelastic duration at all demand-capacity ratios falls below the acceptance curve. On these bases and as discussed in *b(3)* above, Dam-1 responses to the selected earthquake ground motions exhibit negligible nonlinear response in the form of contraction joint opening and closing. The linear time-history method of analysis is therefore acceptable for Dam-1. The results for Dam-2 show that demand-capacity ratios for all earthquake input exceed 2 and that the cumulative inelastic duration, especially for Pacx, Pacb, and Gly, is substantially greater than the acceptance level. This suggests that the selected records cause significant and repeated opening and closing of the contraction joints and that Dam-2 should be analyzed using the nonlinear time-history analysis.

f. Presentation and evaluation. For performance evaluation of arch dams the following results from the linear time-history analysis are required.

(1) Natural frequencies and mode shapes. Natural frequencies and mode shapes of the arch dam-water-foundation system are examined to gain insight into the dynamic characteristics of the dam, its dynamic coupling with the impounded water, and its level of response to earthquake loading. Proximity of the fundamental resonant frequency of the impounded water to fundamental frequency of the dam indicates a strong coupling between the dam and water, thus requiring a more refined dam-water interaction analysis

described in Chapter 2. The frequency range of significant lower modes of vibration should be determined and used in spectrum scaling of the natural earthquake records for dynamic analysis as described in *b(1)* above. The presence of lower modes in the ascending slope of the earthquake response spectra shows an increase in the

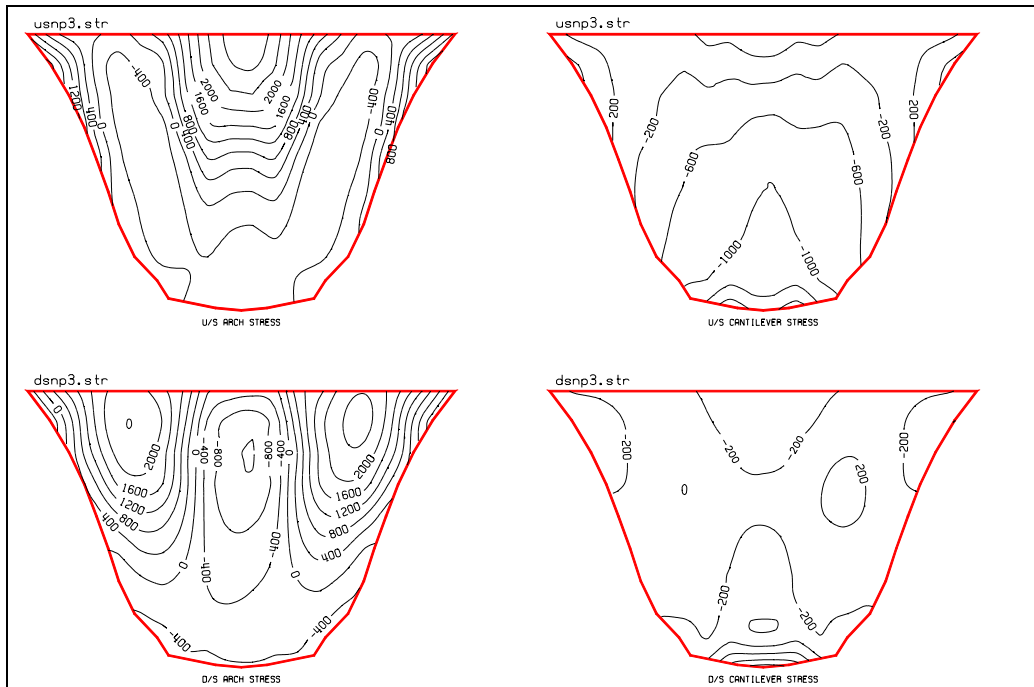


Figure 4-19. Concurrent stresses at the time of maximum arch stress due to Gilroy record (Dam-2)

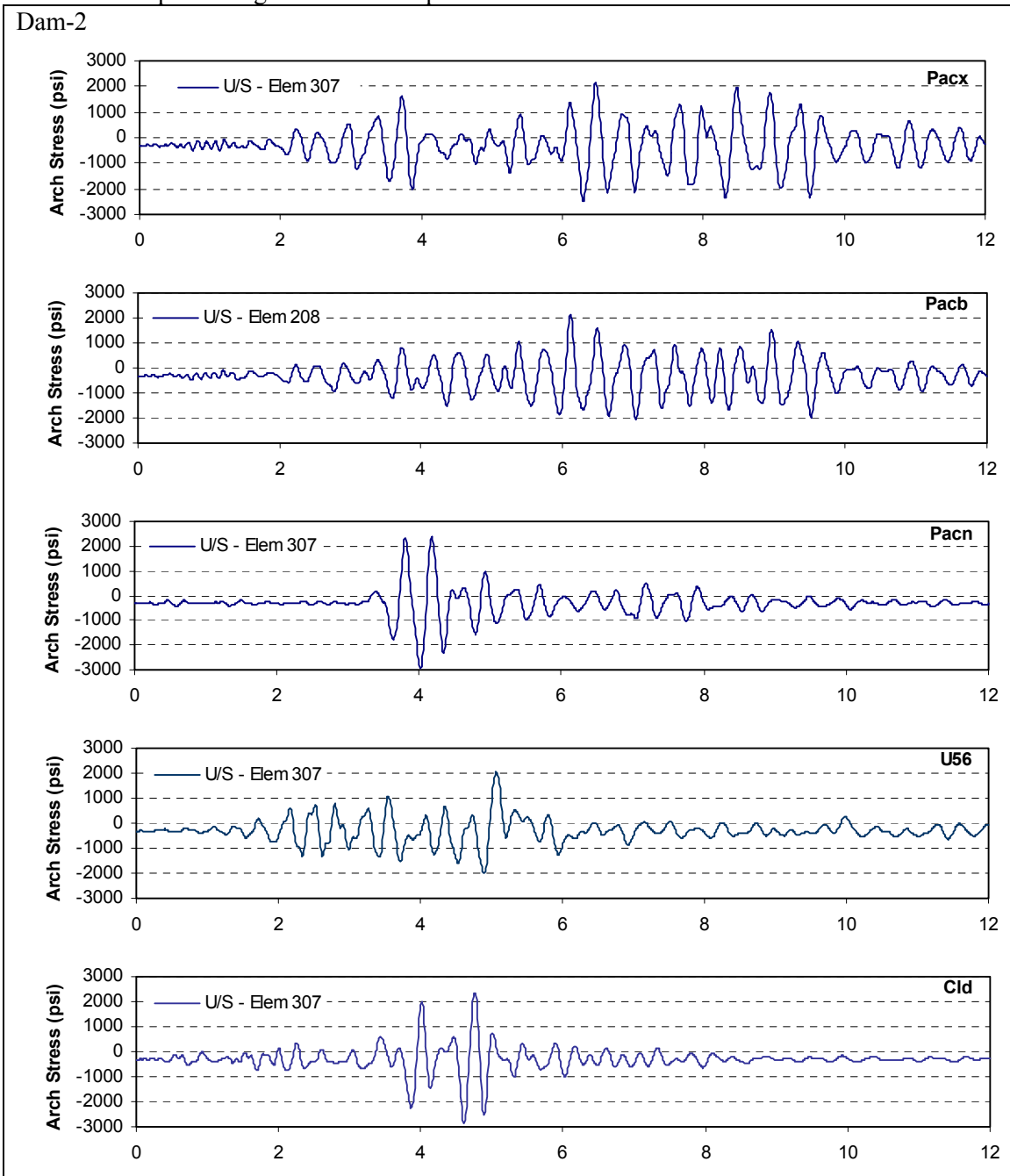
seismic demand if the dam experiences nonlinear response, while the presence of the same in the descending slope indicates reduction of seismic forces.

(2) Displacement histories. The magnitudes and time-histories of nodal displacements at the crest and lower elevations should be presented and examined. Even though displacement magnitudes are not directly used in the performance criteria, their patterns provide a visual means of validating the results and their magnitudes can be employed to assess the overall stability of the dam.

(3) Maximum and minimum stress contours. The maximum and minimum arch and cantilever stresses on the upstream and downstream faces of the dam should be displayed as contour plots and evaluated. The maximum arch and cantilever stress contours show the largest static plus dynamic tensile (positive) stresses that may occur at any location in the dam during the earthquake ground shaking (Figures 4-13 and 4-18). These contours are used to identify critical regions where tensile stresses exceed the tensile or cracking strength of the concrete. Only these regions need to be examined for possible damage. Similarly, contours of the minimum stresses indicate the largest compressive (negative) arch and cantilever stresses that may develop in the dam. The magnitudes of extreme compressive stresses should be compared with the allowable compressive stress to ensure that they meet the required factors of safety. It should be obvious that the maximum and minimum stresses at different locations generally occur at different instants of time and thus are not concurrent.

(4) Time-histories of critical arch and cantilever stresses. Time-histories of the most critical arch and cantilever stresses identified in (3) above should be displayed and evaluated. For each critical arch or cantilever stress point, a pair of stress time-histories, one for the critical point and another for a similar point

on the opposite face of the dam, should be provided. An examination of an arch or cantilever stress pair shows whether the dam undergoes the flexural bending, extension, or a combination of the bending and extension. A pure bending exposes only one-half of the dam cross section to tension, while a pure extension shows the whole section is experiencing tension or compression.



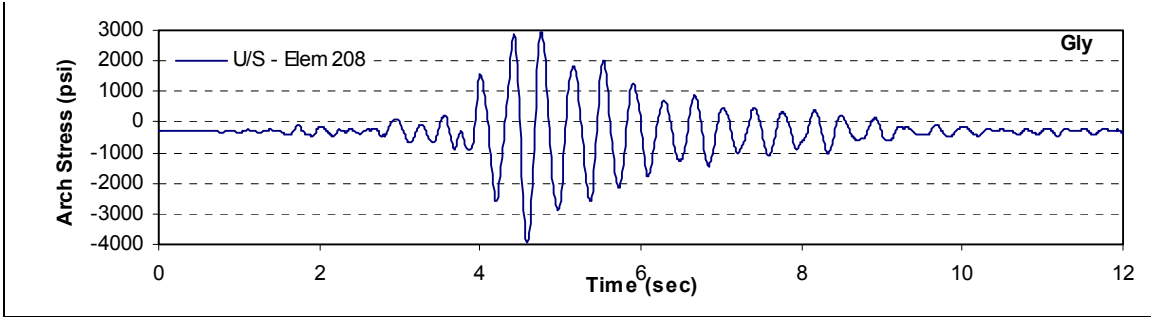
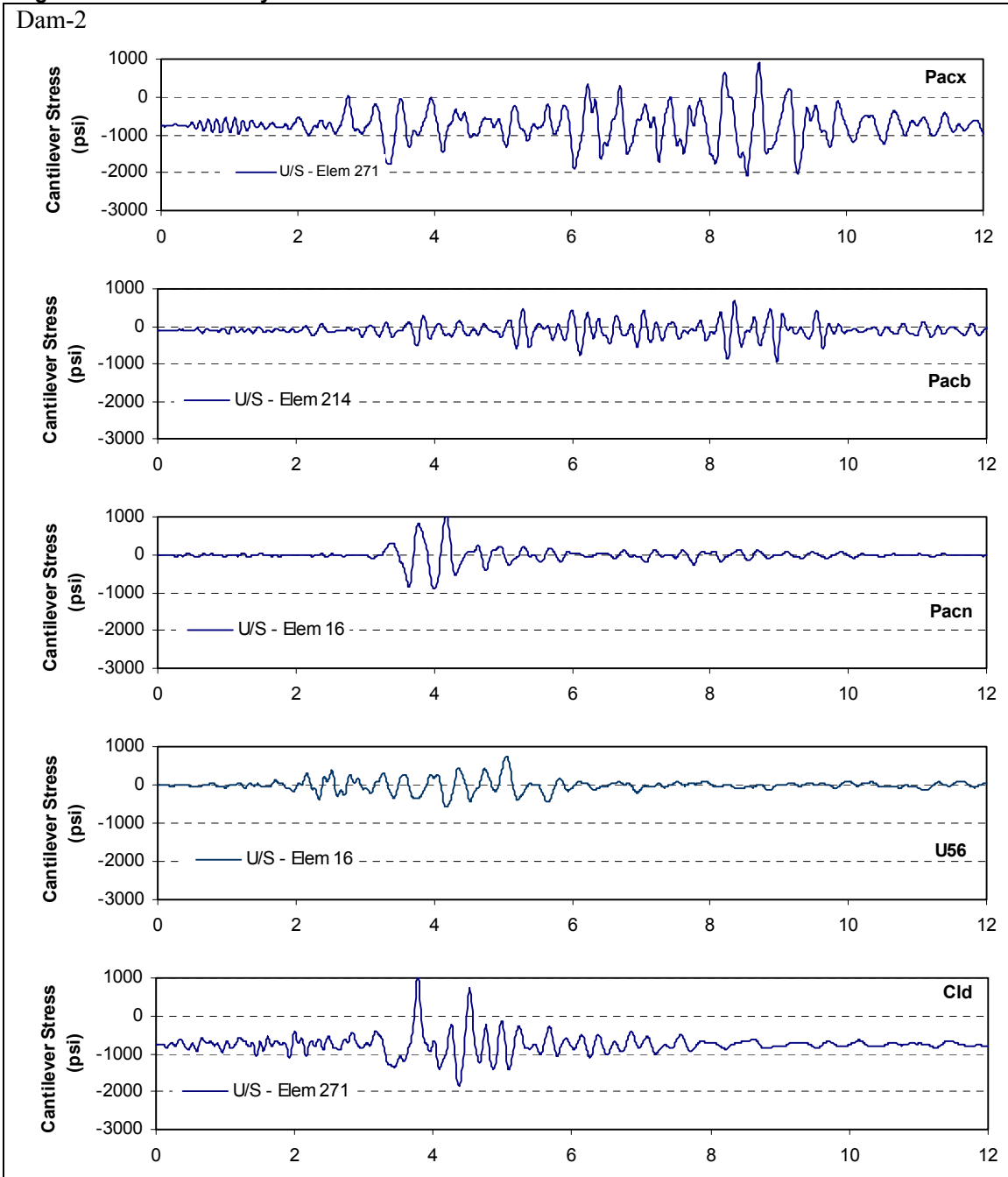


Figure 4-20. Time-history of maximum arch stresses for Dam-2



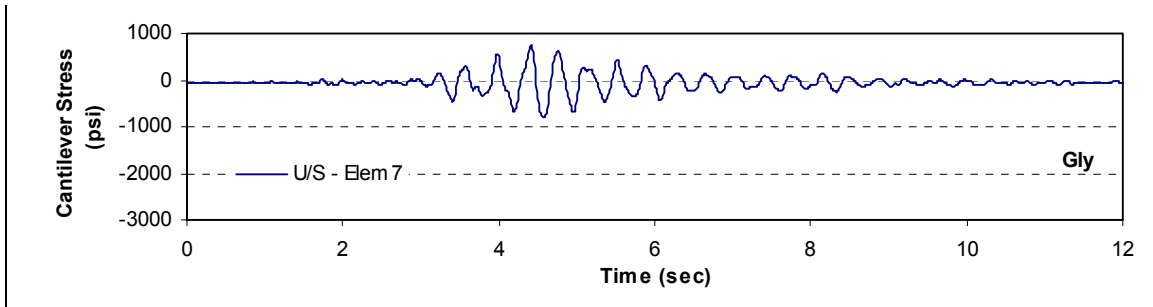


Figure 4-21. Time-history of maximum cantilever stresses for Dam-2

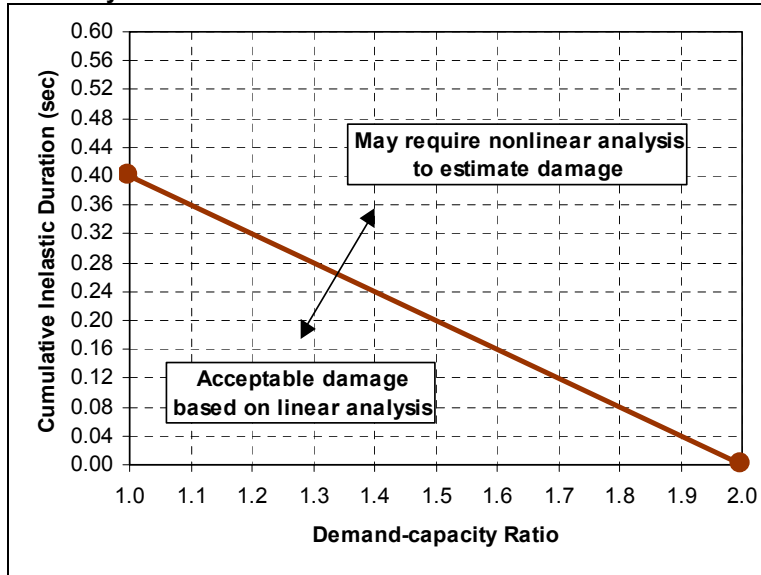


Figure 4-22. Performance curve for linear elastic analysis of arch dams

Table 4-7
Load Combination Cases for Combining Static and Dynamic Stresses for Multicomponent Excitation

Case	Seismic Loads			Static Loads
	Cross-stream Horizontal (H1)	Vertical (V)	Stream Horizontal (H2)	
1 ¹	+	+	+	+
2	+	+	-	+
3	+	-	+	+
4	+	-	-	+
5	-	+	+	+
6	-	+	-	+
7	-	-	+	+
8	-	-	-	+

Note: The (+) and (-) signs indicate the loads are multiplied by +1 or -1 to account for the most unfavorable earthquake direction.
¹ Case-1: Static + H1 + V + H2

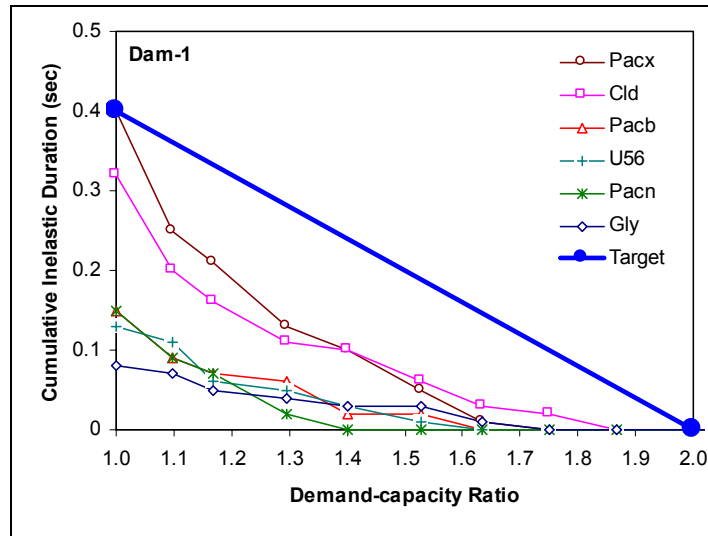


Figure 4-23. Performance assessment of example Dam-1

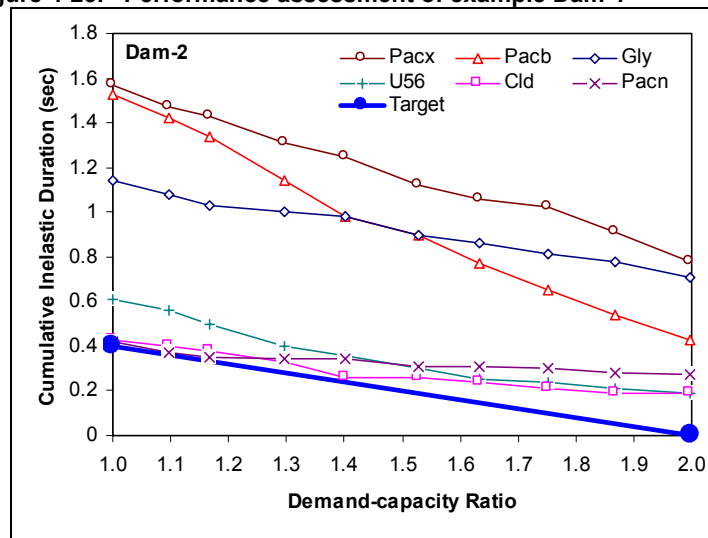


Figure 4-24. Performance assessment of example Dam-2

(5) Concurrent stresses at the time of maximum stresses. The envelopes of maximum stresses in (3) above serve to identify the overstressed regions, critical stress points, and the associated time-histories. From the time-histories of the critical arch and cantilever stresses, the times at which the critical stresses reach their peak values can be determined. The times of maximum arch and maximum cantilever stresses are then used to retrieve simultaneous stress values and prepare concurrent or snapshot stress contours (Figures 4-14, 4-19). The concurrent stresses are evaluated similar to the envelope maximum stresses, except that they represent stress values and are not necessarily all tension.

(6) Demand-capacity ratios. The maximum arch and cantilever stresses in (3) above could also be displayed as plots of the demand-capacity ratios by dividing the computed stresses by the tensile strength of the concrete.

4-5. Navigation Locks

A typical chamber monolith may be analyzed adequately using a 2-D model of the monolith in the cross-stream direction. Dynamic analyses of a miter gate monolith, however, usually require 3-D models or the use of two separate 2-D models in the cross-stream and the upstream-downstream directions. This paragraph discusses presentation and performance evaluation methodology for a miter gate monolith analyzed using 2-D SSI models (Geomatrix 1999). The 2-D cross-stream model of the monolith is approximated by a smeared model, in which the effects of culverts and corrugated pipes are taken into account using appropriate adjustments of the mass and elastic modulus of the concrete. The 2-D model of the monolith in the upstream-downstream direction is also developed the same way by appropriate smearing of the mass and elastic modulus of the concrete and collapsing of the entire monolith into a unit-thick slice. The cross-stream model is analyzed for the vertical and cross-stream components and the upstream-downstream model for the vertical and upstream-downstream components of the MDE ground motion. The results of such analyses include peak values and time-histories of pile forces and moments, lock stresses, and lock section forces and moments at selected critical sections, as well as pile and lock deflections. The pile forces and moments and concrete section forces from each model are then combined to obtain the resulting demands for the design and/or evaluation of the structure, as discussed in the following subparagraphs.

a. Performance criteria. The earthquake performance of reinforced concrete navigation locks is evaluated on the basis of demand-capacity ratios computed for the foundation piles and the concrete sections. The basic approach is to perform linear time-history analysis (with equivalent linear soil modulus) using the load combination cases defined in paragraph 4-5*b* and then compute demand-capacity ratios following procedures described in paragraphs 4-5*c* and 4-5*d* to identify the magnitude and distribution of nonlinear response in various components of the structure. If all computed demand-capacity ratios are less than or equal to 1.0, then the lock structure and piles are expected to respond elastically with no damage. Otherwise demand-capacity ratios of greater than 1.0 show the structure will experience nonlinear behavior in the form of yielding of steel members and cracking or crushing of the concrete. In linear time-history analysis the level of damage or nonlinear behavior will be acceptable if the yielding and associated cumulative yield duration fall below the performance curves provided in Figures 4-25 and 4-26. Regions above the performance curves indicate that the linear time-history analysis is no longer valid and that nonlinear analysis should be employed to assess the damage. The performance curves are given for “Extreme Allowable,” “Minimum Yield,” and “Expected Yield” cases described in paragraph 4-5*c*. In the case of “Minimum Yield,” the performance criteria indicate that yielding should be limited to less than 56 percent of piles and that the peak demand-capacity ratio should not exceed 1.45. The corresponding cumulative yield duration for demand-capacity ratios greater than 1 and 1.45 should be less than 1.52 and 0.02 sec, respectively (Tables 4-8 and 4-9).

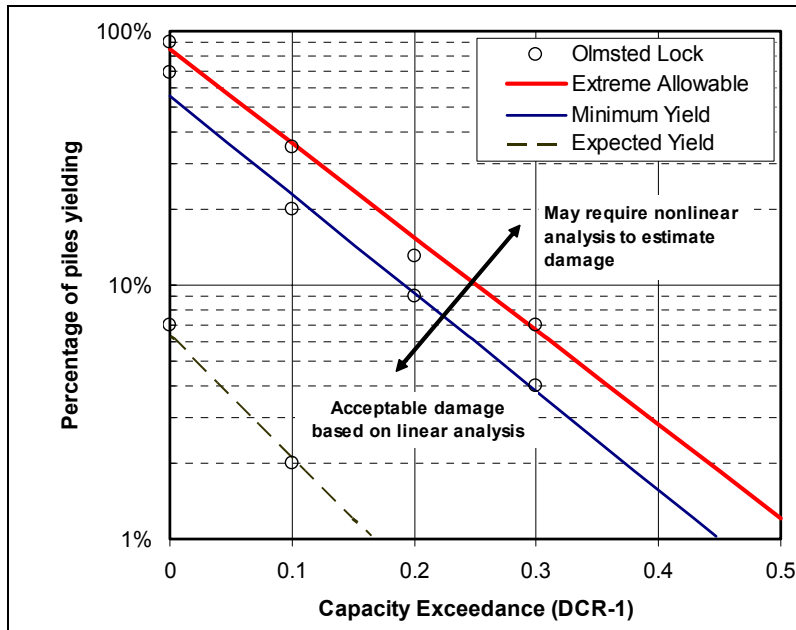


Figure 4-25. Acceptable percentage of pile yielding as a function of demand-capacity ratio levels in linear time-history analysis

b. Load combination cases. Two-dimensional cross-stream and upstream-downstream models of the miter gate monolith are designed or evaluated for two horizontal and vertical excitations plus the effects of usual static loads as described in paragraph 1-6d. Each component of the earthquake input is assumed to have a phasing equal to zero or 180 deg in order to identify the most critical earthquake direction that would give the largest structural response. According to this simple procedure, a total of eight combination cases would be required when all three components of the earthquake input are considered, as listed in Table 4-10.

c. Pile interaction factors (demand-capacity ratios). Performance of the pile-foundation under the MDE loading combination is evaluated using interaction factors or demand-capacity ratios computed in accordance with Equation 4-1.

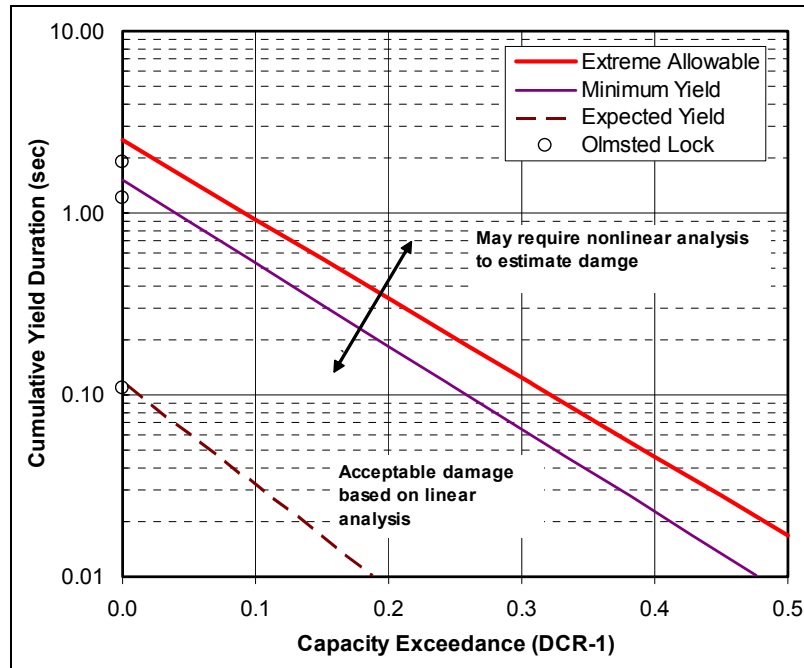


Figure 4-26. Acceptable cumulative yield duration as a function of demand-capacity ratio levels in linear time-history analysis

Table 4-8
Peak Allowable Percentages of Piles Exceeding Various Level of Interaction Factors

Level of Interaction Factor	Extreme Allowable		Minimum Yield 248 MPa (36 ksi)		Expected Yield 303 MPa (44 ksi)	
	Load Combination Case	Percent	Load Combination Case	Percent	Load Combination Case	Percent
1.0	Most Critical	85	Most Critical	56	Most Critical	6
1.1	Most Critical	36	Most Critical	24	Most Critical	2
1.2	Most Critical	16	Most Critical	9		
1.3	Most Critical	7	Most Critical	4		
1.4	Most Critical	3	Most Critical	<2		
1.5	Most Critical	1				

Table 4-9
Peak Allowable Cumulative Yield Duration at Which Pile Interaction Factors Exceed Unity

Level of Interaction Factor	Extreme Allowable		Minimum Yield 248 MPa (36 ksi)		Expected Yield 303 MPa (44 ksi)	
	Load Combination Case	Duration sec	Load Combination Case	Duration Sec	Load Combination Case	Duration sec
1.0	Most Critical	2.5	Most Critical	1.52	Most Critical	0.11
1.1	Most Critical	0.92	Most Critical	0.56	Most Critical	0.03
1.2	Most Critical	0.34	Most Critical	0.18	Most Critical	< 0.01
1.3	Most Critical	0.12	Most Critical	0.07		-
1.4	Most Critical	0.04	Most Critical	0.02		-
1.5	Most Critical	0.02		-		-

Table 4-10
Load Combination Cases for Combining Static and Dynamic Interaction Factors for Multicomponent Excitation

Case	Seismic Loads			Static Loads (Moment / Axial Load)
	Cross-stream Horizontal (H1)	Vertical (V)	Stream Horizontal (H2)	
1 ¹	+	+	+	+
2	+	+	-	+
3	+	-	+	+
4	+	-	-	+
5	-	+	+	+
6	-	+	-	+
7	-	-	+	+
8	-	-	-	+

Note: + = seismic input is multiplied by +1 (zero phase)
 - = seismic input is multiplied by -1 (180-deg phase)
¹ Case-1: Static + H1 + V + H2

$$I_p = \left(\frac{f_a}{F_a} + \frac{m_x}{M_x} + \frac{m_y}{M_y} \right)_{static} + \left(\frac{f_a}{F_a} + \frac{m_x}{M_x} + \frac{m_y}{M_y} \right)_{dynamic} \quad (4-1)$$

where

I_p = pile interaction factor

f_a, m_x, m_y = the axial force and bending moments (force and moment demands) computed either from the static or dynamic analysis

F_a = allowable axial force (force capacity) for combining with allowable moment (moment capacity)

M_x, M_y = allowable moments (moment capacities), respectively, about the strong and weak axes of the pile

For a complete performance evaluation of the piles the three performance cases in Table 4-11 may be considered. The “Extreme Allowable” case is based on EM 1110-2-2906, which requires a factor of safety (FS) of 1.15 for the extreme loading combination and an ASTM A36 for the yield strength. The “Extreme Allowable” case with an FS of 1.15 is considered appropriate when the SPSI effects are modeled approximately and the earthquake input is developed using standard or empirical relationships. However, the use of yield strength (i.e., FS = 1) in computing pile capacities can be justified if dynamic SPSI analyses are employed and extensive geotechnical and site-specific seismic hazard studies are performed. In the absence of measured data a minimum yield strength of 248 MPa (36 ksi) and an FS of 1.0 should be used. This performance case is called “Minimum Yield” case. In situations where testing of steel piles consistently indicates yield strengths of greater than 248 MPa (36 ksi), the average measured yield strength may be employed in the final evaluation. The performance condition based on the expected yield strength is called “Expected Yield” case.

Case	Condition	Yield Strength	Factor of Safety (FS)
I	Extreme Allowable	Nominal: 248 MPa (36 ksi)	1.15
II	Minimum Yield	Nominal: 248 MPa (36 ksi)	1.0
III	Expected Yield	Measured: 303 MPa (44 ksi)	1.0

d. *Allowable pile deflection.* The allowable pile lateral deflection is determined by a separate analysis of the pile-soil system incorporating measured data from the pile load tests (U.S. Army Engineer District, Louis-

ville, 1994b). The allowable deflection or “deflection capacity” is usually selected as a fraction of the pile head deflection that initiates first yielding of the pile. In determining the allowable deflection value, consideration should be given to rebounding of the pile. The study by U.S. Army Engineer District, Louisville (1994b) indicates that as long as the piles do not reach yield condition, a 50 percent rebound of the pile can be expected.

e. Interaction diagrams (demand-capacity ratios) for concrete sections. The axial force-bending moment interaction diagram, plotted in terms of ultimate axial loads as ordinates and ultimate moments as abscissas, characterizes the strength of a reinforced concrete section. Interaction diagrams therefore provide a means for comparing the required strengths (force demands) due to the loading combination cases defined in paragraph 4-5*b* with the design strengths (force capacities) of reinforced concrete sections. The nominal strength and design strength of a reinforced concrete section can be determined using the CORPS library program CSTAR for reinforced concrete design and investigation. For a given section the force capacities are determined from the intersection of the design strength curve with a line drawn from the origin to the required axial force-moment pair computed for the section.

f. Presentation and performance evaluation.

(1) Pile deflections. Pile deflections refer to relative dynamic displacements between pile head and pile tip. The maximum vertical and horizontal pile deflections resulting from the applied loads should be limited to allowable values to ensure integrity of the structure.

(2) Pile forces and moments. Pile axial forces and bending moments are used in accordance with Equation 4-1 to compute pile interaction factors in time domain for the eight combination cases of the static and seismic loads listed in Table 4-10. For each performance criteria case shown in Table 4-11, the resulting time-histories of interaction factors should be processed and presented according to the following list to facilitate performance evaluation and estimation of probable damage:

(a) Peak dynamic pile forces and moments.

(b) Pile forces and moments for static, static plus dynamic values at peak moment, static plus dynamic values at peak axial, and static plus dynamic values at peak shear.

(c) Pile forces and moments for static plus peak dynamic values.

(d) Table of peak interaction factors and associated forces and moments corresponding to the most critical load combination.

(e) Graph of peak interaction factors for the most critical load combination (Figures 4-27 to 4-29).

(f) Time-history of interaction factors for the most critical piles (Figure 4-30).

(g) Duration or number of time-steps that the interaction factors for each pile exceed unity.

(h) Time-history plots of the percentages of piles having an interaction factor (DCR) exceeding 1.0, 1.1, 1.2, and 1.3.

(i) Table of peak percentages of piles having an interaction factor exceeding 1.0, 1.1, 1.2, and 1.3 (Table 4-12)

(j) Table of peak duration at which pile interaction factors exceed unity (Table 4-13).

Extreme Allowable Case

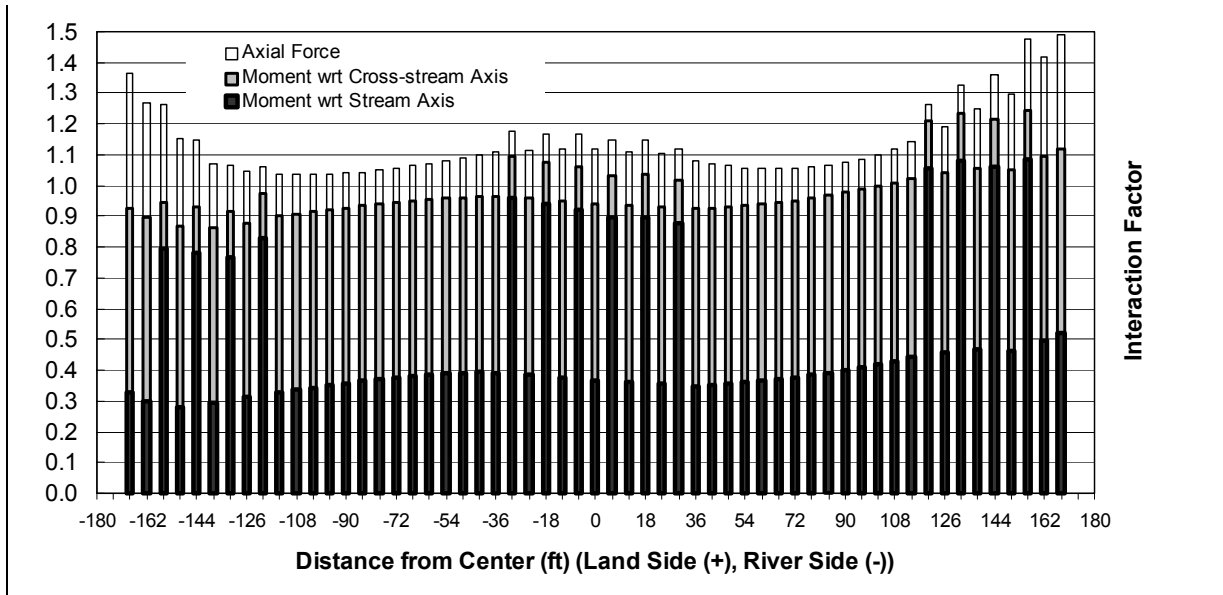


Figure 4-27. Combined static and dynamic interaction factors for H-piles under lower miter gate monolith subjected to MDE; extreme allowable case, FS = 1.15; distance to downstream face = 17 m (56.74 ft)

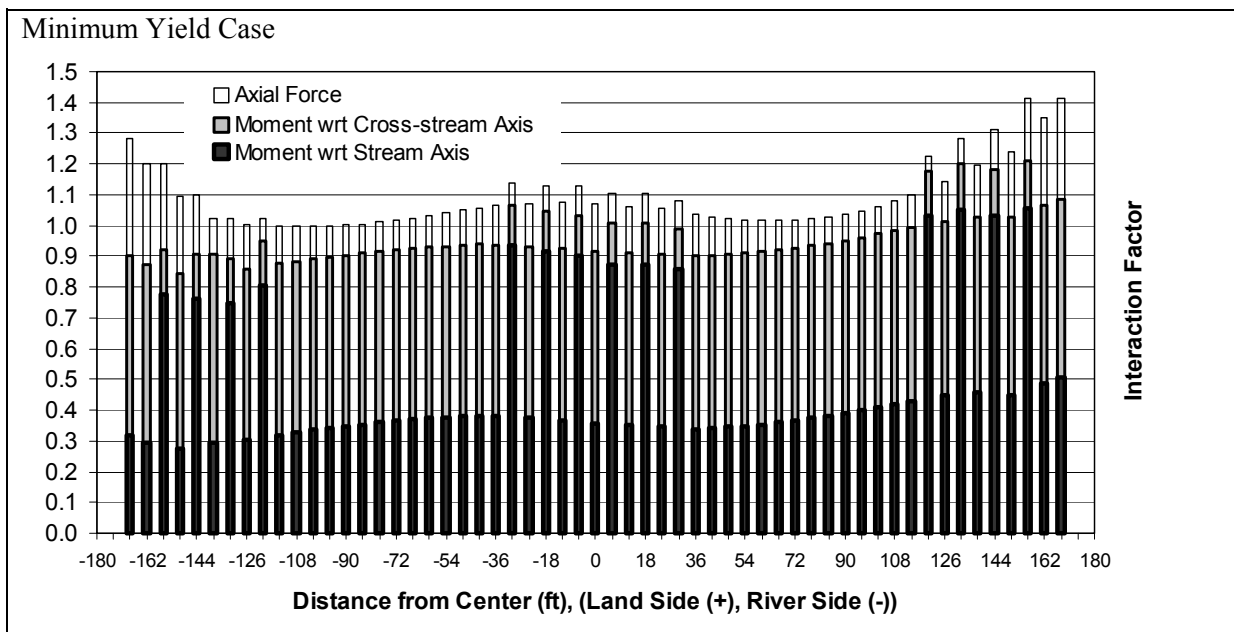


Figure 4-28. Combined static and dynamic interaction factors for H-piles under lower miter gate monolith subjected to MDE; minimum yield case, FS = 1.0; distance to downstream face = 17 m (56.74 ft)

The evaluation process starts with comparison of peak pile forces and moments ((b) and (c) above), acting individually, with the allowable values set forth in EM 1110-2-2906. The combined axial forces and bending moments are assessed using the interaction factors and information described under (d) to (j) above. For three

Expected Yield Case

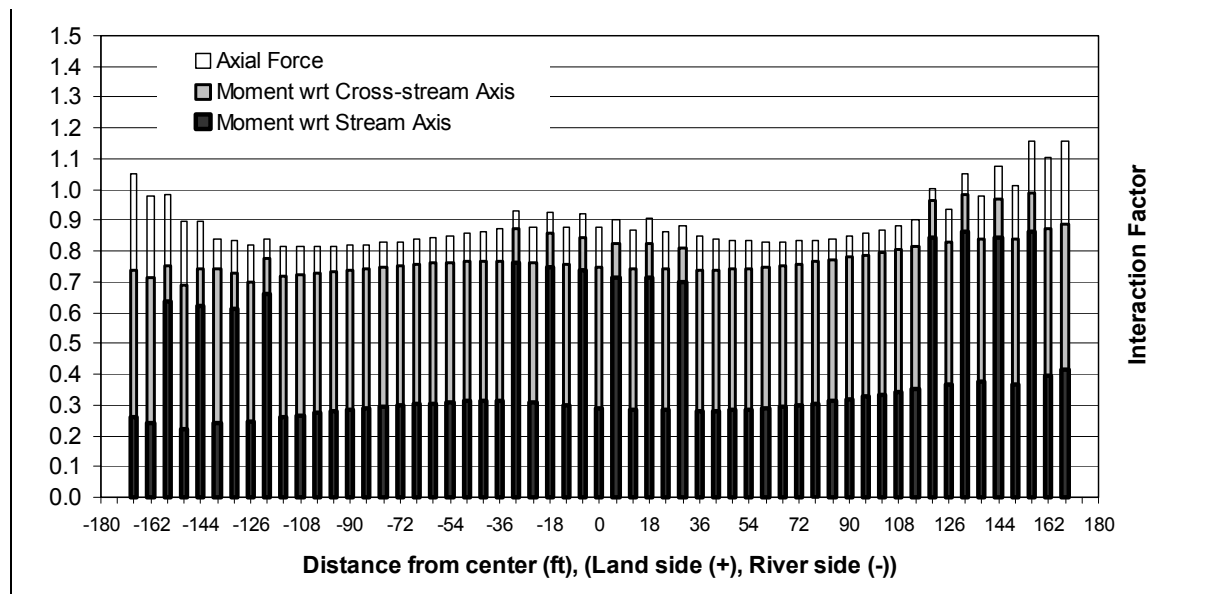


Figure 4-29. Combined static and dynamic interaction factors for H-piles under lower mitergate monolith subjected to MDE; expected yield case, FS = 1.0; distance to downstream face = 17 m (56.74 ft)

performance cases of Extreme Allowable, Minimum Yield, and Expected Yield, the graphs of peak interaction factors (Figures 4-27 to 4-29) provide a snapshot of the peak demand-capacity ratios (interaction factors) that each pile might experience at some instant of time during the earthquake shaking. In the Extreme Allowable Case, if all demand-capacity ratios are less than or equal to unity, all piles remain elastic and satisfy the required factor of safety (FS = 1.15). No further evaluation of piles is therefore necessary. Otherwise some piles might yield, requiring an evaluation on the basis of the minimum or expected yield strength of the pile (i.e., FS = 1) in accordance with paragraph 4-5c. In either case demand-capacity ratios ≤ 1 indicate a satisfactory performance with no need for additional evaluation. Otherwise percentage of piles whose combined demand-capacity ratios exceeding 1.0, 1.1, 1.2, and 1.3 (Figures 4-31 to 4-33) and the corresponding duration of demand-capacity ratio cycles whose values exceed each of these levels should be determined and compared with the performance curves. For comparison percentage of piles showing yielding and the corresponding cumulative yield duration for the Olmsted lower miter gate monolith are shown on the performance curves and summarized in Tables 4-12 and 4-13.

(3) Lock deflections and stresses. Dynamic displacements at the top and base of the lock walls should be computed and the relative displacements between the top and the base determined. The computed peak relative displacements should be within 0.1 percent of the lock height in order to limit the damage.

(4) Lock section forces and moments. Time-histories of dynamic forces and moments at selected concrete sections (Figure 4-34) are combined with the corresponding static forces and moments. Displayed as scatter plots, the resulting force demands are directly compared with the axial force-bending moment interaction diagrams discussed in *e* above. Figures 4-35 and 4-36 are examples of such scatter plots for Sections 1 and 4 (see Figure 4-33) of the Olmsted lower miter gate monolith for four loading combinations discussed in *b* above. The results indicate that the peak demand-capacity ratios for Section 1 are equal to unity and for Section 4 are much less than unity, an indication that the response of the monolith is essentially elastic or nearly elastic. Should the demand-capacity ratios for the concrete sections exceed unity, the performance criteria in *a* above must be followed to assess the severity of nonlinear response or damage.

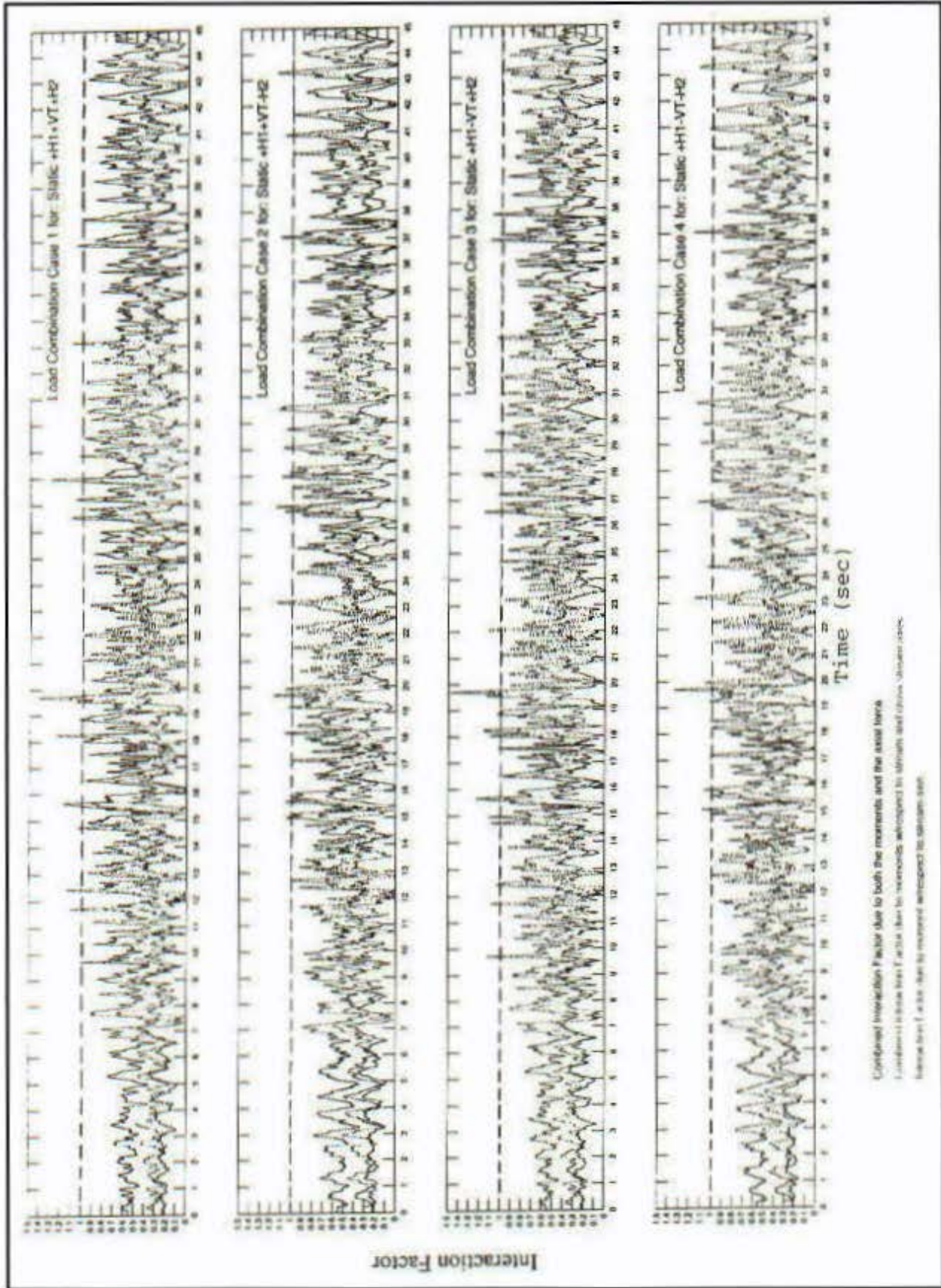


Figure 4-30. Time-history of interaction factors for the most critical piles

Table 4-12
Peak Percentages of Piles Exceeding Various Levels of Interaction Factors

Level of Interaction Factor	Extreme Allowable		Minimum Yield		Expected Yield	
	Load Combination Case	Percent	Load Combination Case	Percent	Load Combination Case	Percent
1.0	3	91	3	69	3	7
1.1	3	35	3	20	3	2
1.2	3	13	3	9	-	-
1.3	6	7	3	4	-	-

Table 4-13
Peak Accumulated Duration at Which Pile Interaction Factors Exceed Unity

Level of Interaction Factor	Extreme Allowable		Minimum Yield		Expected Yield	
	Load Combination Case	Duration sec	Load Combination Case	Duration sec	Load Combination Case	Duration sec
1.0	3	1.90	3	1.21	6	0.11

4-6. Free-Standing Intake Towers

The approximate level of earthquake damage in free-standing intake towers can be assessed using the linear time-history analysis procedures. A typical free-standing intake tower is modeled and evaluated as a 2- or 3-D cantilever column with appropriate stiffness, lumped masses, and damping. As outlined in Chapter 2, the lumped masses include the surrounding and contained water as well as the self-weight of the structure. The dynamic response is obtained for a minimum of three sets of site-specific earthquake-ground-acceleration time-histories as the input. Each set includes one vertical and two orthogonal horizontal components. For free-standing intake towers, the effects of vertical component of ground motion can usually be ignored, unless the tower exhibits significant rocking response. The results of analysis include peak values and time-histories of displacements and element forces. Other parameters of importance to damage assessment include demand-capacity ratios, cumulative duration of force excursions above the strength capacity, and the length of tower over which the strength capacity is exceeded. The procedure for estimation of the probable level of damage for free-standing intake towers was formulated using the results from linear time-history analyses of an example intake tower subjected to four different sets of earthquake ground motions. The accuracy of the procedure was verified by several nonlinear time-history analyses, which employed an elastic-plastic moment-rotation relationship for the structural members.

a. Nonlinear behavior and modes of failure. Figure 4-37 provides some examples of probable modes of failure for free-standing intake towers due to overstressing and structural instability conditions. Different combinations and sequence of failure modes shown in Figure 4-37a, b, c, and d are also conceivable. The desired mode of behavior is the moderate flexural yielding of the base region, which controls the strength, inelastic deformation, and energy dissipation capability of the tower during the earthquake shaking. This is because concrete structures with adequate reinforcement and detailing exhibit more ductile behavior in bending than in shear due to yielding of the flexural reinforcements. The behavior of reinforced concrete walls, with seismic response behavior similar to that of towers, indicates that the largest energy dissipation with the smallest strength degradation is feasible through flexural hinging but not shear (Paulay and Priestley 1992). This superior performance therefore makes the bending the most desirable mode of nonlinear behavior (Figure 4-37a). By contrast, shear failures tend to be nonductile, and can often lead to severe damage and even collapse of the structure. Failure modes such as diagonal tension/compression cracks (4-33b), shear or bond failure along the construction joints and anchorage (4-33c), and rocking (4-33d) are undesirable due to small energy dissipation and rapid strength degradation and should be avoided whenever possible. The shear forces, therefore, are not permitted to exceed the shear capacities of the members. Modes of failure and nonlinear response of intake towers depend largely on the arrangement and the amount of vertical and shear reinforcements (Dove 1998).

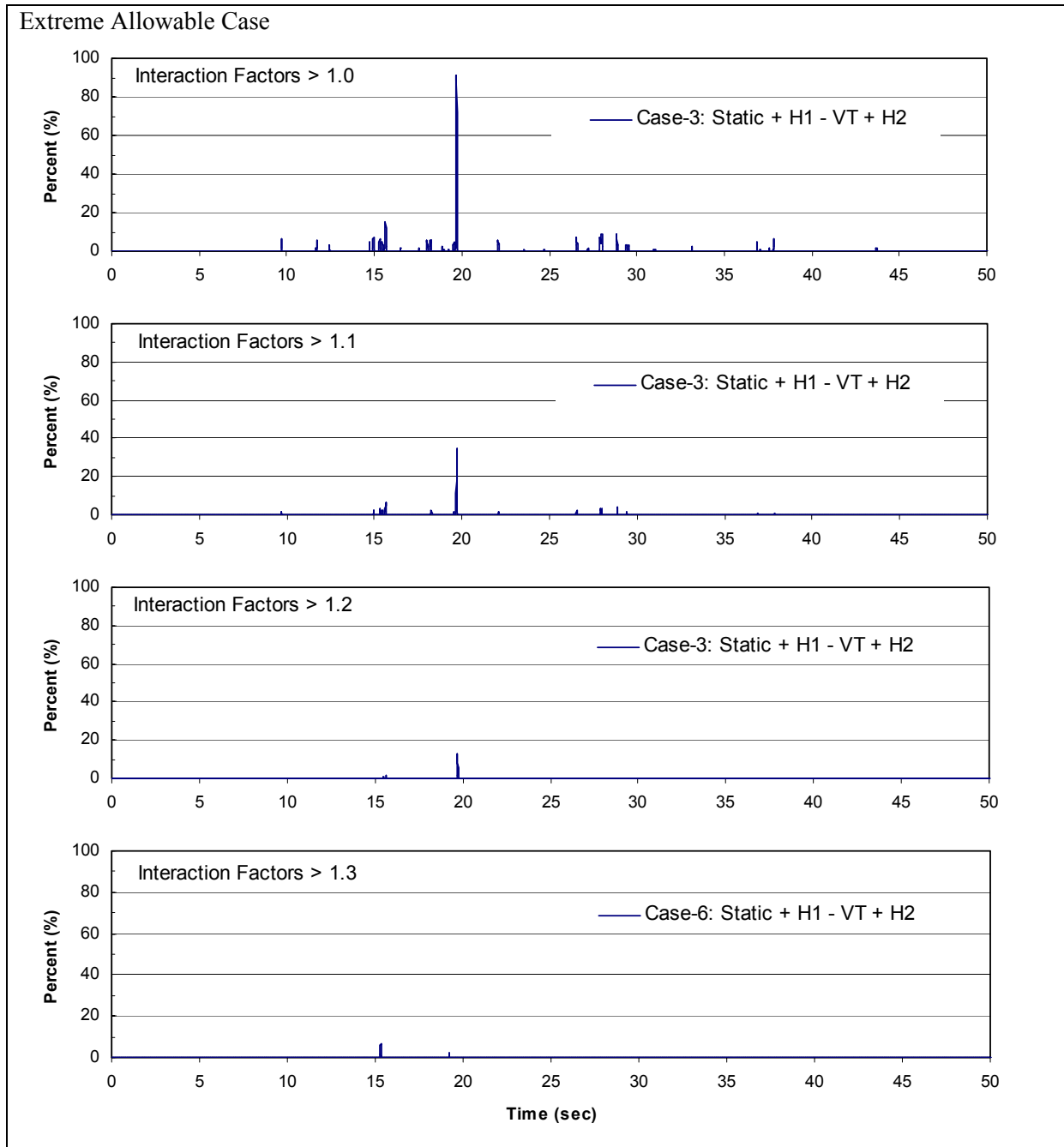


Figure 4-31. Peak percentage of H-piles whose combined interaction values exceed 1.0, 1.1, 1.2, and 1.3; extreme allowable case; lower miter gate monolith for MDE

In nonlinear analyses, the effects of reinforcements should be modeled appropriately in order to capture the most likely mode of behavior. For example, lightly reinforced concrete towers may offer limited ductility with prevailing sliding and/or overturning modes of failure (Figure 4-37c and d).

b. Influence of earthquake ground motion. The magnitude and characteristics of earthquake ground motions can significantly affect the dynamic response and the level of damage that could occur in an intake

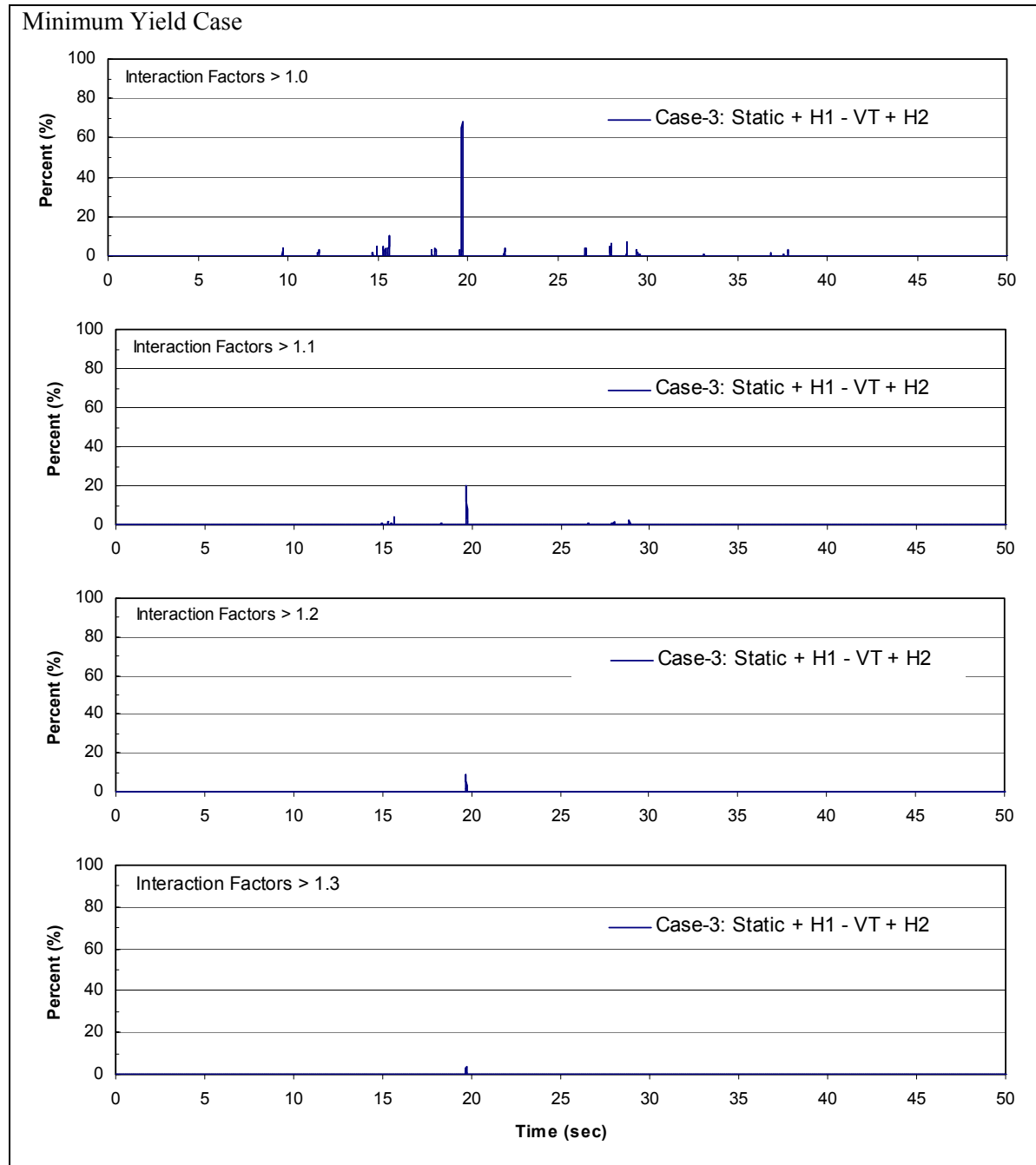


Figure 4-32. Peak percentage of H-piles whose combined interaction factor values exceed 1.0, 1.1, 1.2, and 1.3; minimum yield case; lower miter gate monolith for MDE

tower. The probable level of damage for the example intake tower was therefore evaluated for four sets of recorded acceleration time-histories selected from four different earthquake events having a moment magnitude M_w in the range of 6.0 to 6.9. As shown in Table 4-14, the style of faulting also varied for each event and included a strike-slip, an oblique, or a reverse fault. In general, recordings from these earthquakes showed differences in the frequency content, duration, energy content, and pulse sequencing, all of which were considered in the formulation of damage criteria discussed in *c* below.

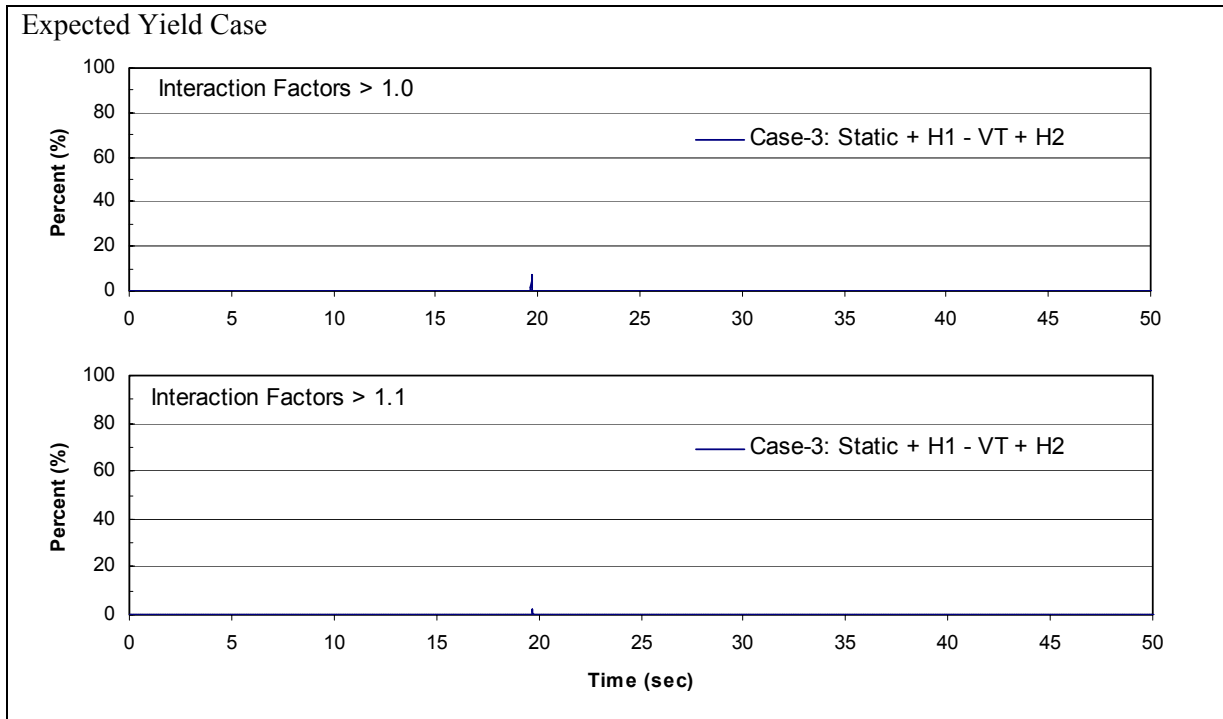


Figure 4-33 Peak percentage of H-piles whose combined interaction factor values exceed 1.0 and 1.1; expected yield case; lower miter gate monolith for MDE

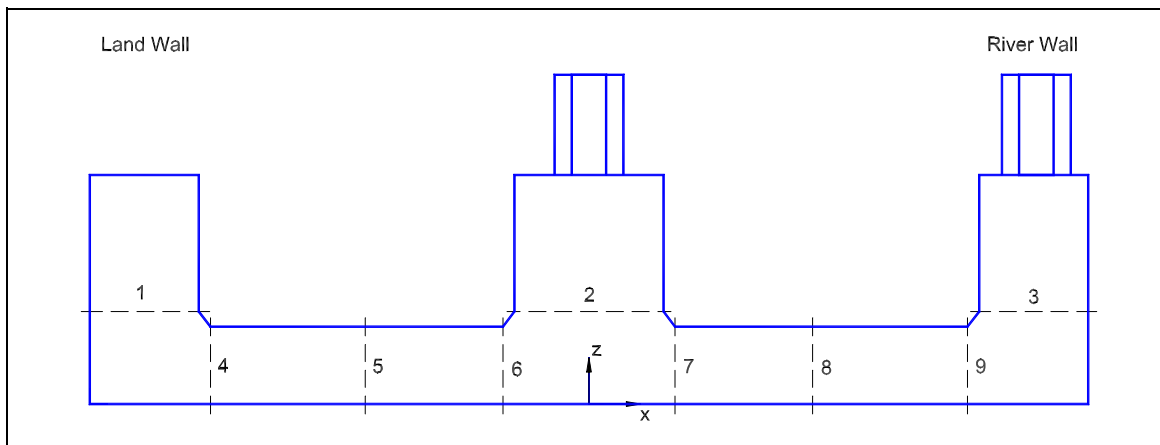


Figure 4-34. Critical lock sections for assessment of forces and moments

(1) Selected earthquake ground motions. Table 4-14 lists the four earthquake ground motion records with their corresponding characteristics and the scaling factors used in this study. These natural records were scaled such that the average of ordinates for the response spectra of all four records would match a smooth design response spectrum in the period range of 0.03 to 0.6 sec important to the example problem. The smooth design response spectrum was developed representative of the median ground motions corresponding to an earthquake M_w 6.5 at a distance of 5 km. Figures 4-38 and 4-39 provide comparisons between the smooth response spectrum with response spectra of the scaled primary and secondary natural records. Time-histories of the scaled records are displayed in Figures 4-40 to 4-43.

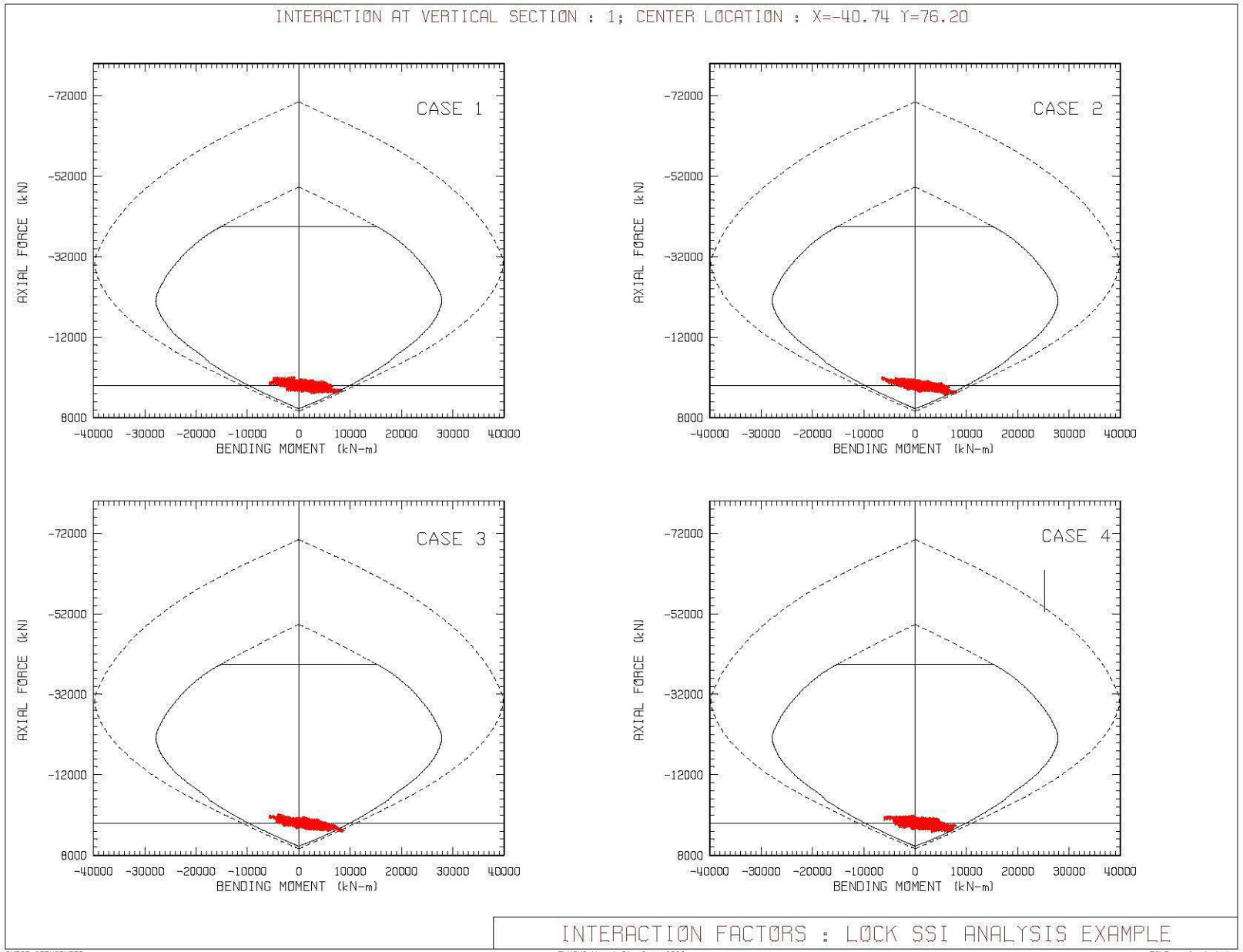


Figure 4-35. Axial force versus bending moment of concrete Section 1

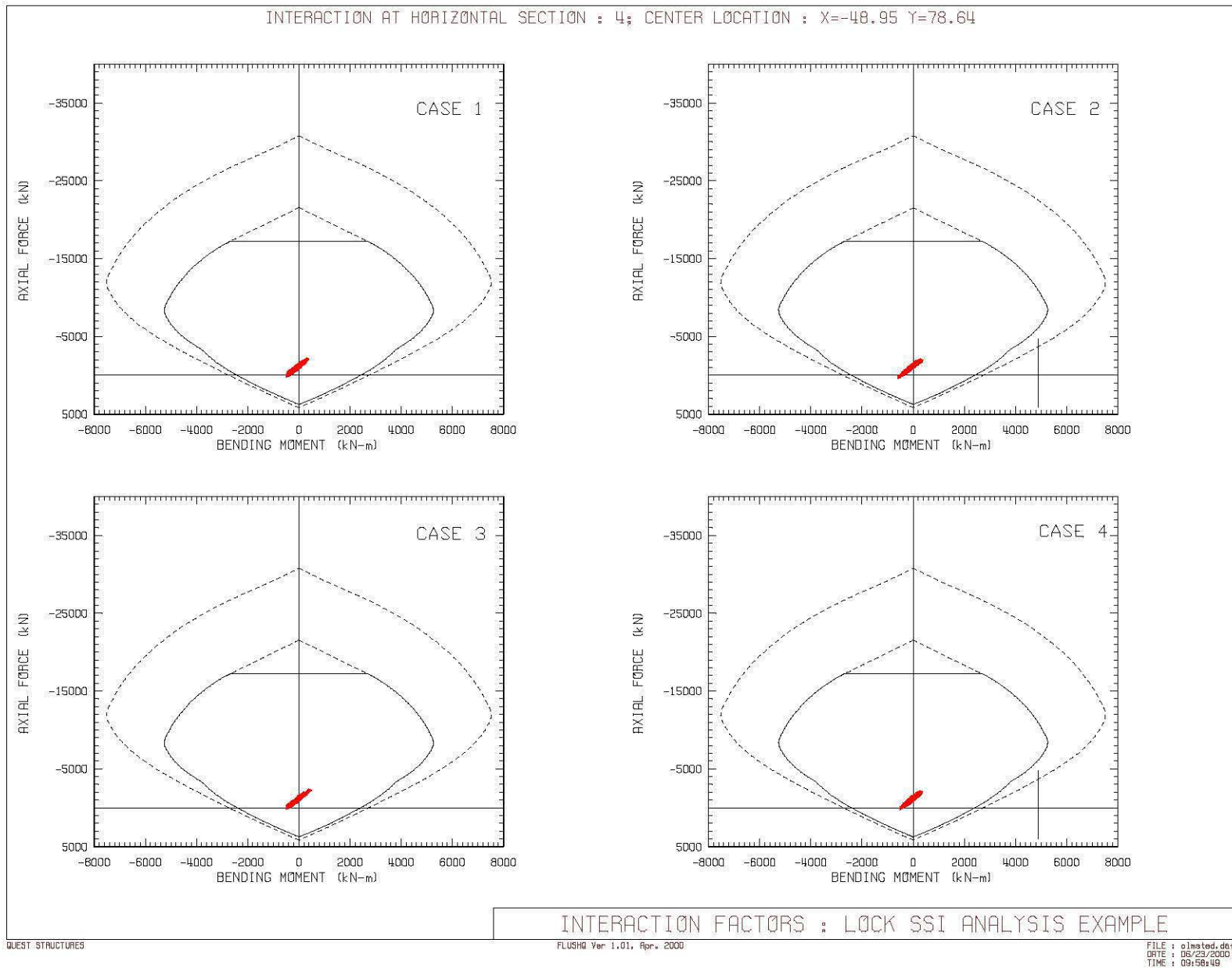


Figure 4-36. Axial force versus bending moment of concrete Section 4

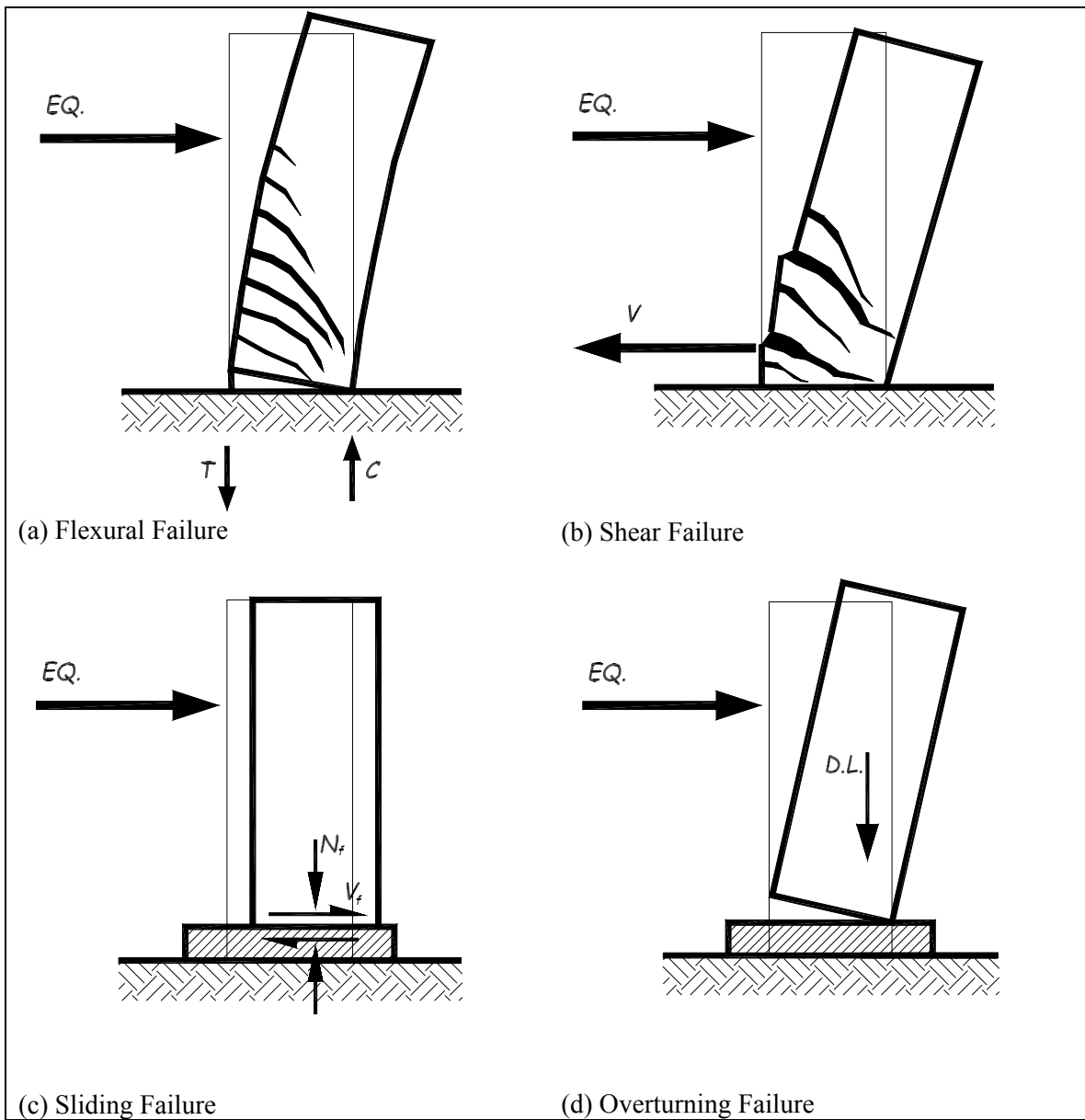


Figure 4-37. Probable modes of failure for free-standing towers where *EQ.* = lateral earthquake load, *T* = tensile base reaction force, *C* = compressive base reaction force, *V* = base shear, *N_f* = normal force at the base, *V_f* = shear friction, and *D.L.* = dead load

Time-History No.	Earthquake Record	<i>M_w</i>	Style of Faulting	Distance, km	Scaling Factor
1	Cholame #8, 1966 Parkfield	6.1	Strike-Slip	9.2	1.7962
2	Garvey Reservoir, 1987 Whittier Narrows	6.0	Reverse	12.1	0.8987
3	Gavilan College, 1989 Loma Prieta	6.9	Oblique	11.2	1.3596
4	Pacoima Dam, 1971 San Fernando	6.6	Reverse	2.8	0.4915

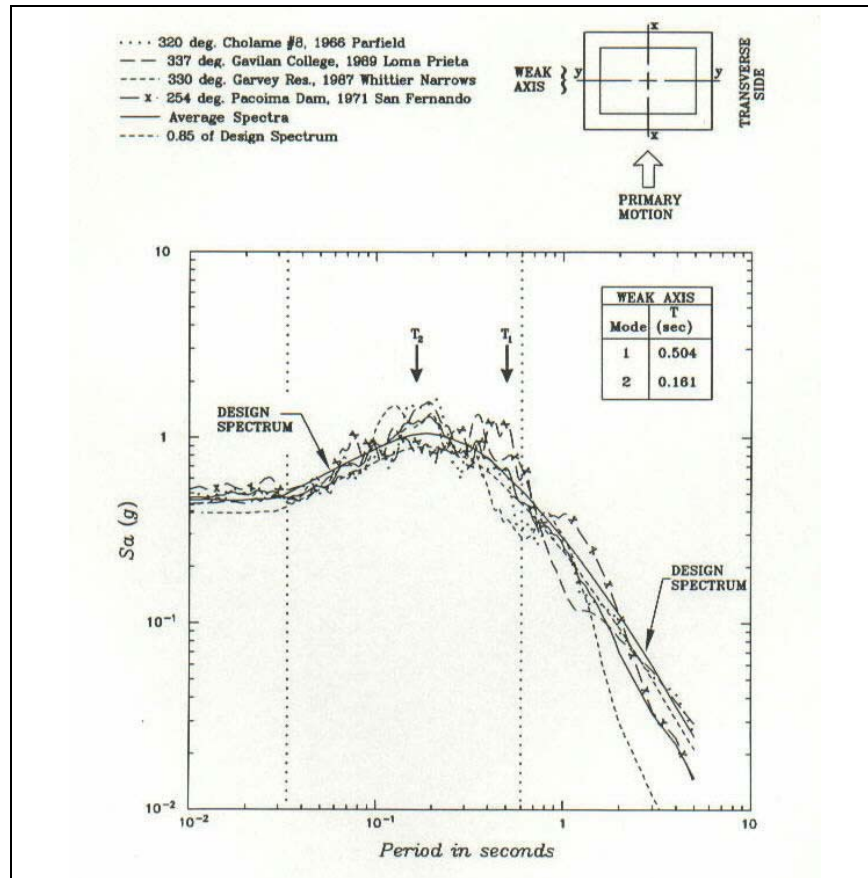


Figure 4-38. Horizontal design spectrum and the four scaled natural time-histories of the primary set with 5 percent damping

(2) Description of example intake tower. The geometry of the example free-standing intake tower is shown in Figure 4-44. The tower is 60.96 m (200 ft) high with base dimensions of 14.63 m by 11.28 m (48 ft by 37 ft). The wall thickness decreases in five steps from 1.83 m (6.0 ft) at the base to 0.61 m (2.0 ft) at the top. The water surface is at elevation 1,016.81 m (3,336 ft) corresponding to outside and inside water depths of 41.45 m (126 ft) and 39.62 m (130 ft), respectively. The material parameters of the concrete and reinforcing steel are summarized in Table 4-15. The transverse and longitudinal nominal and cracking moments and the shear capacities are listed in Table 4-16. To keep the analysis and damage formulation simple the following assumptions were made:

Tower elements do not reach their shear or axial load capacity.

Rocking or sliding modes of failure are not considered.

The vertical component of the earthquake ground motions is ignored.

The effects of gravity load are not included in the dynamic analysis.

(3) Linear time-history earthquake response. The earthquake response of the tower was computed for all four earthquake ground motions described in (1) above. The time-history analysis was carried out separately for excitation in the transverse and longitudinal directions. In each direction, the 10 lowest modes of vibration

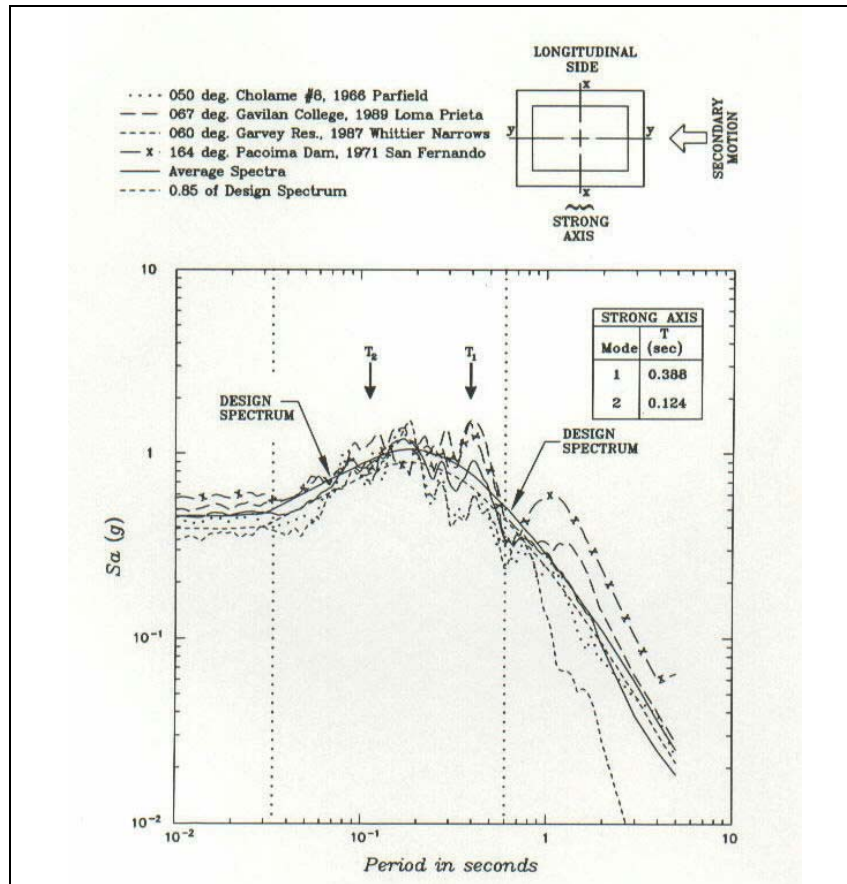


Figure 4-39. Horizontal design spectrum and the four scaled natural time-histories of the secondary set with 5 percent damping

with a modal damping ratio of 5 percent were considered in computation of the dynamic response. The periods of the five lowest transverse modes of vibration ranged from 0.529 to 0.034 sec. For the longitudinal direction, the periods of the five lowest modes were in the range of 0.041 to 0.026 sec. Table 4-17 summarizes maximum lateral displacements at the top of the tower and maximum bending moments and shear forces at the base of the tower. Figures 4-45 to 4-52 present time-histories of displacements, shears V_x and V_y , and bending moments M_x and M_y for the selected earthquake ground motions. The results show that the shear capacity is not reached but the bending moment capacity of the tower is exceeded for all four earthquake records, an indication that some nonlinear behavior and damage could be expected, as discussed next in *c* below.

c. Damage criteria for linear time-history analysis. The damage for lightly reinforced free-standing intake towers is evaluated on the basis of demand-capacity ratios described in *f* below. The basic procedure is to perform linear time-history analysis with appropriate amount of damping to obtain bending moment demand-capacity ratios for all tower elements. Initially a damping ratio of 5 percent is used. If the computed demand-capacity ratios are less than or equal to 1.0, the tower is considered to respond essentially within the linear elastic range with negligible or no damage. For MDE earthquake ground motions, however, it is likely that demand-capacity ratios will exceed 1.0, indicating that the tower would suffer some damage. In this situation, the damping for the linear analysis should be increased to 7 percent if demand-capacity ratios are approaching 2 and to 10 percent if they exceed 2. After adjustment for the damping, the damage is considered moderate and acceptable if the following conditions are met:

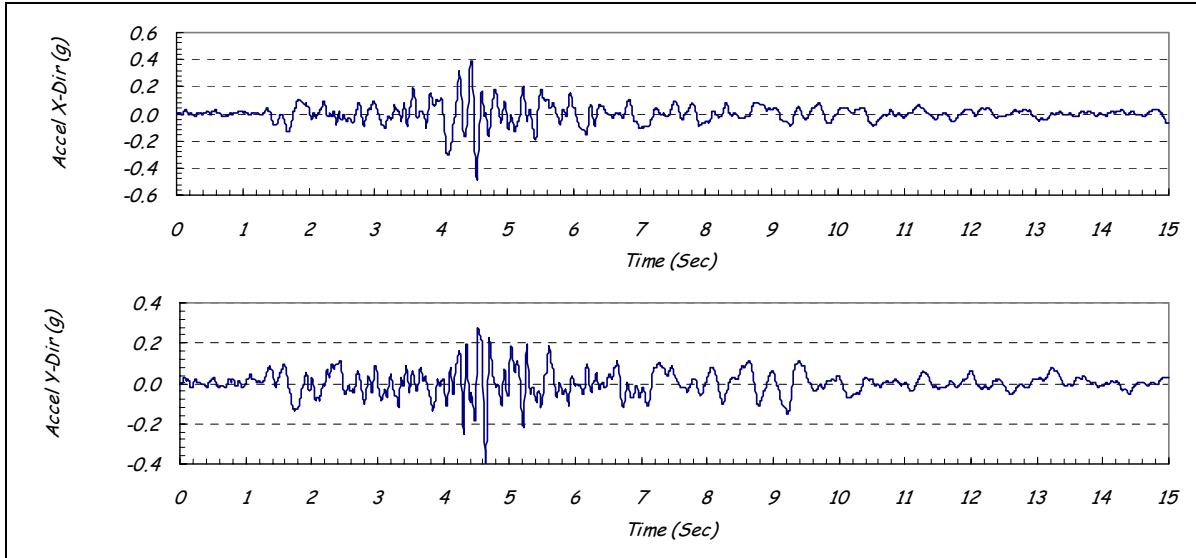


Figure 4-40. Cholame #8, 1966 Parkfield Earthquake (scaled by 1.7962)

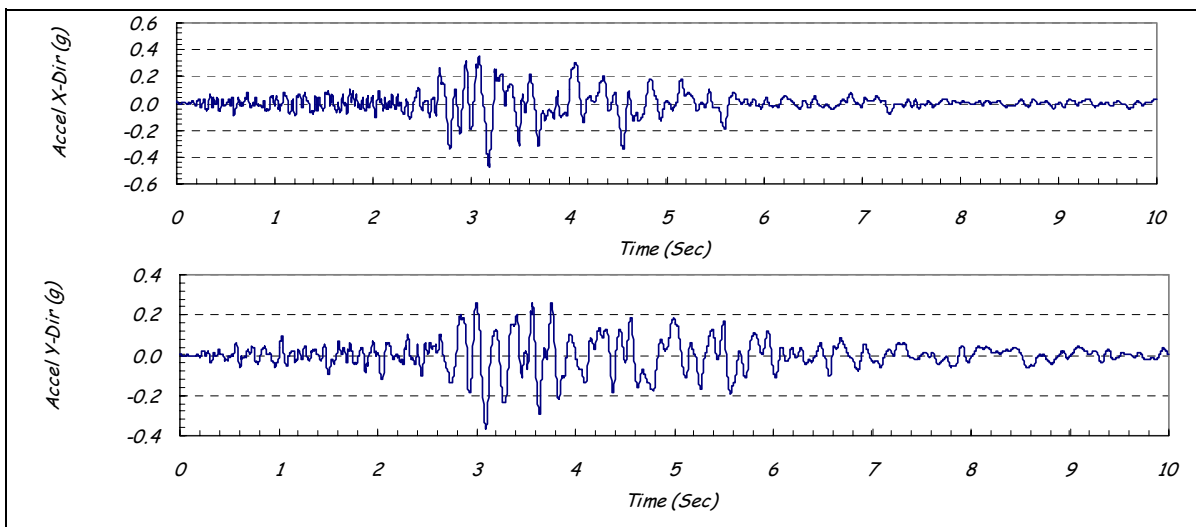


Figure 4-41. Garvey Reservoir, 1987 Whittier Narrows Earthquake (scaled by 0.8987)

- Bending moment demand-capacity ratios computed on the basis of linear time-history analysis remain less than 2.
- Cumulative duration of bending-moment excursions above demand-capacity ratios of 1 to 2 fall below the acceptance curve given in Figure 4-53.
- The extent of yielding along the height of tower (i.e., plastic hinge length for demand-capacity ratios of 1 to 2) is limited and falls below the acceptance curve.

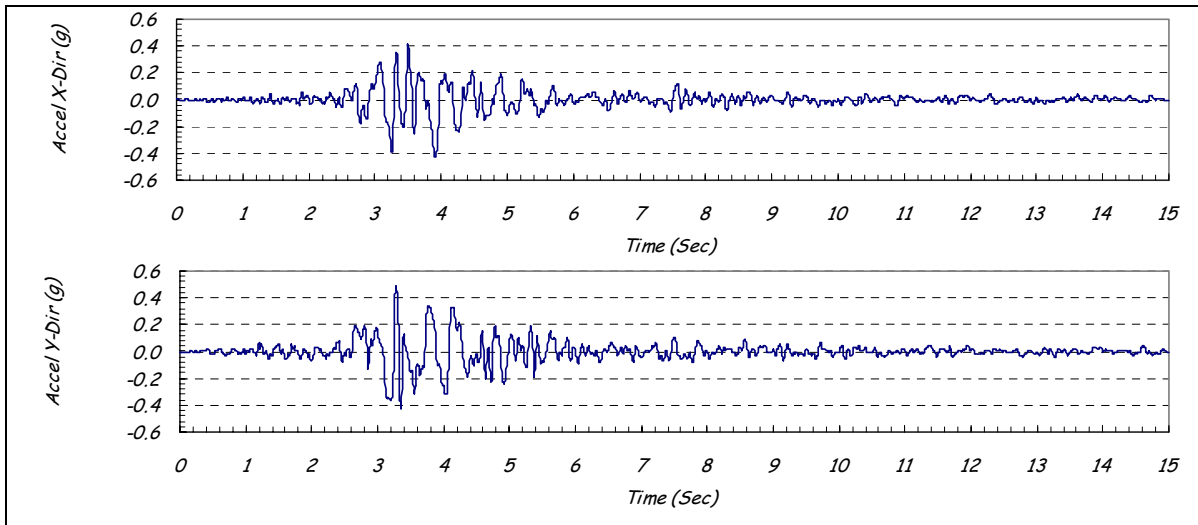


Figure 4-42. Gavilan College, 1989 Loma Prieta Earthquake (scaled by 1.3596)

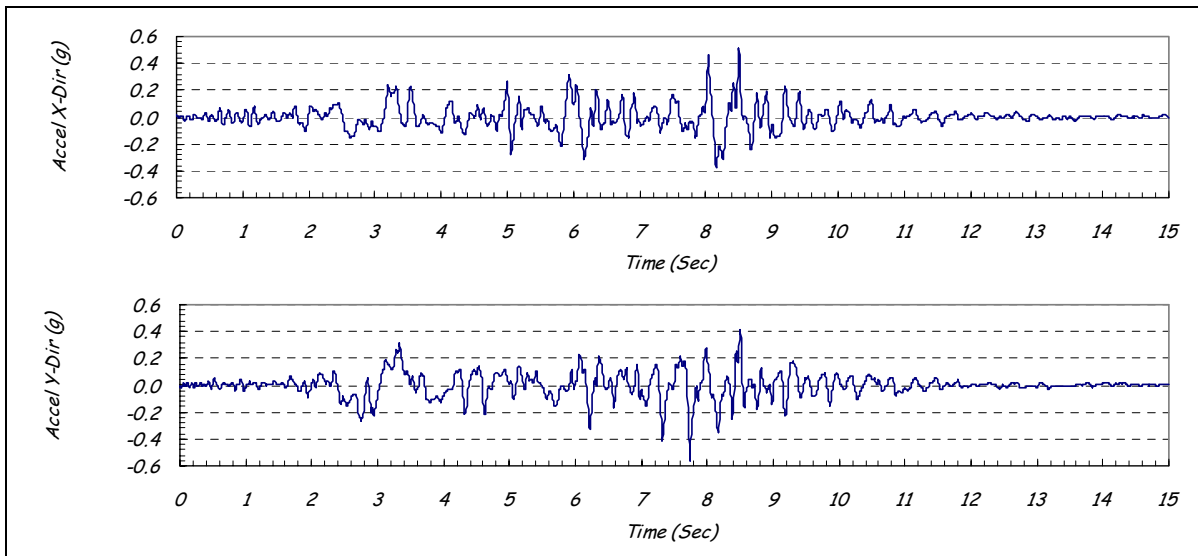


Figure 4-43. Pacoima Dam, 1971 San Fernando Earthquake (scaled by 0.4915)

The acceptance criteria state that as long as demand-capacity ratios are less than 2 and the cumulative inelastic duration and yielded height ratios fall below the acceptance curves, the level of damage will be moderate and can be approximated by the linear analysis procedures. If demand-capacity ratios exceed 2.0 or the cumulative duration and the yield lengths rise above the acceptance curves, the damage is considered to be severe and should be assessed using nonlinear analysis procedures. The term cumulative inelastic duration is defined as the total time of bending moment excursions above a particular capacity corresponding to demand-capacity ratios of 1 to 2. As shown in Figure 4-53, the cumulative inelastic duration for free-standing towers varies from 0.75 to 0.0 sec for demand-capacity ratios of 1 and 2, respectively. The yield height ratio refers to the yielded length of tower normalized with respect to the tower height. To keep the damage to a moderate level, the yield length should be less than one-third of the tower height, as shown in Figure 4-53.

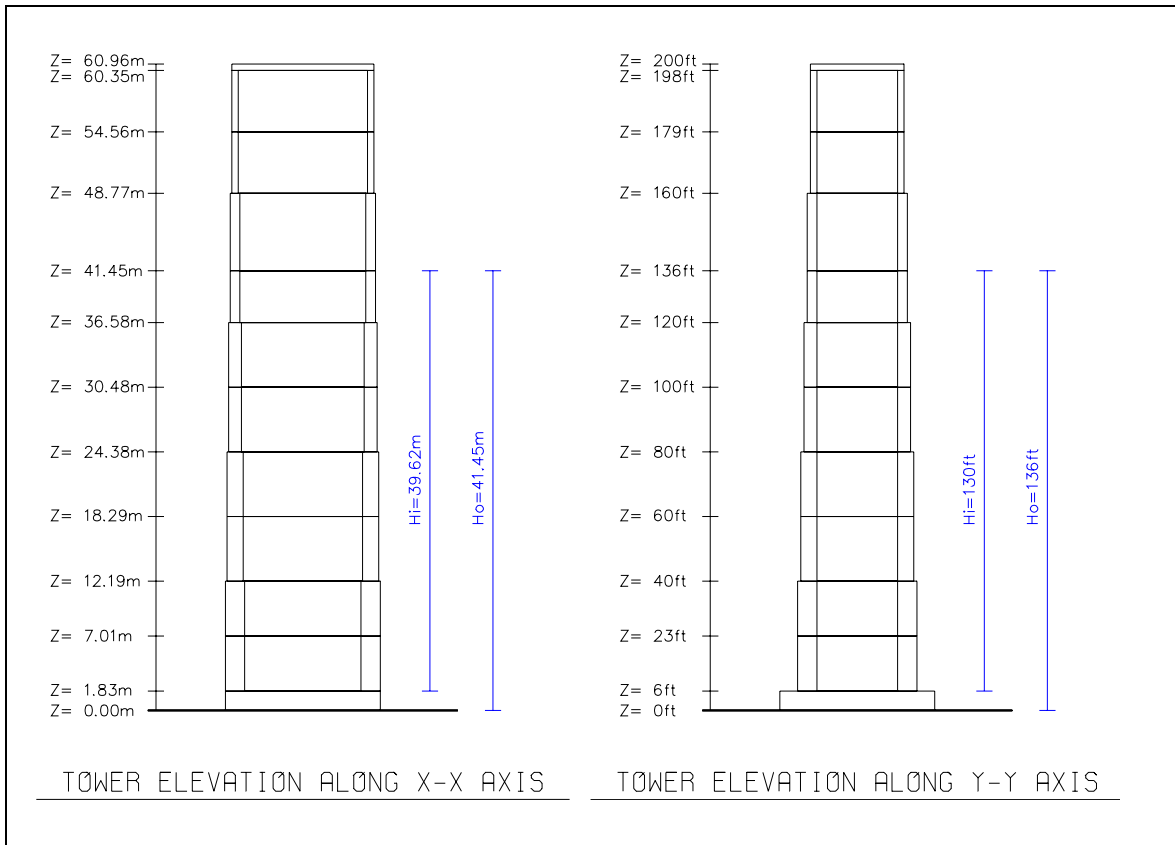


Figure 4-44. Basic geometry of the example tower

Table 4-15 Material Parameters Used in the Study		
Parameter	Value	
Re-bar Material Properties		
Modulus of Elasticity E_s	199,958.46 MPa	29,000.00 ksi
Yield Strength f_y	413.71 MPa	60.00 ksi
Strain Hardening	0.80 %	0.80 %
Steel Ultimate Stress	517.13 MPa	75.00 ksi
Steel Ultimate Strain	5.00 %	5.00 %
Concrete Material Properties		
Modulus of Elasticity E_c	21,526.56 MPa	3,122.00 ksi
Shear Modulus G	8,969.40 MPa	1,300.83 ksi
Poisson's Ratio ν	0.20	0.20
Concrete Strength f'_c	20.69 MPa	3.00 ksi
Modulus of Rupture F_r	2.83 MPa	0.41 ksi
Concrete Ultimate Strain ϵ_c	0.30 %	0.30 %

Table 4-16
Nominal Moment, Cracking Moment, and Shear Capacities for Bottom Three Sections of Tower

Parameter	Section 2	Section 3	Section 4
Height z, m (ft)	1.83-12.19 (6-40)	12.19-24.38 (40-80)	24.38-36.58 (80-120)
Nominal Moment MN_y , kN-m (k-ft)	937,490 (691,421)	881,969 (650,473)	827,955 (610,636.39)
Nominal Moment MN_x , kN-m (k-ft)	719,711 (530,803)	653,529 (481,993)	590,377 (435,417.19)
Cracking Moment Mcr_y , kN-m (k-ft)	814,736 (600,887)	673,358 (496,617)	534,792 (394,421.967)
Cracking Moment Mcr_x , kN-m (k-ft)	675,194 (497,971)	548,840 (404,783)	429,125 (316,489.629)
Shear Capacity Vn_y , kN (kips)	15,537,443 (3,492,773)	12,849,069 (2,888,434)	10,209,724 (2,295,116.85)
Shear Capacity Vn_x , kN (kips)	12,137,049 (2,728,384)	9,756,294 (2,193,187)	7,523,491 (1,691,259.3)

Table 4-17
Calculated Maximum Displacements and Element Forces

Time History No.	Earthquake Record	Maximum Top Displacement, cm (in.)	Maximum Bending Moment, kN-m (k-ft)	Maximum Shear kN (kips)
X-Component of Earthquake Ground Motion (X-Direction)				
1	Cholome #8, 1966 Parkfield	4.96 (1.95)	1,832,986 (1,351,870)	58,492 (13,149)
2	Garvey Reservoir, 1987 Whittier Narrows	5.43 (2.14)	1,970,798 (1,453,510)	68,045 (15,296)
3	Gavilan College, 1989 Loma Prieta	12.18 (4.80)	4,578,458 (3,376,720)	148,169 (33,308)
4	Pacoima Dam, 1971 San Fernando	10.86 (4.28)	3,769,250 (2,779,910)	128,902 (28,977)
Y-Component of Earthquake Ground Motion (Y-Direction)				
1	Cholome #8, 1966 Parkfield	7.76 (3.05)	2,058,380 (1,518,030)	108,066 (24,293)
2	Garvey Reservoir, 1987 Whittier Narrows	6.32 (2.49)	1,375,739 (1,014,640)	64,100 (14,410)
3	Gavilan College, 1989 Loma Prieta	11.59 (4.56)	3,016,094 (2,224,440)	113,106 (25,426)
4	Pacoima Dam, 1971 San Fernando	15.08 (5.94)	3,246,487 (2,394,360)	96,683 (21,734)

d. *Validation of damage criteria.* It is apparent from Figures 4-45 to 4-52 that the bending capacities of the example tower are exhausted and demand-capacity ratios for all the four earthquake records exceed 1. To estimate the expected damage, the performance evaluation curves are developed for all earthquake responses and illustrated in Figure 4-54. In this figure demand-capacity ratio is defined as the ratio of moment demand M_x or M_y to moment capacity M_{xu} or M_{yu} . Based on these results only the recording from the 1966 Parkfield earthquake applied in the longitudinal direction produces damage parameters within the acceptable range. The application of the 1966 Parkfield record in the transverse direction and the other three records in either direction produces significant nonlinear behavior well beyond the acceptable levels set forth for the linear analysis. To validate such findings the example tower was analyzed using nonlinear time-history procedures. The nonlinear analyses were conducted for all four earthquake records using the computer program DRAIN-2DX. The results of nonlinear analyses are summarized in the form of a global displacement ductility factor defined as the ratio of the maximum to yield displacements at the top of the tower (i.e., $m_D = D_m / D_y$). The yield displacement refers to displacement of the top of the tower at the time of the first yield. The global ductility factors listed in Table 4-18 are generally lower than the demand-capacity ratios indicated by linear analysis (Figure 4-54). This is because nonlinear analysis involves both the elastic and hysteretic damping, while linear analysis employs only the elastic damping. Since both the linear and nonlinear analyses show nonlinear deformation in the example tower, it would be prudent to increase the damping for the linear analysis from 5 to 10 percent. On this basis, the linear analyses were repeated with 10 percent modal

damping for all earthquake records. The results of these linear analyses in the form of structural performance curves

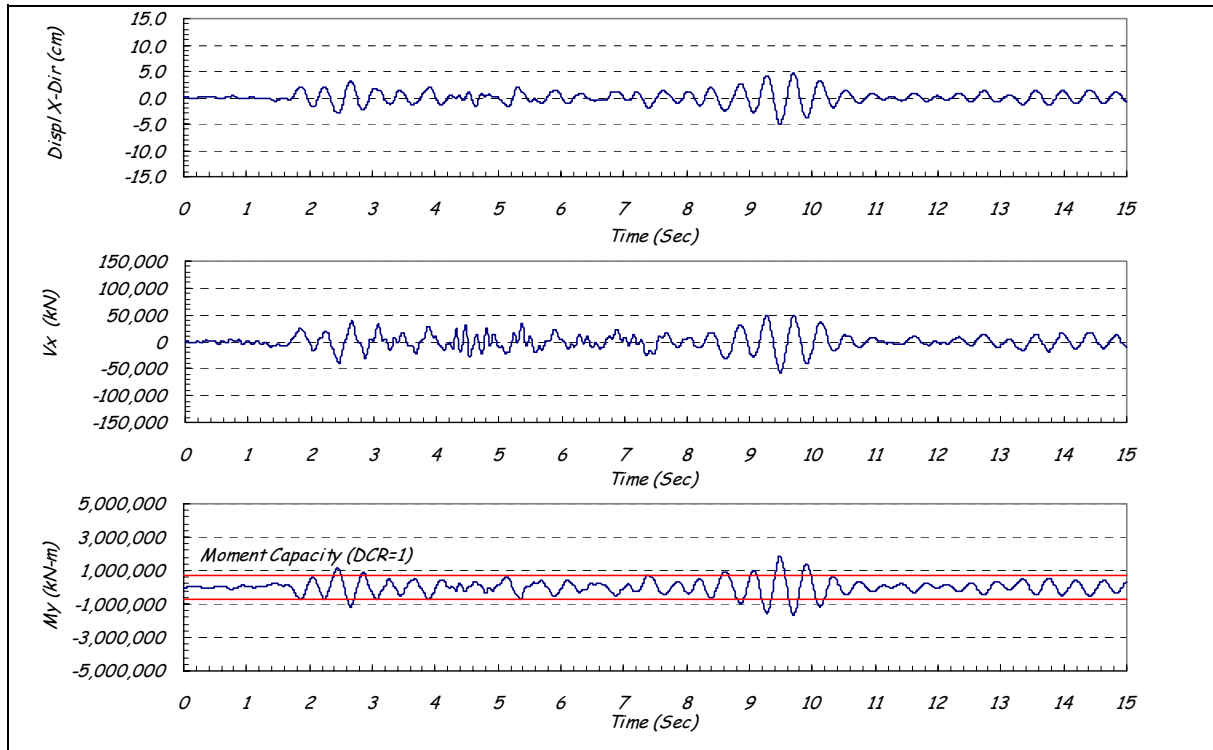


Figure 4-45. Response of the tower in x-direction due to 1966 Parkfield earthquake

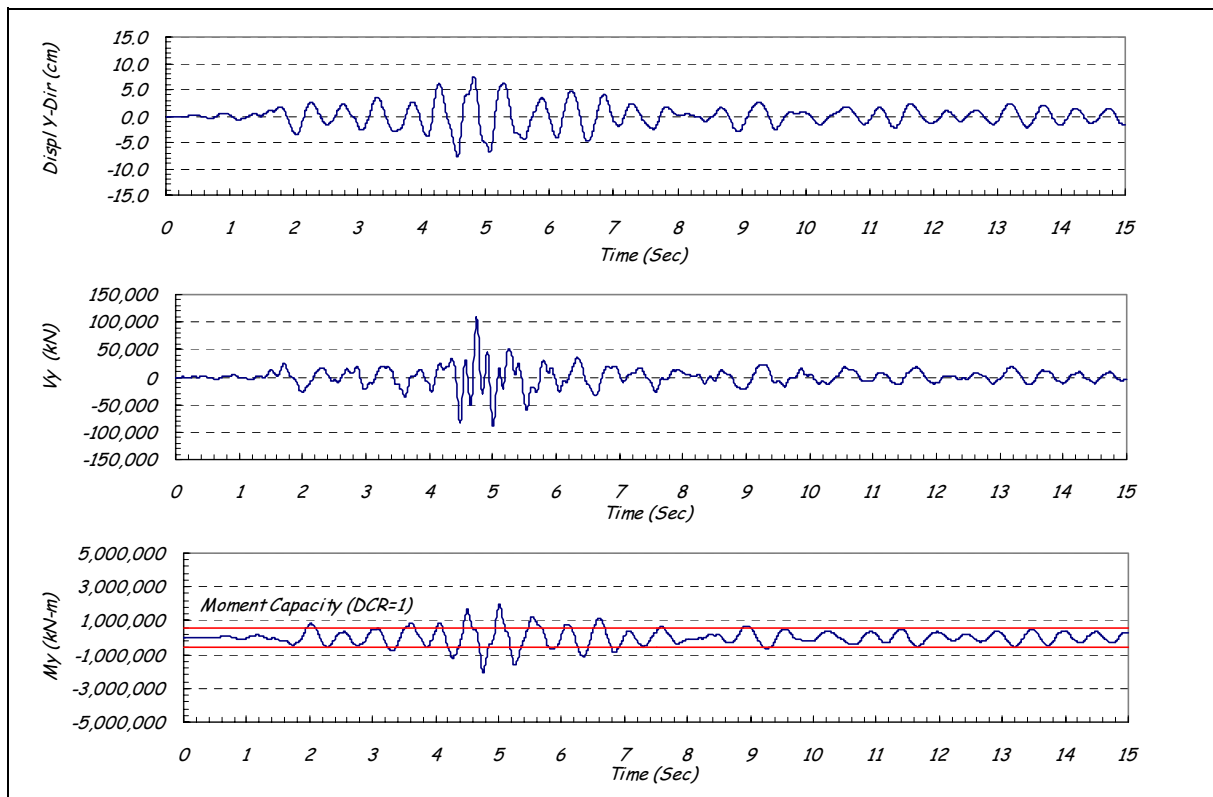


Figure 4-46. Response of the tower in y-direction due to 1966 Parkfield earthquake

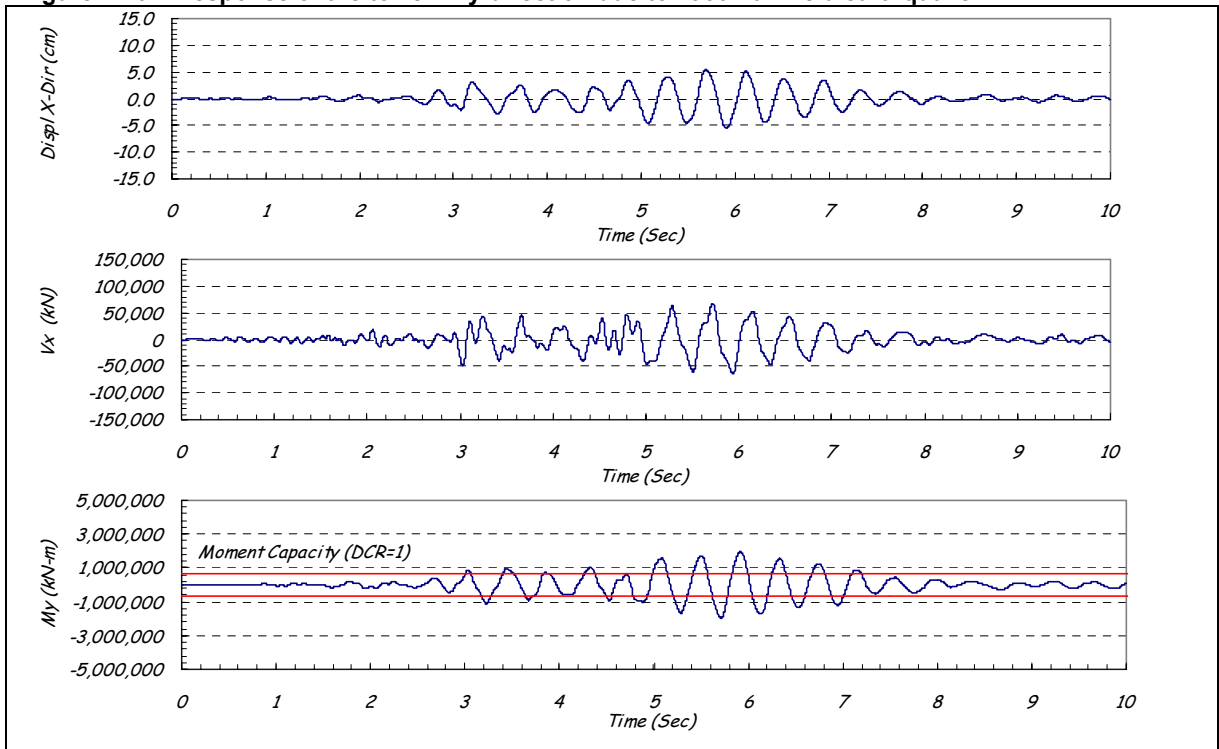


Figure 4-47. Response of the tower in x-direction due to Whittier Narrows earthquake

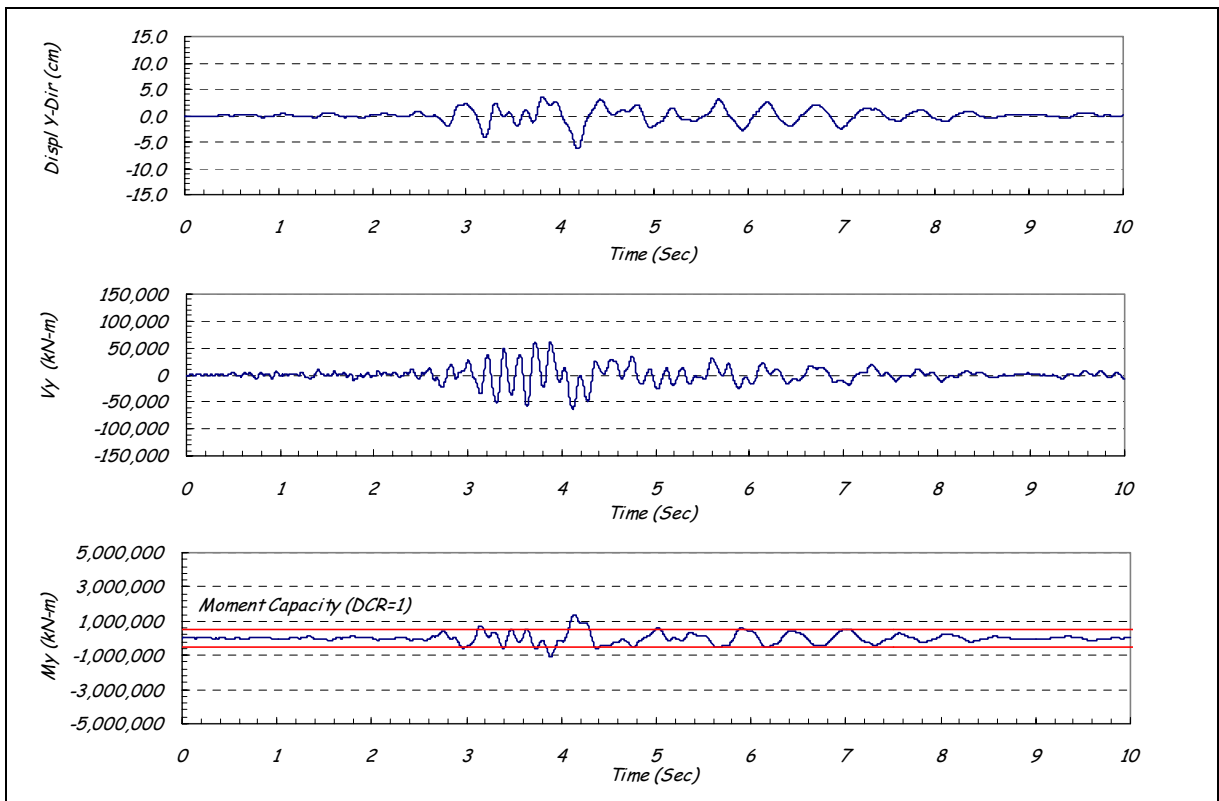


Figure 4-48. Response of the tower in y-direction due to Whittier Narrows earthquake

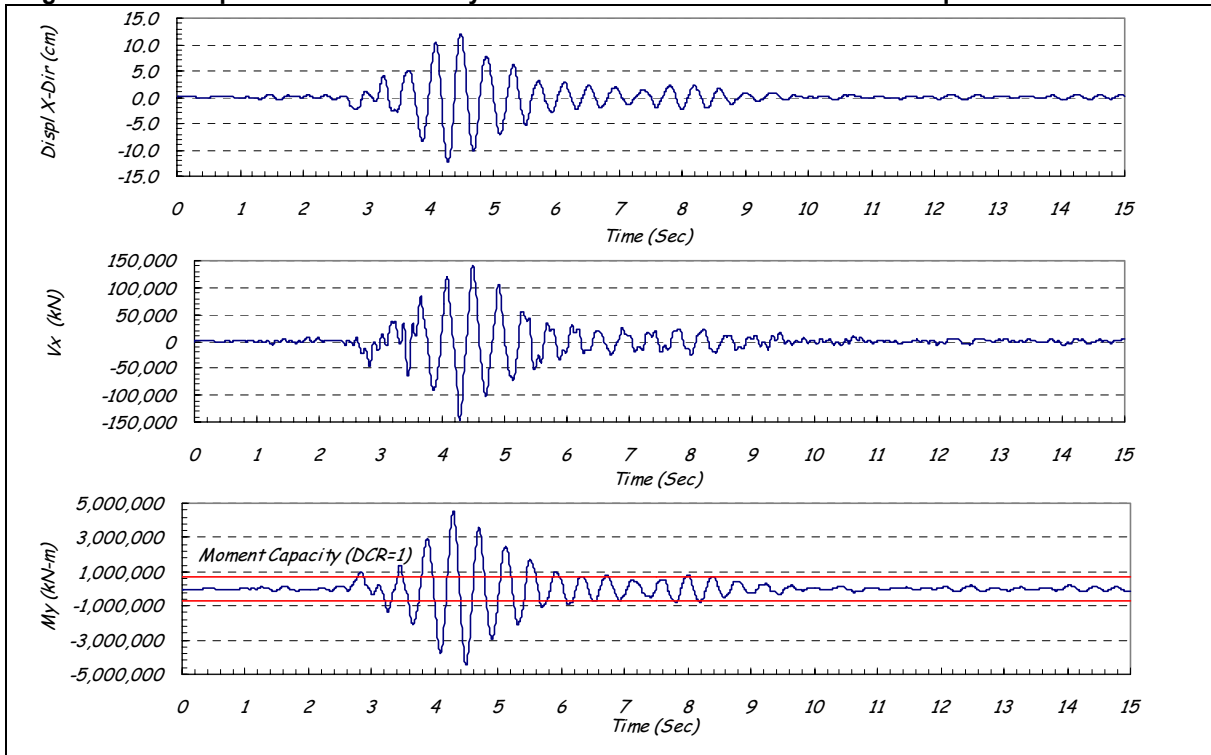


Figure 4-49. Response of the tower in x-direction due to 1989 Loma Prieta earthquake

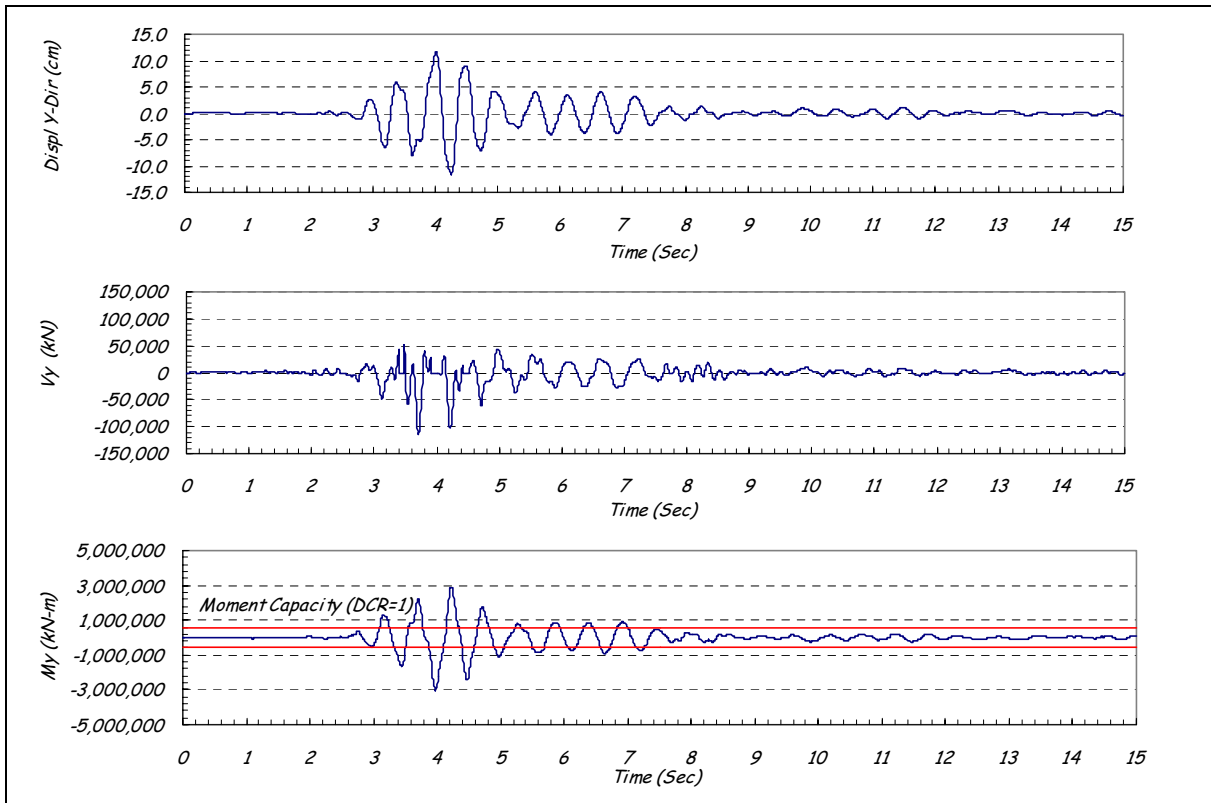


Figure 4-50. Response of the tower in y-direction due to 1989 Loma Prieta earthquake

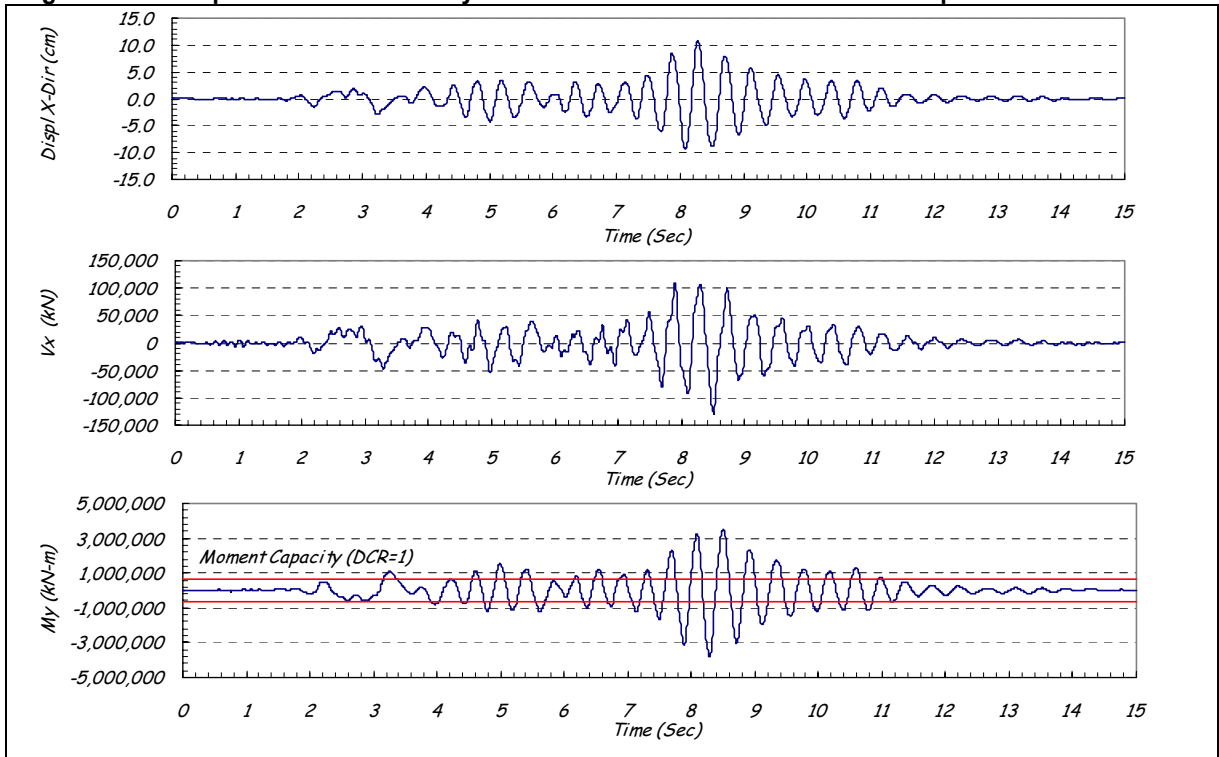


Figure 4-51. Response of the tower in x-direction due to 1971 San Fernando earthquake

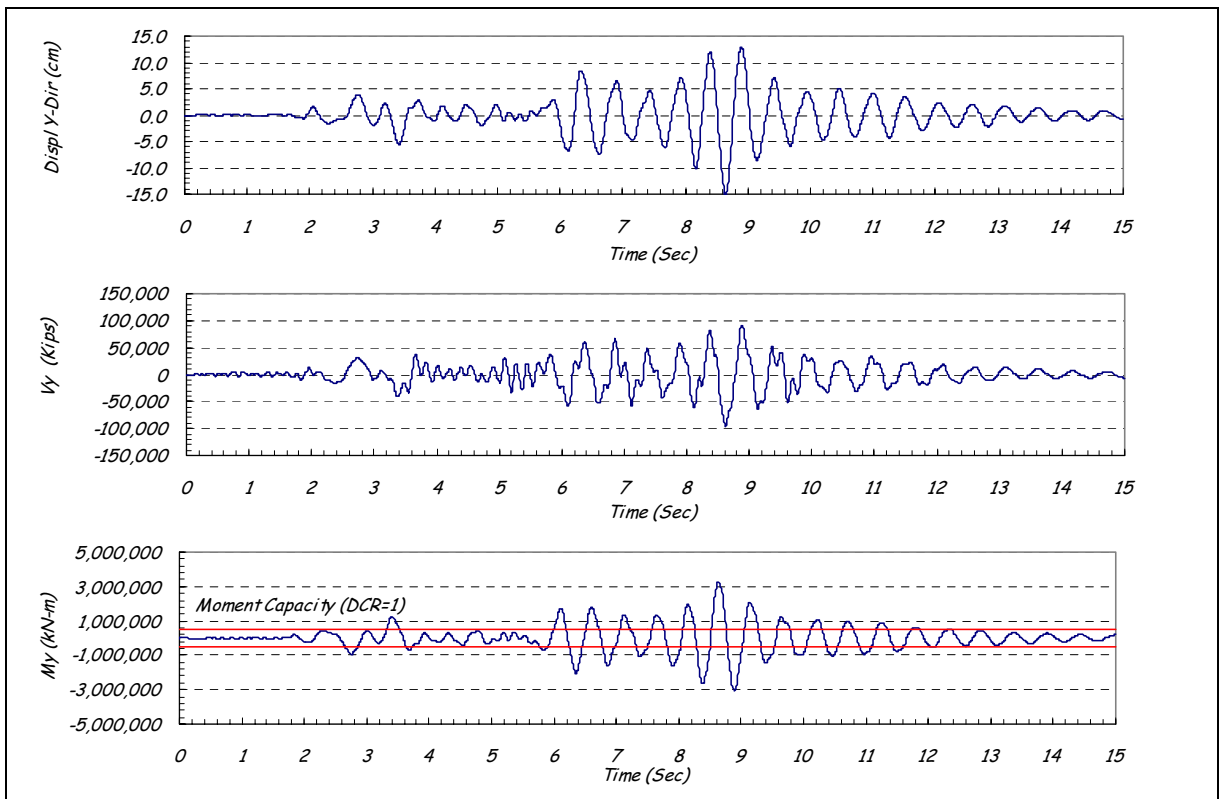


Figure 4-52. Response of the tower in y-direction due to 1971 San Fernando earthquake

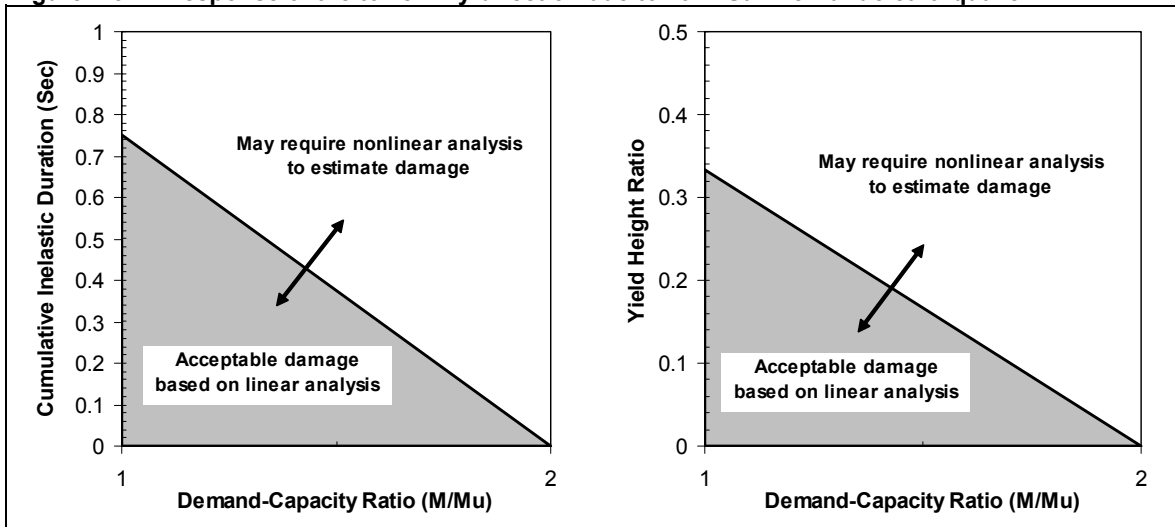


Figure 4-53. Structural performance assessment for free-standing reinforced concrete intake towers based on linear-elastic time-history analysis

(Figure 4-55) show reasonable agreement with the results of nonlinear analyses. The performance curves for the 1966 Parkfield and 1987 Whittier Narrows records fall below the acceptance curves, except for yield height ratios due to the 1966 Parkfield record applied in the transverse direction. The performance curves for the 1989 Loma Prieta and 1971 San Fernando records, even after using a 10 percent damping, rise above the acceptance curves. These results show reasonable agreement with the results of nonlinear analyses, thus validating the accuracy of the damage criteria.

e. Load combination cases. Gravity load in the form of self-weight should be combined with the earthquake ground motion when the analysis includes one or more of the following: axial force-bending moments interaction, vertical component of ground motion, P-delta effect, rocking, or sliding. Furthermore, the rocking or sliding analysis, if required, should include the uplift pressure at the base of the tower as well as the load due to weight of the contained water. Other static loads (i.e., hydrostatic and ice) could be neglected if their effects are negligible.

f. Demand-capacity ratios. The demand-capacity ratio for tower elements is defined as the ratio of calculated maximum force to the corresponding element capacity limit. Demand-capacity ratio should be computed for bending moments as well as axial and shear forces. Under no conditions should the shear or axial forces exceed their capacity limit. When the effects of axial or shear force are critical, the nonlinear analysis should be undertaken to estimate the damage, regardless of the bending moment demand-capacity ratio.

g. Presentation and performance evaluation. An example intake tower was analyzed using four different earthquake records to demonstrate the performance evaluation process discussed in *a*, *b*, and *c* above. The overall process involves presentation and evaluation of the following results:

(1) General description and load combinations. General description of the computer model and all applicable loads and load combinations should be provided. Exclusion of any particular load or load combinations should be discussed and justified.

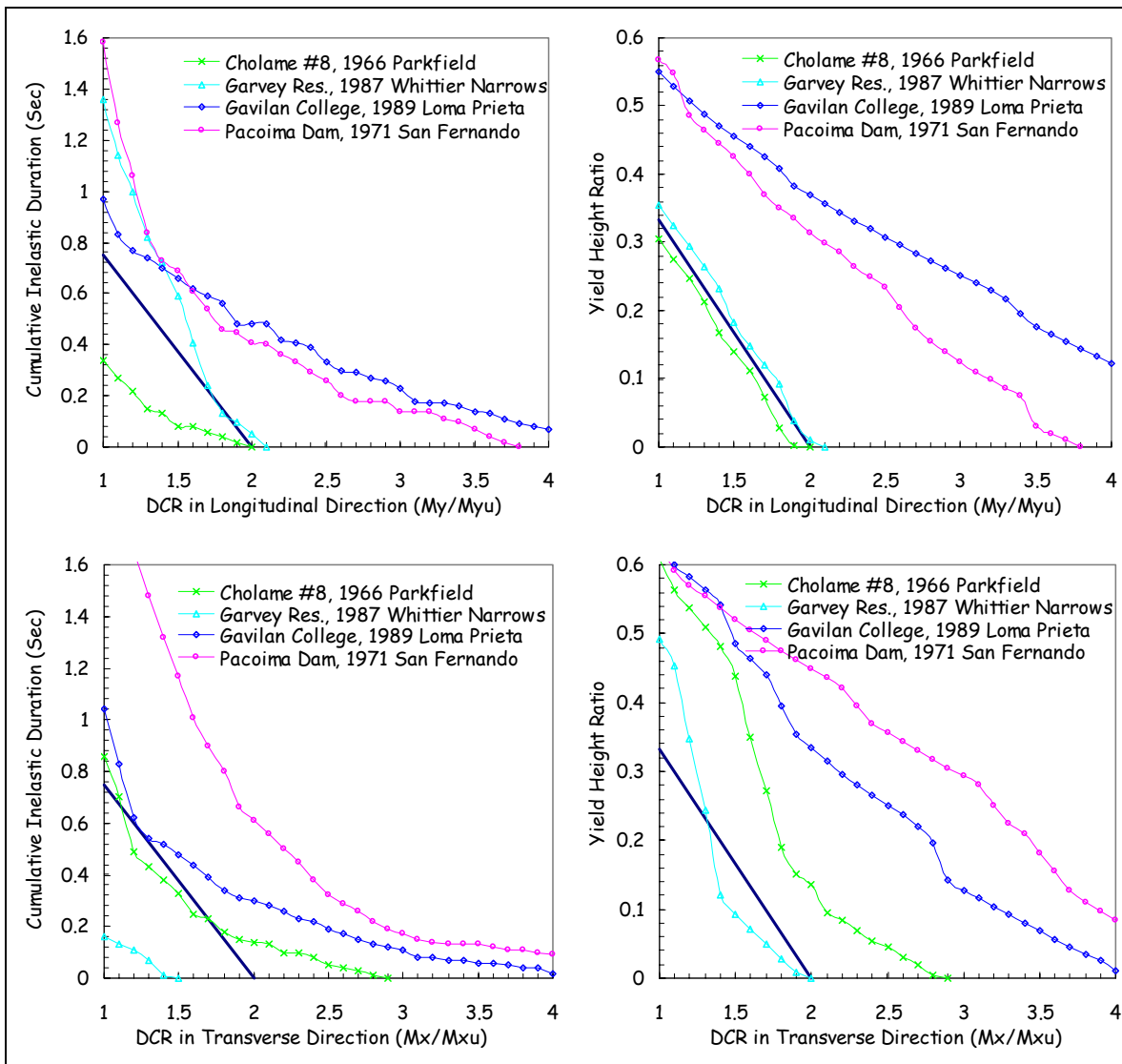


Figure 4-54. Structural performance assessment curves with 5 percent damping

Table 4-18
Global Ductility Factors for Various Ground Excitations

Time-History No.	Earthquake Record	Global Ductility	
		X-Dir.	Y-Dir.
1	Cholame #8, 1966 Parkfield	1.33	1.90
2	Garvey Res. 1987 Whittier Narrows	1.41	1.22
3	Gavilan College, 1989 Loma Prieta	2.96	4.22
4	Pacoima Dam, 1971 San Fernando	2.49	4.45

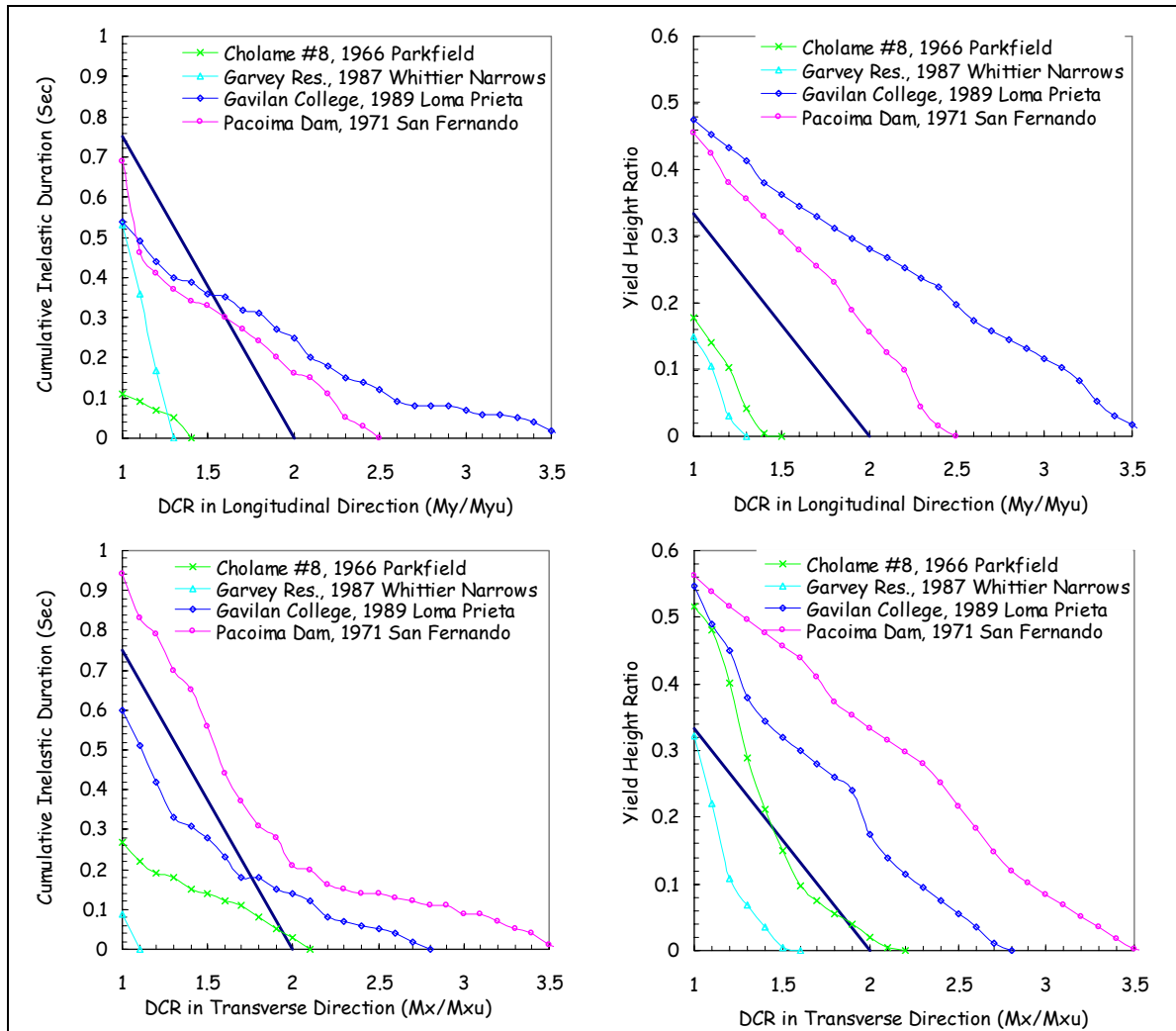


Figure 4-55. Structural performance assessment curves with 10 percent damping

(2) Natural frequencies and mode shapes. Natural frequencies and mode shapes are presented to gain insight into the dynamic characteristics of the tower. The natural frequencies are also used to ensure that the earthquake input is sufficiently energetic in the frequency range of importance to the tower.

(3) Displacement time-history response. The magnitudes and time-histories of displacements at the critical locations, usually at the top of the tower, should be presented.

(4) Time-history of element forces. The magnitudes and time-histories of the section forces exceeding their corresponding capacities should be presented and employed to compute the cumulative inelastic duration.

(5) Demand-capacity ratios. The maximum bending moments and shear and axial forces should be computed and incorporated in plots for comparison with the acceptance performance curves.

Chapter 5 Development of Acceleration Time-Histories

5-1. Introduction

a. Purpose and scope. This chapter describes procedures for the development of site-specific acceleration time-histories of ground motions for seismic analyses of hydraulic structures throughout the United States.

b. Objective of acceleration time-history development. The overall objective in developing acceleration time-histories is to have a set or sets of time-histories that are representative of site ground motions for the design earthquake(s) and that are appropriate for the types of analyses planned for specific structures.

c. Organization of chapter. Paragraph 5-2 provides an overview of the approach to and process of developing time-histories. Paragraph 5-3 describes criteria for the initial selection of acceleration time-histories. Paragraphs 5-4 and 5-5 describe two alternative methodologies for final development of design time-histories using the time-histories selected as described in paragraph 5-3. Paragraph 5-6 provides guidance for modifying time-histories for the response of local site conditions. Appendices B through D provide further details on various aspects of time-history development.

5-2. Overview of Approach for Time-History Development

This paragraph outlines the recommended general approach for developing acceleration time-histories for the seismic analysis of hydraulic structures. The process outlined below is described in greater detail in subsequent paragraphs of this chapter. The process is summarized in chart form in Figure 5-1.

a. Initial selection of candidate time-histories. Before time-histories are developed, design earthquakes and design ground motion characteristics are developed for the project. This process includes characterizing the tectonic environment of the site; characterizing the design earthquake(s) in terms of magnitude(s), distance(s) from the site, and other factors (e.g., type of faulting); characterizing the local site conditions; and developing design site ground motion characteristics for the design earthquakes. For the seismic design of concrete hydraulic structures, the design ground motion characteristics typically include smooth design response spectra (which also include the zero-period acceleration that is equal to the peak ground acceleration), duration of strong shaking, and special ground motion characteristics (e.g., near-source pulsive motions). Guidelines for the development of site-specific design response spectra of ground motions are presented in EM 1110-2-6050. Given these characteristics of the design earthquakes and ground motions, time-history records are then selected from the available database of recorded ground motions that are reasonably consistent with the design parameters and conditions. If sufficient recorded motions are lacking, simulated-recorded time-histories can be developed using ground motion modeling methods.

b. Modification of time-history records and development of final sets of time-histories.

(1) Although the time-histories are initially selected to be reasonably consistent with the seismic setting, design earthquake, and design ground motions, these time-histories and their response spectra may still differ substantially in amplitude from the design ground motion levels. This is because design ground motion characteristics are typically defined on the basis of statistical analysis of ground motion data, and these data

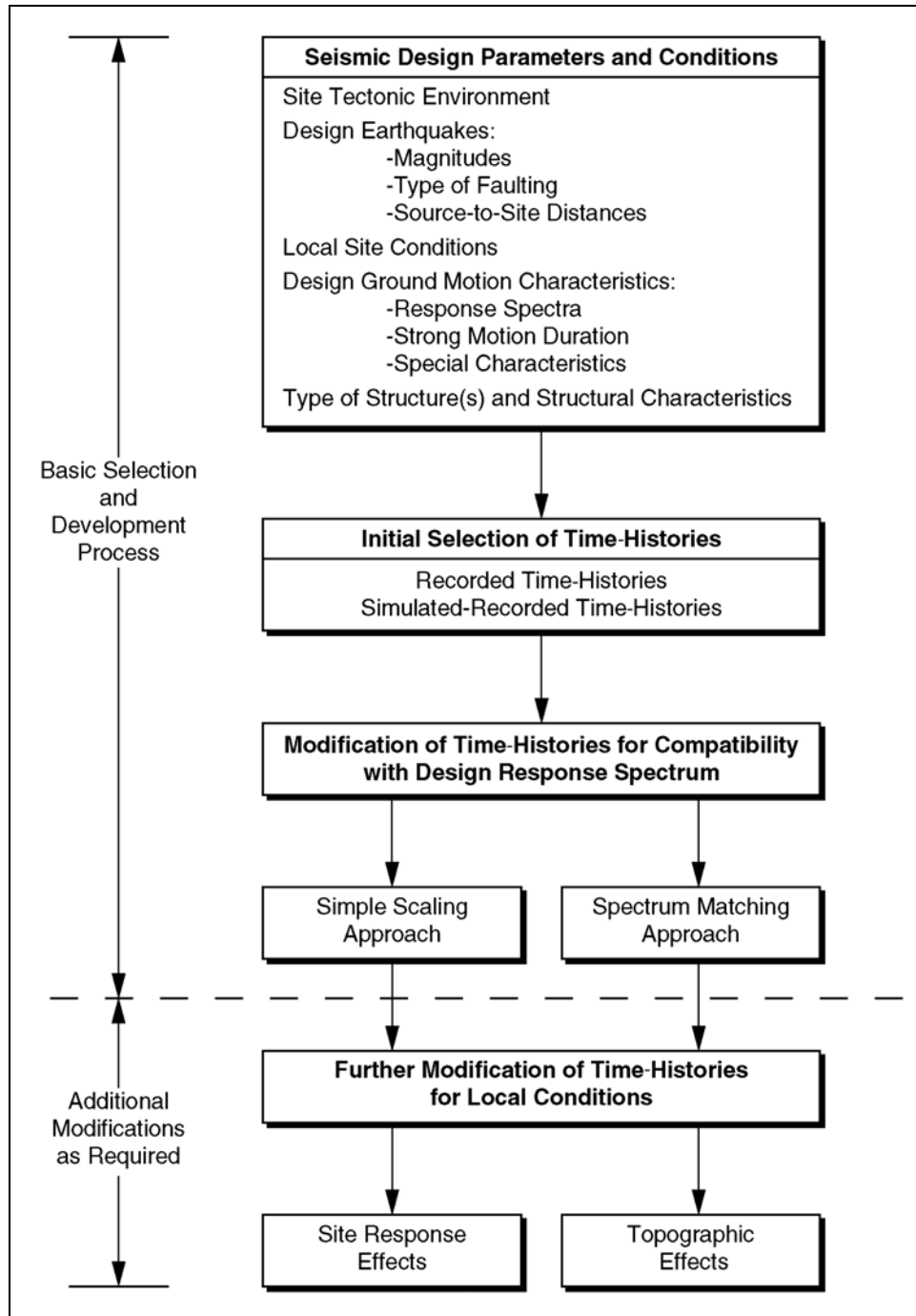


Figure 5-1. Process for developing time-histories for seismic analysis and design

exhibit considerable scatter. Therefore, any single ground motion record may have characteristics that lie above or below mean ground motions defined statistically for a given design earthquake.

(2) Two approaches may be used to adjust or modify the selected time-histories to be closer to the design ground motion conditions. In the first approach, the only modification to a given time-history is simple scaling (by a single factor) of the time-history so that its spectrum is at the approximate level of the design response spectrum in the period range of significance to structural response. Because the spectrum of any

recorded time-history has peaks and valleys, it is likely that this scaling will result in a spectrum that exceeds the smooth design spectrum at some periods and is lower than the design spectrum at other periods. Therefore, additional time-histories will probably need to be selected and scaled so that the spectra of the set of time-histories provide an aggregate match or fit to the design spectrum. In the second approach, a time-history is first scaled and its frequency content then modified so that its spectrum is a good match to the smooth design spectrum (spectrum matching approach).

c. Further modification of time-histories for local conditions. If time-histories in *b* above are developed for bedrock underlying a site and it is desirable to modify them for the overlying soil profile, then site response analyses may be conducted in which the rock time-histories are propagated through an analytical model of the site soil profile. Because it is usually assumed that the acceleration time-histories developed in *b* above are representative of ground motions on level ground, an analysis could also be considered to account for topographic effects at a site that has very irregular topography.

5-3. Initial Selection of Time-Histories

a. Use of recorded and simulated-recorded time-histories. When available for the parameters and conditions of a design earthquake, actual earthquake time-history records should be selected as the initial time-histories that are subject to further scaling or modification for use in seismic analysis. However, in some cases, few or no time-histories may have been recorded during earthquakes similar to the design earthquake. Conditions for which there are relatively few actual earthquake recordings include the following:

- Moderate- to large-magnitude earthquakes in the central and eastern United States.
- Large-magnitude (i.e., magnitude ≥ 8) shallow crustal earthquakes.
- Near-source, large-magnitude (magnitude ≥ 7) earthquakes (although the number of recordings for magnitude $.6-1/2$ to 7 earthquakes has significantly increased in recent years, and the number of recordings for magnitude >7 earthquakes has been greatly increased by the 1999 earthquakes in Taiwan and Turkey).

In cases where suitable recordings are lacking, consideration should be given to developing initial ground motion time-histories using theoretical (numerical) ground motion modeling methods that simulate the earthquake rupture and the source-to-site seismic wave propagation. The methods are being increasingly used to develop time-histories, especially where ground motion data are lacking. Appendix B summarizes the overall approaches involved in ground motion simulation and examples of the application of these approaches.

b. Selection criteria for time-histories. The selection of recorded acceleration time-histories should be guided by the following criteria:

(1) Tectonic environment. Candidate time-histories should have been recorded in a tectonic environment similar to that for the design earthquake. Within the United States the following tectonic environments are generally recognized as being somewhat distinct: shallow crustal fault earthquakes in the western United States (WUS); subduction zone earthquakes along coastal northwest California, Oregon, Washington, and Alaska; and earthquakes in the central and eastern United States (CEUS) (roughly east of the Rocky Mountains).

(2) Earthquake magnitude and type of faulting. Magnitudes of earthquakes generating selected time-histories should be close to (within approximately one-half magnitude unit of) the design earthquake

magnitude. The type of faulting (i.e., strike-slip, reverse, normal, oblique) for the earthquake preferably should be the same as that postulated for the design event, but this is less important than selecting time-histories from earthquakes of similar magnitude.

(3) Earthquake source-to-site distance. The source-to-site distances of earthquakes for selected time-histories should be similar to the design source-to-site distance. The preferred source-to-site distances for the selected time-histories should be within a factor of 2 of the design distance. However, for design source-to-site distances of less than 10 km, it is desirable to select time-histories recorded at distances from 0 to about 10 km in order to have near-source characteristics in the time-histories.

(4) Subsurface conditions. The subsurface conditions for the selected time-histories preferably should be similar to the project site condition for which design time-histories are desired (e.g., rock, deep firm soil). However, if a sufficient number of recordings for the same site condition are not available, records from firm soil sites can substitute for those recorded on rock and vice versa.

(5) Response spectrum characteristics of time-histories. Ideally, the response spectrum of an acceleration time-history selected for use in seismic analysis would have amplitudes similar to those of the design response spectrum. However, some amount of scaling of the time-history is usually required to bring its spectrum to the approximate level of the design spectrum. As a general guideline, it is desirable that time-histories selected for seismic analysis not require scaling upward or downward by more than a factor of about 2 to bring their spectra on average to the approximate level of the design spectrum in the period range of significance for structural response.

(6) Duration of strong shaking.

(a) The duration of strong shaking should be specified for the design earthquake. For the time-histories selected for analysis, strong motion duration should generally be within a factor of 1.5 of the duration specified for the design earthquake. It is more important that the duration not be underestimated than that it be overestimated. For prediction of strong motion duration on rock in the WUS, the correlation of significant duration with magnitude developed by Dobry, Idriss, and Ng (1978) and shown in Figure 5-2 can be used. The correlation is considered by the authors to be valid for the magnitude range of 4.5 to 7.6. The distance distribution of the data used by the authors suggests that the correlation is reasonably applicable within about 50 km of the earthquake source. An increase in duration with distance may be expected for greater distances. In Figure 5-2, the equation for the median prediction of duration is given; the standard deviation for the logarithm (base 10) of duration is equal to 0.13. In this correlation, duration is defined as the time required to build up from 5 to 95 percent of the integral

$$\int_{t=0}^{t=t_f} a^2 dt \quad (5-1)$$

where t_f is the total duration of a time-history and a is acceleration. Arias (1970) showed that this integral is a measure of the energy of an accelerogram. Figure 5-3 illustrates this definition of strong motion duration in the form of a Husid plot (after Husid 1969), which shows the buildup of the energy of an accelerogram with time and the time interval for 5 to 95 percent energy buildup. Duration on soil sites tends to be longer than on rock sites and is more widely scattered. Based on data presented by Dobry, Idriss, and Ng (1978), duration on soil sites may be approximated as 1.5 to 2 times the value estimated for rock sites.

(b) Lack of strong motion data has prevented development of a correlation similar to that in Figure 5-2 for the CEUS. Figure 5-2 and the characterizations discussed in the preceding paragraph may be used to approximately characterize the duration of strong shaking in the CEUS.

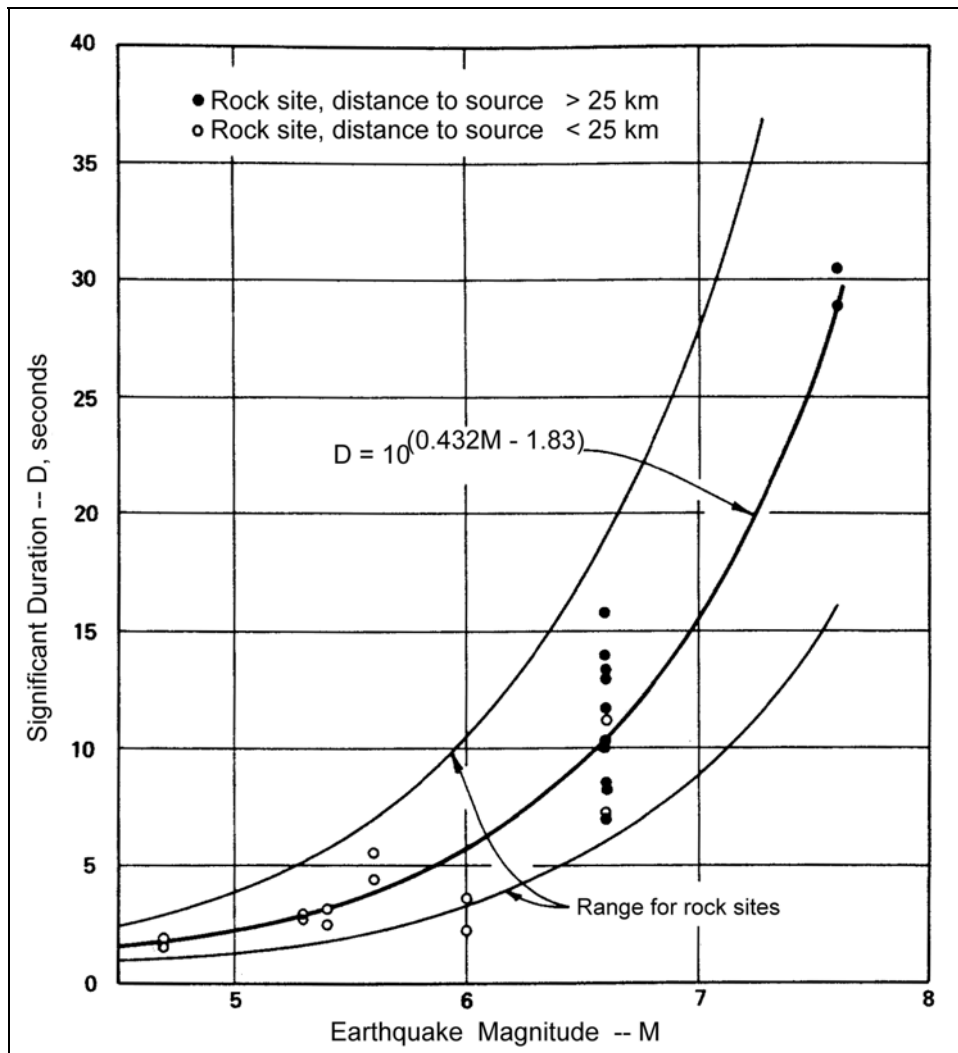


Figure 5-2. Correlation for duration of strong shaking on rock in the western United States (from Dobry, Idriss, and Ng 1978, courtesy of *Seismological Society of America*)

(7) Pulse characteristics and sequencing. No general correlations exist relating how the characteristics and sequencing of acceleration pulses vary with earthquake characteristics, distance, or site conditions. It is well known, however, that in the near-fault region, ground motion time-histories often contain a strong intermediate- to long-period pulse that is a result of the fault rupture process. Therefore, at least some of the acceleration time-histories used for design in the near-source region (i.e., within about 10 km of the fault rupture) should contain a strong ground motion pulse. It has also been found that this pulse is directional in nature, being stronger in the direction perpendicular to the fault strike (i.e., fault-normal component) than parallel to the fault strike (i.e., fault-parallel component) (e.g., Somerville et al. 1997). The ground motion pulse near faults is illustrated in Figure 5-4 for the Rinaldi recording obtained during the 1994 Northridge earthquake. Guidelines for characterizing the response spectral content of near-source pulsive ground motions are presented by Somerville et al. (1997). A limited amount of research has also been conducted on the time-domain characteristics of the near-source pulse; results are presented by Somerville (1998) on the period and peak amplitude of the velocity pulse.

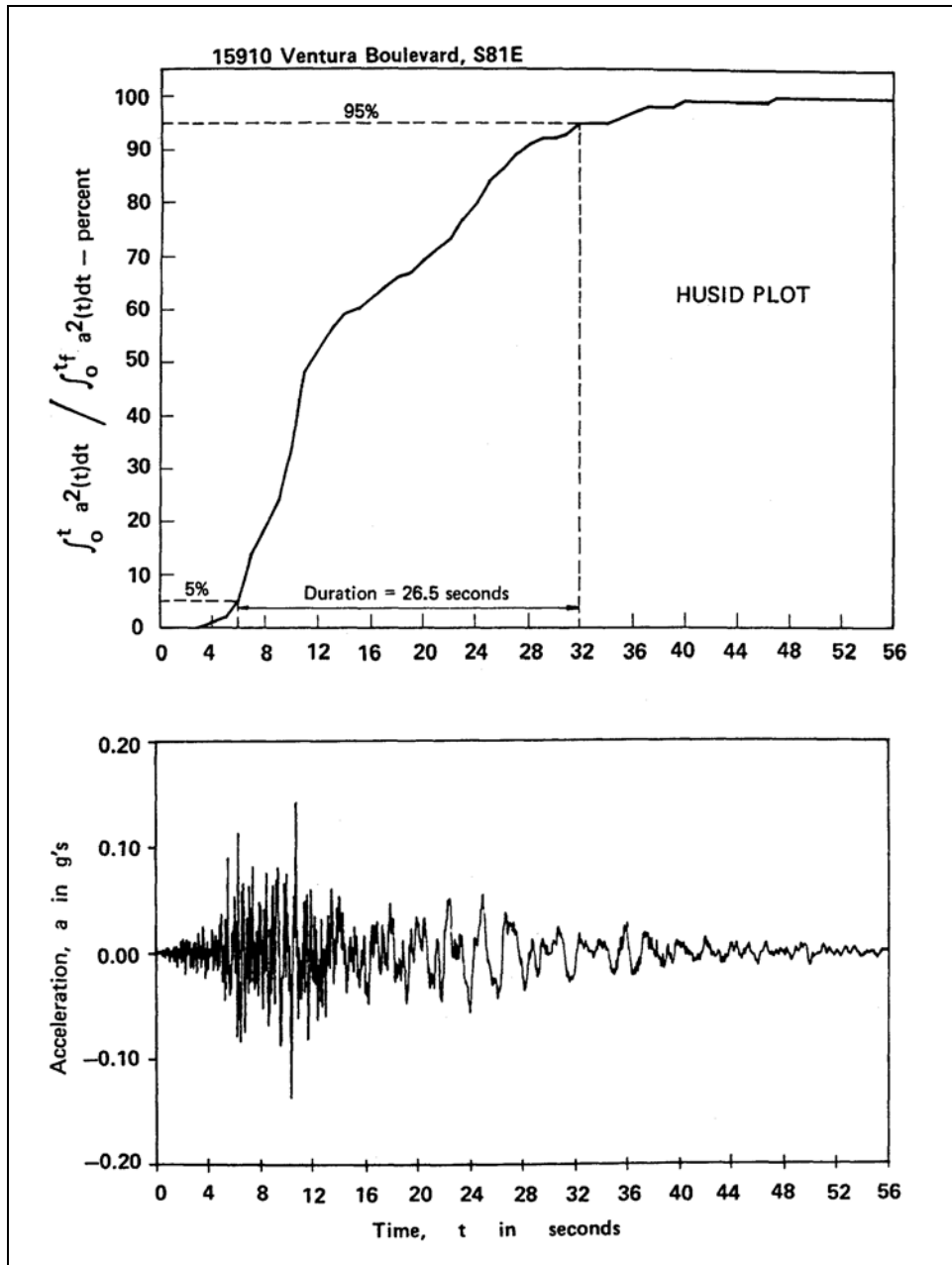


Figure 5-3. Typical Husid plot and duration as defined by Trifunic and Brady (1975) and Dobry, Idriss, and Ng (1978) (from Idriss 1979, courtesy of American Society of Civil Engineers)

c. Selection of records for deterministically defined and probabilistically defined earthquakes.

(1) Application of these guidelines is straightforward when design earthquakes are expressed deterministically, i.e., in terms of magnitude, faulting type, and source-to-site distance. However, the application of the guidelines is less straightforward when the design earthquake ground motions (typically the response spectrum) are derived from a probabilistic ground motion analysis (often termed a probabilistic seismic hazard analysis or PSHA). From this type of analysis, which is described in detail in EM 1110-2-6050, the design response spectrum for a certain selected probability of exceedance in a design time period (or, equivalently,

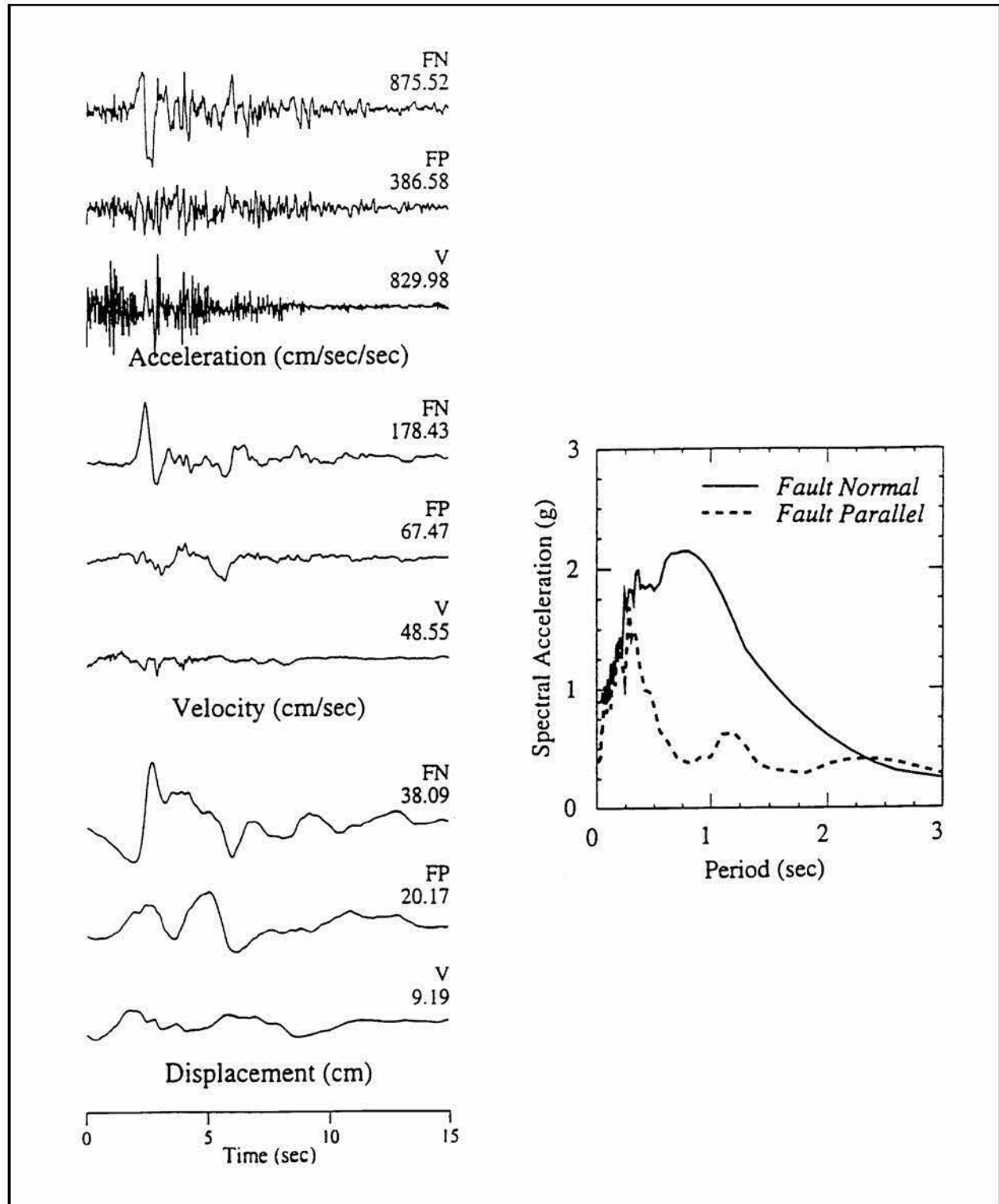


Figure 5-4. Time-histories and horizontal response spectra (5 percent damping) for the strike-normal and strike-parallel components of ground motion for the Rinaldi recording obtained 4.5 miles (7.5 km) from the fault rupture during the 1994 Northridge, California, earthquake (Somerville 1997)

for a design return period) reflects the contribution of different earthquake magnitudes and distances to the probabilities of exceedance. Therefore, when the design response spectrum is probabilistically based, the PSHA should be deaggregated to define the relative contributions of different magnitudes and distances to the ground motion hazard. Furthermore, the deaggregation should be done for probability values or return periods that correspond to those of the design earthquake and for response spectral periods of vibration of significance for seismic structural response because the relative contributions of different magnitudes and distances may vary significantly with return period and period of vibration.

(2) Figure 5-5 illustrates deaggregation of seismic hazard at a site in the western United States located close to highly active faults. The variation in relative contributions of different magnitudes and distances with return period (RP) and period of vibration T is evident. In the example in Figure 5-5, if the design return period is 1,000 years and the periods of interest for structural response are short periods close to 0.3 sec, then the center lower panel of the figure indicates that contributions would be strongly centered about magnitude 6.5 and distances within 10 km. Therefore this magnitude and distance range should be considered representative in selecting time-histories and defining strong motion duration.

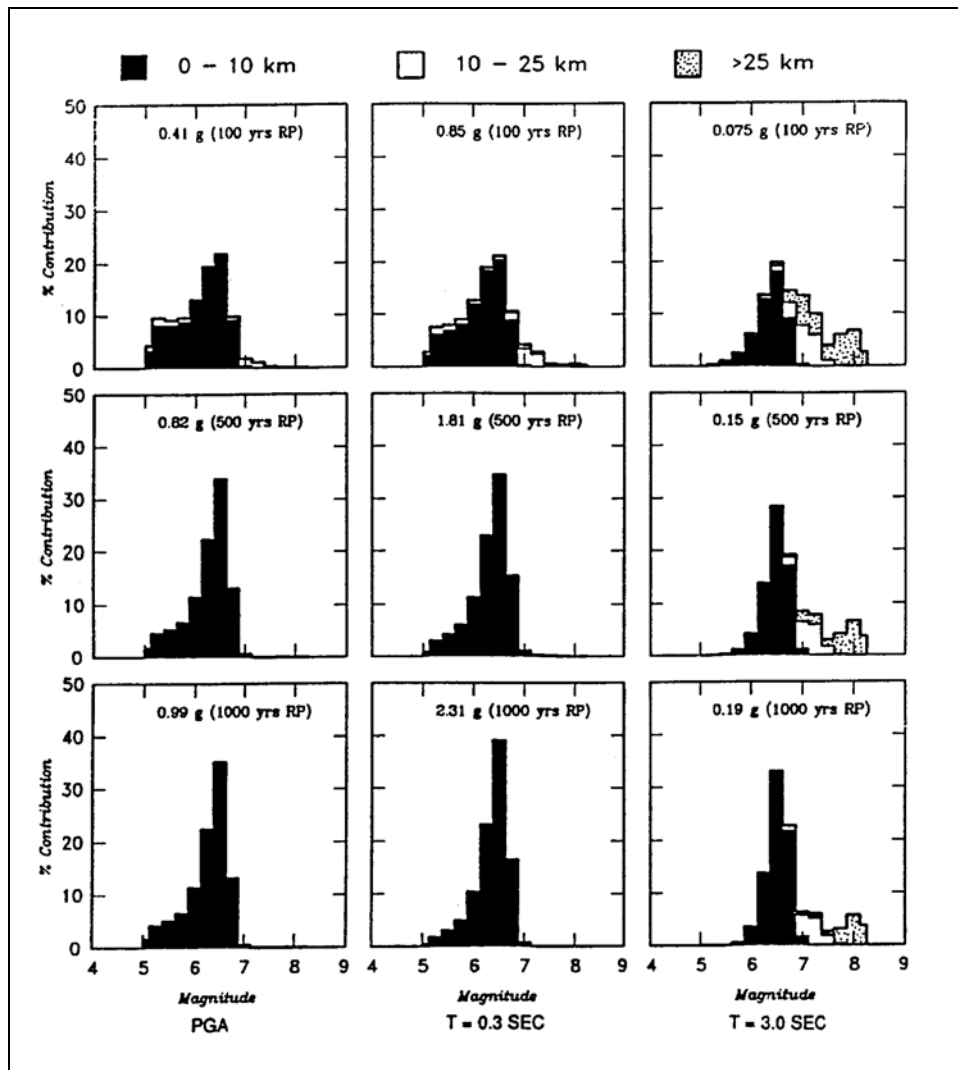


Figure 5-5. Example of deaggregation of seismic hazard from a probabilistic seismic hazard analysis in the western United States

(3) Figure 5-6 illustrates deaggregation of seismic hazard at a site in the eastern United States located in a low-seismicity area in which seismic sources are characterized as source zones. In this example, for a design return period of 2,500 years, earthquake magnitudes in the range of about 5 to 6.5 and distances in the range of 0 to 50 km dominate contributions to a 0.3-sec hazard. In this case, it would be appropriate to select a magnitude of about 5.5 to 6 and a distance of about 15 km as the average magnitude and distance to consider for selecting (or synthesizing) time-history records.

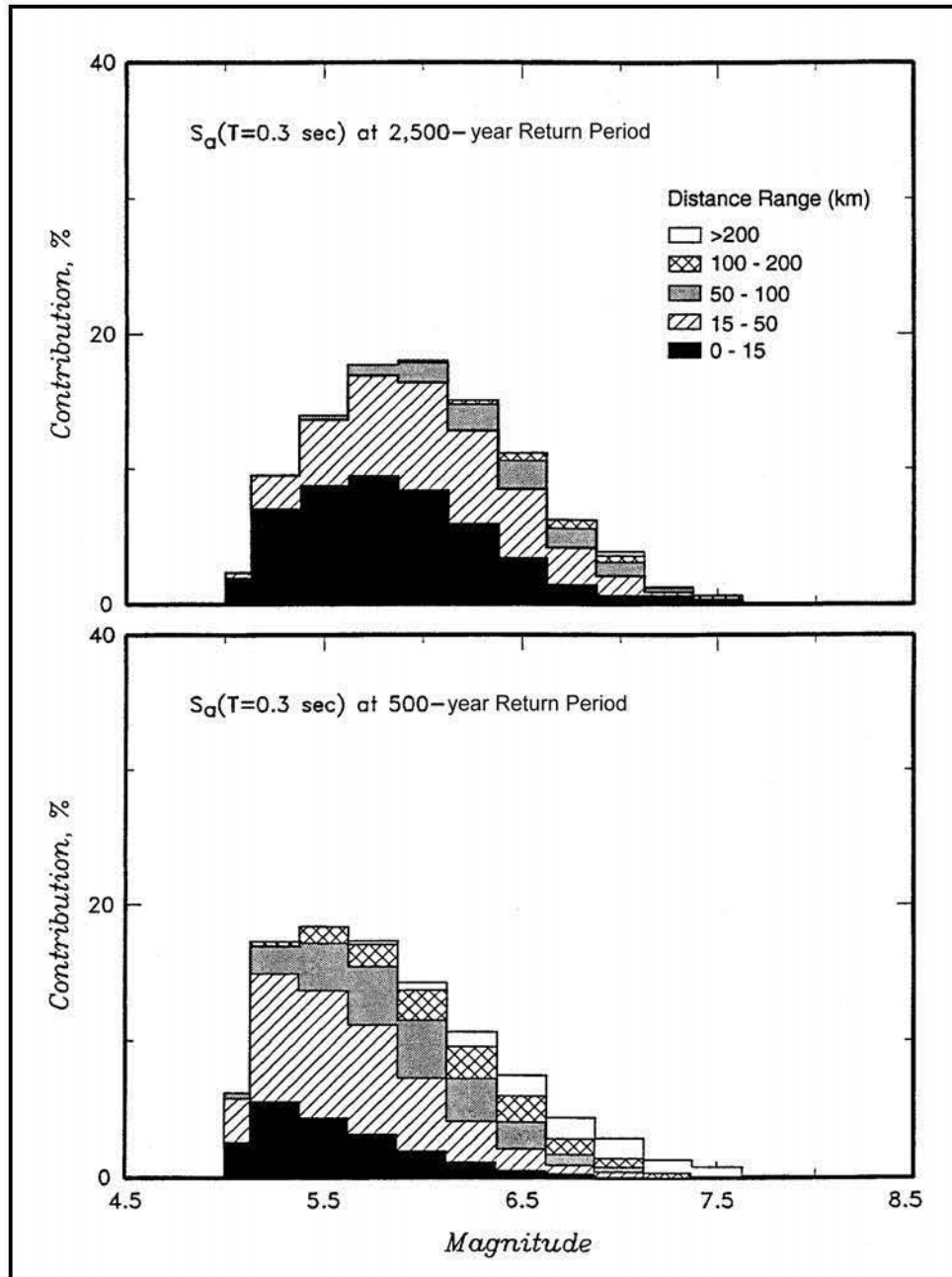


Figure 5-6. Example of deaggregation of seismic hazard from a probabilistic seismic hazard analysis in the eastern United States

(4) Note that for probabilistic analyses at some sites, for a given return period, relative magnitude and distance contributions may vary significantly with period of vibration within the period range of significance for structural response (generally the influences of larger magnitudes and larger distances increase with increasing period of vibration). Where this is the case, consideration should be given to selecting different time-history sets for the earthquakes contributing to different parts of the period range. However, this variation of magnitude and distance contributions with period of vibration is less significant for stiff concrete hydraulic structures having low fundamental periods of vibration than for long-period structures. In some other cases, deaggregation of a PSHA may show a distinct bimodal contribution to the hazard for certain periods of vibration (e.g., major contributions from both nearby moderate-magnitude earthquakes and distant large-magnitude earthquakes). In these cases, it may be appropriate to select time-history sets for both earthquakes. Again, this type of result of a PSHA is usually seen for long periods of vibration and not the shorter periods that are typical of concrete hydraulic structures.

5-4. Simple Scaling Approach to Final Development of Acceleration Time-Histories

a. General. Time-histories to be considered for seismic analysis are those initially selected as described in paragraph 5-3. Using the simple scaling approach, each selected time-history is then scaled by a single factor so that the response spectrum of the scaled time-history is approximately at the level of the design smooth response spectrum in the period range of significance to structural response. Since a recorded (or simulated recorded) time-history typically contains peaks and valleys at different periods, it is likely that, after scaling, the degree of agreement of the smooth design spectrum and the spectrum of the scaled time-history will vary greatly with period. In the following subparagraphs, guidelines are presented for the minimum number of time-histories to be used for seismic analysis and the degree of agreement of the fit of spectra of the time-histories to the design spectrum.

b. Number of time-histories.

(1) Time-histories for use in linear dynamic analysis. For use in linear dynamic analysis, at least three time-histories (for each component of motion) should be used for each design earthquake.

(2) Time-histories for use in nonlinear dynamic analysis. For use in nonlinear dynamic analysis, at least five time-histories should be used (for each component of motion) for each design earthquake. Fewer time-histories are required for linear dynamic analysis than for nonlinear analysis because the dynamic response of a linear structure is determined largely by the response spectral content of the motion, whereas the response of a nonlinear structure may be importantly influenced by the time domain character of the time-history (e.g., shape, sequence, and number of pulses) in addition to the response spectrum characteristics. Since these time domain characteristics may vary greatly for time-histories having similar spectral content, more time-histories are required for nonlinear analysis to capture the variability in response. If the nonlinear response is found to be significantly sensitive to the time-history characteristics for the records selected, then the set of time-histories should be expanded.

c. Degree of spectrum fit of time-histories used with the design spectrum.

(1) Spectrum fit for individual time-histories. Each time-history should be scaled to the approximate level of the design response spectrum. As a guideline, the scaling factor should be initially selected such that the sum of the differences (calculated period by period) of the logarithms of the spectral accelerations of the scaled time-history and the logarithms of the design response spectrum is approximately equal to zero over the period range of significance to structural response. Although it is desirable to implement this guideline quantitatively, it is also satisfactory to implement it qualitatively by obtaining an average, visual fit of the spectrum of the scaled time-history to the design response spectrum. Note that the scaling and resulting

spectrum fit for individual time-histories may have to be adjusted in order to satisfy the aggregate fit requirements stated in (2) below.

(2) Aggregate spectrum fit requirements for time-history sets. For each component of motion used in the analysis, a mean spectrum of the individual spectra of the time-histories should be calculated period by period. The mean spectrum should not be more than 15 percent lower than the design response spectrum at any period in the defined period range of significance to structural response. Furthermore, over the defined period range of significance, the average of the ratios of the mean spectrum to the design spectrum should be equal to or greater than unity. Figure 5-7 illustrates a comparison of spectra of four scaled time-histories with a design spectrum that satisfies these aggregate fit requirements over the period range 0 to 0.6 sec (selected in this example as the period range of significance to structural response). The individual time-histories in this example were initially scaled according to the quantitative guideline stated in paragraph (1) above, and the scaling factors were then adjusted for the time-histories to meet the aggregate fit requirements of this paragraph.

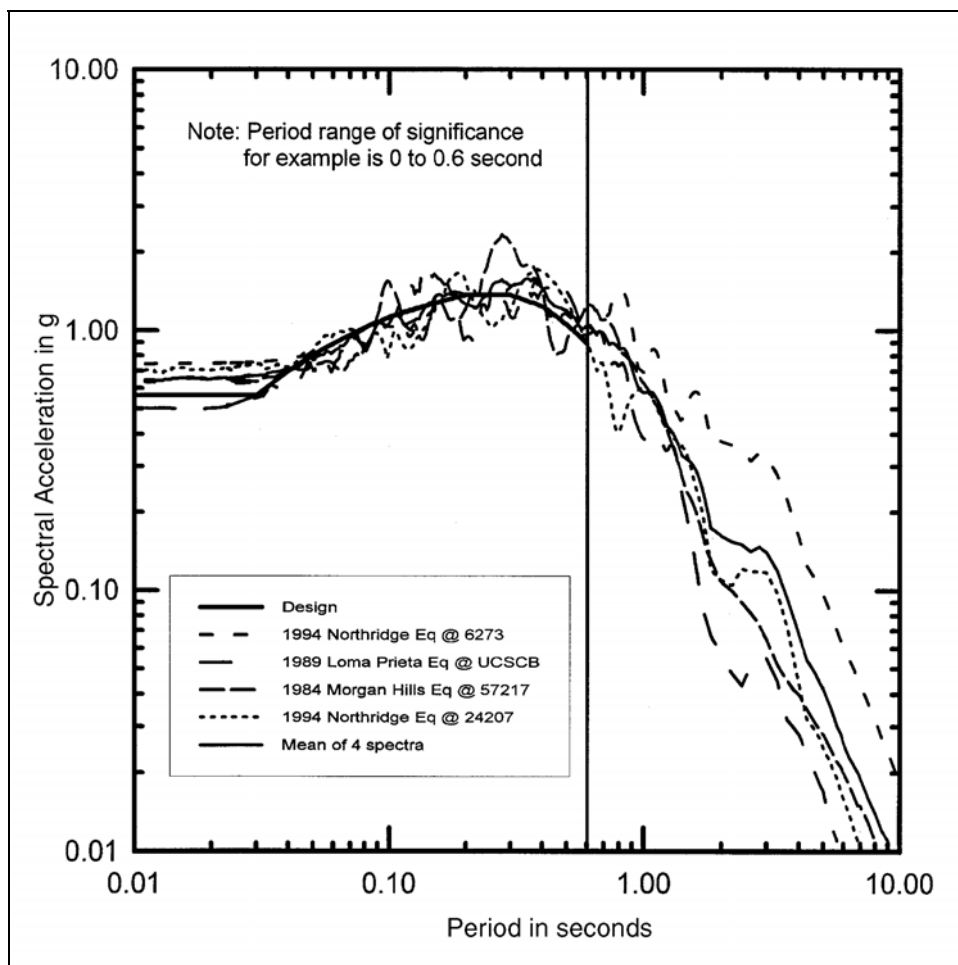


Figure 5-7. Illustrative comparison of spectra for four scaled time-histories and the mean spectrum with a designed spectrum in a period range of significance to structural response

d. *Considerations for dynamic analysis for multiple components of motion.* The criteria presented in c(2) above for the degree of spectrum fit are applicable for a single component of motion from each ground

motion record used in the analysis. There are additional considerations and alternatives when the seismic analysis requires more than one component of motion (i.e., 1 horizontal + 1 vertical; 2 horizontal; or 2 horizontal + 1 vertical components). In these cases, the following alternatives may be considered for scaling the different components of each ground motion record.

(1) Use same scaling factors for each component. With this approach, the scaling factors for the component that is most important to response (e.g., the horizontal component to be applied perpendicular to the axis of a dam) are applied to the selected time-histories such that the fit criteria in *c(2)* above are satisfied. The same scaling factors are then used for the other component(s) of motion required for the analysis. This approach has the advantage that the relative amplitudes of different components of the same record are preserved. However, the aggregate fit to the design spectrum for the other component(s) of motion may be poorer than the fit for the primary component (i.e., aggregate fit in *c(2)* above may not be satisfied for the other components). This approach may be considered when structural response is dominated by one component of motion. The aggregate fit for the other components should be examined by the seismic analyst with respect to its influence on structural response. If the structural response is not adequately captured, additional scaling of the time-histories should be performed.

(2) Using different scaling factors for each component. With this approach, different scaling factors are applied as required to each component of motion. The aggregate fit criteria stated in *c(2)* are applied to each component. This approach has the advantage that for each component of motion, a good aggregate spectral fit will be obtained. The disadvantage is that the relative amplitudes of different components of the same record are not preserved. This approach is acceptable but is less desirable than the approach of alternative (1).

5-5. Spectrum-Matching Approach to Final Development of Acceleration Time-Histories

a. General. Using the time-histories selected as described in paragraph 5-3, the first step is to scale the time-histories to be the approximate level of the design response spectrum in the period range of greatest significance to structural response. This step is the same as that described in paragraph 5-4c(1) for the scaling approach. Then, the spectral content of the time-histories is modified to provide a close match to the design spectrum using spectrum-matching techniques. The following subparagraphs present guidelines for the number of time-histories to be used for seismic analysis and the degree of agreement of the fit of the spectra of the time-histories with the design spectrum, describe different types of spectrum matching methods and periods of vibration to be used for matching, and summarize the advantages and disadvantages of the spectrum matching approach versus the simple scaling approach.

b. Number of time-histories.

(1) Time-histories for use in linear dynamic analysis. Because the response of a structure in a linear dynamic analysis is determined by the spectral content of the time-history and because it is possible to obtain a very close fit to the design spectrum using spectrum-matching methods, it is sufficient to have a single time-history for each component of motion for each design earthquake.

(2) Time-histories for use in nonlinear dynamic analysis. Because the nonlinear structural response may be strongly affected by the time-domain character of the time-histories even if the spectra of different time-histories are nearly identical, the requirements for numbers of time-histories are the same as for the simple scaling approach. At least five time-histories (for each component of motion) should be used for each design earthquake.

c. Degree of spectrum fit of time-histories used with design spectrum. When multiple time-histories are used (for a single component) for each design earthquake, a mean spectrum of the individual spectra of time-histories should be calculated. The requirements for the fit of this mean spectrum are the same as for the

simple scaling approach stated in paragraph 5-4c(2): the mean spectrum should not be more than 15 percent lower than the design response spectrum in the period range of significance to structural responses; and the average of the ratios of the mean spectrum to the design spectrum should be equal to or greater than unity over this same period range. If a single time-history is used (for a single component), then the degree of fit of the spectrum of this time-history should be the same as stated in this paragraph for the mean of the spectra of multiple time-histories.

d. Considerations for dynamic analysis for multiple components of motion. In cases where two or three components of motion are needed for dynamic analysis, the objective for each component is to have a close match to the design horizontal and vertical spectrum. Therefore, for each component, time-histories should initially be scaled to the approximate level of the design spectrum as stated in *a* above and then spectrum matching carried out to provide the degree of fit stated in paragraph *c* above.

e. Spectrum-matching methods.

(1) Spectrum matching methods include methods in which the time-history adjustments are made in the time domain and those in which the adjustments are made in the frequency domain. These methods are described and illustrated in Appendix C. As illustrated therein, either method is capable of producing design time-histories that not only have spectra that are a close match to a design response spectrum but also have time-histories that, in most cases, maintain fairly well the basic time-domain character of the recorded or simulated recorded time-histories with respect to shape, sequence, and number of pulses.

(2) To minimize changes to the time-domain character of the recorded time-histories when using the spectrum-matching approach, it is desirable that

- The overall shape of the spectrum of the recorded (or simulated recorded) time-history not differ greatly from the shape of the design response spectrum.
- As stated in *a* above, the time-history initially be scaled so that its spectrum is at the approximate level of the design spectrum to minimize the changes that occur to the time-history during the subsequent spectrum-matching process.

Figures 5-8 and 5-9 are examples of a design time-history developed using the spectrum-matching approach. Shown in these figures are the scaled time-histories (acceleration time-history and the corresponding velocity and displacement time-histories) before and after spectrum matching (Figure 5-8) and the corresponding acceleration response spectrum compared with the design response spectrum (Figure 5-9). The close spectrum match can be noted as well as the similar appearance of the time-histories before and after spectrum matching. As shown in Figure 5-9, spectrum matching was carried out in the period range 0 to 2 sec for this example. Appendix D presents an examination of the effect of the spectrum-matching process on several ground motion characteristics for ten time-histories. The appendix illustrates that the process is capable of producing time-histories having characteristics that generally do not differ greatly from those of scaled recorded motions.

f. Periods of vibration for spectrum-matching. It is important that spectrum matching be carried out for a sufficiently fine grid of periods or frequencies of vibration that the response spectrum of a matched time-history is also smooth and nearly the same as the design spectrum at intervening periods. A recommended

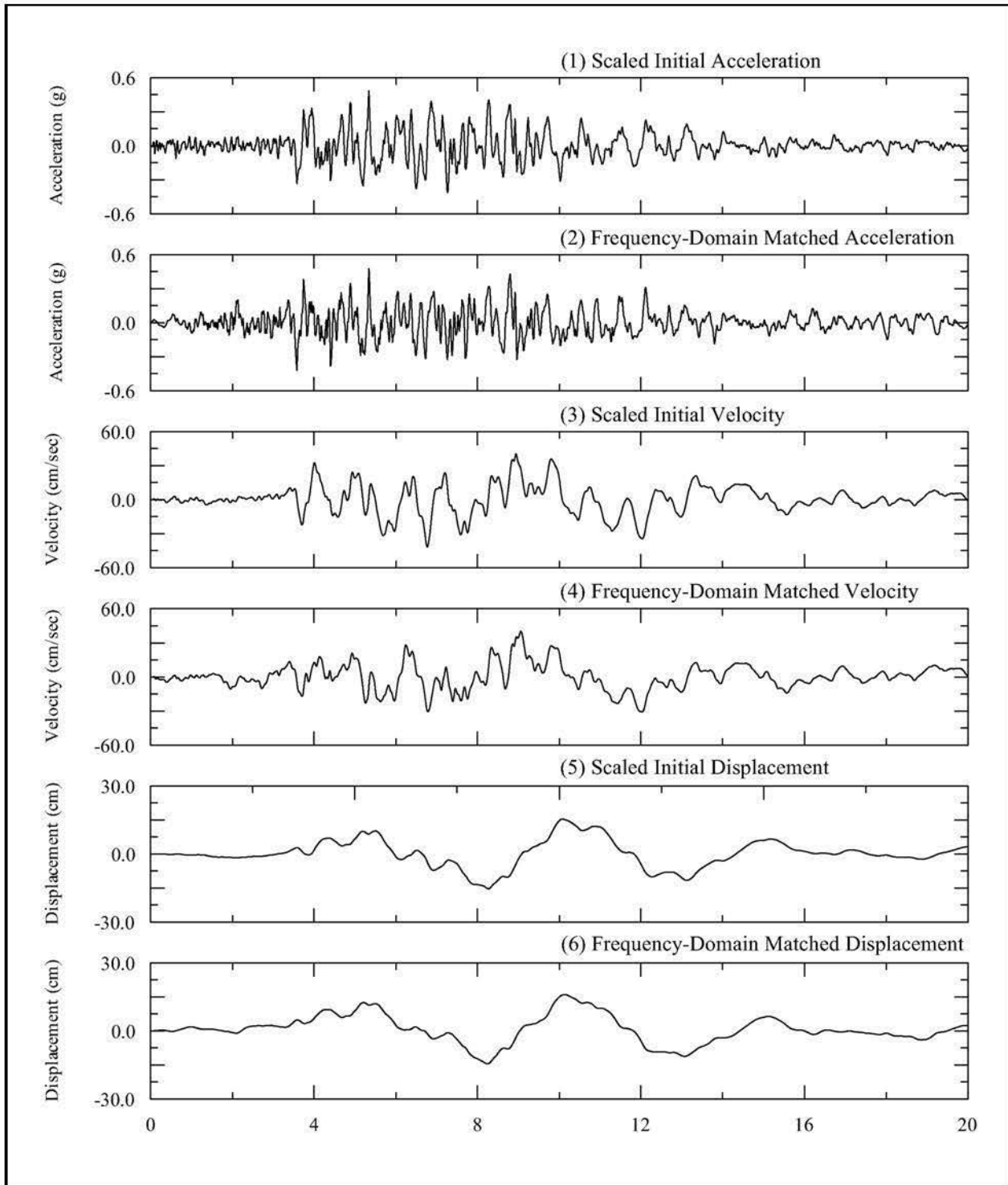


Figure 5-8. Comparisons of scaled time-histories from the 1971 San Fernando earthquake at Griffith Park (270E) to the frequency-domain matched time-histories

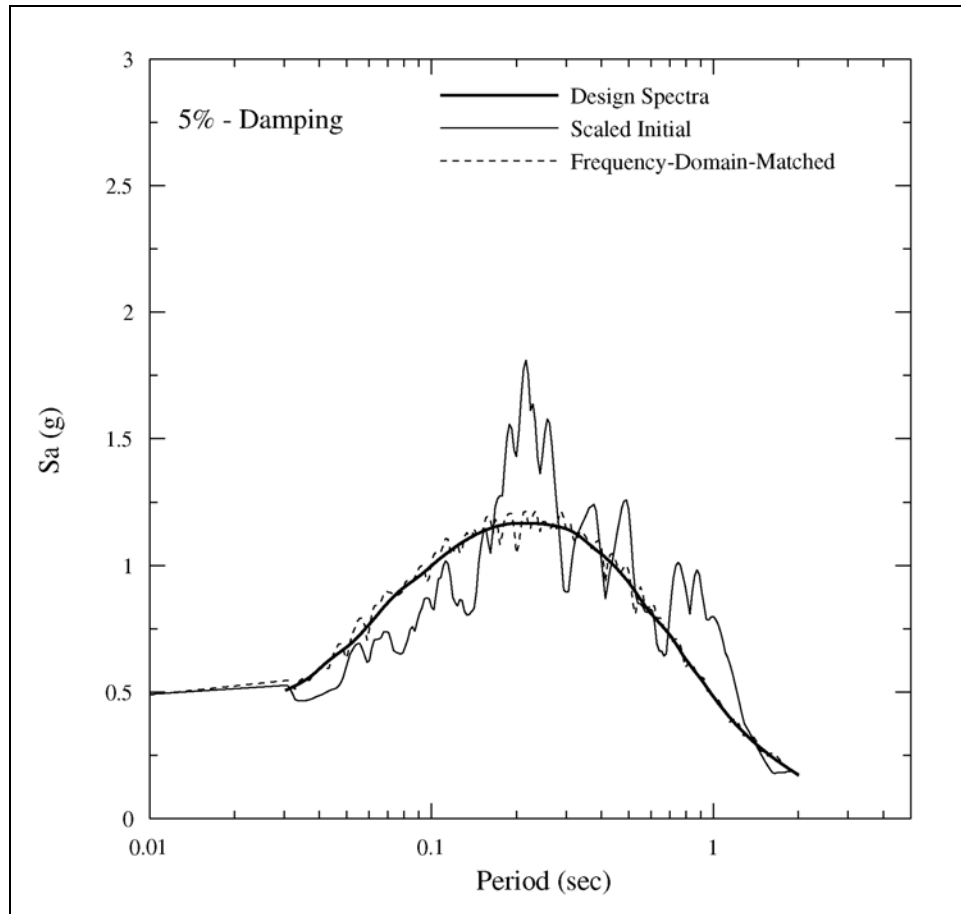


Figure 5-9. Comparisons of response spectra from the scaled 1971 San Fernando earthquake at Griffith Park (270E) and the frequency-domain matched acceleration time-history

grid of frequencies for spectrum matching to achieve this objective is 120 frequencies per decade (equally spaced on the log frequency axis).

g. Relative advantages and disadvantages of spectrum matching and simple scaling approaches for developing design time-histories. The simple scaling approach has the advantage that the time-histories are truly “natural” and represent time-domain and spectral characteristics of actual recordings (or simulated recordings), except for the scaling of the records. On the other hand, some of the “natural” quality is lost if different components of the same record are scaled by different factors (paragraph 5-4d). The spectrum matching approach has the advantage that fewer time-histories are required, at least for linear analysis. The disadvantage is that the time-domain character of the record is altered to some degree through the spectrum-matching process. The results in Appendices C and D indicate that, if the spectra of the selected scaled time-histories do not differ greatly from the design spectrum (i.e., spectral peaks and valleys of the time-histories oscillate about the design spectrum) then the changes induced by spectrum matching on the time-domain character of the time-histories are generally fairly small. Appendix D also indicates that the spectrum-matching process does not greatly change the energy of a time-history, if the spectrum of the scaled time-histories does not differ too much from the design spectrum. In summary, both the simple scaling approach and the spectrum-matching approach are acceptable provided that the guidelines for time-history selection and development presented in this chapter are followed.

5-6. Modifying Time-Histories for Site Response Effects

a. *General.* The two approaches for accounting for site soil response effects at a project site on acceleration time-histories are as follows:

- Selecting and developing the design time-histories to be representative of the type of soil conditions present at the project site using the procedures presented in the previous paragraphs of this chapter.
- Selecting and developing design time-histories for rock conditions underlying a site (using the procedures presented in the previous paragraphs) and then modifying the time-histories by propagating them through an analytical model of the site soil profile.

Either approach can be used; the choice of the approach depends on the subsurface conditions at a site and the preferences of the seismic analyst and principal design engineer. If deep and stiff soil conditions exist at a site, the depth to bedrock is not well defined, and the dynamic properties of the soil are not well defined, then generally approach 1 would be preferred. If a well-defined bedrock exists beneath a site and the stratigraphy and dynamic properties of the site can be adequately characterized, then generally approach 2 would be preferred. Approach 1 is described in the preceding paragraphs of this chapter. The additional steps involved in approach 2 are summarized below. It is noted that in many cases it may be appropriate to carry out the analyses in approach 2 as part of the dynamic analysis of the structure, rather than as an analysis only to modify the bedrock time-histories for the site soil conditions. In such cases, the dynamic analysis is of the modeled soil and structure system to the design rock time-history (soil-structure-interaction analysis).

b. *Conducting site soil response analyses.* Conducting an analysis of the response of a site soil profile to an input design rock motion time-history is schematically illustrated in Figure 5-10 and is summarized below.

(1) Modeling the soil profile. The stratigraphy and dynamic properties (dynamic moduli and damping characteristics) of the soil profile are modeled. If the soil depth is reasonably constant beneath the structure and the soil layers and ground surface reasonably flat, then a one-dimensional site-response soil model and analysis method can be used as illustrated in Figure 5-10. Two- or three-dimensional models of the site soils can be used where these conditions are not met. Unless the soil properties are very well constrained by a field and laboratory testing program, a range of properties should be defined for the soil layers to account for the uncertainties in the properties.

(2) Analysis and calculation of top-of-soil time-histories. The design bedrock time-histories are input to the soil model, the response of the model is calculated, and the corresponding top-of-soil time-histories are obtained. The rock motions are assigned to a hypothetical rock outcrop at the site rather than to the rock at depth beneath the soil column. This assignment is made because actual rock motion recordings are usually obtained at the ground surface rather than at depth and, unless the rock is rigid, the rock motion beneath a soil column will differ from the rock outcrop motion. Analysis techniques to be used (and corresponding models of soil properties) should incorporate nonlinear soil behavior either through the equivalent linear method or true nonlinear analysis methods. Computer codes that may be considered for one-dimensional analysis include equivalent linear codes SHAKE (Schnabel, Seed, and Lysmer 1972; Idriss and Sun 1992) or WESHAK (Sykora, Wahl, and Wallace 1992); and nonlinear codes DESRA-2 (Lee and Finn 1978), DESRA-MUSC (Qiu 1998), SUMDES (Li, Wang, and Shen 1992), MARDES (Chang et al. 1990) D-MOD (Matasovic 1993), and TESS (Pyke 1992). Computer codes that may be considered for 2- or 3-D analyses include equivalent linear codes FLUSH (2-D) (Lysmer et al. 1975), QUAD4M (Hudson, Idriss, and Beikae 1994), and SASSI (2-D or 3-D) (Lysmer et al. 1991) (in SASSI, equivalent linear analysis is possible only through successive external

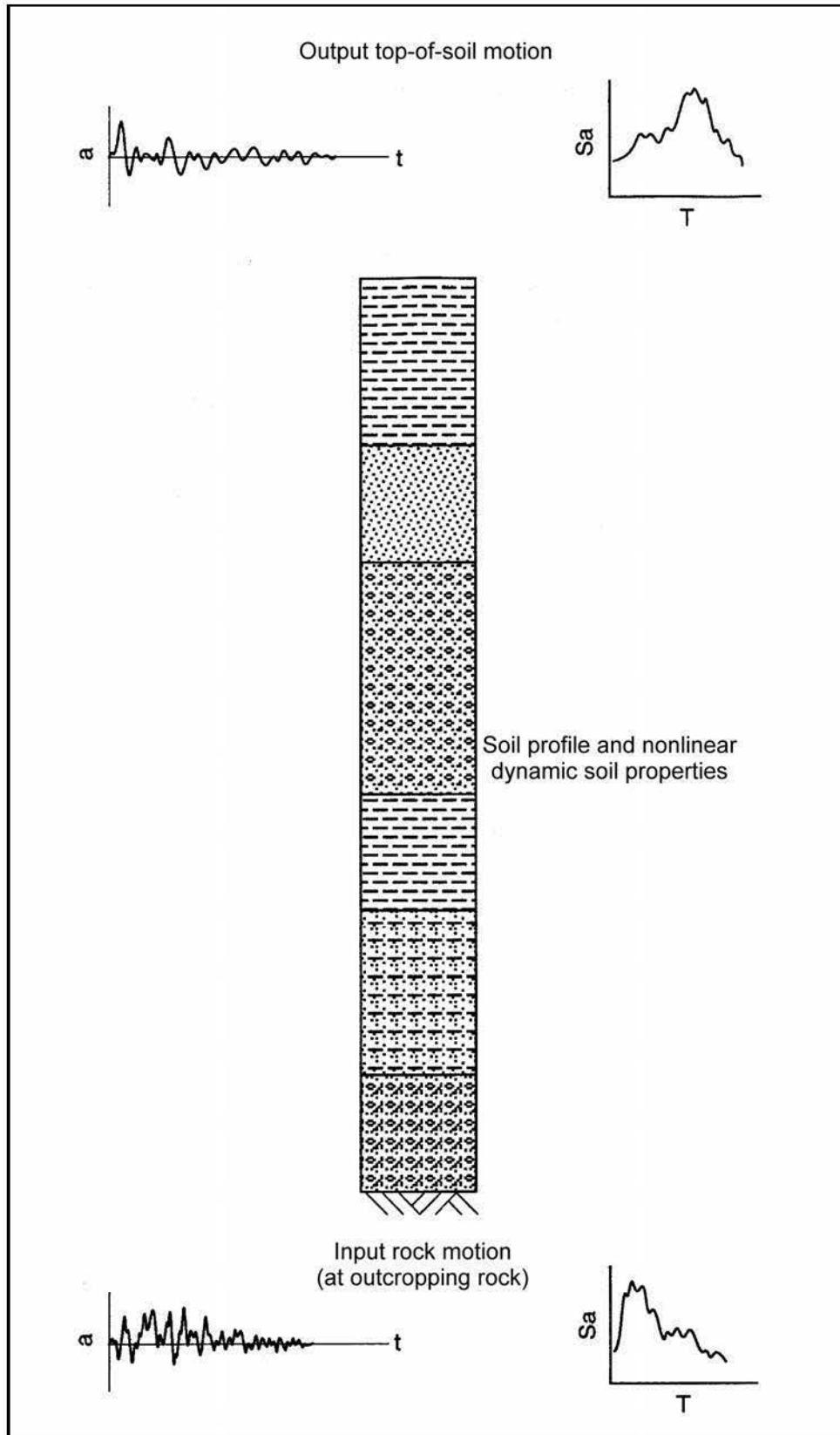


Figure 5-10. Schematic of one-dimensional site response analysis

adjustment of soil properties and iterative analysis); and nonlinear codes FLAC (Itasca 1998; Wang and Makdisi 1999), and TENSIMUSC (Martin 1998). Analyses should be carried out for a range of soil dynamic properties unless the properties are very well constrained as stated in the preceding paragraph. Soil time-histories obtained from the analyses should be baseline-corrected before using them for dynamic structural analysis.

c. Conducting other types of analyses for local site effects. Conceptually, a 3-D analysis could be carried out to determine the effect of an irregular surface topography on the ground motions, such as at an arch dam site. The topographic effects could include amplification and deamplification, differences in frequency content, and out-of-phase arrivals of the ground motions at different locations of the interface of the ground and the structure. At present, such analyses are not commonly performed because realistic modeling of the site with the irregular topography and geology would be either too costly or not well constrained by data on the characteristics of the geologic materials.

Chapter 6 Earthquake Response Evaluation of Concrete

6.1 Folsom Dam Nonoverflow Monolith

6.1-1 Background

The structure selected for this numerical example corresponds to a monolith of the concrete gravity section of the Folsom Dam and Reservoir Project, located on the American River, about 32 km (20 miles) northeast of the city of Sacramento, CA. The reservoir serves a variety of purposes. It is used to provide flood control, irrigation, and power generation. The construction of the dam, which spanned almost 8 years, was completed in 1956. The gravity dam section consists of 28 monoliths, 15.2 m (50 ft) wide each. The section selected for this numerical example corresponds to the tallest nonoverflow monolith, which was identified as the critical section in earlier studies (Hall, Woodson, and Nau 1989).

6.1-2 Purpose and Objectives

The purpose of this section is to illustrate the application of linear time-history analysis to earthquake response computation of a 2-D concrete gravity dam section. The objectives of this study are to evaluate the dynamic characteristics of the 2-D model, and to compute the seismic response of the system when subjected to horizontal ground motion using different earthquake records. Several ground acceleration records were selected to evaluate the influence of the ground excitation characteristics on the resulting dynamic performance of the structural system.

6.1-3 Scope

The scope of the study included the following:

- Definition of ground acceleration time-histories.
- Development of the 2-D finite element model of the system.
- Computation of the dynamic characteristics of the system.
- Time-history analysis of seismic performance and evaluation of results.

6.1-4 Earthquake Ground Motions

Several natural ground motions were considered for the analysis, all of them scaled up to the same value of peak acceleration. The records considered are defined in Table 6.1-1. The time-histories for these acceleration records are indicated in Figure 6.1-1, and the corresponding response spectra (3 percent damping) are shown in Figure 6.1-2.

Event	Record	Component, deg	Peak Acceleration, g's
1966 Parkfield Earthquake	Cholame #8	320	0.30
1989 Loma Prieta Earthquake	Gavilan College	337	0.30
1987 Whittier Narrows Earthquake	Garvey Reservoir	330	0.30
1971 San Fernando Earthquake	Pacoima Dam	254	0.30

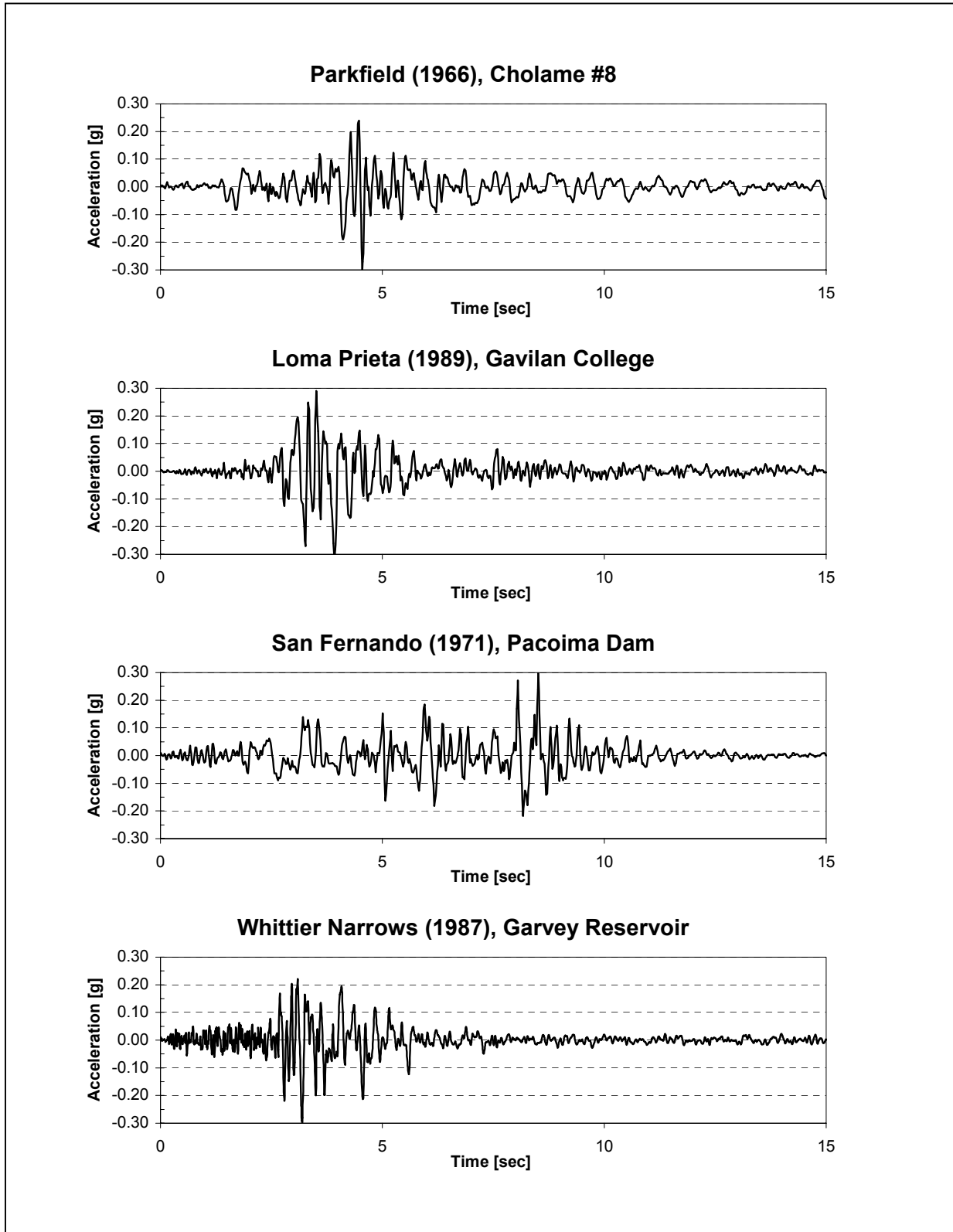


Figure 6.1-1. Ground motion acceleration time-histories used for analysis

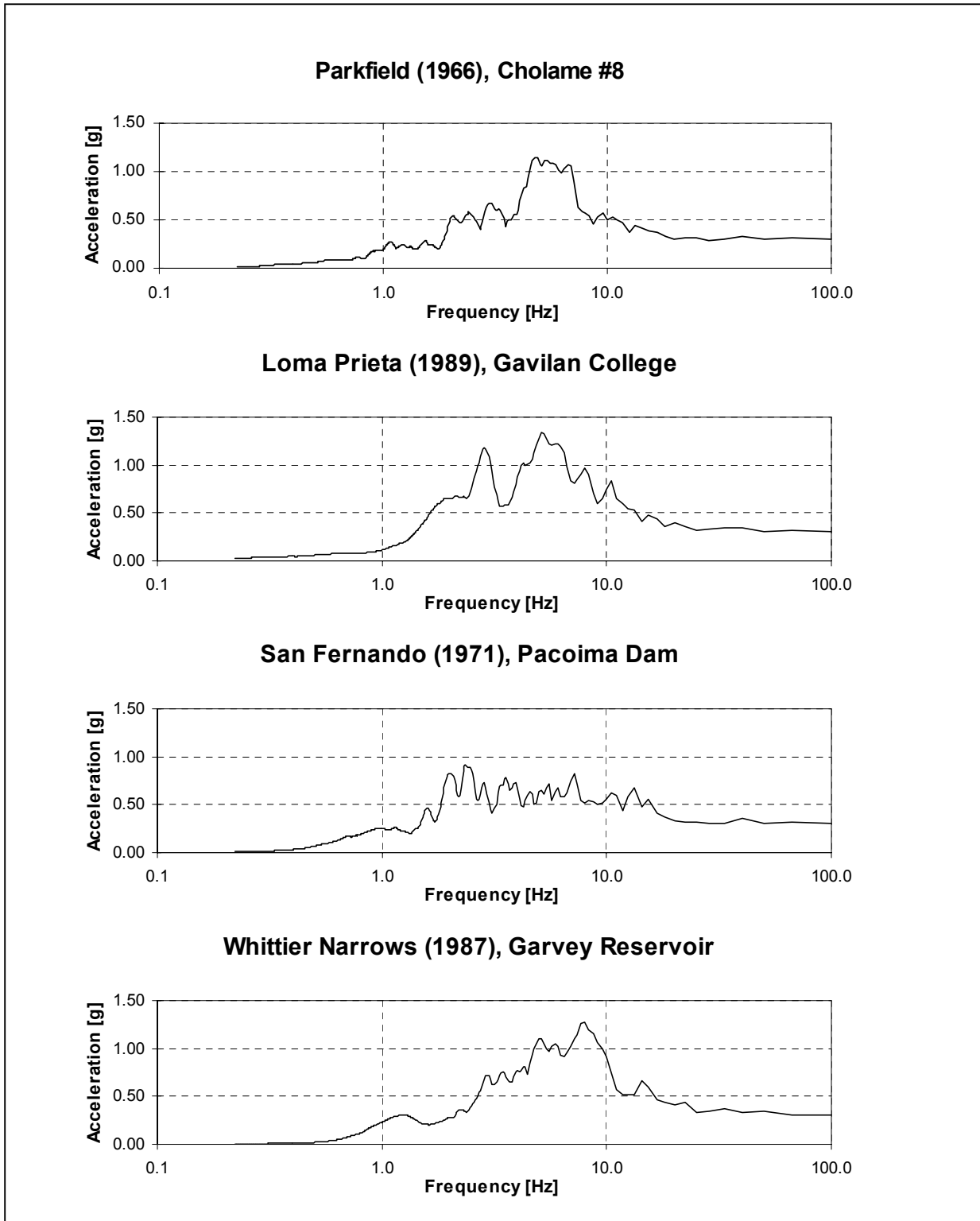


Figure 6.1-2. Response spectra for the ground motion acceleration time-histories used for analysis

6.1-5 Finite Element Analysis

The analysis in this study was restricted to the determination of the in-plane response of the critical section, which corresponds to the tallest nonoverflow monolith (monolith 11). This section was analyzed using a 2-D finite element model. The height of the monolith is 82.4 m (270.5 ft), the base is about 61 m (200 ft), and the downstream face of the section exhibits a constant-radius transition between the crest and the main body. Figure 6.1-3 shows the geometry and the finite element mesh used for the analysis. The 2-D section was modeled with 260 eight-node isoparametric elements. The foundation was assumed rigid. Assuming incompressibility of the fluid, the presence of the reservoir was incorporated into the model by a consistent added mass matrix. Linear viscous damping was represented using a proportional damping, and a 5 percent damping ratio was selected for the fundamental mode. The analyses were performed using the computer program, which computes the dynamic response of the system by implicit direct time integration of the equations of motion.

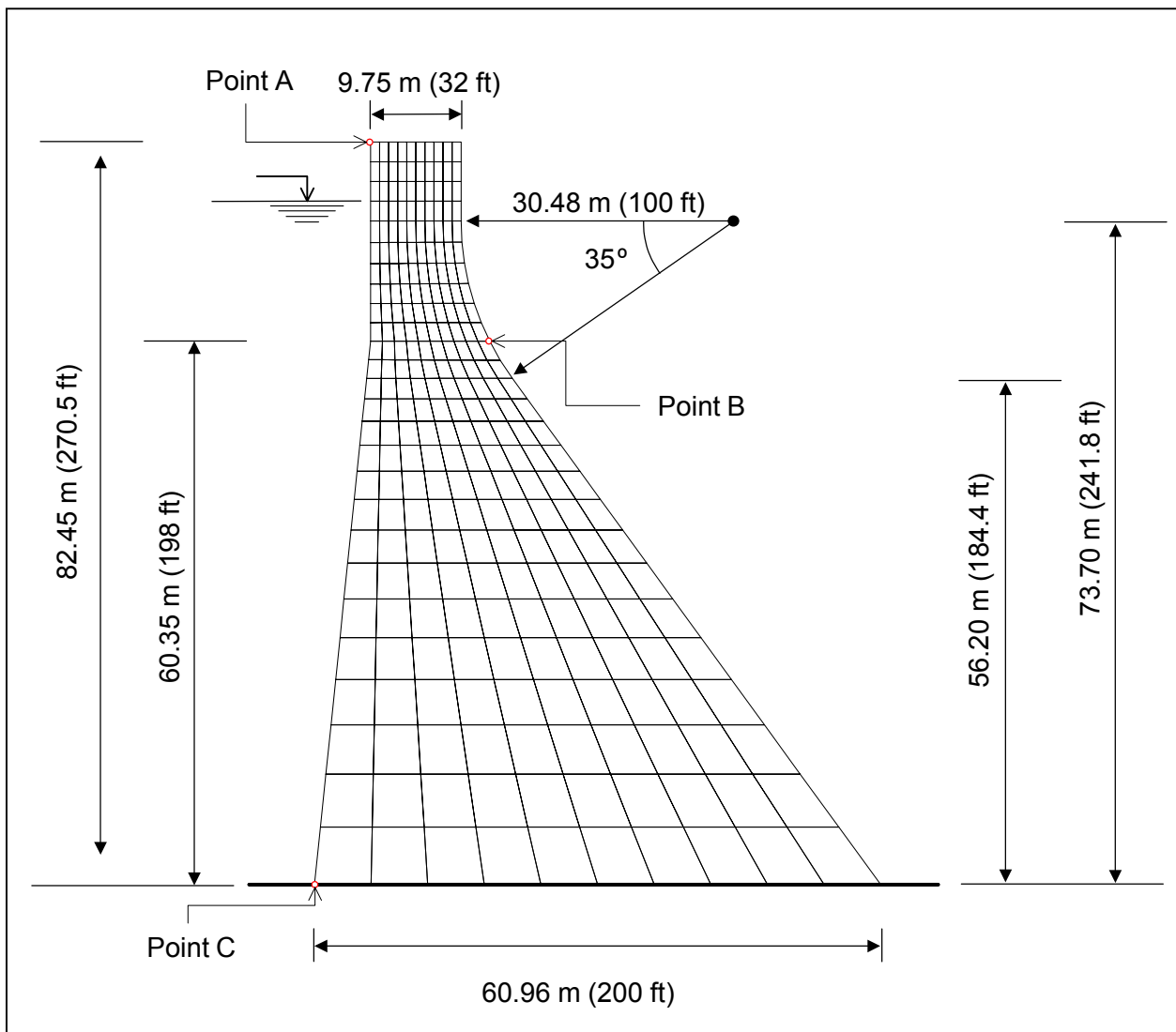


Figure 6.1-3. Section geometry and finite element model

6.1-6 Material Properties

Extensive studies have been performed to characterize the material properties of the concrete (Hall, Woodson, and Nau 1989). A summary of the results corresponding to the series of tests performed at the University of California at Berkeley is presented in Table 6.1-2.

Parameter	Value	
Modulus of elasticity	Static	37,576 MPa (5.45 10 ⁶ psi)
	Dynamic	41,024 MPa (5.95 10 ⁶ psi)
Poisson's ratio	Static	0.18
	Dynamic	0.20
Splitting tensile strength	Static	2.50 MPa (363 psi)
	Dynamic	3.72 MPa (539 psi)

The values of the material properties used in this numerical study are shown in Table 6.1-3. The values selected for the elastic modulus and the Poisson's ratio are based on the values recommended in the study by Raphael (1986).

Parameter	Value
Modulus of elasticity	40,679 MPa (5.90 10 ⁶ psi)
Poisson's ratio	0.19
Unit weight (concrete)	24,820 N/m ³ (158 lb/ft ³)
Unit weight (water)	9,802 N/m ³ (62.4 lb/ft ³)

6.1-7 Dynamic Characteristics

The first ten natural frequencies are shown in Table 6.1-4, corresponding to both empty and full reservoir conditions. The mode shapes corresponding to the first four natural frequencies are shown in Figures 6.1-4 and 6.1-5. Note that the third mode is associated with mostly vertical motion. This association explains the fact that the third natural frequency appears not to be affected significantly by the presence of the reservoir. Figure 6.1-6 shows the relative change in frequency associated with the presence of the full reservoir for the first 10 natural frequencies. It can be observed that in general the frequencies are reduced about 80 percent with respect to the dry condition, with the exception of those corresponding to the third and sixth mode shapes, which are less sensitive to the presence of the reservoir.

Mode	Empty		Full	
	Period, sec	Frequency, Hz	Period, sec	Frequency, Hz
1	0.1802	5.5484	0.2218	4.5087
2	0.0817	12.2374	0.0996	10.0376
3	0.0580	17.2467	0.0591	16.9204
4	0.0440	22.7424	0.0549	18.2103
5	0.0290	34.5188	0.0374	26.7100
6	0.0271	36.9271	0.0296	33.7884
7	0.0208	47.9964	0.0277	36.0522
8	0.0198	50.4299	0.0252	39.7354
9	0.0189	52.9105	0.0245	40.8106
10	0.0172	58.1441	0.0220	45.3576

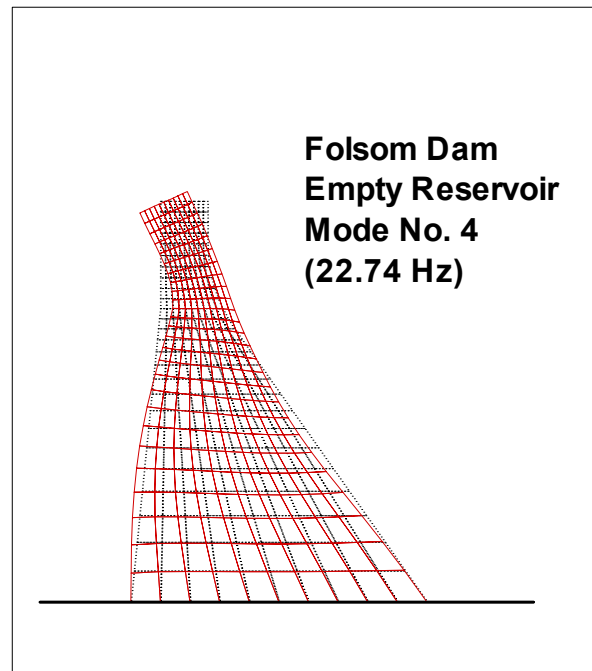
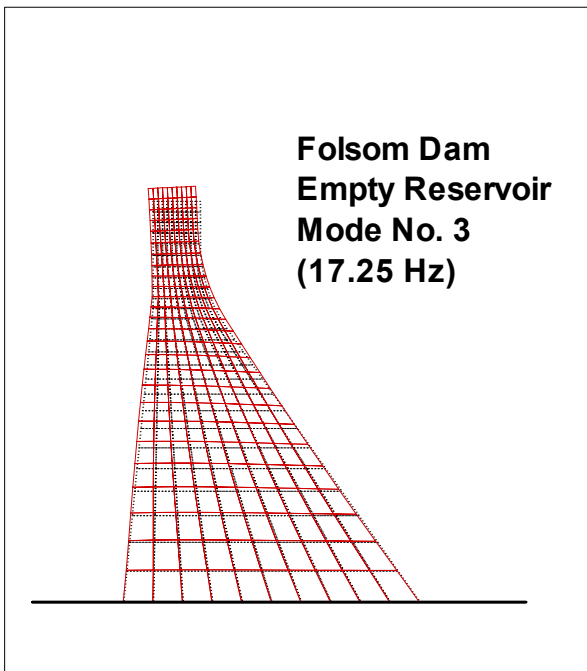
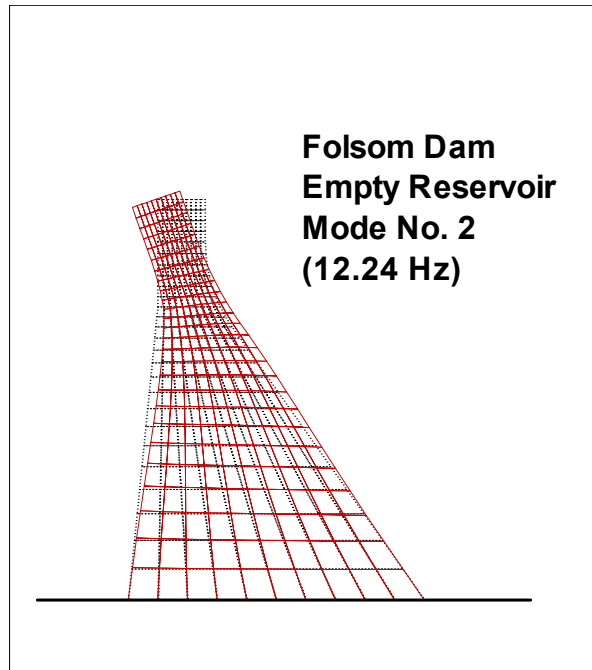
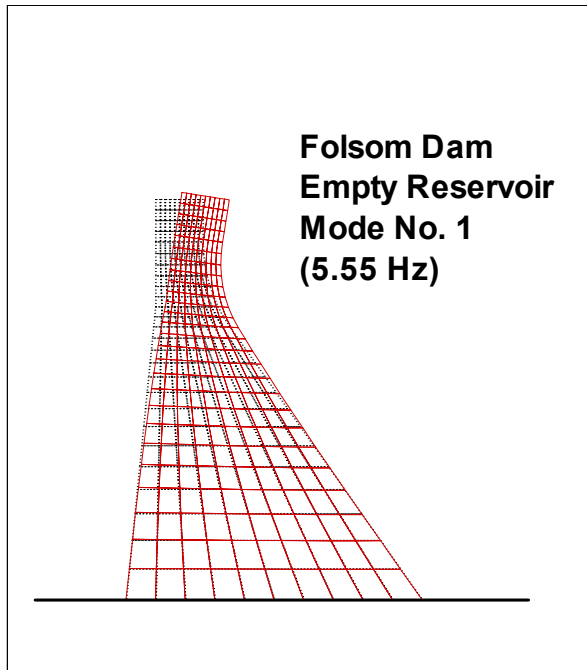


Figure 6.1-4. Mode shapes (empty reservoir)

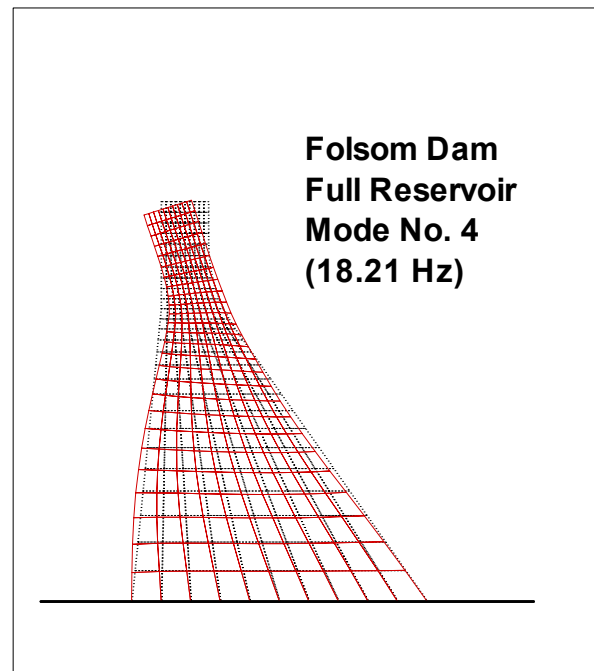
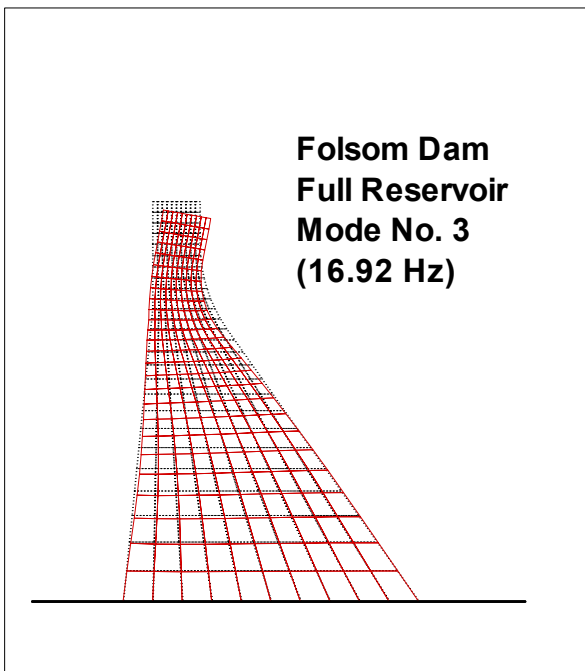
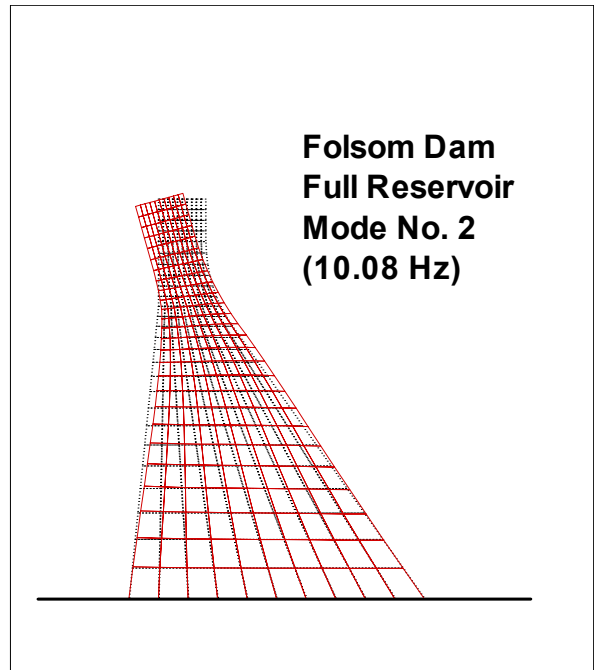
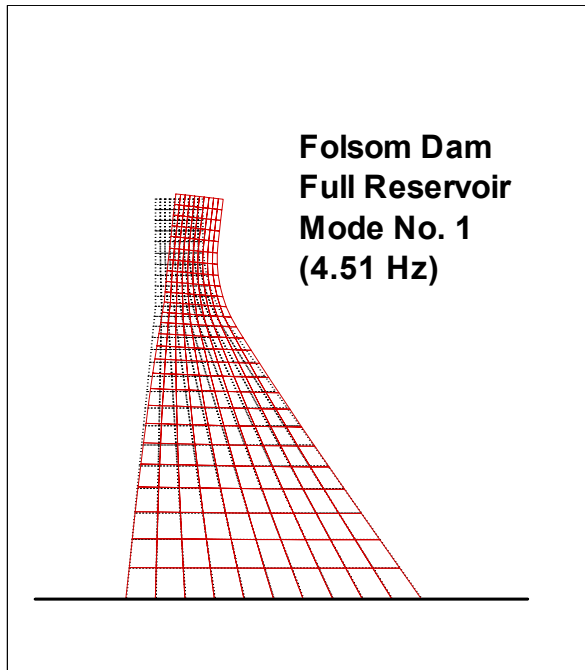


Figure 6.1-5. Mode shapes (full reservoir)

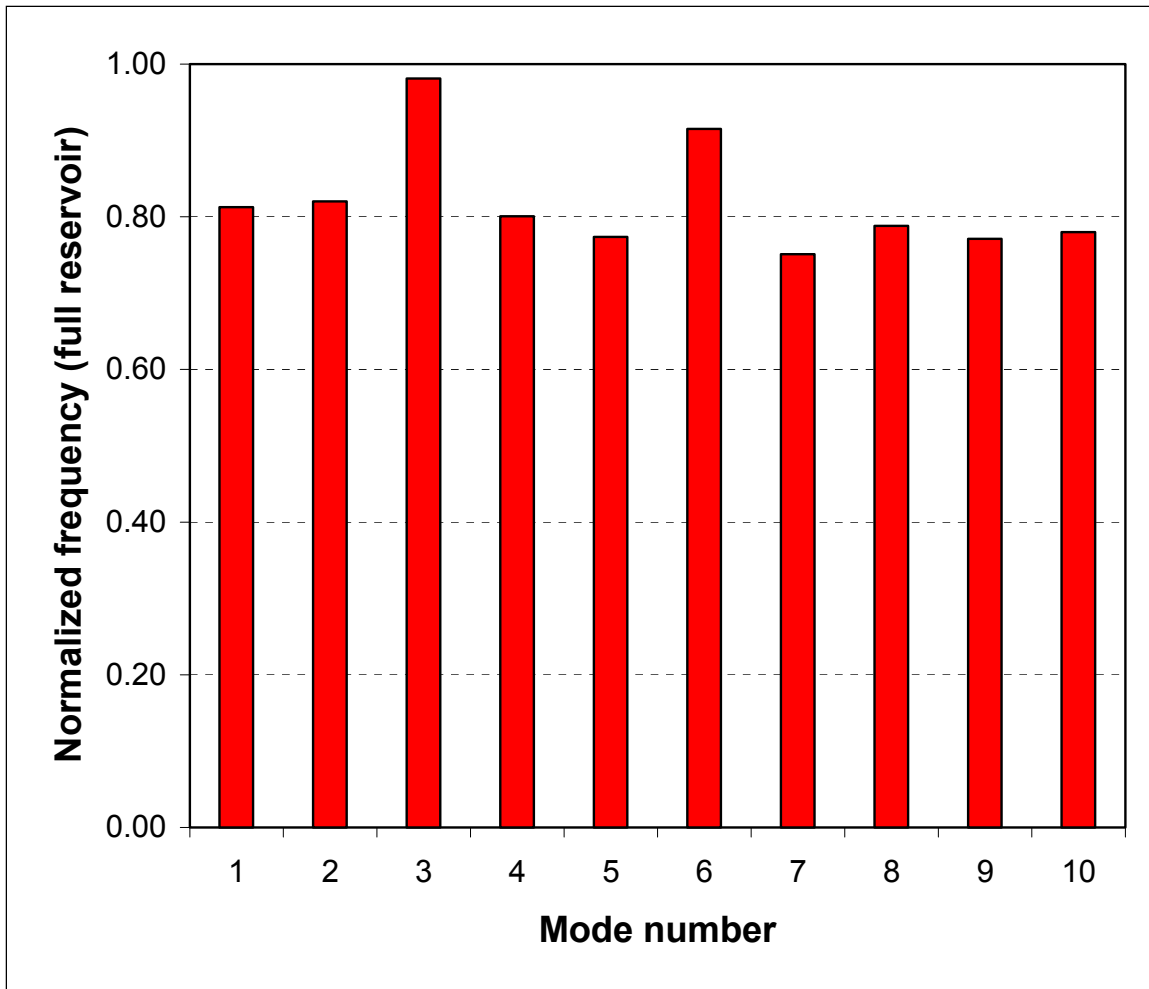


Figure 6.1-6. Effect of full reservoir condition on natural frequencies

6.1-8 Time-History Analysis

a. This section describes the results of the time-history analyses of the system subjected to different horizontal ground motions. Since the structure is not symmetric, the dynamic stresses on the upstream and downstream faces depend on the sign convention used to scale the ground acceleration record. To identify the critical loading condition, two analyses were performed for each earthquake, combining the initial static loading with the two opposite directions of horizontal excitation. Since the damage to a concrete dam is essentially associated with the development of tensile stresses, the critical loading condition for each earthquake is defined as the load combination that generates the higher tensile stress values in the section.

b. Table 6.1-5 compares the dynamic performance of the dam when subjected to the Loma Prieta earthquake for two different reservoir conditions. The presence of the reservoir not only affects the initial static loading condition through the incorporation of the corresponding hydrostatic forces, but it also modifies the dynamic characteristics of the system, as indicated previously. The table shows the peak value of horizontal dynamic displacement at the crest of the dam (Figure 6.1-3, point A), and the peak value of horizontal absolute acceleration at the same location. The table also shows the maximum value of total principal stress within the section, including the static loading contribution. The results show that the system

exhibits an overall increase in the response quantities associated with the full reservoir condition. In particular, the displacement and total

**Table 6.1-5
Performance for Different Reservoir Conditions (Loma Prieta)**

Reservoir Condition	Peak Crest Displacement (Dynamic)	Peak Crest Acceleration	Maximum Principal Stress (Including Static Loads)
Empty reservoir	1.85 cm (0.73 in)	2.45 g	4.62 MPa (669.84 psi)
Full reservoir	2.59 cm (1.02 in)	2.80 g	6.77 MPa (981.57 psi)

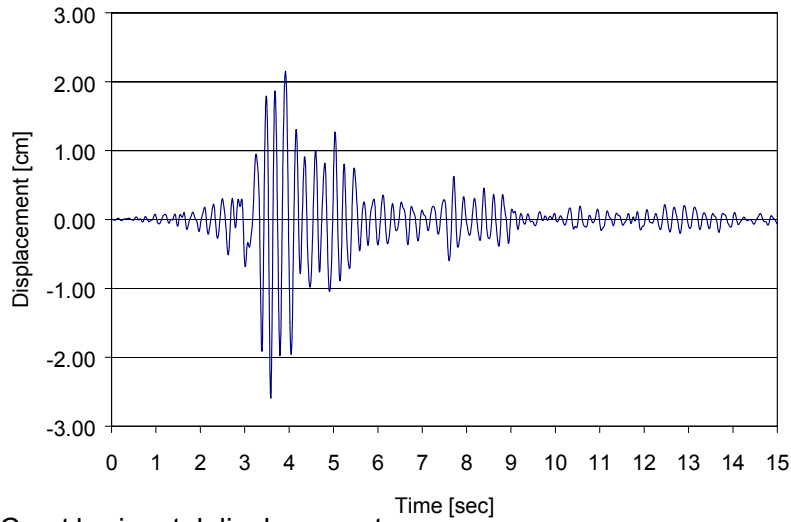
stress responses represent an increase of 134 and 146 percent, respectively, with respect to the response quantities associated with the empty reservoir condition.

c. Next, the dynamic performance of the section was investigated for different input ground motions for the full reservoir condition. The results are presented in Figures 6.1-7 to 6.1-10 for each ground motion. These figures show the time-histories for the horizontal components of displacement and absolute acceleration at the crest of the dam. The crest displacement is measured with respect to the base motion, and only the dynamic component of the displacement is considered in the figures. The figures also show the time evolution of the maximum principal stress at point B (Figure 6.1-3). The initial (static) loading state is included in the total stress computations. As indicated below, point B represents the critical location for the Loma Prieta, Parkfield, and Whittier Narrows ground motions. It is observed that for these ground motions, the principal stress time-histories show some pulses exceeding the recommended value of apparent tensile strength, 4.83 MPa (Raphael 1986). However, for this level of ground excitation (0.3 g), these tensile pulses are isolated and do not represent a continuous series of excursions beyond the tensile strength threshold.

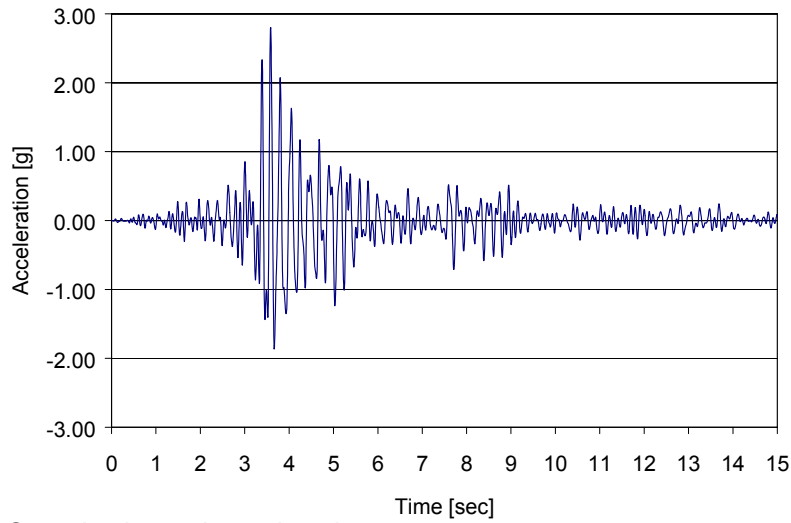
d. Figures 6.1-11 to 6.1-14 show the contours of maximum principal stress corresponding to each earthquake, including the initial (static) loading. These stress contours represent the distribution of the peak values reached by the maximum principal stress at each point within the section. The figures show that the highest values of tensile stress occur along the downstream and upstream faces. The contour plots also show the stress concentration induced by the downstream transition between the crest and the main body of the section. The time-history results are summarized in Table 6.1-6. The four ground motions used in the analysis are indicated in the first column of the table. The second column shows the peak value of the dynamic crest displacement for each ground motion, whereas the third column shows the corresponding dynamic magnification, defined as the ratio between the peak absolute values of crest and base absolute acceleration. The fourth column shows the peak value of the maximum principal stress within the section. For the Loma Prieta, Parkfield, and Whittier Narrows ground motions, this critical value exceeded the value of apparent tensile strength and it occurred on the upper part of the transition region on the downstream face, about 22.6 m (74 ft) below the crest (Figure 6.1-3, point B). On the other hand, the critical tensile stress value corresponding to the San Fernando ground motion did not exceed the tensile strength, and it occurred at the upstream base location (Figure 6.1-3, point C).

6.1-9 Conclusions

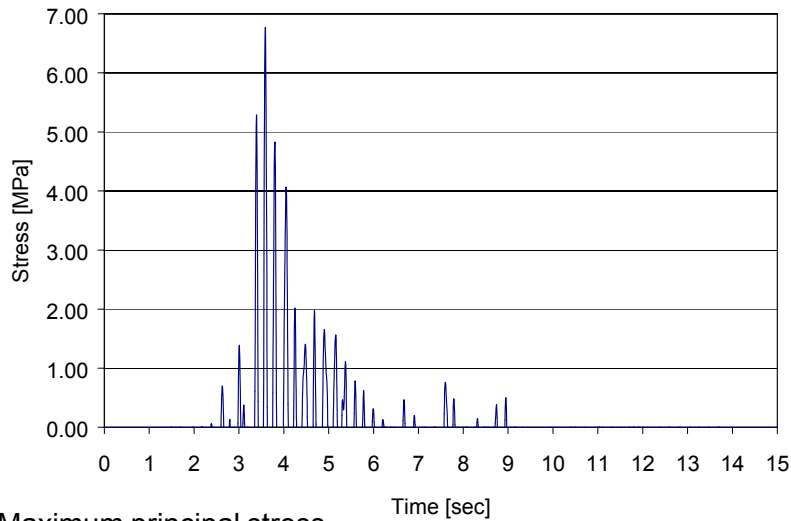
This numerical example confirms the importance of the ground motion selection for the accurate evaluation of the seismic performance of concrete gravity dams. The different earthquake records used in this numerical study (Loma Prieta, Parkfield, Whittier Narrows, and San Fernando) were scaled up to the same peak ground acceleration level. For this example, the Loma Prieta and Parkfield ground motions represent a more severe loading condition than the other two ground motions. The results show that the dynamic performance can exhibit significant variations in selected response quantities (peak crest displacement and acceleration, and critical maximum principal stress). This highlights the importance of the frequency characteristics of the ground motion to the response of the structural system.



a. Crest horizontal displacement

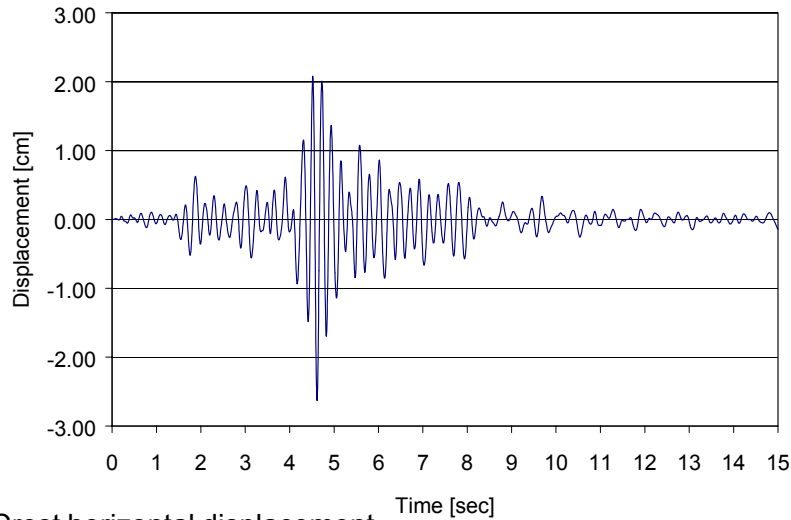


b. Crest horizontal acceleration

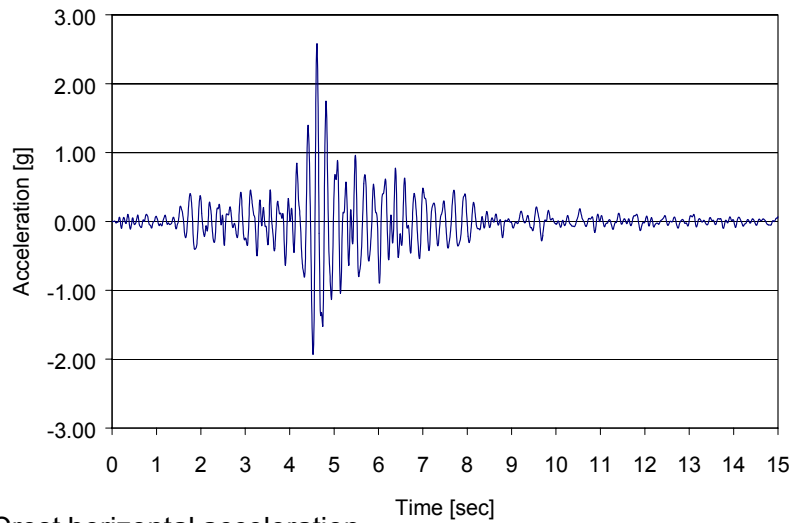


c. Maximum principal stress

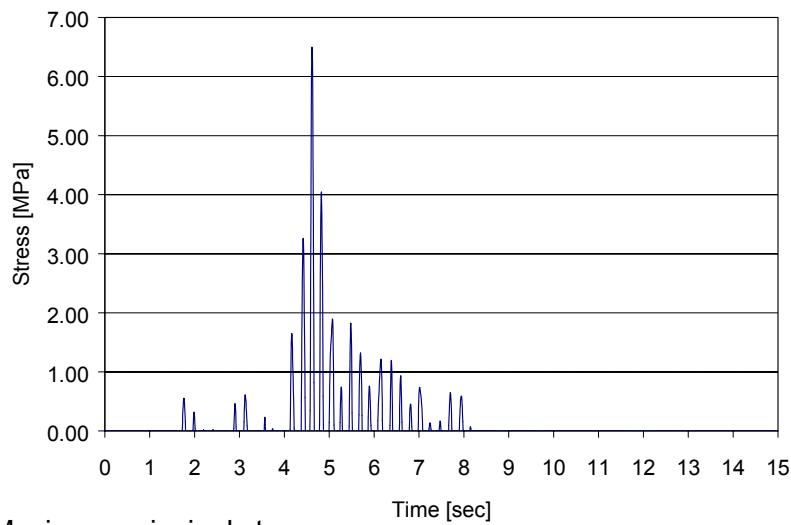
Figure 6.1-7. Relative displacement and absolute acceleration time-histories at the crest, and maximum principal stress history at point B (Loma Prieta ground motion)



a. Crest horizontal displacement

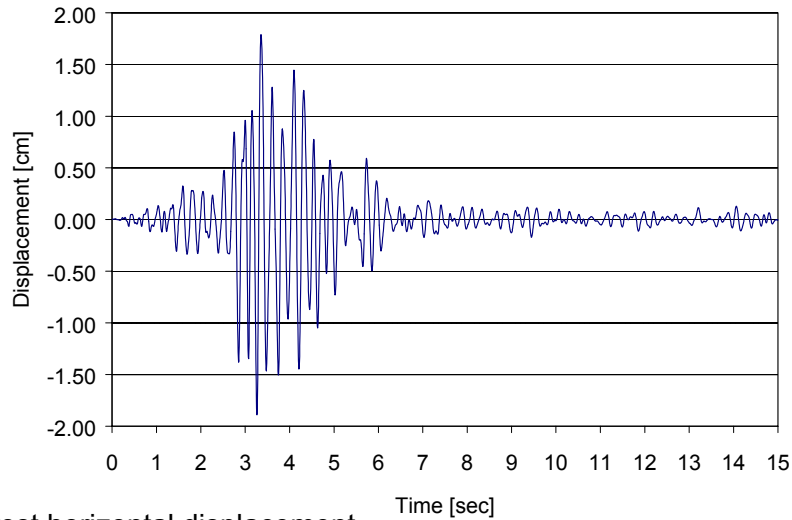


b. Crest horizontal acceleration

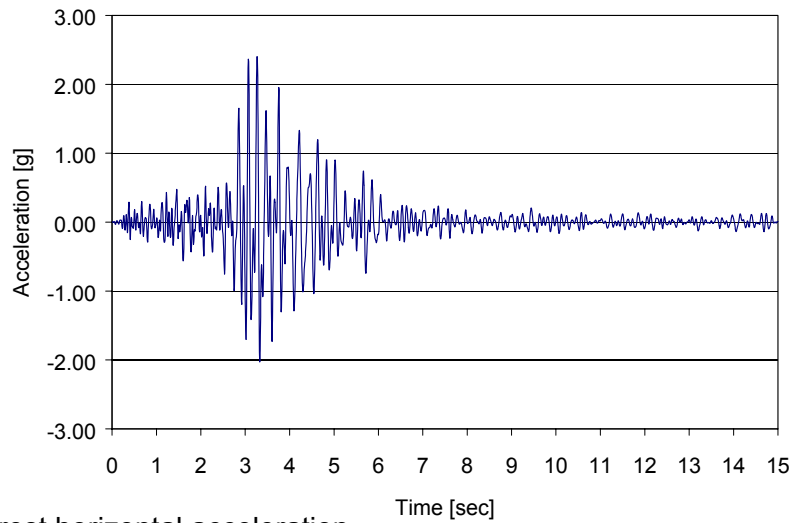


c. Maximum principal stress

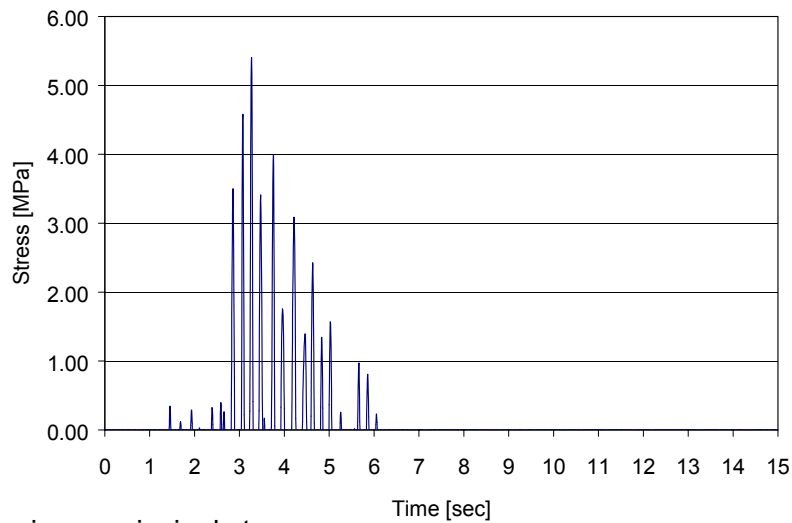
Figure 6.1-8. Relative displacement and absolute acceleration time-histories at the crest and maximum principal stress history at point B (Parkfield ground motion)



a. Crest horizontal displacement



b. Crest horizontal acceleration



c. Maximum principal stress

Figure 6.1-9. Relative displacement and absolute acceleration time-histories at the crest and maximum principal stress history at point B (Whittier Narrows ground motion)

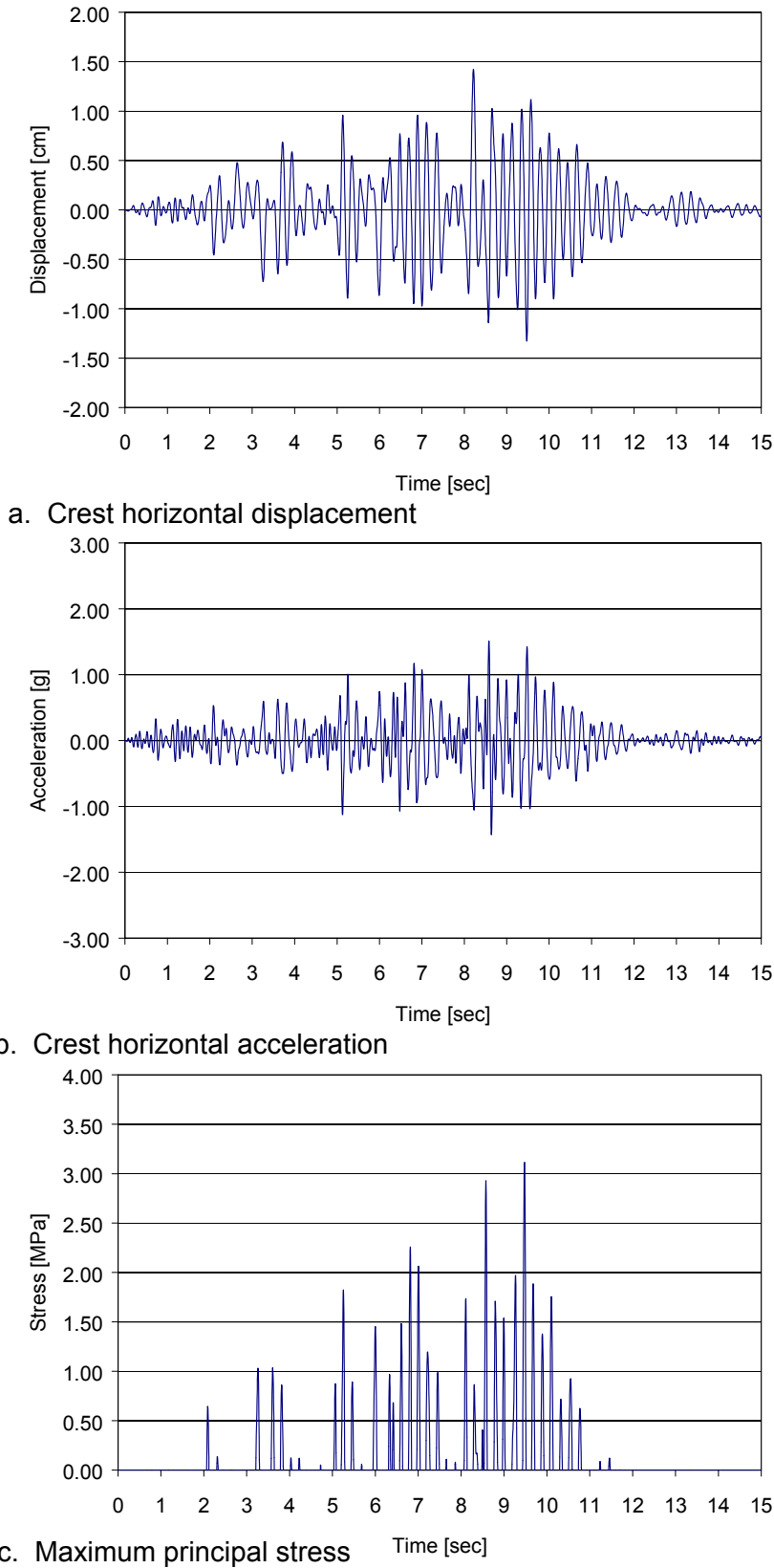


Figure 6.1-10. Relative displacement and absolute acceleration time-histories at the crest and maximum principal stress history at point B (San Fernando ground motion)

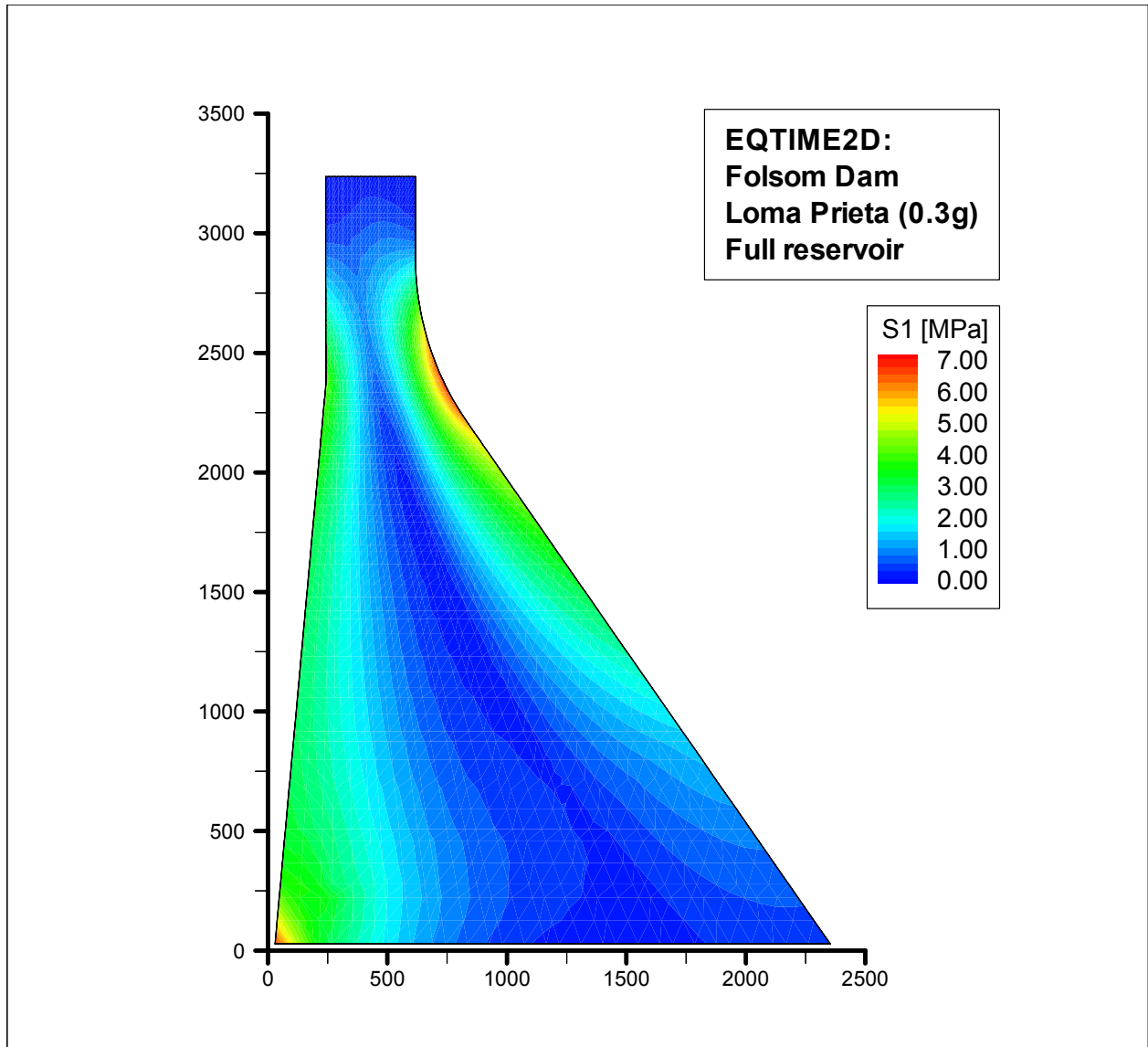


Figure 6.1-11. Maximum principal stress contour (Loma Prieta)

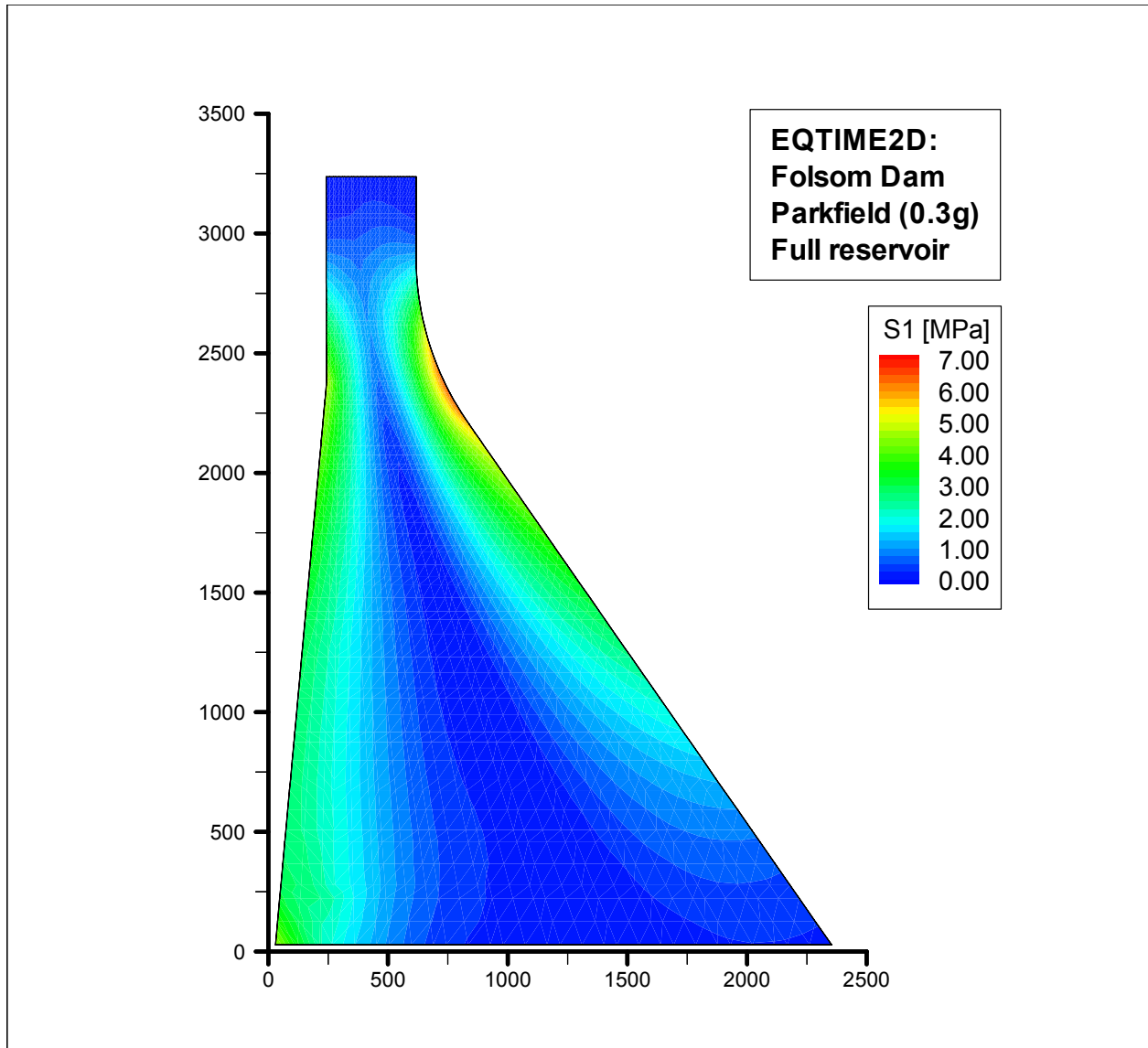


Figure 6.1-12. Maximum principal stress contour (Parkfield)

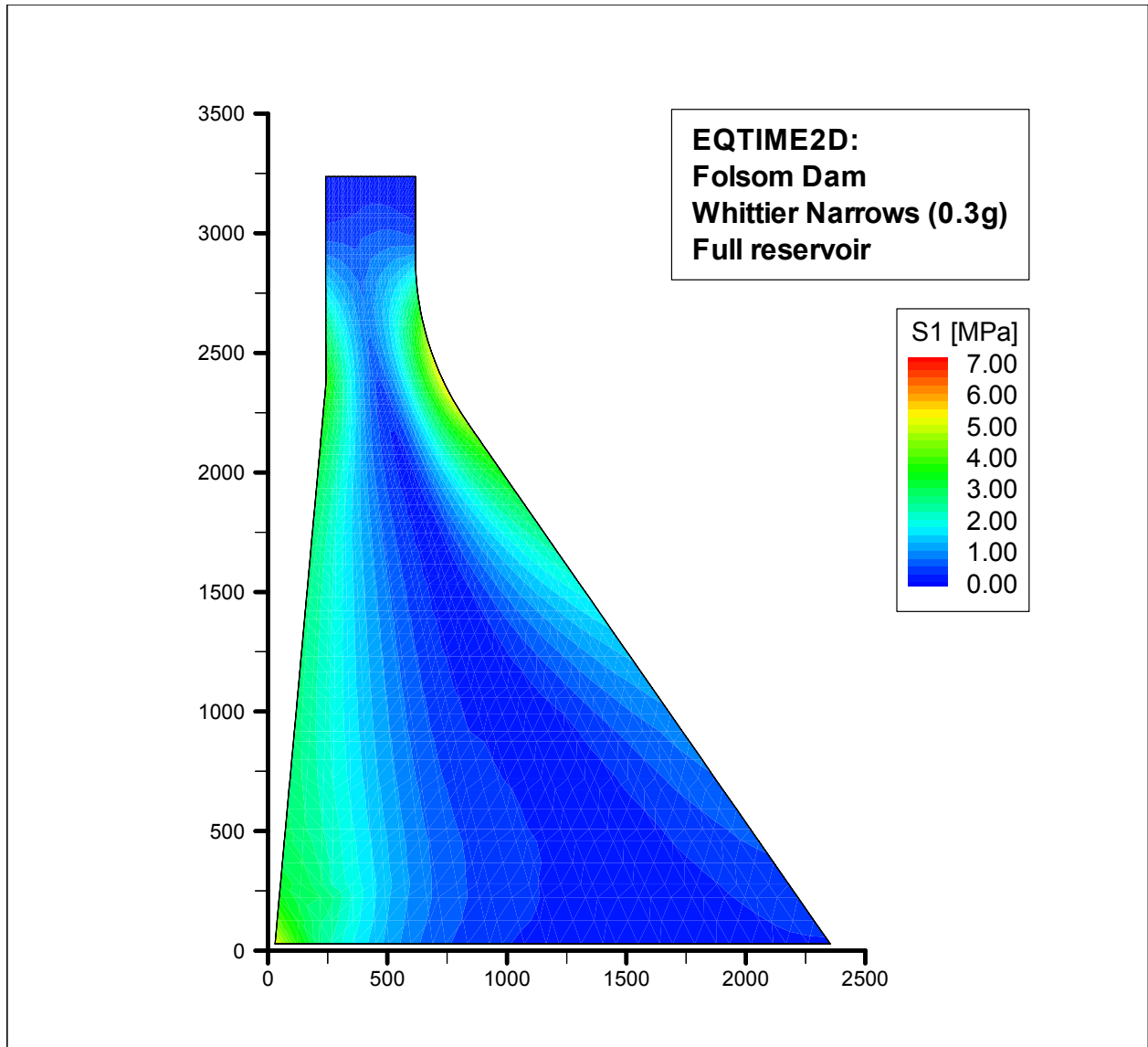


Figure 6.1-13. Maximum principal stress contour (Whittier Narrows)

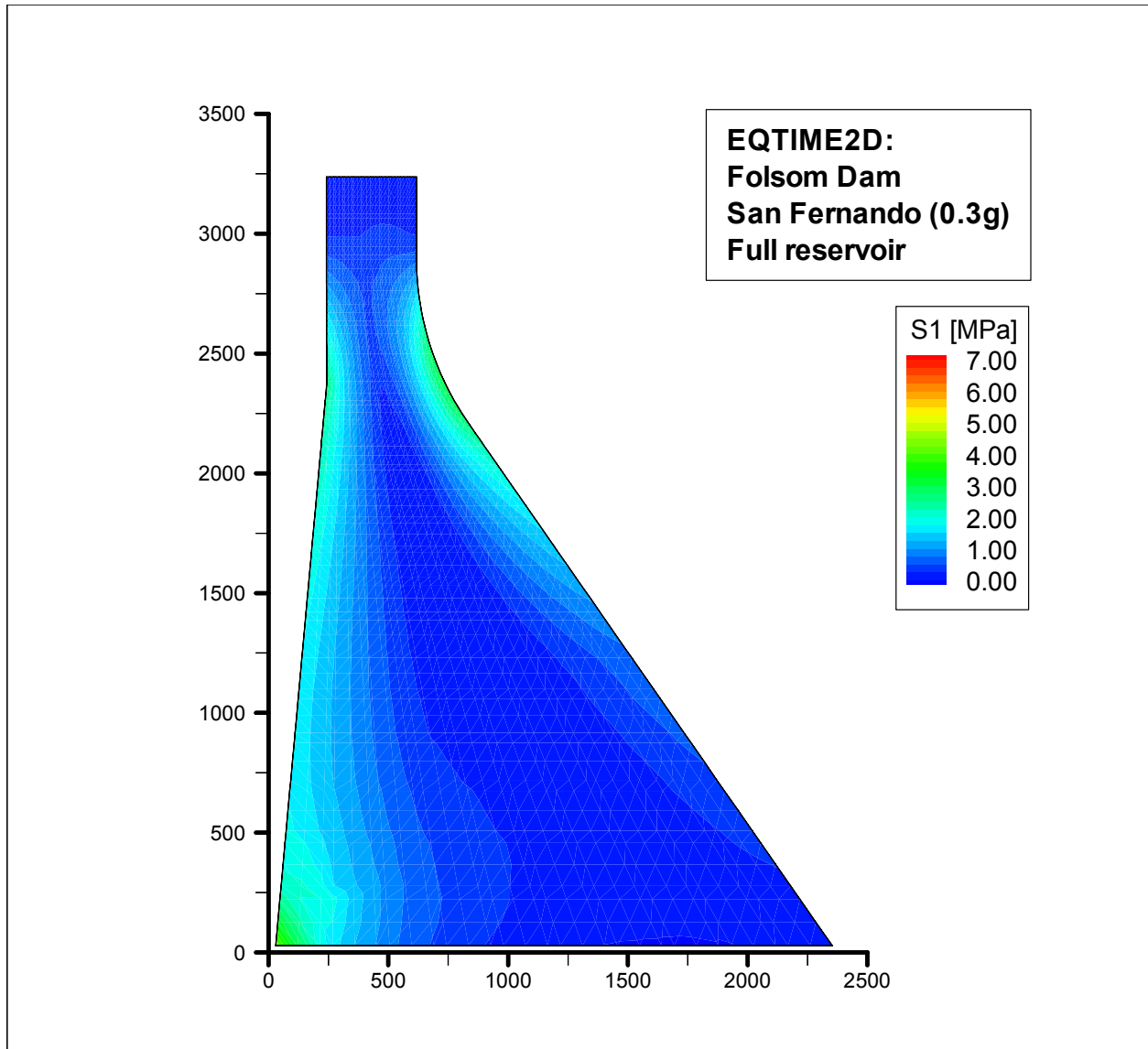


Figure 6.1-14. Maximum principal stress contour (San Fernando)

Table 6.1-6 Performance Comparison for Different Earthquakes			
Ground Motion	Peak Crest Displacement (Dynamic)	Dynamic Magnification¹	Maximum Principal Stress (Including Static Loads)
Loma Prieta	2.59 cm (1.02 in)	9.33	6.77 MPa (981.57 psi)
Parkfield	2.64 cm (1.04 in)	8.61	6.50 MPa (942.63 psi)
Whittier Narrows	1.88 cm (0.74 in)	8.01	5.41 MPa (785.05 psi)
San Fernando	1.42 cm (0.56 in)	5.03	4.24 MPa (614.27 psi)

¹ Ratio between peak absolute values of crest and base absolute acceleration.

6.2 Portugues Arch Dam

6.2-1 Background

Designed by the U.S. Army Engineer District, Jacksonville, Portugues Dam is a double-curvature three-centered arch dam to be built on the Portugues River approximately 4.5 km (2.8 miles) northwest of the city of Ponce, in south-central Puerto Rico. The 82.5-m- (270.6-ft-) high Portugues Dam is a multipurpose dam to be constructed in two phases. Initially, it will be built to a height of 67 m (219.6 ft) as a flood-control dam, and later it will be raised to its full height of 82.5 m and a crest length of 458.72 m (1,505 ft) for additional water supply and recreational benefits. The full-height Portugues Dam used in this example is 3.66 m (12 ft) thick at the crest and 12.20 m (40 ft) thick at the base. The dam includes an ungated, 45.7-m- (150-ft-) wide ogee spillway to the left of the crown section. In addition to the usual, unusual, and extreme static loading combinations, the dam was also designed to withstand the MCE and the 100-year OBE described in Section 6.2.4. The dam was initially analyzed using the response spectrum method of analysis, and later both the linear and nonlinear time-history analyses were also performed as a confirmation for the MCE.

6.2-2 Purpose and Objectives

The purpose of this section is to illustrate the application of linear time-history analysis to earthquake response computation of Portugues Arch Dam. The objectives of the time-history analysis are to compute dynamic characteristics of the dam-water-foundation system consisting of all significant vibration mode shapes and frequencies; to compute dam displacement and stress response histories under the combined vertical and two horizontal components of earthquake ground motions; and to present the results in the form of stress contour plots and stress time-histories for assessing the earthquake performance of the dam.

6.2-3 Scope

The scope of the study included the following:

- Definition of acceleration time-histories of design ground motion.
- Development of finite element models of the dam-water-foundation system.
- Computation of mode shapes and frequencies of the dam-water-foundation system.
- Analysis of static loading.
- Analysis of dynamic loading for four sets of earthquake acceleration time-histories.
- Evaluation of dam stresses under combined static and dynamic loads and their sensitivity to characteristics of acceleration time-histories. ‘

6.2-4 Earthquake Ground Motions

Based on a seismotectonic evaluation and earthquake ground motion assessment conducted for the Portugues Dam Site (Geomatrix Consultants 1988), two earthquakes were selected as the MCE and one earthquake as the OBE for design of the dam. The MCE ground motions were selected deterministically based on the maximum earthquake magnitudes on both near field and distant sources, the source-to-site distance, and attenuation effects. The OBE was selected based on these parameters and the earthquake(s) producing the

maximum ground motions at the site once in 100 years. The earthquakes selected for the design of Portugues Dam are listed in Table 6.2-1.

Table 6.2-1 Design Earthquakes for Portugues Arch Dam	
MCE	M6-1/2 Earthquake on Salinas Fault at Distance = 18 km M8.0 Earthquake on Muertos Trough at Distance = 50 km
OBE	M7-3/4 Earthquake on Puerto Rico Trench at Distance = 85 km

The mean horizontal and vertical smooth response spectra for the controlling MCE ground motion associated with an M6-1/2 earthquake on Salinas Fault at a distance of 18 km from the dam are given in Figure 6.2-1. Also included in this figure are periods of vibration for Modes 1, 5, 10, and 20, so their respective spectral accelerations can be noted and compared.

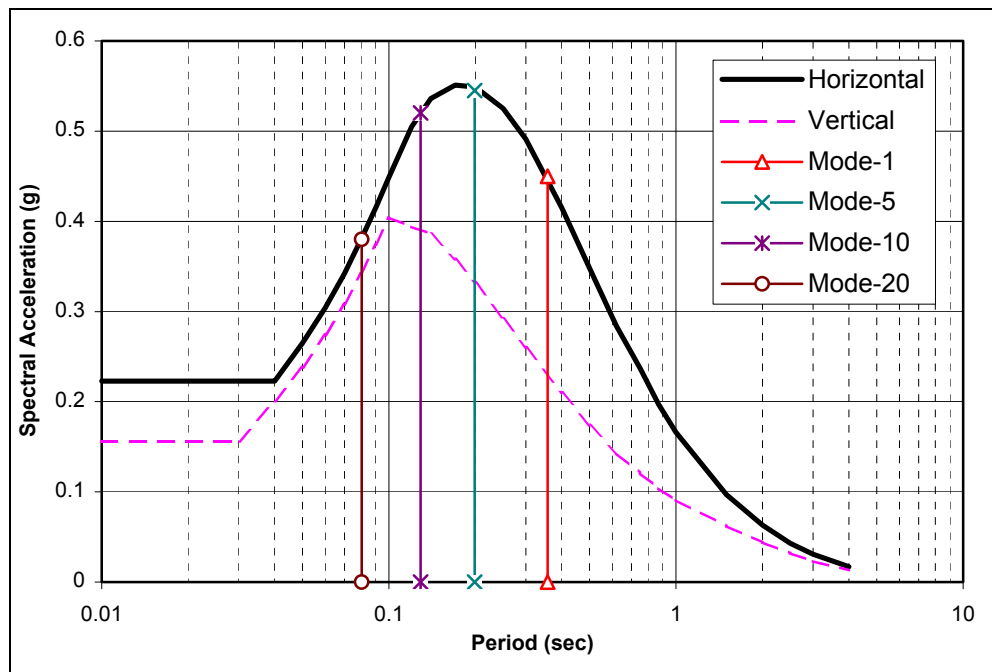


Figure 6.2-1. Horizontal and vertical smooth response spectra for MCE, M6-1/2 at distance of 18 km on the Salinas Fault (5 percent damping)

The acceleration time-histories employed in the design analysis (U.S. Army Engineer District (USAED), Jacksonville, 1990) were a set of spectrum-matched records shown in bottom graphs of Figures 6.2-2 to 6.2-4. The earthquake ground motions selected for this example consisted of the same spectrum-matched record and four additional natural records (Table 6.2-2). The natural records were scaled such that their response spectra in the range of significant periods of vibration of the dam are approximately at the level of the smooth design response spectra, in accordance with procedures outlined in Chapter 5. The natural records were selected from earthquakes with magnitudes in the range of 6.0 to 6-1/2, nearly the same as that for the controlling MCE event discussed previously. The acceleration time-histories of the scaled natural records and the spectrum-matched record are presented in Figures 6.2-2 to 6.2-4. Variation of these records in terms of frequency contents, duration of strong shaking, pulse sequencing, and the period of dominant pulses can easily be observed.

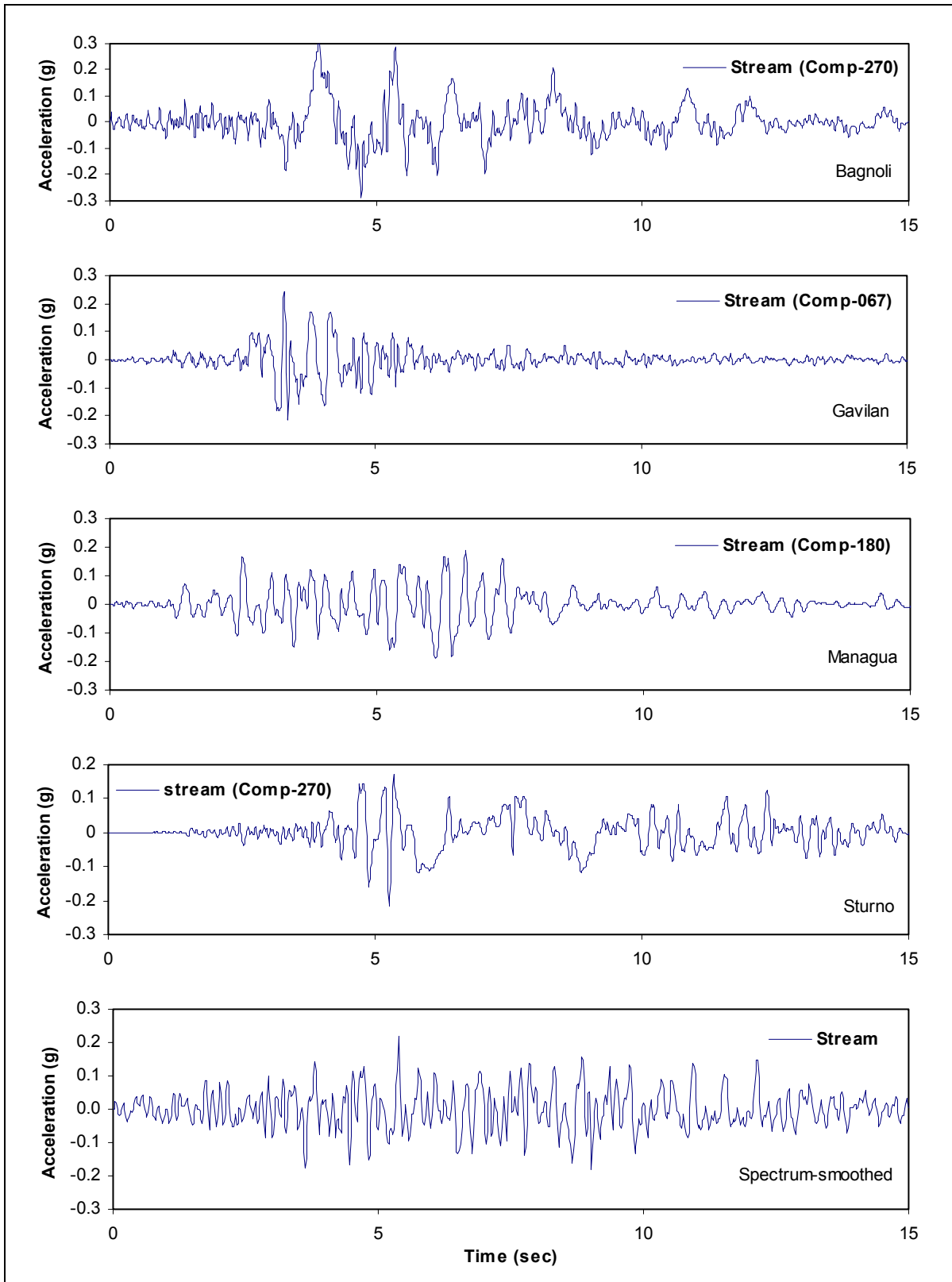


Figure 6.2-2. Acceleration time-histories of different sets of earthquake input ground motions applied in the stream direction

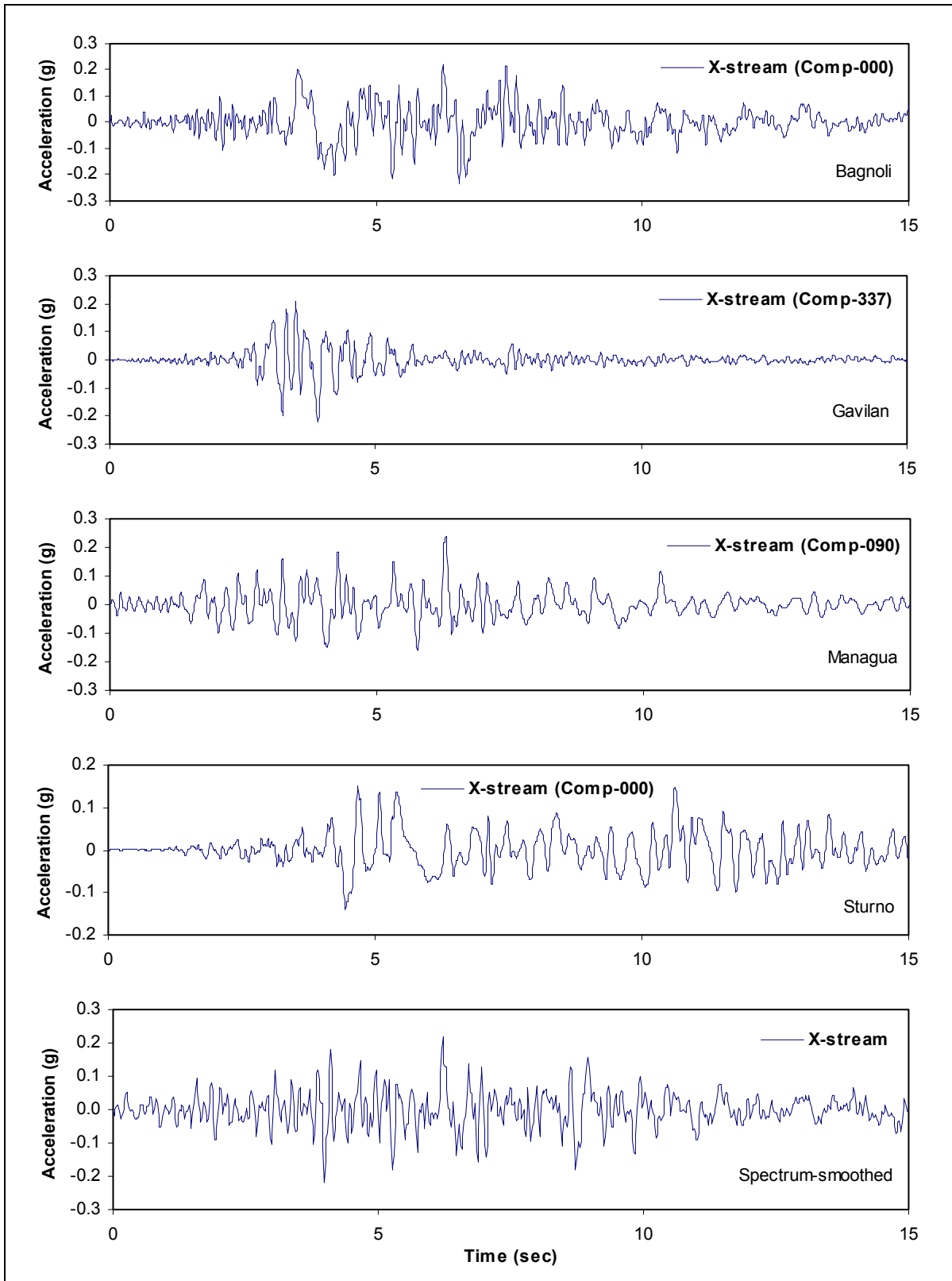


Figure 6.2-3. Acceleration time-histories of different sets of earthquake input ground motions applied in the cross-stream direction

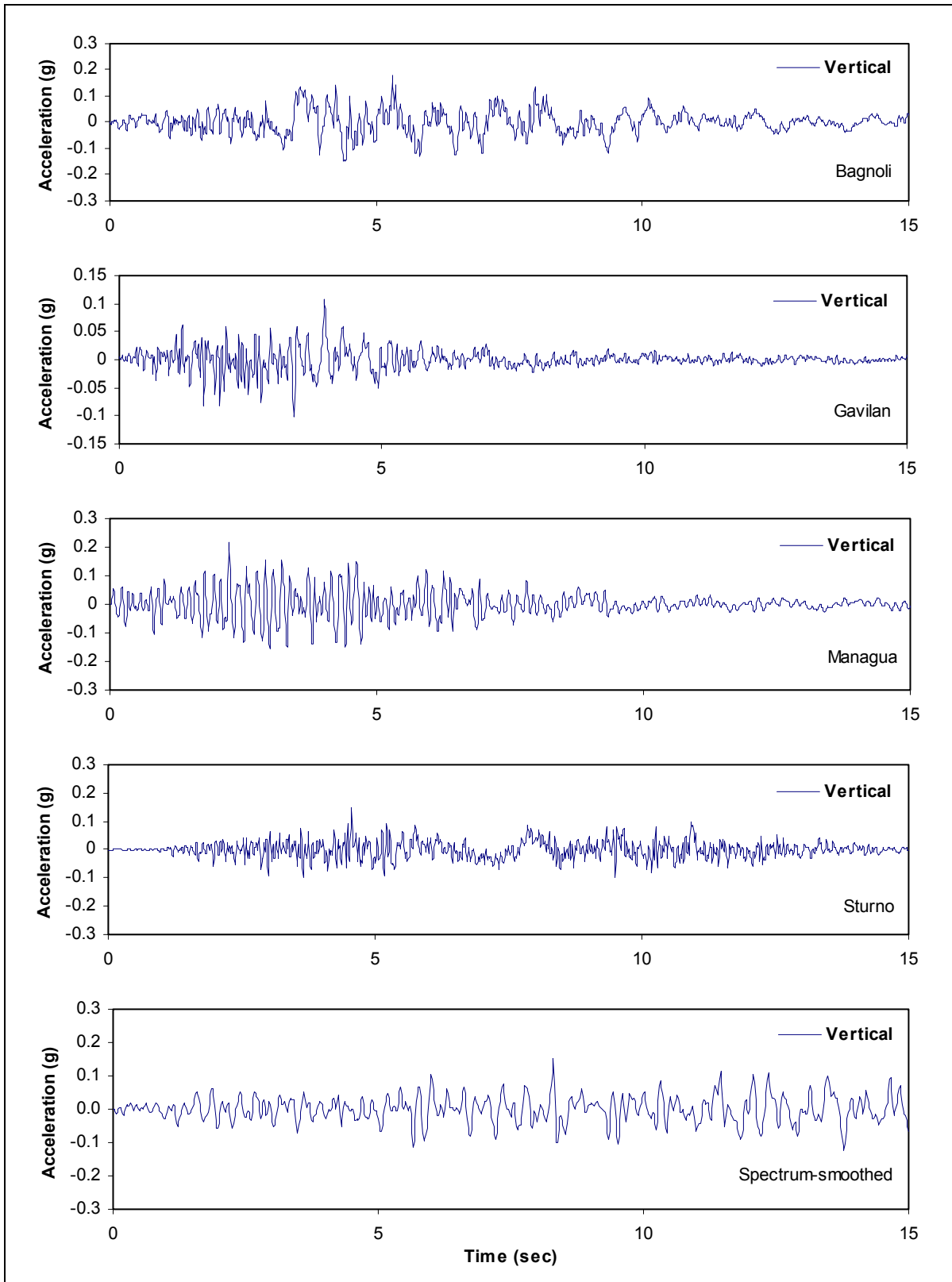


Figure 6.2-4. Acceleration time-histories of different sets of earthquake input ground motions applied in the vertical direction

Table 6.2-2
Natural Earthquake Records for Time-History Analysis

Station	Earthquake	Magnitude
Bagnoli Irpino	1980 Irpinia, Italy	6.5
Gavilan College	1989 Loma Prieta, California	6.0
Managua	1972 Nicaragua	6.2
Sturno	1980 Irpinia, Italy	6.5

6.2-5 Selection of Analysis Procedures

The linear-elastic time-history analysis of arch dams is currently based on 3-D finite element procedures discussed in Chapter 2. Finite element models for the concrete arch, foundation rock, and the impounded water as well as loading combinations are developed according to criteria established in EM 1110-2-2201. Material properties are selected based on laboratory or in situ tests with the dynamic material properties reflecting the appropriate increases due to rapid rate of seismic loading. The ground motion acceleration time-history inputs for the dynamic analysis are developed or selected based on an earthquake hazard assessment of the site following the procedures discussed in Chapter 4. Interaction effects of the impounded water and foundation rock with the dam are included in the finite element stress analyses by modeling a sufficiently large portion of the foundation rock and the impounded water. Depending on the dynamic characteristics of the dam and the impounded water, a compressible or incompressible fluid mesh may be employed. When water compressibility is considered, the energy loss capability of the reservoir boundary arising from the absorption of pressure waves should be taken into account. Structural damping effects are included using a viscous damping coefficient proportional in scale to the severity of dam shaking during the earthquake. The performance of the dam is evaluated based on contours showing the extreme and instantaneous stress distribution over the entire dam at critical instants of time, as well as stress time-histories indicating magnitude and number of excursions of peak stresses beyond maximum allowable values and their relationship to surrounding stresses.

6.2-6 Finite Element Models

As described in Chapter 2, computer modeling and time-history analysis of Portugues Dam were performed using the computer program GDAP (Ghanaat 1993a). A brief description of the finite element models is given in the following section.

a. Dam model.

(1) The finite element model of Portugues Dam for this example was developed identical to that constructed by USAED, Jacksonville (1990), as shown in Figure 6.2-5. The arch structure was modeled using 56 thick-shell and 24 3-D-shell elements available in the computer program GDAP (Ghanaat 1993b). The use of a single layer of shell elements through the dam thickness was considered adequate for this thin arch dam. The thick-shell elements were employed to model the interior region of the dam where the shell behavior is dominant. The regions near the abutments were represented by 3-D-shell elements, which also facilitated the connection between the thick-shell and the solid elements of the foundation rock model.

(2) Both thick-shell and 3-D-shell elements are based on an isoparametric formulation and use quadratic geometry and displacement interpolation in the dam surface directions and linear interpolation through the thickness. The geometry of shell elements is defined by 16 nodes, 8 on each face. For thick-shell elements the 16 surface nodes are reduced to 8 midsurface nodes, each having five degrees of freedom (three translations and two rotations), while all the 16 surface nodes for the 3-D-shell elements, each having three translational degrees of freedom, are retained.

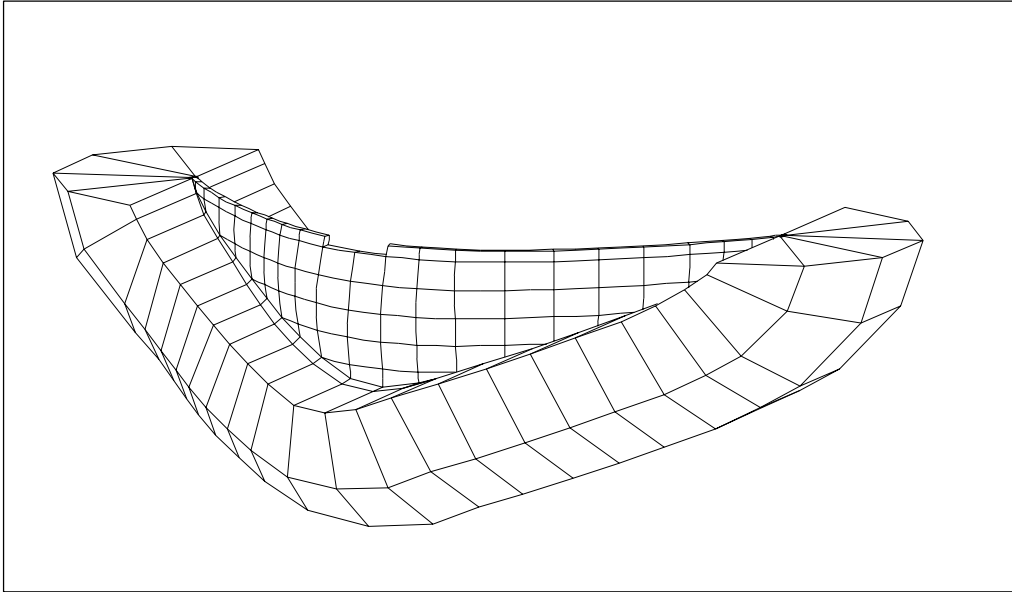


Figure 6.2-5. Finite element representation of Portugues Arch Dam and foundation rock

b. Foundation model. The finite element model of the foundation rock was constructed on the semicircular planes cut into the canyon walls perpendicular to the dam-foundation interface (Figure 6.2-5). The radius of the semicircle was selected equal to the height of the dam. The foundation mesh therefore extended one dam height in the upstream, downstream, and downward directions. Considering that the modulus ratio of rock to concrete was greater than 0.5, this foundation mesh size was judged adequate (EM 1110-2-2201). The foundation model included 176 eight-node solid elements with each node having three translational degrees of freedom. The foundation model was assumed to be massless, the assumption commonly used in practice to eliminate reflection of seismic waves at the fixed boundaries of the foundation model and to apply the earthquake records measured at the ground surface directly at the base of the foundation model.

c. Reservoir water model.

(1) The fundamental frequency for the impounded water at Portugues Dam with a maximum water depth of 56 m was estimated to be about 8.5 Hz. This frequency is more than twice the fundamental mode of the dam without water (2.97 Hz), indicating that the effects of water compressibility can be neglected (EM 1110-2-2201). Consequently the inertia forces of the impounded water were represented by the equivalent added-mass matrix coefficients applied to the upstream concrete nodes. The added mass of water was computed using a finite element mesh of incompressible water developed on the basis of site topography, as shown in Figure 6.2-6.

(2) The finite element mesh consisted of four layers of incompressible fluid elements that extended four times the water depth in the upstream direction. The fluid nodes at the dam-water interface matched the concrete nodes, and the nodes within the reservoir water were selected on one cylindrical section near the dam and on three plane sections away from the dam controlled by topography of the reservoir bottom. The dam-water interface includes forty 8-node curvilinear 2-D fluid elements, and the body of water was represented by one hundred sixty 16-node fluid elements. Both elements are based on isoparametric formulation and are described in Ghanaat (1993b).

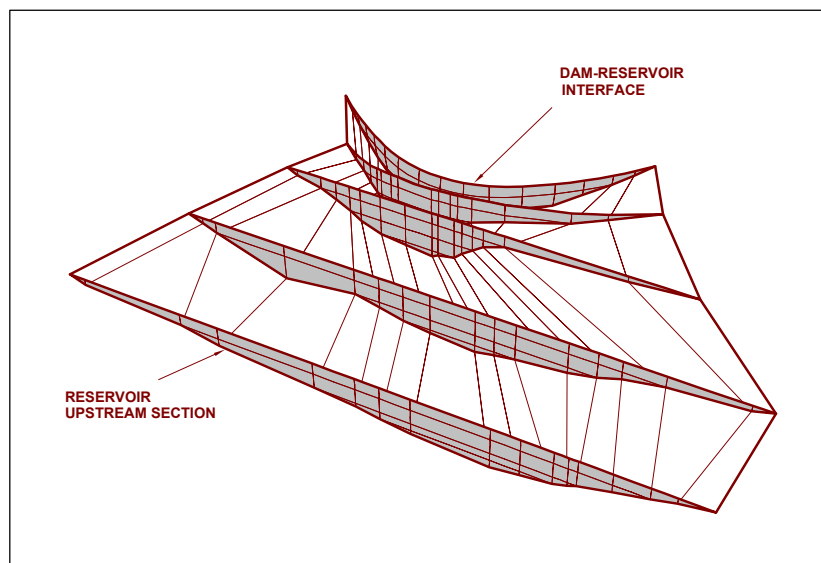


Figure 6.2-6. Finite element model of incompressible reservoir water

6.2-7 Material Properties

The material properties of the concrete dam and foundation rock for this example were based on test results published by USAED, Jacksonville (1986, 1988a, 1988b). The concrete material properties under static and dynamic loading are summarized in Table 6.2-3. These included modulus of elasticity, Poisson's ratio, and unit weight. A coefficient of thermal expansion of $5.4 \times 10^{-6}/\text{EF}$ was used. The compressive and tensile strengths of the concrete also presented in Table 6.2-3 were employed for evaluation of the results. The foundation rock properties used in the analysis included a uniform deformation modulus of 13,793 MPa (2.0×10^6 psi) and a Poisson's ratio of 0.2 for both static and dynamic analyses.

Table 6.2-3 Concrete Material Properties		
Concrete	Static	Dynamic
Modulus of elasticity, MPa (psi)	13,790 (2,000,000)	33,095 (4,800,000)
Compressive strength, MPa (psi)	27.5 (4,000)	37.0 (5,400)
Tensile strength, MPa (psi)	3.1 (450 ¹)	5.75 (833 ²)
Poisson's ratio	0.152	0.152
Weight density, kg/m ³ (pcf)	2,476 (154.6)	2,476 (154.6)

¹ USAED, Jacksonville (1988a).
² Apparent tensile strength obtained based on the results of modulus of rupture tests and modifications suggested by Raphael (1984).

6.2-8 Computation of Earthquake Response

The earthquake response of Portugues Arch Dam to various ground motions was obtained using the mode-superposition time-history method discussed in Chapter 1. The analysis usually consists of computation of vibration periods and mode shapes, evaluation of response of each individual mode to earthquake input using the step-by-step integration procedure (Chapter 3), and finally combination of the modal responses at each time-step in order to obtain the total response.

22 Dec 03

a. *Dynamic characteristics of dam.*

(1) The vibration frequencies and mode shapes required for the time-history earthquake analysis of Portuges Dam were obtained using the finite element models described in 6.2.6. The 20 lowest vibration frequencies and mode shapes were computed for both the empty and full reservoir conditions, as shown in Table 6.2-4. The results show that Portuges Dam has numerous closely spaced modes, 14 of which for the case with water are below 10 Hz and are expected to produce significant response to earthquake loading.

Table 6.2-4
Vibration Frequencies of Portuges Dam-Water-Foundation System

Mode No.	Without Water		With Water	
	Period, sec	Frequency, Hz	Period, sec	Frequency, Hz
1	0.337	2.966	0.354	2.823
2	0.280	3.568	0.291	3.440
3	0.255	3.920	0.272	3.684
4	0.230	4.356	0.234	4.282
5	0.196	5.116	0.198	5.056
6	0.169	5.923	0.171	5.862
7	0.148	6.772	0.153	6.551
8	0.130	7.679	0.147	6.822
9	0.128	7.799	0.131	7.643
10	0.117	8.540	0.129	7.741
11	0.114	8.780	0.116	8.626
12	0.103	9.673	0.112	8.930
13	0.102	9.803	0.106	9.425
14	0.099	10.076	0.103	9.724
15	0.096	10.423	0.098	10.161
16	0.093	10.794	0.095	10.488
17	0.087	11.523	0.093	10.774
18	0.083	11.984	0.084	11.862
19	0.080	12.564	0.081	12.297
20	0.077	12.993	0.080	12.444

(2) The computed mode shapes for the 10 lowest modes are displayed in the form of deflected shapes along the arch section, as shown in Figure 6.2-7. These modes represent various arch harmonic deflected shapes accompanied primarily by the first cantilever and a couple of second cantilever bending modes. The second cantilever bending means that the upper and lower parts of the dam deflect in the opposite directions (Modes 8 and 10).

b. *Displacement results.*

(1) Magnitudes of the maximum dam displacements are listed in Table 6.2-5, and the corresponding displacement histories for the stream direction are displayed in Figure 6.2-8. The results show that the displacements for the scaled Gavilan and Managua earthquake records are the largest with the maximum reaching a value of 38 mm at a location near the midcrest of the dam.

(2) An examination of the displacement histories indicates a predominant response frequency of about 3.5 Hz corresponding to the fundamental symmetric mode of the dam (see mode shapes in Figure 6.2-7). In particular, the displacement histories due to Gavilan and Managua excitations exhibit a much stronger and sustained harmonic response at 3.5 Hz, apparently caused by the presence of a predominant seismic pulse of about the same frequency in these earthquake records (Figure 6.2-2).

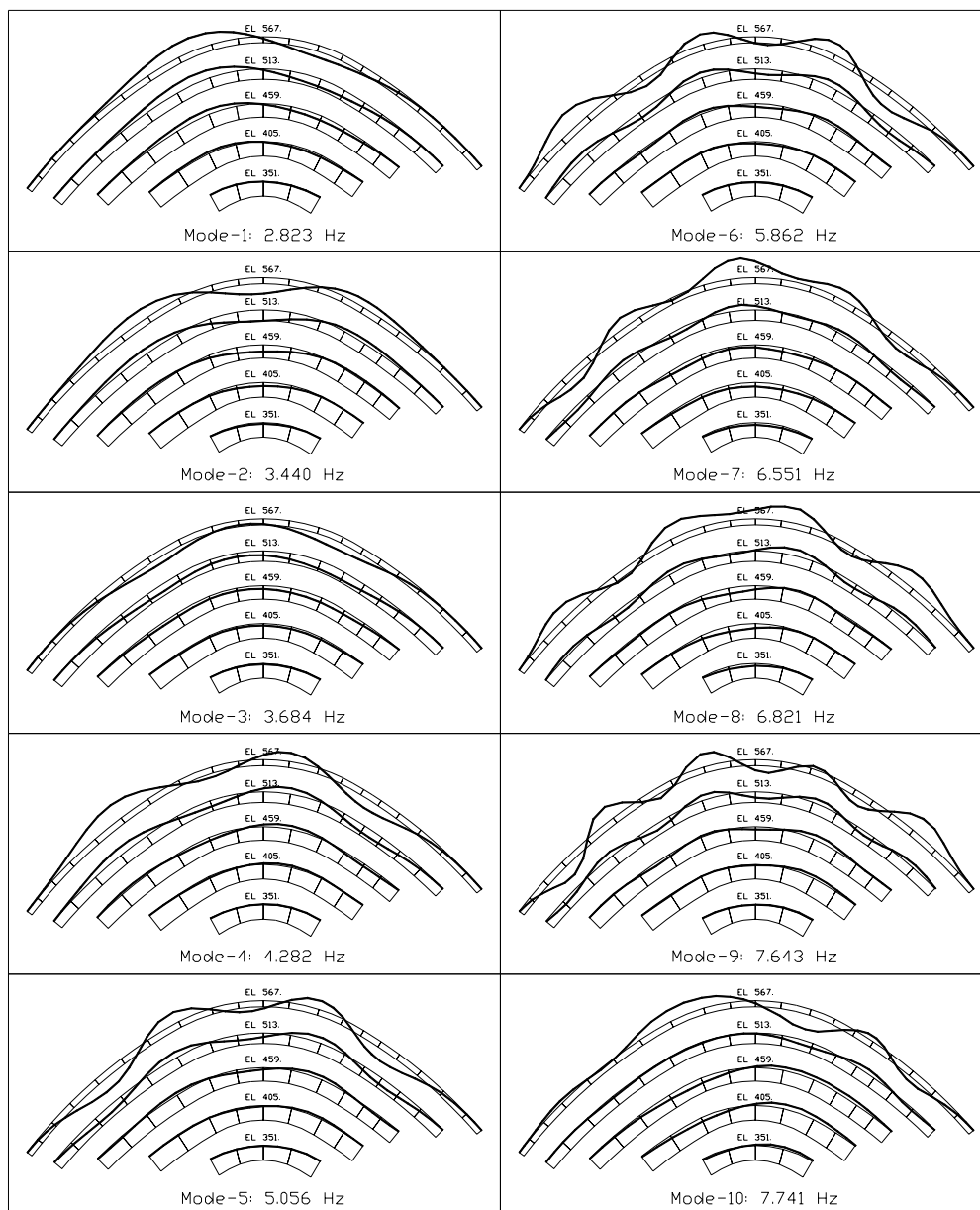


Figure 6.2-7. Ten lowest mode shapes of Portugues dam-water-foundation system

Table 6.2-5
Maximum Dynamic Displacements for Various Input Ground Motions, mm

Ground Motion	Node Number	X-stream	Stream	Vertical
Scaled Bagnoli	393 ¹	8	22	2
Scaled Gavilan	637 ²	15	38	3
Scaled Sturno	637	11	29	3
Scaled Managua	637	15	38	3
Spectrum-matched	393	12	30	3

¹ At spillway crest elevation on right side of dam center.

² At spillway crest elevation on left side of dam center.

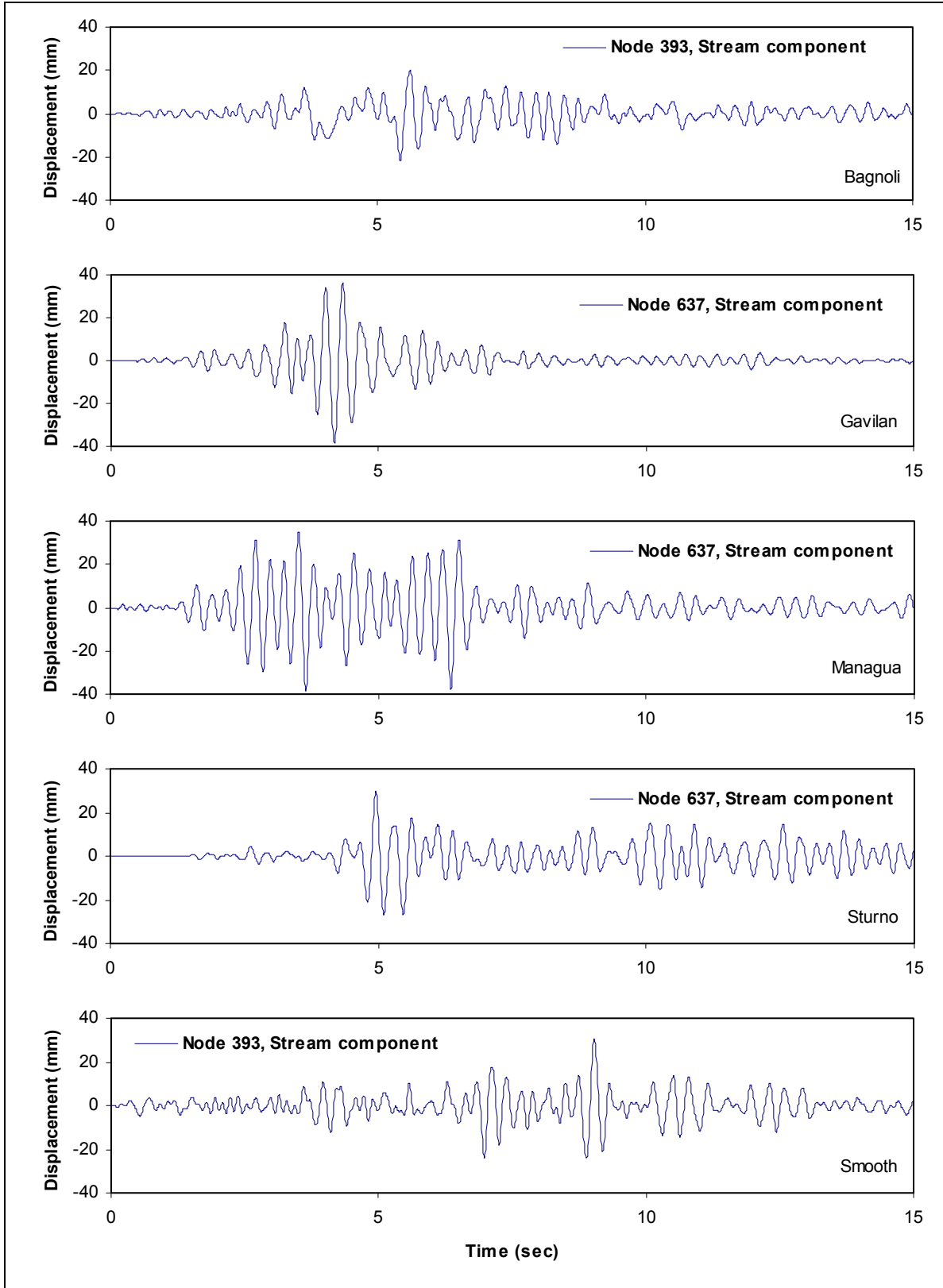


Figure 6.2-8. Maximum dynamic displacement histories due to different sets of three-component earthquake ground motions

c. *Stress results.*

(1) For evaluation of earthquake performance of the dam, the seismic stresses must be combined with stresses induced by the usual static load combination. The usual static load combination for Portugues Dam consisted of the gravity load due to the dead weight of the concrete, hydrostatic pressures of the impounded water, and the usual concrete temperatures. These loads were applied in a separate static analysis of the dam using the same finite element described in paragraph 6.2.6. The gravity loads were applied to individual cantilevers because they act on cantilever monoliths prior to the grouting of the vertical joints, while the hydrostatic pressures and temperature loads were applied to the monolithic structure.

(2) The maximum total stresses for the earthquake excitation plus the usual static load combination are summarized in Table 6.2-6. These represent the largest maximum arch and cantilever stresses that occur on the upstream and downstream faces of the dam during the particular earthquake excitation. Consistent with the displacement response histories discussed in *b* above, the Managua record gives the highest and Gavilan the second highest maximum tensile stresses.

Ground Motion	Scale Factor	Arch Stress MPa (psi)		Cantilever Stress MPa (psi)	
		Upstream	Downstream	Upstream	Downstream
Scaled Bagnoli	1.6526	3.9 (565)	4.0 (580)	2.2 (319)	3.5 (507)
Scaled Gavilan	0.6914	5.9 (855)	5.1 (740)	3.7 (536)	4.5 (652)
Scaled Managua	0.5682	6.8 (986)	6.8 (986)	4.4 (638)	4.6 (667)
Scaled Sturno	0.6106	4.3 (623)	3.4 (493)	3.0 (435)	2.8 (406)
Spectrum matched	1	4.9 (710)	4.7 (681)	2.7 (391)	3.3 (478)

(3) The minimum static plus seismic stresses were also evaluated to obtain the peak compressive stresses. The peak compressive stresses were well within the compressive strength of the concrete and thus are not discussed here.

(4) For each earthquake input, the stress results are also presented in the form of the envelopes of the maximum stresses, the concurrent or simultaneous stresses at critical time-steps, and the time-histories of critical tensile stresses. The envelopes of the maximum arch and cantilever stresses that usually occur at different times during the earthquake excitation are displayed in the form of stress contours, as shown in Figures 6.2-9 to 6.2-13. Each figure includes four contours showing the maximum tensile arch and cantilever stresses on the upstream (U/S) and downstream (D/S) faces of the dam. The results show that the peak tensile arch stresses occur primarily in the central region of the dam near the crest and peak tensile cantilever stresses at the dam-abutment contact regions and also at the base of the dam on the upstream side.

(5) These maximum tensile stresses are not concurrent; they rather show the maximum stresses that occur at any given locations some time during the earthquake ground shaking. For evaluation of the performance of the dam the concurrent or simultaneous stresses at the critical time-steps should also be examined. Thus for each earthquake input the concurrent stresses at the time of peak tensile arch stress were determined and are presented as stress contours in Figures 6.2-14 to 6.2-18. These so-called stress “snapshots” show that for Portugues Dam the critical tensile arch stresses occur simultaneously on both faces of the dam but are accompanied by compressive arch stresses on the lower part of the dam and compressive cantilever stresses on the upstream face.

(6) The significance of the tensile stresses in terms of producing joint opening or cracking is assessed from examination of the time-histories of the maximum tensile stresses. Stress time-histories corresponding

to the highest maximum tensile arch and cantilever stresses are displayed in Figures 6.2-19 to 6.2-23. Each figure includes two separate time-history graphs, one for arch stresses and another for cantilever stresses. The top graph shows the time-history of the maximum tensile arch stresses plotted together with arch stresses at the same location on the opposite face of the dam. Similarly, the bottom graph shows the time-history of the maximum cantilever stresses together with the cantilever stresses on the opposite face of the dam.

6.2-9 Evaluation of Results

a. Evaluation of the linear-elastic time-history analysis results for arch dams is based on the comparison of the computed stresses with the allowable values and consideration of several factors and engineering judgment. The factors commonly considered include the extent of overstressed regions, number and duration of stress cycles exceeding the allowable values, the ratio of computed to allowable limits, computed displacements, and the simultaneous stress distributions.

b. Usually two sets of allowable stress limits are specified, one for static and another for seismic, which accounts for the fast rate of seismic loading. A detailed description of allowable stress limits is given in EM 1110-2-2201. The Portugues Dam stress limits for the usual static and dynamic loads are listed in Table 6.2-7 (USAED, Jacksonville 1990). The allowable compressive stresses are obtained from the compressive strength of the concrete by applying an appropriate factor of safety, whereas the allowable tensile stresses are taken equal to the tensile strength of the concrete (EM 1110-2-2201).

Concrete	Static MPa (psi)	Dynamic MPa (psi)
Compressive strength	27.5 (4,000)	37.0 (5,400)
Tensile strength	3.10 (450)	5.75 (833)
Allowable compressive stress	7.0 (1000)	24.8 (3,600)
Allowable tensile stress	3.10 (450)	5.75 (833)

c. A comparison of the maximum tensile stresses in Table 6.2-6 and Figures 6.2-9 to 6.2-13 with the allowable limits given in Table 6.2-7 indicates that only arch tensile stresses for the Gavilan and Managua earthquake excitations exceed the dynamic tensile strength of the concrete. However, it is important to note that the tension resistance capability of the vertical contraction joints in arch dams is limited and is expected to be much less than the tensile strength of the intact concrete. As a result the presence of net tension across the vertical contraction joints may be interpreted as the contraction joint opening. In the case of Portugues Dam, the concurrent stress contours in Figures 6.2-14 to 6.2-18 show tensile arch stresses on both faces of the dam, an indication that momentary joint opening would occur. The time-histories of arch stresses in Figures 6.2-19 to 6.2-23 demonstrate that although the joint opening may occur repeatedly during the earthquake excitation, duration of each joint opening is only a fraction of a second and should not cause any significant damage. The fact that Portugues Dam would safely withstand such joint opening was verified by a nonlinear time-history analysis of the dam that permitted contraction joints to open whenever nonzero tension forces were indicated across the joints (QUEST Structures 1990). The amount of joint opening is expected to be the highest for the Managua record and the second highest for the Gavilan record.

d. The maximum tensile cantilever stresses for all earthquake excitation cases meet the required dynamic tensile strength of 5.75 MPa for the concrete. Furthermore, the time-histories and concurrent cantilever stresses demonstrate that the significant tensile cantilever stresses are accompanied by compressive cantilever stresses on the opposite face of the dam. Therefore, should any cracks occur due to the cantilever bending, they would be minor and shallow and limited to small regions near the dam-foundation contact.

6.2-10 Conclusion and Recommendations

a. Three-dimensional finite element analysis including dam-water and dam-foundation interaction is essential for the design and evaluation of concrete arch dams. For successful analyses, realistic structural modeling, proper selection of material properties, appropriate loading combinations, and reasonable design or evaluation of earthquake ground motion(s) are among important issues that need to be carefully examined and addressed.

b. In cases similar to Portugues Dam, a finite element incompressible liquid mesh is usually adequate for modeling the dam-water interaction effects. For dams higher than 100 m and reservoirs with significant amounts of accumulated sediment, a refined dam-water interaction model including water compressibility and reservoir boundary absorption effects may be more desirable. The standard foundation model for seismic analysis of arch dams is a massless model. Such a simplified model is considered adequate for practical purposes especially where the modulus of the foundation rock is about the same as or exceeds that of the concrete. The earthquake input for time-history analysis of arch dams is defined in terms of three-component acceleration time-histories. The spectrum-matched and/or scaled natural earthquake acceleration records may be employed. As demonstrated in this example problem, the result for the spectrum-matched earthquake inputs may be considered as the average response, whereas the dam response to the scaled natural records may fall in a wide range representing both the lower and upper bound as well as the average values.

c. Following the procedures illustrated in this example, the performance of arch dams subjected to earthquake loading can be adequately analyzed and evaluated. Although only the linear-elastic response of the dam was computed, it was still possible to estimate what mode of behavior and level of damage could be expected. The results also demonstrate that even for the linear-elastic analysis the use of one set of spectrum-matched records commonly used in practice may not be sufficient. It is recommended that the spectrum-matched records be supplemented by at least three additional scaled natural records having different waveforms and frequency contents.

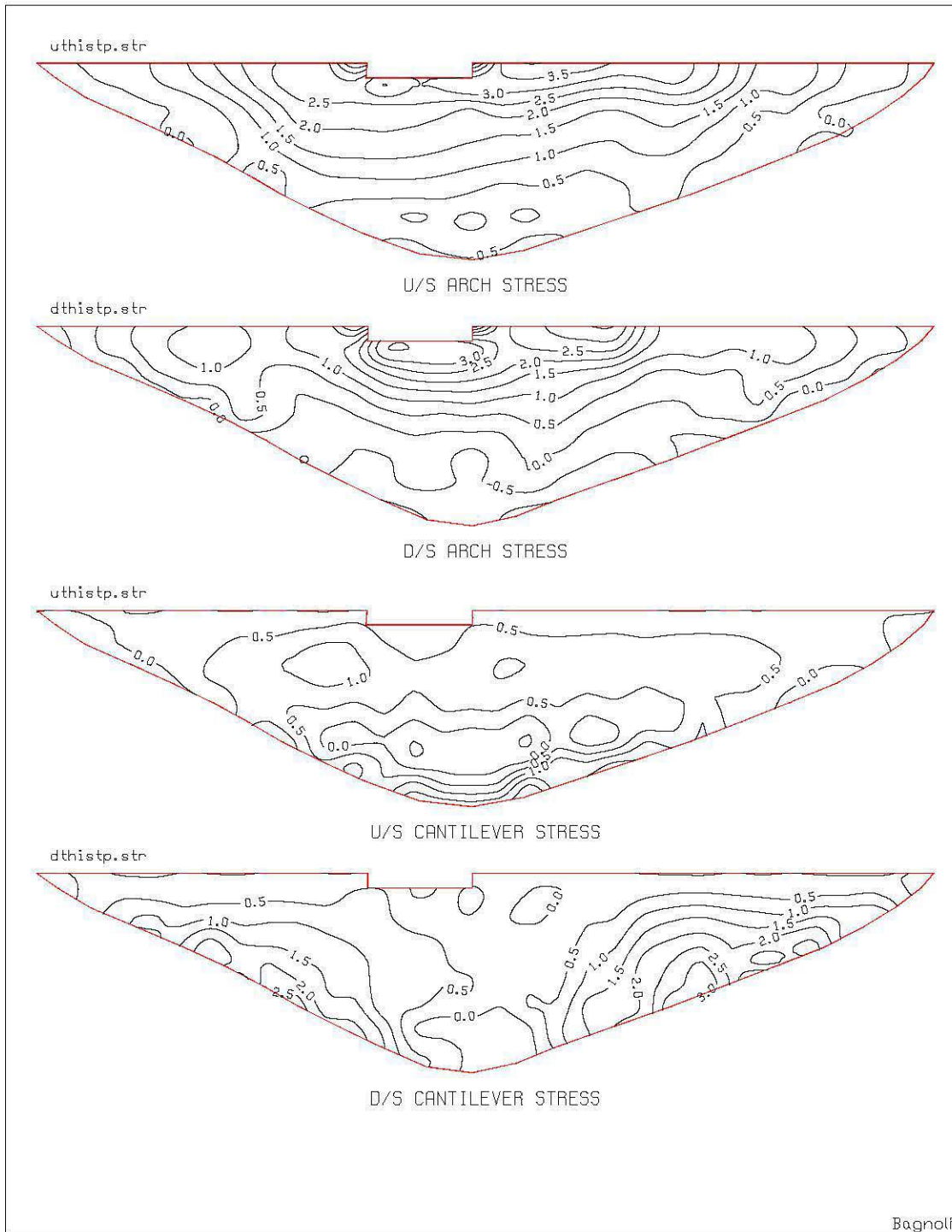


Figure 6.2-9. Envelopes of maximum stresses due to Bagnoli record plus static loads

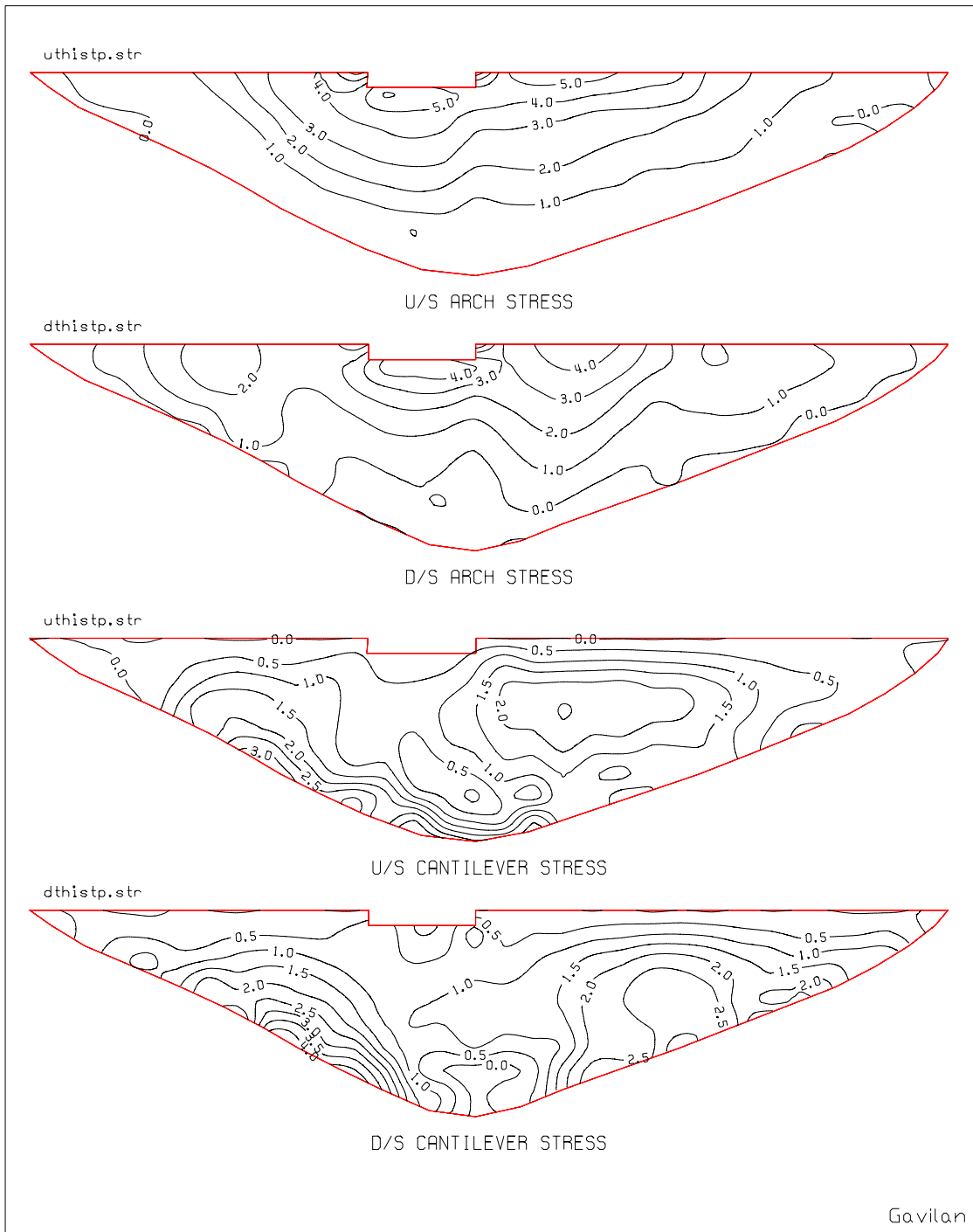


Figure 6.2-10. Envelopes of maximum stresses due to Gavilan record plus static loads

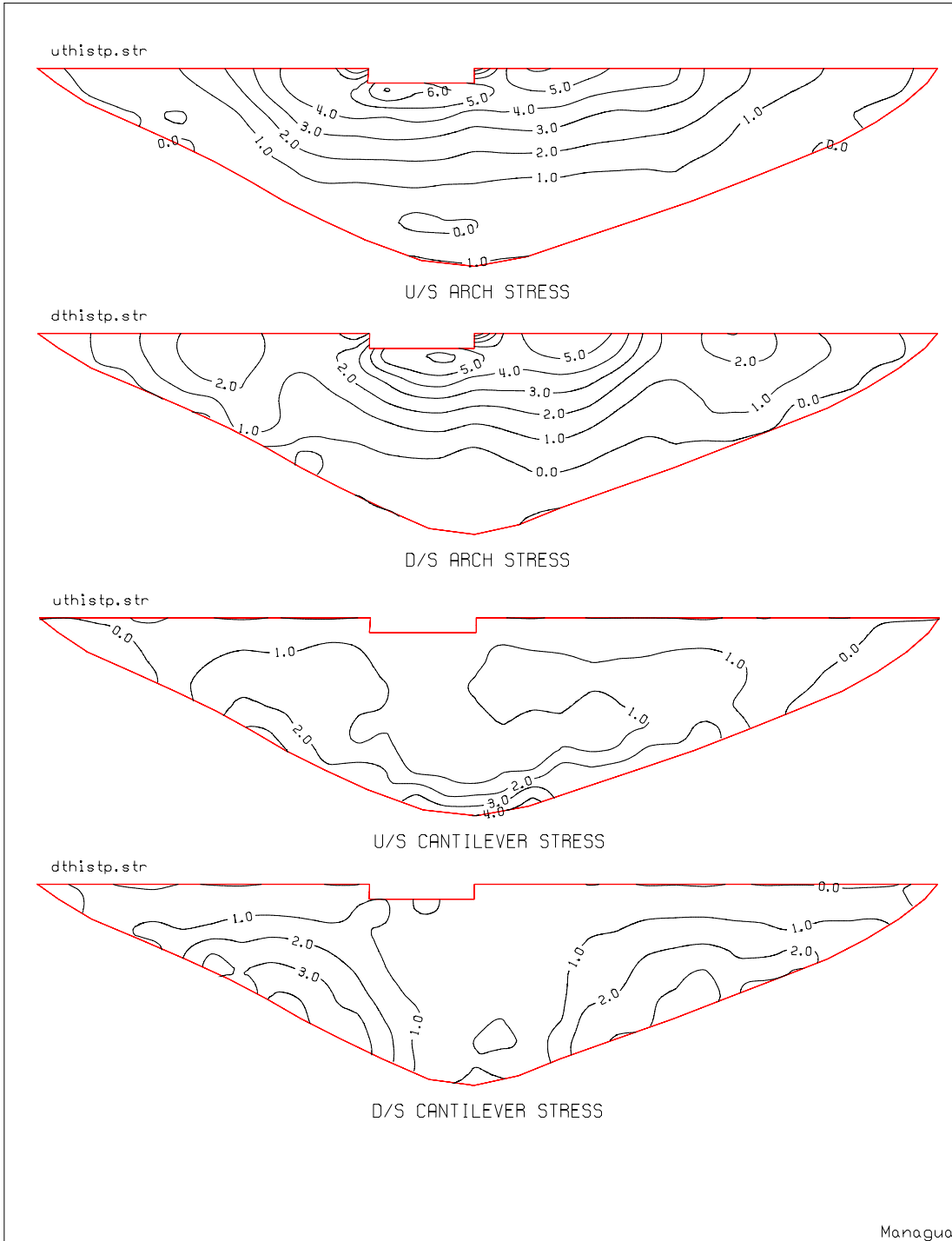


Figure 6.2-11. Envelopes of maximum stresses due to Managua record plus static loads

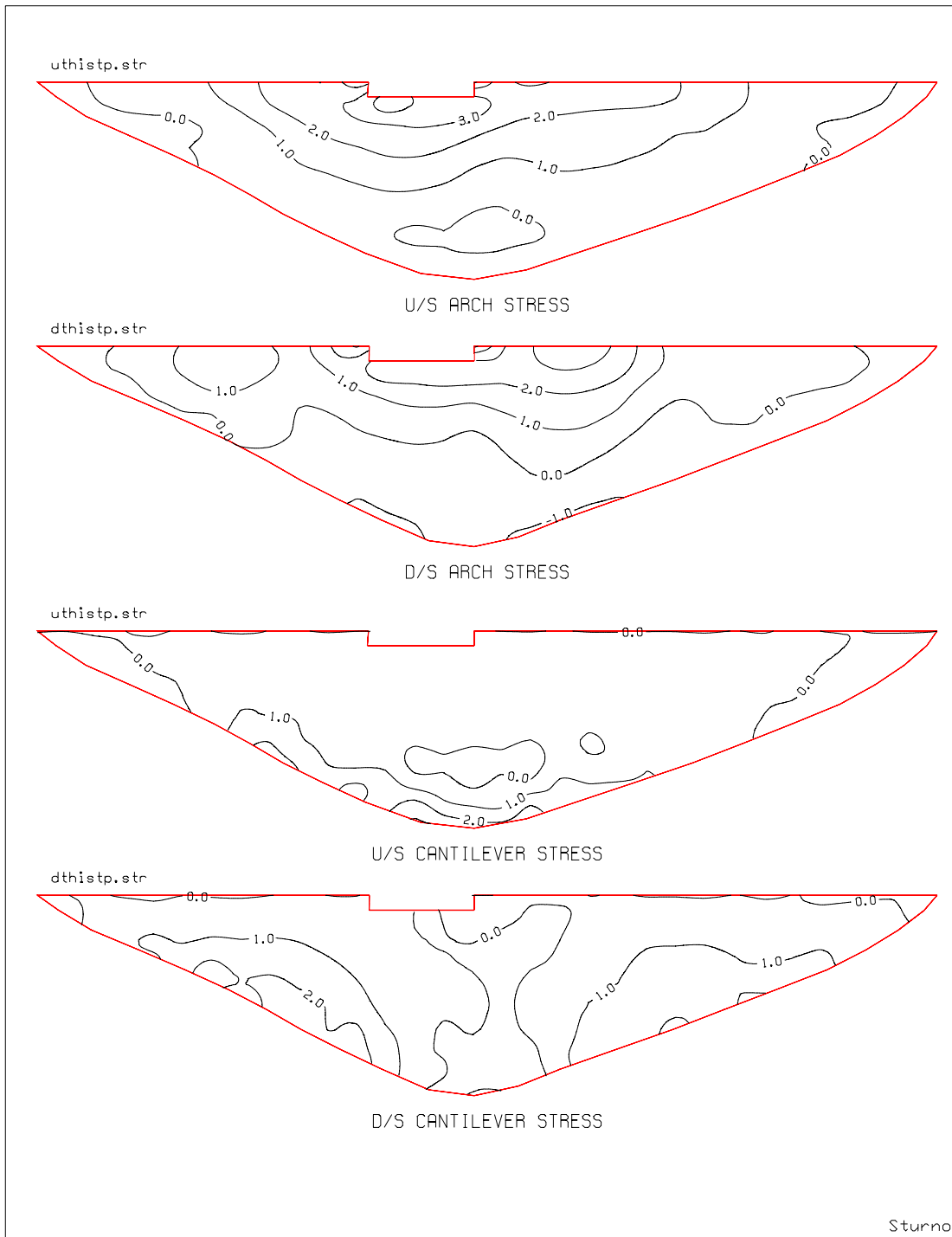


Figure 6.2-12. Envelopes of maximum stresses due to Sturmo record plus static loads

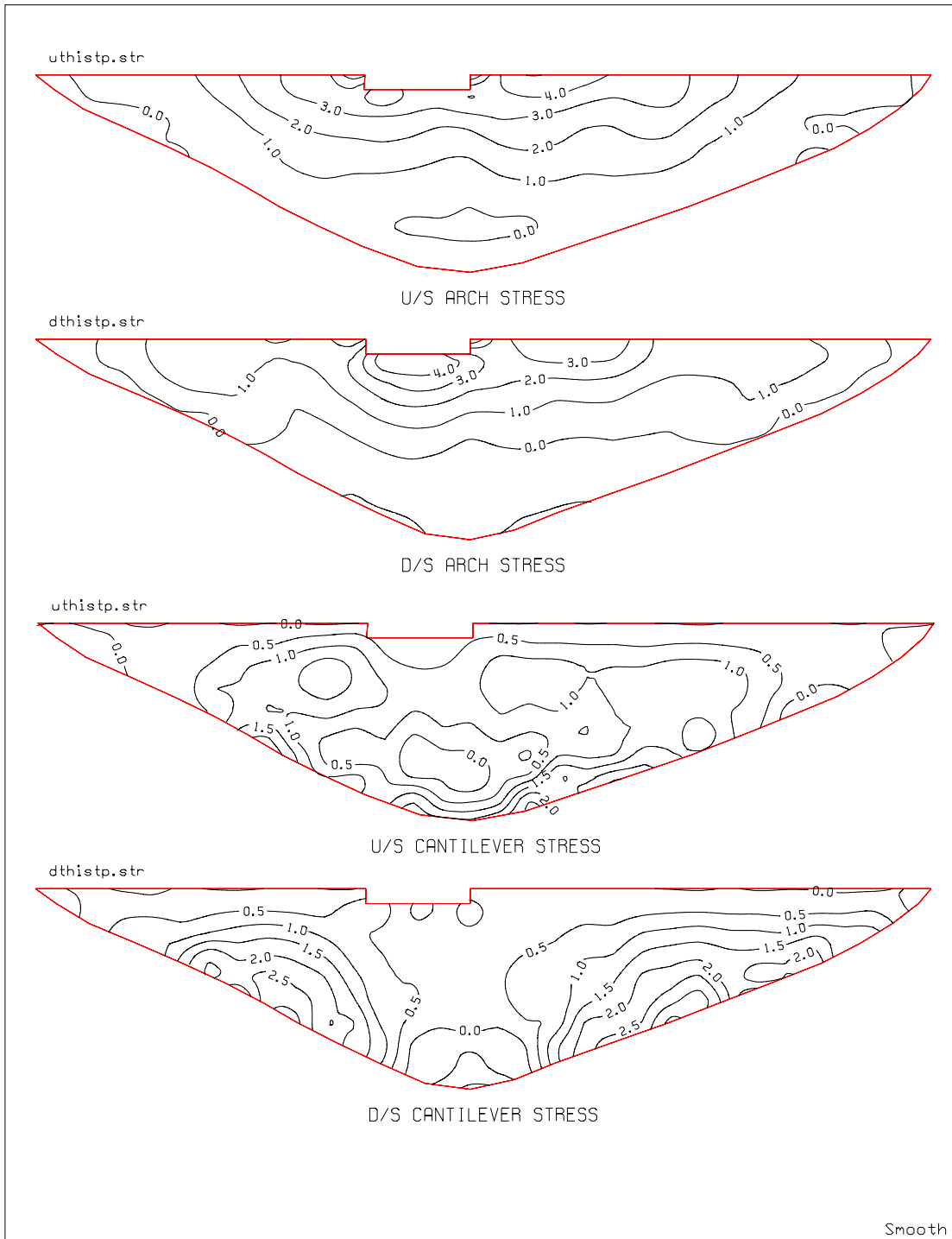


Figure 6.2-13. Envelopes of maximum stresses due to spectrum-matched record plus static loads

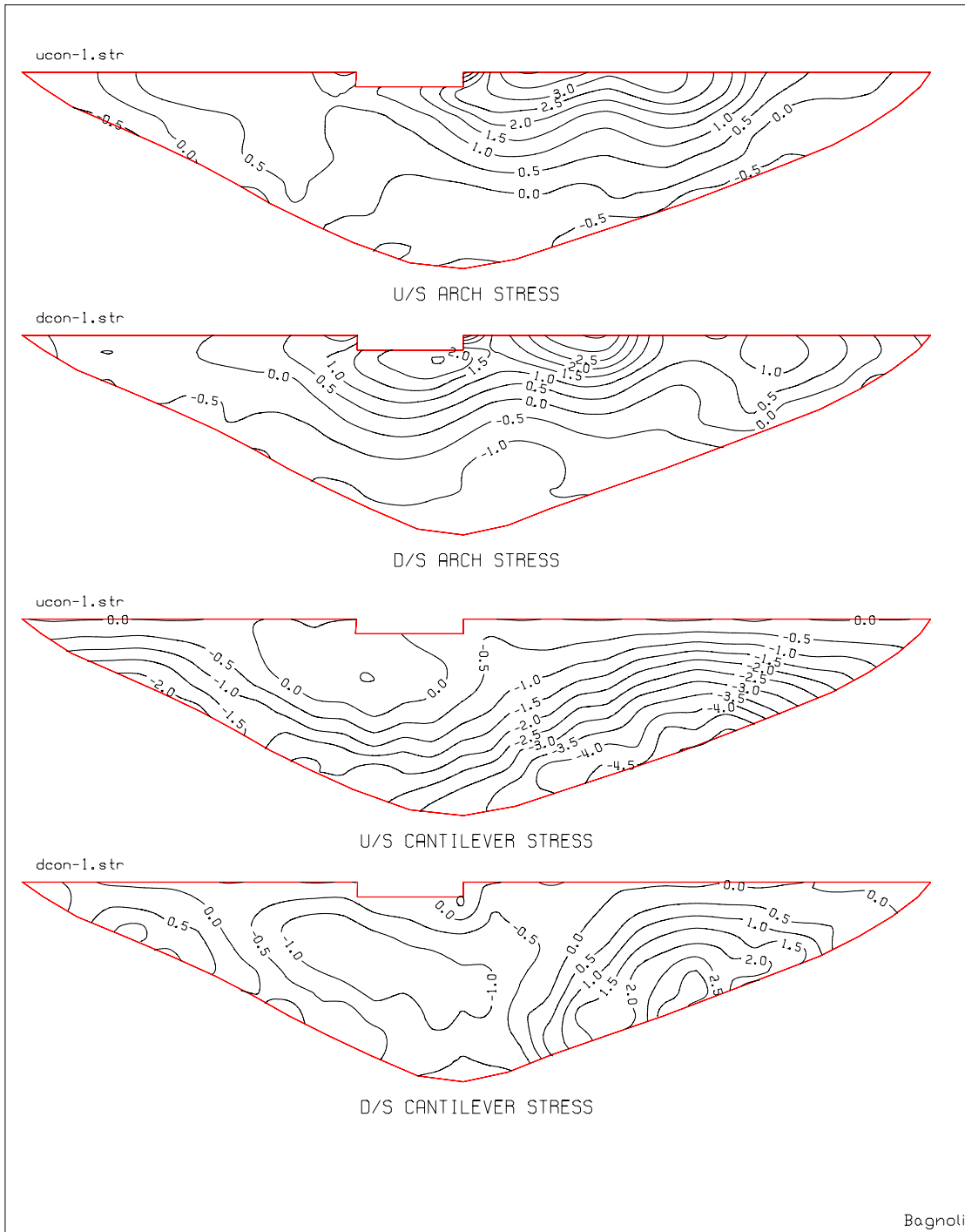


Figure 6.2-14. Concurrent stresses due to Bagnoli record plus static loads at the time of maximum arch stress

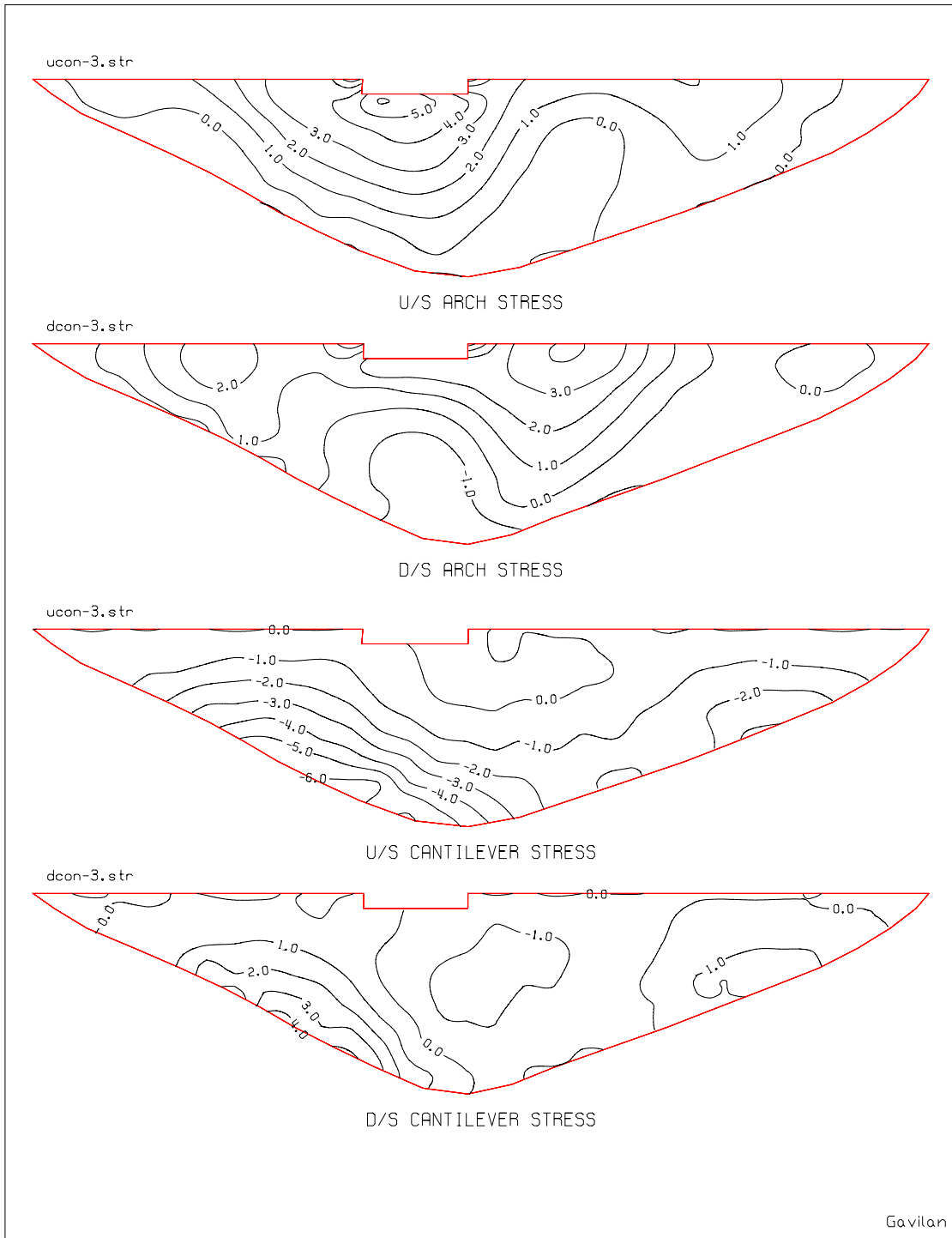


Figure 6.2-15. Concurrent stresses due to Gavilan record plus static loads at the time of maximum arch stress

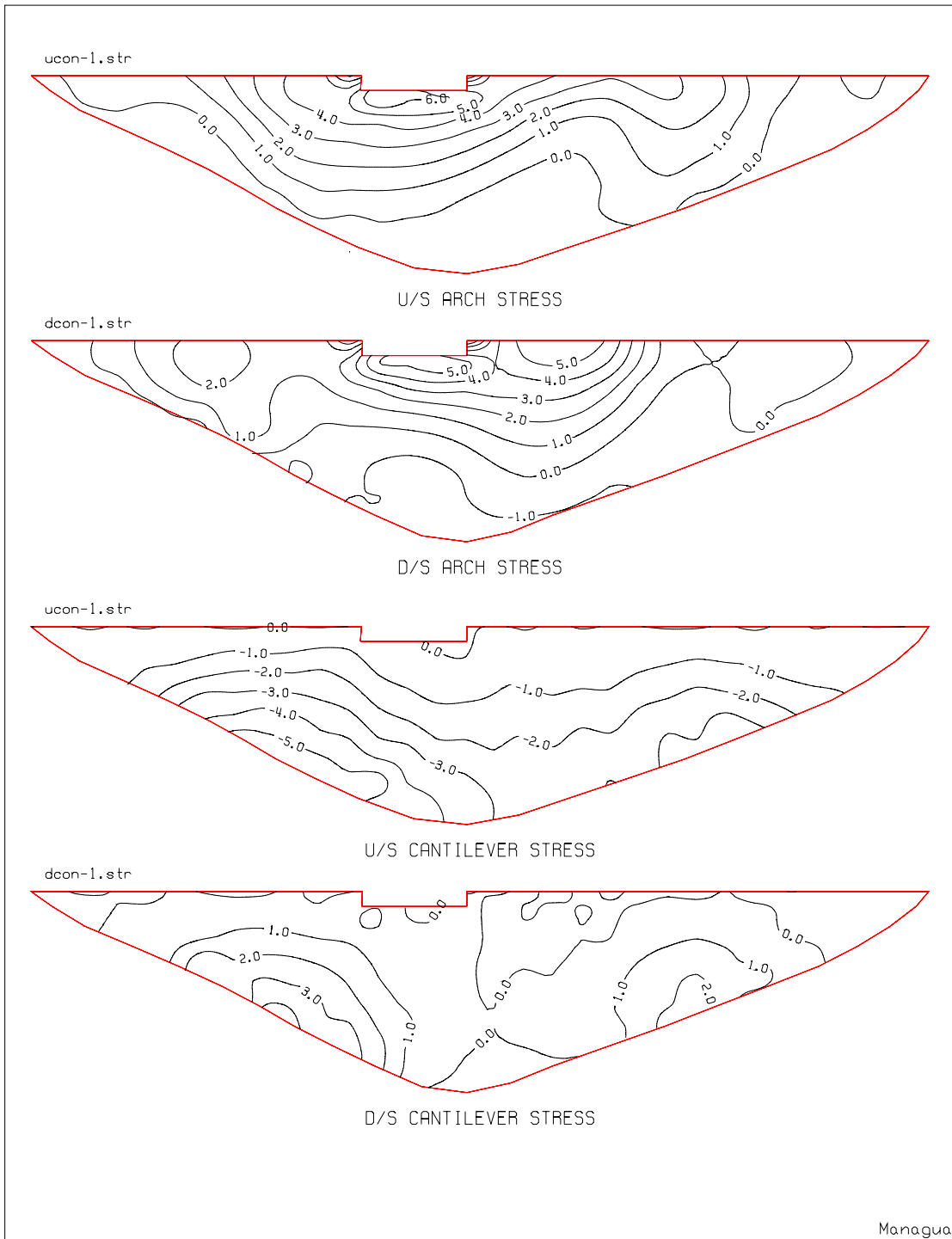


Figure 6.2-16. Concurrent stresses due to Managua record plus static loads at the time of maximum arch stress

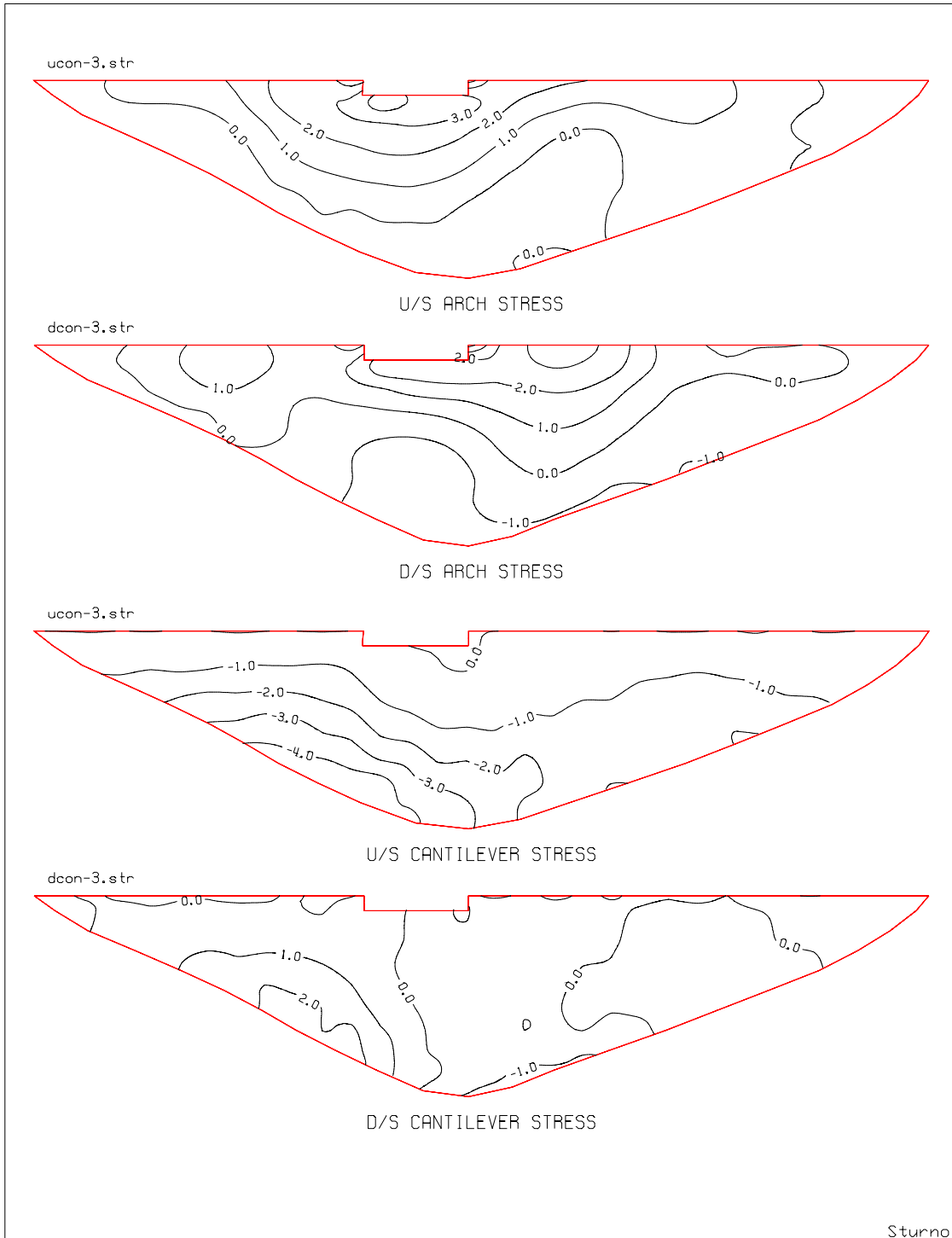


Figure 6.2-17 Concurrent stresses due to Sturmo record plus static loads at the time of maximum arch stress

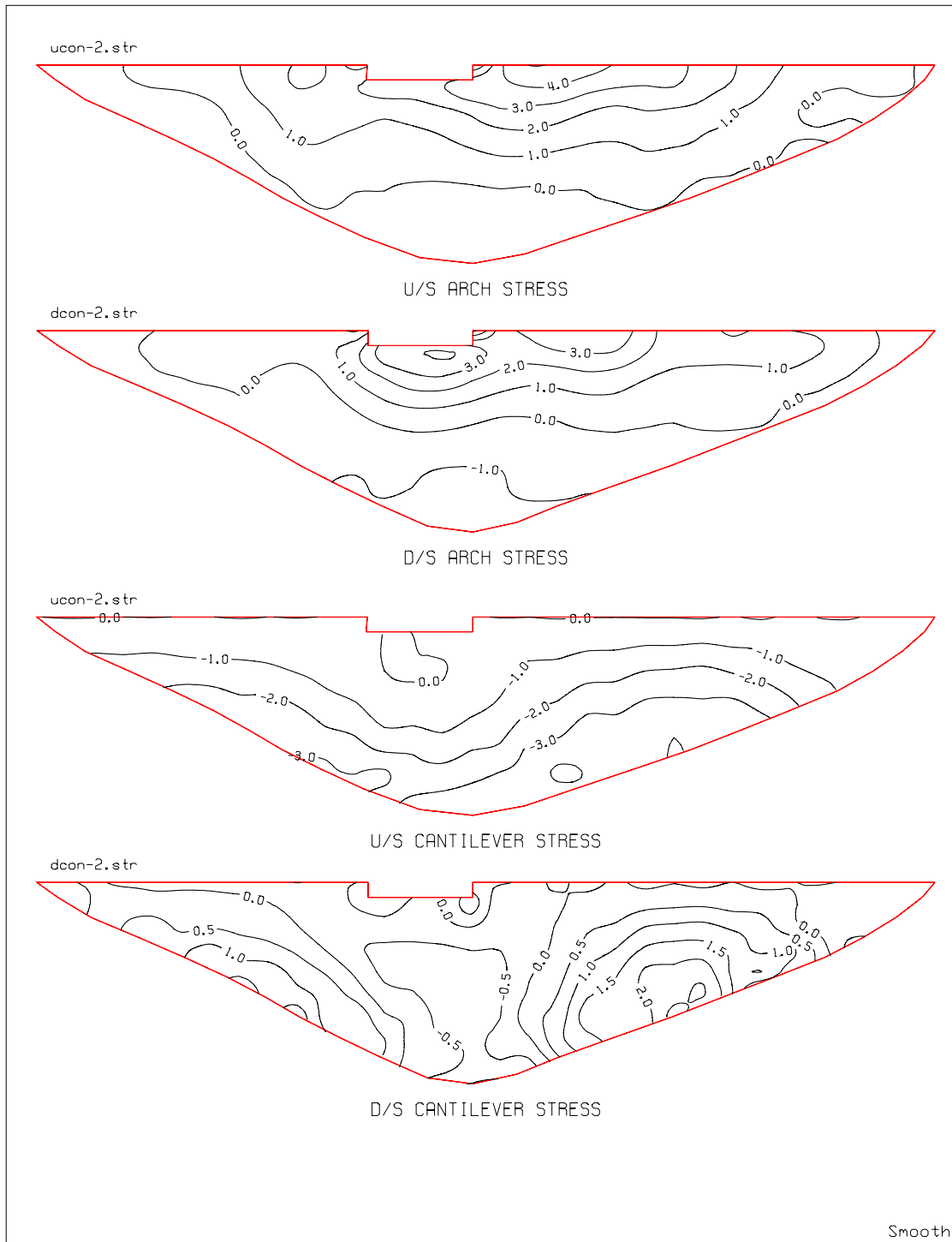


Figure 6.2-18. Concurrent stresses due to spectrum-matched record plus static loads at the time of maximum arch stress

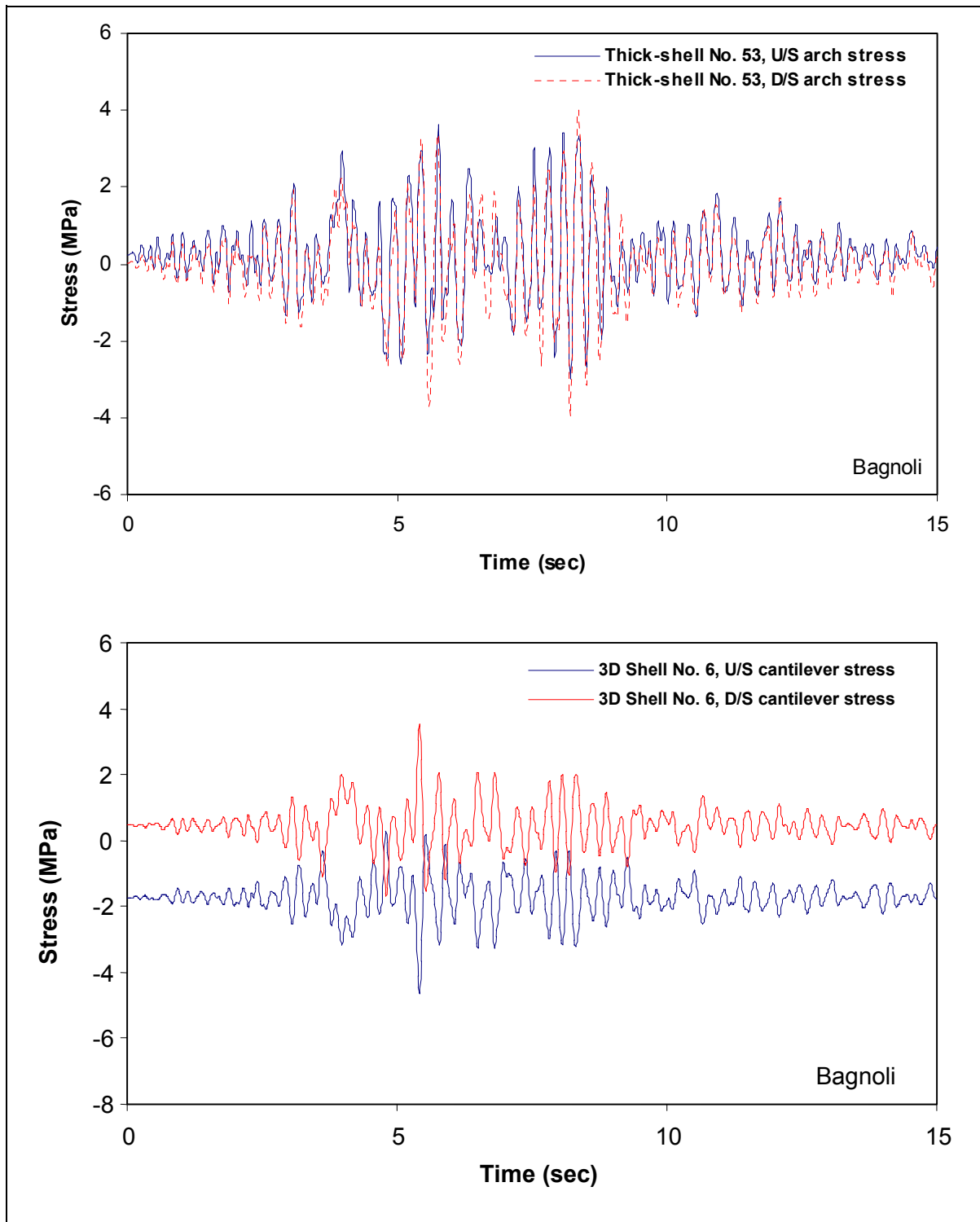


Figure 6.2-19. Time-histories of maximum arch and cantilever stresses and corresponding stresses on opposite face of the dam due to Bagnoli record plus static loads

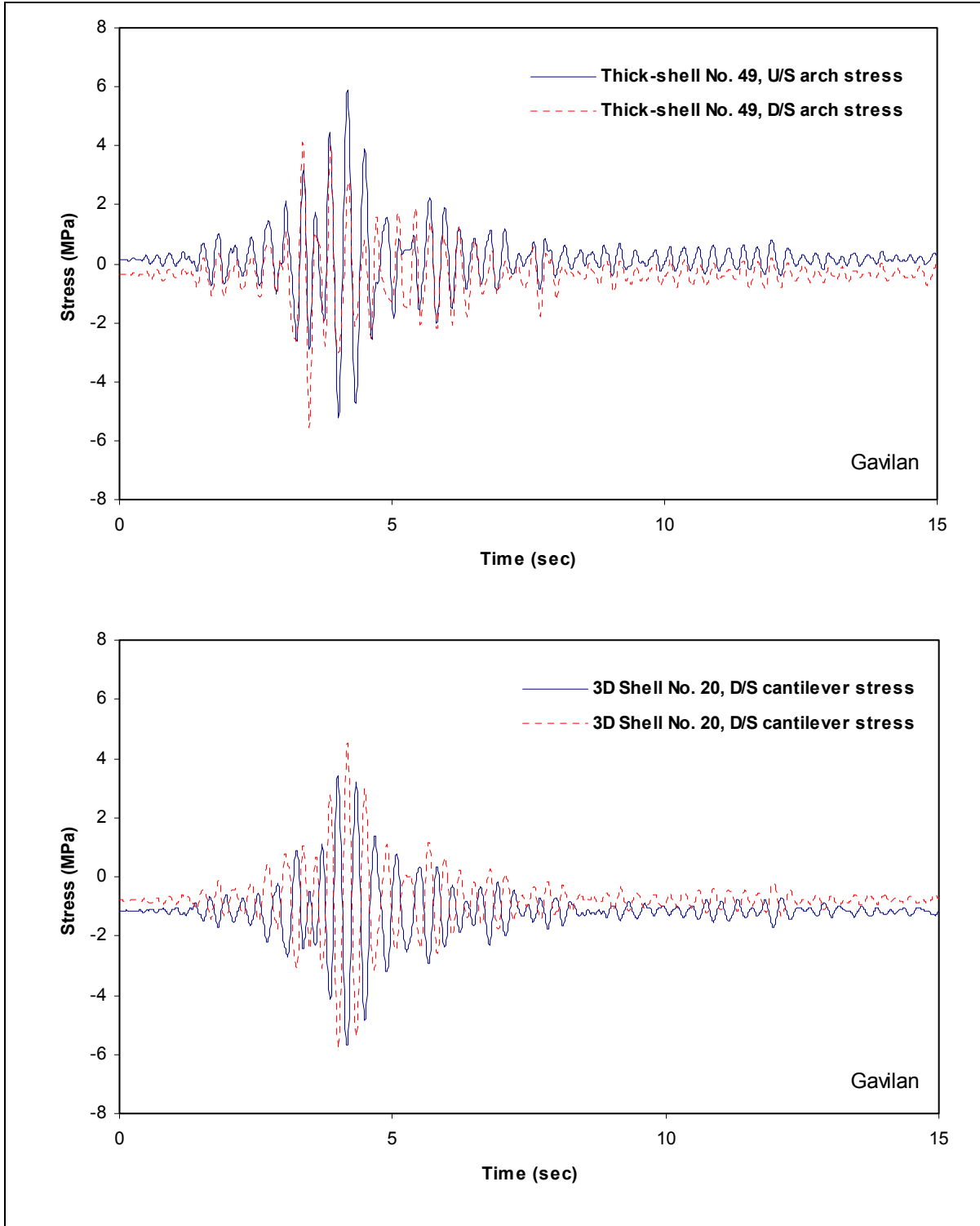


Figure 6.2-20. Time-histories of maximum arch and cantilever stresses and corresponding stresses on opposite face of the dam due to Gavilan record plus static loads

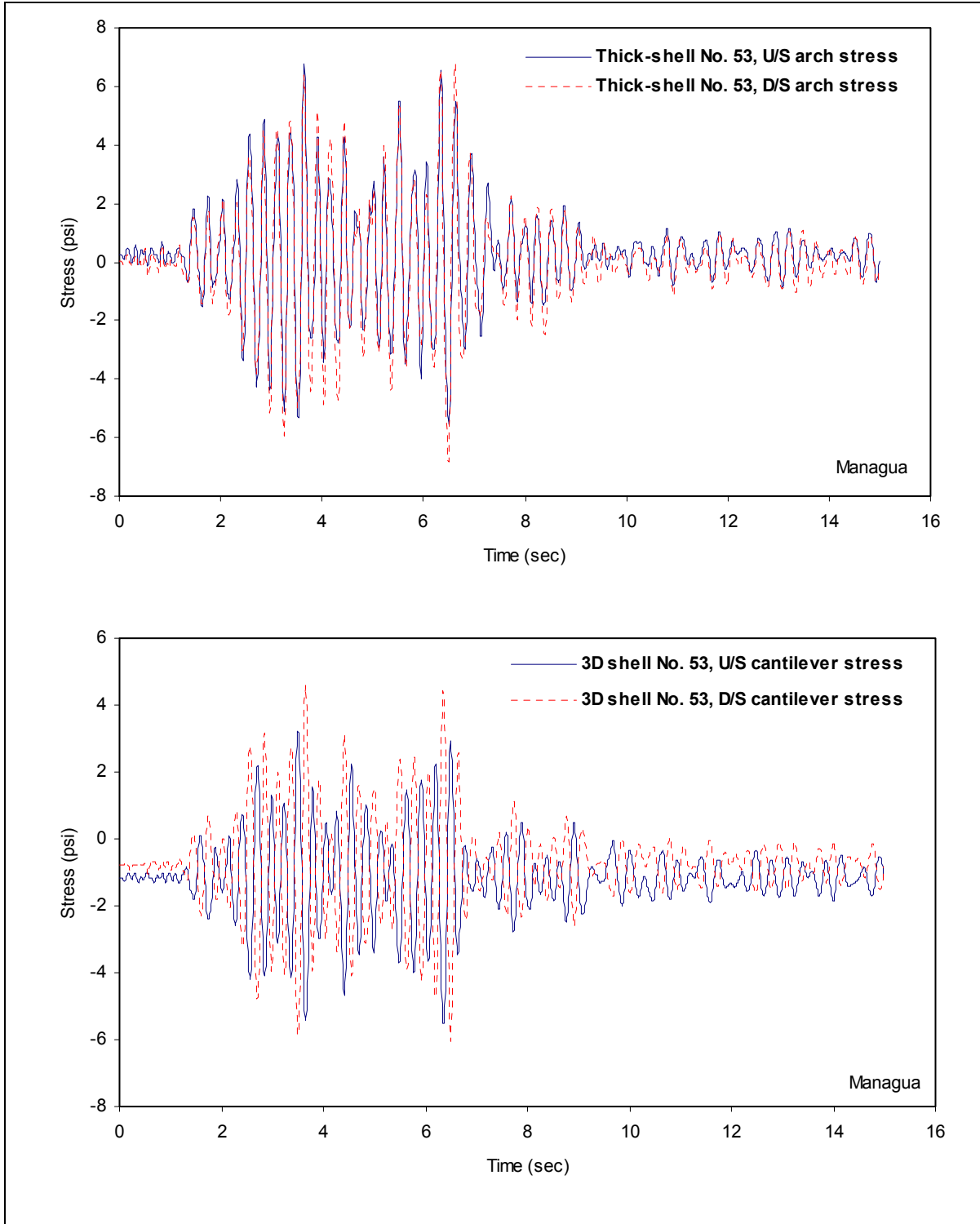


Figure 6.2-21. Time-histories of maximum arch and cantilever stresses and corresponding stresses on opposite face of the dam due to Managua record plus static loads

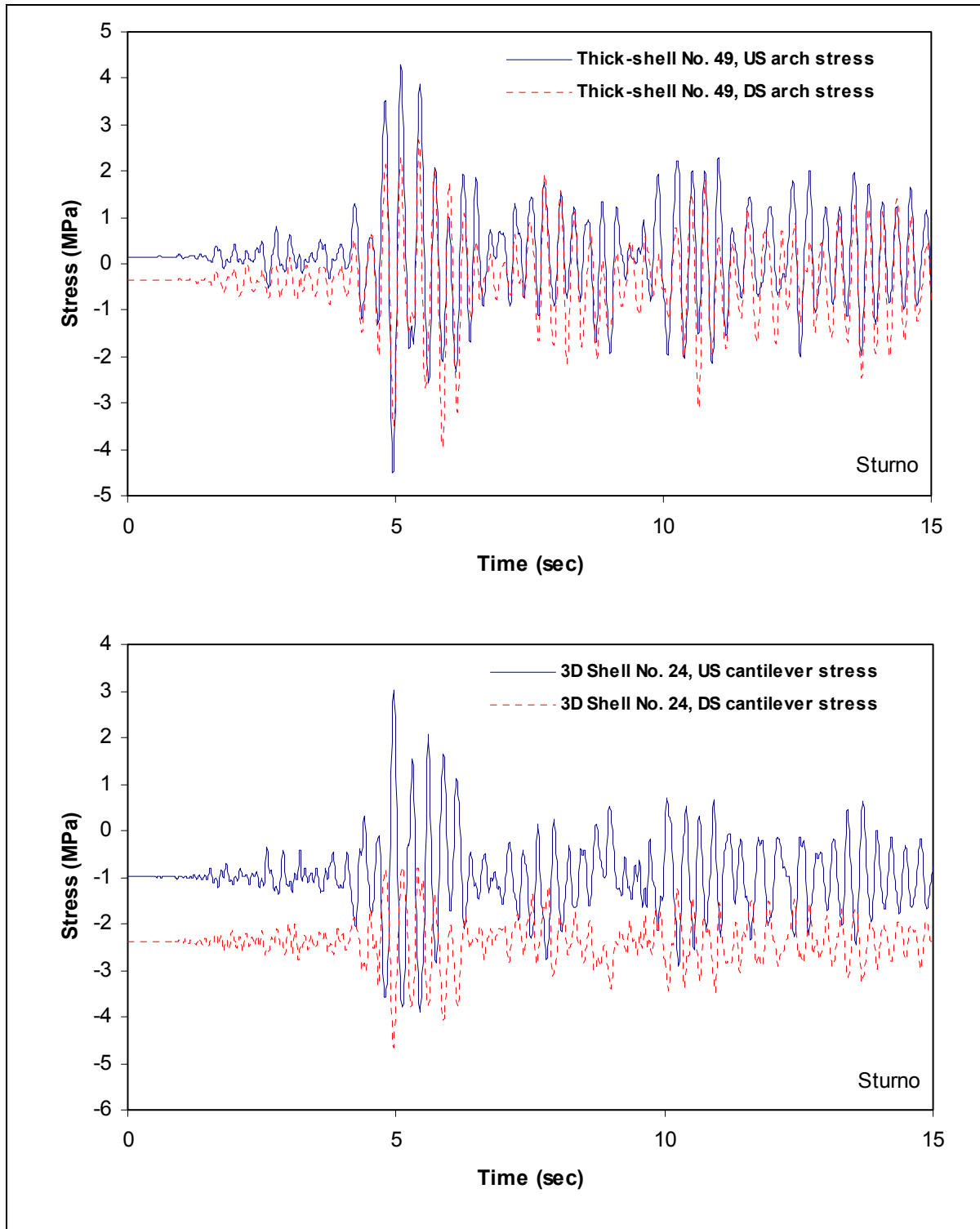


Figure 6.2-22. Time-histories of maximum arch and cantilever stresses and corresponding stresses on opposite face of the dam due to Sturmo record plus static loads

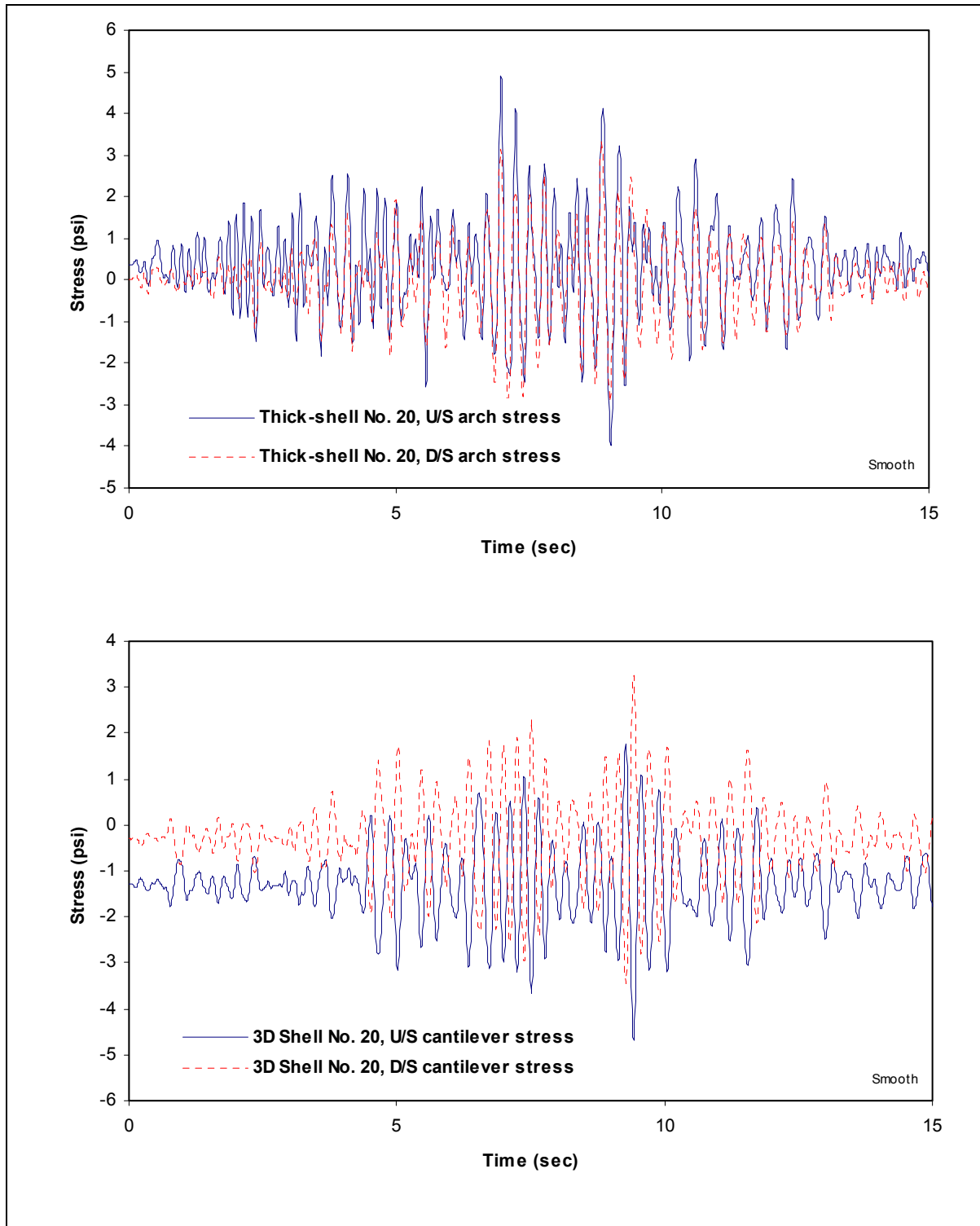


Figure 6.2-23. Time-histories of maximum arch and cantilever stresses and corresponding stresses on opposite face of the dam due to spectrum-matched record plus static loads

6.3 DYNAMIC SOIL-STRUCTURE INTERACTION ANALYSIS OF OLMSTED LOCK CHAMBER MONOLITH

6.3-1 Background

The Olmsted Locks and Dam Project replaces existing Lock and Dam 52 and 53 and is located at Ohio River Mile 964.4, approximately 2.9 km (1.8 miles) downstream of Lock and Dam 53, near Olmsted, Illinois. The lock structure consists of two 33.5-m by 365.8-m (110-ft by 1200-ft) locks adjacent to the Illinois bank (Figure 6.3-1). The locks are supported by more than 11,700 H-piles (HP 14×117) spaced 1.5 to 2.1 m (5 to 7 ft) in the upstream-downstream direction and 1.8 to 3.8 m (6 to 12.5 ft) in the cross-stream direction. The H-piles are about 12.2 to 13.7 m (40 to 45 ft) long and penetrate into the McNairy I formation, which is found to be highly over-consolidated toward the ground surface. For the chamber monoliths, the landside lock wall is backfilled to the top of the wall at El +3101. This results in about 20.1 m (66 ft) of the backfill behind the landside lock wall on the Illinois bank. The riverside lock wall is embedded to El +285 (i.e., 12.5 m (41-ft) embedment).

6.3-2 Purpose and Objectives

The purpose of this example is to illustrate an approach used to perform dynamic soil-pile-structure-interaction (SPSI) analysis for the chamber monolith of the Olmsted Locks using time-history analysis. The objectives of the SPSI analysis are:

- a. To compute peak values and time histories of dynamic pile forces and moments for the combined horizontal and vertical earthquake excitations
- b. To evaluate pile interaction factors for assessing demand/capacity ratio of piles
- c. To compute peak values and time histories of dynamic section forces and moments at critical sections of the lock structure for reinforcement design

6.3-3 Scope

The scope of this example included consideration of one set of seismic input acceleration time histories and involved the following:

- Definition of time histories for design ground motion
- Idealization of site soil profiles and estimates of dynamic soil properties
- Development of finite element models of the soil-pile-lock structure system
- Analysis of static loading
- Analysis of dynamic loading
- Evaluation of response of pile foundation and concrete sections for static plus earthquake loads

Note that in a true seismic evaluation one needs to use more than one set of acceleration time histories to account for uncertainties in earthquake ground motions.

¹ All elevations (El) cited in this section are in feet referred to the National Geodetic Vertical Datum. To convert to meters, multiply by 0.3048.

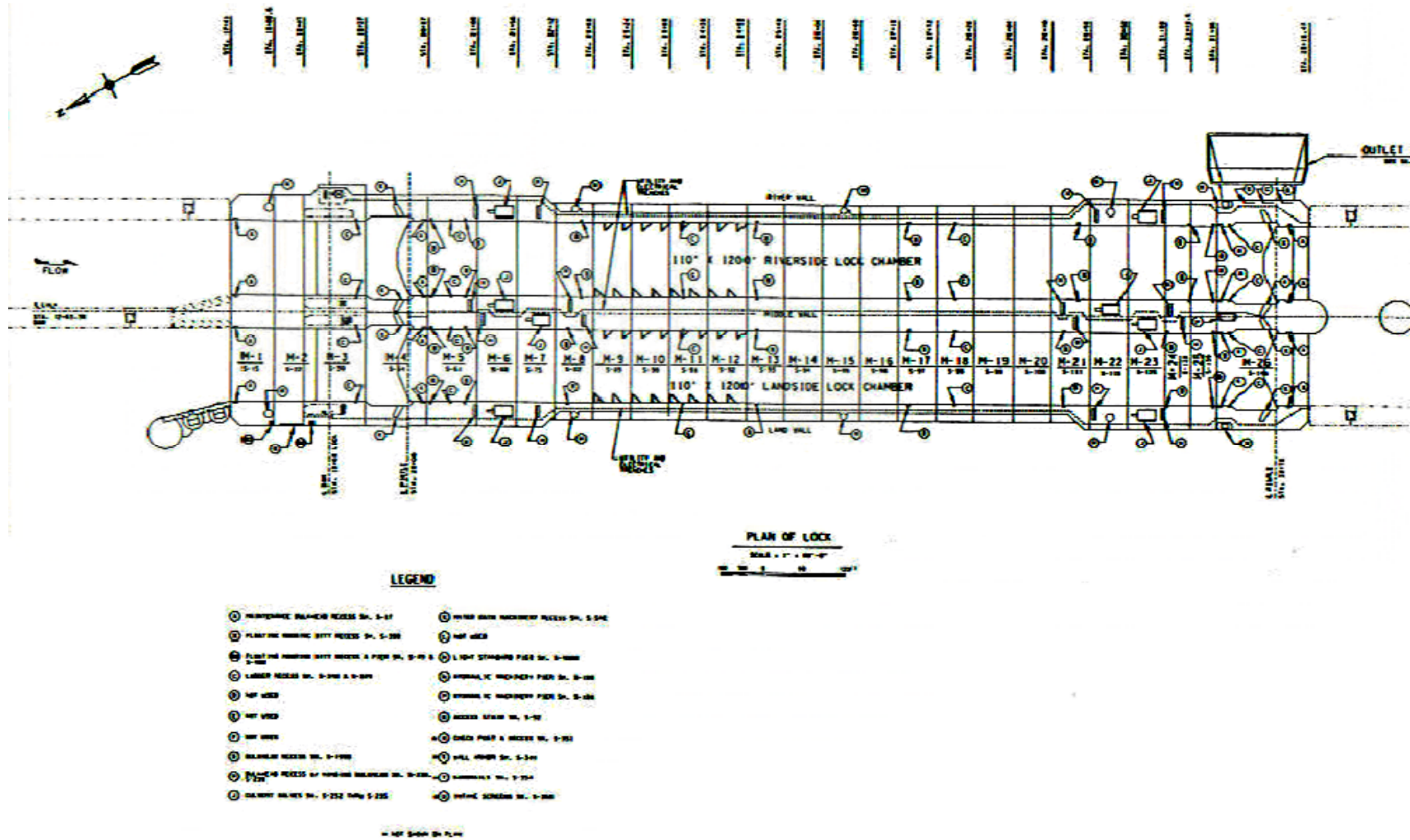


Figure 6.3-1. Plan View of Olmsted Locks

6.3-4 election of Analysis Procedures

Mainly two procedures are available for analysis of SPSI: soil spring versus soil continuum. In the soil spring procedure, the structure is supported by a series of nonlinear soil springs simulating soil-pile interaction and is loaded by lateral soil pressures acting on the embedded lock walls. In the soil continuum procedure, the structure is supported by a series of piles idealized as beam elements embedded and connected with quadrilateral soil elements beneath and surrounding the lock structure. Advantages and limitations of each analysis procedure are described in *a* and *b* below.

a. Soil spring procedure

(1) The soil spring procedure is generally based on a sub-structuring method of analysis. The lock structure is supported by a series of springs at the lock base representing the pile foundation and on the lock wall representing lateral soil pressures. The soil springs at the lock base are nonlinear and are generally approximated by nonlinear pile-head load-deflection curves. The pile-head load-deflection curves are generally developed by modeling the piles supported by a series of independent nonlinear axial (t-z) and lateral (p-y) soil springs along the length of the pile. These nonlinear axial and lateral soil springs are based on empirical relationships developed from back calculation of static axial and lateral pile load tests. For closely spaced pile foundations (e.g., pile center-to-center spacing of less than three pile diameters), pile-to-pile interaction or pile group effects are approximated by semi-empirical interaction factors. Thus, the nonlinear soil-pile interaction is approximated by nonlinear pile head stiffness through an iterative procedure.

(2) The soil spring procedure has the following limitations:

- Axial and lateral soil-pile springs are uncoupled and are generally developed for static loading conditions and used for seismic loading conditions.
- Kinematic soil-structure interaction cannot be rigorously accounted for in the analysis.
- Wave propagation phenomena and soil-pile interaction under seismic loading conditions are generally not rigorously accounted for; thus, there are uncertainties related to pile response under seismic loading conditions.
- Pile group effects on the computed response are accounted for through the use of p-multiplier based on limited empirical static pile load test data, and its modeling accuracy has not been validated.
- Soil-embedment effects especially on the landside lock wall cannot be easily accounted for.

b. Soil continuum procedure

(1) The soil continuum procedure is a direct method in which the lock structure, piles, and surrounding soil media to basement rock can be modeled and analyzed as a complete system. Using this procedure, both kinematic and inertial interaction and wave propagation phenomena are accounted for directly. Depending on the size or number of piles, the soil-pile-structure system may be approximated by a 3- or 2-D model. For a long pile-supported lock structure such as the Olmsted chamber monolith, the response of the lock in the transverse direction (cross-stream direction) can be reasonably approximated by a 2-D model. Both the lock structure and soil media are modeled by 2-D quadrilateral elements. Piles are modeled by beam elements connected to the quadrilateral soil or concrete elements. Wave propagation, pile group effects, and soil embedment effects on the lock response are rigorously accounted for in this procedure.

(2) The soil continuum procedure has the following limitations:

- For a large pile foundation, due to limitations in computing resource, the pile foundation can be approximated only by a 2-D model
- Nonlinear soil-pile interaction can only be approximated by equivalent linear techniques; thus, strong nonlinear soil-pile interaction, if present, cannot be realistically modeled.

c. Modeling procedure selected

(1) For the Olmsted locks, the soil continuum procedure implemented in the computer program FLUSH (Lysmer et al. 1975) was selected to model SPSI and the effects of deep soil embedment at the land-side on the response of the lock-pile system. In the subsequent sections, analysis steps followed and the results obtained are described.

(2) The dynamic SPSI analyses were performed using QFLUSH (QUEST Structures, www.WebDams.com), an enhanced version of FLUSH with pre- and post-processing capabilities. The analyses were performed in the frequency domain for vertically propagating shear and compression waves (horizontal and vertical excitations). Analyses for the horizontal and vertical excitations were performed separately and then combined. The nonlinear soil behavior was approximated by the equivalent linear techniques described in 5-6b(2) through iterative procedures for the horizontal excitation. The results for the horizontal and vertical excitations were transformed from the frequency domain back to the time domain. The time-domain results were subsequently combined to obtain the total response for simultaneous horizontal and vertical (shear- and compression-wave) excitations. For the QFLUSH analyses, the input motion at the rigid base is required. The input motion was derived as an interface motion at the boundary between the free-field soil/rock column and basement rock from the site response analysis using the program SHAKE (Schnabel et al. 1972).

6.3-5 Finite Element Modeling

a. The computer model for the SPSI analyses consisted of the lock structure, supporting soil, and the piles. The lock structure and the foundation soil were modeled by plain-strain 2-D quadrilateral solid elements. Each individual pile was modeled by a series of beam elements whose translational degrees of freedom were connected to surrounding soil or concrete elements. The finite element representation of the chamber monolith and its pile foundation is shown in Figure 6.3-2. The rigid connection between the pile head and the lock basemat was simulated by extending pile elements 1.2 m (4 ft) into the basemat. The pile foundation model included 43 piles; each modeled by 17 beam elements. The finite element model of the complete soil-pile-lock structure is shown in Figure 6.3-3. Two rock layers were incorporated in the model to minimize the effects of the rigid base on the computed response. The vertical dimensions of the soil elements depend on the maximum frequency of the motion to be retained in the analysis, and were established as suggested by Lysmer et al. (1975). It was estimated that the maximum frequency of importance to the structural response was about 10 to 12 Hz. In the analyses, the vertical dimensions of the soil elements were selected to retain a maximum frequency of 20 Hz for the horizontal excitation and at least 30 Hz for the vertical excitation. The finite element model consisted of 3,740 solid elements, 739 beam elements, and 4,716 nodal points.

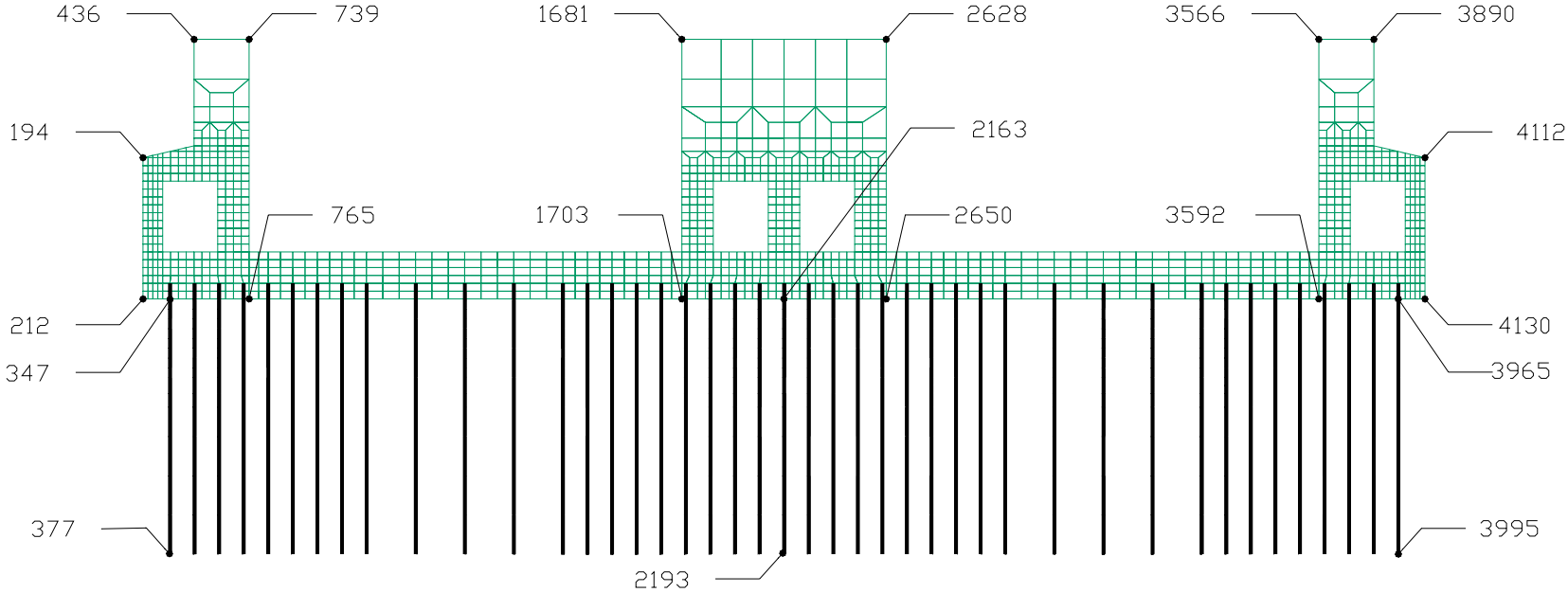


Figure 6.3-2. Finite element model of lock and piles

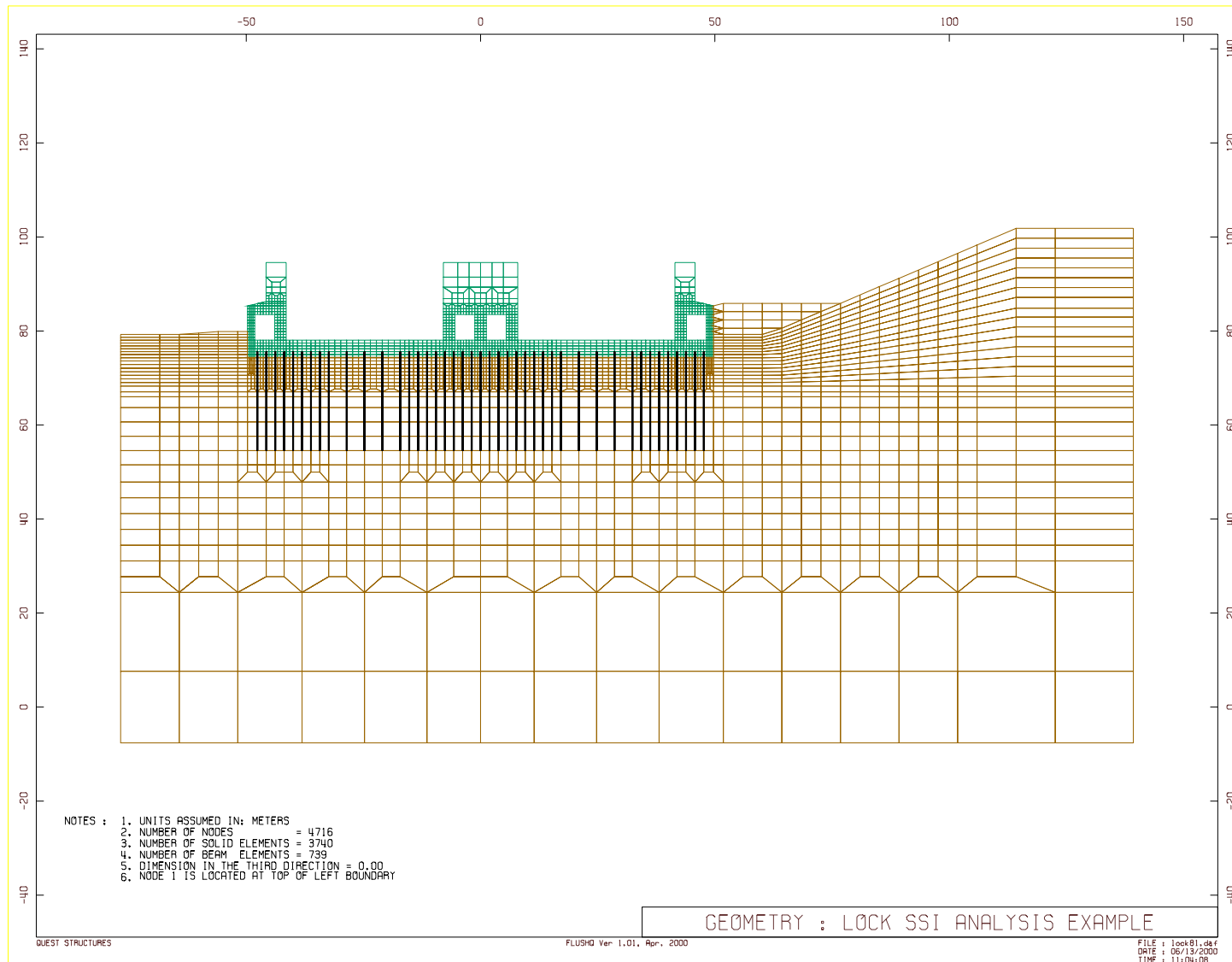


Figure 6.3-3. Finite-element mesh representation of the soil-pile-lock system

b. An energy-transmitting boundary was specified on the left side (i.e., riverside) of the model. A displacement boundary condition consisting of horizontal rollers for the horizontal excitation and vertical rollers for the vertical excitation was specified on the right side boundary (i.e., bank side).

c. The finite element model incorporated a thin soft-soil layer, 76-mm (3-in.) in thickness, beneath the lock basemat in order to compute conservative values of forces and moments at pile heads. The soft-soil layer simulates a condition where primarily piles would carry seismic loads.

6.3-6 Material Parameters

a. Stratigraphic Profile

(1) The Olmsted lock structure considered for SPSI studies is situated along the Illinois bank of the Ohio River. Subsurface soil conditions of the Illinois bank generally consist of a surficial layer of colluvium/alluvium overlying McNairy Zone I and McNairy Zone II formations. Granular backfill will be placed on both sides of the lock (river and bank sides). The McNairy Zone I formation is described in USAED, Louisville (1989 and 1990) as “a complex assemblage of interbedded partings and bands of micaceous clays, silts, and very fine to fine sands.” Results of pressure meter tests performed in 1997 indicated that the McNairy I formation is highly over consolidated. The McNairy Zone II formation is described as “predominantly a clayey silt with varying amounts of organics; contains numerous gravel size fragments of black chert with some extensive layers of highly jointed indurated clayey silt to siltstone; material is rock-like in some locations and soil-like in others.” Bedrock, described as a Paleozoic-age shale, was encountered at approximately Elevation 27.43 m (90 ft) immediately underlying the McNairy Zone II formation.

(2) To perform SPSI analyses, a typical stratigraphic profile through the chamber monolith was developed. Subsurface soil conditions (and associated geotechnical data) encountered in borings within reasonable proximity to the chamber monoliths were used to characterize the profile. The resulting stratigraphic profile, with the proposed lock structure superimposed, is illustrated in Figure 6.3-4.

b. Dynamic Soil Properties

(1) Geotechnical data available for the project site and experience with properties of other soils for similar conditions were used to characterize the dynamic soil properties (low-strain and strain-dependent) within the SPSI finite element model.

(2) At the Olmsted site, an empirical correlation was developed between the corrected blow counts and the normalized shear-wave velocity measured at both the Illinois and Kentucky banks (U.S. Army Engineer District, Louisville, 1994). The correlation was used to estimate low-strain shear-wave velocity or shear modulus of soils beneath the monolith using the blow counts estimated for the idealized soil profiles shown in Figure 6.3-4. The estimated low-strain shear-wave velocity profiles at the free field on the riverside are shown in Figure 6.3-5. Shear-wave velocity estimates for the McNairy Zone II materials were assumed not to be dependent on density or effective stress as are the Zone I soils. This is because of the tendency of the Zone II materials to be indurated, as described in the boring logs. Therefore, for McNairy Zone II, values of shear-wave velocities were selected based directly on interpretations of the geophysical measurements.

(3) Soil stiffness (shear modulus) and energy absorption (damping) characteristics are soil properties that have been shown by innumerable studies to be strain-level dependent. Various researchers (Seed et al. 1984; Sun et al. 1988; Vucetic and Dobry 1991) also have shown the strain dependency to be related to soil type, stress history, density state, and other factors. For SPSI analyses, a set of modulus reduction and damping curves based on data for similar soils (i.e., clayey soils with a plasticity index (PI) in a range of 10 to 30) was selected and is shown in Figure 6.3-6. In this figure, G is soil shear modulus and G_{max} is soil shear modulus at low strain (strain less than 10^{-4} percent).

(4) Comparison of shear and compression wave velocities measured at the project site indicates that Poisson's ratios for the site soils are very close to a value of 0.50. To maintain numerical stability in the finite element SPSI analyses, Poisson's ratios were limited to a value of 0.49 for the soils.

c. Dynamic properties of concrete and pile elements

Dynamic properties of the concrete elements representing the lock structure and of the beam elements representing the piles are summarized in Table 6.3-1.

Table 6.3-1
Dynamic Properties of Concrete Elements for Lock Structure and Beam Elements for Piles

Material	Shear Modulus MPa (ksf)	Poisson's Ratio	Density kN/m ³ (pcf)	Damping Ratio	Section Area cm ² (in ²)	Moment of Inertia m ⁴ (in ⁴)		Effective Shear Area m ² (in ²)
						X-X Axis	Y-Y Axis	
Concrete Elements for Lock Structure	9,774.07 (204,125)	0.15	23.56 (150.00)	0.05	-	-	-	-
Beam Elements for Piles (HP14x117)	76,909.31 (1,606,200)	0.30	76.82 (489.00)	0.03	222.19 (34.44)	7,925.79 (1,228.50)	2,858.70 (443.10)	66.65 (10.33)

Note: To obtain section area and moment inertia per foot along the axis of the lock, the total area and moment inertia are divided by the pile spacings

6.3-7 Loading Conditions

a. Static Loads. Analyses of static pile forces and moments and static concrete stresses of the lock structure were conducted for the normal operating condition consisting of the dead weight, normal water pressures, and the backfill earth pressures. A 2D model consisting of the foundation soil, piles, backfill soil, and the lock structure was developed and analyzed using the computer program SAP2000. The foundation and backfill soils were represented by 2D solid elements. Piles were modeled by beam elements, and lock section by solid elements with concrete properties. The SAP2000 model for static analysis was later converted to a QFLUSH model for dynamic soil-structure-interaction analysis. The static and dynamic finite-element models, therefore, were identical in terms of geometry, mesh, and element types to facilitate combination of the static with dynamic results.

b. Earthquake ground motion. The MDE ground motions were used as the seismic input. Response spectra of the MDE ground motions were derived from a probabilistic seismic hazard assessment (Geomatrix Consultants, Inc., 1996) as the equal-hazard spectra having a return period of 1,000 years. The 5-percent-damped MDE response spectra for the horizontal and vertical components of rock motion are shown in Figure 6.3-7. Time histories of the horizontal and vertical components of rock motion (i.e. H1, H2, and V)

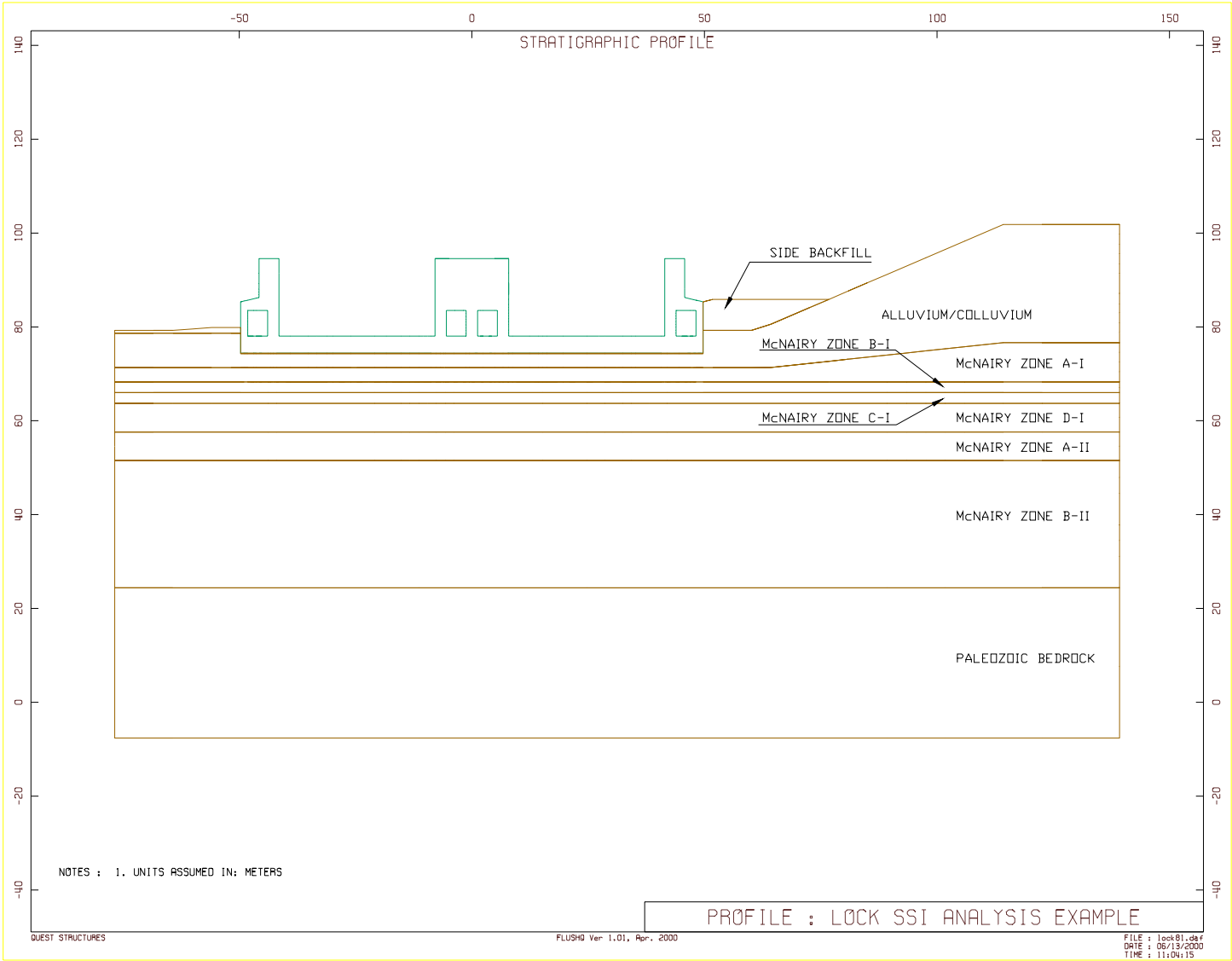


Figure 6.3-4. Idealized stratigraphic profile at Olmsted Locks and Dam site

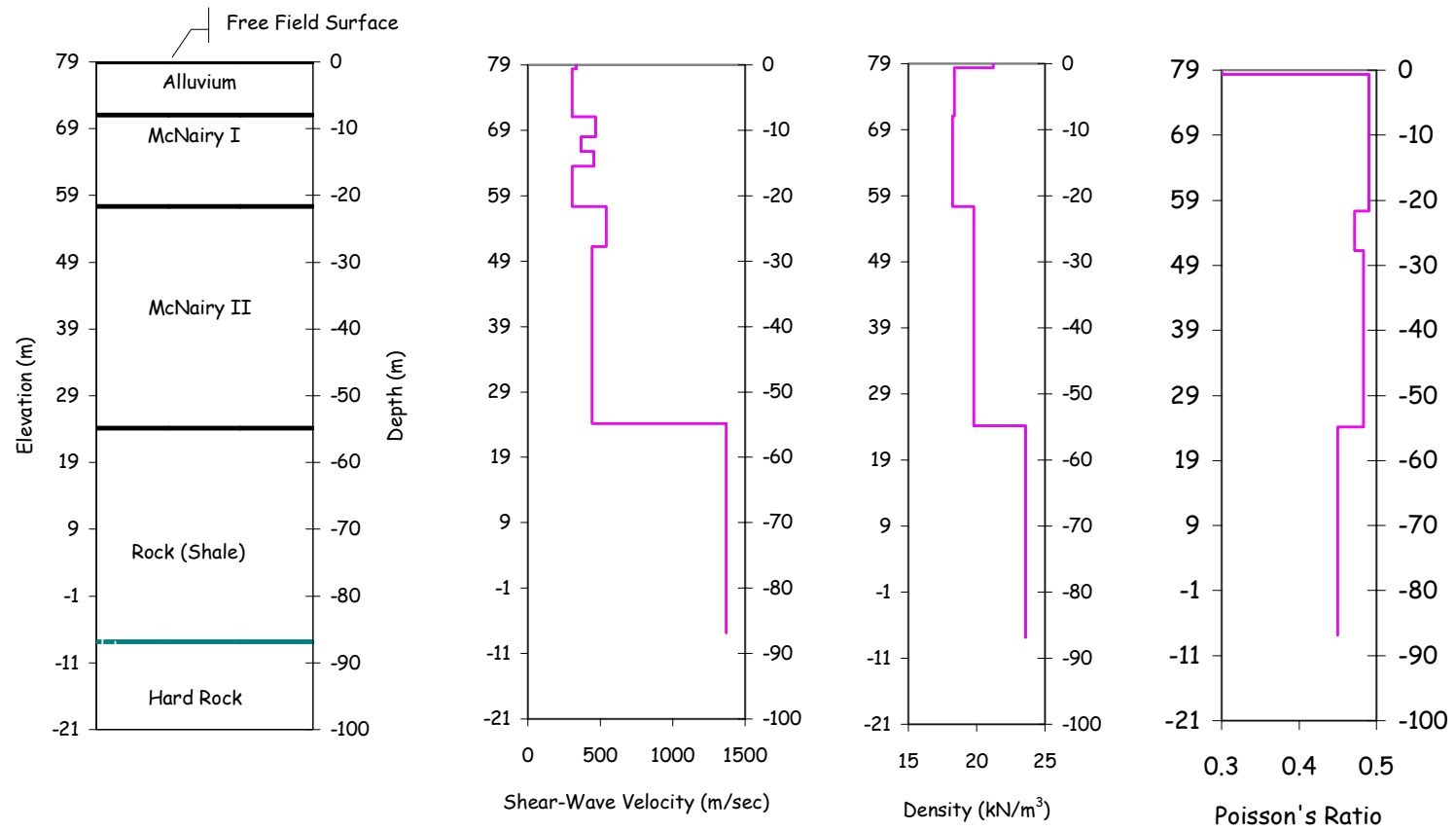


Figure 6.3-5. Estimated low-strain shear-wave velocity profile in the free field on the river side

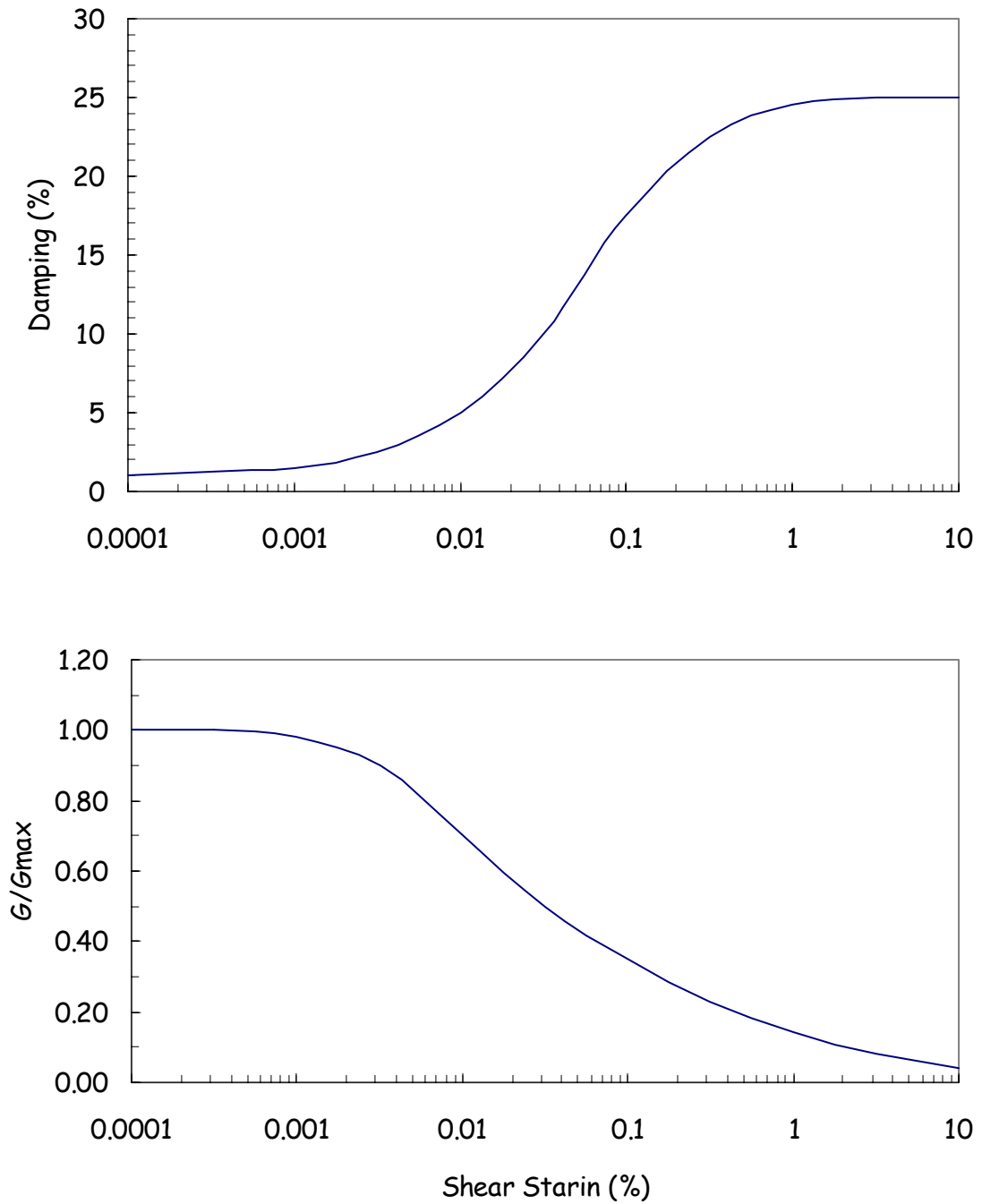


Figure 6.3-6. Damping curves and shear modulus reduction for soils

were developed to envelop the 1000-year design response spectra. Figure 6.3-7 shows that the resulting rock motion time histories have a return period in the range of 1000 to 1500 years. These time histories and their corresponding Fast Fourier Transform (FFT) are shown in Figures 6.3-8 through 6.3-10. The FFT results indicate that the rock motion energy is mainly in the frequency range of less than 15 Hz.

Time histories of the horizontal and vertical components of rock motion (i.e. H1 and V) were used as the outcrop motion at the basement rock of a free-field soil/rock column. As described previously, the seismic input for QFLUSH analyses, referred to as interface motion, was obtained at an elevation higher than the basement rock (i.e. at the fixed base of the finite-element model). The interface motion was computed from a separate free-field site response analysis. Because of large velocity contrast at the top of the basement rock, the interface motions are similar when computed from the free-field site response analyses at the river and bank sides.

c. Hydrodynamic forces

(1) Earthquake ground motions generate two types of dynamic fluid pressures in a lock structure – impulsive and convective. The impulsive pressure represents the effects of that portion of the fluid that moves in unison with the lock; the convective pressure represents the effects of the sloshing action of the fluid.

(2) The calculated fundamental period of water sloshing for the Olmsted Lock chamber is 7.07 sec (0.411 Hz). At this long period, the sloshing hydrodynamic pressures induced during earthquake excitation are two orders of magnitude smaller than the impulsive hydrodynamic pressures. Therefore, the sloshing effects were considered negligible and were not considered in this study.

(3) The impulsive pressures exerted on the lock walls during earthquake ground shaking were computed and compared using three different procedures: the velocity potential method, the Westergaard method, and the Housner method. The velocity potential method computes hydrodynamic pressure distributions on the lock walls by solving the Laplace equation for the velocity potential with appropriate boundary conditions. As with the Westergaard and Housner methods, the lock walls were assumed rigid.

(4) The hydrodynamic pressures obtained from the velocity potential method were used in the SPSI analyses. First, the hydrodynamic pressures were converted into nodal lumped masses according to the tributary area associated with each node. Then they were added to the lock wall nodal points as additional masses to account for the water inertia forces during earthquake excitation. The computed nodal added masses for the center, bank, and river walls of the example monolith are shown in Table 6.3-2. For the river wall, the added masses were computed for the inside and outside faces of the wall.

(5) Impulsive pressures are also exerted on the lock floor, but the added masses associated with the floor pressures must be considered active only in the vertical direction. The original version of FLUSH applies the added mass assigned to a nodal point to both the horizontal and vertical translational degrees of freedom associated with that node. To apply added masses to appropriate degrees of freedom, the original FLUSH was modified. The revised and enhanced version of the program (QFLUSH) allows added masses to be either applied to the horizontal or vertical, or both horizontal and vertical degrees of freedom.

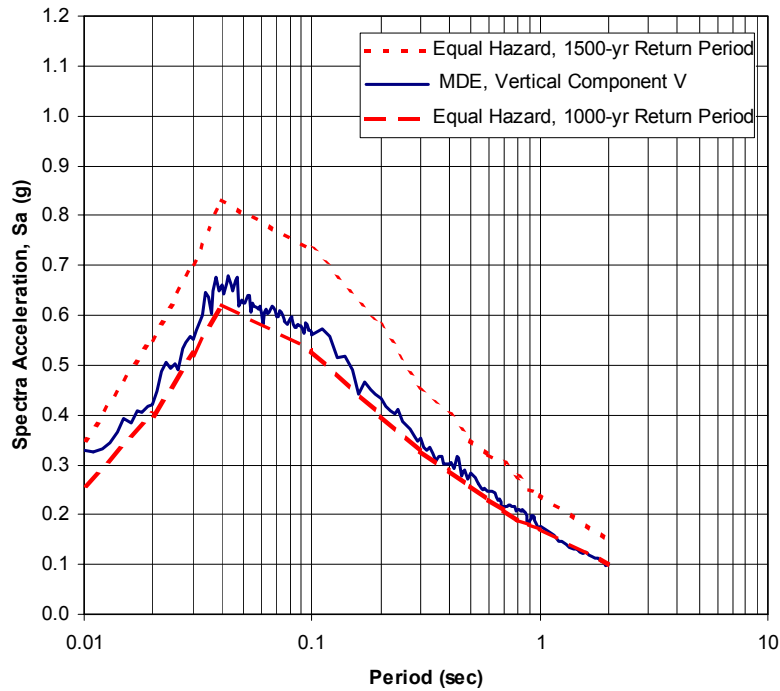
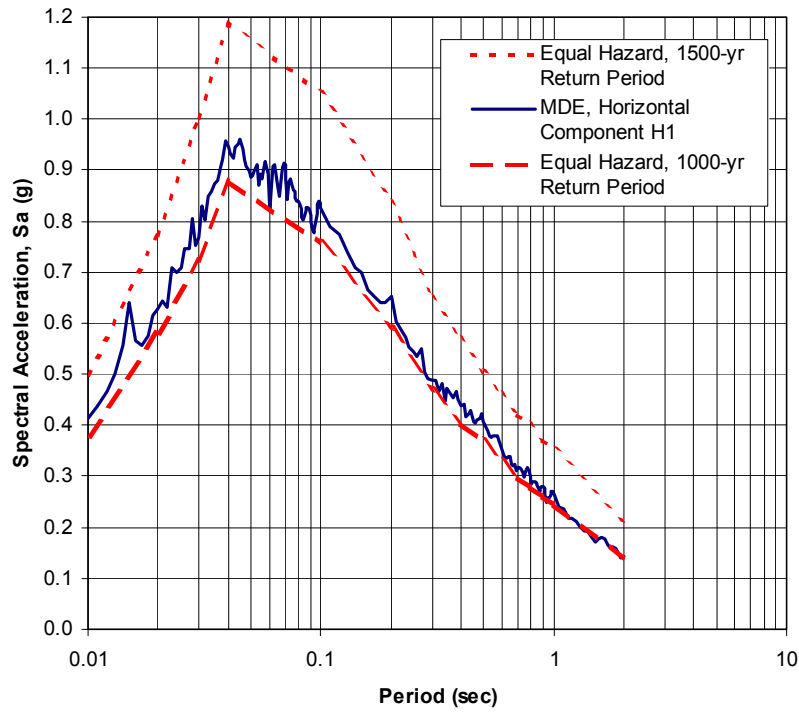


Figure 6.3-7. Comparison of 5%-damped rock motion response spectra with equal-hazard spectra

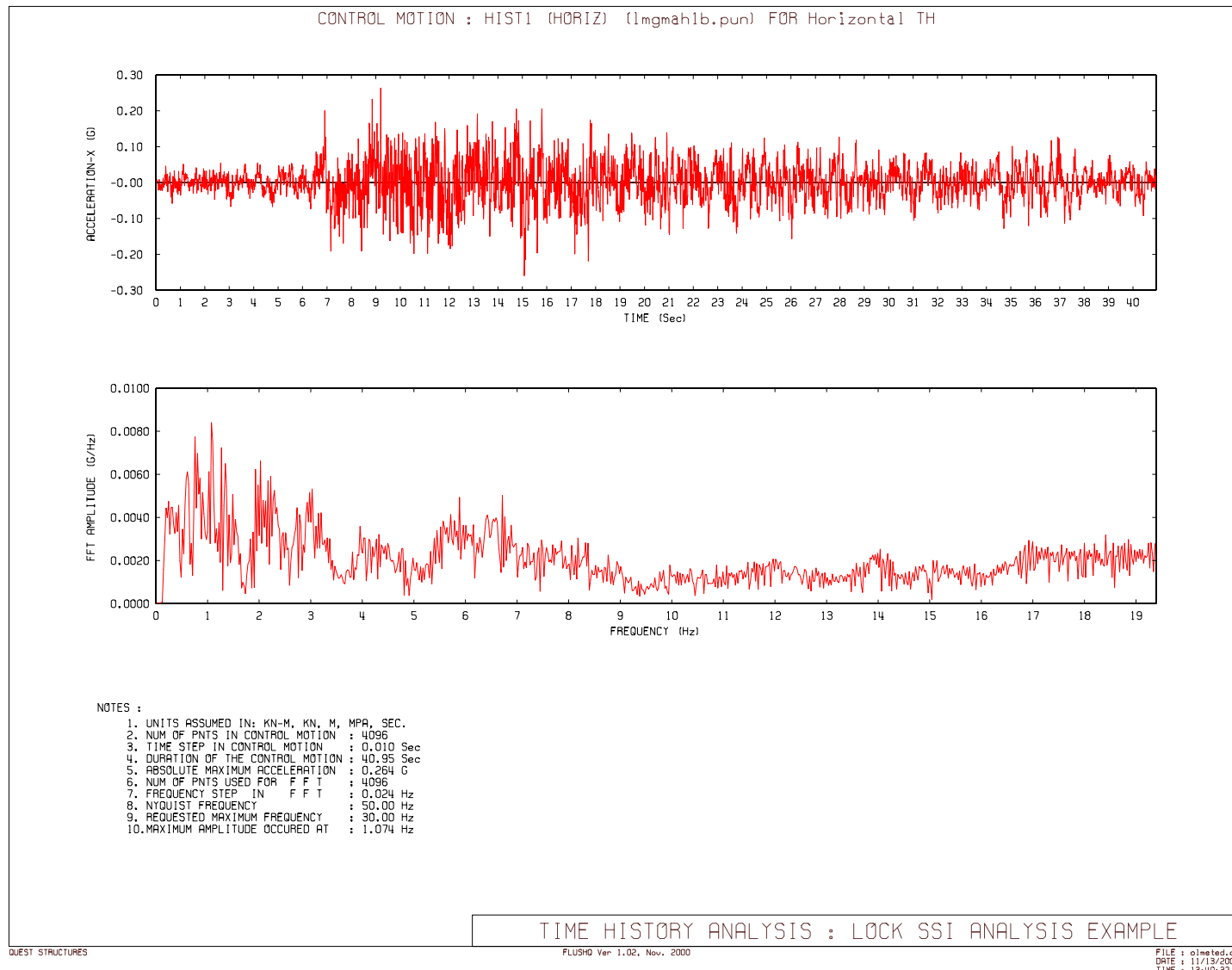


Figure 6.3-8. Time history and FFT of rock outcrop motion at Olmsted Locks and Dam (Horizontal component H1)

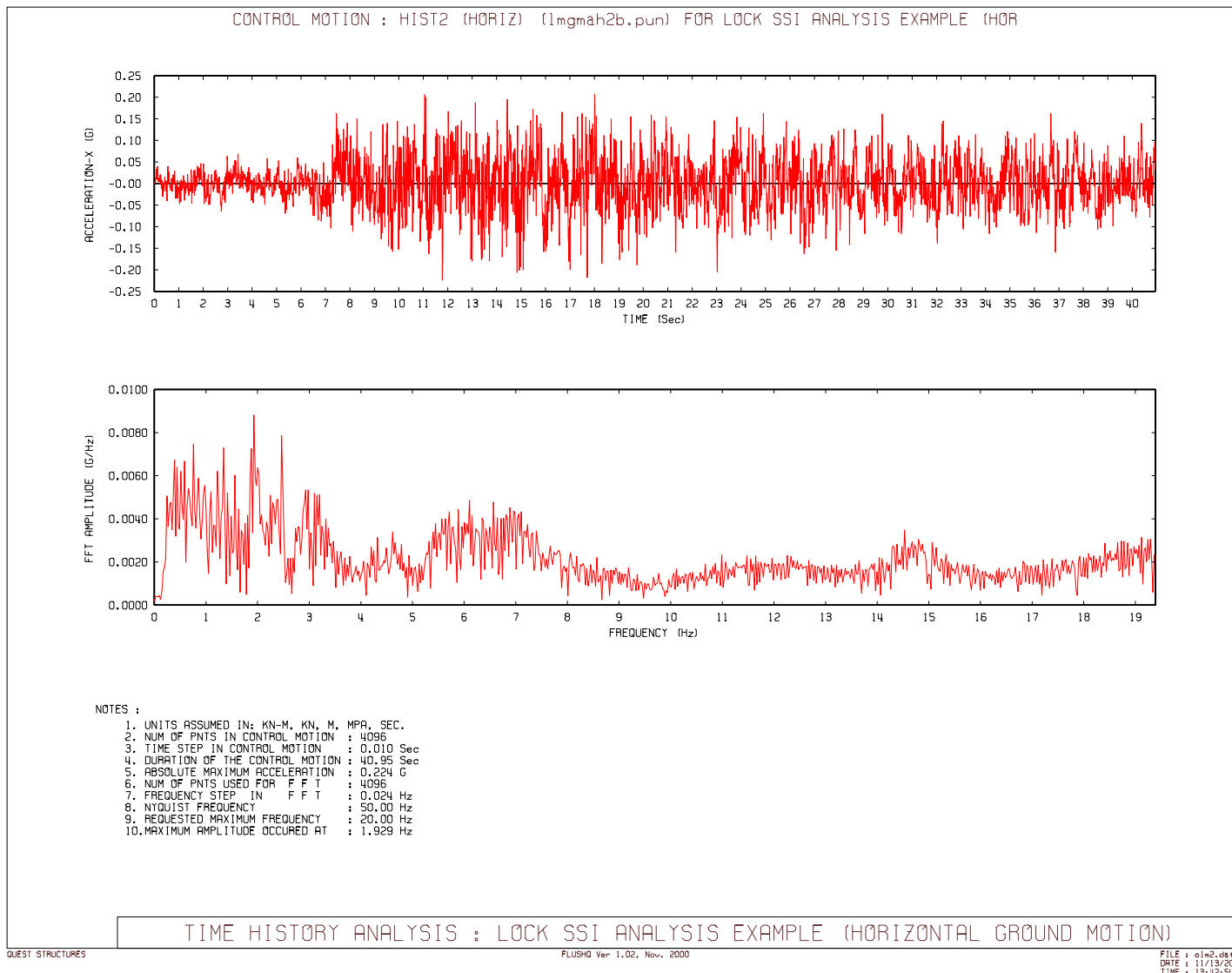


Figure 6.3-9. Time history and FFT of rock outcrop motion at Olmsted Locks and Dam (Horizontal component H2)

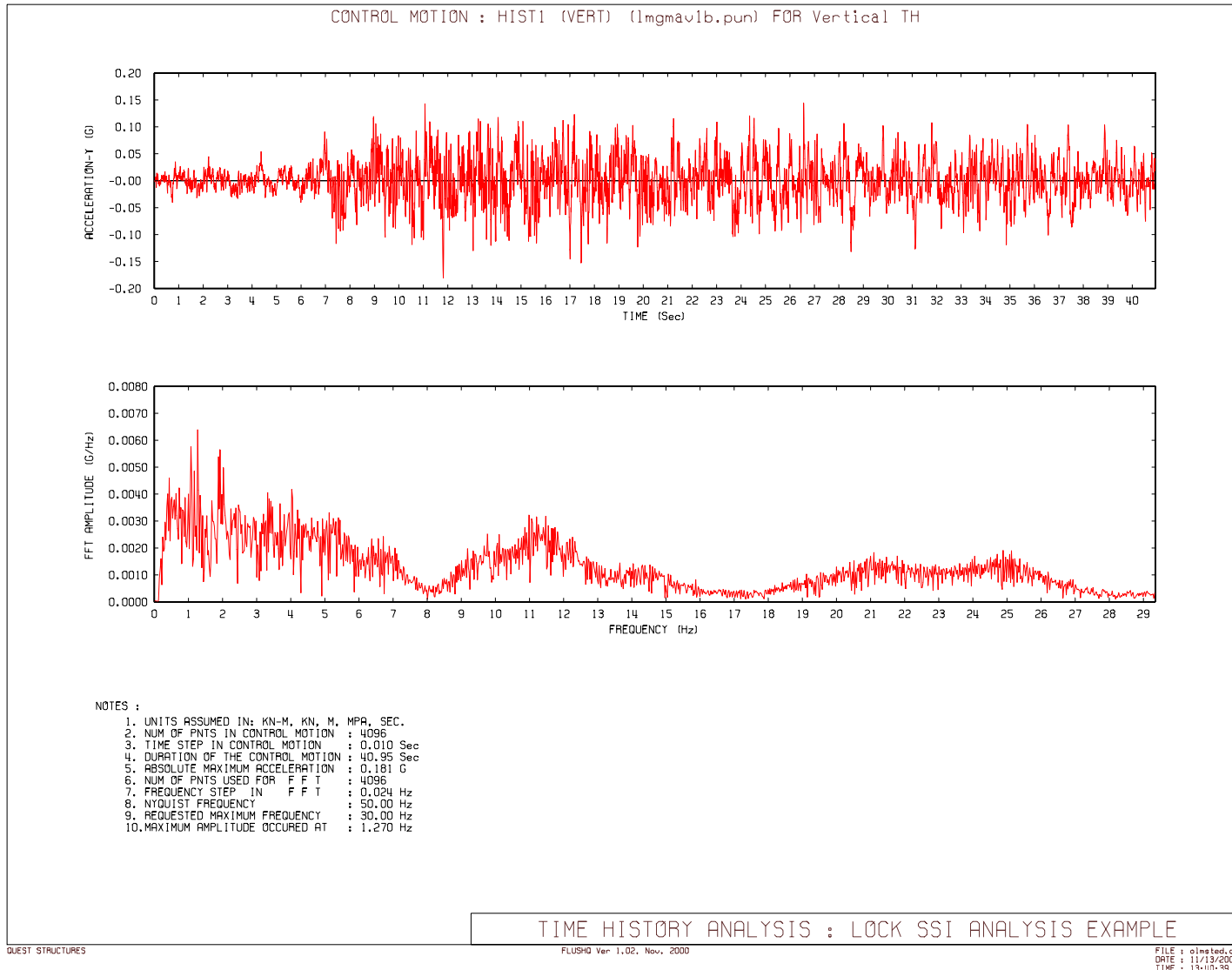


Figure 6.3-10. Time history and FFT of rock outcrop motion at Olmsted Locks and Dam (Vertical component V)

Table 6.3-2
Calculated Added Mass Values for 1-ft-thick Lock Chamber Monolith

Node Elevation m (ft)	Bank and River Walls (Inside Face)		Center Walls		River Wall (Outside Face)		Bank Wall (Outside Face)	
	Horizontal Mass kN-sec ² /m (lb-sec ² /ft)	Vertical Mass kN-sec ² /m (lb-sec ² /ft)	Horizontal Mass kN-sec ² /m (lb-sec ² /ft)	Vertical Mass kN-sec ² /m (lb-sec ² /ft)	Horizontal Mass kN-sec ² /m (lb-sec ² /ft)	Vertical Mass kN-sec ² /m (lb-sec ² /ft)	Horizontal Mass kN-sec ² /m (lb-sec ² /ft)	Vertical Mass kN-sec ² /m (lb-sec ² /ft)
91.44 (300.00)	2.31 (158.60)		2.31 (158.60)					
89.31 (293.00)	4.91 (336.64)		6.70 (459.05)					
88.09 (289.00)	2.95 (202.47)							
87.48 (287.00)	2.06 (141.04)							
86.87 (285.00)	2.14 (146.79)		6.10 (417.80)					
86.26 (283.00)	1.87 (128.41)				0.21 (14.15)	0.06 (3.88)	0.10 (6.60)	0.06 (3.88)
86.12 (282.54)					0.09 (5.89)	0.14 (9.54)	0.04 (2.75)	0.14 (9.54)
85.98 (282.08)					0.09 (6.42)	0.17 (11.33)	0.04 (2.99)	0.17 (11.33)
85.84 (281.62)	1.69 (116.00)		3.95 (270.67)		0.10 (6.90)	0.19 (13.12)	0.05 (3.22)	0.19 (13.12)
85.70 (281.15)					0.09 (5.98)	0.18 (12.11)	0.04 (2.79)	0.18 (12.11)
85.61 (280.87)					0.07 (4.77)	0.15 (10.02)	0.03 (2.22)	0.15 (10.02)
85.52 (280.58)					0.07 (4.93)	0.16 (10.71)	0.03 (2.30)	0.16 (10.71)
85.43 (280.29)					0.07 (5.09)	0.17 (11.41)	0.03 (2.37)	0.17 (11.41)
85.34 (280.00)	2.08 (142.52)				0.30 (20.81)	0.09 (6.06)	0.02 (1.22)	0.09 (6.06)
84.73 (278.00)	2.35 (161.23)		3.30 (226.35)		0.63 (43.03)			
84.12 (276.00)	2.40 (164.78)		2.40 (164.78)		0.71 (48.79)			
83.52 (274.00)	2.45 (168.12)		2.45 (168.12)		0.79 (53.94)			
82.91 (272.00)	2.49 (170.86)		2.49 (170.86)		0.86 (58.64)			
82.30 (270.00)	2.52 (172.93)		2.52 (172.93)		0.92 (62.99)			
81.69 (268.00)	2.55 (174.62)		2.55 (174.62)		0.98 (67.06)			
81.08 (266.00)	2.57 (176.27)		2.57 (176.27)		1.03 (70.89)			
80.47 (264.00)	2.60 (177.88)		2.60 (177.88)		1.09 (74.53)			
79.86 (262.00)	2.61 (179.15)		2.61 (179.15)		0.57 (39.00)			
79.25 (260.00)	2.62 (179.81)		2.62 (179.81)					
78.64 (258.00)	2.63 (179.96)		2.63 (179.96)					
78.03 (256.00)	1.31 (89.97)	1.50 (103.03)	1.31 (89.97)	1.63 (111.91)				

EM 1110-2-6051
22 Dec 03

6.3-8 Presentation and Evaluation of the Results

Dynamic SPSI analyses were performed for the primary horizontal component (H1) and for the vertical component (V) of the MDE rock motion described previously. Responses due to the horizontal and vertical excitations were combined in the time domain taking into account differences in phasing between the horizontal and vertical ground motion. Figures 6.3-11 and 6.3-12 show the strain-compatible shear-wave velocity profile and damping ratio profile, respectively, for a free-field soil column at the riverside. Results show that shear wave velocity drops as much as 50% and damping ratio reaches as high as 11% during the MDE excitation. Variation of free-field peak accelerations with depth at the riverside is shown in Figure 6.3-13. An amplification of about 2 is observed between the peak ground surface and interface accelerations.

a. Dynamic response of the soil-pile-lock structure system. Dynamic response of the soil-pile-lock structure was examined in terms of transfer functions between the top and bottom of the lock walls and between the top of lock walls and the free field ground surface at the riverside. These transfer functions are shown on Figure 6.3-14. As shown on this figure the river wall appears to have a fundamental frequency of about 4 Hz and the middle wall a fundamental frequency of about 6.2 Hz. The land wall appears to have a higher fundamental frequency of about 9 Hz because of the resistance of the backfill. The fundamental frequency of the foundation soil appears to be about 1 Hz and that of the soil-pile-lock system about 2.5 Hz.

b. Design criteria. The design criteria for the pile foundation and the lock structure are described in USAED, Louisville (1992). Allowable stresses and loads for HP 14x117 piles and allowable stresses for the reinforced concrete used in this study are summarized below.

c. Allowable stresses and loads for HP 14x117 (A-36 grade). For the extreme loading conditions (MDE), the allowable loads and allowable deflections are summarized in Table 6.3-3.

Axial Compression at Pile Tips F_a kN (kips)	Axial Tension ¹ F_b kN (kips)	Allowable Loads			Allowable Deflection	
		Bending kN-m (k-ft)	Combined Axial and Bending ² kN (kips) kN-m (k-ft)	Shear F_v kN (kips)	Vertical cm (in)	Horizontal cm (in)
3,212 (722)	1,548 (348)	$M_x = 680 (502)$ $M_y = 236 (174)$	$(F_a)_c = 4,824 (1,084)$ $M_x = 680 (502)$ $M_y = 236 (174)$	1,068 (240)	<1.12 (<0.44)	<2.29 (<0.9)

¹ Soil is limiting factor.
² $(F_a)_c$ = allowable axial force for combination with allowable moment.

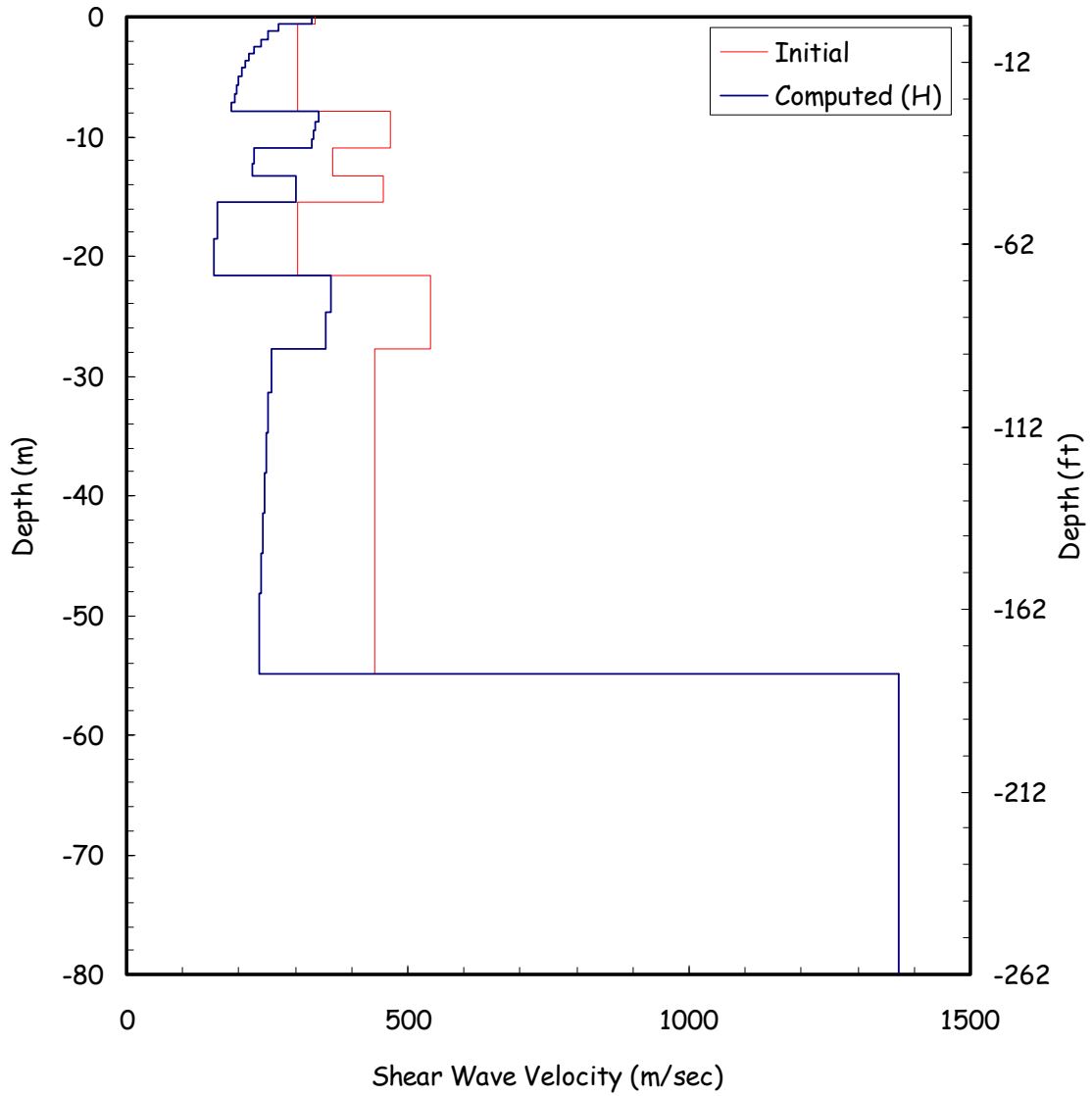


Figure 6.3-11. Comparison of initial shear-wave velocity with strain-compatible shear-wave velocity obtained from MDE excitation.

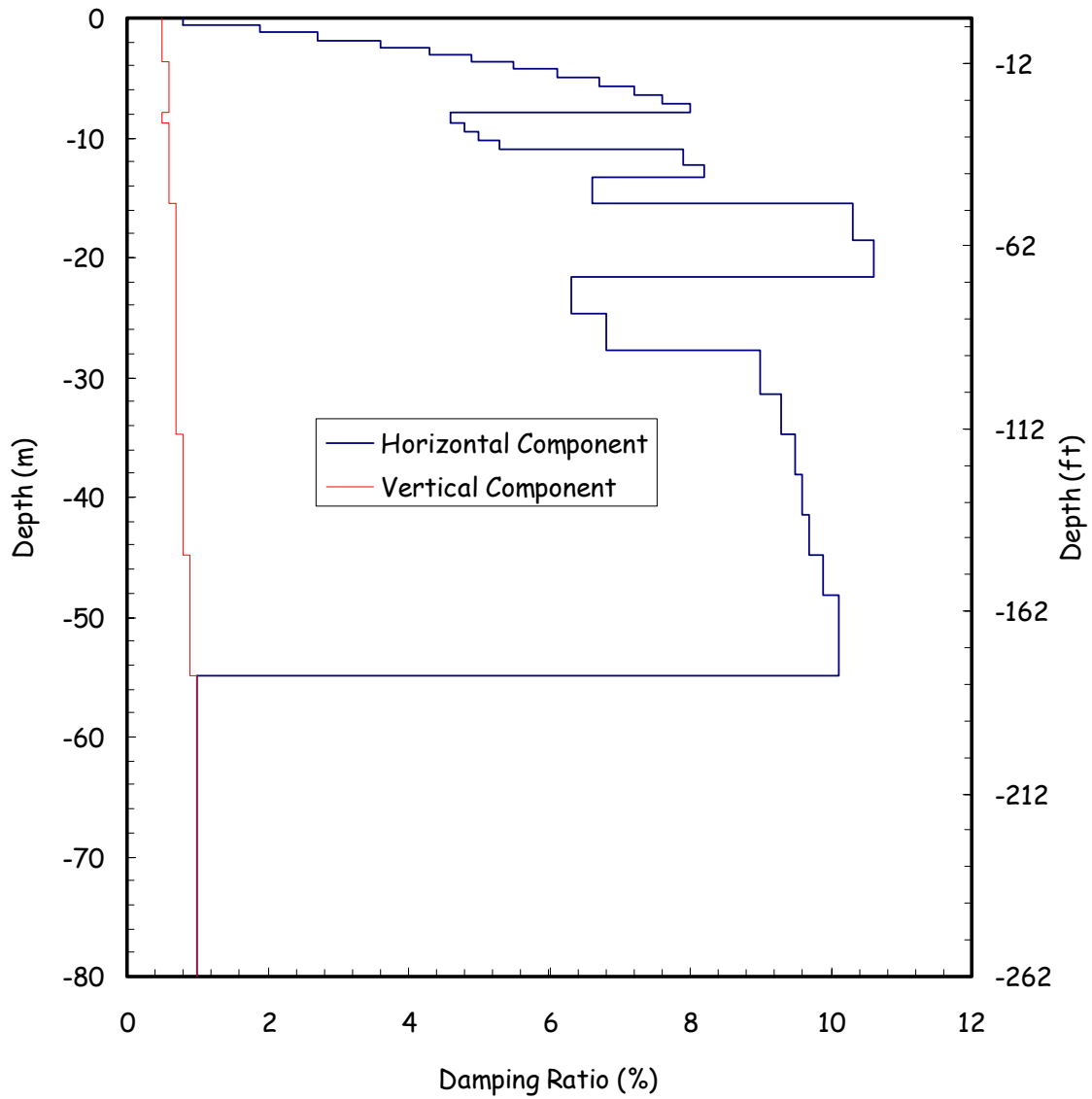


Figure 6.3-12. Strain-compatible damping ratio profile obtained from MDE excitation.

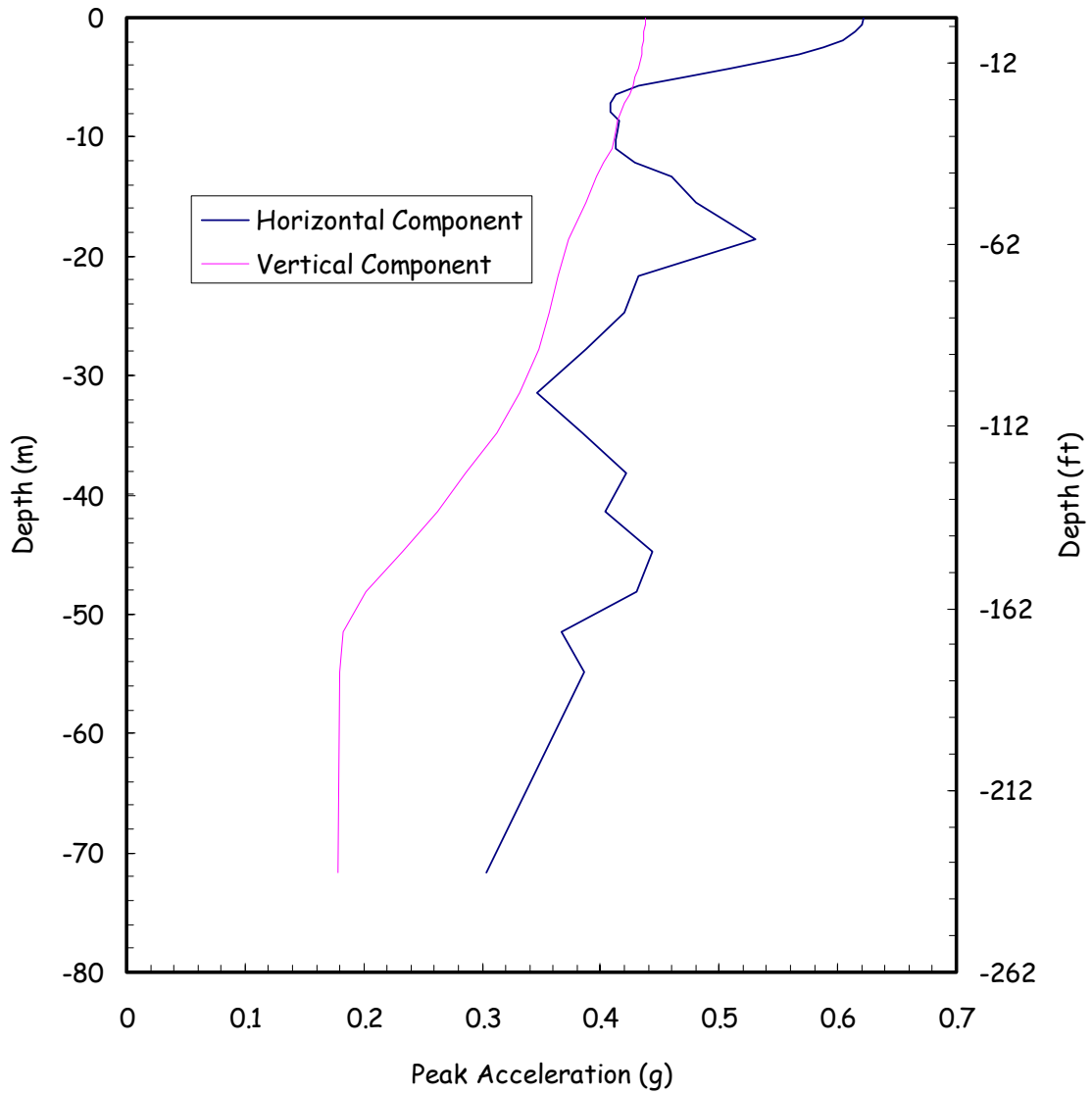


Figure 6.3-13. Variation of peak acceleration with depth for MDE excitation

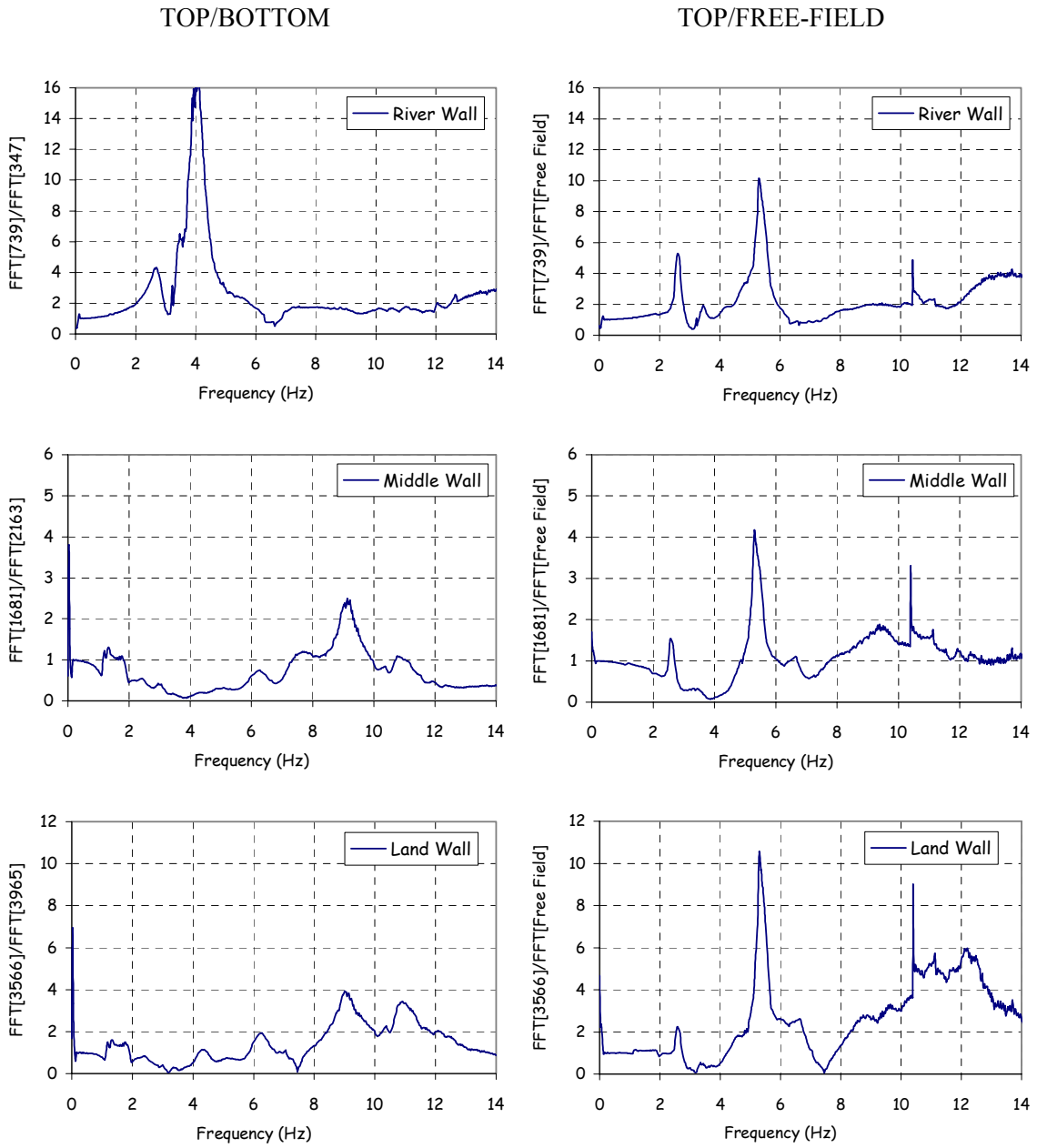


Figure 6.3-14. Transfer functions between top and bottom of lock walls, and top of lock walls and free field ground surface

d. Allowable stresses for reinforced concrete. The design of the lock concrete structure is in accordance with the strength design requirements for reinforced concrete hydraulic structures contained in EC 1110-2-267. The design of the concrete components of the lock is based on a minimum concrete compressive strength of 3,000 psi. Reinforced concrete design is based on billet steel bars conforming to the yield strength of 60,000 psi. Main reinforcement that is required by analysis is at a minimum as limited by ACI 318. Maximum tension reinforcement is as required by EC 1110-2-267.

e. Pile forces and moments.

(1) To consider possible phasing of the horizontal and vertical motions when the response from the horizontal and vertical excitations are combined with static loads, four loading combinations summarized in Table 6.3-4 are used.

Tabel 6.3-4
Various Static and Seismic Loads Combinaitons Evaluated

Case	Seismic Loads		Static Loads	
	Horizontal Excitation	Vertical Excitation	Bending Moment	Axial Force
1	+	+	+	+
2	+	-	+	+
3	-	+	+	+
4	-	-	+	+

(2) Table 6.3-5 shows peak values of static plus dynamic pile forces and moments for all piles for the load combination Case 3. Also shown in Table 6.3-5 are values of axial and shear forces at times of peak moments, values of moments and shear forces at times of peak axial forces, and values of moments and axial forces at times of peak shear forces. It is noted that peak moments and peak shear forces occur at the same time. However, peak moments and peak axial forces do not occur at the same time. The peak axial and shear forces shown in Table 6.3-5 indicate that they are substantially lower than the allowable values.

(3) To evaluate demand/capacity ratios for the H-piles, interaction factors of each pile I_p beneath the chamber monolith are computed in accordance with Equation (4-1). The interaction factors for the maximum pile moments and axial forces for the four load combination cases were computed and plotted, as shown in Figure 6.3-15. The interaction factors for load combination Case 3 are listed in the last column of Table 6.3-5. Figure 6.3-15 shows that the interaction factors depend on the phasing of the ground motion. To obtain maximum interaction factors for all possible ground motion phasing, Figure 6.3-16 was generated by selecting the maximum interaction factor for each individual piles from the four cases shown in Figure 6.3-15. The interaction factors were also computed in time domain for all the four combination cases. The resulting interaction factors at each time step for three typical piles located at the two extreme edges (i.e., river and bank sides) and at the center of the lock are shown in Figures 6.3-17 through 6.3-19. The results in Figures 6.3-16 through 6.3-19 show that values of the interaction factor are less than 0.82 with an average value of about 0.6, indicating the piles have adequate factors of safety.

f. Pile deflection. Relative displacements between selected locations of the lock structure (i.e., top and bottom of the lock walls, middle level of lock and lock base), and between pile head and pile tip computed from the combined horizontal and vertical excitations are summarized in Table 6.3.6. Relative displacements between the pile head and pile tip are slightly higher than the allowable values shown in Table 6.3-3.

g. Concrete section forces and moments

(1) Section forces and moments for critical sections shown on Figure 6.3-20 were computed from time histories of the concrete element stresses. Table 6.3-7 shows peak static plus dynamic forces and moments for the critical sections. Also shown in Table 6.3-7 are values of forces when the peak moments occur or values of moments when the peak forces occur. These data indicate that due to differences in phasing, the peak values of force and moment generally do not occur at the same time. However, peak values of shear force and moment tend to occur about the same time. Table 6.3-8 summarizes static section forces and moments used in combination with the dynamic section forces and moments.

(2) Time histories of the dynamic section forces and moments (combined horizontal and vertical excitations) for the selected sections are combined with the static forces and moments. The reinforced concrete strengths (the nominal strength and design strength) were computed in accordance with ACI-318 for each section using the post processing capabilities of QFLUSH. Examples of the interaction diagrams for concrete vertical sections 1, 3, 4, and 6 are shown on Figures 6.3-21 to 6.3-24 and for horizontal sections 4, 5, 15, and 16 are shown in Figures 6.3-25 to 6.3-28. Also shown on these figures for comparison are the nominal strength (dashed line) and design strength (solid line) envelopes of the reinforced concrete of the respective sections. The data shown on Figures 6.3-21 and 6.3-28 were used for the reinforcement design and evaluation. The results show that axial force-moment demand pairs for all sections fall within the interaction capacity diagrams, except for vertical Sections 1 and 6. At these sections less than 10% of axial force-moment pairs fall outside the interaction diagrams. This response behavior, however, is acceptable because the high axial-force demand pairs are associated with transient moments with little damage potential, as illustrated by the time histories of the axial force-bending moment interaction factors in Figure 6.3.29. Thus the reinforced concrete design, represented by the interaction diagrams, is considered adequate for the computed seismic demands.

6.3-9 Conclusions

In this section, an example of seismic time-history analysis of a pile-supported lock structure was illustrated. The procedure was used to analyze the seismic response of the Olmsted Locks under the MDE loading conditions and to provide data for the design of the pile foundation and the reinforcement steel of the concrete sections.

**Table 6.3-5
Combined Static and Dynamic Pile Forces, Moments, and Interaction Factors for MDE Loading**

LOAD COMBINATION: -1.0(Horizontal) + 1.0(Vertical) + 1.0(Static)

Pile	X-Coordinate m (ft)	Time History Peak values			At Peak Moment		At Peak Axial		At Peak Shear		Peak Interaction Factor
		Moment kN-m (k-ft)	Axial Force kN (kips)	Shear Force kN (kips)	Axial Force kN (kips)	Shear Force kN (kips)	Moment kN-m (k-ft)	Shear Force kN (kips)	Moment kN-m (k-ft)	Axial Force kN (kips)	
1	-47.63 (-156.27)	-283.25 (-208.90)	-1,581.87 (-355.60)	606.77 (136.40)	-1,403.04 (-315.40)	606.77 (136.40)	47.28 (34.87)	-148.44 (-33.37)	-283.25 (-208.90)	-1,403.04 (-315.40)	0.74
2	-45.72 (-150.00)	-246.37 (-181.70)	-1,088.98 (-244.80)	467.09 (105.00)	-979.55 (-220.20)	467.09 (105.00)	30.95 (22.83)	-78.92 (-17.74)	-246.37 (-181.70)	-979.55 (-220.20)	0.59
3	-43.82 (-143.77)	-232.40 (-171.40)	-854.10 (-192.00)	446.62 (100.40)	-742.89 (-167.00)	446.62 (100.40)	34.86 (25.71)	-104.41 (-23.47)	-232.40 (-171.40)	-742.89 (-167.00)	0.52
4	-41.91 (-137.50)	-223.72 (-165.00)	-758.02 (-170.40)	446.18 (100.30)	-544.49 (-122.40)	433.77 (97.51)	-65.14 (-48.04)	173.31 (38.96)	-202.30 (-149.20)	-663.26 (-149.10)	0.49
5	-40.01 (-131.27)	-212.87 (-157.00)	-739.33 (-166.20)	475.10 (106.80)	-436.30 (-98.08)	412.46 (92.72)	-67.04 (-49.44)	191.19 (42.98)	-210.98 (-155.60)	-692.18 (-155.60)	0.47
6	-38.10 (-125.00)	-218.43 (-161.10)	-734.88 (-165.20)	480.88 (108.10)	-655.26 (-147.30)	480.88 (108.10)	-60.49 (-44.61)	166.68 (37.47)	-218.43 (-161.10)	-655.26 (-147.30)	0.47
7	-36.19 (-118.73)	223.72 (165.00)	-129.81 (-29.18)	-316.20 (-71.08)	-127.67 (-28.70)	-316.20 (-71.08)	222.77 (164.30)	-314.73 (-70.75)	223.72 (165.00)	-127.67 (-28.70)	0.36
8	-34.29 (-112.50)	234.03 (172.60)	-129.32 (-29.07)	-327.41 (-73.60)	-125.31 (-28.17)	-327.41 (-73.60)	231.31 (170.60)	-323.40 (-72.70)	234.03 (172.60)	-125.31 (-28.17)	0.37
9	-32.39 (-106.27)	250.30 (184.60)	-134.97 (-30.34)	-346.89 (-77.98)	-127.18 (-28.59)	-346.89 (-77.98)	238.09 (175.60)	-329.19 (-74.00)	250.30 (184.60)	-127.18 (-28.59)	0.40
10	-28.58 (-93.77)	275.25 (203.00)	-141.95 (-31.91)	-381.59 (-85.78)	-126.02 (-28.33)	-381.59 (-85.78)	124.44 (91.78)	-167.66 (-37.69)	275.25 (203.00)	-126.02 (-28.33)	0.43
11	-24.76 (-81.23)	272.67 (201.10)	-150.80 (-33.90)	-377.72 (-84.91)	-120.60 (-27.11)	-377.72 (-84.91)	130.49 (96.24)	-177.05 (-39.80)	272.67 (201.10)	-120.60 (-27.11)	0.43
12	-20.95 (-68.73)	269.14 (198.50)	-126.74 (-28.49)	-372.87 (-83.82)	-98.36 (-22.11)	-372.87 (-83.82)	181.15 (133.60)	-249.38 (-56.06)	269.14 (198.50)	-98.36 (-22.11)	0.42
13	-17.15 (-56.27)	248.13 (183.00)	-133.77 (-30.07)	-344.04 (-77.34)	-93.11 (-20.93)	-344.04 (-77.34)	-138.30 (-102.00)	200.85 (45.15)	248.13 (183.00)	-93.11 (-20.93)	0.39
14	-15.24 (-50.00)	234.98 (173.30)	-141.42 (-31.79)	-323.00 (-72.61)	-92.93 (-20.89)	-323.00 (-72.61)	-125.41 (-92.49)	186.61 (41.95)	234.98 (173.30)	-92.93 (-20.89)	0.37
15	-13.34 (-43.77)	228.60 (168.60)	-163.53 (-36.76)	-312.28 (-70.20)	-77.85 (-17.50)	-312.28 (-70.20)	-115.98 (-85.54)	175.63 (39.48)	228.60 (168.60)	-77.85 (-17.50)	0.37
16	-11.43 (-37.50)	221.96 (163.70)	-179.94 (-40.45)	-302.09 (-67.91)	-74.51 (-16.75)	-302.09 (-67.91)	-105.27 (-77.64)	162.01 (36.42)	221.96 (163.70)	-74.51 (-16.75)	0.36
17	-9.53 (-31.25)	210.84 (155.50)	-216.42 (-48.65)	-285.77 (-64.24)	-74.47 (-16.74)	-285.77 (-64.24)	-87.17 (-64.29)	136.17 (30.61)	210.84 (155.50)	-74.47 (-16.74)	0.35
18	-7.62 (-25.00)	192.81 (142.20)	-251.65 (-56.57)	-259.48 (-58.33)	-109.12 (-24.53)	-259.48 (-58.33)	-73.58 (-54.27)	108.81 (24.46)	192.81 (142.20)	-109.12 (-24.53)	0.34
19	-5.72 (-18.75)	183.32 (135.20)	-210.95 (-47.42)	-249.65 (-56.12)	-142.84 (-32.11)	-249.65 (-56.12)	-63.65 (-46.94)	90.53 (20.35)	183.32 (135.20)	-142.84 (-32.11)	0.31
20	-3.81 (-12.50)	180.47 (133.10)	-189.01 (-42.49)	-250.14 (-56.23)	-135.59 (-30.48)	-250.14 (-56.23)	99.83 (73.63)	-137.68 (-30.95)	180.47 (133.10)	-135.59 (-30.48)	0.30
21	-1.91 (-6.25)	175.45 (129.40)	-187.37 (-42.12)	-243.02 (-54.63)	-136.70 (-30.73)	-243.02 (-54.63)	98.11 (72.36)	-135.63 (-30.49)	175.45 (129.40)	-136.70 (-30.73)	0.30
22	0.00 (0.00)	170.84 (126.00)	-195.29 (-43.90)	-235.81 (-53.01)	-163.17 (-36.68)	-235.81 (-53.01)	96.89 (71.46)	-134.92 (-30.33)	170.84 (126.00)	-163.17 (-36.68)	0.29
23	1.91 (6.25)	-173.55 (-128.00)	-1,179.29 (-265.10)	401.70 (90.30)	-1,022.26 (-229.80)	401.70 (90.30)	-76.21 (-56.21)	166.64 (37.46)	-173.55 (-128.00)	-1,022.26 (-229.80)	0.50
24	3.81 (12.50)	-176.81 (-130.40)	-1,265.59 (-284.50)	410.10 (92.19)	-1,098.77 (-247.00)	410.10 (92.19)	-79.59 (-58.70)	173.09 (38.91)	-176.81 (-130.40)	-1,098.77 (-247.00)	0.52
25	5.72 (18.75)	-182.64 (-134.70)	-1,383.91 (-311.10)	413.97 (93.06)	-1,209.98 (-272.00)	413.97 (93.06)	-86.37 (-63.70)	182.61 (41.05)	-182.64 (-134.70)	-1,209.98 (-272.00)	0.56
26	7.62 (25.00)	-201.62 (-148.70)	-1,482.67 (-333.30)	462.64 (104.00)	-1,304.73 (-293.30)	462.64 (104.00)	-106.60 (-78.62)	235.59 (52.96)	-201.62 (-148.70)	-1,304.73 (-293.30)	0.60
27	9.53 (31.25)	-228.20 (-168.30)	-1,464.88 (-329.30)	556.95 (125.20)	-1,295.39 (-291.20)	556.95 (125.20)	-135.47 (-99.91)	338.84 (76.17)	-228.20 (-168.30)	-1,295.39 (-291.20)	0.64
28	11.43 (37.50)	-236.87 (-174.70)	-1,331.42 (-299.30)	561.40 (126.20)	-1,157.04 (-260.10)	561.40 (126.20)	-144.54 (-106.60)	349.34 (78.53)	-236.87 (-174.70)	-1,157.04 (-260.10)	0.62
29	13.34 (43.77)	-237.96 (-175.50)	-1,246.01 (-280.10)	551.61 (124.00)	-969.76 (-218.00)	550.27 (123.70)	-143.86 (-106.10)	336.13 (75.56)	-237.15 (-174.90)	-1,053.39 (-236.80)	0.61
30	15.24 (50.00)	-237.15 (-174.90)	-1,211.31 (-272.30)	541.38 (121.70)	-905.26 (-203.50)	541.38 (121.70)	-137.89 (-101.70)	321.18 (72.20)	-237.15 (-174.90)	-905.26 (-203.50)	0.60
31	17.15 (56.27)	-241.48 (-178.10)	-1,380.36 (-310.30)	697.96 (156.90)	-990.67 (-222.70)	697.96 (156.90)	-130.99 (-96.61)	390.00 (87.67)	-241.48 (-178.10)	-990.67 (-222.70)	0.64
32	20.95 (68.73)	-255.31 (-188.30)	-1,517.81 (-341.20)	859.00 (193.10)	-1,012.02 (-227.50)	859.00 (193.10)	-141.15 (-104.10)	482.66 (108.50)	-255.31 (-188.30)	-1,012.02 (-227.50)	0.69
33	24.76 (81.23)	-248.26 (-183.10)	-1,429.73 (-321.40)	836.75 (188.10)	-907.48 (-204.00)	836.75 (188.10)	-135.03 (-99.59)	465.75 (104.70)	-248.26 (-183.10)	-907.48 (-204.00)	0.66
34	28.58 (93.77)	-233.21 (-172.00)	-1,333.20 (-299.70)	794.49 (178.60)	-716.65 (-161.10)	794.49 (178.60)	97.08 (71.60)	-349.29 (-78.52)	-233.21 (-172.00)	-716.65 (-161.10)	0.62
35	32.39 (106.27)	-206.23 (-152.10)	-1,076.08 (-241.90)	576.96 (129.70)	-278.38 (-62.58)	569.40 (128.00)	85.57 (63.11)	-275.27 (-61.88)	-199.45 (-147.10)	-402.10 (-90.39)	0.53
36	34.29 (112.50)	-194.30 (-143.30)	-884.35 (-198.80)	443.16 (99.62)	-195.82 (-44.02)	443.16 (99.62)	84.17 (62.08)	-196.89 (-44.26)	-194.30 (-143.30)	-195.82 (-44.02)	0.47
37	36.19 (118.73)	-187.66 (-138.40)	-875.01 (-196.70)	469.31 (105.50)	-159.08 (-35.76)	464.42 (104.40)	80.28 (59.21)	-252.85 (-56.84)	-185.89 (-137.10)	-145.55 (-32.72)	0.46
38	38.10 (125.00)	183.86 (135.60)	-143.95 (-32.36)	-258.28 (-58.06)	-6.14 (-1.38)	-258.28 (-58.06)	-131.37 (-96.89)	189.50 (42.60)	183.86 (135.60)	-6.14 (-1.38)	0.30
39	40.01 (131.27)	178.30 (131.50)	-178.56 (-40.14)	-247.38 (-55.61)	2.16 (0.49)	-247.38 (-55.61)	-71.58 (-52.79)	108.05 (24.29)	178.30 (131.50)	2.16 (0.49)	0.30
40	41.91 (137.50)	170.03 (125.40)	-177.67 (-39.94)	-231.28 (-51.99)	-19.28 (-4.34)	-231.28 (-51.99)	-12.16 (-8.97)	16.60 (3.73)	170.03 (125.40)	-19.28 (-4.34)	0.29
41	43.82 (143.77)	167.05 (123.20)	-152.94 (-34.38)	-226.96 (-51.02)	-60.54 (-13.61)	-226.96 (-51.02)	-82.80 (-61.07)	121.98 (27.42)	167.05 (123.20)	-60.54 (-13.61)	0.28
42	45.72 (150.00)	183.32 (135.20)	-1,548.51 (-348.10)	-395.47 (-88.90)	-725.10 (-163.00)	-395.38 (-88.88)	120.54 (88.90)	-229.99 (-51.70)	181.01 (133.50)	-747.79 (-168.10)	0.59
43	47.63 (156.27)	230.23 (169.80)	-2,308.75 (-519.00)	-589.87 (-132.60)	-1,098.77 (-247.00)	-589.87 (-132.60)	179.25 (131.20)	-463.53 (-104.20)	230.23 (169.80)	-1,098.77 (-247.00)	0.82

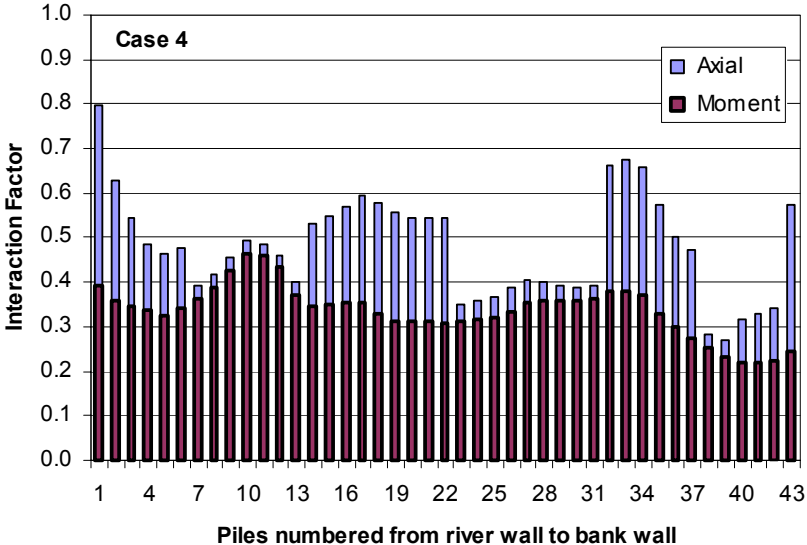
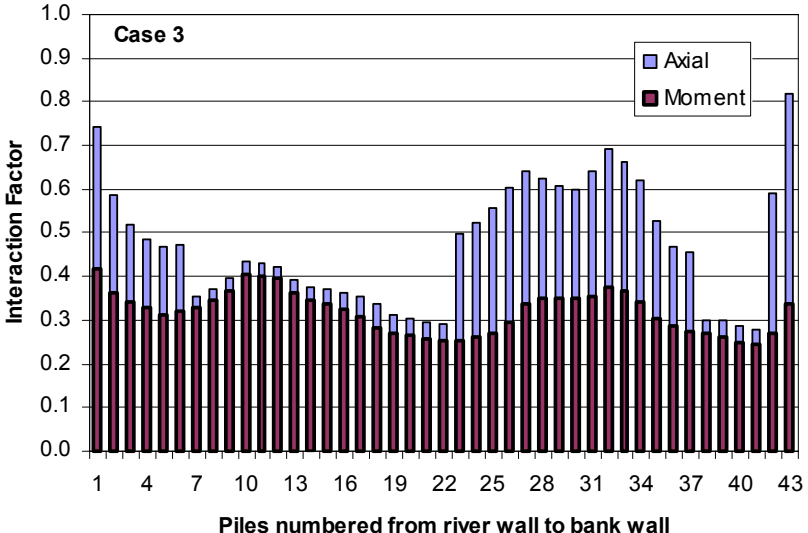
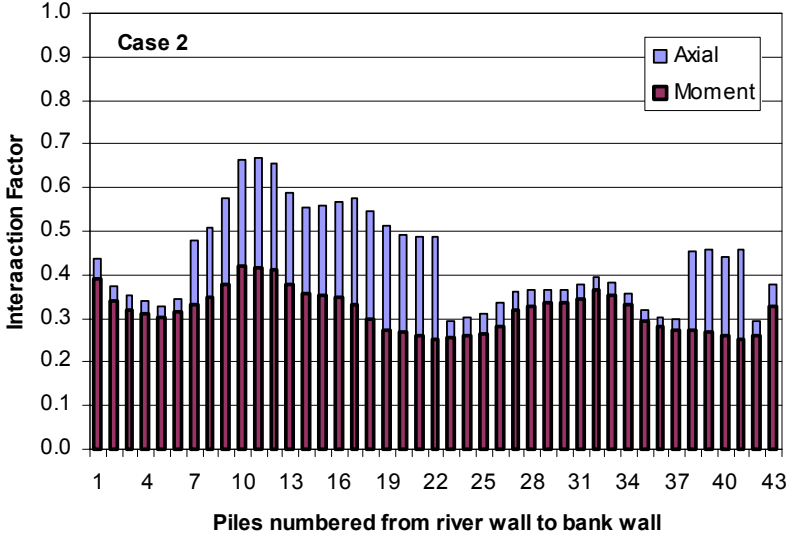
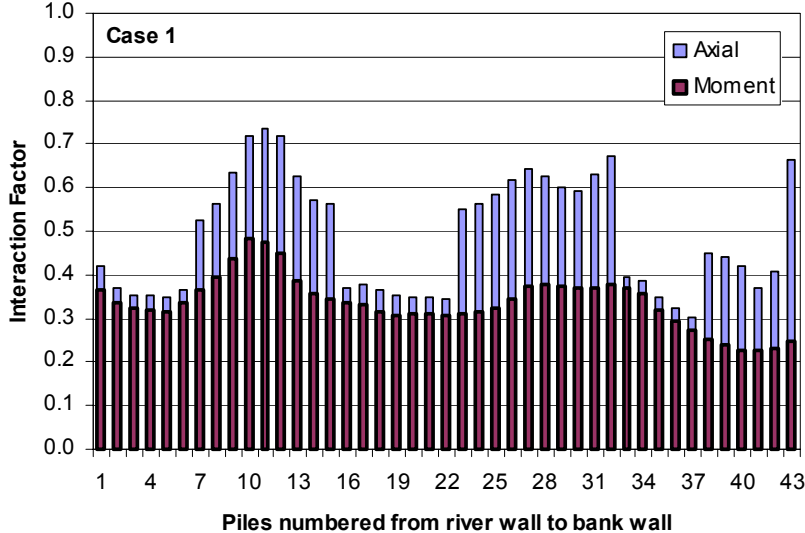


Figure 6.3-15. Maximum piles interaction factors for each load combination case listed in Table 6.3-4.

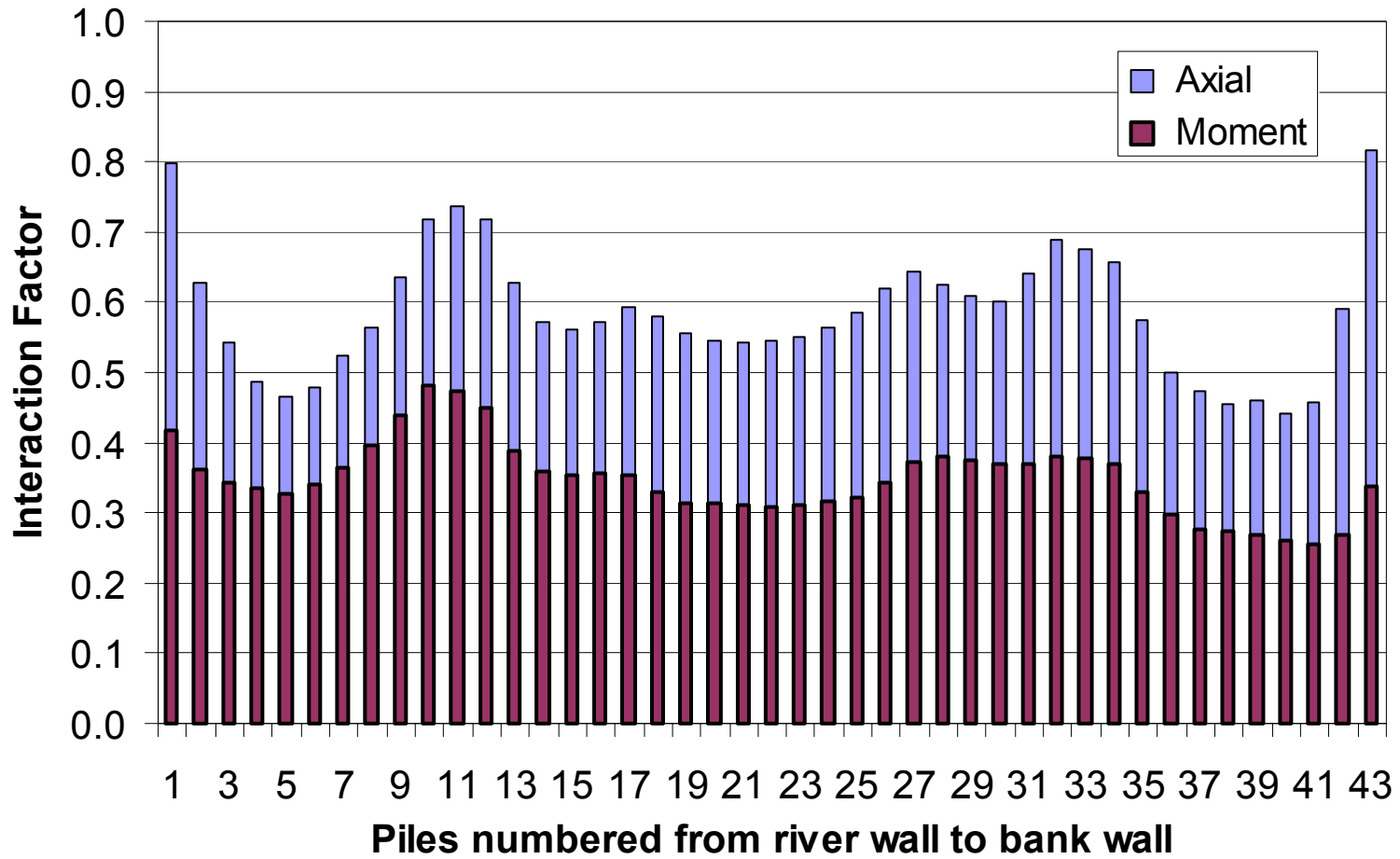


Figure 6.3-16. Envelopes of Maximum piles interaction factors for all load combination cases

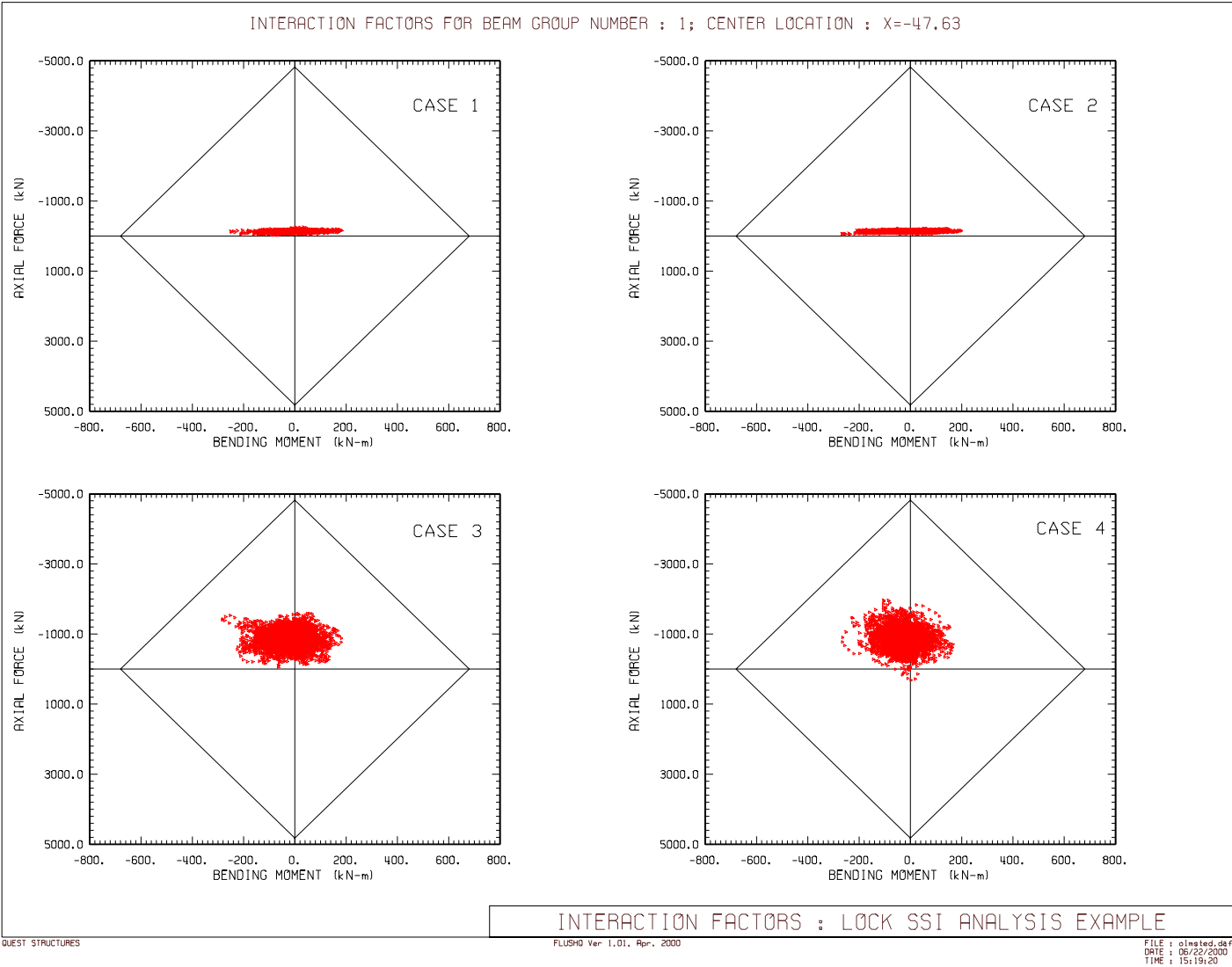


Figure 6.3-17. Comparison of Pile 1 (river side) bending moment-axial force demands with bending-moment-axial force capacities for load combination cases shown in Table 6.3-4.

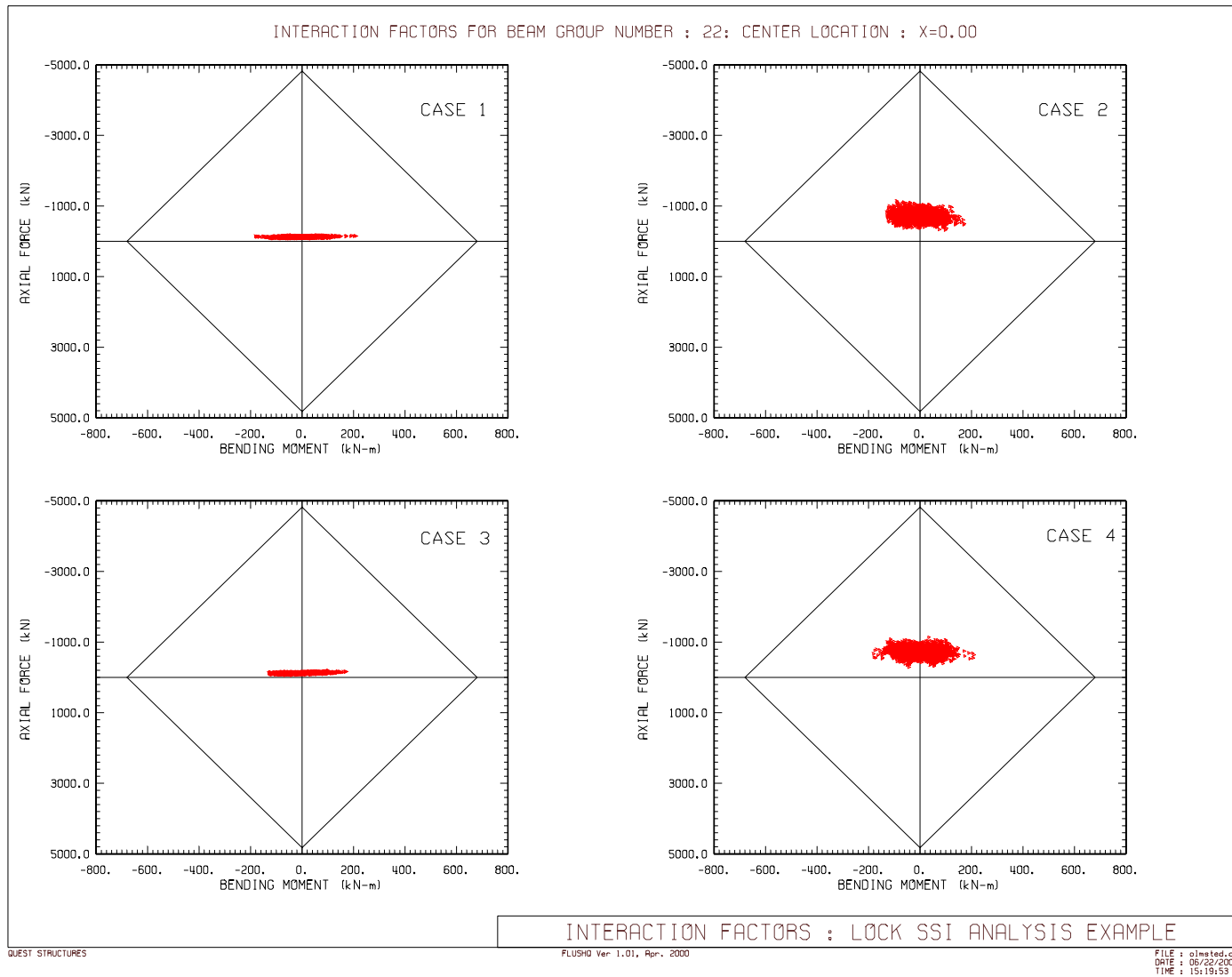


Figure 6.3-18. Comparison of Pile 22 (center) bending moment-axial force demands with bending moment-axial force capacities for load combination cases shown in Table 6.3-4.

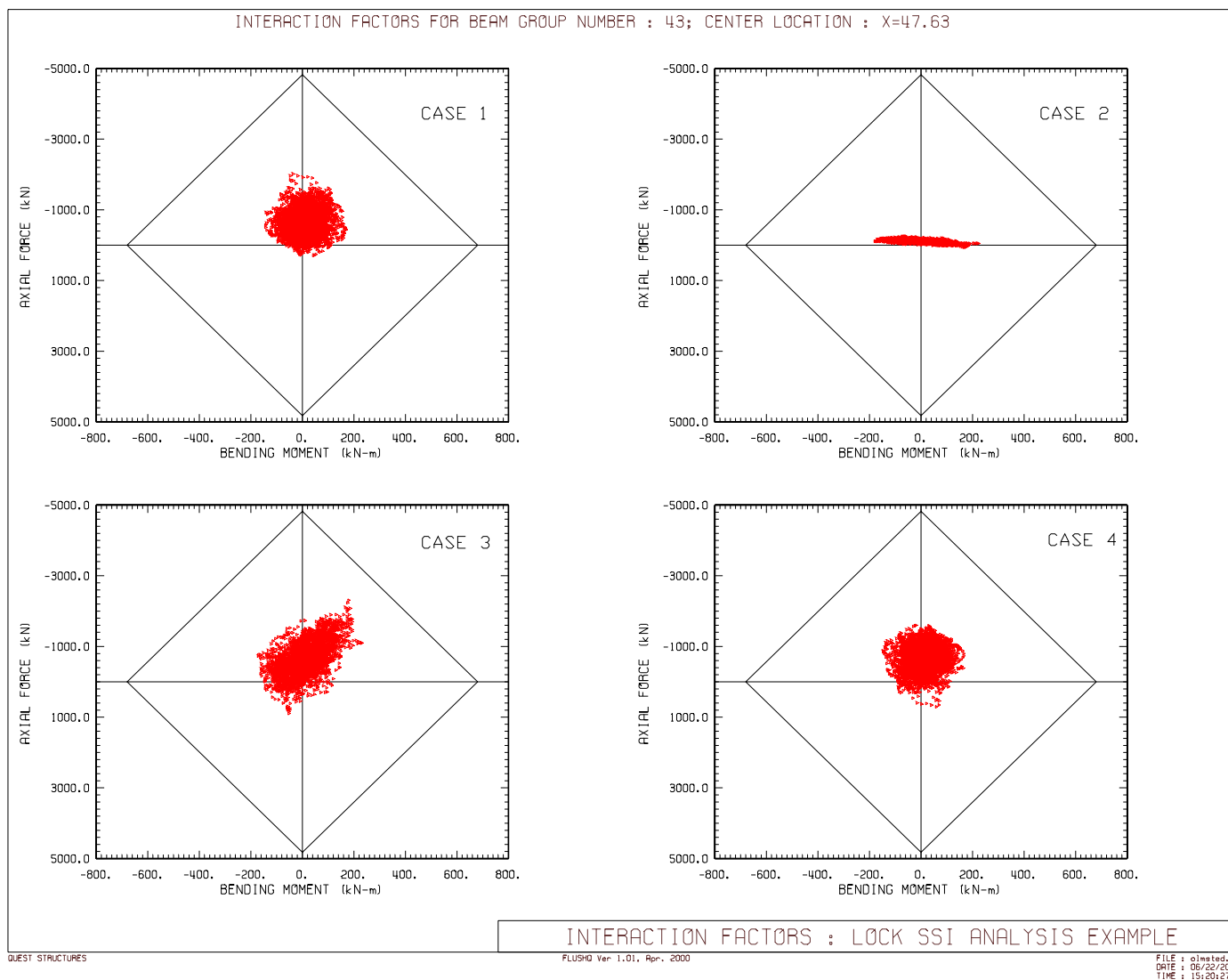


Figure 6.3-19. Comparison of Pile 43 (land side) bending moment-axial force demands with bending moment-axial force capacities for load combination cases shown in Table 6.3-4.

Table 6.3-6

Absolute and relative displacements at selected piles and lock walls locations of chamber monolith for MDE excitation

					(TH Horizontal) + (TH Vertical) + Static				(TH Horizontal) - (TH Vertical) + Static			
	Location				Horizontal Displacement cm (in)		Vertical Displacement cm (in)		Horizontal Displacement cm (in)		Vertical Displacement cm (in)	
	Node	X, m	Y, m	Absolute	Relative	Absolute	Relative	Absolute	Relative	Absolute	Relative	
Pile Displacement	Left	347	-47.63	74.37	8.65 (3.40)	2.59 (1.02)	5.74 (2.26)	0.66 (0.26)	8.47 (3.34)	2.21 (0.87)	5.39 (2.12)	0.48 (0.19)
		377	-47.63	54.56	6.06 (2.39)		5.09 (2.00)		6.26 (2.46)		4.91 (1.93)	
	Middle	2163	0.00	74.37	8.82 (3.47)	2.77 (1.09)	5.26 (2.07)	0.38 (0.15)	8.67 (3.41)	2.86 (1.13)	5.41 (2.13)	0.36 (0.14)
		2193	0.00	54.56	6.05 (2.38)		4.88 (1.92)		5.81 (2.29)		5.05 (1.99)	
	Right	3965	47.63	74.37	8.83 (3.48)	2.62 (1.03)	5.84 (2.30)	0.67 (0.26)	8.70 (3.42)	2.64 (1.04)	6.13 (2.41)	0.70 (0.27)
		3995	47.63	54.56	6.21 (2.45)		5.17 (2.04)		6.05 (2.38)		5.43 (2.14)	
Lock Displacement	Left Wall	194	-49.71	85.34	9.34 (3.68)	0.70 (0.28)	6.01 (2.37)	0.07 (0.03)	9.22 (3.63)	0.75 (0.30)	5.52 (2.17)	0.05 (0.02)
		212	-49.71	74.37	8.64 (3.40)		5.94 (2.34)		8.47 (3.34)		5.46 (2.15)	
		739	-41.48	94.53	9.94 (3.91)	1.25 (0.49)	5.54 (2.18)	0.06 (0.02)	9.90 (3.90)	1.39 (0.55)	5.48 (2.16)	0.05 (0.02)
		765	-41.48	74.37	8.69 (3.42)		5.48 (2.16)		8.51 (3.35)		5.43 (2.14)	
	Middle Wall	1681	-7.93	94.53	9.43 (3.71)	0.63 (0.25)	5.29 (2.08)	0.04 (0.01)	9.28 (3.65)	0.62 (0.24)	5.24 (2.06)	0.02 (0.01)
		1703	-7.93	74.37	8.80 (3.47)		5.25 (2.07)		8.66 (3.41)		5.22 (2.06)	
		2628	7.93	94.53	9.43 (3.71)	0.55 (0.21)	5.32 (2.10)	0.06 (0.02)	9.28 (3.65)	0.55 (0.22)	5.66 (2.23)	0.07 (0.03)
		2650	7.93	74.37	8.89 (3.50)		5.26 (2.07)		8.73 (3.44)		5.59 (2.20)	
	Right Wall	3566	41.48	94.53	12.01 (4.73)	3.13 (1.23)	5.20 (2.05)	-0.07 (-0.03)	11.98 (4.72)	3.23 (1.27)	5.33 (2.10)	-0.10 (-0.04)
		3592	41.48	74.37	8.88 (3.50)		5.27 (2.07)		8.76 (3.45)		5.43 (2.14)	
		4112	49.71	85.34	10.51 (4.14)	1.67 (0.66)	6.15 (2.42)	0.09 (0.04)	10.47 (4.12)	1.77 (0.70)	6.50 (2.56)	0.10 (0.04)
		4130	49.71	74.37	8.84 (3.48)		6.06 (2.39)		8.70 (3.43)		6.40 (2.52)	

Table 6.3-6
Continued

					- (TH Horizontal) + (TH Vertical) + Static				- (TH Horizontal) - (TH Vertical) + Static			
	Location				Horizontal Displacement cm (in)		Vertical Displacement cm (in)		Horizontal Displacement cm (in)		Vertical Displacement cm (in)	
		Node	X, m	Y, m	Absolute	Relative	Absolute	Relative	Absolute	Relative	Absolute	Relative
Pile Displacement	Left	347	-47.63	74.37	9.04 (3.56)	2.40 (0.95)	8.95 (3.52)	3.72 (1.46)	9.21 (3.63)	2.30 (0.90)	6.22 (2.45)	0.61 (0.24)
		377	-47.63	54.56	6.63 (2.61)		5.23 (2.06)		6.92 (2.72)		5.61 (2.21)	
	Middle	2163	0.00	74.37	9.07 (3.57)	2.86 (1.12)	5.22 (2.05)	0.38 (0.15)	9.22 (3.63)	2.76 (1.09)	5.33 (2.10)	0.37 (0.15)
		2193	0.00	54.56	6.21 (2.44)		4.84 (1.91)		6.46 (2.54)		4.96 (1.95)	
	Right	3965	47.63	74.37	8.96 (3.53)	2.92 (1.15)	4.60 (1.81)	-0.29 (-0.12)	9.09 (3.58)	2.90 (1.14)	5.49 (2.16)	0.59 (0.23)
		3995	47.63	54.56	6.04 (2.38)		4.89 (1.93)		6.20 (2.44)		4.90 (1.93)	
Lock Displacement	Left Wall	194	-49.71	85.34	10.54 (4.15)	1.49 (0.59)	6.02 (2.37)	0.06 (0.03)	10.65 (4.19)	1.44 (0.56)	6.50 (2.56)	0.06 (0.02)
		212	-49.71	74.37	9.05 (3.56)		5.96 (2.35)		9.22 (3.63)		6.44 (2.54)	
		739	-41.48	94.53	11.90 (4.69)	2.82 (1.11)	5.52 (2.17)	0.02 (0.01)	11.95 (4.70)	2.69 (1.06)	5.54 (2.18)	-0.06 (-0.02)
		765	-41.48	74.37	9.08 (3.58)		5.51 (2.17)		9.26 (3.65)		5.59 (2.20)	
	Middle Wall	1681	-7.93	94.53	9.75 (3.84)	0.63 (0.25)	5.41 (2.13)	0.06 (0.02)	9.90 (3.90)	0.64 (0.25)	5.59 (2.20)	0.06 (0.02)
		1703	-7.93	74.37	9.12 (3.59)		5.35 (2.11)		9.27 (3.65)		5.52 (2.17)	
		2628	7.93	94.53	9.75 (3.84)	0.69 (0.27)	5.14 (2.02)	0.06 (0.02)	9.91 (3.90)	0.69 (0.27)	5.13 (2.02)	0.01 (0.00)
		2650	7.93	74.37	9.06 (3.56)		5.08 (2.00)		9.21 (3.63)		5.12 (2.02)	
	Right Wall	3566	41.48	94.53	9.99 (3.93)	0.99 (0.39)	5.36 (2.11)	0.01 (0.01)	10.02 (3.94)	0.90 (0.36)	5.39 (2.12)	0.03 (0.01)
		3592	41.48	74.37	8.99 (3.54)		5.35 (2.10)		9.12 (3.59)		5.36 (2.11)	
		4112	49.71	85.34	9.53 (3.75)	0.57 (0.23)	5.62 (2.21)	0.06 (0.02)	9.57 (3.77)	0.49 (0.19)	5.65 (2.22)	0.06 (0.02)
		4130	49.71	74.37	8.95 (3.52)		5.56 (2.19)		9.09 (3.58)		5.59 (2.20)	

Table 6.3-7
Combined Static and Dynamic Concrete Section Forces and Moments for Load Combination Case 3
LOAD COMBINATION: -1.0(Horizontal) + 1.0(Vertical) + 1.0(Static)

Section	Time History Peak values			At Peak Moment		At Peak Axial		At Peak Shear	
	Moment kN-m (k-ft)	Axial Force kN (kips)	Shear Force kN (kips)	Axial Force kN (kips)	Shear Force kN (kips)	Moment kN-m (k-ft)	Shear Force kN (kips)	Moment kN-m (k-ft)	Axial Force kN (kips)
H 1	-2,191.31 (-492.60)	-911.73 (-62.47)	-1,878.33 (-128.70)	-661.58 (-45.33)	339.33 (23.25)	-989.78 (-222.50)	-165.80 (-11.36)	2,048.07 (460.40)	-668.00 (-45.77)
H 2	-665.04 (-149.50)	-1,311.91 (-89.89)	-268.54 (-18.40)	-1,307.54 (-89.59)	-268.54 (-18.40)	-657.48 (-147.80)	-267.67 (-18.34)	-665.04 (-149.50)	-1,307.54 (-89.59)
H 3	-754.46 (-169.60)	-2,710.23 (-185.70)	-741.41 (-50.80)	-410.40 (-28.12)	128.45 (8.80)	587.20 (132.00)	-691.20 (-47.36)	721.54 (162.20)	-2,705.85 (-185.40)
H 4	-433.06 (-97.35)	-2,107.47 (-144.40)	-367.64 (-25.19)	-89.98 (-6.17)	-331.44 (-22.71)	407.75 (91.66)	-11.32 (-0.78)	-333.63 (-75.00)	-379.32 (-25.99)
H 5	3,381.27 (760.10)	-2,294.28 (-157.20)	-1,465.30 (-100.40)	88.15 (6.04)	1,255.58 (86.03)	-1,881.25 (-422.90)	-1,243.17 (-85.18)	-2,148.16 (-482.90)	-2,193.58 (-150.30)
H 6	-1,616.57 (-363.40)	-2,295.74 (-157.30)	-584.81 (-40.07)	-1,954.23 (-133.90)	-584.81 (-40.07)	-1,437.30 (-323.10)	-569.63 (-39.03)	-1,616.57 (-363.40)	-1,954.23 (-133.90)
H 7	-1,481.78 (-333.10)	-2,241.74 (-153.60)	-430.98 (-29.53)	-1,590.82 (-109.00)	-373.77 (-25.61)	729.55 (164.00)	-430.98 (-29.53)	729.55 (164.00)	-2,241.74 (-153.60)
H 8	-1,874.13 (-421.30)	-2,533.63 (-173.60)	-662.01 (-45.36)	560.73 (38.42)	315.97 (21.65)	650.36 (146.20)	-550.07 (-37.69)	984.89 (221.40)	-2,497.15 (-171.10)
H 9	-2,772.72 (-623.30)	-2,669.37 (-182.90)	-1,748.44 (-119.80)	-260.51 (-17.85)	721.27 (49.42)	1,647.71 (370.40)	-1,344.17 (-92.10)	1,352.33 (304.00)	-2,419.80 (-165.80)
H 10	1,482.67 (333.30)	-1,936.71 (-132.70)	-708.13 (-48.52)	-1,137.95 (-77.97)	-226.51 (-15.52)	-562.73 (-126.50)	-390.85 (-26.78)	17.29 (3.89)	-1,308.41 (-89.65)
H 11	2,723.79 (612.30)	-2,786.12 (-190.90)	-1,520.76 (-104.20)	419.45 (28.74)	677.63 (46.43)	-1,852.78 (-416.50)	-1,117.08 (-76.54)	-2,336.77 (-525.30)	-2,720.45 (-186.40)
H 12	-1,868.35 (-420.00)	-932.31 (-63.88)	-1,974.66 (-135.30)	-447.03 (-30.63)	-1,590.82 (-109.00)	-1,165.50 (-262.00)	-1,555.79 (-106.60)	-1,456.87 (-327.50)	-594.29 (-40.72)
H 13	1,932.41 (434.40)	-2,707.31 (-185.50)	-1,161.44 (-79.58)	99.58 (6.82)	593.13 (40.64)	-1,217.99 (-273.80)	-1,154.73 (-79.12)	-1,136.14 (-255.40)	-2,634.34 (-180.50)
H 14	-1,003.13 (-225.50)	-2,241.74 (-153.60)	-328.09 (-22.48)	736.59 (50.47)	-131.85 (-9.03)	812.29 (182.60)	-139.99 (-9.59)	-351.38 (-78.99)	-608.45 (-41.69)
H 15	-4,684.22 (-1,053.00)	-2,508.82 (-171.90)	-2,324.93 (-159.30)	325.75 (22.32)	1,901.69 (130.30)	4,417.76 (993.10)	-2,270.93 (-155.60)	4,492.94 (1,010.00)	-2,412.50 (-165.30)
H 16	-875.90 (-196.90)	-2,726.28 (-186.80)	-675.59 (-46.29)	-2,726.28 (-186.80)	594.73 (40.75)	-875.90 (-196.90)	594.73 (40.75)	804.73 (180.90)	756.30 (51.82)
V 1	8,696.73 (1,955.00)	1,728.01 (118.40)	1,620.01 (111.00)	1,108.47 (75.95)	1,620.01 (111.00)	4,056.55 (911.90)	659.39 (45.18)	8,696.73 (1,955.00)	1,108.47 (75.95)
V 2	-1,896.38 (-426.30)	-2,482.55 (-170.10)	-909.83 (-62.34)	1,065.70 (73.02)	-650.92 (-44.60)	-347.65 (-78.15)	-674.42 (-46.21)	-1,221.10 (-274.50)	-199.80 (-13.69)
V 3	-5,960.93 (-1,340.00)	3,574.23 (244.90)	-2,275.31 (-155.90)	-1,771.79 (-121.40)	-2,043.25 (-140.00)	4,016.07 (902.80)	382.53 (26.21)	-5,871.96 (-1,320.00)	-920.92 (-63.10)
V 4	-5,404.87 (-1,215.00)	-3,095.53 (-212.10)	-2,964.18 (-203.10)	-2,012.60 (-137.90)	-2,956.88 (-202.60)	-3,085.45 (-693.60)	-2,244.66 (-153.80)	-5,289.21 (-1,189.00)	-2,304.50 (-157.90)
V 5	-2,306.97 (-518.60)	3,885.10 (266.20)	-986.16 (-67.57)	-2,700.01 (-185.00)	-675.59 (-46.29)	-1,648.60 (-370.60)	-515.19 (-35.30)	-186.79 (-41.99)	1,000.61 (68.56)
V 6	10,876.47 (2,445.00)	4,925.70 (337.50)	-2,886.83 (-197.80)	4,919.86 (337.10)	2,034.50 (139.40)	10,823.09 (2,433.00)	1,993.63 (136.60)	-7,851.52 (-1,765.00)	-3,836.94 (-262.90)
V 7	425.49 (95.65)	-299.92 (-20.55)	748.12 (51.26)	62.64 (4.29)	690.47 (47.31)	-118.28 (-26.59)	-686.68 (-47.05)	370.42 (83.27)	105.96 (7.26)
V 8	-850.10 (-191.10)	-1,186.98 (-81.33)	-992.73 (-68.02)	738.93 (50.63)	-992.73 (-68.02)	67.66 (15.21)	113.74 (7.79)	-850.10 (-191.10)	738.93 (50.63)

H = Horizontal Section, V = Vertical Section

Note: Metric-unit forces and moments are for 1-m thick slice and those of English units are for 1-ft thick slice

Table 6.3-8
Static Concrete Section Forces and Moments

LOAD COMBINATION: Static

Section	X-Coordinate m (ft)	Y-Coordinate m (ft)	Static Values		
			Moment kN-m (k-ft)	Axial Force kN (kips)	Shear Force kN (kips)
H 1	-43.61 (-143.08)	86.91 (285.14)	-318.69 (-71.64)	-649.75 (-44.52)	-579.85 (-39.73)
H 2	-48.95 (-160.60)	82.91 (272.01)	82.25 (18.49)	13.23 (0.91)	-41.05 (-2.81)
H 3	-42.70 (-140.09)	82.91 (272.01)	80.52 (18.10)	-1,668.17 (-114.30)	-356.11 (-24.40)
H 4	-48.95 (-160.60)	78.64 (258.01)	-74.42 (-16.73)	-977.55 (-66.98)	-170.90 (-11.71)
H 5	-42.70 (-140.09)	78.64 (258.01)	186.88 (42.01)	-1,206.25 (-82.65)	-204.33 (-14.00)
H 6	-6.71 (-22.00)	82.91 (272.01)	-253.52 (-56.99)	-905.31 (-62.03)	-161.13 (-11.04)
H 7	0.00 (0.00)	82.91 (272.01)	37.26 (8.38)	-1,557.25 (-106.70)	-349.10 (-23.92)
H 8	6.71 (22.00)	82.91 (272.01)	-298.27 (-67.05)	-1,266.67 (-86.79)	-232.64 (-15.94)
H 9	-6.71 (-22.00)	78.64 (258.01)	-543.60 (-122.20)	-1,239.09 (-84.90)	-509.50 (-34.91)
H 10	0.00 (0.00)	78.64 (258.01)	37.05 (8.33)	-1,197.93 (-82.08)	-326.04 (-22.34)
H 11	6.71 (22.00)	78.64 (258.01)	-145.42 (-32.69)	-1,471.14 (-100.80)	-516.94 (-35.42)
H 12	43.61 (143.08)	86.91 (285.14)	-13.57 (-3.05)	-576.34 (-39.49)	-494.61 (-33.89)
H 13	42.70 (140.09)	82.91 (272.01)	157.88 (35.49)	-1,306.22 (-89.50)	-355.67 (-24.37)
H 14	48.95 (160.60)	82.91 (272.01)	-176.16 (-39.60)	-702.30 (-48.12)	-130.96 (-8.97)
H 15	42.70 (140.09)	78.64 (258.01)	346.53 (77.90)	-1,096.06 (-75.10)	-338.30 (-23.18)
H 16	48.95 (160.60)	78.64 (258.01)	63.84 (14.35)	-799.20 (-54.76)	-111.40 (-7.63)
V 1	-40.74 (-133.66)	76.20 (250.00)	1,139.69 (256.20)	57.39 (3.93)	-92.91 (-6.37)
V 2	-24.76 (-81.23)	76.20 (250.00)	-130.65 (-29.37)	178.93 (12.26)	-674.27 (-46.20)
V 3	-8.73 (-28.63)	76.20 (250.00)	-560.06 (-125.90)	-11.54 (-0.79)	-885.60 (-60.68)
V 4	8.73 (28.63)	76.20 (250.00)	-1,128.13 (-253.60)	31.15 (2.13)	-1,605.41 (-110.00)
V 5	24.76 (81.23)	76.20 (250.00)	-109.39 (-24.59)	106.51 (7.30)	-682.74 (-46.78)
V 6	40.74 (133.66)	76.20 (250.00)	685.51 (154.10)	148.72 (10.19)	-610.06 (-41.80)
V 7	-47.57 (-156.07)	84.72 (277.95)	138.70 (31.18)	-49.51 (-3.39)	150.18 (10.29)
V 8	47.57 (156.07)	84.72 (277.95)	-237.06 (-53.29)	-138.36 (-9.48)	-159.08 (-10.90)

Note: Metric-unit forces and moments are for 1-m thick slice and those of English units are for 1-ft
H = Horizontal Section, V = Vertical Section

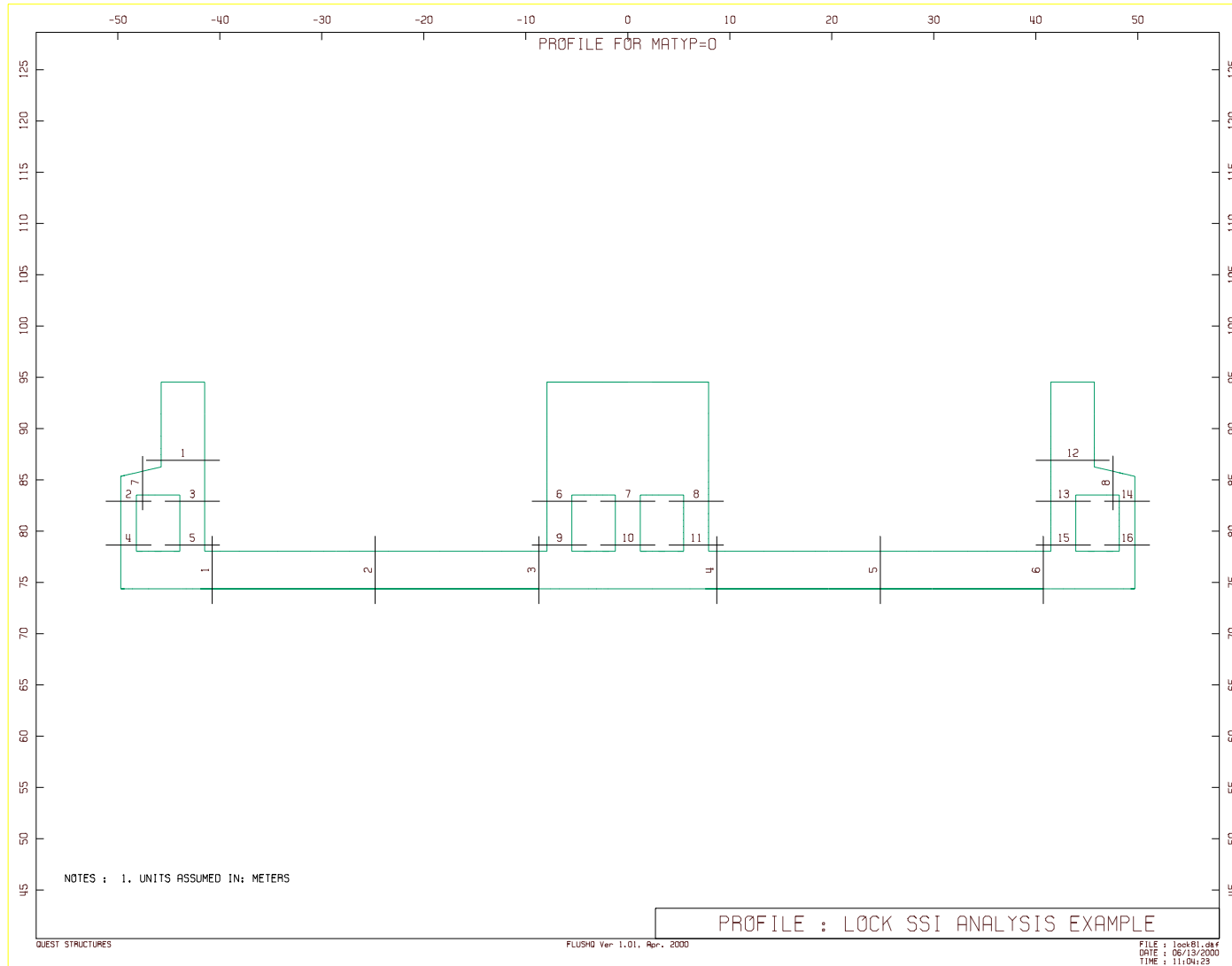


Figure 6.3-20. Critical sections for reinforced concrete forces and moments

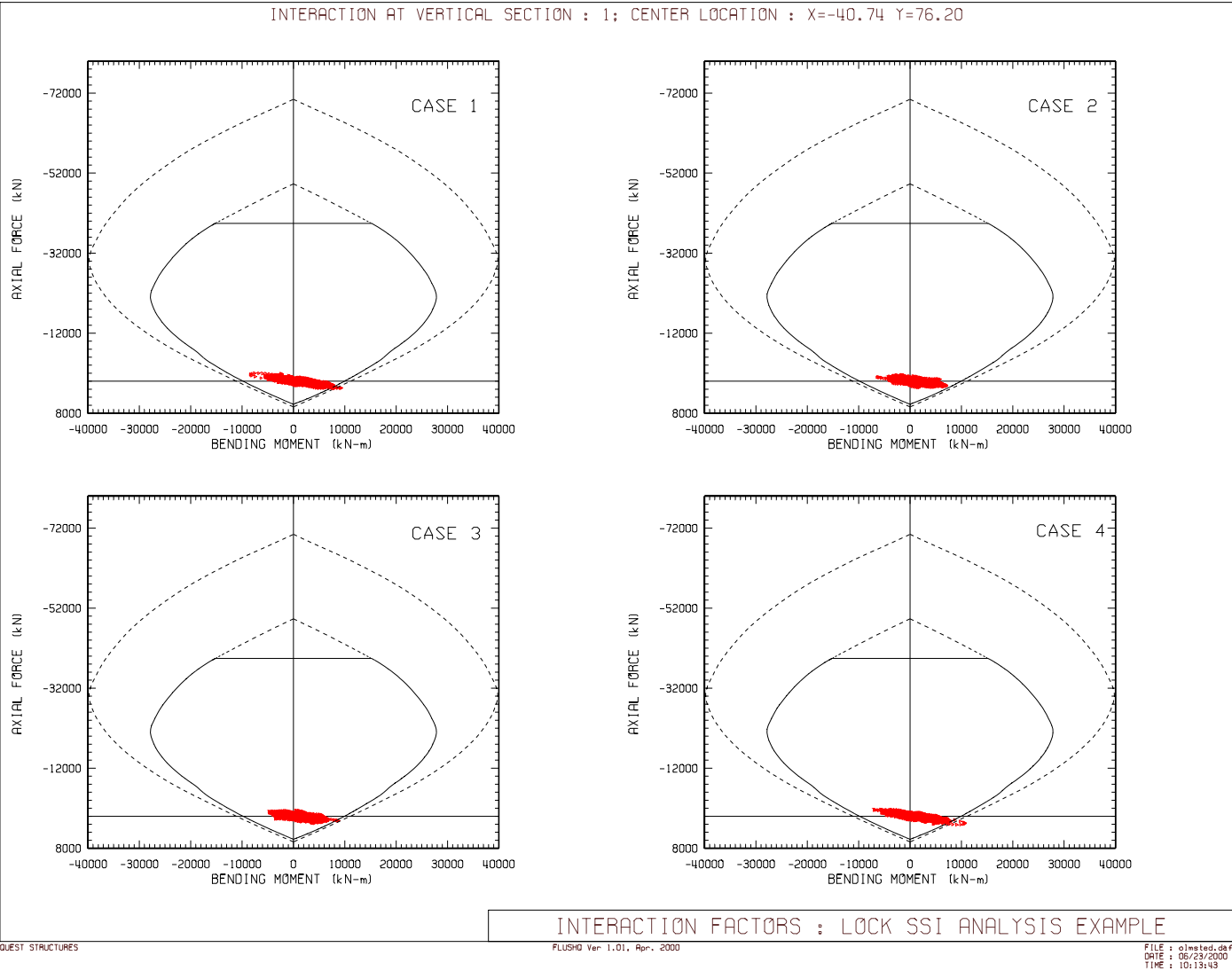


Figure 6.3-21. Combined static and seismic axial force vs. bending moment for concrete vertical section 1 shown in Figure 6.3-20)

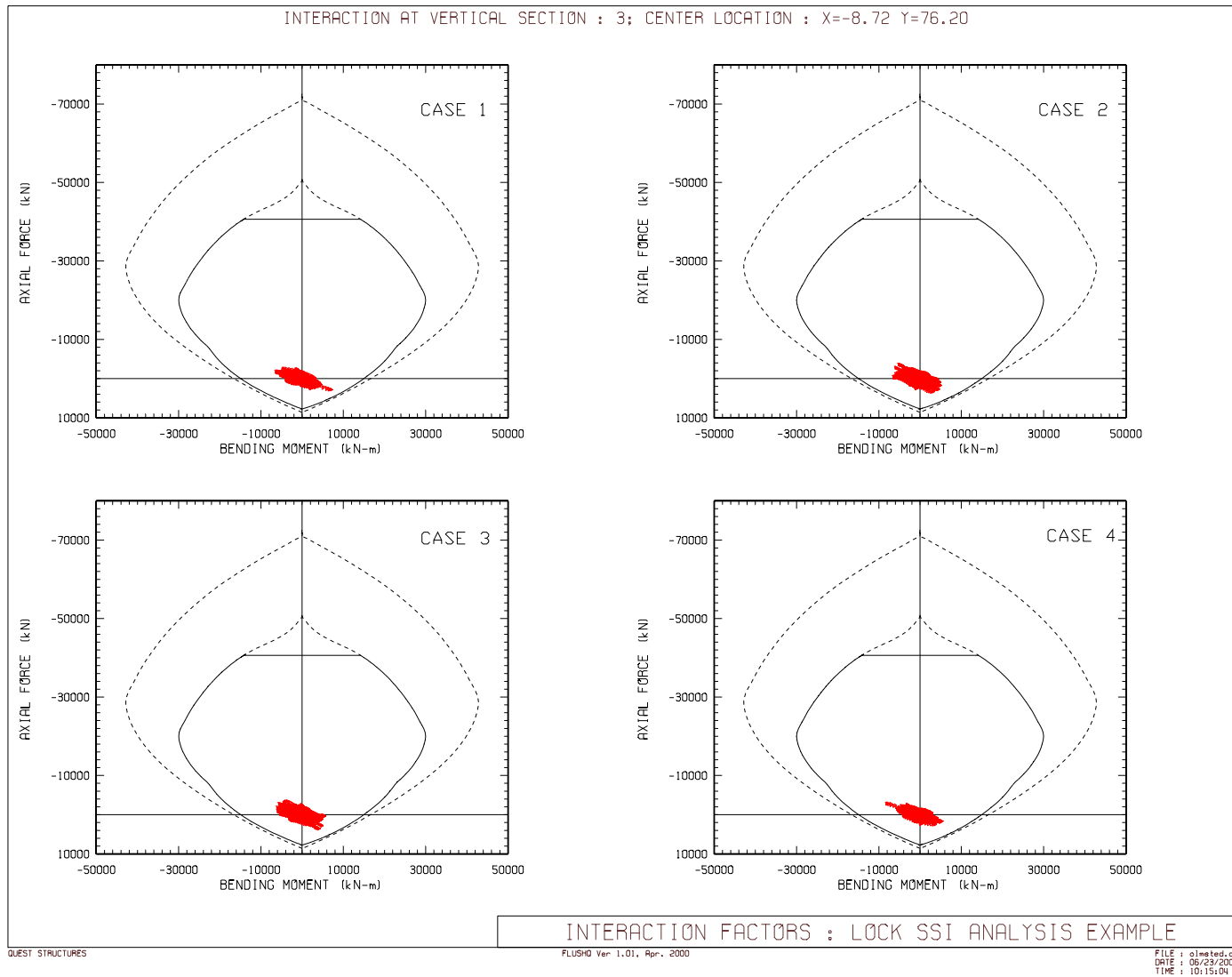


Figure 6.3-22. Combined static and seismic axial force vs. bending moment for concrete vertical section 3 (see Figure 6.3-20)

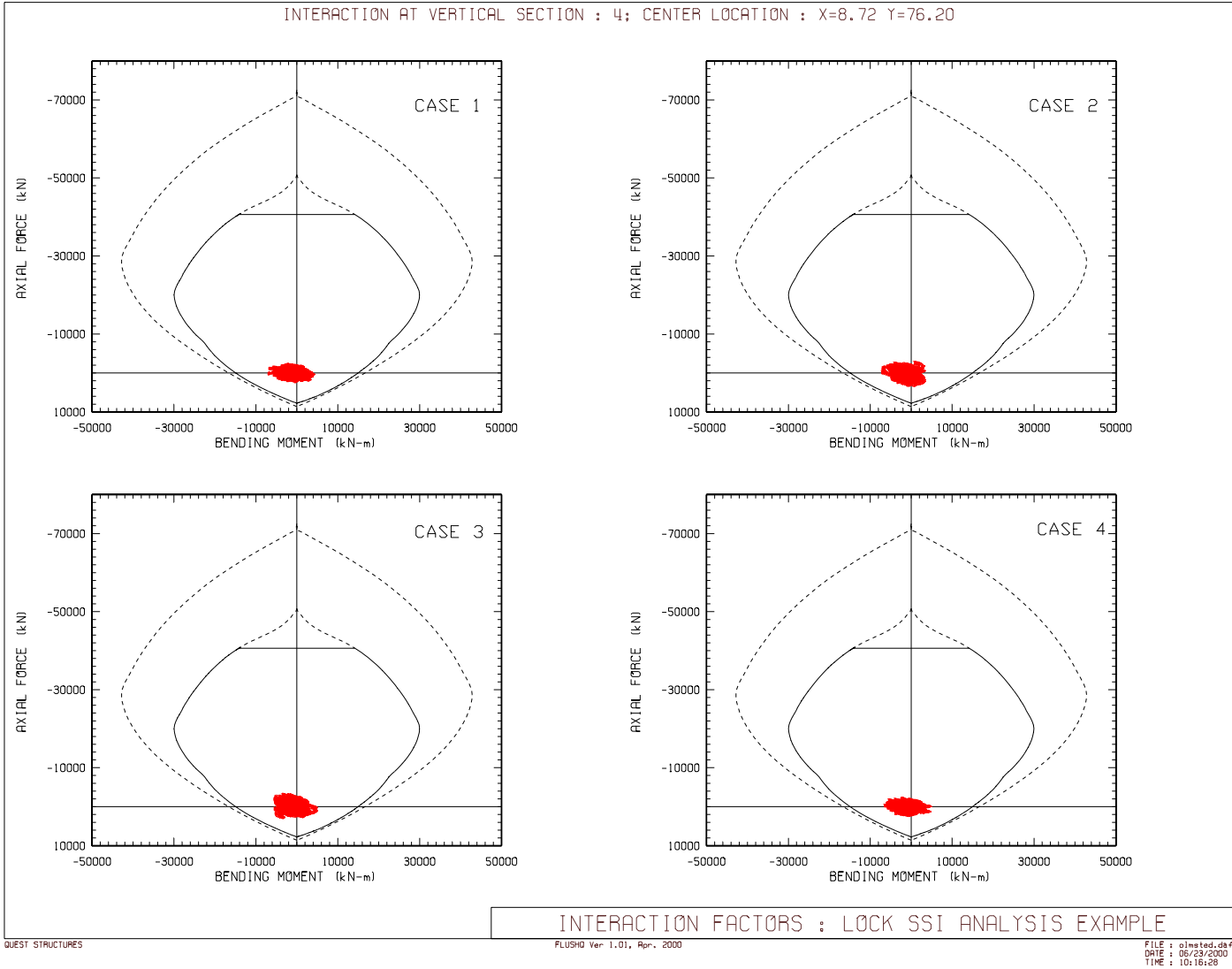


Figure 6.3-23. Combined static and seismic axial force vs. bending moment for concrete vertical section 4 (see Figure 6.3-20)

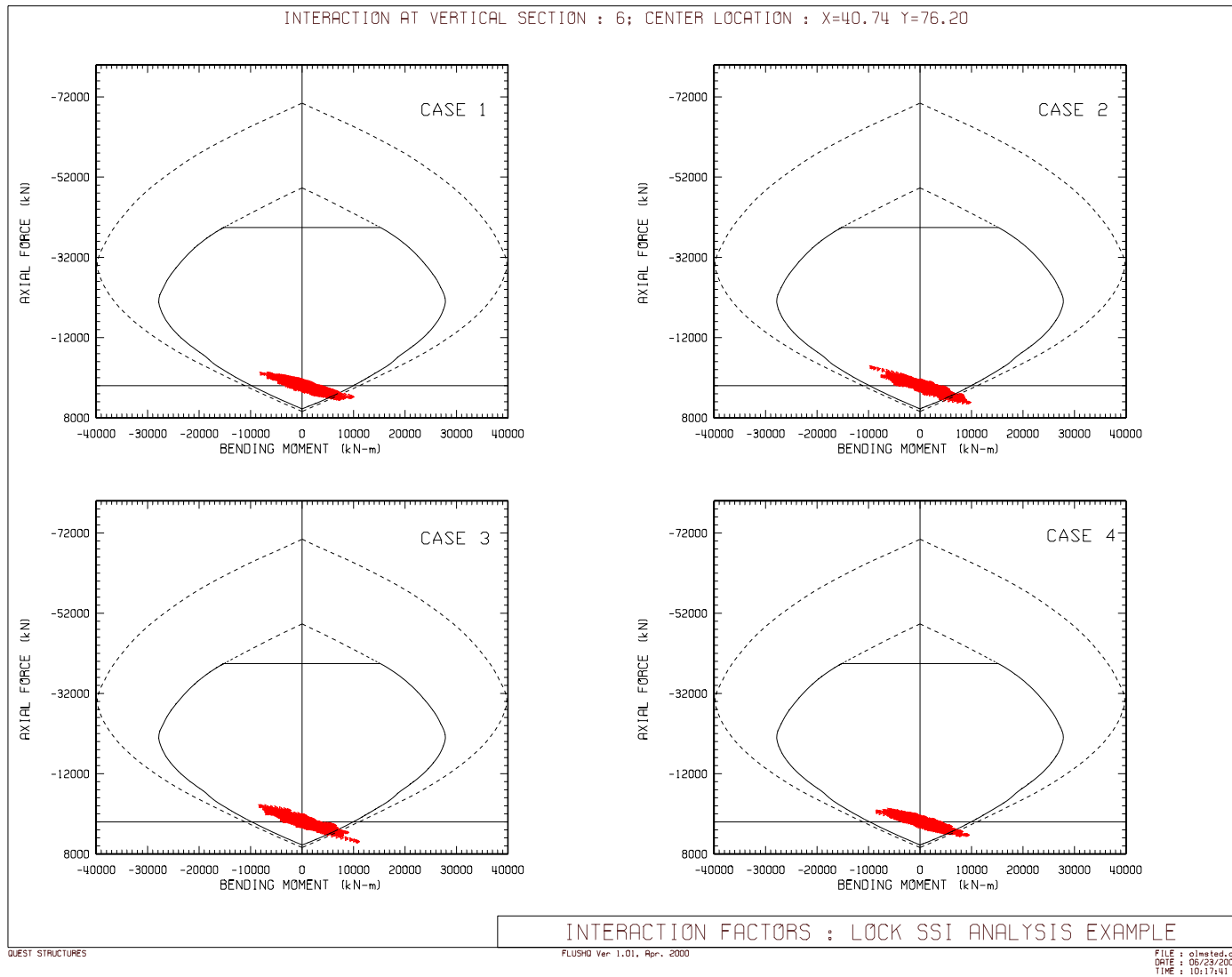


Figure 6.3-24. Combined static and seismic axial force vs. bending moment for concrete vertical section 6 (see Figure 6.3-20)

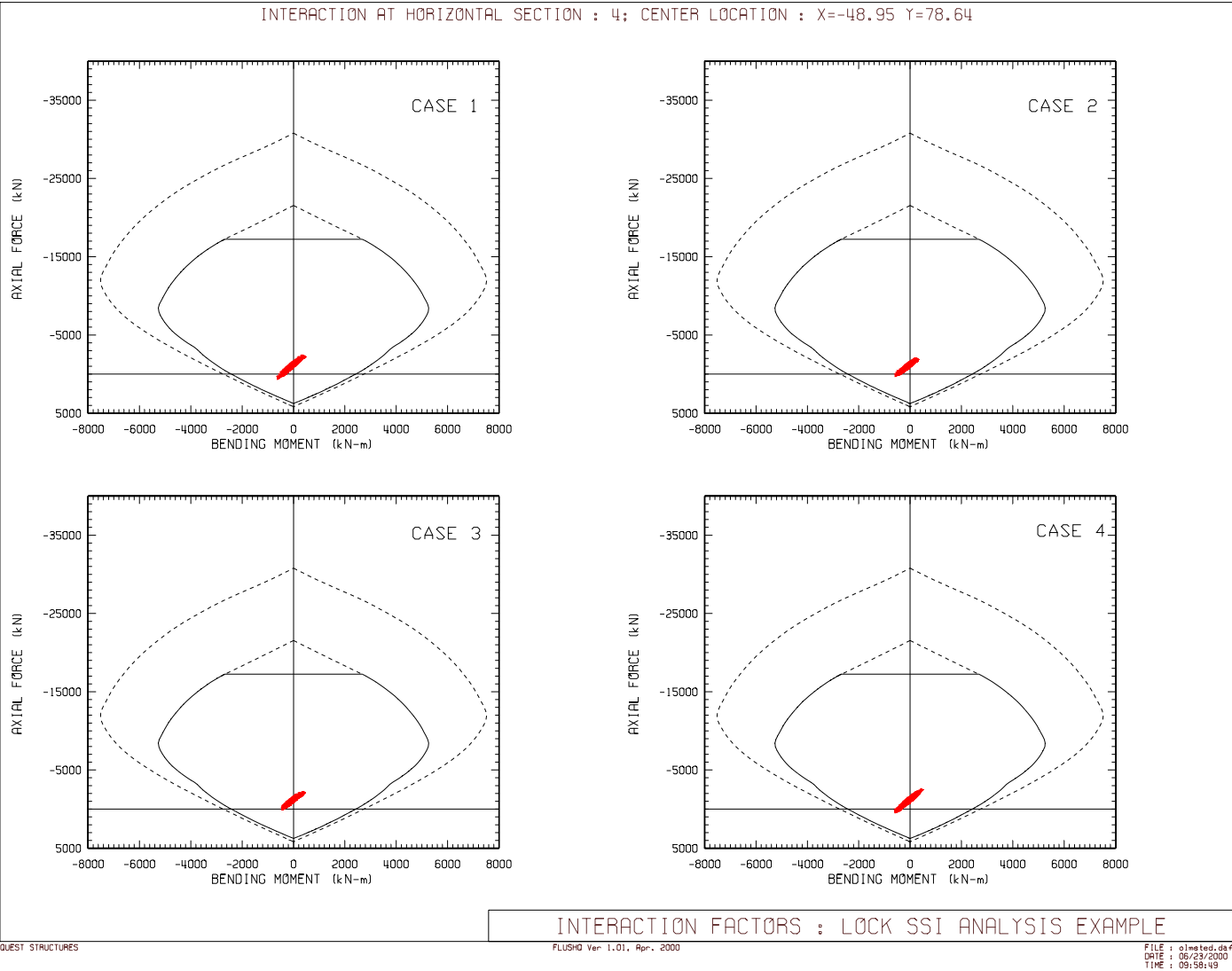


Figure 6.3-25. Combined static and seismic axial force vs. bending moment for concrete horizontal section 4 (see Figure 6.3-20)

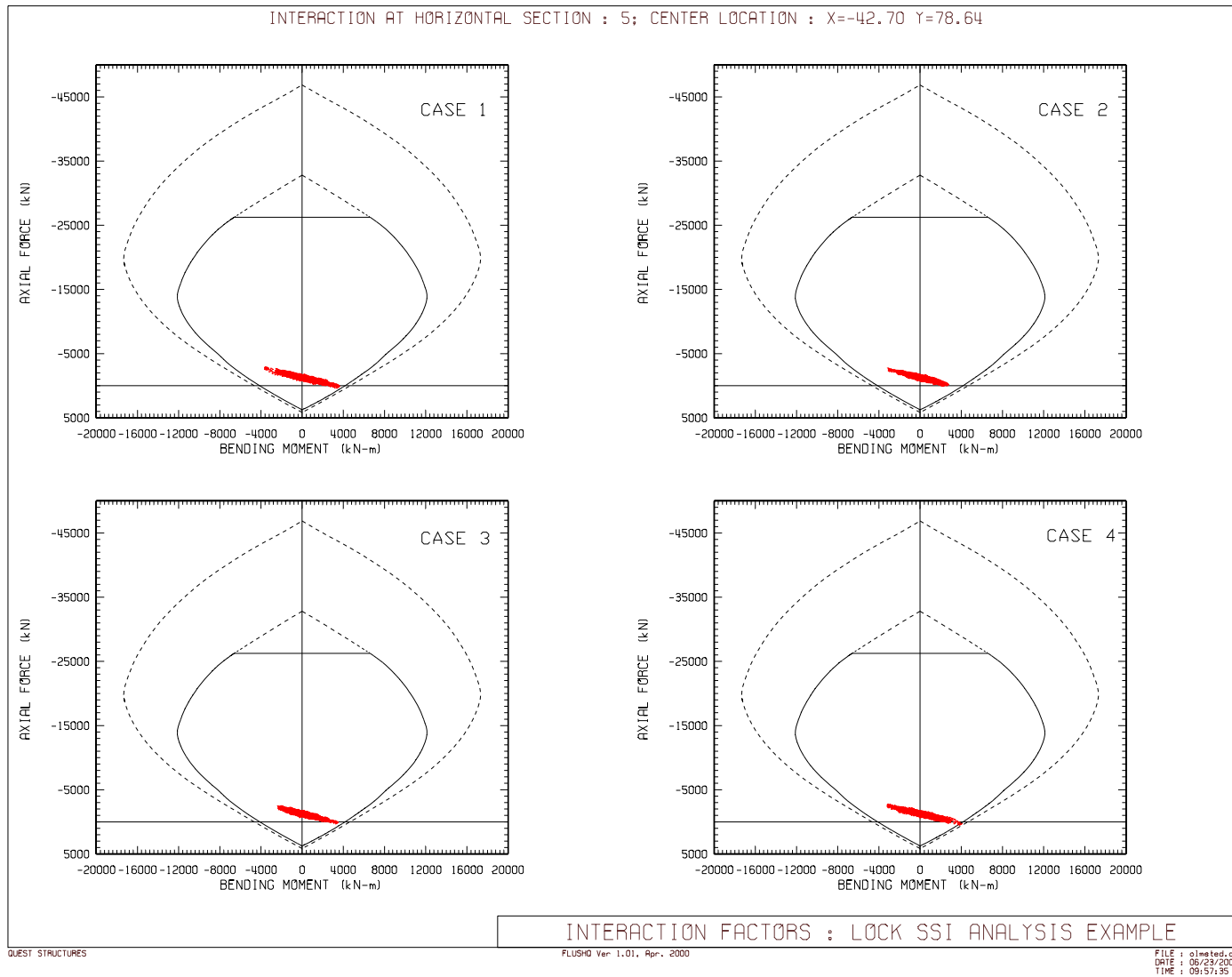


Figure 6.3-26. Combined static and seismic axial force vs. bending moment for concrete horizontal section 5 (see Figure 6.3-20)

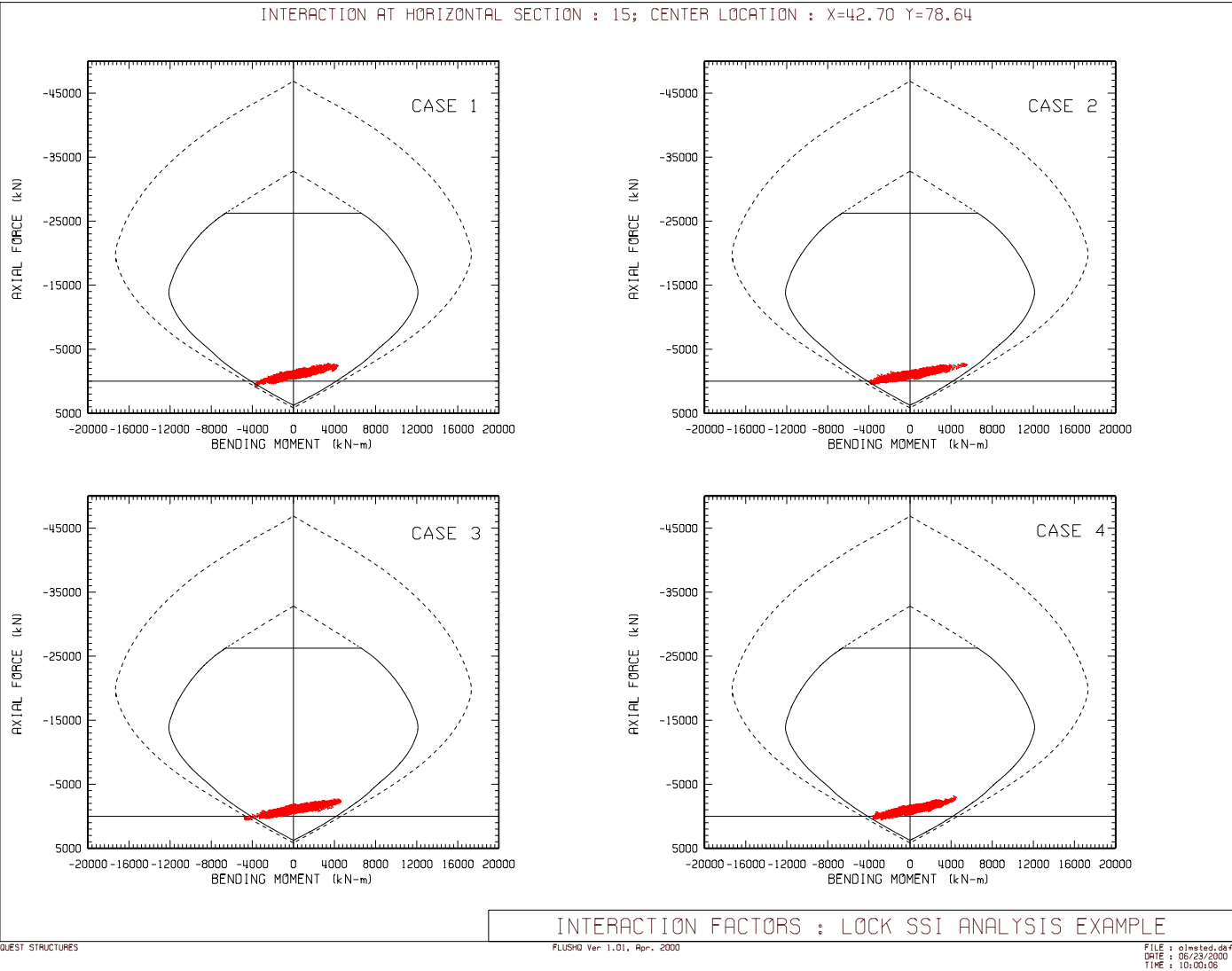


Figure 6.3-27. Combined static and seismic axial force vs. bending moment for concrete horizontal section 15 (see Figure 6.3-20)

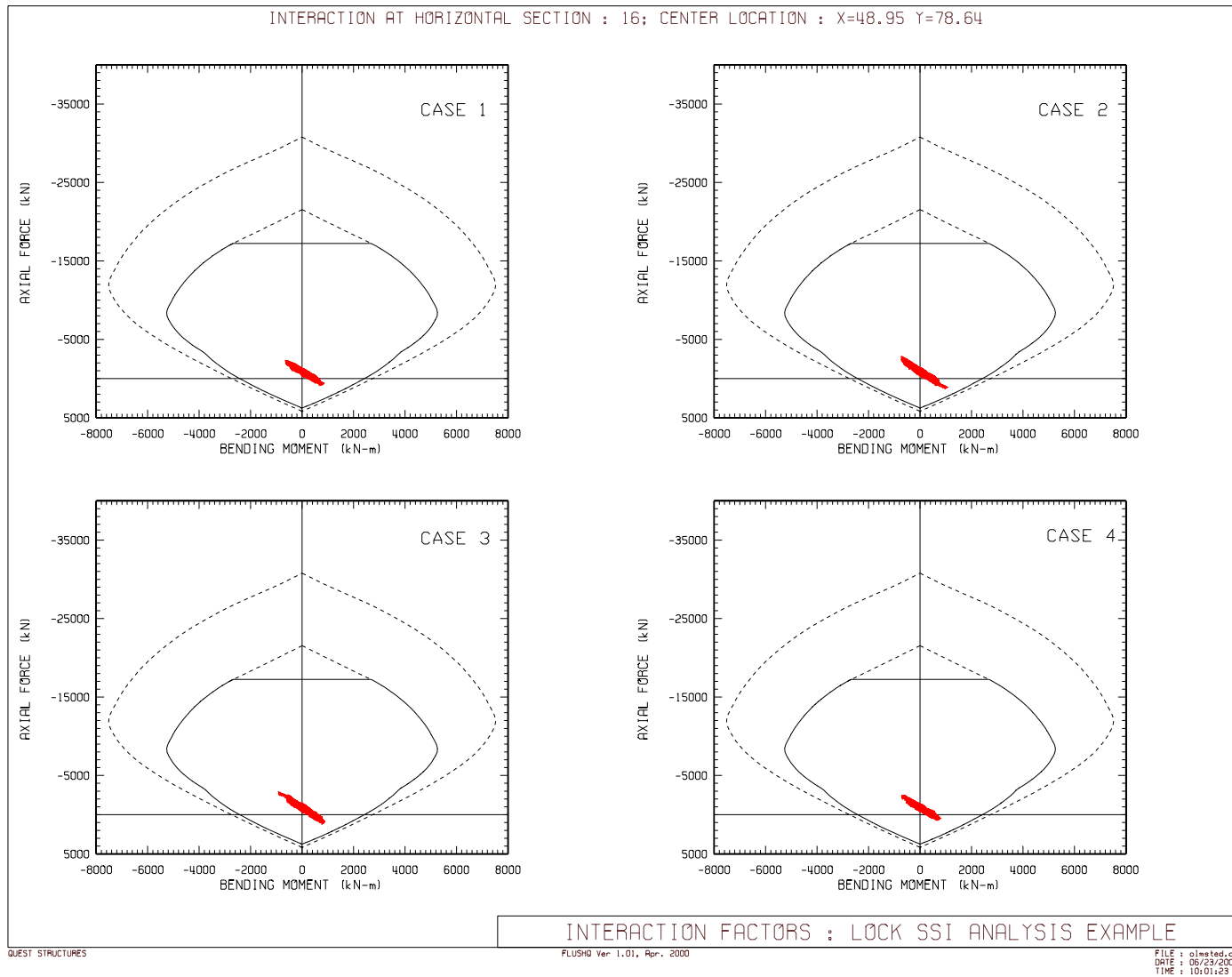
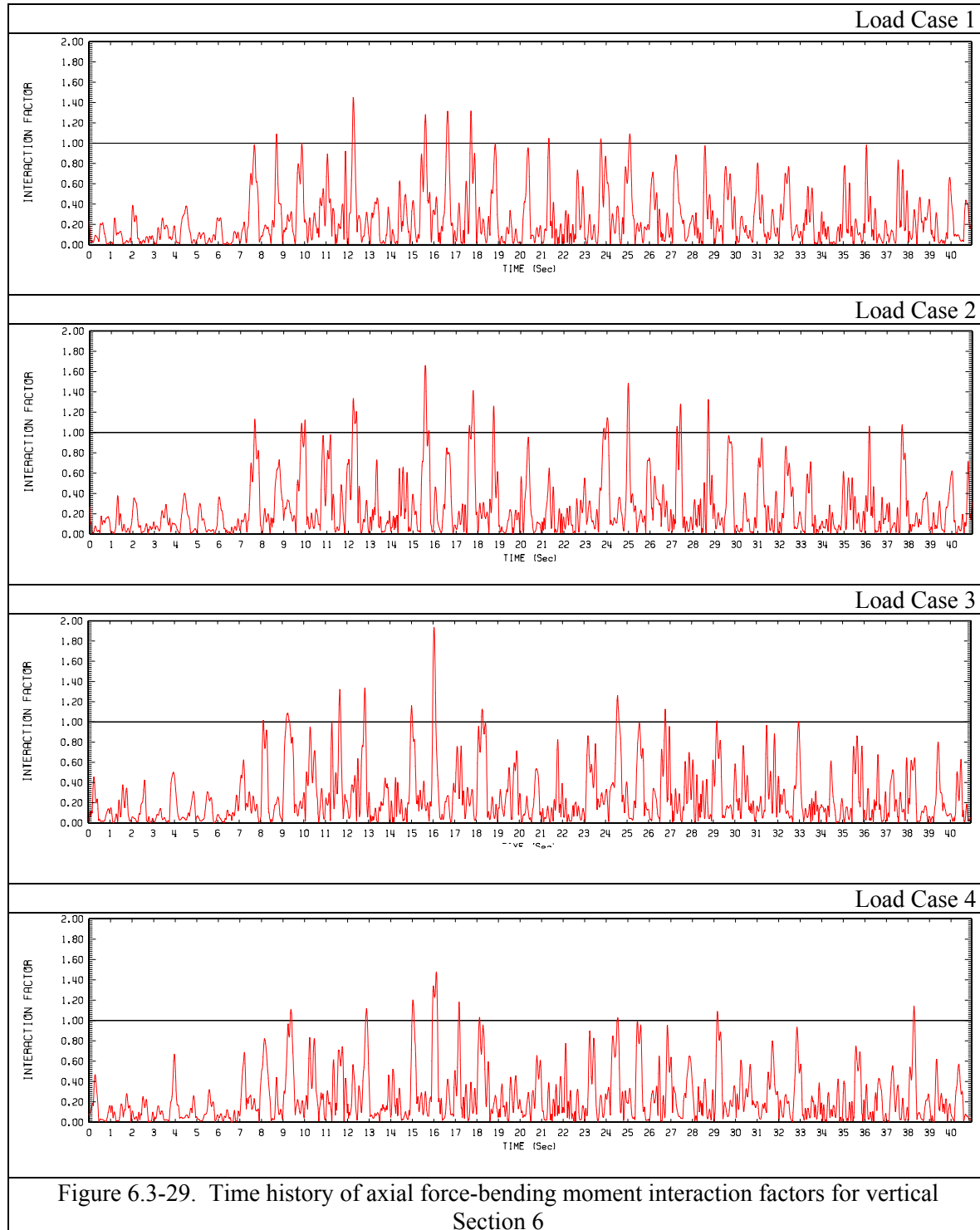


Figure 6.3-28. Combined static and seismic axial force vs. bending moment for concrete horizontal section 16 (see Figure 6.3-20)



6.3-10 Unit Conversion Table

Table 6.3-9

Unit Conversion Table

1 in	=	0.0254 m	1 m	=	39.3701 in
1 ft	=	0.3048 m	1 m	=	3.2808 ft
1 lb	=	0.4536 kg	1 kg	=	2.2046 lb
1 lbf	=	4.4485 N	1 N	=	0.2248 lbf
1 psi	=	6,895.12 Pa	1 Pa	=	1.45E-04 psi
1 k-ft	=	1.3559 kN-m	1 kN-m	=	0.7375 k-ft
1 ksi	=	6,895.12 kPa	1 kPa	=	1.45E-04 ksi
1 ksi	=	6.8951 mPa	1 mPa	=	0.1450 ksi
1 ksf	=	47.8828 kPa	1 kPa	=	0.0209 ksf
1 k-s ² /ft	=	14.5947 kN-s ² /m	1 kN-s ² /m	=	0.0685 k-s ² /ft
1 kcf	=	157.0957 kN/m ³	1 kN/m ³	=	0.0064 kcf

6.4 Seven Oaks Inclined Intake Tower

6.4-1 Background

This section provides an example time-history analysis for intake towers requiring three-dimensional finite-element evaluation. The example tower is the Seven Oaks Dam Intake Tower located in Santa Ana River Basin, San Bernardino County, California. The main feature of the tower is that it is inclined against the abutment and partially embedded into the foundation rock. The 68.6-m (225-foot) high tower was anchored to the inclined rock slope and designed to withstand the earthquake forces generated by a maximum probable earthquake (OBE) and the maximum credible earthquake (MCE) events. The structure is located 1.92 km (1.2 miles) from a branch of San Andreas Fault, capable of producing a magnitude M8+ earthquake. This tower was chosen for this analysis because of its unique 3D features and that a 3D model of the tower was available from previous analyses by Waterways Experiment Station. The structural response of the tower is primarily rotation about its most vertical centroidal axis (torsion), and resulting forces are transferred to the rock abutment by tension in steel rods anchored in the rock and extending into the tower. Because of the torsional response and the fact that the tower has no plane of symmetry, 3-D analyses were required. The accelerations used in the following five analyses are not the design accelerations for the tower, but results from a previous analysis using the Seven Oaks design acceleration records are also presented for reference.

6.4-2 Purpose and Scope

a. The main purpose of this example is illustration of the time-history analysis in evaluation of the global behavior of an inclined intake tower and its abutment anchorage system to seismic loading. Additional objectives include demonstration of the dominant torsional response, the importance of higher modes of vibration, and the effects of multiple ground motions that are essential in dynamic response analysis of inclined towers but may not be necessary for free-standing towers. The example, however, does not consider the local behavior and section capacities needed for the reinforcing steel design.

b. The time-history analysis is applied to earthquake response computation of the Seven Oaks Intake Tower. The analyses are carried out for five sets of acceleration time histories to investigate sensitivity of the dynamic response to characteristics of the earthquake ground motion. Design earthquakes and the selected acceleration time-histories are described; the structural modeling details, including three-dimensional finite-element representation of the tower, surrounding water, and the foundation-abutment are presented; the dynamic characteristics of the tower dominated by torsion and contribution from higher modes are determined; the tower responses to five sets of three-component earthquake acceleration time-histories are computed; and results in the form of stress contours, section force and moment demands, and anchor force demands are presented and discussed. The results for the five acceleration time-histories selected in this example are compared with the results from the design analyses.

6.4-3 Description of Intake tower

a. The U.S. Army Engineer District, Los Angeles, designed the intake structure for the Seven Oaks Dam, shown in Figure 6.4-1. The structure is a reinforced concrete intake tower inclined against and anchored to the rock abutment, as shown in Figure 6.4-2. The tower is partially embedded in the rock formation at the bottom. The maximum vertical height of the structure is 68.7m (225.5 ft), extending from elevation (El.) 2,080 ft at the foundation to El. 2305.5 ft at the top of the parapet. The high-level intake height is 50.3 m (165 ft) based on an expected sediment deposition over the project life from El. 2,100 ft to El. 2,265 ft. Structure configuration, starting from the foundation, includes a 6.1-meter-thick (20-foot-thick) concrete footing embedded into rock, a 50.3-meter-high (165-foot-high) semicircular structure with an 11-meter-diameter (36-foot-diameter) wet well inclined at a 4V on 1H slope against the abutment, and an 11.3-meter-high (37-foot-high) vertical circular high-

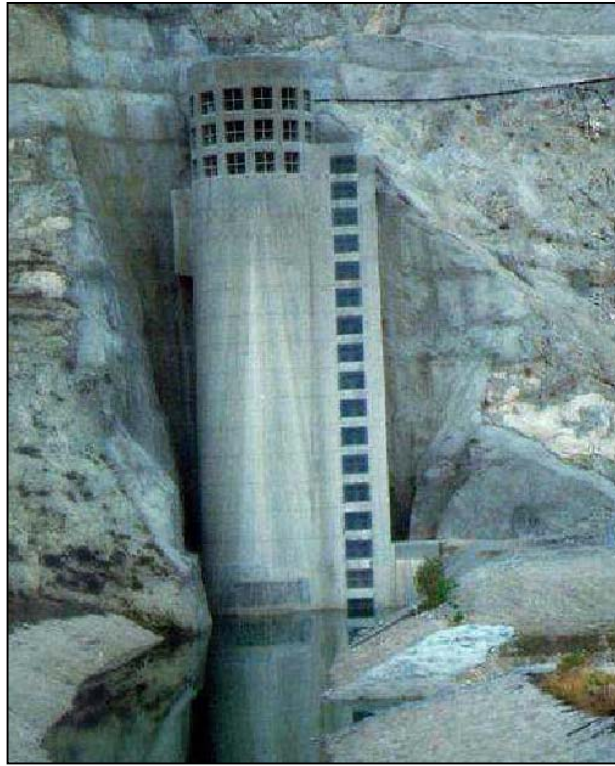


Figure 6.4-1 Seven Oaks Dam Intake Tower (Courtesy of Rayw Dewey, Portland District)

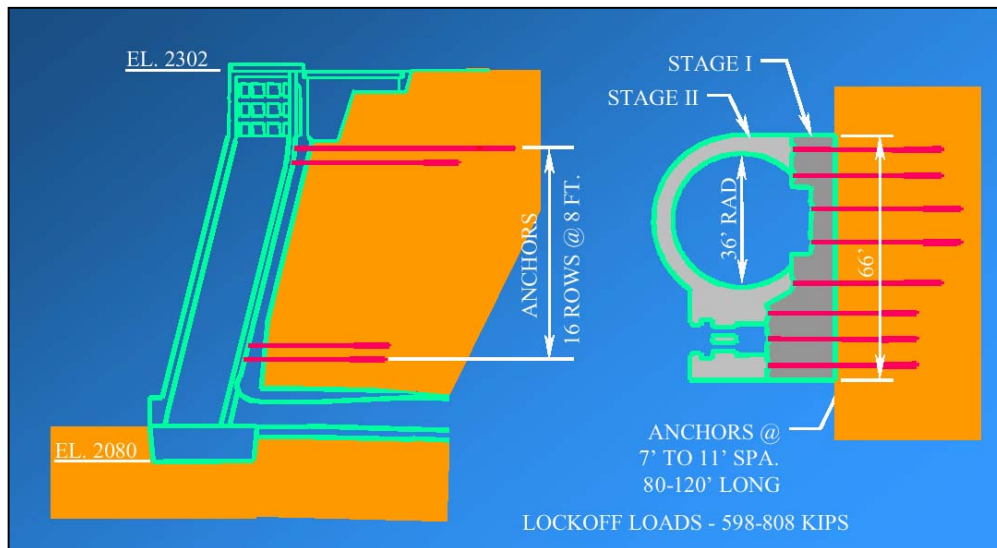


Figure 6.4-2 Seven Oaks Intake Tower Anchorage System (Courtesy of Ray Dewey, Portland District)

level intake covered with a maintenance deck. A trash structure surrounds the high-level intake and a 15.2-meter-long (50-foot-long) bridge connects the maintenance deck to an access road from the embankment dam.

b. A total of 128 anchors were used to fasten tower to the abutment. They were arranged in 16 rows of 8 post-tensioned anchors, as shown in Figure 6.4-2. Each post-tensioned anchor included seven low relaxation 0.6-in diameter tendons rated at 1,862 MPa (270 ksi). The intake structure was constructed in two stages. First the back-face concrete was placed against the sloping rock face followed by installation and pre-stressing of the anchors. Then the front-face concrete was placed to complete the construction.

6.4-4 Earthquake Ground Motions

Seven Oaks Intake Tower was designed for the Maximum Credible Earthquake (MCE) and Operational Earthquake (OBE). The MCE was a magnitude M8+ earthquake on a branch of San Andreas Fault located 1.92 km (1. miles) from the site. The peak ground acceleration for the MCE was estimated at 0.7g. The seismic performance for the MCE included inelastic response with cracking and yielding, but maintaining the ability to lower the pool in controlled manner. The OBE was chosen as the maximum probable earthquake (MPE) with 1% chance of occurrence per year (63% in 100 years). The MPE was postulated as an M7.5 to 8 earthquake on a fault located 19 km (12 miles) from the site, capable of producing a peak ground acceleration of 0.5g. The seismic performance for the OBE included a nearly elastic response, where the tower remains fully operational with minor damage not requiring extensive repair. The OBE performance requirements turned out to be more stringent and thus the OBE controlled the design.

a. No attempt was made to use the design ground motions described above in this example. Instead a generic target response spectrum representative of the southern California seismic environment was developed and used to select five sets of acceleration time histories for this example. Two methods were used to develop acceleration records for the analyses:

- Four of the records were scaled from existing earthquake records to a best fit of the target response spectrum.
- One set of spectrum-compatible was developed to closely match the target spectra.

Table 6.4-1 lists all five earthquake records and corresponding scaling factors. All acceleration records with the exception of SMPAC include two horizontal and one vertical component. Vertical component of SMPAC was not computed and is not included in this example. The smooth target spectrum and the spectra for the scaled motions in the primary (x) direction are compared in Figure 6.4-3. The scale factor for both horizontal components of direction in each of the four scaled record sets was based on a fit of x acceleration data to the target spectrum shown in Figure 6.4-3. Spectrum fits for the y-direction for the four-scaled sets are shown in Figure 6.4-4. Acceleration time-histories for the five records are shown in [Figures 6.4-5 to 6.4-9](#). While maximum accelerations are similar in the x-direction for all records and have been scaled to 0.5g, significant differences exist in the y-direction due to the use of the x-direction scaling factor for both horizontal records.

b. The “design” accelerations used in the original analysis of the tower are shown in [Figure 6.4-10](#) for comparison and reference only. They are in no way related to the target spectra of [Figures 6.4-3](#) and [6.4-4](#). The design acceleration time histories included records in the x-, y-, and z-directions. These accelerations and results from this analysis are included only for reference.

Table 6.4-1 Earthquake Records for Example Analyses			
Record Name	Component deg	Scale Factor	Analysis Designation
1966 Parkfield Earthquake, Cholame #8 (CHO)	320 50 up	1.7962	CHO
1989 Loma Prieta Earthquake, Gavilan College (GGC)	337 67 up	1.3596	GGC
1987 Whittier Narrows Earthquake, Garvey Reservoir (GRV)	330 60 up	0.8987	GRV
1971 San Fernando Earthquake, Pacoima Dam (PAC)	254 164 up	0.4915	PAC
Spectrum-matched Pacoima Dam (SMPAC)	Both	None	SMPACX

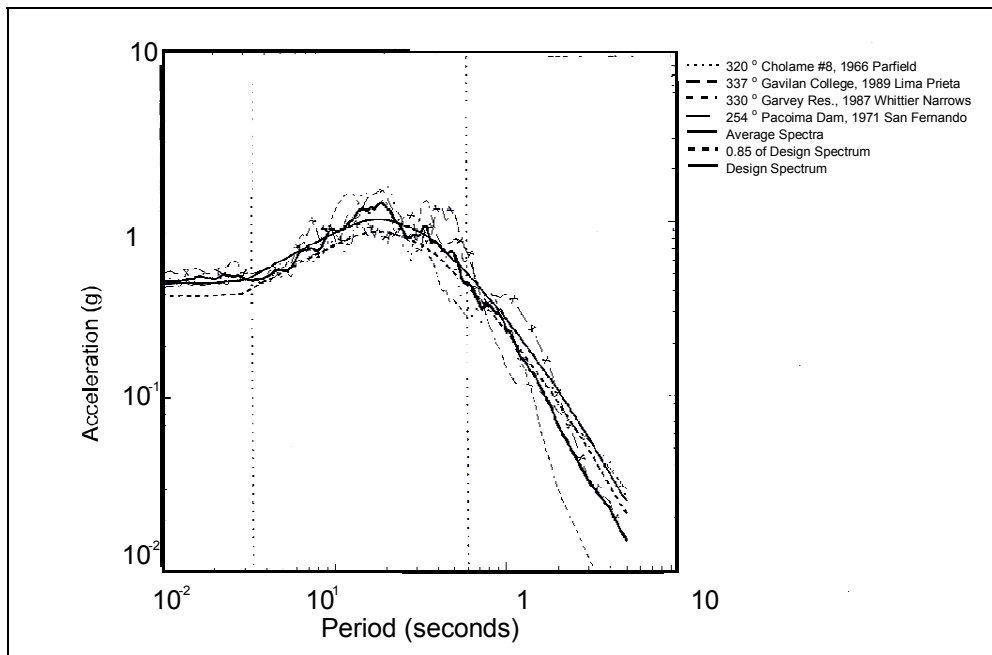


Figure 6.4-3. Target and scaled spectra, x-direction

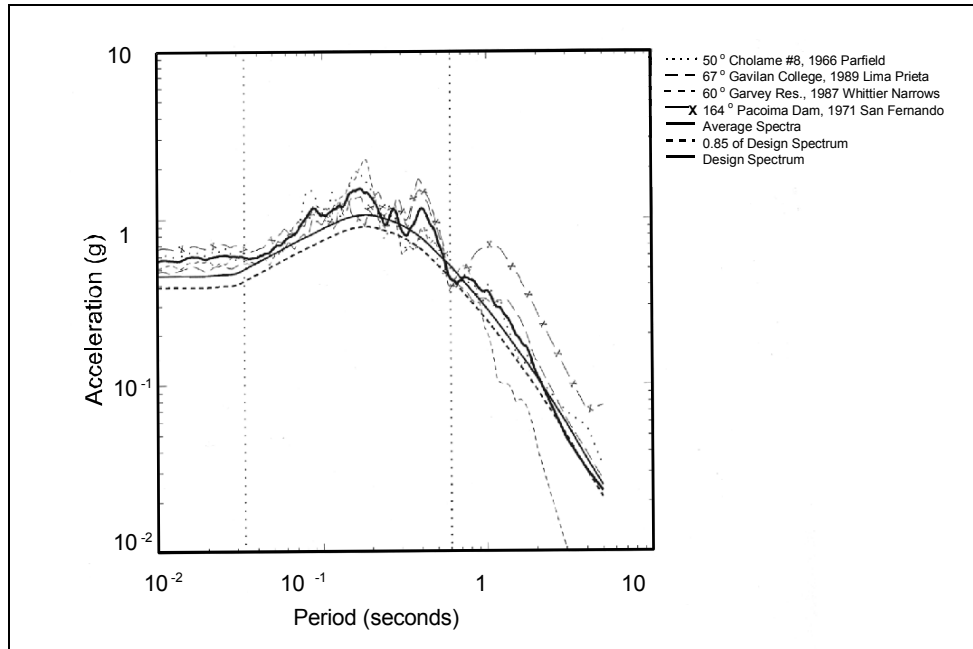


Figure 6.4-4. Target and scaled spectra, y-direction

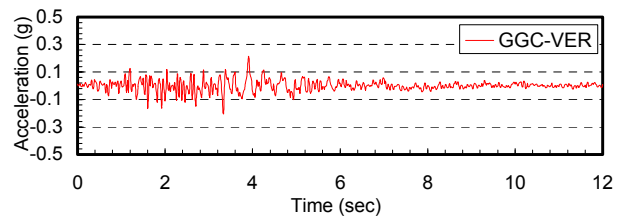
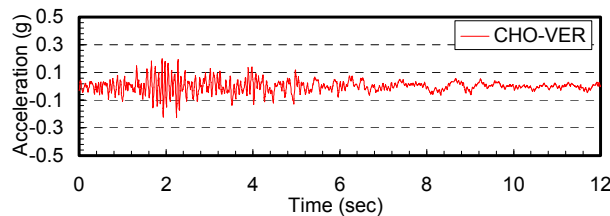
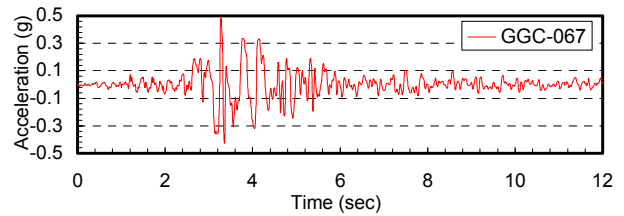
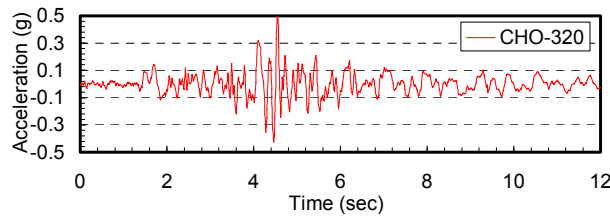
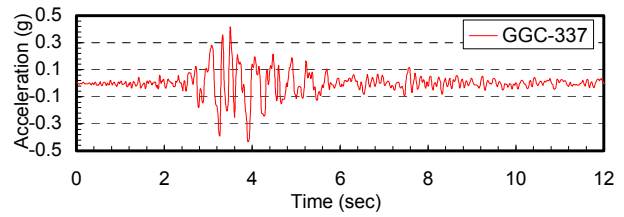
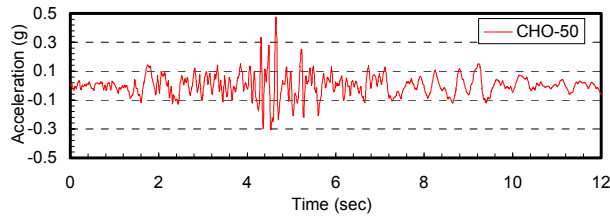


Figure 6.4-5. 1966 Parkfield earthquake,
Cholame #8 (CHO)

Figure 6.4-6. 1989 Loma Prieta earthquake,
Gavilan College (GGC)

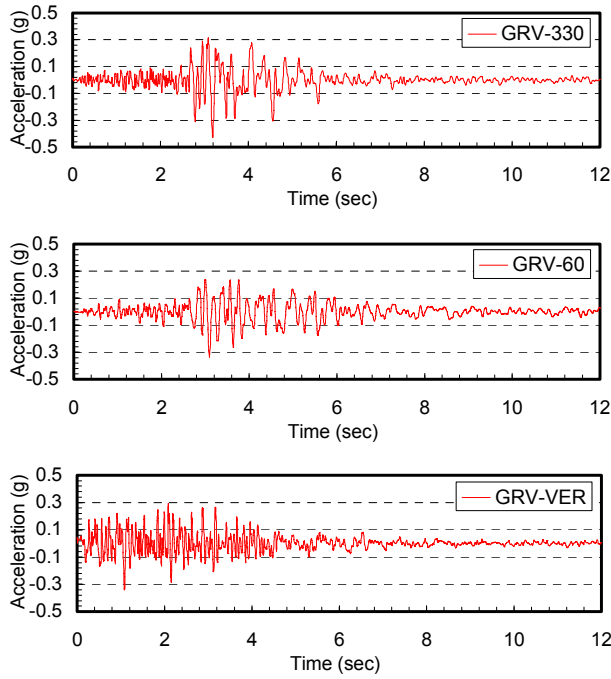


Figure 6.4-7. 1987 Whittier Narrows earthquake, Garvey Reservoir (GRV)

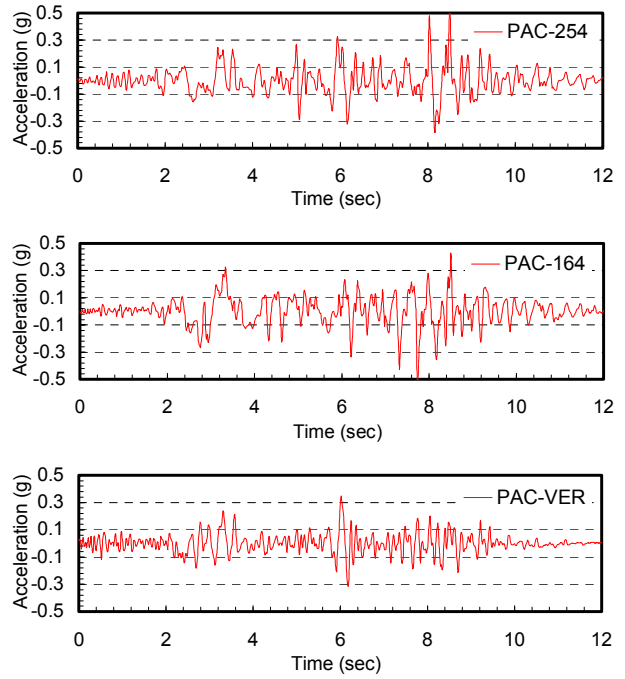


Figure 6.4-8. 1971 San Fernando earthquake, Pacoima Dam (PAC)

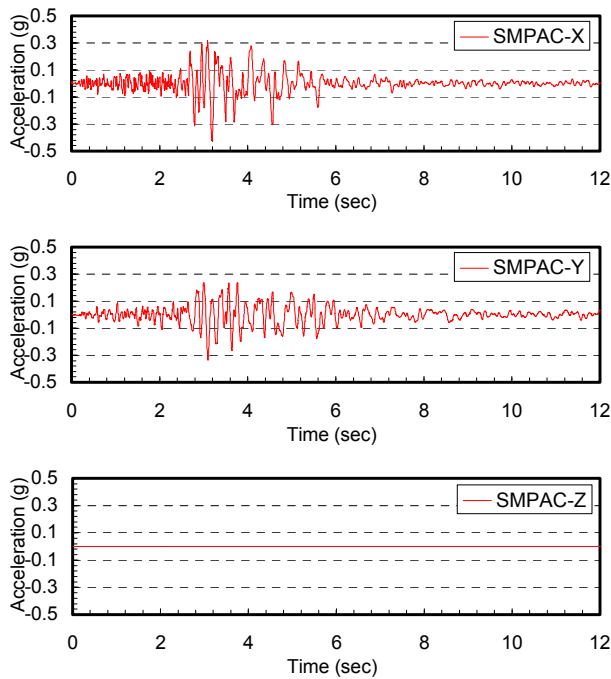


Figure 6.4-9. Spectrum matched PAC (SMPAC)

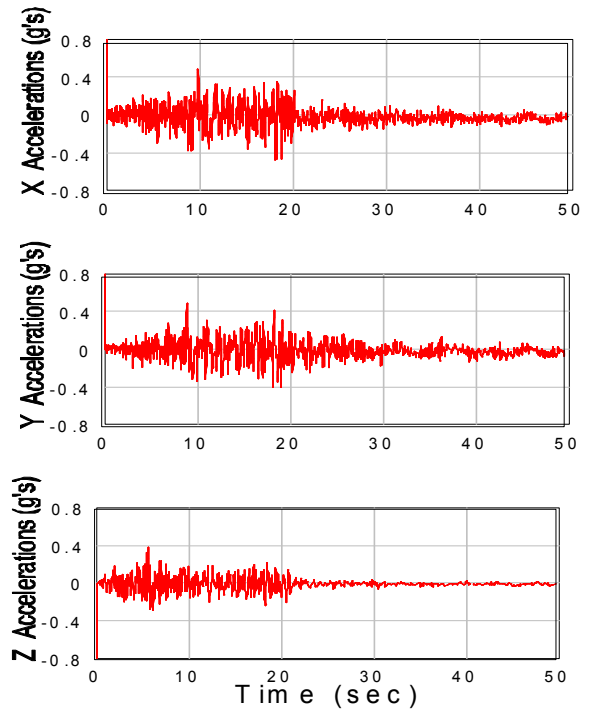


Figure 6.4-10. Seven Oaks design accelerations

6.4-5 Structural Model

The three-dimensional geometry of the tower, severe seismic demand, and the substantial hydrodynamic forces acting on the tower requires a 3D finite-element (FE) model which includes the tower- water and the tower-foundation-abutment interaction effects.

a. The concrete intake tower (see Figure 6.4-11 and Figure 6.4-13) was modeled using 2,084 eight-node solid elements and 169 beam elements. Solid elements were used in the body of the tower and beam elements were used to model the trash-rack. Moments in the trash-rack were transmitted to the solid elements by extending beams into the solid elements. The eight-node solids are linear isoparametric elements using linear geometry and displacement interpolation functions.

b. The foundation rock was modeled using 2,642 eight-node solid elements. The minimum width of the foundation model was three times the base width of the tower. Foundation rock was included in the model from the rock/concrete interface to a distance approximately equal to the height of the tower, and from the base of the tower downward to a distance of approximately half of the height of the tower. All outer nodes of the foundation model (i.e. nodes at the bottom, sides and back of the model) were fixed in space. Accelerations in the global x, y, and z directions were applied to the outer rock boundaries (see Figure 6.4-12). Foundation elements were assigned zero mass to eliminate erroneous wave reflections at the fixed boundaries due to finite size of the foundation model.

c. The tower-rock interface consisted of 240 nodes shared by the abutting concrete and rock elements. Normal and tangential forces at these nodes were used to check the adequacy of steel anchors between the tower and the abutment rock.

d. The inertia forces of the impounded water were represented by the equivalent hydrodynamic added-mass lumped to the submerged exterior and interior nodes of the tower. The added-mass coefficients of the surrounding water were those computed for design of the tower using boundary element method described in Section 2-20.c. The added-mass coefficients for the water inside the wet well were approximately obtained from the weight of water.

e. Static loads consisted of the gravity due to self-weight and hydrostatic pressures of the inside and outside water. Note that due to unsymmetrical cross-section of the tower, hydrostatic pressures generally do not cancel out and should be considered in the analysis. The water loads were applied as hydrostatically varying pressures on surfaces of the submerged elements.

f. Earthquake loads were applied as ground acceleration time-histories in x, y, and z directions along the outer foundation boundaries. Structural damping was assumed to be 5% of critical.

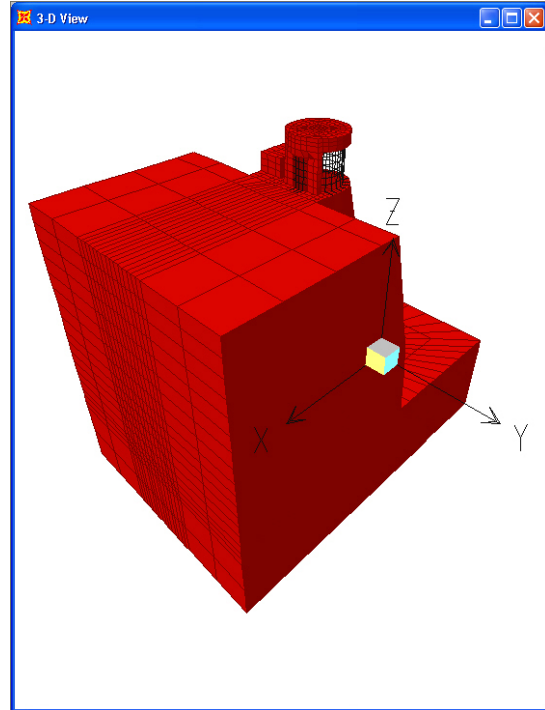
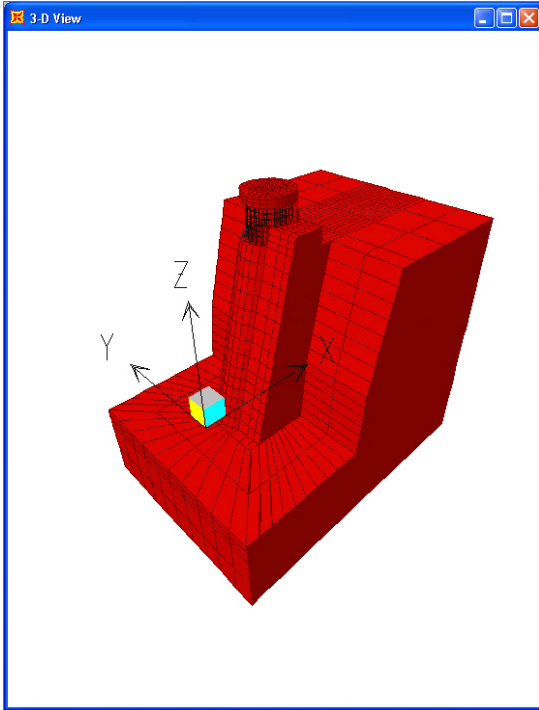


Figure 6.4-11. 3-D views of tower-foundation-abutment finite-element model

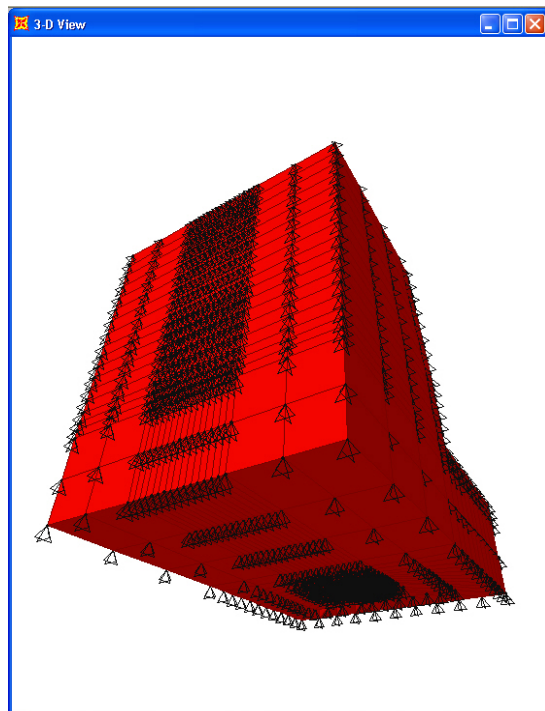
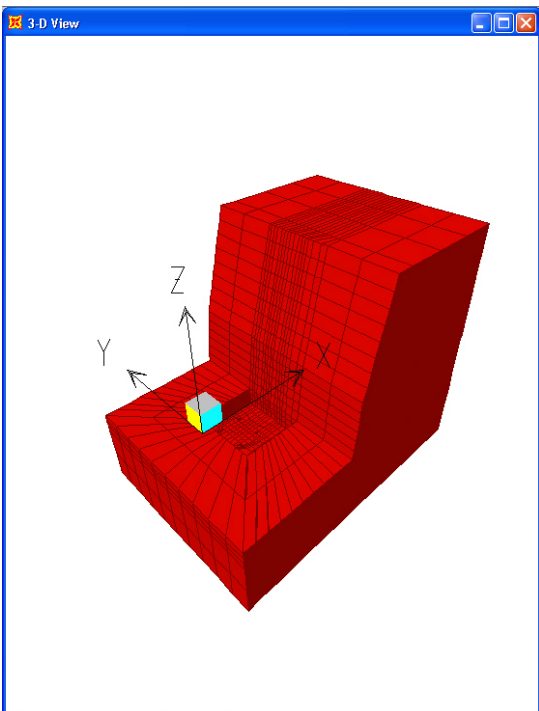


Figure 6.4-12. 3-D views of foundation-abutment finite-element model

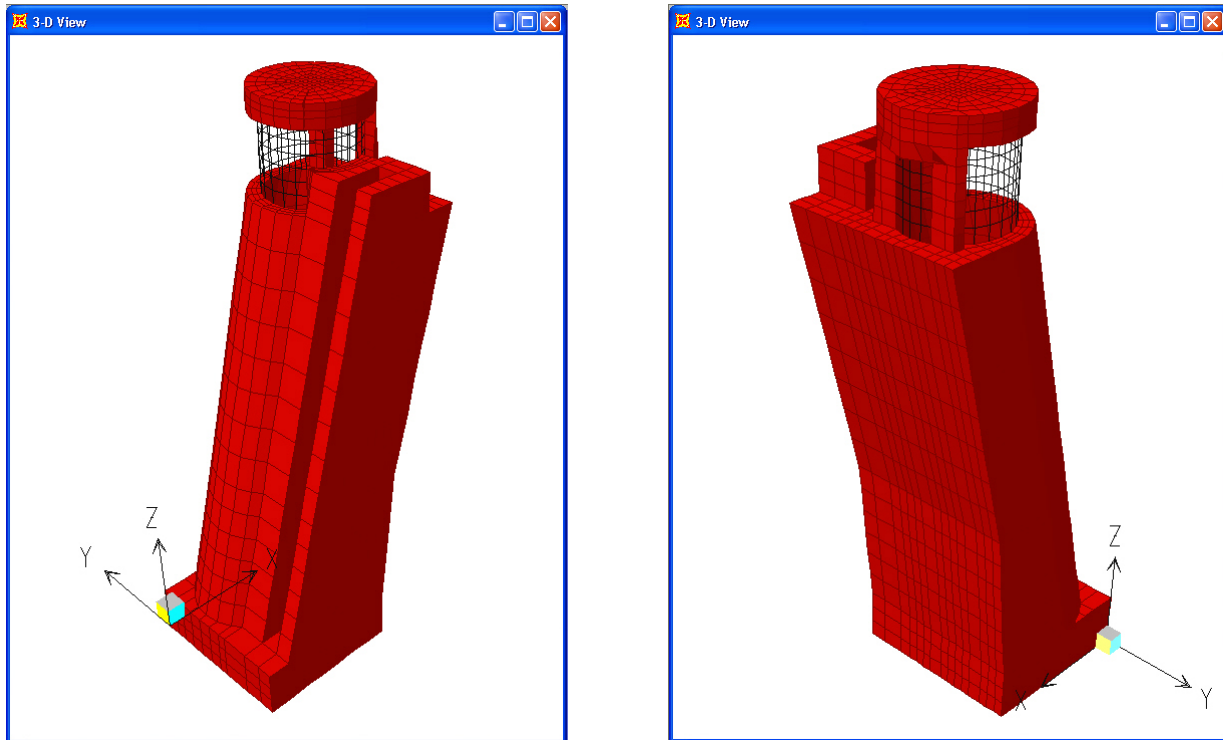


Figure 6.4-13. 3-D views of tower finite-element model

6.4-6 Computation of Earthquake Response

a. Dynamic characteristics of tower. The natural periods and mode shapes of the tower were obtained using the finite-element model described above. The Ritz-Vector feature of SAP2000 was employed to obtain 100 mode shapes and periods for the full reservoir. The resulting vibration periods and the associated modal participation factors are given in Table 6.4-2. The results show that 100 percent modal participation was achieved in all three orthogonal x, y, and z directions. Figures 6.4-14 and 6.4-15 show deflected shapes for the 8 lowest modes of vibration. Modes 1 and 2 involve bending of the high-level intake in directions perpendicular (x-direction) and parallel to the abutment (y-direction), respectively. Modes 3 to 8 and higher (not shown) indicate dominant torsion response. That the vibration response involves torsion is a result of the restraint along the height of the tower. The results show that an important characteristic of the dynamic response of the Seven Oaks Tower is that 65 modes were necessary to achieve a 90% mass participation in all three global directions (see Table 6.4-2), as opposed to dynamic characteristics of freestanding towers that is dominated by the two lowest modes of vibration.

b. Earthquake response of tower. Earthquake response of Seven Oaks intake tower was computed for the five ground motions discussed in 6.4.4. A 5 percent modal damping ratio was used. The tower response for structural evaluation included maximum and minimum stresses within the tower and at the tower-abutment interface for identification of overstressed regions, section forces and moments along the height for comparison with section capacities, and anchor forces to assess adequacy of the anchorage system. Each of these response quantities are discussed below.

c. Stress contours. Maximum and minimum stress values are presented in the form of contour plots for determining locations and magnitudes of high stresses. These plots generally provide a cursory assessment of overstressed regions, their damage potential, and effects on stability of the tower. Better estimate of damage

requires careful study of other parameters discussed in Chapter 4. In this example only normal stresses at the tower-abutment interface and vertical stresses within the tower are presented. However, shear stresses should always be examined to assure that shear failure would not occur.

(1) Tower-abutment interface stresses. Figure 6.4-15 shows node numbers at the tower-abutment interface used to compute anchor forces. Figure 6.4-16 through Figure 6.4-20 display contour plots of maximum and minimum normal stresses at the tower-abutment interface for the five seismic input employed in this example. Results show that peak maximum (tension) and minimum (compression) stresses occur at the edges of the back face and then dropping toward the centerline of the semicircular wet well. This type of stress distribution clearly indicates a torsion response behavior. The peak tensile stress reaches 2 MPa (300 psi) and peak compressive stress -1.4 MPa (-200 psi) at about mid-height of the back face.

(2) Stresses within the tower. Figures 6.4-21 through 6.4-28 show maximum and minimum vertical stresses within the tower for the Pacoima Dam (PAC) record of the 1971 San Fernando earthquake. Stress contours are presented for the back face (downstream), right face, front face (upstream), and the left face of the tower and high-level intake. Localized high vertical stresses develop at the edges of the back face of the tower and near the bottom of the high-level intake main supports (Figures 6.4-21 and 6.4-22). The high vertical stresses for the wet well occur at the bottom and 1/3 height of the right and front faces of the tower (Figure 6.4-24 and 6.4-26). For the multi-level intake structure, high vertical stresses are confined to the base of the structure (Figure 6.4-26 and 6.4-28). However, for the tower peak stresses are well below tensile and compressive strengths of concrete. Peak tensile stresses as high as 7 MPa (1,000 psi) develop at the base of the high-level intake supports, but reinforcing steels built into the design of tower can easily resist them.

c. *Tower section forces and moments.* For design and evaluation of the tower, section forces and moments should be computed and examined along the height of the tower. Section forces may be computed from stresses of the elements forming the section using a spreadsheet program. Alternatively, the section forces and moments can be computed directly by the structural analysis program should the program have such capability. In this example SAP2000 capability to compute group joint forces was used to determine section forces and moments. Figure 6.4-29 through 6.4-34 show the maximum and minimum section forces and moments along the height of the tower for each of the ground motions. The computed section forces and moments are usually compared with the ultimate section capacities to estimate reinforcing steels for new designs or assess adequacy of existing structures. The results in Figures 6.4-29 to 6.4-31 show that horizontal shear forces (F_x and F_y) for various input ground motions vary much less than the normal section forces (F_z). This is because horizontal section forces arise mainly from the horizontal components of ground motions that were scaled to remain at the approximate level of the horizontal smooth response spectra. The resulting scale was then applied to the corresponding vertical components of the ground motions without any further adjustment. Consequently variations of vertical components of ground motions are by far greater than those of the horizontal components. Such greater variation in vertical ground motion is expected to affect the axial or normal section forces, as illustrated in Figure 6.4-31. This figure also shows that the embedded portion of the tower remains in compression and that magnitudes of maximum compressions along the height of the tower are greater than magnitudes of maximum tensions. The peak section shear forces occur near the bottom of the tower and they are twice larger in the direction normal to the abutment (x-dir.) than they are in the direction parallel to the abutment (y-dir.). Figures 6.4-32 to 6.4-34 show peak section moments also occur near the bottom and that torsion response produces the largest moment or torque (M_z). The positive bending moments with respect to x-axis (M_x) are substantially greater than positive bending moments with respect to y-axis (M_y). This indicates that the tower primarily bends toward the multi-level intake than into the abutment.

d. *Anchor Forces.* To avoid separation and pounding between the tower and abutment during earthquake ground shaking, the tower was securely attached to the abutment rock. The attachment was accomplished by 128 post-tensioned steel anchors, each penetrating into the rock a length required to mobilize a rock mass

equal to the dynamic tensile design force of the anchor (Figure 6.4-2). The anchor design forces were estimated as summation of the direct tensile force demands and the normal forces required resisting shear force demands computed for the tower-abutment interface nodal points. To assess adequacy of existing steel anchors, the earthquake force demands at the tower-abutment interface nodal points should be computed and compared with the anchor capacities. This evaluation is conducted in two steps. First envelopes of maximum interface forces are obtained and compared with the total strength capacity of all steel anchors. Second time-history force demands are compared with the individual capacity of the anchors.

(1) Envelope Forces. Envelopes of maximum and minimum normal and shear forces at the tower-abutment interface are computed from the interface normal and shear stresses. In this example SAP2000 capability of group joint forces was used to compute these forces for the entire tower-abutment interface. Figure 6.4-35 to 6.4-37 show computed group forces per unit tributary length. In Figure 6.4-35 interface normal forces are compared with the normalized anchor capacities along the height of the tower. The comparison shows that tensile normal force demands are well the capacity of the anchors.

(2) Time-history of anchor forces.

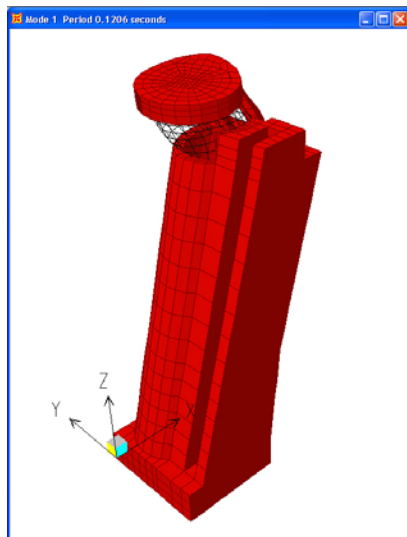
(3) Figure 6.4-38 displays maximum normal force time-histories for all five input ground motions at the location of Node 1733 (see Figure 6.4-15). These forces are to be resisted by the anchors and can be compared with capacity of the anchor closest to this location. The design force for the anchor closest to Node 1733 is 4,825 kN (1,085 kips), which well above the maximum normal force of 2,000 kN (450 kips) at this location. Time histories of normal forces for all interface nodal points were also computed and are compared with the total capacity of all 128 anchors in Figure 6.4-39. This figure shows that total interface normal force demand remains adequately below the anchor design load of 497,044 kN (111,740 kips), except for a momentary instance of less than one-hundredth of a second for the Pacoima Dam record (PAC). Note that this negligible exceedance of extremely short duration has no structural significance.

Table 6.4-2
Vibration periods and modal participation factors

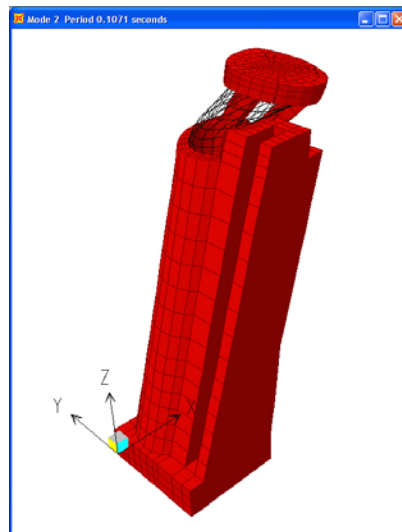
Mode	Period (sec)	Individual Mode			Cumulative		
		UX	UY	UZ	UX	UY	UZ
1	0.1206	0.55	0.18	0.01	0.55	0.18	0.01
2	0.1070	0.00	1.91	0.00	0.55	2.10	0.02
3	0.0985	1.31	3.08	0.00	1.86	5.17	0.02
4	0.0799	12.32	0.84	0.01	14.18	6.02	0.03
5	0.0745	11.33	0.39	0.28	25.52	6.40	0.30
6	0.0663	0.08	0.22	0.24	25.60	6.63	0.55
7	0.0644	0.58	0.05	0.81	26.18	6.68	1.36
8	0.0617	2.58	0.25	5.11	28.76	6.92	6.47
9	0.0558	1.44	0.24	20.01	30.20	7.17	26.48
10	0.0550	16.77	0.85	10.18	46.97	8.02	36.66
11	0.0519	0.06	0.16	4.60	47.02	8.18	41.26
12	0.0499	2.82	0.25	4.49	49.84	8.43	45.75
13	0.0496	1.44	0.76	0.03	51.28	9.18	45.78
14	0.0468	1.58	0.04	8.53	52.86	9.22	54.30
15	0.0446	0.00	0.01	0.23	52.86	9.23	54.54
16	0.0435	0.09	0.78	1.74	52.95	10.01	56.28
17	0.0428	0.17	4.35	0.56	53.12	14.35	56.83
18	0.0423	0.15	18.50	1.49	53.27	32.85	58.33
19	0.0408	0.07	1.77	0.03	53.34	34.62	58.36
20	0.0396	0.02	8.44	1.48	53.35	43.07	59.84
21	0.0392	1.46	0.11	0.00	54.82	43.18	59.84
22	0.0379	0.02	0.23	0.07	54.84	43.41	59.91
23	0.0377	2.65	0.47	3.07	57.49	43.87	62.98
24	0.0368	2.89	5.10	0.34	60.38	48.97	63.32
25	0.0367	0.32	0.01	0.38	60.69	48.98	63.70
26	0.0358	0.11	0.00	0.14	60.80	48.98	63.84
27	0.0352	0.15	4.89	0.05	60.95	53.88	63.89
28	0.0348	4.96	2.89	0.13	65.91	56.77	64.02
29	0.0343	2.57	0.47	0.51	68.48	57.23	64.53
30	0.0340	0.03	2.04	0.54	68.51	59.27	65.06
31	0.0336	0.25	1.97	0.40	68.76	61.24	65.46
32	0.0330	4.75	5.11	0.34	73.51	66.36	65.80
33	0.0321	0.99	0.26	0.54	74.50	66.62	66.34
34	0.0318	0.05	0.29	0.02	74.55	66.91	66.36
35	0.0315	1.30	1.60	0.11	75.85	68.51	66.46
36	0.0313	0.21	0.20	2.69	76.06	68.71	69.15
37	0.0310	1.95	1.35	0.59	78.01	70.06	69.75
38	0.0306	0.48	3.80	4.56	78.49	73.86	74.30
39	0.0304	2.32	0.04	1.88	80.81	73.90	76.19
40	0.0302	0.06	0.01	0.21	80.87	73.91	76.40
41	0.0302	0.07	2.42	0.56	80.93	76.34	76.96
42	0.0295	0.31	3.56	0.81	81.25	79.90	77.77
43	0.0293	0.60	0.61	0.53	81.85	80.51	78.30
44	0.0288	0.05	0.16	0.19	81.90	80.67	78.49
45	0.0284	0.37	0.58	0.35	82.27	81.25	78.83
46	0.0282	0.15	0.13	0.00	82.42	81.38	78.84
47	0.0279	0.01	0.02	0.10	82.43	81.40	78.94
48	0.0277	0.00	0.62	0.00	82.43	82.02	78.94
49	0.0272	0.10	0.79	0.02	82.53	82.80	78.96
50	0.0268	0.00	0.47	1.04	82.53	83.27	80.00

Table 6.4-2 Continued
Vibration periods and modal participation factors

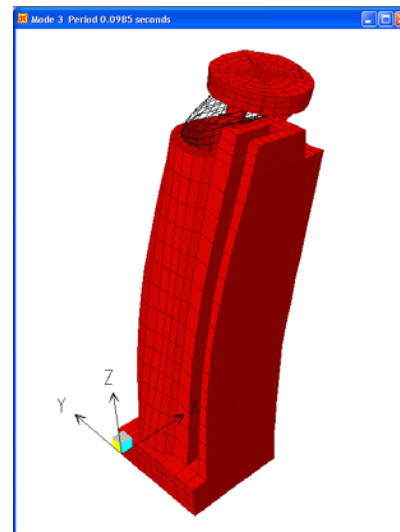
Mode	Period (sec)	Individual Mode			Cumulative		
		UX	UY	UZ	UX	UY	UZ
51	0.0266	0.00	1.02	0.85	82.54	84.28	80.84
52	0.0262	0.33	0.49	0.30	82.87	84.77	81.14
53	0.0260	0.95	0.07	0.70	83.82	84.84	81.84
54	0.0256	0.15	1.14	0.62	83.98	85.97	82.46
55	0.0254	1.76	0.37	0.45	85.74	86.35	82.90
56	0.0247	0.96	0.70	0.46	86.70	87.05	83.36
57	0.0242	0.04	0.43	0.73	86.73	87.49	84.08
58	0.0240	1.61	0.14	0.17	88.35	87.63	84.25
59	0.0236	0.01	1.37	0.05	88.36	89.00	84.31
60	0.0235	0.09	0.05	4.33	88.45	89.05	88.64
61	0.0230	2.02	0.04	0.15	90.47	89.09	88.79
62	0.0222	0.25	0.23	3.01	90.73	89.32	91.79
63	0.0219	0.70	0.19	0.84	91.42	89.51	92.64
64	0.0218	0.73	0.31	0.34	92.16	89.82	92.98
65	0.0212	0.11	0.33	0.85	92.27	90.15	93.83
66	0.0208	0.13	0.46	0.49	92.40	90.61	94.32
67	0.0204	2.74	0.05	0.00	95.14	90.66	94.32
68	0.0195	0.57	0.39	0.50	95.71	91.05	94.82
69	0.0193	1.50	0.00	0.46	97.20	91.06	95.28
70	0.0191	0.23	0.81	0.33	97.44	91.86	95.61
71	0.0183	0.04	0.54	0.54	97.48	92.41	96.15
72	0.0180	0.06	0.64	0.27	97.54	93.04	96.42
73	0.0178	0.86	0.17	0.01	98.40	93.21	96.43
74	0.0167	0.10	0.40	0.14	98.50	93.60	96.57
75	0.0164	0.28	0.02	0.21	98.78	93.63	96.77
76	0.0163	0.18	0.43	0.06	98.95	94.06	96.83
77	0.0149	0.22	0.79	0.02	99.17	94.85	96.85
78	0.0148	0.11	0.62	0.47	99.28	95.47	97.32
79	0.0146	0.03	1.65	0.39	99.31	97.12	97.72
80	0.0140	0.01	2.50	0.05	99.32	99.62	97.77
81	0.0135	0.10	0.04	0.94	99.42	99.66	98.71
82	0.0134	0.36	0.06	0.03	99.78	99.72	98.74
83	0.0126	0.01	0.18	0.11	99.79	99.90	98.86
84	0.0121	0.01	0.00	0.85	99.80	99.90	99.71
85	0.0119	0.09	0.01	0.08	99.89	99.91	99.79
86	0.0107	0.00	0.00	0.14	99.89	99.91	99.93
87	0.0104	0.05	0.01	0.01	99.94	99.92	99.94
88	0.0103	0.03	0.02	0.00	99.97	99.94	99.94
89	0.0090	0.00	0.00	0.04	99.97	99.94	99.98
90	0.0087	0.02	0.01	0.00	99.99	99.95	99.98
91	0.0085	0.00	0.04	0.00	99.99	99.98	99.98
92	0.0072	0.00	0.00	0.01	99.99	99.99	99.99
93	0.0070	0.00	0.01	0.00	99.99	100.00	99.99
94	0.0067	0.01	0.00	0.00	100.00	100.00	99.99
95	0.0053	0.00	0.00	0.00	100.00	100.00	100.00
96	0.0051	0.00	0.00	0.00	100.00	100.00	100.00
97	0.0048	0.00	0.00	0.00	100.00	100.00	100.00
98	0.0040	0.00	0.00	0.00	100.00	100.00	100.00
99	0.0037	0.00	0.00	0.00	100.00	100.00	100.00
100	0.0036	0.00	0.00	0.00	100.00	100.00	100.00



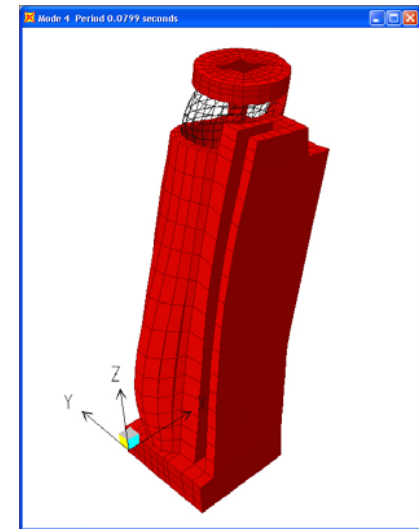
Mode 1. T = 0.1206 sec.



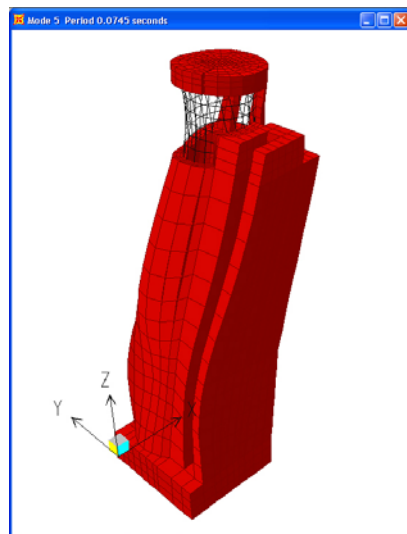
Mode 2. T = 0.1071 sec.



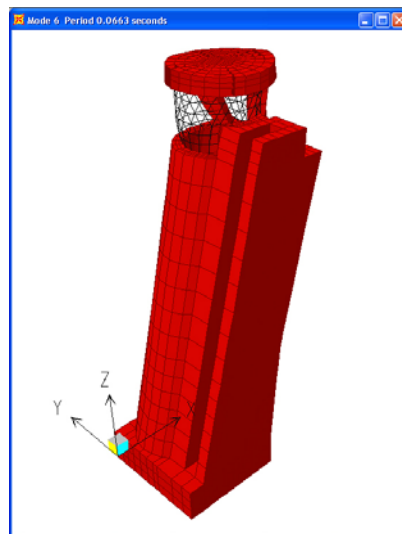
Mode 3. T = 0.0985 sec.



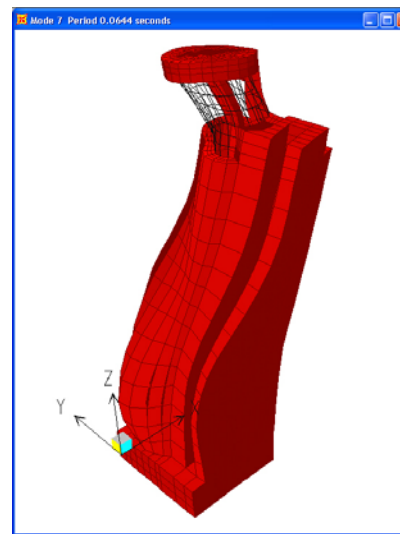
Mode 4. T = 0.0799 sec.



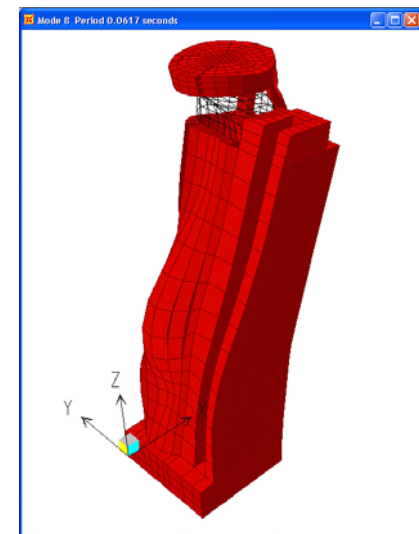
Mode 5. T = 0.0745 sec.



Mode 6. T = 0.0663 sec.



Mode 7. T = 0.0644 sec.



Mode 8. T = 0.0617 sec.

Figure 6.4-14 Vibration mode shapes

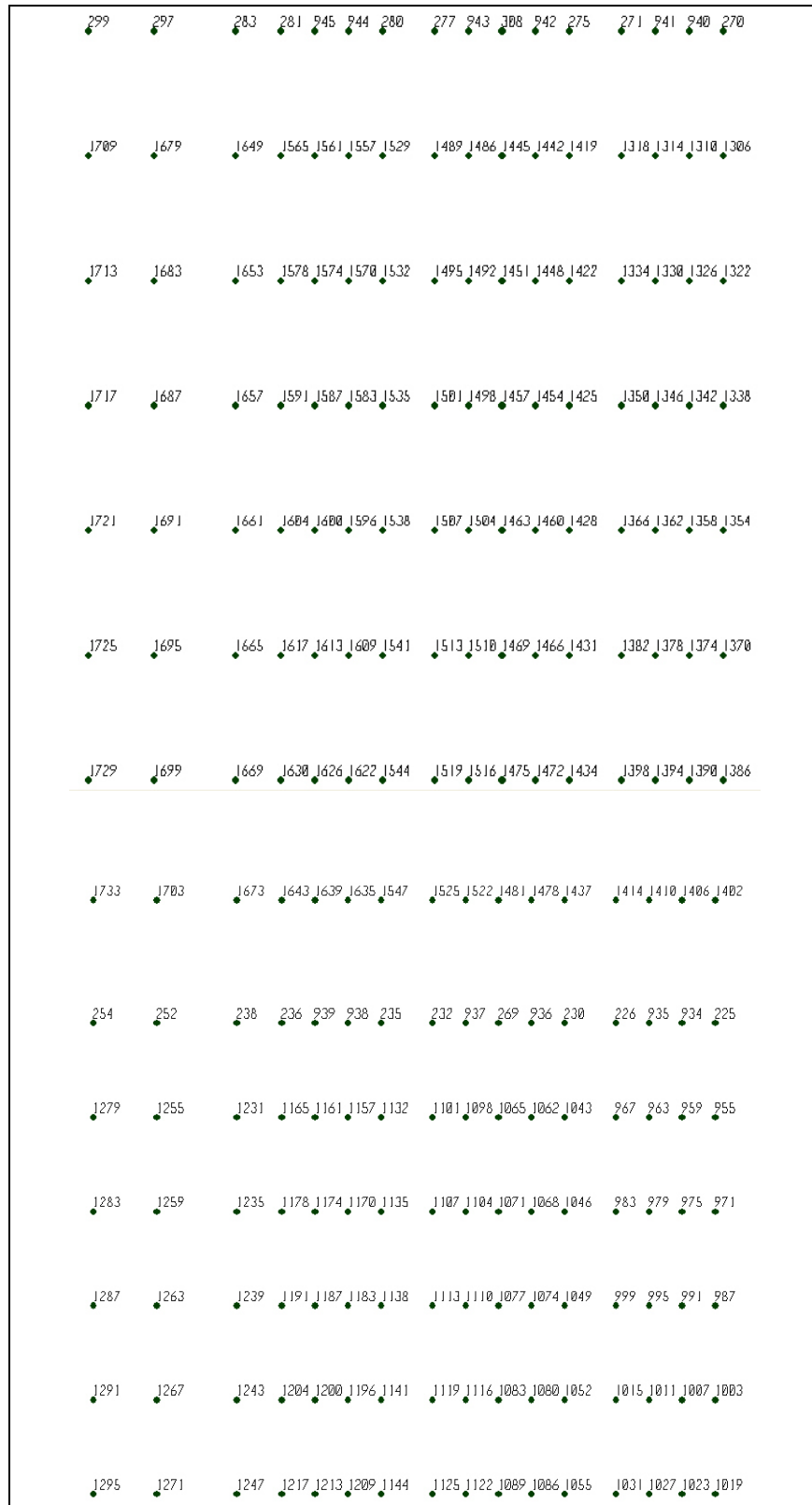
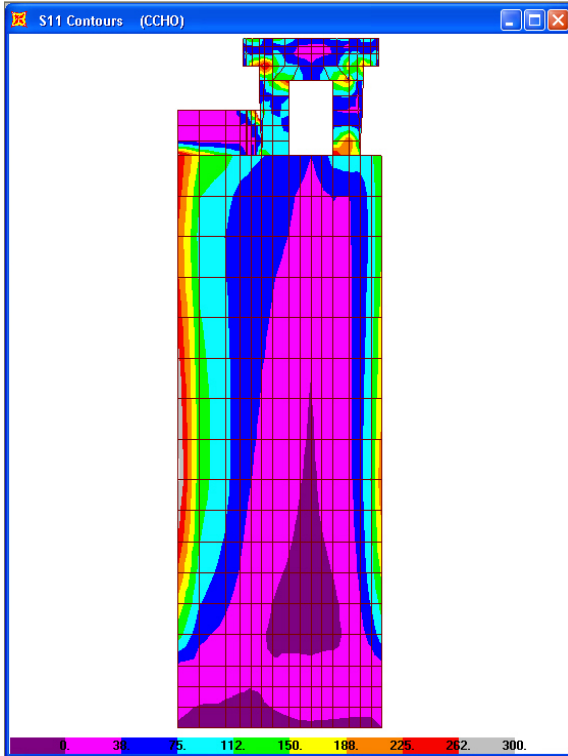
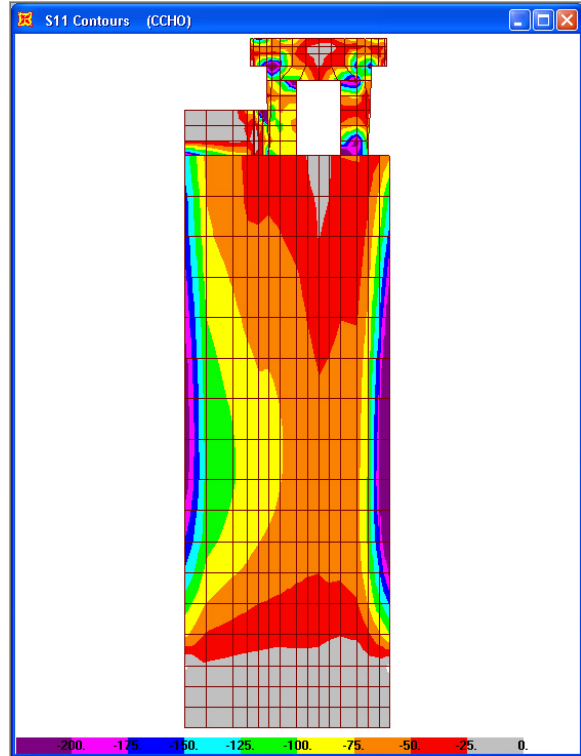


Figure 6.4-15. Node numbering at tower-rock interface

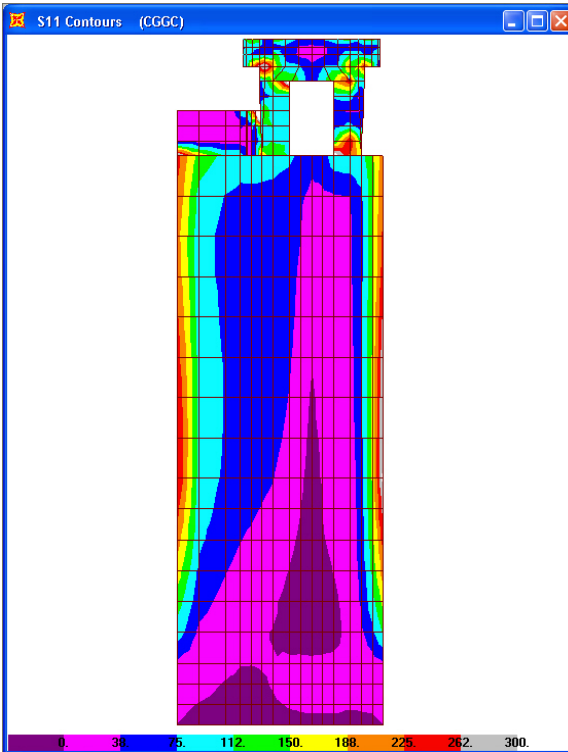


CHO Maximum Stresses (psi)

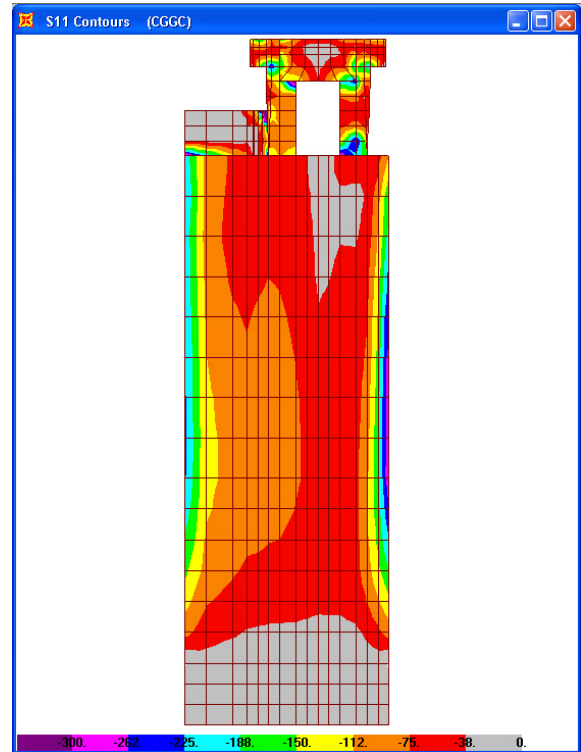


CHO Minimum Stresses (psi)

Figure 6.4-16. Normal stress contours at tower-abutment interface for CHO

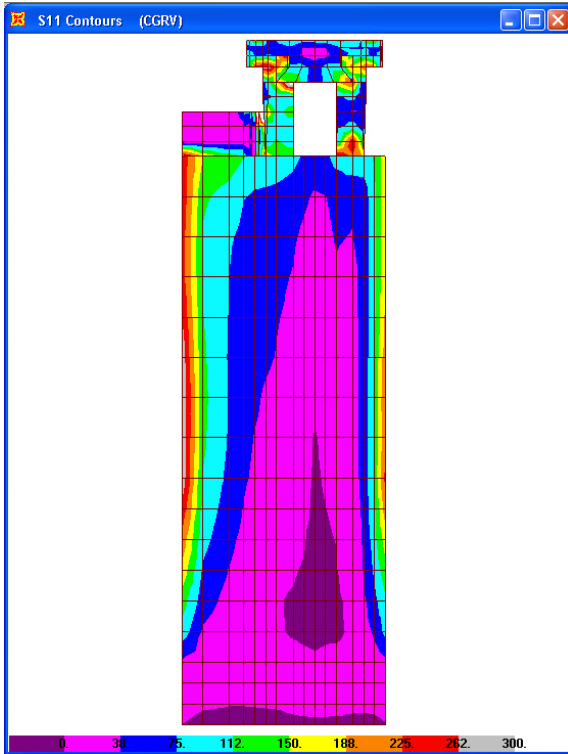


GGC Maximum Stresses (psi)

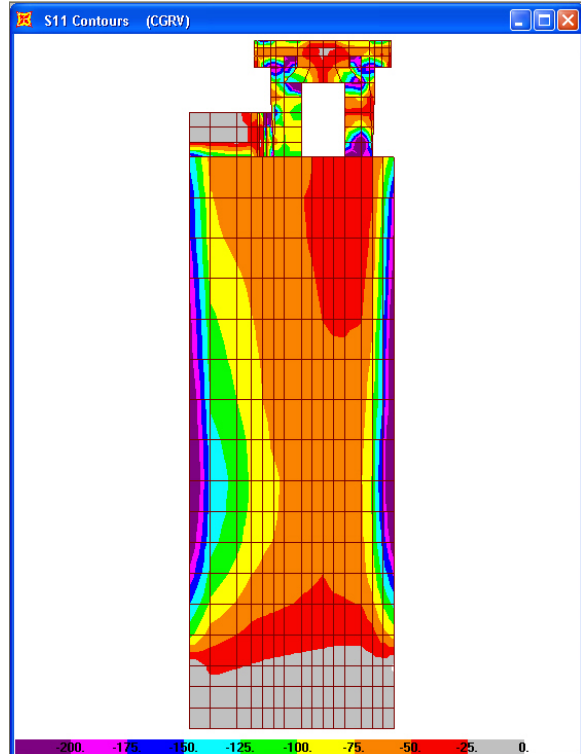


GGC Minimum Stresses (psi)

Figure 6.4-17. Normal stress contours at tower-abutment interface for GGC

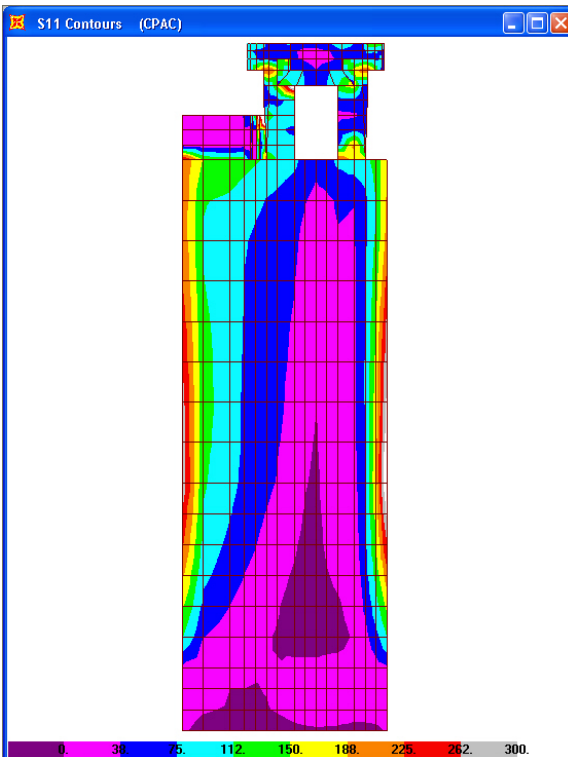


GRV Maximum Stresses (psi)

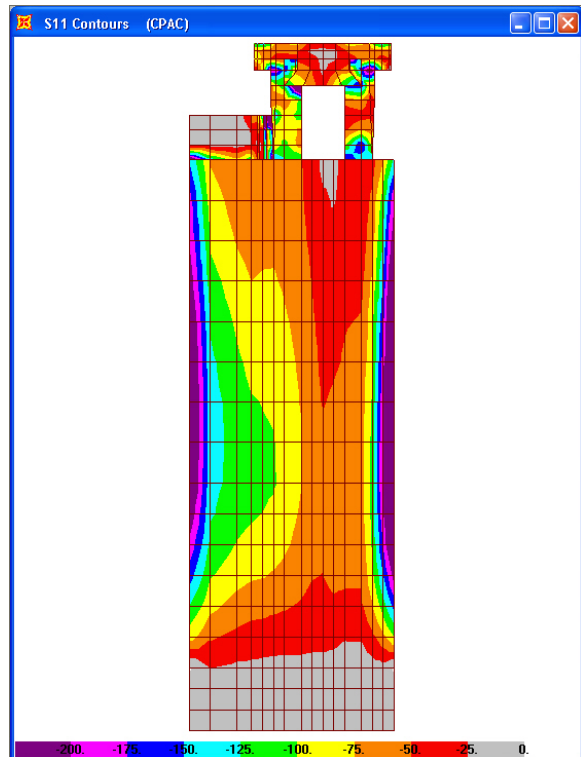


GRV Minimum Stresses (psi)

Figure 6.4-18. Normal stress contours at tower-abutment interface for GRV

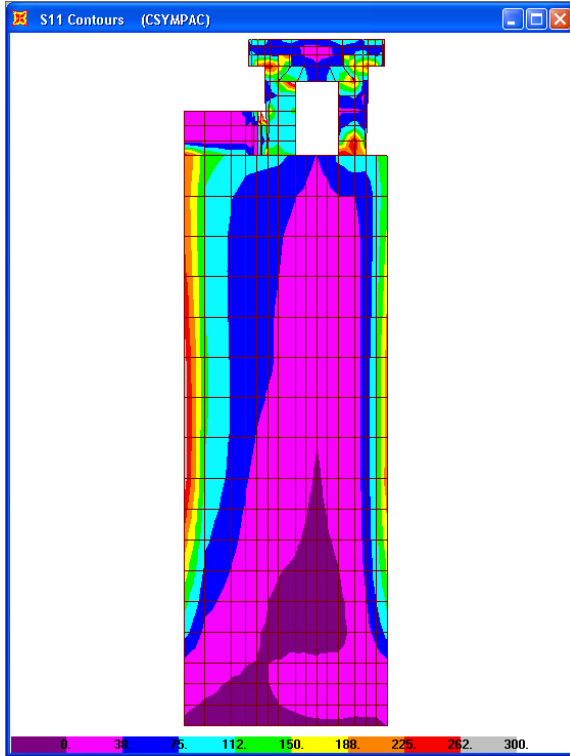


PAC Maximum Stresses (psi)

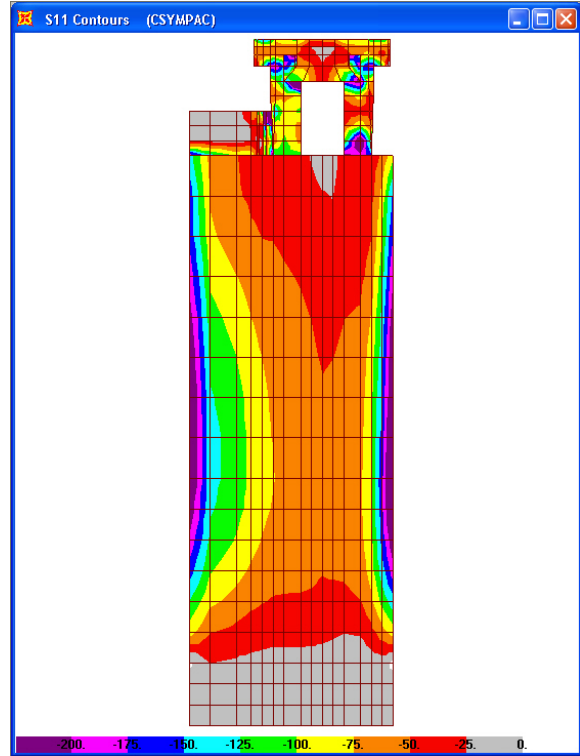


PAC Minimum Stresses (psi)

Figure 6.4-19. Normal stress contours at tower-abutment interface for PAC

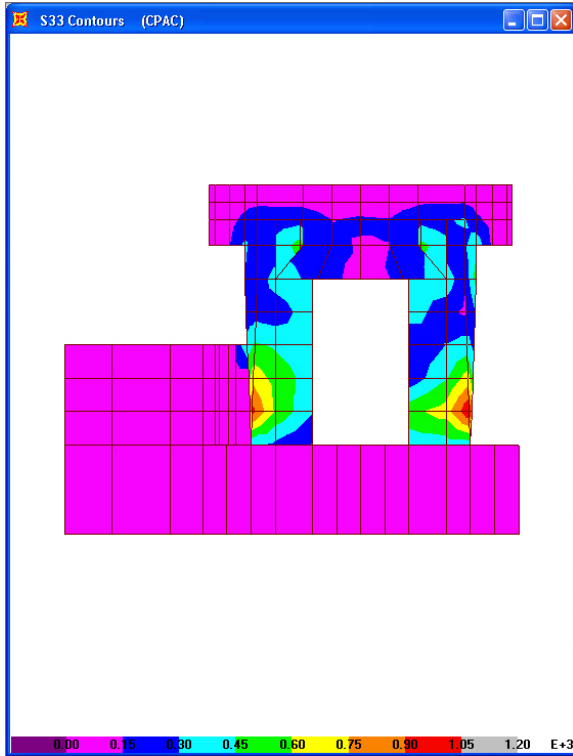


SMPAC Maximum Stresses (psi)

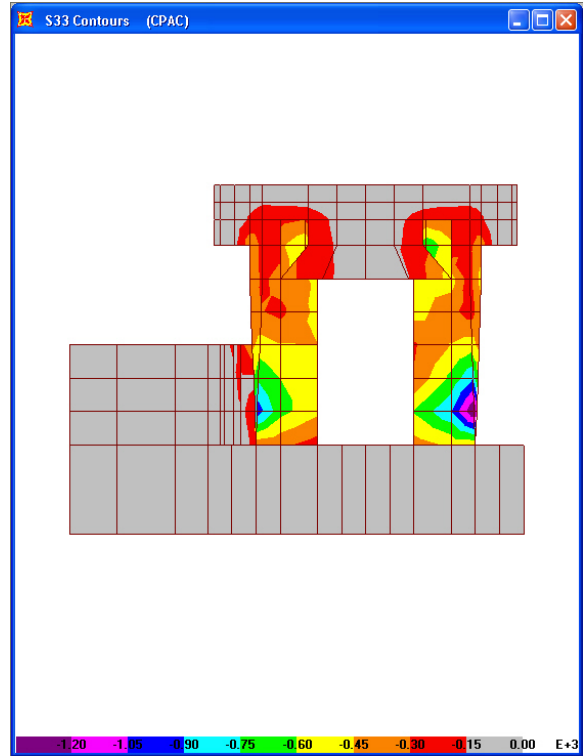


SMPAC Minimum Stresses (psi)

Figure 6.4-20. Normal stress contours at tower-abutment interface for SMPAC

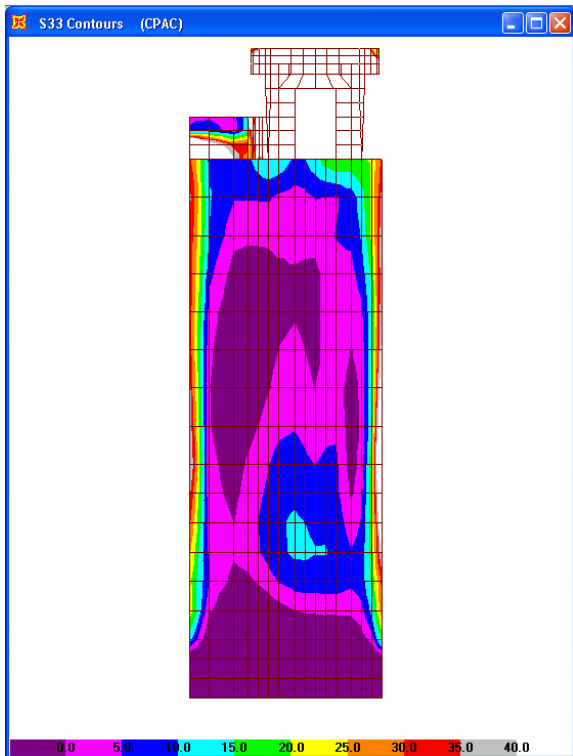


PAC Maximum Stresses (psi)

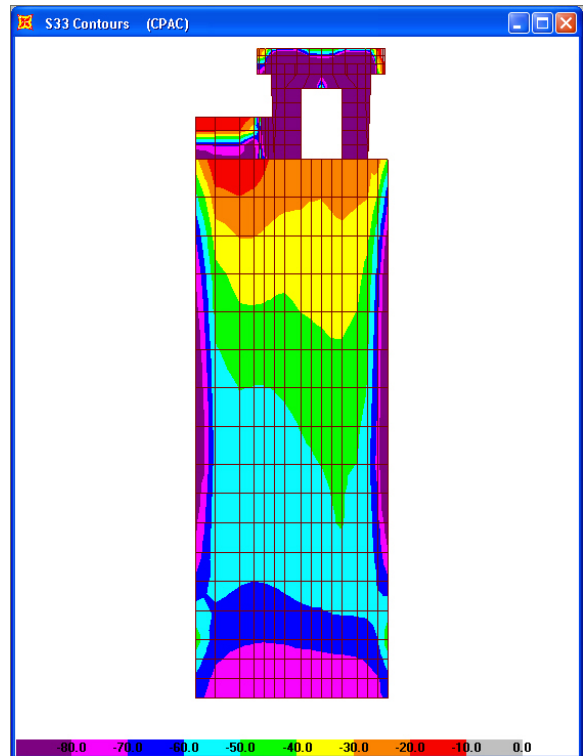


PAC Minimum Stresses (psi)

Figure 6.4-21. Vertical stresses in back face (downstream) of high-level intake for PAC

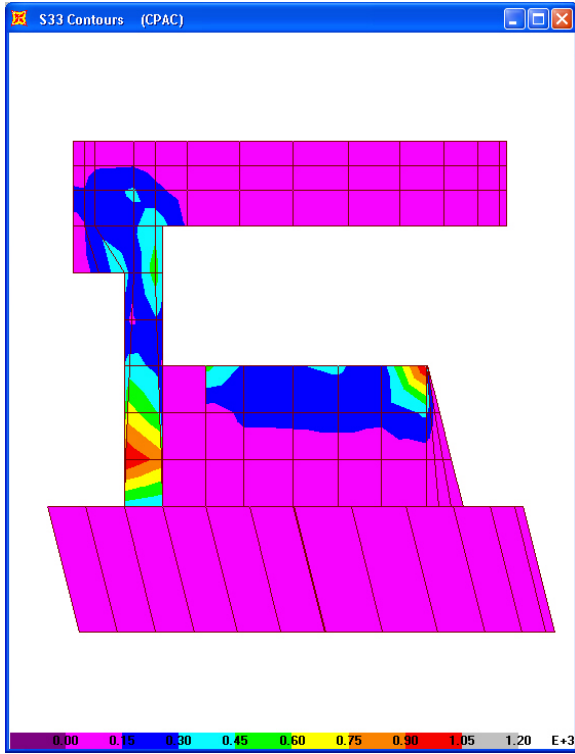


PAC Maximum Stresses (psi)

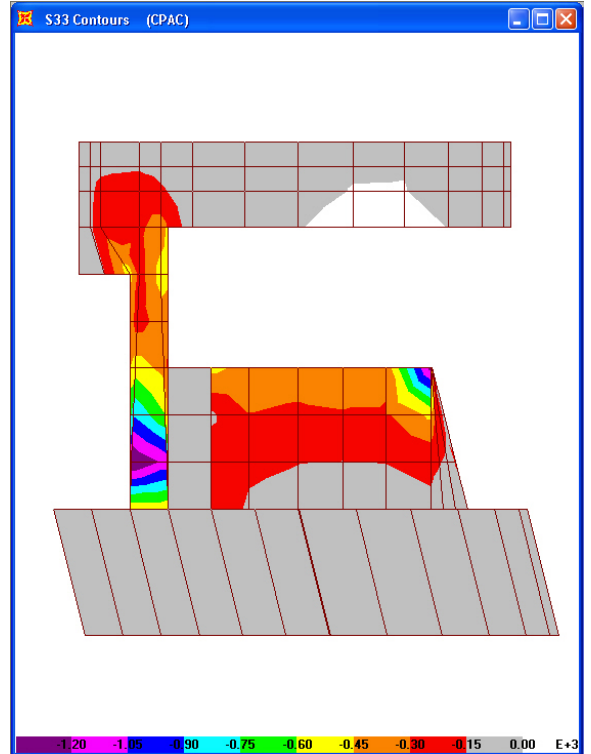


PAC Minimum Stresses (psi)

Figure 6.4-22. Vertical stresses in back face (downstream) of tower for PAC

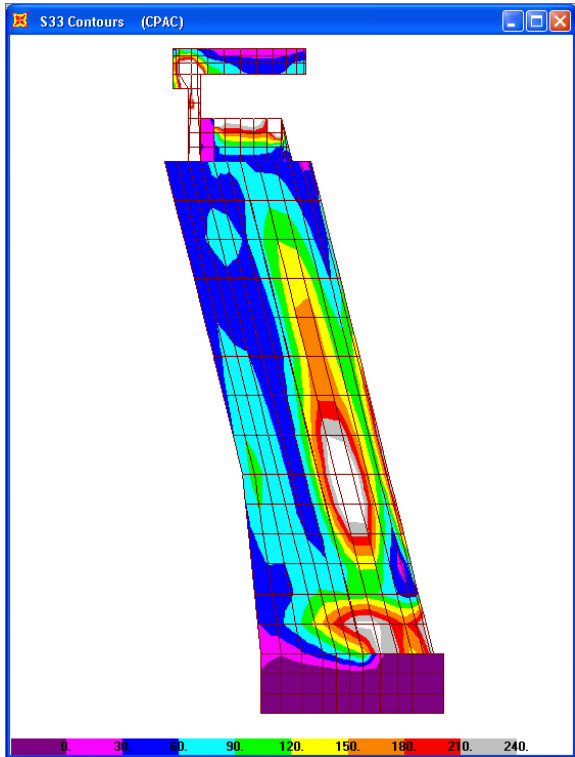


PAC Maximum Stresses (psi)

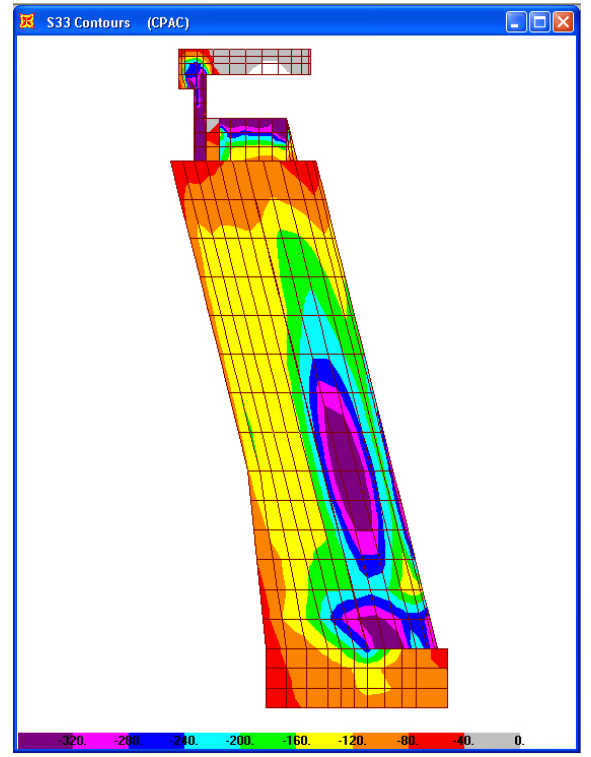


PAC Minimum Stresses (psi)

Figure 6.4-23. Vertical stresses in right face of high-level intake for PAC

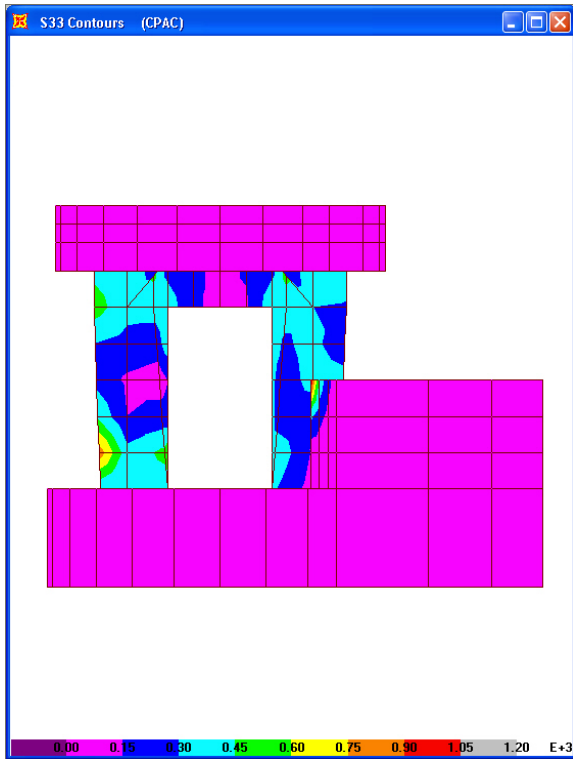


PAC Maximum Stresses (psi)

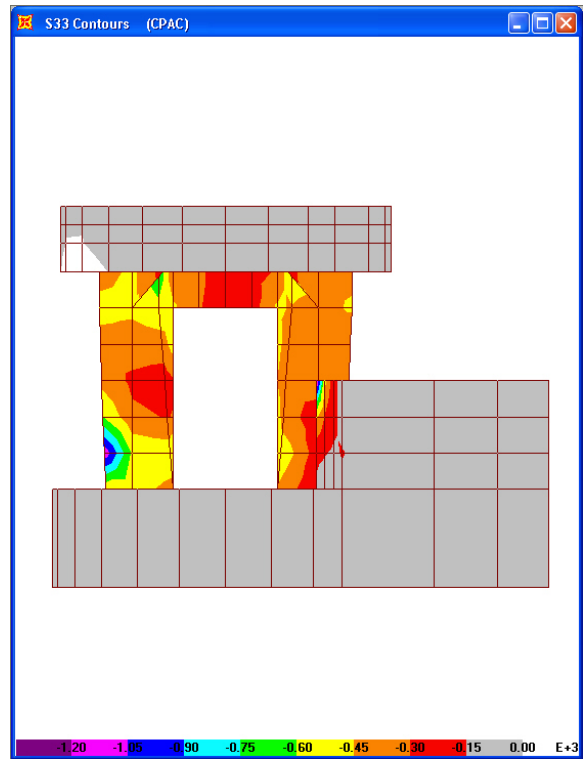


PAC Minimum Stresses (psi)

Figure 6.4-24. Vertical stresses in right face of tower for PAC

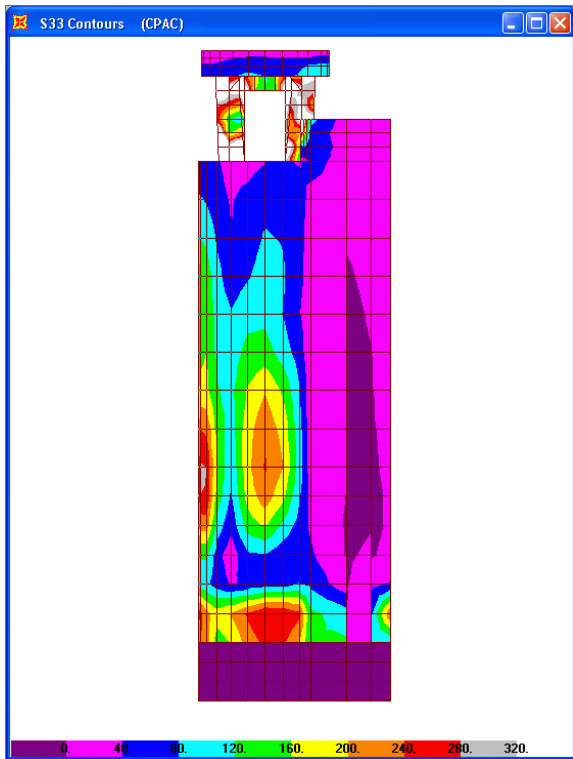


PAC Maximum Stresses (psi)

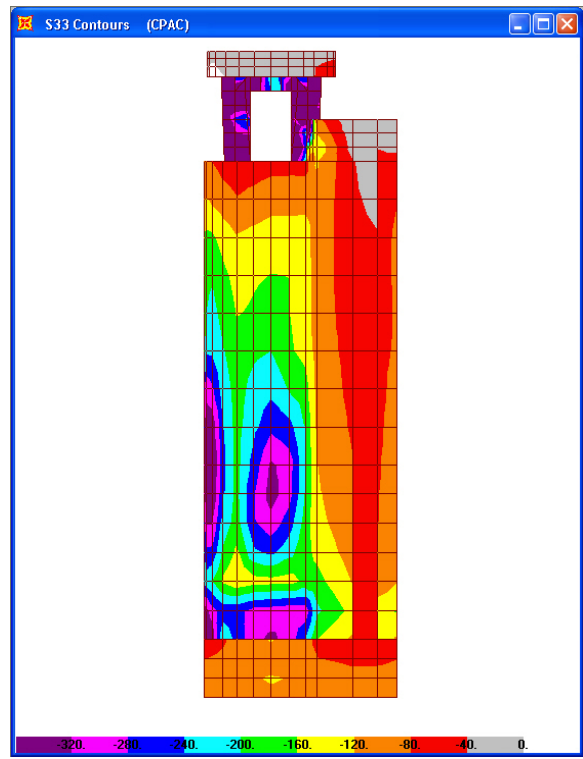


PAC Minimum Stresses (psi)

Figure 6.4-25. Vertical stresses in front face (upstream) of high-level intake for PAC

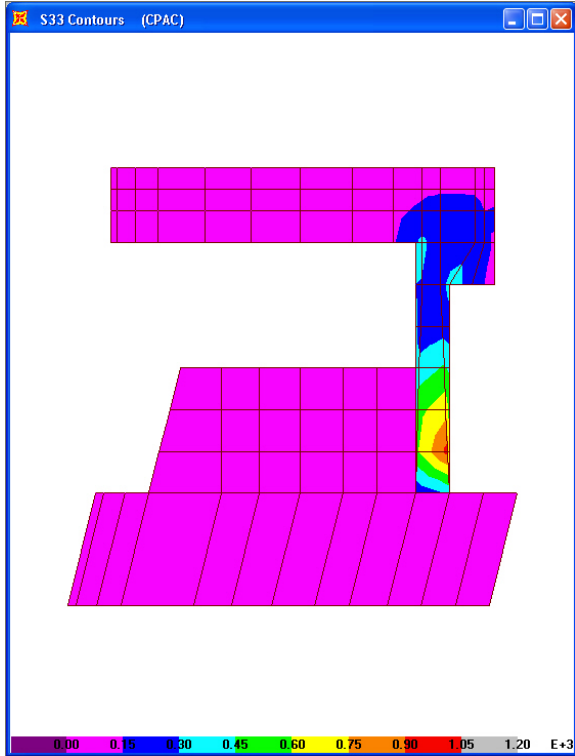


PAC Maximum Stresses (psi)

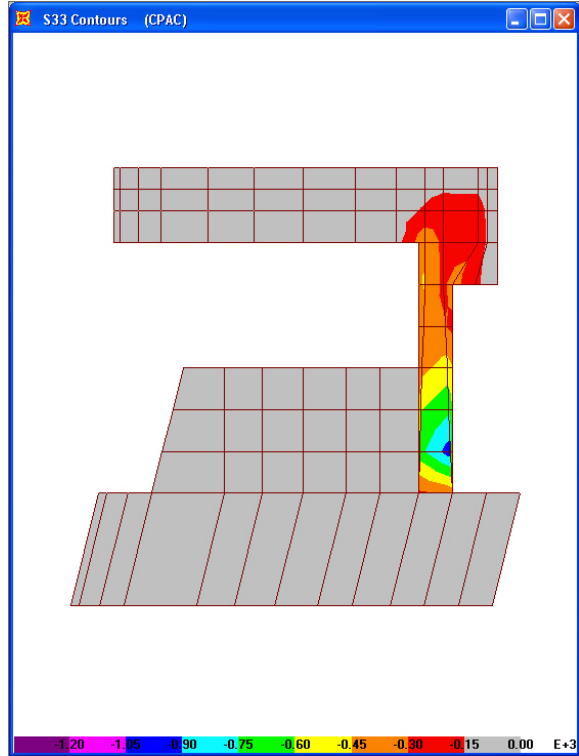


PAC Minimum Stresses (psi)

Figure 6.4-26. Vertical stresses in front face (upstream) of tower for PAC

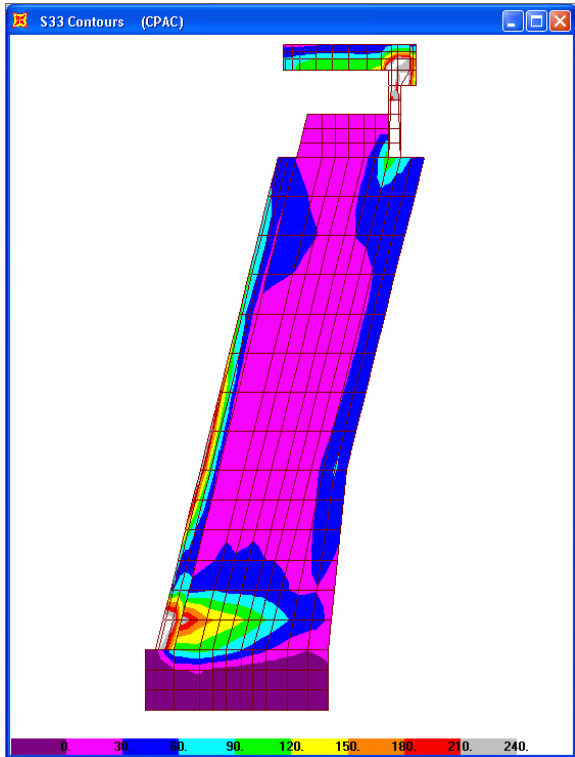


PAC Maximum Stresses (psi)

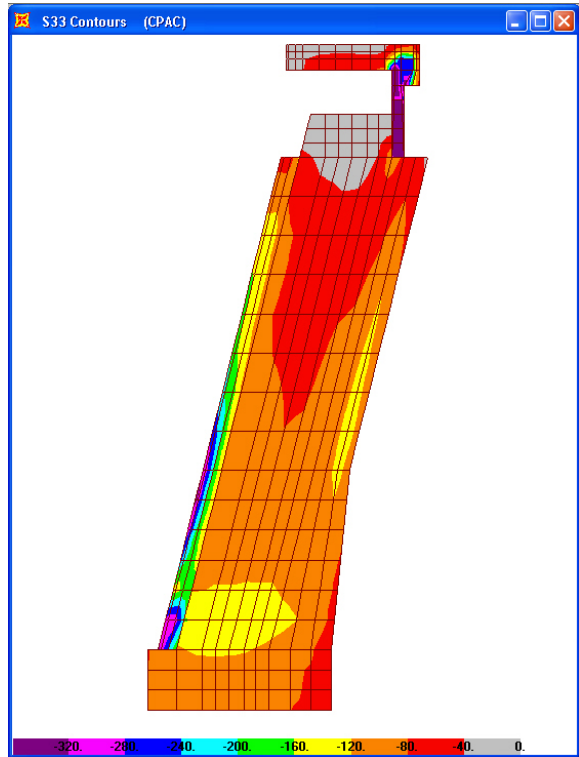


PAC Minimum Stresses (psi)

Figure 6.4-27. Vertical stresses in left face of high-level intake for PAC



PAC Maximum Stresses (psi)



PAC Minimum Stresses (psi)

Figure 6.4-28. Vertical stresses in left face of tower for PAC

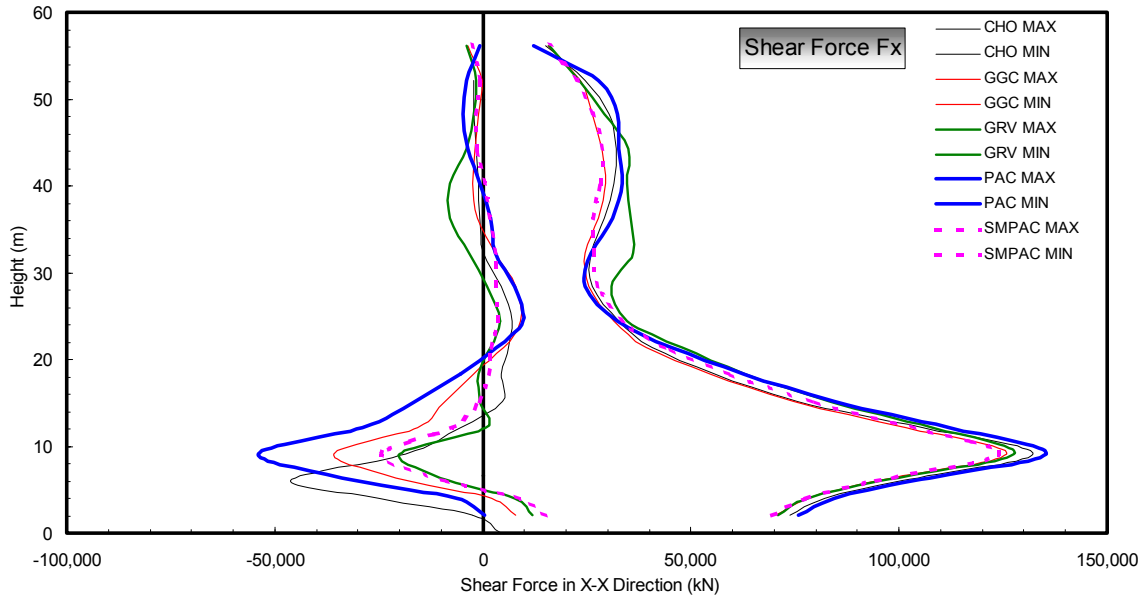


Figure 6.4-29. F_x shear force diagram (normal to abutment)

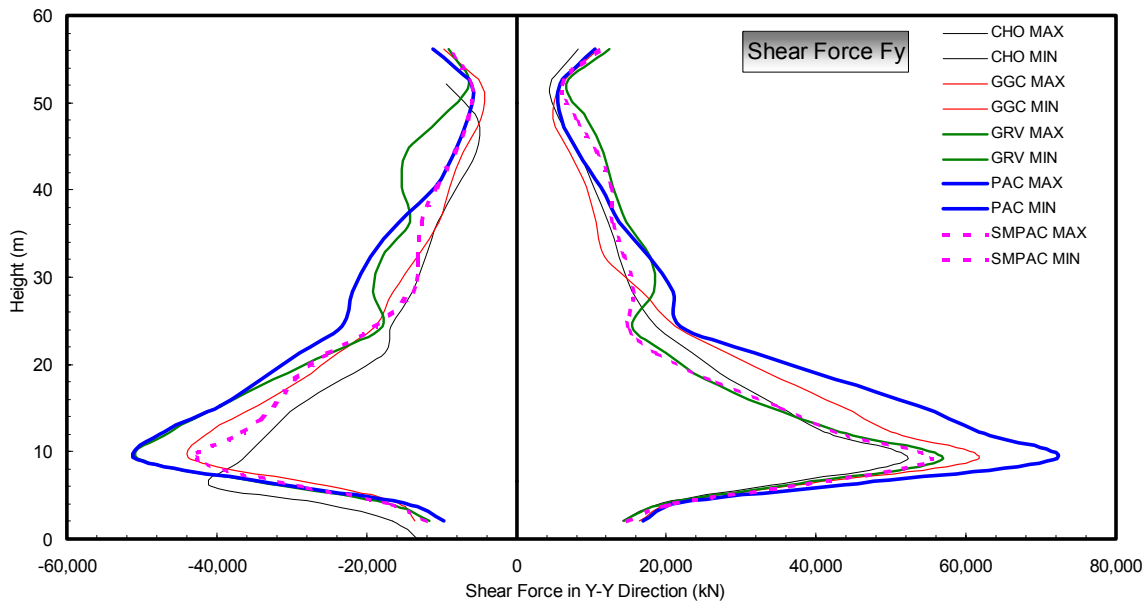


Figure 6.4-30. F_y shear force diagram (parallel to abutment)

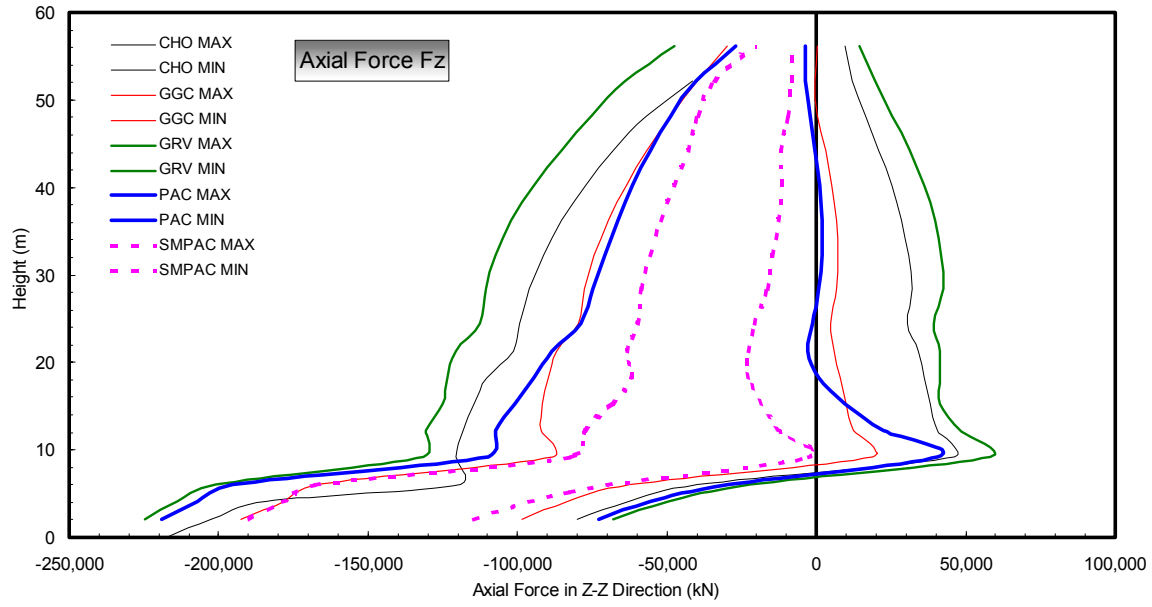


Figure 6.4-31. F_z (vertical) axial force diagram (+ = tension, - = compression)

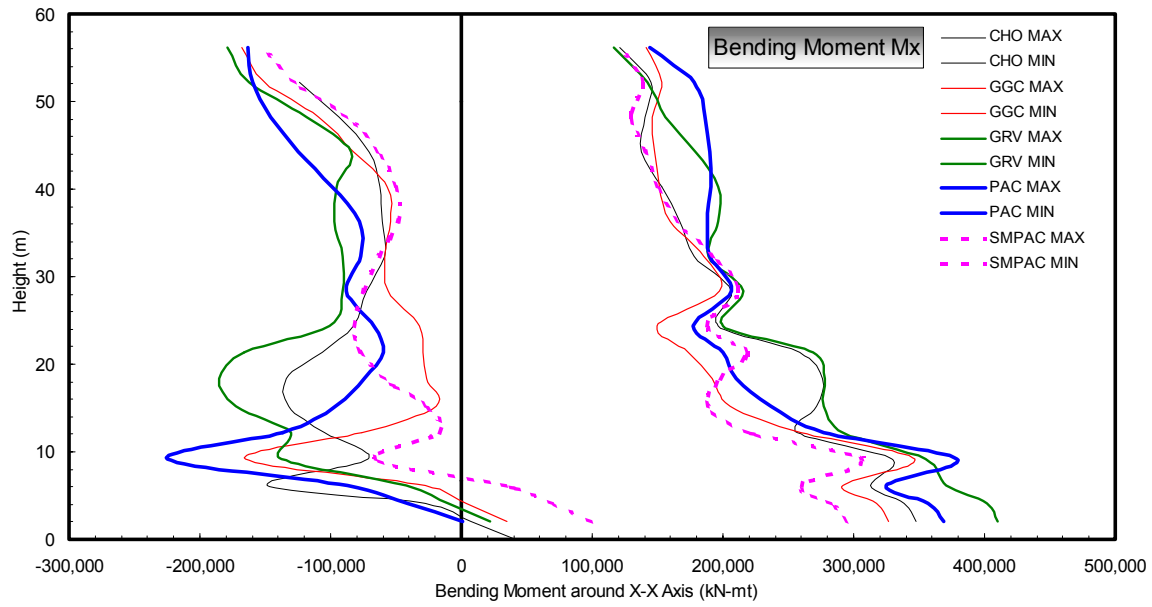


Figure 6.4-32. M_x bending moment diagram

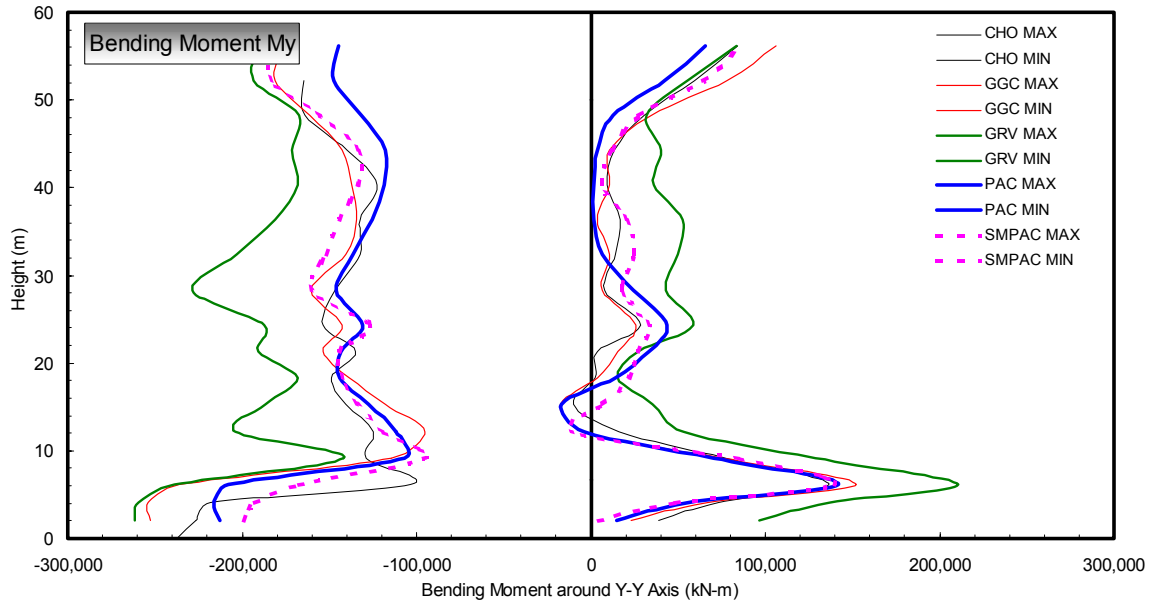


Figure 6.4-33. M_y bending moment diagram

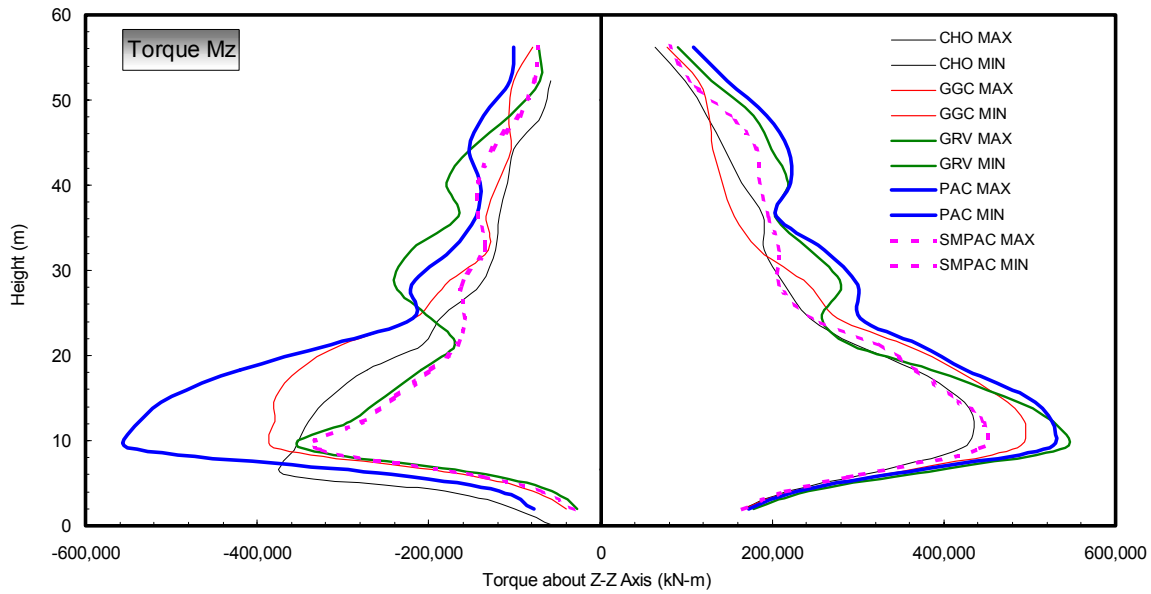


Figure 6.4-34. M_z torque moment diagram

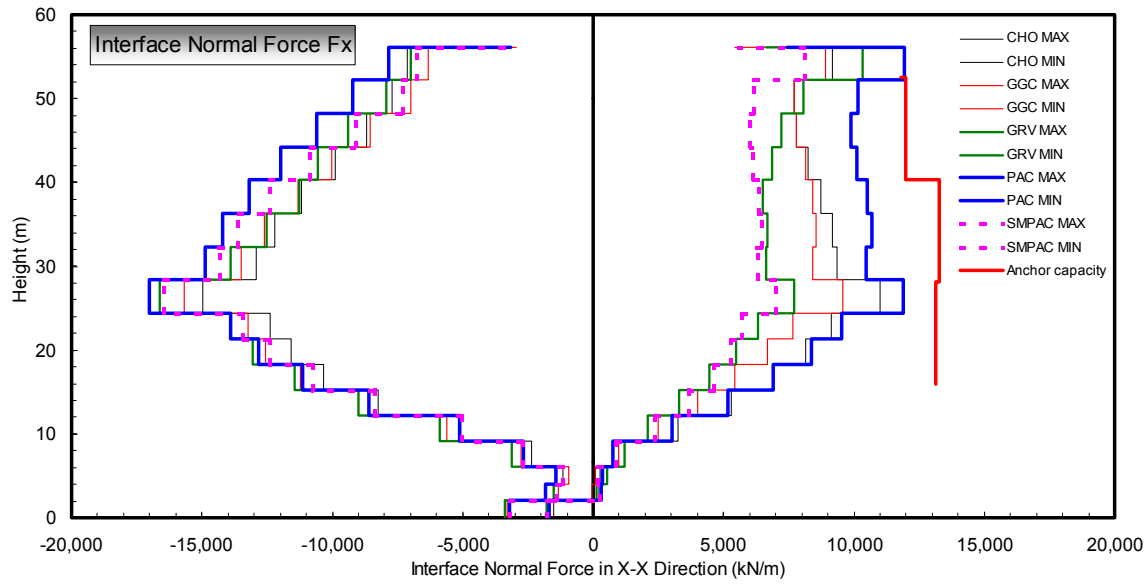


Figure 6.4-35. Tower-abutment interface normal forces

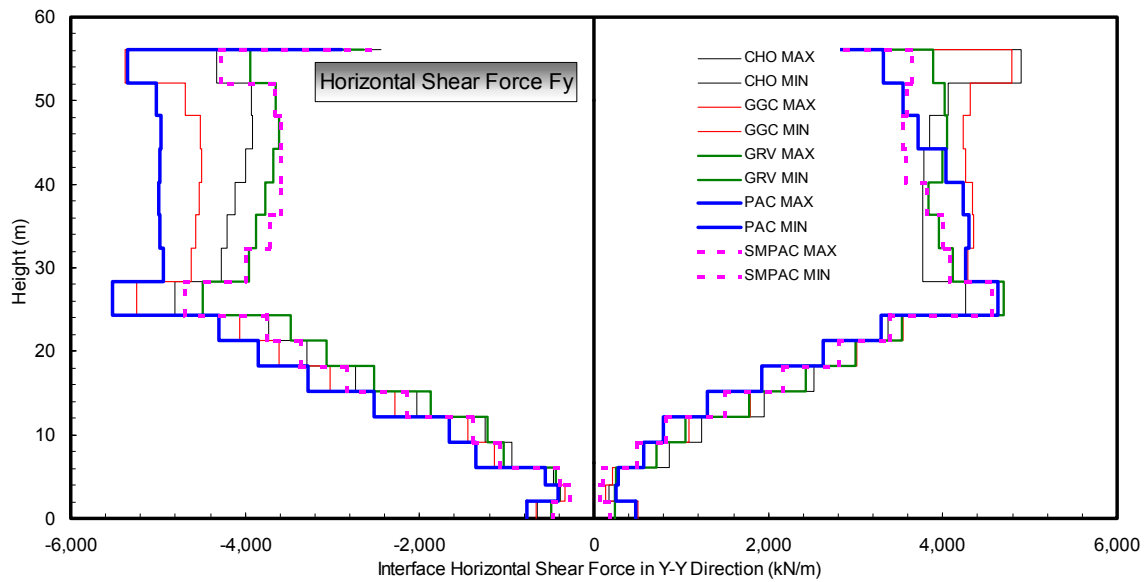


Figure 6.4-36. Tower-abutment interface horizontal shear forces

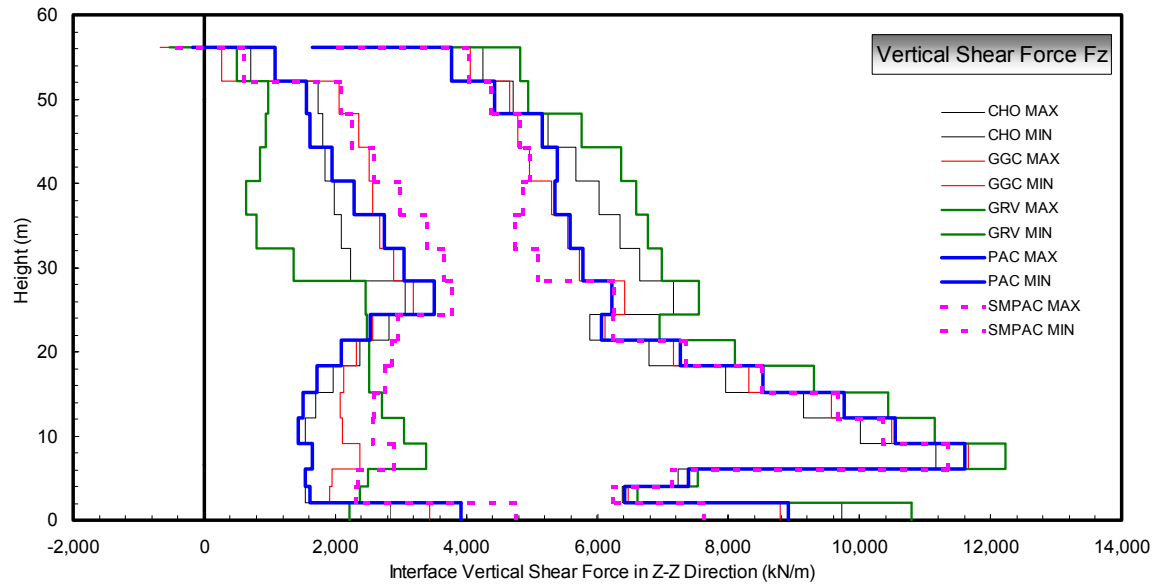


Figure 6.4-37. Tower-abutment interface vertical shear forces

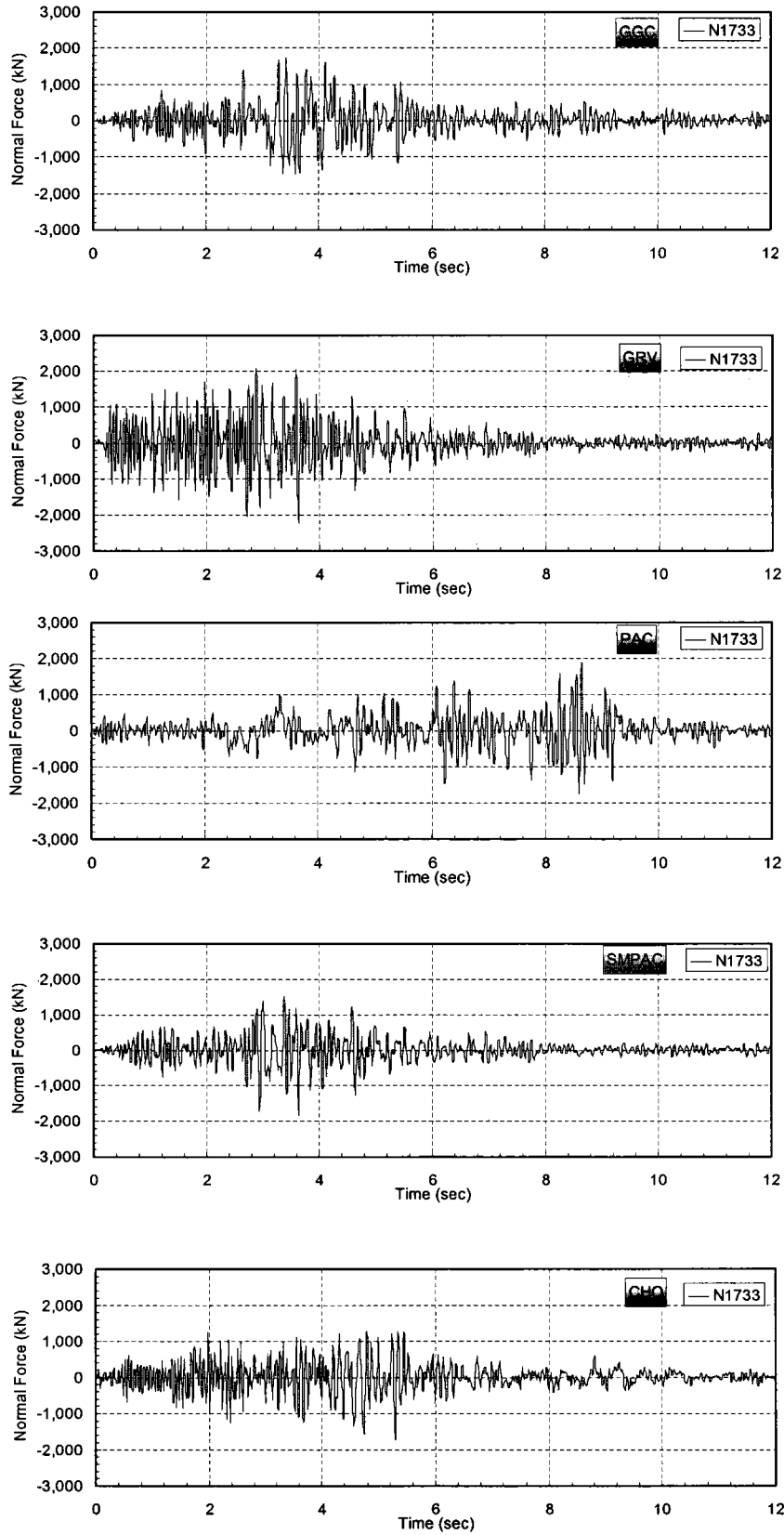


Figure 6.4-38. Time-history of anchor forces at Node N1733

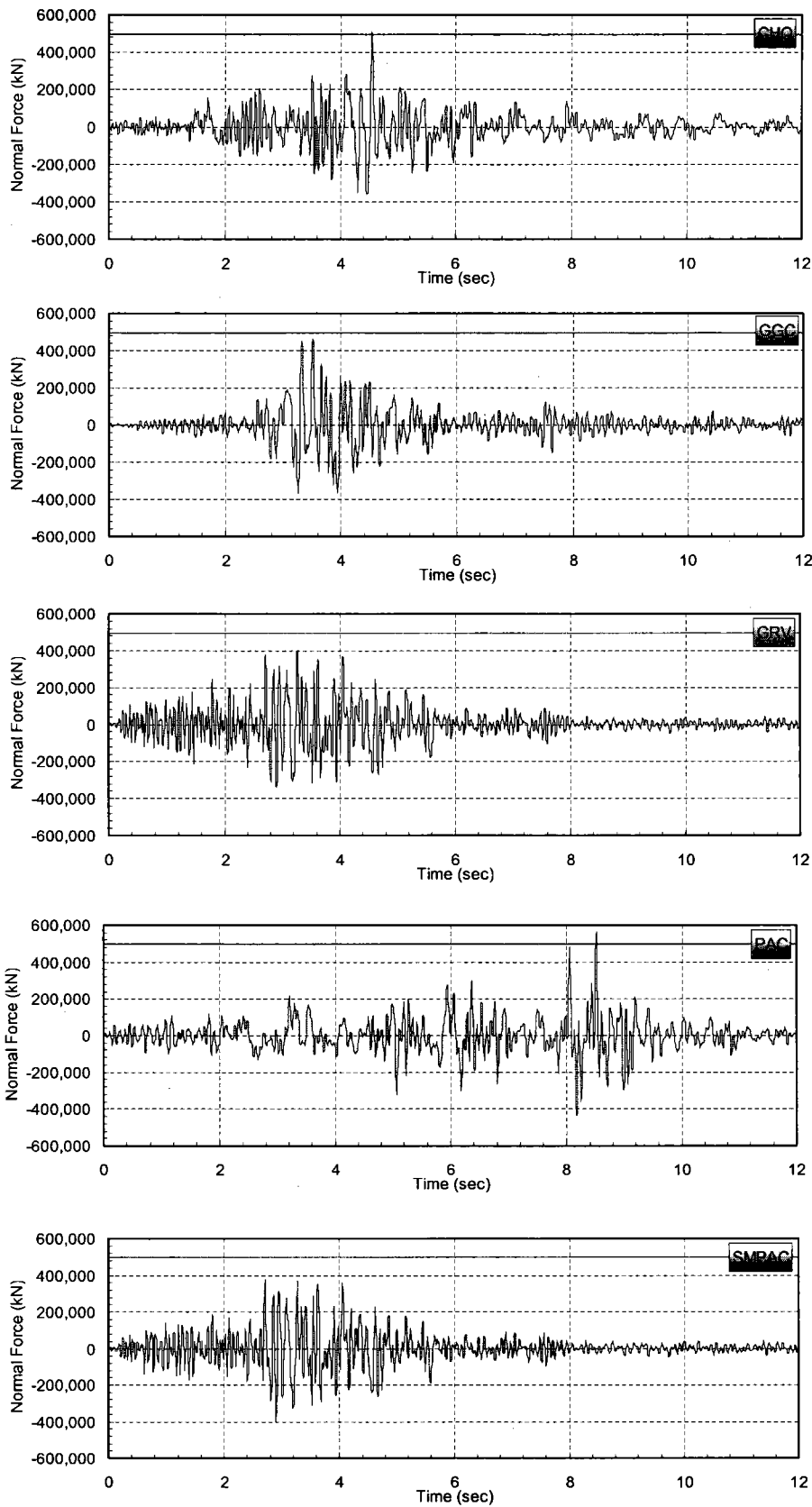


Figure 6.4-39. Comparison of time-history of total interface normal force with anchor design force

Appendix A References

ER 1110-2-1806

Earthquake Design and Evaluation of Civil Works Projects

EM 1110-2-2104

Strength Design for Reinforced-Concrete Hydraulic Structures

EM 1110-2-2201

Arch Dam Design

EM 1110-2-2906

Design of Pile Foundations

EM 1110-2-6050

Response Spectra and Seismic Analysis for Concrete Hydraulic Structures

Abrahamson 1992

Abrahamson, N. A. 1992. "Non-stationary Spectral Matching," *Seismological Research Letters*, Vol 63, No. 1, p 30.

Abrahamson, Somerville, and Cornell 1990

Abrahamson, N. A., Somerville, P. G., and Cornell, C. A. 1990. "Uncertainties in Numerical Strong Motion Predictions," *Proceedings, 4th U.S. National Conference on Earthquake Engineering*, Earthquake Engineering Research Institute, Oakland, CA, 1, 407-416.

ADINA 1997

ADINA. 1997. "Automatic Dynamic Incremental Nonlinear Analysis Program for Structures, Heat Transfer, and CFD," ADINA R&D, Inc., Watertown, MA.

Aki and Richards 1980

Aki, K., and Richards, P. G. 1980. *Quantitative Seismology, Theory, and Methods*, W.H. Freeman, San Francisco, 932 pp.

Aki et al. 1995

Aki, K., Martin, G. R., Chin, B. H., Abrahamson, N., Cornell, A. C., and Mahdyiar, M. 1995. "Final Task Report on the Characteristics of Earthquake Ground Motions for Seismic Design; Task H-7, Probabilistic Seismic Hazard Analysis and Development of Earthquake Scenario Time Histories for Southern California Sites," Southern California Earthquake Center, University of Southern California, Los Angeles, CA.

Alarcon, Dominguez, and Del Cano 1980

Alarcon, E., Dominguez, J., and Del Cano, F. 1980. "Dynamic Stiffness of Foundations," *Proceedings of the 2nd International Seminar, Recent Advances in BEM*, C.A. Brebia, ed., pp 264-288.

American Concrete Institute 1989

American Concrete Institute. 1989. "Building Code Requirements for Reinforced Concrete," ACI-318, Farmington Hills, MI.

Arias 1970

Arias, A. 1970. "A Measure of Earthquake Intensity," *Seismic Design for Nuclear Power Plants*, R. Hanson, ed., Massachusetts Institute of Technology Press, Cambridge, MA.

ASTM A36

American Society for Testing and Materials. "Standard Specification for Structural Steel," ASTM A36, West Conshohocken, PA.

ASTM C496

American Society for Testing and Materials. "Standard Test Method for Splitting Tensile Strength of Cylindrical Concrete Specimens," ASTM C496, West Conshohocken, PA.

Bathe and Wilson 1976

Bathe, K. J., and Wilson, E. L. 1976. *Numerical Methods in Finite Element Analysis*, Prentice-Hall, Englewood Cliffs, NJ.

Beresnev and Atkinson 1997

Beresnev, I. A., and Atkinson, G. M. 1997. "Modeling Finite-Fault Radiation from the Tⁿ Spectrum," *Bulletin of the Seismological Society of America*, Vol 87, pp 67-84.

Bolt and Gregor 1993

Bolt, B. A., and Gregor, N. J. 1993. "Synthesized Strong Ground Motions for the Seismic Condition Assessment of the Eastern Portion of the San Francisco Bay Bridge," Report UCB/EERC-93/12, University of California, Earthquake Engineering Research Center, Berkeley, CA.

Boore 1983

Boore, D. M. 1983. "Stochastic Simulation of High-Frequency Ground Motions Based on Seismological Models of the Radiated Spectra," *Bulletin of the Seismological Society of America*, Vol 73, pp 1865-1894.

Boore 1996

Boore, D. M. 1996. "SMSIM – Fortran Programs for Simulating Ground Motions from Earthquakes: Version 1.0," Open File Report 96-80-A, U.S. Geological Survey.

Brune 1970

Brune, J. N. 1970. "Tectonic Stress and the Spectra of Seismic Shear Waves from Earthquakes," *Journal of Geophysical Research*, Vol 75, pp 4997-5009.

CASTR 1993

CASTR. 1993. "User's Guide for Concrete Strength Investigation and Design," CORPS Library Program X0067, U.S. Army Engineer Waterways Experiment Station, Vicksburg, MS.

Chang et al. 1990

Chang, C.-Y., Mok, C. M., Power, M. S., Tang, Y. K., Tang, H. T., and Stepp, J. C. 1990. "Equivalent Linear Versus Nonlinear Ground Response Analyses at Lotung Seismic Experiment Site," *Proceedings, Fourth U.S. National Conference on Earthquake Engineering*, Palm Springs, CA, May 20-24, 1990, Earthquake Engineering Research Institute, El Cerrito, CA, Vol 1, pp 327-336.

Chopra 1987

Chopra, A. K. 1987. "Earthquake Analysis, Design, and Safety Evaluation of Concrete Dams," *Proceedings, 5th Canadian Conference on Earthquake Engineering*, Ottawa, Ontario, Canada, A. A. Balkema, Rotterdam, The Netherlands, pp 39-62.

Chopra 1988

Chopra, A. K. 1988. "Earthquake Response Analysis of Concrete Dams," *Advanced Dam Engineering for Design, Construction, and Rehabilitation*, Chapter 15, Robert B. Jansen, ed., Van Nostrand Reinhold, New York.

Chopra 1995

Chopra, A. K. 1995. *Dynamics of Structures: Theory and Applications to Earthquake Engineering*, Prentice-Hall, Englewood Cliffs, NJ.

Chopra and Chakrabarti 1981

Chopra, A. K., and Chakrabarti, P. 1981. "Earthquake Analysis of Concrete Gravity Dams Including Dam-Water-Foundation Interaction," *Earthquake Engineering and Structural Dynamics*, Vol 9, No. 4, pp 363-383.

Chopra and Fok 1984

Chopra, A. K., and Fok, K. L. 1984. "Evaluation of Simplified Earthquake Analysis Procedures for Intake-Outlet Towers," *8th World Conference on Earthquake Engineering*, San Francisco, Vol 7, pp 467-474.

Clough and Penzien 1993

Clough, R. W., and Penzien, J. 1993. *Dynamics of Structures*, 2d ed., McGraw-Hill, New York.

Clough et al. 1984a

Clough, R. W., Chang, K. T., Chen, H. -Q., Stephen, R. M., Wang, G. -L., and Ghanaat, Y. 1984a. "Dynamic Response Behavior of Xiang Hong Dian Dam," Report No. UCB/EERC-84/02, Earthquake Engineering Research Center, University of California, Berkeley.

Clough et al. 1984b

Clough, R. W., Chang, K. T., Chen, H. -Q., Stephen, R. M., Ghanaat, Y., and Qi, J. -H. 1984b. "Dynamic Response Behavior of Quan Shui Dam," Report No. UCB/EERC-84/20, Earthquake Engineering Research Center, University of California, Berkeley.

Cooley and Tukey 1965

Cooley, P.M., and Tukey, J.W. 1965. "An algorithm for the machine computation of complex Fourier series," *Mathematics and Computation*, Vol 19, No. 4, pp 297-301.

Dasgupta and Chopra 1979

Dasgupta, G., and Chopra, A. K. 1979. "Dynamic Stiffness Matrices for Viscoelastic Half Planes," *Journal of the Engineering Mechanics Division*, ASCE, Vol 105, No. EM5, pp 729-745.

Dobry, Idriss, and Ng 1978

Dobry, R., Idriss, I. M., and Ng, E. 1978. "Duration Characteristics of Horizontal Components of Strong-Motion Earthquake Records," *Bulletin of the Seismological Society of America*, Vol 68, No. 5, pp 1487-1520.

Dove 1998

Dove, R. C. 1998. "Performance of Lightly Reinforced Concrete Intake Towers under Selected Loading," Technical Report SL-98-1, U.S. Army Engineer Waterways Experiment Station, Vicksburg, MS.

Ebeling 1992

Ebeling, R. M. 1992. "Introduction to the Computation of Response Spectrum for Earthquake Loading," Technical Report ITL-92-11, U.S. Army Engineer Waterways Experiment Station, Vicksburg, MS.

Ebeling and Morrison 1992

Ebeling, R. M., and Morrison, E. E. 1992. "The Seismic Design of Waterfront Retaining Structures," Technical Report ITL-92-11, U.S. Army Engineer Waterways Experiment Station, Vicksburg, MS.

Ebeling, Green, and French 1997

Ebeling, R. M., Green, R. A., and French, S. E. 1997. "Accuracy of Response of Single-Degree-of-Freedom Systems to Ground Motion," Technical Report ITL-97-7, U.S. Army Engineer Waterways Experiment Station, Vicksburg, MS.

Electric Power Research Institute 1995

Electric Power Research Institute. 1995. *Proceedings of Workshop on Modeling Earthquake Ground Motion at Close Distances*, September 5-6, 1990, EPRI Report TR-104975, Palo Alto, CA.

Epstein 1976

Epstein, H. I. 1976. "Seismic Design of Liquid-Storage Tanks," *Journal of the Structures Division*, ASCE, Vol 102, No. ST9, pp 1659-1673.

Fenves and Chopra 1984a

Fenves, G., and Chopra, A. K. 1984a. "EAGD-84: A Computer Program for Earthquake Analysis of Concrete Gravity Dams," Report No. UCB/EERC-84/11, Earthquake Engineering Research Center, University of California, Berkeley.

Fenves and Chopra 1984b

Fenves, G., and Chopra, A. K. 1984b. "Earthquake Analysis and Response of Concrete Gravity Dams," Report No. UCB/EERC-84/10, Earthquake Engineering Research Center, University of California, Berkeley.

Fenves and Chopra 1986

Fenves, G., and Chopra, A. K. 1986. "Simplified Analysis for Earthquake Resistant Design of Concrete Gravity Dams," Report No. UCB/EERC-85-10, Earthquake Engineering Research Center, University of California, Berkeley.

Fok and Chopra 1985

Fok, K. -L., and Chopra, A. K. 1985. "Earthquake Analysis and Response of Concrete Arch Dams," Report No. UCB/EERC-85-07, Earthquake Engineering Research Center, University of California, Berkeley.

Fok, Hall, and Chopra 1986

Fok, K. -L., Hall, J. F., and Chopra, A. K. 1986. "EACD-3D, A Program for Three-dimensional Earthquake Analysis of Concrete Dams," Report No. UCB/EERC-86-09, Earthquake Engineering Research Center, University of California, Berkeley.

French, Ebeling, and Strom 1994

French, S. E., Ebeling, R. M., and Strom, R. 1994. "Dynamics of Intake Towers and Other MDOF Structures Under Earthquake Loads: A Computer-Aided Approach," Technical Report ITL-94-4, U.S. Army Engineer Waterways Experiment Station, Vicksburg, MS.

French, Ebeling, and Strom 1996

French, S. E., Ebeling, R. M., and Strom, R. 1996. "Dynamics Analysis of Distributed-Mass Intake Towers Using the Rayleigh Method," *Proceedings, Corps of Engineers Structural Engineering Conference*, San Antonio, TX, 28-30 August 1995, U.S. Army Engineer Waterways Experiment Station, Vicksburg, MS, Vol 2, pp 821-837.

Gasparini and Vanmarcke 1976

Gasparini, D., and Vanmarcke, E. H. 1976. "SIMQKE: A Program for Artificial Motion Generation," Department of Civil Engineering, Massachusetts Institute of Technology, Cambridge, MA.

Geomatrix Consultants 1988

Geomatrix Consultants. 1988. "Geological-Seismological Evaluation to Assess Potential Earthquake Ground Motions for the Portugues Dam, Puerto Rico," Report prepared for U.S. Army Engineer District, Jacksonville, Jacksonville, FL.

Geomatrix Consultants 1996

Geomatrix Consultants, Inc. 1996. "Probabilistic Seismic Hazard Assessment, Olmsted Locks and Dam Site," report prepared for U.S. Army Engineer District, Louisville, Louisville, KY.

Geomatrix Consultants 1999

Geomatrix Consultants. 1999. "Final Report: Seismic Analysis and Evaluation of Lower Mitergate Monolith, M26 Olmsted Locks and Dam, Ohio River, Illinois and Kentucky," performed for U.S. Army Engineer District, Louisville.

Geotechnical and Structures Laboratory (in preparation)

Geotechnical and Structures Laboratory. "EQTIME2D: Time-History Analysis of 2D Concrete Gravity Dam Sections" (in preparation), Engineering Research and Development Center, Vicksburg, MS.

Ghanaat 1992

Ghanaat, Y. 1992. "Added-mass Matrix for Seven Oaks Intake Tower," prepared for U.S. Army Engineer Waterways Experiment Station, Vicksburg, MS.

Ghanaat 1993a

Ghanaat, Y. 1993a. "GDAP -- Graphics-based Dam Analysis Program," Instruction Report ITL-93-3, U.S. Army Engineer Waterways Experiment Station, Vicksburg, MS.

Ghanaat 1993b

Ghanaat, Y. 1993b. "Theoretical Manual for Analysis of Arch Dams," Instruction Report ITL-93-1, U.S. Army Engineer Waterways Experiment Station, Vicksburg, MS.

Ghanaat et al. 1993

Ghanaat, Y., Chen, H. -Q., Redpath, B. B., and Clough, R. W. 1993. "Experimental Study of Dongjiang Dam for Dam-Water-Foundation Interaction," QUEST Structures Report No. QS93-03, submitted to National Science Foundation, Orinda, CA.

Ghanaat and Redpath 1995

Ghanaat, Y., and Redpath, B. B. 1995. "Measurement of Reservoir-Bottom Reflection Coefficient at Seven Concrete Dam Sites," QUEST Structure Report No. QS95-01, submitted to the U.S. Army Engineer Waterways Experiment Station, Vicksburg, MS, and Bureau of Reclamation.

Ghanaat et al. 1999

Ghanaat, Y., Chen, H. -Q., Redpath, B. B., Hall, R. L., and Marjanishvili, S. M. 1999. "Measurement and Prediction of Dam-Water-Foundation Interaction at Longyangxia Dam," QUEST Structures Report No. QS99-05 submitted to National Science Foundation, Orinda, CA.

Ghanaat 2002

Ghanaat, Y. 2000. "Seismic Performance and Damage Criteria for Concrete Dams," Proceedings of the 3rd US-Japan Workshop on Advanced Research on Earthquake Engineering for Dams, San Diego, California, June 22-23, 2002.

Goodman and Shi 1985

Goodman, R. E., and Shi, G.-H. 1985. *Block Theory and Its Application to Rock Engineering*, Prentice-Hall, Englewood Cliffs, NJ.

Goyal and Chopra 1989

Goyal, A., and Chopra, A. K. 1989. "Earthquake Analysis and Response of Intake-Outlet Towers," Report No. UCB/EERC-89/04, Earthquake Engineering Research Center, University of California, Berkeley.

Hall and Chopra 1980

Hall, J. F., and Chopra, A. K. 1980. "Dynamic Response of Embankment, Concrete Gravity and Arch Dams Including Hydrodynamic Interaction," Report No. UCB/EERC-80/39, Earthquake Engineering Research Center, University of California, Berkeley.

Hall, Woodson, and Nau 1989

Hall, R. L., Woodson, S. C., and Nau, J. M. 1989. "Seismic Stability Evaluation of Folsom Dam and Reservoir Project; Report 3, Concrete Gravity Dam," Technical Report GL-87-14, U.S. Army Engineer Waterways Experiment Station, Vicksburg, MS.

Haroun 1984

Haroun, M. A. 1984. "Stress Analysis of Rectangular Walls Under Seismically Induced Hydrodynamic Loads," *Bulletin of the Seismological Society of America*, Vol 74, No. 3, pp 1031-1041.

Hartzell 1978

Hartzell, S. 1978. "Earthquake Aftershocks as Green's Functions," *Geophysical Research Letter*, Vol 5, pp 1-4.

Hartzell 1985

Hartzell, S. 1985. "The Use of Small Earthquake as Green's Functions," *Strong Motion Simulation and Earthquake Engineering Applications*, Publication 85-02, R. E. Scholl and J. L. King, ed., Earthquake Engineering Research Institute, El Centro, CA, pp 22-1—22-8.

Hartzell, Frazier, and Brune 1978

Hartzell, S., Frazier, G. A., and Brune, J. N. 1978. "Earthquake Modeling in a Homogeneous Half-Space," *Bulletin of the Seismological Society of America*, Vol 68, pp 301-316.

Herrero and Bernard 1994

Herrero, A., and Bernard, P. 1994. "A Kinematic Self-Similar Rupture Process for Earthquake," *Bulletin of the Seismological Society of America*, Vol 83, pp 1216-1228.

Horton and Jacob 1997

Horton, S., and Jacob, K. 1997. Analysis of duration of ground motion in the central and eastern United States: preliminary report submitted to National Center for Earthquake Engineering Research (NCEER) for the NCEER Highway Project.

Housner 1957

Housner, G. W. 1957. "Dynamic Pressures on Accelerated Fluid Containers," *Bulletin of the Seismological Society of America*, Vol 47, pp 15-35.

Hudson 1979

Hudson, D. E. 1979. "Reading and Interpreting Strong Motion Accelerograms," Monograph, Earthquake Engineering Research Institute, Oakland, CA.

Hudson, Idriss, and Beikae 1994

Hudson, M., Idriss, I. M., and Beikae, M. 1994. "User's Manual for QUAD4M, a Computer Program to Evaluate the Seismic Response of Soil Structures Using Finite Element Procedures and Incorporating a Compliant Base," Center for Geotechnical Modeling, University of California, Davis.

Hughes 1987

Hughes, T. J. R. 1987. *The Linear Finite Element Method, Linear Static and Dynamic Finite Element Analysis*, Prentice-Hall, Englewood Cliffs, NJ.

Humar and Jablonski 1988

Humar, J. L., and Jablonski, A. M. 1988. "Boundary Element Reservoir Model for Seismic Analysis of Gravity Dams," *Earthquake Engineering and Structural Dynamics*, Vol 16, pp 1129-1156.

Husid 1969

Husid, R. L. 1969. "Analisis de Terremotos: Analisis General," *Revista del IDIEM*, Universidad de Chile, Santiago, Chile, Vol 8, No. 1, May, pp 21-42.

Hutchings and Wu 1990

Hutchings, L., and Wu, F. 1990. "Empirical Green's Functions from Small Earthquakes – A Waveform Study of Locally Recorded Aftershocks of the San Fernando Earthquake," *Journal of Geophysical Research*, Vol 95, pp 1187-1214.

Idriss 1979

Idriss, I. M. 1979. "Characteristics of Earthquake Ground Motions," *Proceedings of the ASCE Geotechnical Engineering Specialty Conference Earthquake Engineering and Soil Dynamics*, Pasadena, CA, June 19-21, 1978, American Society of Civil Engineers, Vol III pp 1151-1265.

Idriss and Sun 1992

Idriss, I. M., and Sun, J. I. 1992. "User's manual for SHAKE91," Center for Geotechnical Modeling, Department of Civil and Environmental Engineering, University of California, Davis.

Irikura 1983

Irikura, K. 1983. "Semi-Empirical Estimation of Strong Ground Motions During Large Earthquakes," *Bulletin, Disaster Prevention Research Institute*, Kyoto University, Kyoto, Japan, Vol 33, pp 63-104.

Itasca 1998

Itasca. 1998. "FLAC, Fast Lagrangian Analysis of Continua, Version 3.40 User's Guide," Itasca Consulting Group, Inc., Minneapolis, MN.

Jacobson 1949

Jacobson, L. S. 1949. "Impulsive Hydrodynamics of Fluids Inside a Cylindrical Tank and of Fluid Surrounding a Cylindrical Pier," *Bulletin of the Seismological Society of America*, Vol 39, pp 189-204.

Jordan and Dawkins 1990

Jordan, T. D., and Dawkins, W. P. 1990. "User's Guide: Computer Program for Two-Dimensional Analysis of U-Frame or W-Frame Structures (CWFRAM)" (X0091), Instruction Report ITL-90-6, available from U.S. Army Engineer Waterways Experiment Station, 3909 Halls Ferry Road, Vicksburg, MS.

Joyner 1995

Joyner, W. B. 1995. "Stochastic Simulation of Near-Source Earthquake Ground Motion," *Proceedings of Workshop on Modeling Earthquake Ground Motion at Close Distances*, September 5-6, 1990, EPRI Report EPRI TR-104975, Electric Power Research Institute, Palo Alto, CA.

Joyner and Boore 1986

Joyner, W. B., and Boore, D. M. 1986. "On Simulating Large Earthquake by Green's-Function Addition of Smaller Earthquakes," *Earthquake Source Mechanics, Maurice Ewing, Ser.*, S. Das et al., ed., American Geophysical Union, Washington, DC, Vol 6, pp 269-274.

Kennedy et al. 1984

Kennedy, R. P., Short, S. A., Merz, K. L., Tokarz, F. J., Idriss, I. M., Power, M. S., and Sadigh, K. 1984. "Engineering Characterization of Ground Motion Task 1: Effects of Characteristics of Free-Field Motion on Structural Response," Report NURGE/CR-3805, prepared for Division of Engineering Technology, Office of Nuclear Regulatory Research, U.S. Nuclear Regulatory Commission, Washington, DC.

Kotsubo 1965

Kotsubo, S. 1965. "Seismic Force Effect on Submerged Pier with Elliptical Cross-Sections," *Proceedings 3rd World Conference on Earthquake Engineering*, New Zealand, Vol II, pp 342-356.

Kramer 1996

Kramer, S. L. 1996. *Geotechnical Earthquake Engineering*, Prentice-Hall, New Jersey.

Kuo 1982

Kuo, J. S. -H. 1982. "Fluid-Structure Interactions: Added Mass Computations for Incompressible Fluid," Report No. UCB/EERC-82/09, Earthquake Engineering Research Center, University of California, Berkeley.

Lee and Finn 1978

Lee, M. K. W., and Finn, W. D. L. 1978. "DESRA-2, Dynamic Effective Stress Response Analysis of Soil Deposits with Energy Transmitting Boundary Including Assessment of Liquefaction Potential," Soil Mechanics Series No. 36, Department of Civil Engineering, University of British Columbia, Vancouver, Canada.

Leger and Leclerc 1996

Leger, P., and Leclerc, M. 1996. "Evaluation of Earthquake Ground Motions to Predict Cracking Response of Gravity Dams," *Engineering Structures*, Vol 18, No. 3, pp 227-239.

Li, Wang, and Shen 1992

Li, X. S., Wang, Z. L., and Shen, C. K. 1992. "SUMDES, a Nonlinear Procedure for Response Analysis of Horizontally-Layered Sites Subject to Multi-Directional Earthquake Loading," Department of Civil Engineering, University of California, Davis.

Liaw and Chopra 1973

Liaw, C.-Y., and Chopra, A. K. 1973. "Earthquake Response of Axisymmetric Tower Structures Surrounded by Water," Report No. EERC 73-25, Earthquake Engineering Research Center, University of California, Berkeley.

Liaw and Chopra 1974

Liaw, C.-Y. and Chopra, A. K. 1974. "Dynamic of Towers Surrounded by Water," *International Journal of Earthquake Engineering and Structural Dynamics*, Vol 3, No. 1.

Lilhanand and Tseng 1988

Lilhanand, K., and Tseng, W. S. 1988. "Development and Application of Realistic Earthquake Time-Histories Compatible with Multiple-Damping Design Spectra," *Proceedings of the 9th World Conference of Earthquake Engineering*, Tokyo-Kyoto, Japan, August 2-9, Japan Association for Earthquake Disaster Prevention.

Luco and Apsel 1983

Luco, J. E., and Apsel, R. J. 1983. "On the Green's Functions for a Layered Half-Space, I," *Bulletin of the Seismological Society of America*, Vol 73, pp 909-929.

Lysmer 1978

Lysmer, J. 1978. "Analytical Procedures in Soil Dynamics," Report No. UCB/EERC-78/29, University of California at Berkeley, Earthquake Engineering Research Center, Richmond, CA.

Lysmer and Kuhlemeyer 1969

Lysmer, J., and Kuhlemeyer, R. L. 1969. "Finite Dynamic Model for Infinite Media," *Journal of the Engineering Mechanics Division*, ASCE, Vol 95, pp 859-877

Lysmer et al. 1975

Lysmer, J., Ukada, T., Tsai, C.-F., and Seed, H. B. 1975. "FLUSH – A Computer Program for Approximate 3-D Analysis of Soil-Structure Interaction Problems," Report No. EERC/75-30, Earthquake Engineering Research Center, University of California, Berkeley.

Lysmer et al. 1981

Lysmer, J., Raissi, M., Tajirian, F., Vahdani, S., and Ostadan, F. 1981. "SASSI: A System for Analysis of Soil-Structure Interaction," University of California, Berkeley, Geotechnical Report No. 81-02.

Lysmer et al. 1991

Lysmer, J., Ostadan, F., Tabatabaie, M., Tajirian, F., and Vahdani, S. 1991. "SASSI User's Manual: A System for Analysis of Soil-Structure Interaction," Revision 0, University of California at Berkeley.

Mahin and Lin 1983

Mahin, S. A., and Lin, J. 1983. "Construction of Inelastic Response Spectra for Single-Degree-of-Freedom Systems, Computer Program and Applications," Report No. UCB/EERC-83/17, Earthquake Engineering Research Center, University of California, Berkeley.

Martin 1998

Martin, G. R. 1998. "Design Recommendations, Site Response, and Liquefaction," Report for MCEER Highway Project, submitted to Multidisciplinary Center for Earthquake Engineering Research, Buffalo, NY.

Matasovic 1993

Matasovic, N. 1993. "Seismic Response of Composite Horizontally-Layered Soil Deposits," Ph.D. Dissertation, Civil and Environmental Engineering Department, University of California, Los Angeles.

Mononobe and Matuo 1929

Mononobe, N., and Matuo, H. 1929. "On the Determination of Earth Pressures During Earthquakes," *Proceedings, World Engineering Congress*, Tokyo, Japan, 1929, Vol 9, Paper No. 388.

Mosher 1992

Mosher, R. L. 1992. "Three-Dimensional Finite-Element Analysis of Sheet-Pile Cellular Cofferdam," Technical Report ITL-92-1, U.S. Army Engineer Waterways Experiment Station, Vicksburg, MS.

Multidisciplinary Center for Earthquake Engineering Research 1999

Multidisciplinary Center for Earthquake Engineering Research. 1999. *Proceedings of the MCEER Workshop on Ground Motion Methodologies for the Eastern United States*, Memphis, TN, October 16-17, 1997, Technical Report MCEER-99-0016, N. Abrahamson and A. Becker, ed., Buffalo, NY.

Novak and El Hifnawy 1983

Novak, M., and El Hifnawy, L. 1983. "Effect of Soil-Structure Interaction on Damping of Structures," *Earthquake Engineering and Structural Dynamics*, Vol 11, pp 595-621.

Okabe 1924

Okabe, S. 1924. "General Theory of Earth Pressure and Seismic Stability of Retaining Wall and Dam," *Journal, Japan Society of Civil Engineers*, Vol 12.

Olson, Orcutt, and Frazier 1984

Olson, A. H., Orcutt, J., and Frazier, G. 1984. "The Discrete Wave Number/Finite Element Method for Synthetic Seismograms," *Geophysical Journal International of the Royal Astronomical Society*, Vol 77, pp 421-460.

Paulay and Priestley 1992

Paulay, T., and Priestley, M. J. N. 1992. *Seismic Design of Reinforced Concrete and Masonry Buildings*, John Wiley, New York.

Paz 1991

Paz, M. 1991. *Structural Dynamics, Theory and Computation*, 3rd ed., Van Nostrand Reinhold, New York.

Pyke 1992

Pyke, R. M. 1992. "TESS: A Computer Program for Nonlinear Ground Response Analyses," TAGA Engineering Systems and Software, Lafayette, CA.

Qiu 1998

Qiu, P. 1998. "Earthquake-Induced Nonlinear Ground Deformation Analyses," Ph.D. Dissertation, University of Southern California, Los Angeles.

Quest Structures 1990

QUEST Structures. 1990. "Nonlinear Earthquake Analysis of Portugues Dam," Report prepared for U.S. Army Engineer District, Jacksonville, Jacksonville, FL.

Raphael 1984

Raphael, J. M. 1984. "The Tensile Strength of Concrete," *ACI Journal Proceedings*, Vol 81, pp 158-165.

Raphael 1986

Raphael, J. M. 1986. "Mass Concrete Properties for Seismic Evaluation of Engelbright Dam, Folsom Dam, and Pine Flat Dam," prepared under Contract No. DACW05-86-P-1049, for the U.S. Army Engineer District, Sacramento, Sacramento, CA.

Rashed 1982

Rashed, A. 1982. "Dynamic Analysis of Fluid-Structure Systems," Report No. EERL82-03, Earthquake Engineering Research Laboratory, California Institute of Technology, Pasadena.

Reid 1911

Reid, H. F. 1911. "The Elastic-Rebound Theory of Earthquake," *University of California Publications in the Geological Sciences*, Vol 6, pp 413-44.

Schneider, Abrahamson, and Hanks 1996

Schneider, J. F., Abrahamson, N. A., Hanks, T. C. 1996. "Ground Motion Modeling of Scenario Earthquakes at Yucca Mountain: Provisional Draft Final Report for Activity 9.3.1.17.3.3," U.S. Geological Survey.

Schnabel, Seed, and Lysmer 1972

Schnabel, P. B., Seed, H. B., and Lysmer, J. 1972. "SHAKE – A Computer Program for Earthquake Response Analysis of Horizontally Layered Sites," Report No. EERC 72-12, Earthquake Engineering Research Center, University of California, Berkeley.

Seed and Idriss 1969

Seed, H. B., and Idriss, I. M. 1969. "Influence of Soil Conditions on Ground Motions During Earthquakes," *Journal of Soil Mechanics and Foundation Division*, ASCE, Vol 95, No. SM1, pp 99-137.

Seed and Idriss 1970

Seed, H. B., and Idriss, I. M. 1970. "Soil Moduli and Damping Factors for Dynamic Response Analysis," Report No. EERC - 70/10, Earthquake Engineering Research Center, University of California, Berkeley.

Seed et al. 1984

Seed, H. B., Wong, R. T., Idriss, I. M., and Tokimatsu, K. 1984. "Moduli and Damping Factors for Dynamic Analyses of Cohesionless Soils," *Journal of Geotechnical Engineering*, ASCE, Vol 112, No. 11, pp 1016-1032.

Silva and Lee 1987

Silva, W., and Lee, K. 1987. "State-of-the-art for Assessing Earthquake Hazards in the United States; Report 24, WES RASCAL Code for Synthesizing Earthquake Ground Motions," Miscellaneous Paper S-73-1, U.S. Army Engineer Waterways Experiment Station, Vicksburg, MS.

Silva, Chiou, and Somerville 1995

Silva, W., Chiou, S.-J., and Somerville, M. 1995. "Finite and Point Source RVT Modeling," *Proceedings of Workshop on Modeling Earthquake Ground Motion at Close Distances*, September 5-6, 1990, EPRI Report TR-104975, Electric Power Research Institute, Palo Alto, CA.

Silva et al. 1990

Silva, W., Darragh, R., Stark, C., Wong, I., Stepp, J. C., Schneider, J. F., and Chiou, S.-J. 1990. "A Methodology to Estimate Design Response Spectra in the Near-Source Region of Large Earthquake Using the Band-Limited-White Noise Ground Motion Model," *Proceedings, 4th U.S. National Conference on Earthquake Engineering*, Palm Springs, CA, May 20-24, 1990, Earthquake Engineering Research Institute, El Cerrito, CA, Vol 1, pp 487-494.

Somerville 1992

Somerville, P. G. 1992. "Engineering Applications of Strong Motion Simulation," *Tectonophysics*, Vol 218, pp 195-219.

Somerville 1997

Somerville, P. G. 1997. "The Characteristics and Quantification of Near Fault Ground Motion," *Proceedings of the FHWA/NCEER Workshop on the National Representation of Seismic Ground Motion for New and Existing Highway Facilities*, San Francisco, CA, May 29-30. Technical Report NCEER-97-0010, I. M. Friedland, M. S. Power, and R. L. Mayes, ed., National Center for Earthquake Engineering Research, Buffalo, NY.

Somerville 1998

Somerville, P. 1998. "Development of an Improved Representation of Near-Fault Ground Motions," *Proceedings of the SMIP98 Seminar on Utilization of Strong Motion Data*, Oakland, California, California Strong Motion Instrumentation Program, Division of Mines and Geology, California Department of Conservation, Sacramento, CA.

Somerville, Sen, and Cohee 1991

Somerville, P. G., Sen, M. K., and Cohee, B. P. 1991. "Simulations of Strong Ground Motion Recorded During the 1985 Michoacan, Mexico and Valparaiso, Chile, Earthquakes," *Bulletin of the Seismological Society of America*, Vol 81, pp 1-28.

Somerville et al. 1997

Somerville, P. G., Smith, N. F., Graves, R. W., and Abrahamson, N. A. 1997. "Modification of Empirical Strong Ground Motion Attenuation Relations to Include the Amplitude and Duration Effects of Rupture Directivity," *Seismological Research Letters*, Vol 68, No. 1, pp 199-222.

Sun, Golesorkhi, and Seed 1988

Sun, J. I., Golesorkhi, R., and Seed, H. B. 1988. "Dynamic Moduli and Damping Ratios for Cohesive Soils," Report No. EERC 88-15, University of California, Berkeley.

Sykora, Wahl, and Wallace 1992

Sykora, D. W., Wahl, R. E., and Wallace, D. C. 1992. "WESHAKe for Personal Computers; Report 1 (Version 1.0), USACE Geotechnical Earthquake Engineering software," Instruction Report GL-92-4, U.S. Army Engineer Waterways Experiment Station, Vicksburg, MS.

Tan and Chopra 1995

Tan, H., and Chopra, A. K. 1995. "Earthquake Analysis and Response of Concrete Arch Dams," Report No. EERC - 95/07, Earthquake Engineering Research Center, University of California, Berkeley.

Trifunac and Brady 1975

Trifunac, M. D., and Brady, A. G. 1975. "A Study of the Duration of Strong Earthquake Ground Motion," *Bulletin of the Seismological Society of America*, Vol 65, No. 3, pp 581-626.

U.S. Army Engineer District, Jacksonville 1986

U.S. Army Engineer District, Jacksonville. 1986. "Concrete Properties, Portugues and Bucana Project, Puerto Rico," Design Memorandum No. 20, Jacksonville, FL.

U.S. Army Engineer District, Jacksonville 1988a

U.S. Army Engineer District, Jacksonville. 1988a. "Structural Properties and Special Studies, Portugues and Bucana Project, Puerto Rico," Design Memorandum No. 21, Jacksonville, FL.

U.S. Army Engineer District, Jacksonville 1988b

U.S. Army Engineer District, Jacksonville. 1988b. "Foundation Investigations, Portugues and Bucana Project, Puerto Rico," Design Memorandum No. 22, Jacksonville, FL.

U.S. Army Engineer District, Jacksonville 1990

U.S. Army Engineer District, Jacksonville. 1990. "Portugues and Bucana Project, Puerto Rico, Design Memorandum No. 24, Portugues Dam," Jacksonville, FL.

U.S. Army Engineer District, Los Angeles 1992

U.S. Army Engineer District, Los Angeles. 1992. "Appendix C1, Feature Design Memorandum, Seven Oaks Dam Outlet Works," Los Angeles, CA.

U.S. Army Engineer District, Louisville 1989

U.S. Army Engineer District, Louisville. 1989. "General Design Memorandum; Appendix B, Geology and Foundations," Design Memorandum No. 1, Louisville, KY.

U.S. Army Engineer District, Louisville 1990

U.S. Army Engineer District, Louisville. 1990. "Supplement No. 1 of Design Memorandum No. 1, General Design Memorandum," Louisville, KY.

U.S. Army Engineer District, Louisville 1992

U.S. Army Engineer District, Louisville. 1992. "Locks, Feature Design Memorandum, Olmsted Locks and Dam," Design Memorandum No. 7, Louisville, KY.

U.S. Army Engineer District, Louisville 1994a

U.S. Army Engineer District, Louisville. 1994a. "Locks, Feature Design Memorandum, Olmsted Locks and Dam," Design Memorandum No. 7 (Supplement), Louisville, KY.

U.S. Army Engineer District, Louisville 1994b

U.S. Army Engineer District, Louisville. 1994b. "Locks, Feature Design Memorandum," Appendix B, Design Memorandum No. 7 (Supplement), Louisville, KY.

U.S. Army Corps of Engineers 1999

U.S. Army Corps of Engineers. 1999. "EQTIME2D: Nonlinear Time-History Analysis of 2D Concrete Gravity Dam Sections," Engineering Research and Development Center, Waterways Experiment Station, Vicksburg, MS.

Vanmarcke and Lai 1980

Vanmarcke, E. H., and Lai, S. P. 1980. "Strong-motion Duration and RMS Amplitude of Earthquake Records," *Bulletin of the Seismological Society of America*, Vol 70, No. 4, August, pp 1293-1307.

Veletsos and Younan 1994

Veletsos, A. S., and Younan, A. H. 1994. "Dynamic Soil Pressures on Rigid Vertical Walls," *Earthquake Engineering and Structural Dynamics*, Vol 23, pp 275-301.

Vucetic and Dobry 1991

Vucetic, M., and Dobry, R. 1991. "Effects of Soil Plasticity on Cyclic Response," *Journal of Geotechnical Engineering*, ASCE, Vol 117, No. 1.

Wald and Heaton 1994

Wald, D. J., and Heaton, T. H. 1994. "A Dislocation Model for the 1994 Northridge California Earthquake Determined from Strong Ground Motions," Open File Report 94-278, U.S. Geological Survey.

Wang and Makdisi 1999

Wang, Z. L., and Makdisi, F. I. 1999. "Implementing a Bounding Surface Hypoplasticity Model for Sand into the FLAC Program," *FLAC and Numerical Modeling in Geomechanics; Proceedings of the International FLAC Symposium on Numerical Modeling in Geomechanics*, Minneapolis, MN, 1-3 September 1999, Christine Detourney and Roger Hart, ed., Balkema, Rotterdam, The Netherlands.

Westergaard 1933

Westergaard, H. M. 1933. "Water Pressures on Dams During Earthquakes," *Transactions, American Society of Civil Engineers*, Vol 98.

Wolf 1995

Wolf, J. P. 1995. "Discussion on a paper by A. S. Veletsos and A. H. Younan," *Earthquake Engineering and Structural Dynamics*, Vol 24, pp 1287-1291.

Wolf 1988

Wolf, J. P. 1988. *Soil-Structure-Interaction Analysis in Time Domain*, Prentice-Hall, Englewood Cliffs, NJ.

Wolf and Darbre 1984

Wolf, J. P., and Darbre, G. R. 1984. "Dynamic Stiffness Matrix of Soil by the Boundary Element Method," *Earthquake Engineering and Structural Dynamics*, Vol 12, pp 401-416.

Zeng, Anderson, and Yu 1994

Zeng, Y., Anderson, J. G., and Yu, G. 1994. "A Composite Source Model for Computing Realistic Synthetics Strong Ground Motions," *Geophysical Research Letters*, Vol 21, pp 725-728.

Zhang and Chopra 1991

Zhang, L. -P., and Chopra A. K. 1991. "Impedance Functions for Three-dimensional Foundations Supported on an Infinitely Long Canyon of Uniform Cross-Section in a Homogeneous Half-Space," *Earthquake Engineering and Structural Dynamics*, Vol 20, pp 1011-1028.

Appendix B Synthesizing a Suite of Simulated Recorded Motions

B.1 Introduction

a. Using existing time-histories recorded under conditions representative of the design earthquake is an appealing and logical approach to obtain design time-histories. However, there may not always be an adequate suite of recorded motions that are representative of the design earthquake conditions in terms of such factors as the tectonic environment, earthquake magnitude and other characteristics, earthquake source-to-site distance, and subsurface conditions. Despite the significant increase in the number of recordings during the past 25 years, data gaps remain. For example, there is no record representing the near-source region of a large ($M_w \sim 8$) strike-slip earthquake that has a high probability to occur on the San Andreas Fault system in this century. Similarly, in the northwestern United States and Alaska, where a very large subduction zone earthquake ($M_w \sim 9$) is possible, recordings from this type of megathrust earthquake are also unavailable. In the central and eastern United States, there are only a few acceleration time-histories from moderate to large earthquakes at close distances.

b. An alternative or supplement to using recorded time-histories is to develop synthetic time-histories based on the theoretical models of earthquake source processes and seismic wave propagation. These models can be used to produce more realistic time-histories than those produced by methods that do not contain seismological controls. The synthetic motions may be computed for three orthogonal components of acceleration at a site.

c. There is a large diversity of approaches to ground motion simulations. These approaches reflect differences in motivations, degree of simplification, and objectives behind individual approaches. Nevertheless, each method accommodates the common aspects that seismic waves are generated by a ruptured fault of finite dimensions and are propagated through the crust to the site at the surface of the earth. In this appendix, these basic aspects of ground motion simulation are discussed, and information relevant to the generation of time-histories for use in engineering design is presented. The objective is to provide an understanding of the basic ideas behind time-history simulations. Validating the simulation procedures is also discussed in this appendix.

B.2 Ground Motion Simulation Model

The computational model for synthetic seismograms consists of three driving processes: the seismic source process, the process of seismic wave propagation from the source region to the design site, and the process of shallow site response. The issue of site response is discussed in Section 5.6; this appendix focuses on simulations for rock site conditions not including local site response effects. It should be noted that randomness is often introduced, either in the source process or in the wave propagation, to model the complexity of observed seismograms.

a. *Earthquake source process.*

(1) Reid's elastic-rebound theory (Reid 1911) is the foundation of the modern earthquake source model now being widely adapted by the seismological community. Reid's hypothesis explains the origin of earthquakes by a fracture in prestrained crust. In his elastic-rebound theory, strains are accumulated in the crustal rock surrounding the fault. The rock finally reaches a failure point. Rupture then takes place, and the strained rock rebounds on each side of the fault (fault slips) under its own stresses until the strain is largely or completely released. The abrupt fault slip is the cause of seismic waves and hence of macroseismic shaking.

An important notion conveyed by Reid's elastic-rebound theory is that fault rupture takes place at first in a small area and quickly grows into a larger area at a rate not greater than the compressional wave velocity of the rock. Furthermore, a point on the fault starts to slip only when the moving rupture front arrives at that point, and it takes a finite amount of time (rise time) for that point to complete the slip. The propagating rupture front and finite rise time are essential to the explanation of directivity, near-fault velocity pulses, and other important features of the recorded earthquake motions at distances close to a finite fault. Rupture velocity, rupture initiation point, and slip-time functions over the ruptured area are the primary source parameters needed for the simulation of time-histories.

(2) Studies of previous earthquakes suggest that the actual fault rupture process is spatially and temporally complex. Therefore, in ground motion simulations, randomness is often utilized to characterize the source process. A source model is called a deterministic model if there is no randomness in the model parameters. A deterministic model is most appropriate for the regular part of a rupture process that dominates the generation of low-frequency waves. The jerky and irregular part of the rupture processes generates high-frequency waves and is usually characterized as a stochastic process because the rupture is usually too complicated to be described deterministically. It is generally believed that a hybrid source with both deterministic components (for low-frequency waves) and stochastic components (for high-frequency waves) is more robust than a deterministic or a stochastic process alone. Examples of simulation procedures that use stochastic and hybrid source models are given in paragraph B.3.

b. Wave propagation.

(1) Seismic waves propagating away from the ruptured fault undergo geometrical spreading, attenuation of wave amplitude due to inelasticity of the crust, reflection and refraction at the interface of distinct rock types, and scattering from lateral inhomogeneities. To simulate these path effects, a theoretical Green's function¹ can be calculated for a crustal model. The more complicated the crustal model, the more difficult and expensive to compute the Green's function numerically. The important factor determining the computational effort is the highest frequency of the simulated ground motions. Computational time increases almost as a cubic power of the maximum frequency of the simulations.

(2) Computation of the theoretical Green's function requires knowledge of the crustal parameters such as the compressional- and shear-wave velocities, density, and damping factor (or seismic Q factor, where $Q \approx 0.5/\text{damping ratio}$). Different idealizations of the crustal parameter distributions in the earth's crust are being used for time-history simulations. In a homogeneous model, the crustal parameters are uniform throughout the crust, and the model has the simplest exact Green's function with $1/R$ geometrical spreading, where R is the hypocentral distance. This simple Green's function has been used in several stochastic simulation procedures (Boore 1983; Silva and Lee 1987). Green's function for a more realistic model consisting of horizontal layers of rock can also be calculated (Olson, Orcutt, and Frazier 1984; Luco and Apsel 1983). This layered model is now widely used in ground motion simulation practice to capture the first-order path effect of the earth's crust. When the site is in a sedimentary basin or is expected to experience topographic effects, then a crustal model involving lateral variation of rock properties and nonplanar geometry may be used. Complex wave phenomena (such as mode conversions, energy focusing, scattering, and diffraction) resulting from this type of large-scale heterogeneity are often important to the simulated ground motions. Green's function for this kind of complicated crustal model is feasible only via numerical methods such as finite element or finite difference, and these methods are time-consuming and are often limited to low-frequency calculations.

(3) Scattered waves from the small-scale heterogeneities of the earth's crust contribute significantly to the complexity of a recorded time-history. They prolong the ground motion duration, redistribute energies

¹ Green's function is the response of the earth to a seismic point source. It is a function of the site and source locations. A point source is the fundamental source that can be used as a building block to form a more general source.

among the three orthogonal components, and contribute to the spatial incoherence of ground motions. Lack of scattered waves in theoretical models led to the underprediction of strong motion duration of Northridge records by a factor of 1.3 and higher (Aki et al. 1995).

(4) An alternative to the theoretical Green's function is the empirical Green's function (Hartzell 1978, 1985; Irikura 1983; Hutchings and Wu 1990). An empirical Green's function is a recorded three-component set of time-histories of a small earthquake whose source mechanism and propagation path are similar to those of the design earthquake. This definition requires the empirical Green's function to be recorded at the site of interest, and its hypocenter occurs on the fault of interest. In keeping with the concept of Green's function, the magnitude of the event should be small enough that the source approximates a point source. The empirical Green's function is considered more realistic than the theoretical one in the high-frequency range (above 0.5 to 1.0 Hz); at lower frequencies, the signal-to-noise ratio is usually not good enough to make the recording useful. The main difficulty with the empirical Green's function approach is that it requires a sufficient number of them to cover the entire ruptured area. To overcome the lack of empirical Green's functions, approximations by extrapolating or interpolating the available empirical Green's functions are commonly made.

c. Ground motion simulations. Given the fault slip model and Green's functions, ground motions are computed using the representation theorem (Aki and Richards 1980; Hartzell, Frazier, and Brune 1978). The representation theorem involves a time convolution of the slip-time function with the Green's function and a surface integral of the convoluted Green's function over the rupture surface. The representation theorem allows the construction of ground motions from a finite source by integrating ground motions from simple sources (the convoluted Green's functions). In the computer implementation, the surface integral is typically approximated by a summation over a grid of points. Under this approximation, the simulation procedure simply sums a suite of Green's functions lagged in time. The time lag is the delay time caused by the rupture propagation plus the time needed for the seismic waves to travel from the corresponding point source to the site.

B.3 Examples of Simulation Procedures

a. A detailed review of some of the ground motion simulation methods currently in use can be found in reports published by Electric Power Research Institute (1995), Aki et al. (1995), and Schneider, Abrahamson, and Hanks (1996). Motivations behind these procedures are quite diverse. Some are intended mainly to provide an estimate of response spectra, and some are better suited to generating synthetic time-histories. In the following paragraphs, several simulation procedures are discussed, and examples of time-histories computed using these procedures are also given.

b. Boore (1983) developed a Band-Limited-White-Noise model for stochastic simulation of high-frequency ground motions. This simulation procedure does not generate ground motions from a given stochastic slip model. Instead, this procedure generates random white noise, multiplies it by a window function appropriate for the expected source duration, and then filters the windowed white noise to obtain a time-history having a band-limited Fourier amplitude spectrum specified by the T^2 source model (Brune 1970) and incorporating wave propagation effects of a homogeneous crust with $1/R$ geometrical attenuation. Silva and Lee (1987) use a similar formulation for the Fourier amplitude spectrum, but they use the phase spectrum from a natural time-history to generate the synthetic time-history. These stochastic procedures are well calibrated and validated for calculation of response spectra. However, it should be noted that the main motivation of these two stochastic methods is to simulate the average of the two horizontal response spectra, and they are not specifically aimed at generating a three-component set of time-histories that include the near-fault features and wave propagation effects. Related computer codes RASCAL (Silva and Lee 1987) and SMSIM (Boore 1996) are publicly available. In Figure B-1, time-histories obtained using these two programs

are illustrated for an earthquake of magnitude M_w 6.7 at distance of 5 km. The RASCAL simulation uses the Fourier phase spectra from the Newhall record (USC station 56) of the 1994 Northridge earthquake to generate synthetic time-histories. The source model of these two simulation procedures is not a finite-source model because it does not explicitly simulate the propagating rupture of a finite source. Extensions to the finite-source model have been developed by Joyner and Boore (1986), Sliva et al. (1990), Silva, Chiou, and Somerville (1995), and Beresnev and Atkinson (1997).

c. Simulation procedures that use a hybrid slip model and Green's function of a layered crust have shown promise in generating realistic, broad-band three-component seismograms. Examples of this type of procedure include the composite-source approach (Zeng, Anderson, and Yu 1994), the self-similar slip model (Herrero and Bernard 1994; Joyner 1995), and the hybrid theoretical/empirical source approach (Somerville, Sen, and Cohee 1991; Somerville 1992). Two sets of three-component synthetic time-histories generated using the self-similar slip model are shown in Figure B-2. These time-histories were simulated at the Newhall recording station (USC Station 56) for the 1994 Northridge earthquake. Scattered waves are included in the simulations. A hybrid source model is used in the simulation of Set 1 that consists of a stochastic slip distribution superimposed on the deterministic slip model of the Northridge earthquake obtained by modeling the recorded velocity time-histories (Wald and Heaton 1994) at a large number of sites. As a result, Set 1 shows a greater resemblance to the actual Newhall record from the Northridge earthquake than does Set 2, where a slip model unrelated to the Northridge source model is used for the simulation. It is encouraging to see that both sets of synthetics exhibit the near-fault velocity pulse and the stronger fault-normal component (N 32° E) of the velocity pulse (Somerville et al. 1997) that is expected for a near-fault record.

B.4 Controls on Simulation Processes

a. *Validation of simulation procedures.* Before a procedure is used to generate ground motions for engineering applications, it should be formally validated. Systematic validation of a numerical procedure is needed to provide a check that the computational model of the procedure is adequate and to provide estimates of the modeling variability. Abrahamson, Somerville, and Cornell (1990) developed a method for validating numerical simulation procedures. The validation is accomplished by comparing how well the simulation procedure reproduces the characteristics of recorded motions from past earthquakes. Recently, this approach has been used to evaluate several simulation procedures by the Southern California Earthquake Center (Aki et al. 1995), Schneider, Abrahamson, and Hanks (1996), and the Multidisciplinary Center for Earthquake Engineering Research (1999). These validations have been based on the average of two horizontal response spectra. Strong-motion duration has been examined in these studies, but other time-domain characteristics (such as sequencing of various seismic phases and near-fault velocity pulse) have not been considered.

b. *Production and adjustment of simulated time-histories.* Simulated time-histories should be produced for the design earthquake conditions in terms of such factors as magnitude, fault dimensions, strike and dip angles of fault, style of faulting, and tectonic environment. Ground motion characteristics of these simulated time-histories should be similar to those estimated for the design conditions. If there are excessive differences, then one needs to scale the simulated time-history to the desired level and perform spectrum matching if necessary. Scaling and spectrum matching processes are described in Chapter 5. One also needs to make sure the desired special characteristics, such as the near-fault velocity pulse, are present in the simulated ground motions if conditions justify their existence.

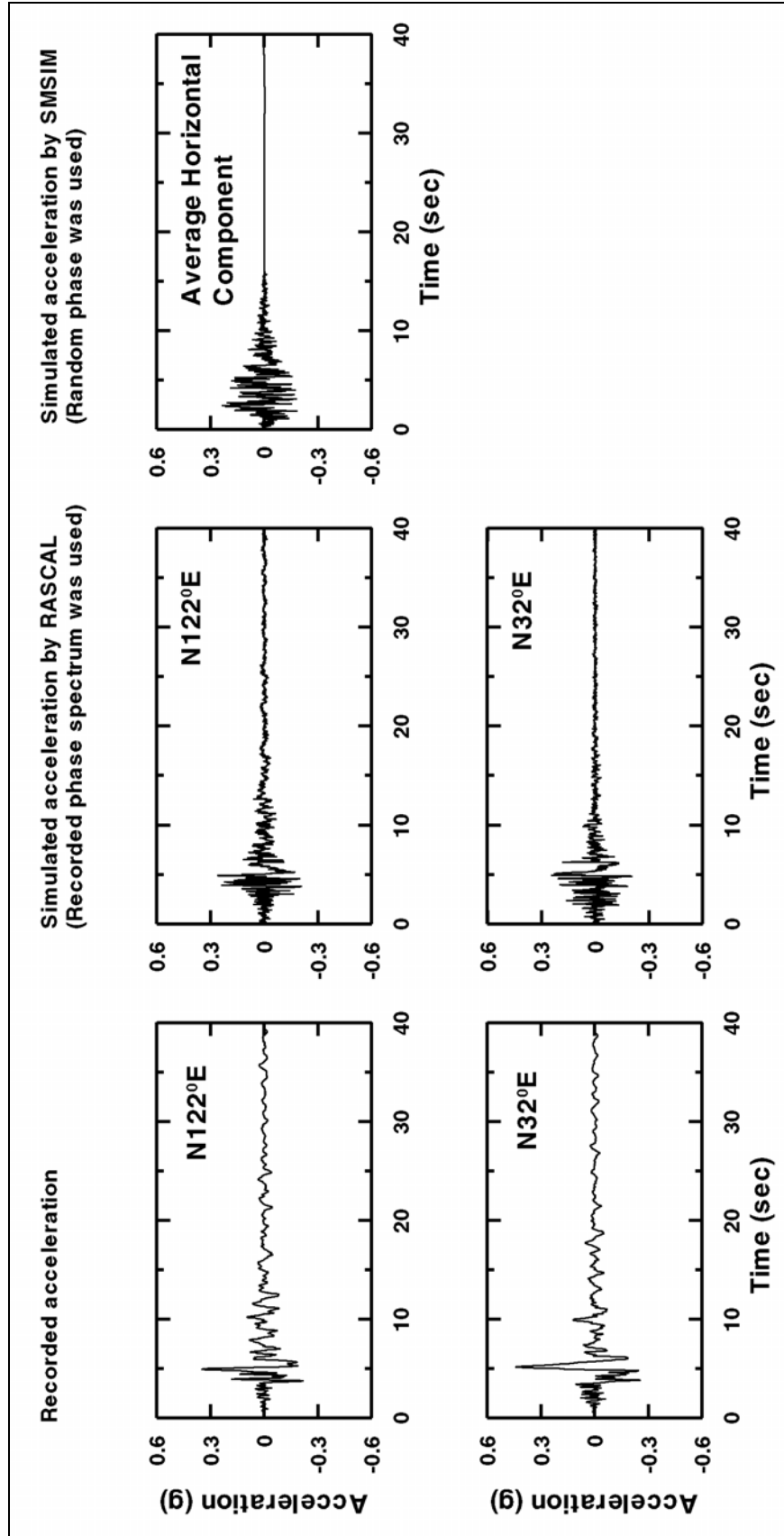


Figure B-1. Comparison of records simulated by stochastic procedure to the records at Newhall (USC Station 56) during the 1994 Northridge earthquake (Continued)

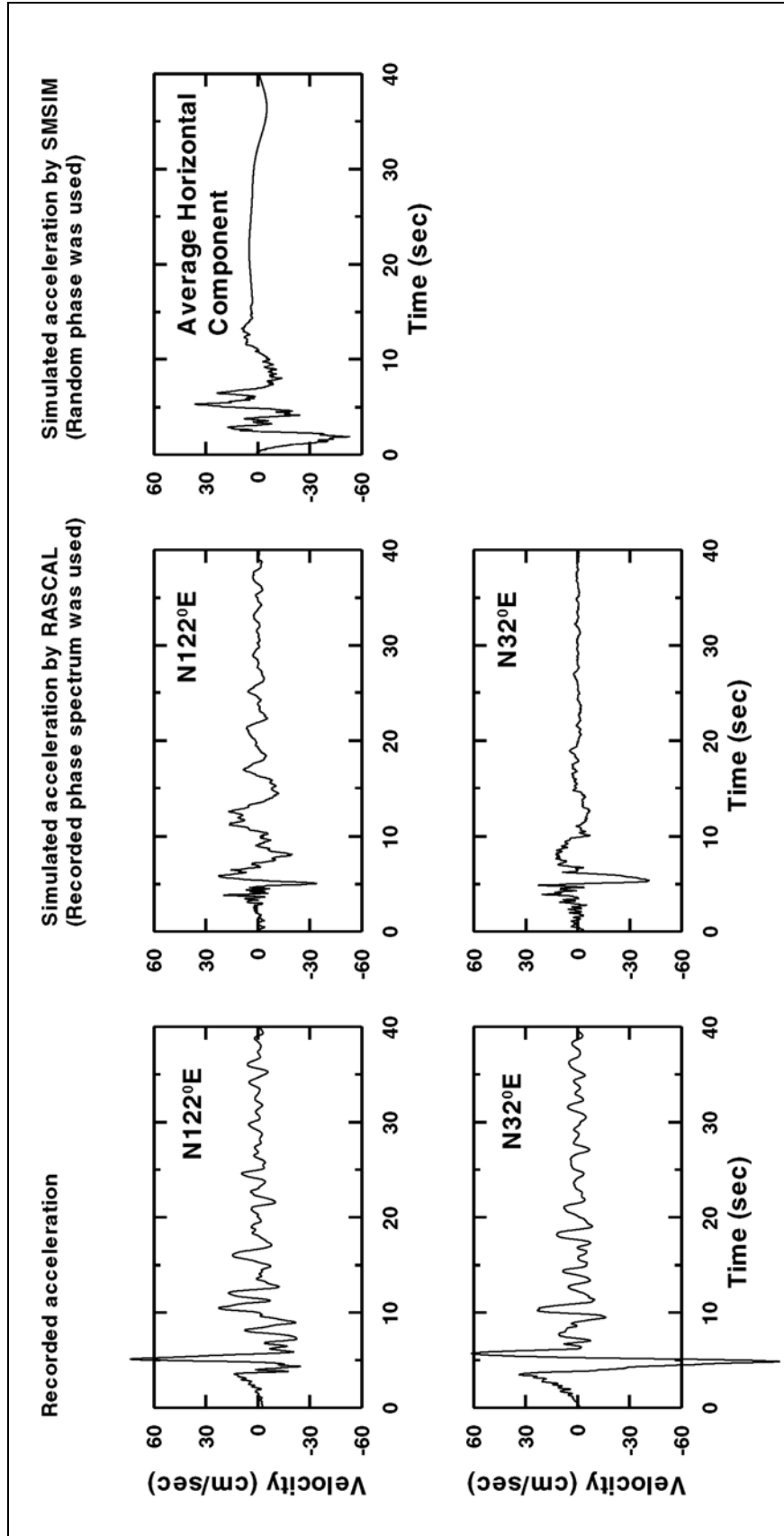


Figure B-1. (Concluded)

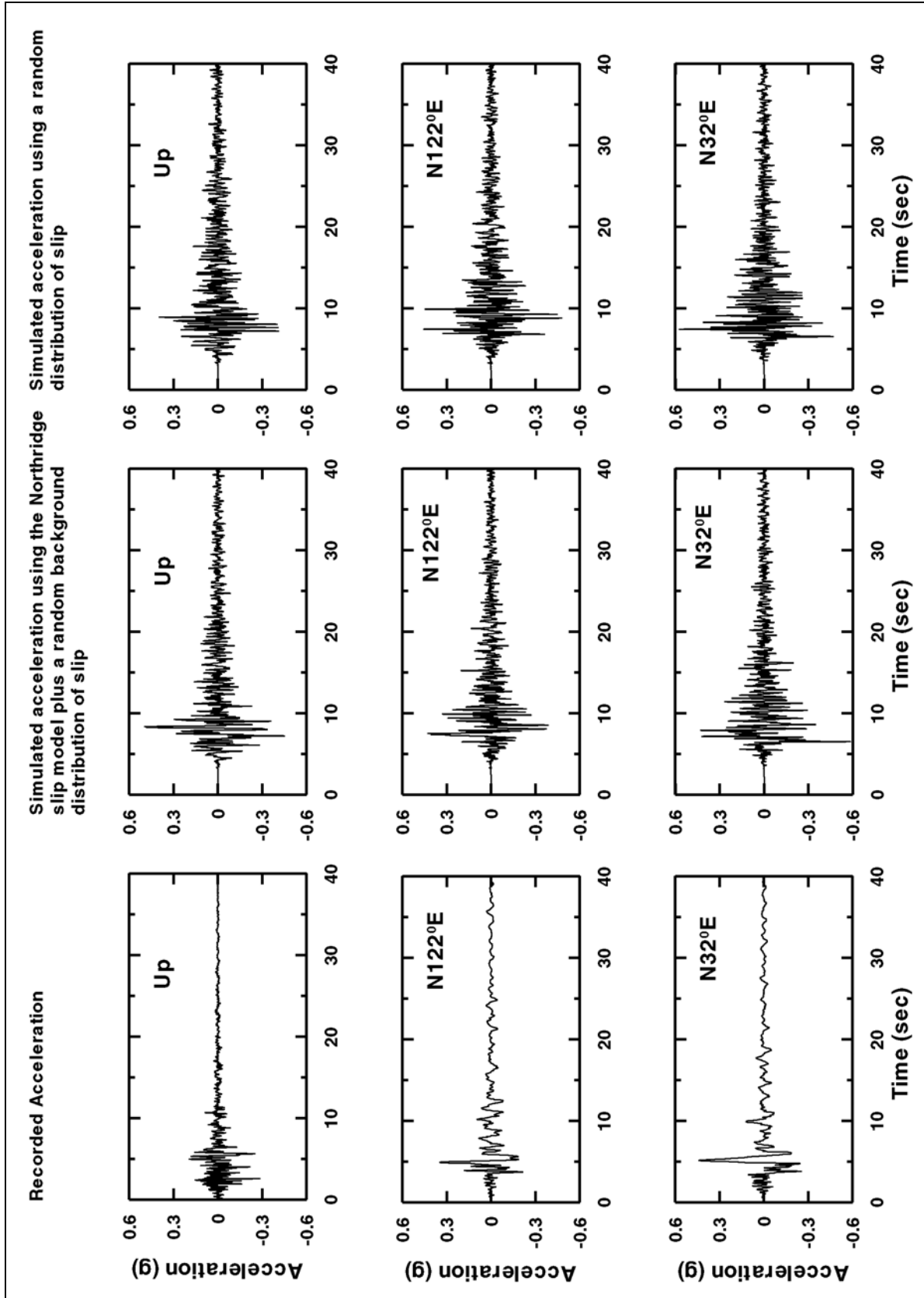


Figure B-2. Comparison of records simulated using a Green function/kinematic slip procedure to the records recorded at Newhall (USC Station 56) during the 1994 Northridge earthquake (Continued)

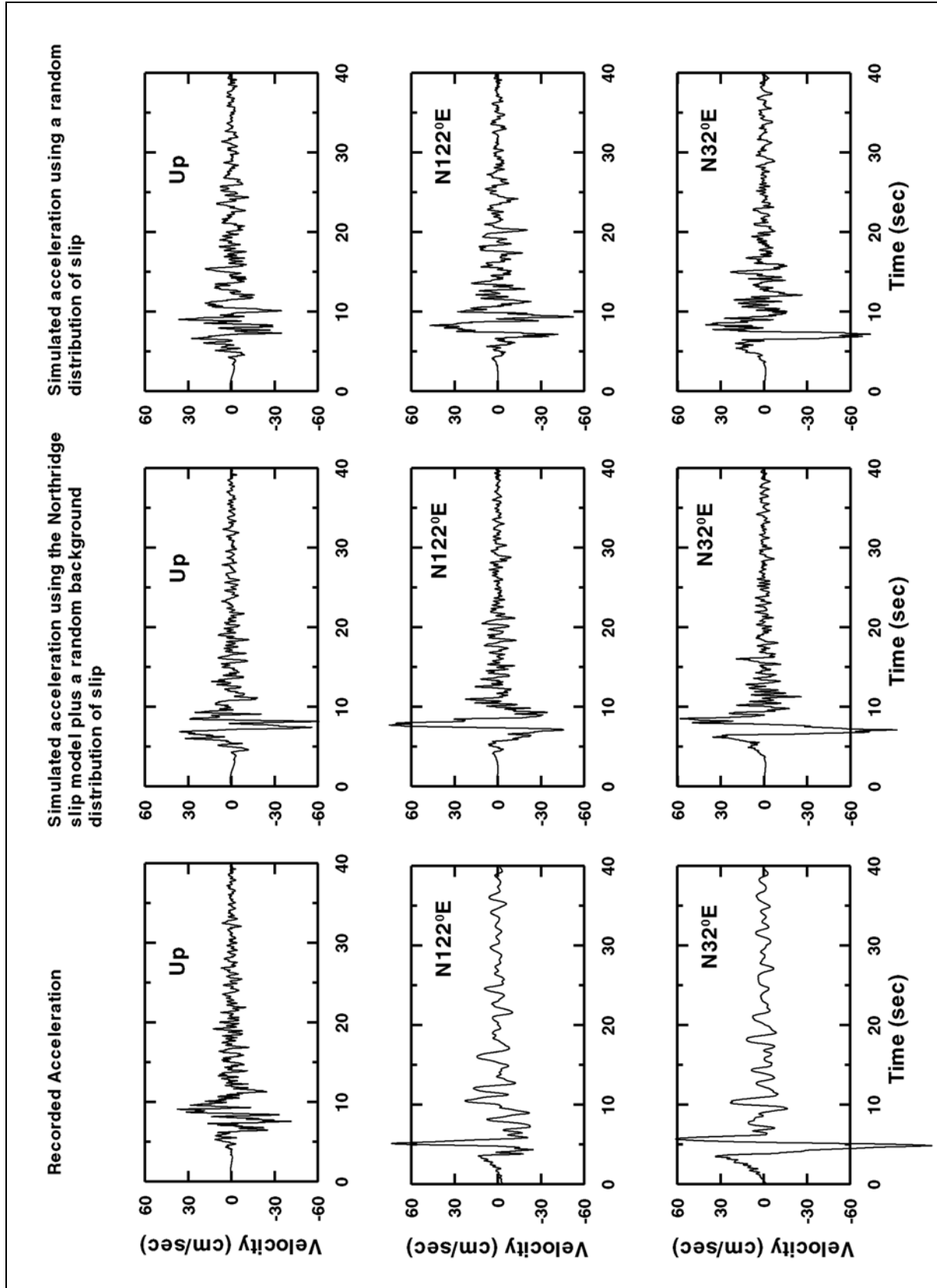


Figure B-1. (Concluded)

Appendix C Spectrum Matching

C.1 Spectrum Matching Process

a. This appendix discusses the generation of realistic acceleration time-histories whose response spectra closely match a smooth design response spectrum. The spectrum-matching procedure begins with an acceleration time-history whose characteristics reasonably represent the ground motions expected for the site. (Guidelines for selecting such an initial time-history are discussed in paragraph 5.3.) This initial time-history has individual spectral peaks and valleys that deviate from the smooth design spectrum. The objective of the matching procedure is to reduce these deviations in the period range important to the structure while preserving the nonstationary characteristics (which are critical to nonlinear analysis) of the initial time-history as much as possible. The design spectral values are generally given at a fine grid of periods so that the response spectrum from the matched time-history is also smooth at the intervening periods (paragraph 5.5*f*). Convergence with the design spectrum is achieved when spectral values of the modified time-history are within specified deviations from the design values at every period being matched (paragraph 5.5*c*).

b. Spectrum matching is conducted by adding (subtracting) elementary wavelets to (from) the initial acceleration time-history. Each wavelet is intended to match the response spectrum at one period. Matching is performed either period by period or simultaneously for a group of periods; the latter usually provides a better convergence property, and it is adopted in this study. Spectral convergence typically requires several iterations of matching. Excessive iterations should be avoided to assure the preservation of nonstationary characteristics of the initial time-history. The existing matching procedures can be divided into two categories.

(1) Time-Domain Approach (Lilhanand and Tseng 1988; Abrahamson 1992). Matching is accomplished by adding (subtracting) finite-duration wavelets to (from) the initial time-history. This approach normally provides a close fit to the target. One representative wavelet is the impulse response time-history of the single-degree-of-freedom oscillator reversed in time. This wavelet abruptly ceases (i.e., becomes zero) after the peak-response time and thus limits the temporal extent of the modification made to the time-history. Another commonly used wavelet is the tapered sinusoid with the level of tapering being period dependent. Timing of these wavelets is selected so that it is in phase with the peak response of the acceleration time-history. Detailed descriptions of the mathematical formulation and the numerical algorithms are given in Lilhanand and Tseng (1988) and Abrahamson (1992).

(2) Frequency-Domain Approach (Gasparini and Vanmarcke 1976; Silva and Lee 1987; Bolt and Gregor 1993). The frequency-domain matching adjusts only the Fourier amplitudes while the Fourier phases are kept unchanged. This procedure is equivalent to adding or subtracting sinusoids (with the Fourier phases of the initial time-history) in the time domain and does not always provide as close a fit to the design spectrum as the time-domain approach. Because the sinusoids extend the entire length of the time-history, the spectrum-compatible motion produced by this procedure shows greater visual differences from the initial time-history than does the time-domain approach.

c. To preserve the nonstationary characteristics of the initial time-history, it is essential to start with an acceleration time-history whose spectrum is as close to the target spectrum as possible in the period range of interest. A close initial fit also ensures a speedy convergence to the design values. In many cases, a good initial match can be obtained by simply applying a single scale factor to the initial time-history. After spectrum matching, the following checks on the resulting acceleration time-history are recommended in addition to checking the spectrum match:

(1) A check should be made for baseline drift in the final time-history. The baseline should be corrected, and the resulting baseline-corrected acceleration time-history should be checked again for spectrum compatibility, then rematched if necessary. Baseline correction typically has little effect on the spectral values in the period ranges of interest.

(2) The acceleration, velocity, and displacement time-histories should be examined to ensure that they are reasonably close to the original or target values in terms of peak values, wave form, strong shaking duration, and other critical features such as the near-fault velocity pulse (fling).

(3) Power spectral density (PSD) functions should be examined to ensure a broad distribution of energy in the final spectrum-compatible motion as a function of Fourier period. There should not be significant deficiencies in the energy at periods important to the structure.

C.2 Examples

a. A target spectrum was specified for 5 percent damping at 220 periods ranging from 0.03 to 2 sec. Ten horizontal acceleration time-histories were selected and matched to the target spectrum using both the time-domain and frequency-domain approaches. The spectral value at the 0.03-sec period was taken as equal to the peak ground acceleration (PGA) value. For these examples, multiple-damping design spectra were not specified. Before matching was done, each record was scaled so that the initial overall fit to the target spectrum was improved. The scale factors, along with other information on the selected records, are given in Table C-1. All of the selected time-histories were recorded close to faults.

b. Computer codes RSPMATCH (Abrahamson 1992) and RASCAL (Silva and Lee 1987) were used to perform time-domain and frequency-domain matching, respectively. For the time-domain matching, the target spectra were extended to a 10-sec period by setting spectral values of the initial scaled time-histories as target values in the period range of 2 to 10 sec. This extension is needed to prevent the matching procedure from unduly modifying the motions at periods longer than 2 sec, which dominate the velocity and displacement time-histories. The number of iterations was restricted to be less than 10. The impulse response of a single-degree-of-freedom system (Lilhanand and Tseng 1988) was used as the adjustment wavelet. The resulting mismatch to the design spectral values was generally less than 10 percent.

c. Baseline-corrected acceleration, velocity, and displacement time-histories for the scaled initial time-histories, the frequency-domain spectrum-matched time-histories, and the time-domain spectrum-matched time-histories are shown in Figures C-1 to C-10. Also shown in these figures are the modifications to the initial time-history. Response spectra are shown in the top plot of Figures C-11 through C-20. The bottom plot of these figures shows the smoothed power spectral density functions. The power spectral density function $PSD(T)$ of an acceleration time-history is estimated as

$$PSD(\omega) = \frac{2 |F(\omega)|^2}{2\pi T_m} \quad (C-1)$$

where

T = Fourier frequency

$|F(T)|$ = Fourier amplitude computed over a time window which contains acceleration that is near maximum and near stationary power

T_m = duration of the time window

The time window used for each record is shown as dashed lines in Figures C-1 to C-10. To remove the irregularity, the smoothed $PSD(T)$ is then obtained by computing the average value over the frequency range from $T - 0.2T$ to $T + 0.2T$.

The following observations on the spectrally matched records are made:

(1) Both matching procedures produce an adequate fit to the target spectra. However, in general, the time-domain matching produces a closer fit than the frequency-domain matching does.

(2) The spectrum-compatible acceleration time-histories are reasonably similar to the initial acceleration time-histories. Modifications introduced by the two matching procedures show quite different time characteristics. The time-domain modification typically has a shorter time span.

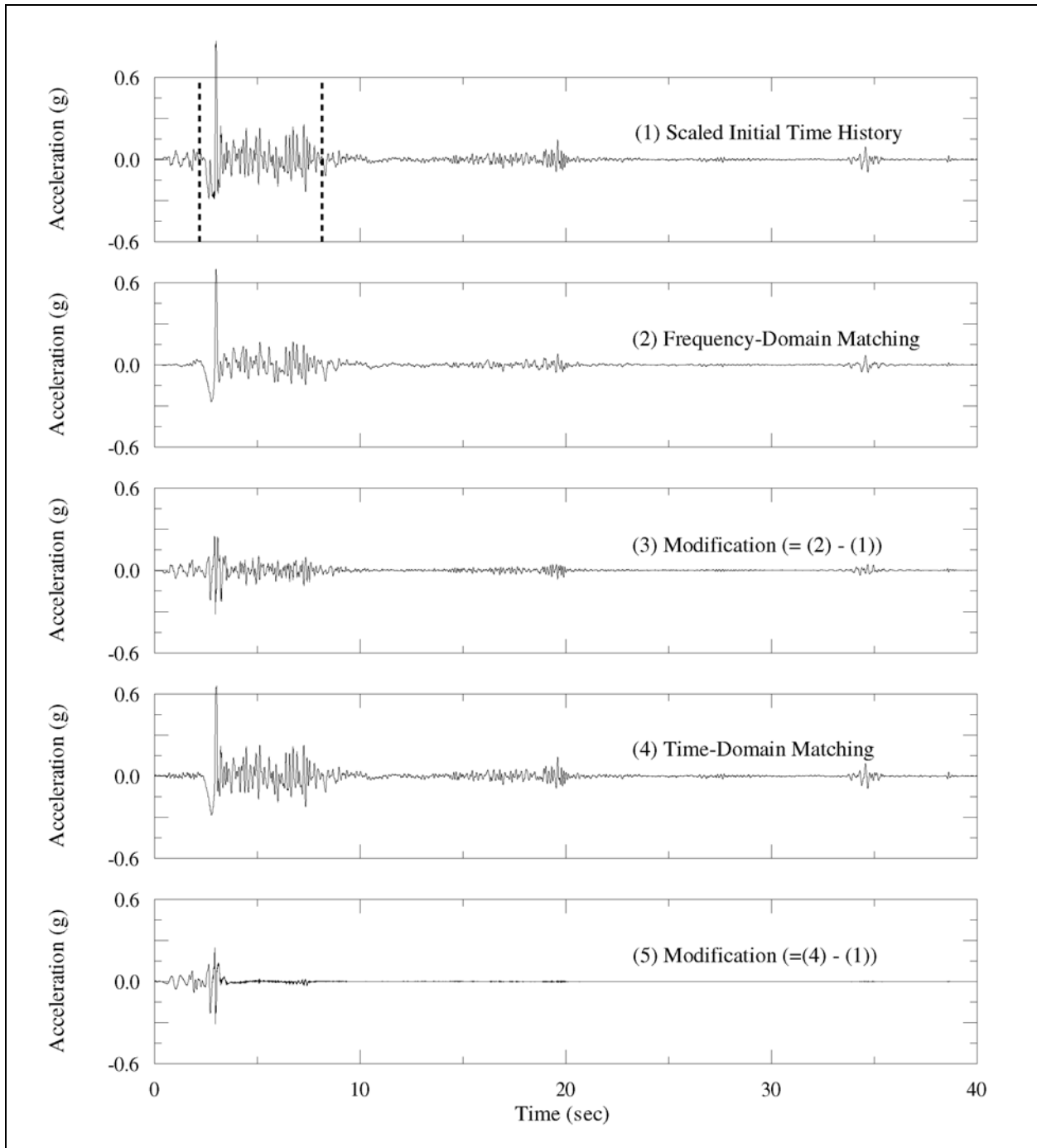
(3) Because matching is performed up to a 10-sec period in the time-domain approach, modification of spectral values at periods longer than the longest period of the target spectra is introduced occasionally. This undesired modification is quite obvious in some of the velocity and displacement time-histories shown in Figures C-1 to C-10, and it can be easily removed by high-pass filtering the spectrum-compatible acceleration time-histories. This is not a problem for the frequency-domain approach. It does not have this problem because it does not alter Fourier amplitudes beyond the longest period of the target spectra.

(4) There is no apparent energy deficiency in the matched records (Figures C-11 to C-20). The matching procedure reduces energy at periods where initial spectra are higher than the target spectra and increases energy at periods where initial spectra are lower.

(5) Both matching procedures are unable to simultaneously fit the PGA and short-period response of the Petrolia record from the 1992 Cape Mendocino earthquake (Figure C-11), despite an almost perfect fit to the target at longer periods. This inability to match is due to the coupling of short-period responses via the large acceleration pulse near the 3-sec time mark (Figure C-1a). This pulse controls the PGA and short-period spectral response (0.03 sec (PGA) to 0.3 sec), and it will not support a lower PGA value while matching the target from the 0.08- to 0.3-sec period. Even though this type of spectral coupling does not occur in the other nine histories used in this appendix, it is encountered occasionally. Special effort is usually needed to break up the spectral coupling.

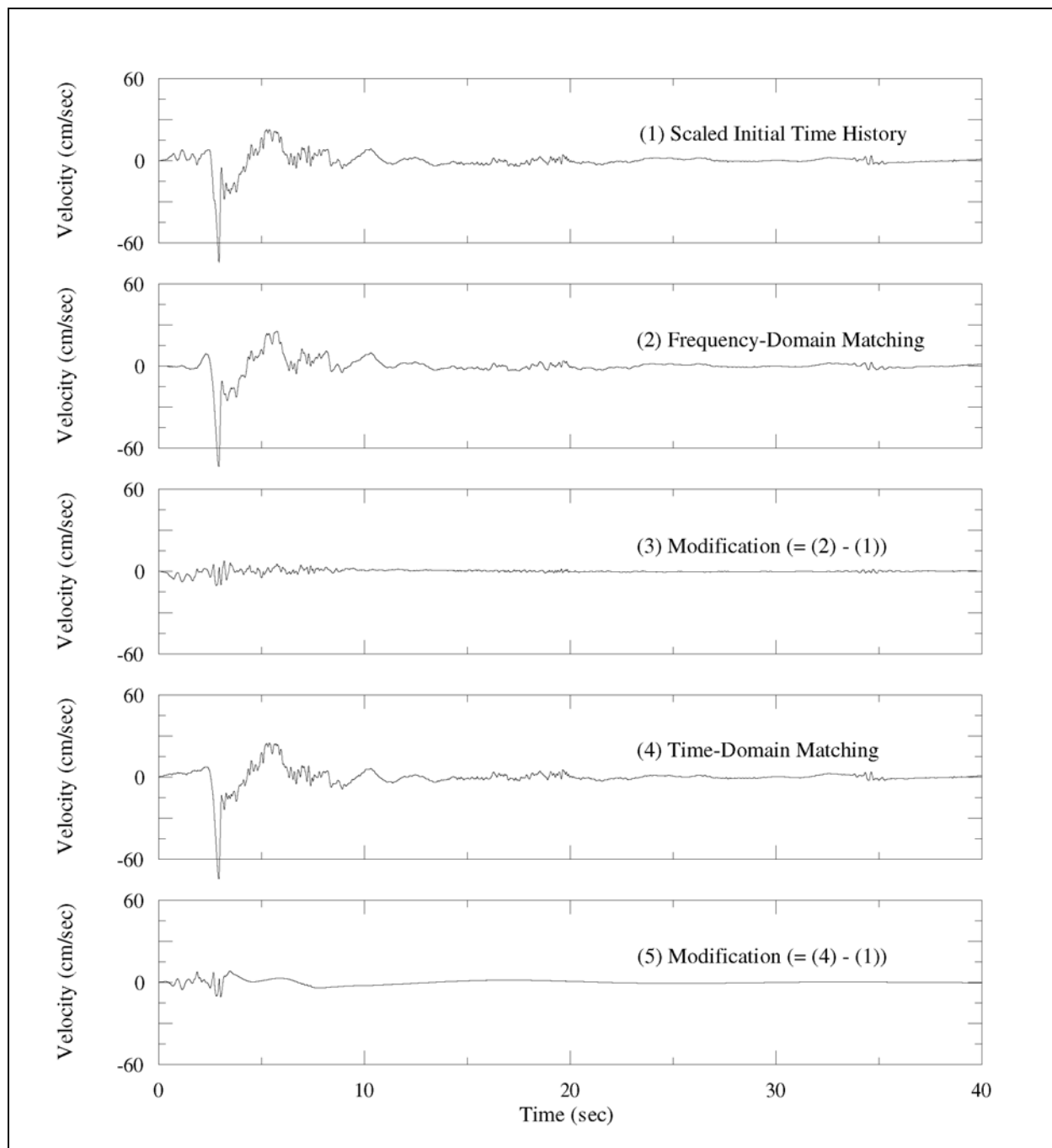
Table C-1
Acceleration Time-Histories Selected for Spectrum Matching

Record	Earthquake	M_w	Closest Distance, km	Component deg	Scale Factor
Petrolia	1992 Cape Mendocino	7.1	8.5	000	0.58
Gilroy	1989 Loma Prieta	6.9	11.6	067	1.43
Griffith Park	1971 San Fernando	6.6	17.4	270	2.85
Halls Valley	1984 Morgan Hill	6.2	3.4	240	2.22
Gazli	1976 Gazli	6.8	3.0	090	0.70
Pacoima	1994 Northridge	6.7	9.8	265	1.34
Coyote Lake Dam	1984 Morgan Hill	6.2	0.1	195	0.66
SCSE	1994 Northridge	6.7	7.8	018	0.85
Pacoima Dam	1971 San Fernando	6.6	2.8	254	0.60
UCSC BRAN	1989 Loma Prieta	6.9	10.3	090	0.83



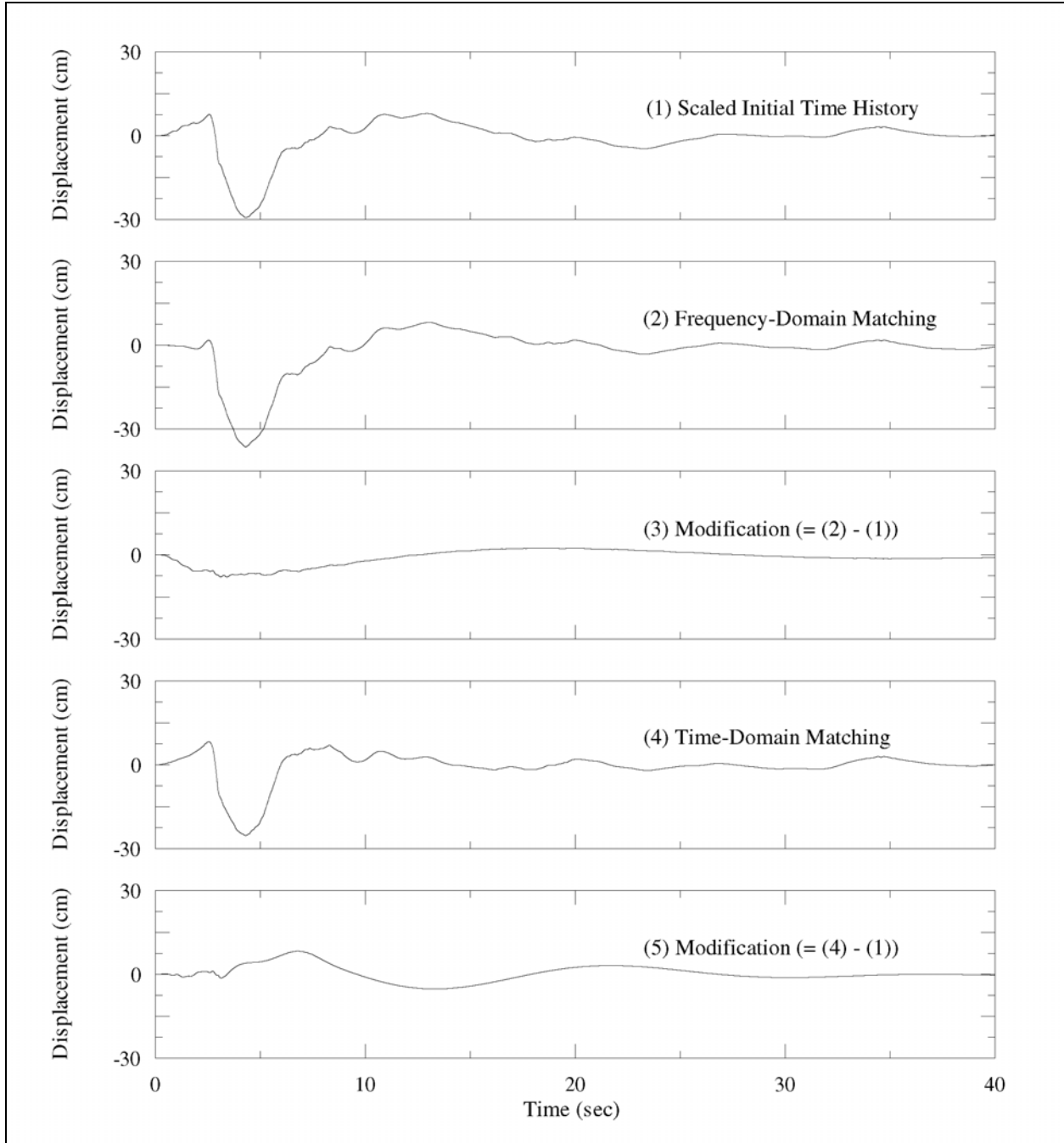
a. Comparison of acceleration time-histories: (1) the scaled initial recorded time-history; (2) frequency-domain-matched time-history; (3) modification to the time-history made by the frequency-domain method; (4) time-domain-matched time-history; (5) modification to the time-history made by time-domain method. Dashed lines indicate the time window used in the calculation of power spectral density function.

Figure C-1. Comparison of time-histories for Petrolia recording (component 000E), 1992 Cape Mendocino earthquake (Sheet 1 of 3)



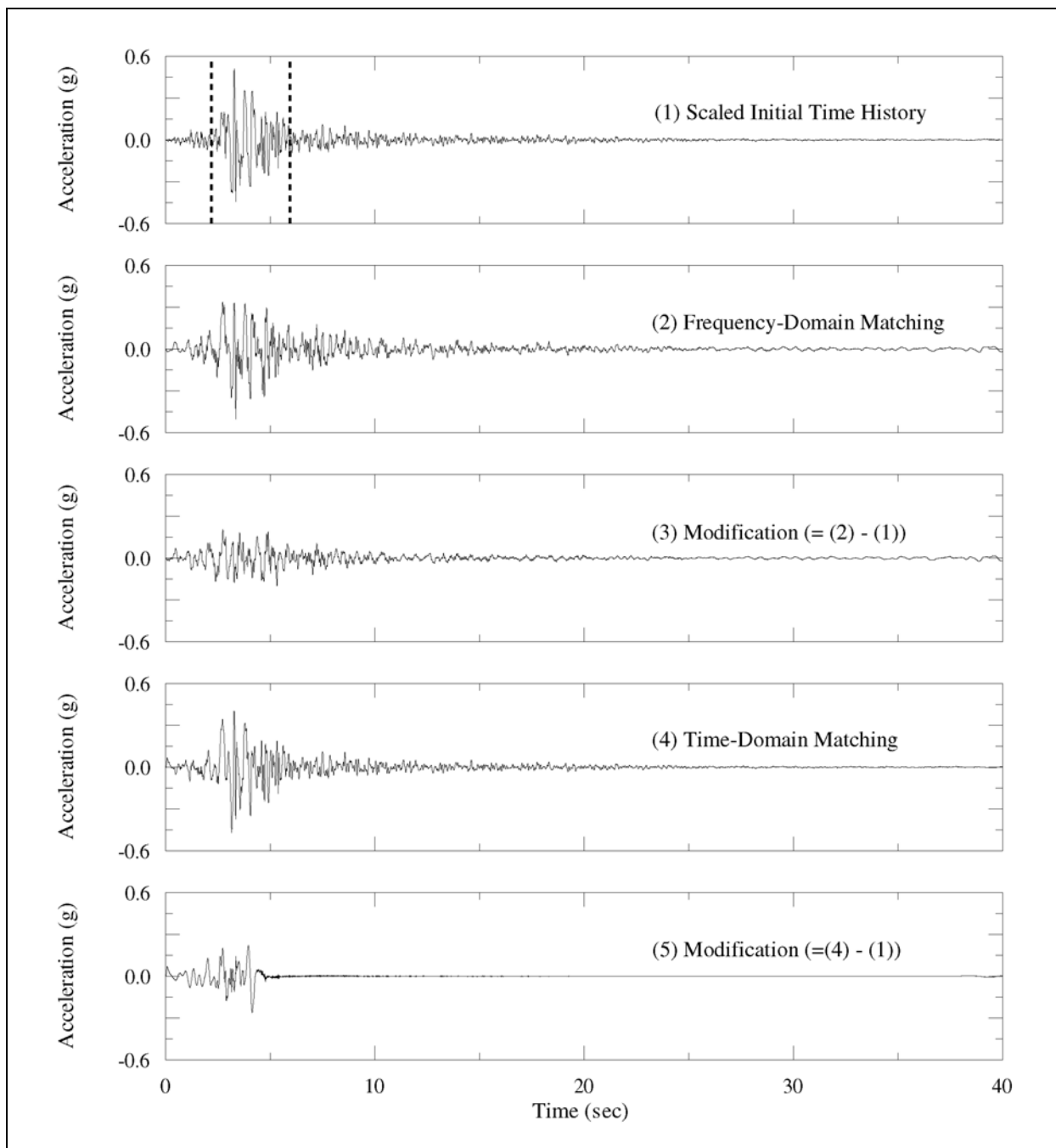
b. Comparison of velocity time-histories: (1) the scaled initial time-history; (2) frequency-domain-matched time-history; (3) modification to the time-history made by the frequency-domain method; (4) time-domain-matched time-history; (5) modification to the time-history made by time-domain method.

Figure C-1. (Sheet 2 of 3)



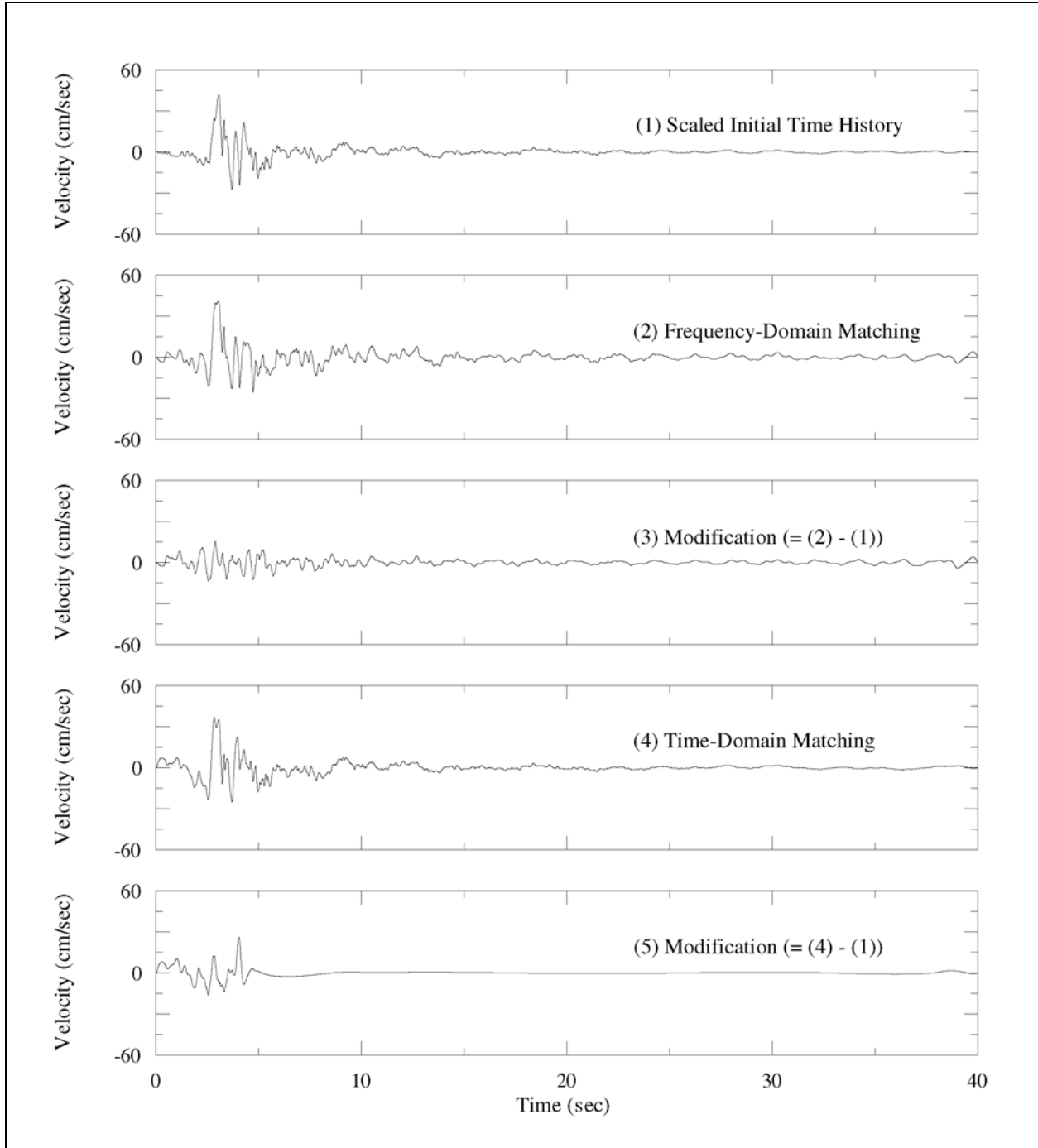
c. Comparison of displacement time-histories: (1) the scaled initial time-history; (2) frequency-domain-matched time-history; (3) modification to the time-history made by the frequency-domain method; (4) time-domain-matched time-history; (5) modification to the time-history made by time-domain method.

Figure C-1. (Sheet 3 of 3)



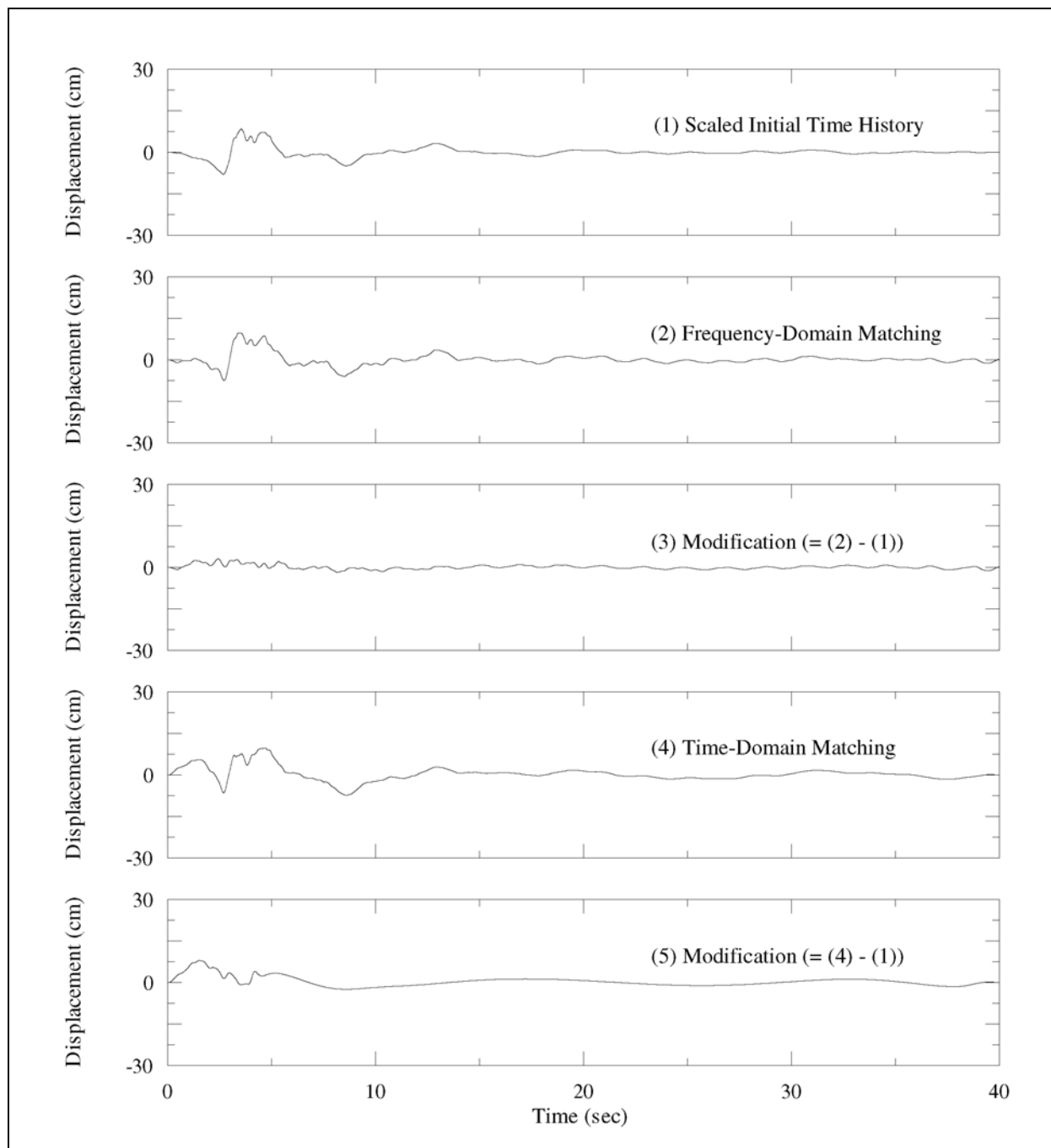
a. Comparison of acceleration time-histories: (1) the scaled initial recorded time-history; (2) frequency-domain-matched time-history; (3) modification to the time-history made by the frequency-domain method; (4) time-domain-matched time-history; (5) modification to the time-history made by time-domain method. Dashed lines indicate the time window used in the calculation of power spectral density function.

Figure C-2. Comparison of time-histories for Gilroy recording (component 067E) 1989 Loma Prieta earthquake (Sheet 1 of 3)



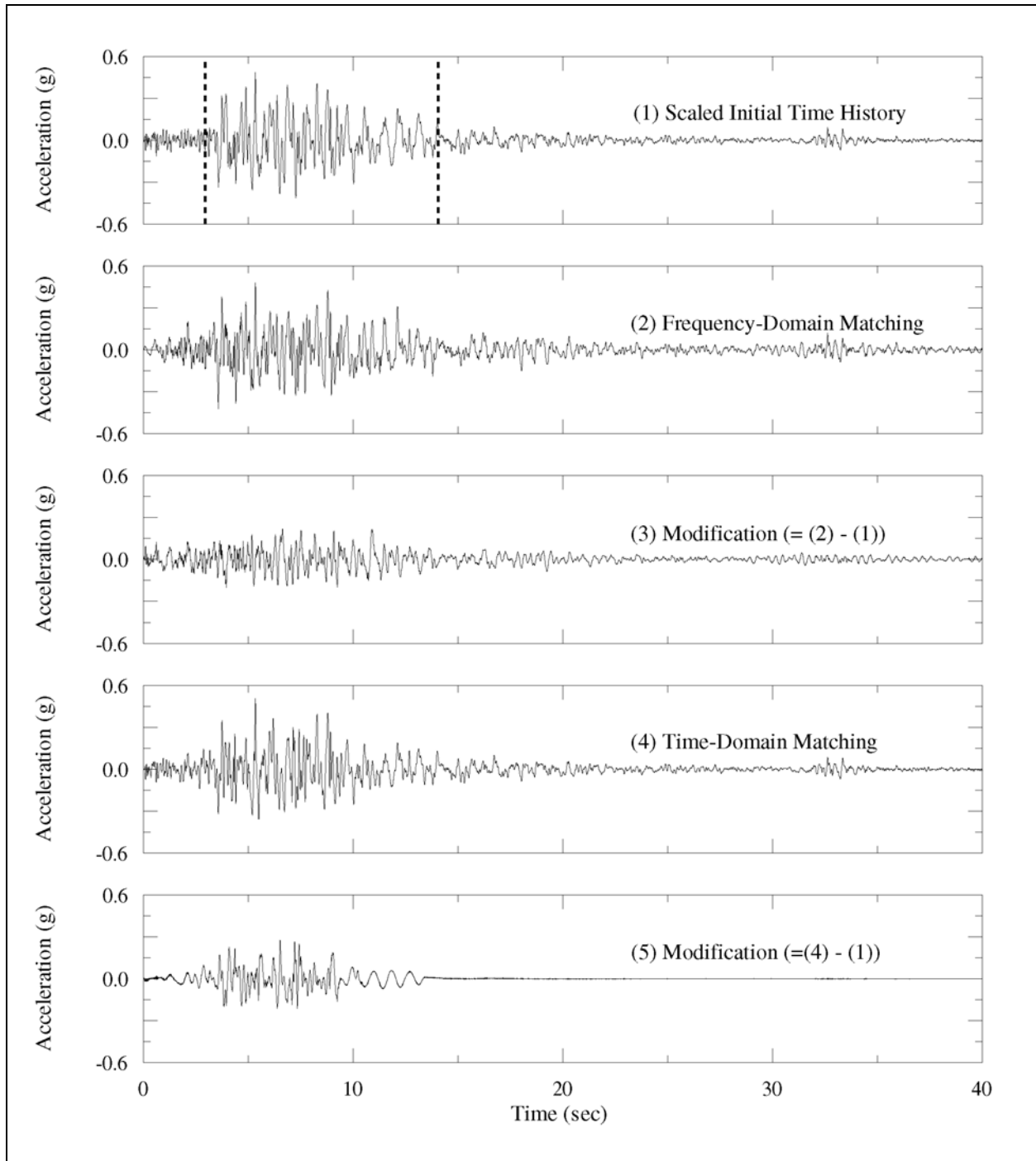
b. Comparison of velocity time-histories: (1) the scaled initial time-history; (2) frequency-domain-matched time-history; (3) modification to the time-history made by the frequency-domain method; (4) time-domain matched time-history; (5) modification to the time-history made by time-domain method.

Figure C-2. (Sheet 2 of 3)



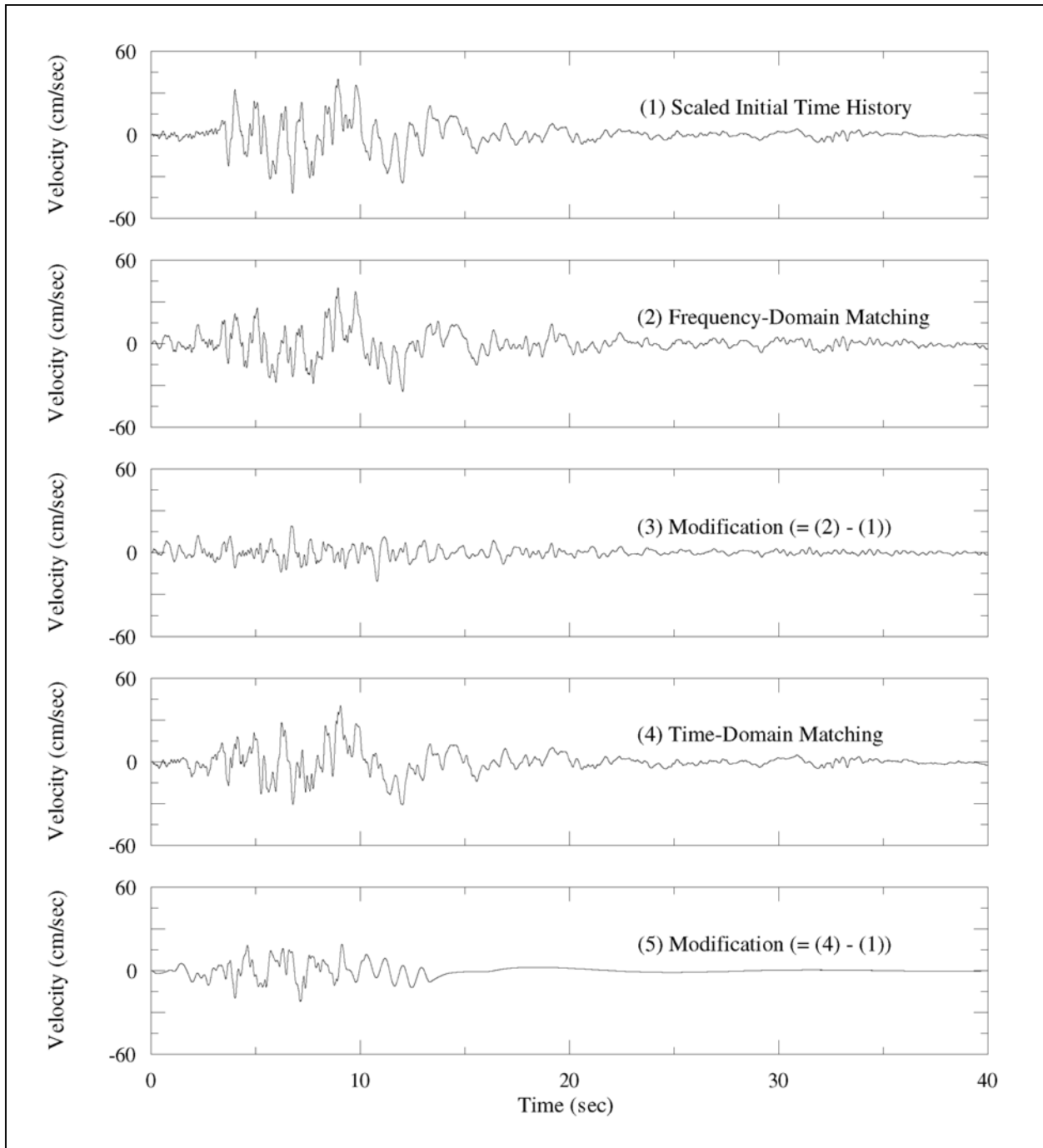
c. Comparison of displacement time-histories: (1) the scaled initial time-history; (2) frequency-domain-matched time-history; (3) modification to the time-history made by the frequency-domain method; (4) time-domain-matched time-history; (5) modification to the time-history made by time-domain method.

Figure C-2. (Sheet 3 of 3)



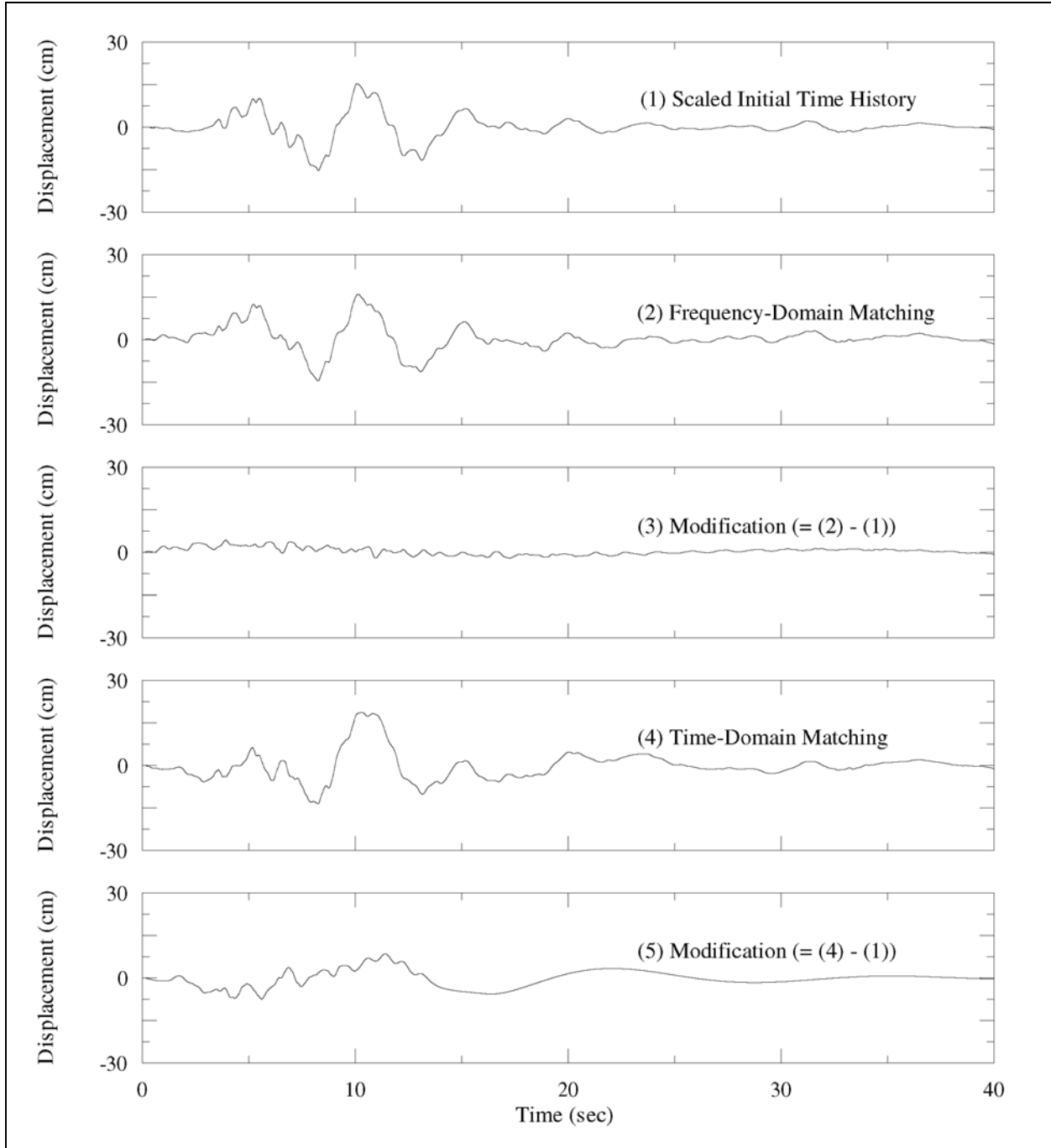
a. Comparison of acceleration time-histories: (1) the scaled initial recorded time-history; (2) frequency-domain-matched time-history; (3) modification to the time-history made by the frequency-domain method; (4) time-domain-matched time-history; (5) modification to the time-history made by time-domain method. Dashed lines indicate the time window used in the calculation of power spectral density function.

Figure C-3. Comparison of time-histories for Griffith Park recording (component 270E), 1971 San Fernando earthquake (Sheet 1 of 3)



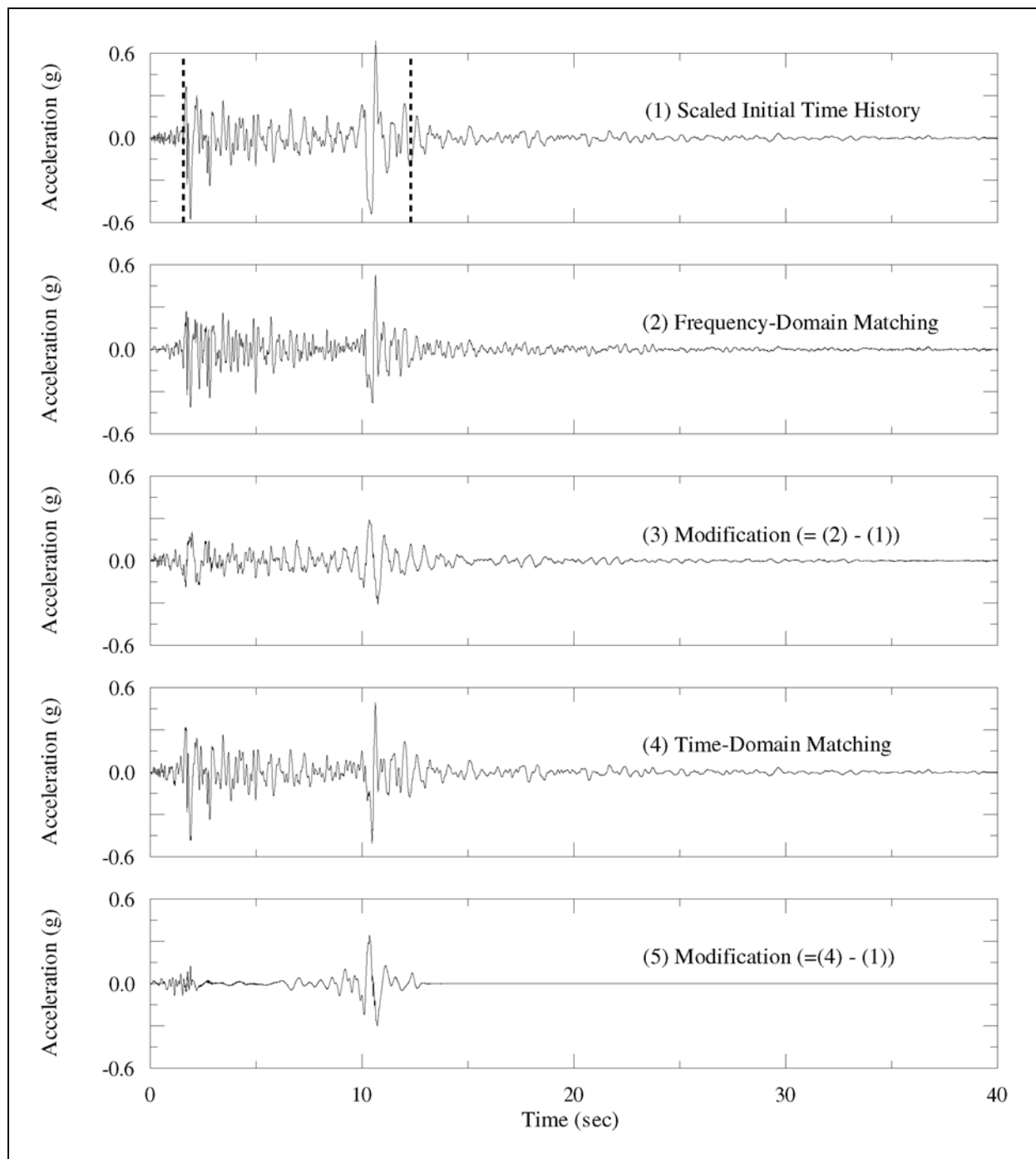
b. Comparison of velocity time-histories: (1) the scaled initial time-history; (2) frequency-domain-matched time-history; (3) modification to the time-history made by the frequency-domain method; (4) time-domain matched time-history; (5) modification to the time-history made by time-domain method.

Figure C-3. (Sheet 2 of 3)



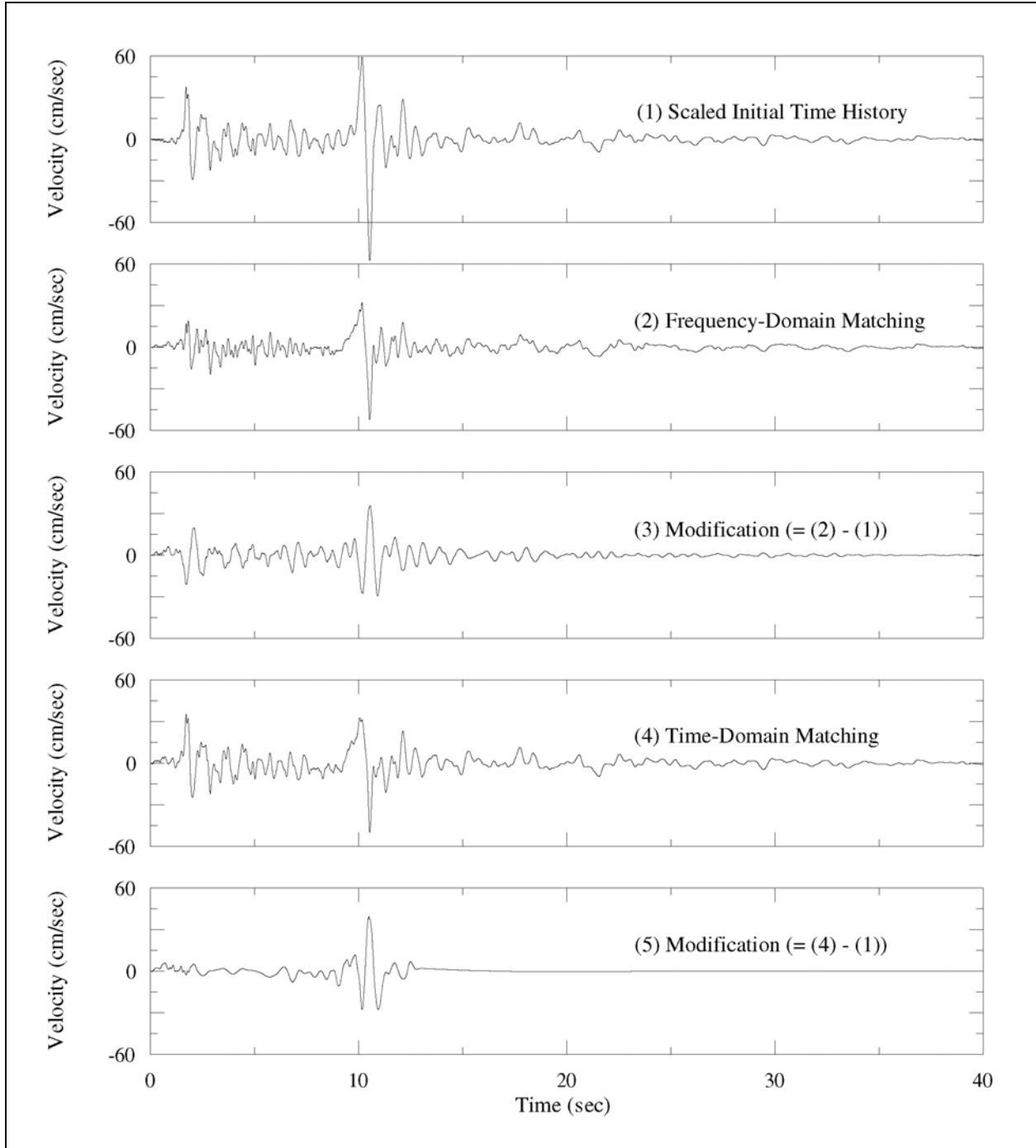
c. Comparison of displacement time-histories: (1) the scaled initial time-history; (2) frequency-domain-matched time-history; (3) modification to the time-history made by the frequency-domain method; (4) time-domain-matched time-history; (5) modification to the time-history made by time-domain method.

Figure C-3. (Sheet 3 of 3)



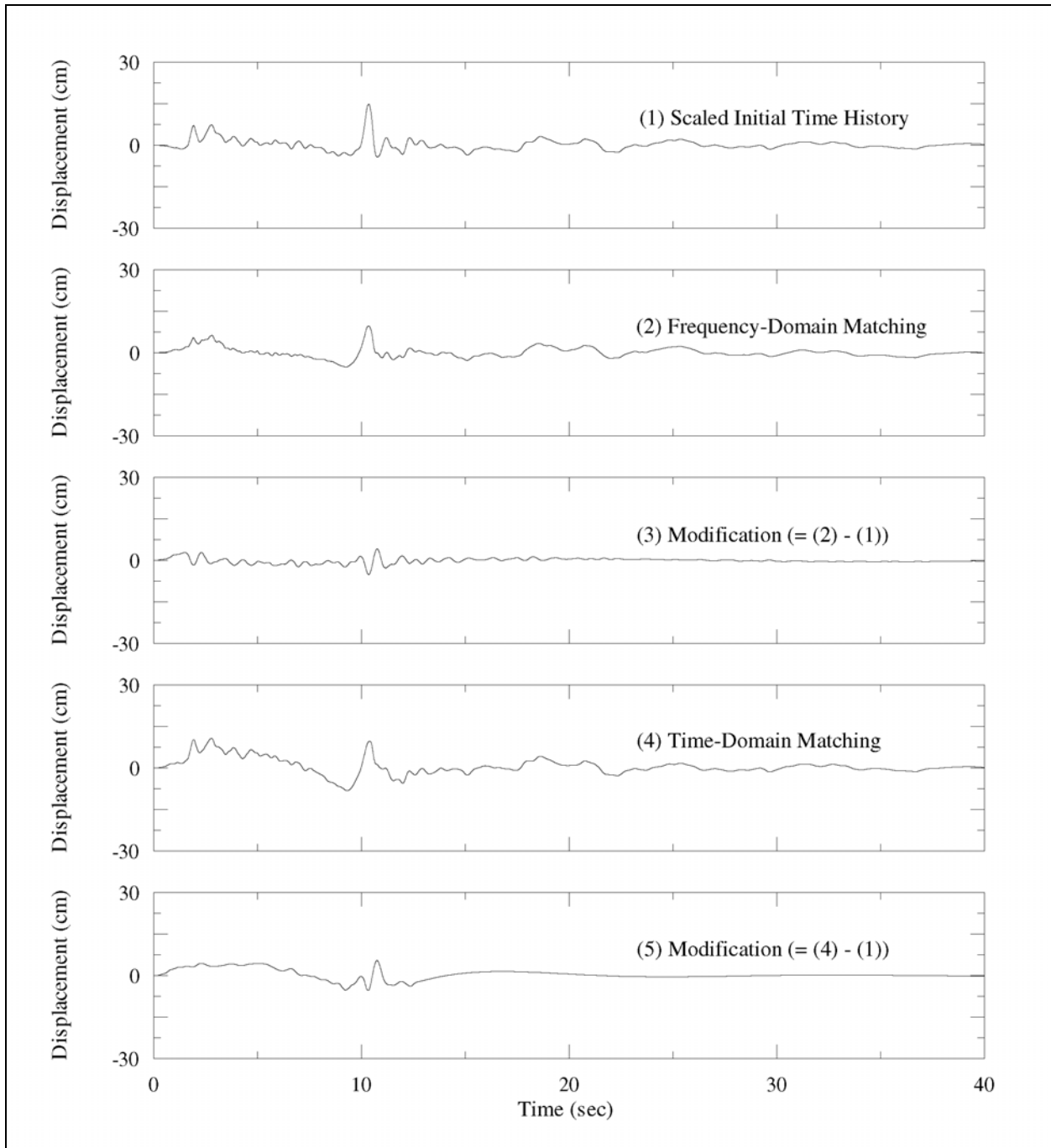
a. Comparison of acceleration time-histories: (1) the scaled initial recorded time-history; (2) frequency-domain-matched time-history; (3) modification to the time-history made by the frequency-domain method; (4) time-domain-matched time-history; (5) modification to the time-history made by time-domain method. Dashed lines indicate the time window used in the calculation of power spectral density function.

Figure C-4. Comparison of time-histories for Halls Valley recording (component 240E), 1984 Morgan Hill earthquake (Sheet 1 of 3)



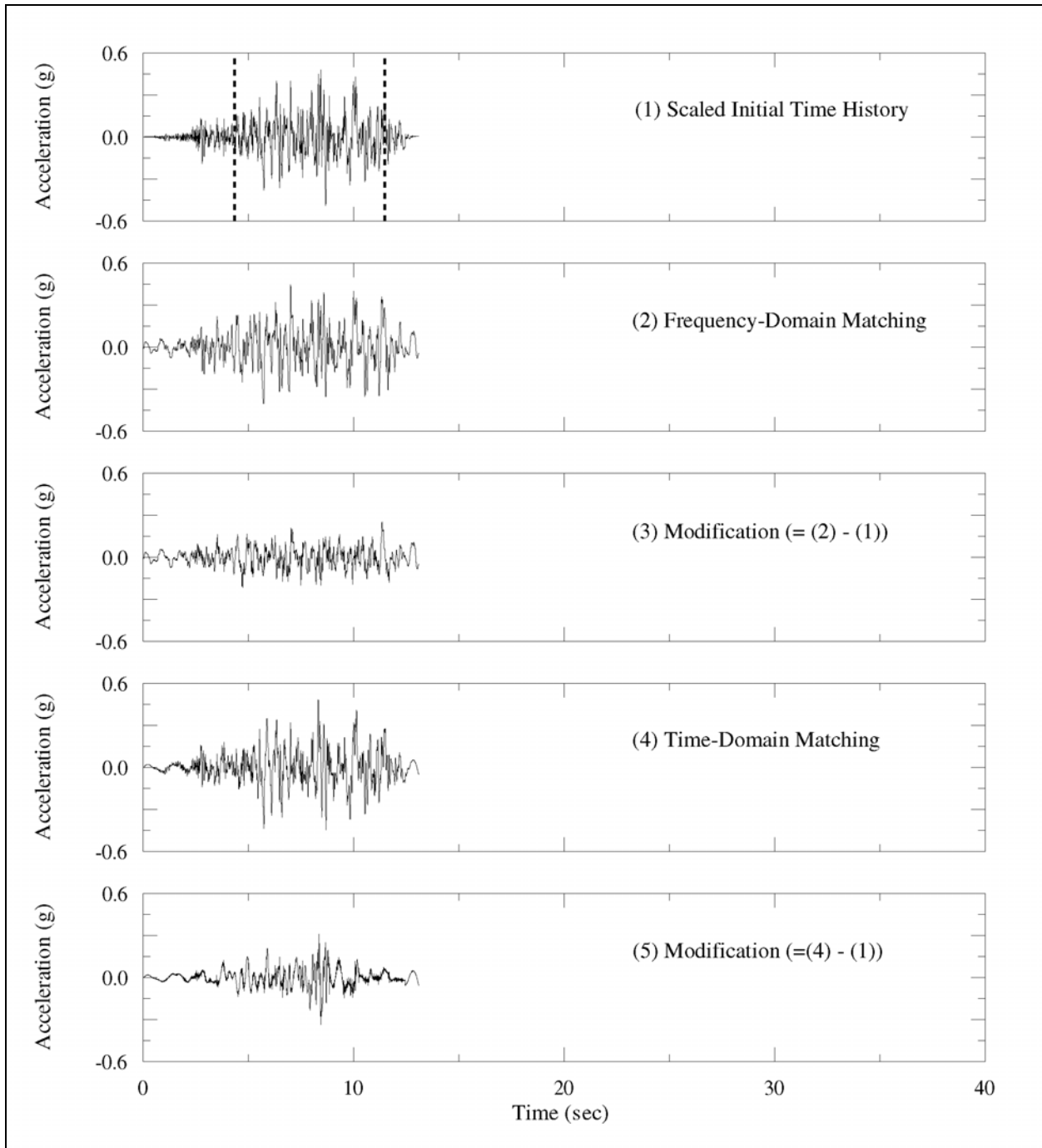
b. Comparison of velocity time-histories: (1) the scaled initial time-history; (2) frequency-domain-matched time-history; (3) modification to the time-history made by the frequency-domain method; (4) time-domain matched time-history; (5) modification to the time-history made by time-domain method.

Figure C-4. (Sheet 2 of 3)



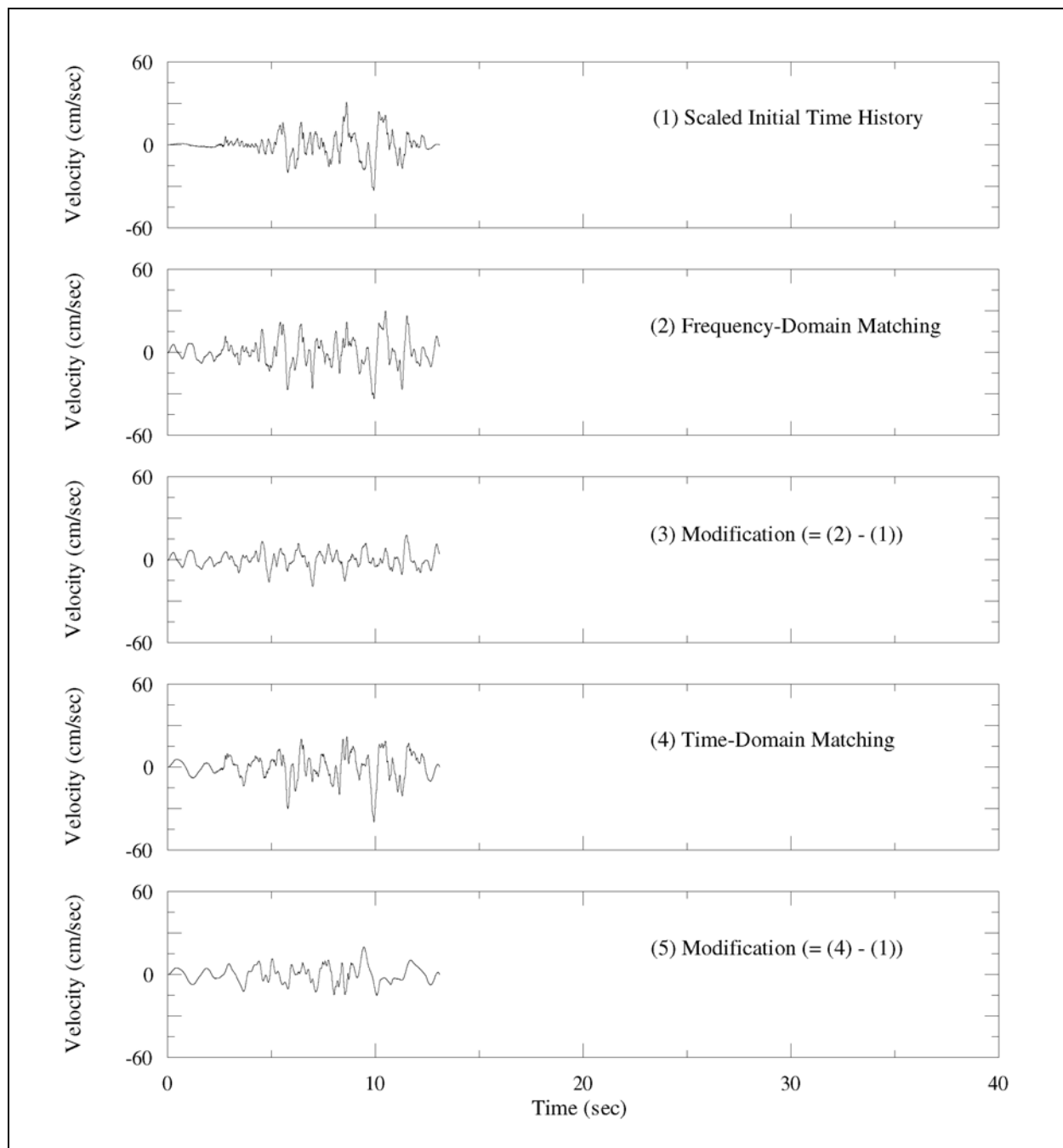
c. Comparison of displacement time-histories: (1) the scaled initial time-history; (2) frequency-domain-matched time-history; (3) modification to the time-history made by the frequency-domain method; (4) time-domain-matched time-history; (5) modification to the time-history made by time-domain method.

Figure C-4. (Sheet 3 of 3)



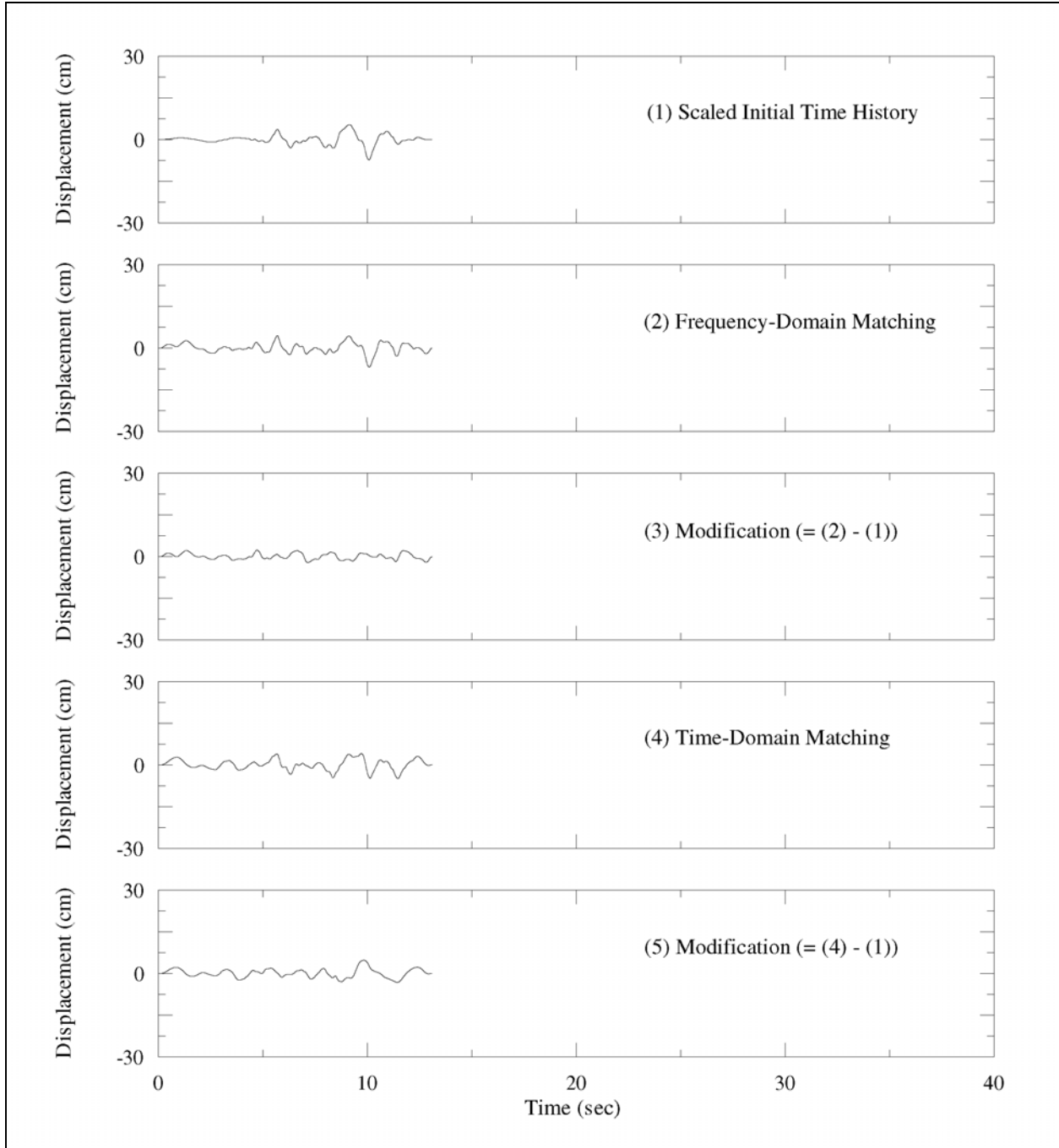
a. Comparison of acceleration time-histories: (1) the scaled initial recorded time-history; (2) frequency-domain-matched time-history; (3) modification to the time-history made by the frequency-domain method; (4) time-domain-matched time-history; (5) modification to the time-history made by time-domain method. Dashed lines indicate the time window used in the calculation of power spectral density function.

Figure C-5. Comparison of time-histories for Gazli recording (component 090E), 1976 Gazli earthquake (Sheet 1 of 3)



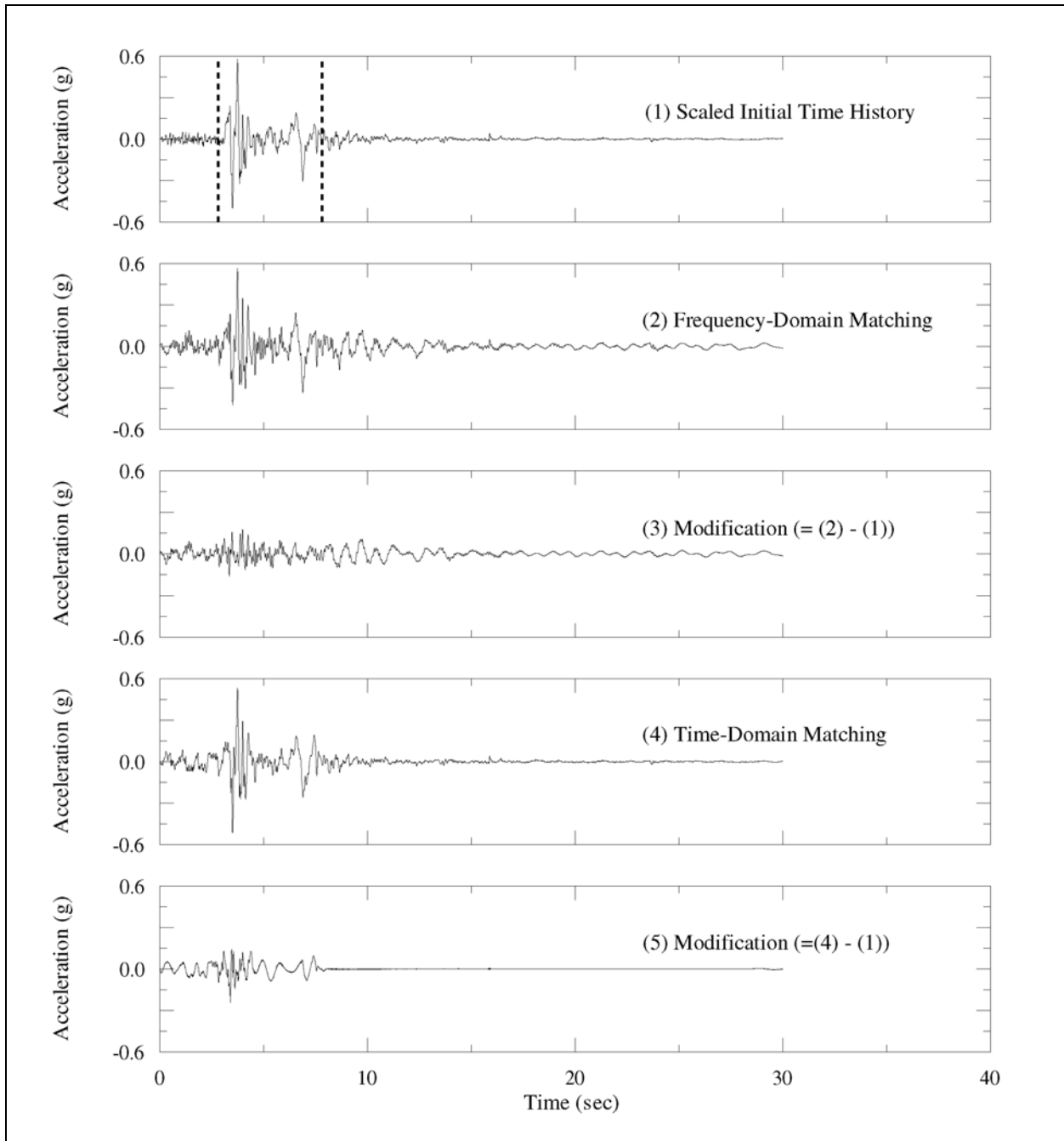
b. Comparison of velocity time-histories: (1) the scaled initial time-history; (2) frequency-domain-matched time-history; (3) modification to the time-history made by the frequency-domain method; (4) time-domain matched time-history; (5) modification to the time-history made by time-domain method.

Figure C-5. (Sheet 2 of 3)



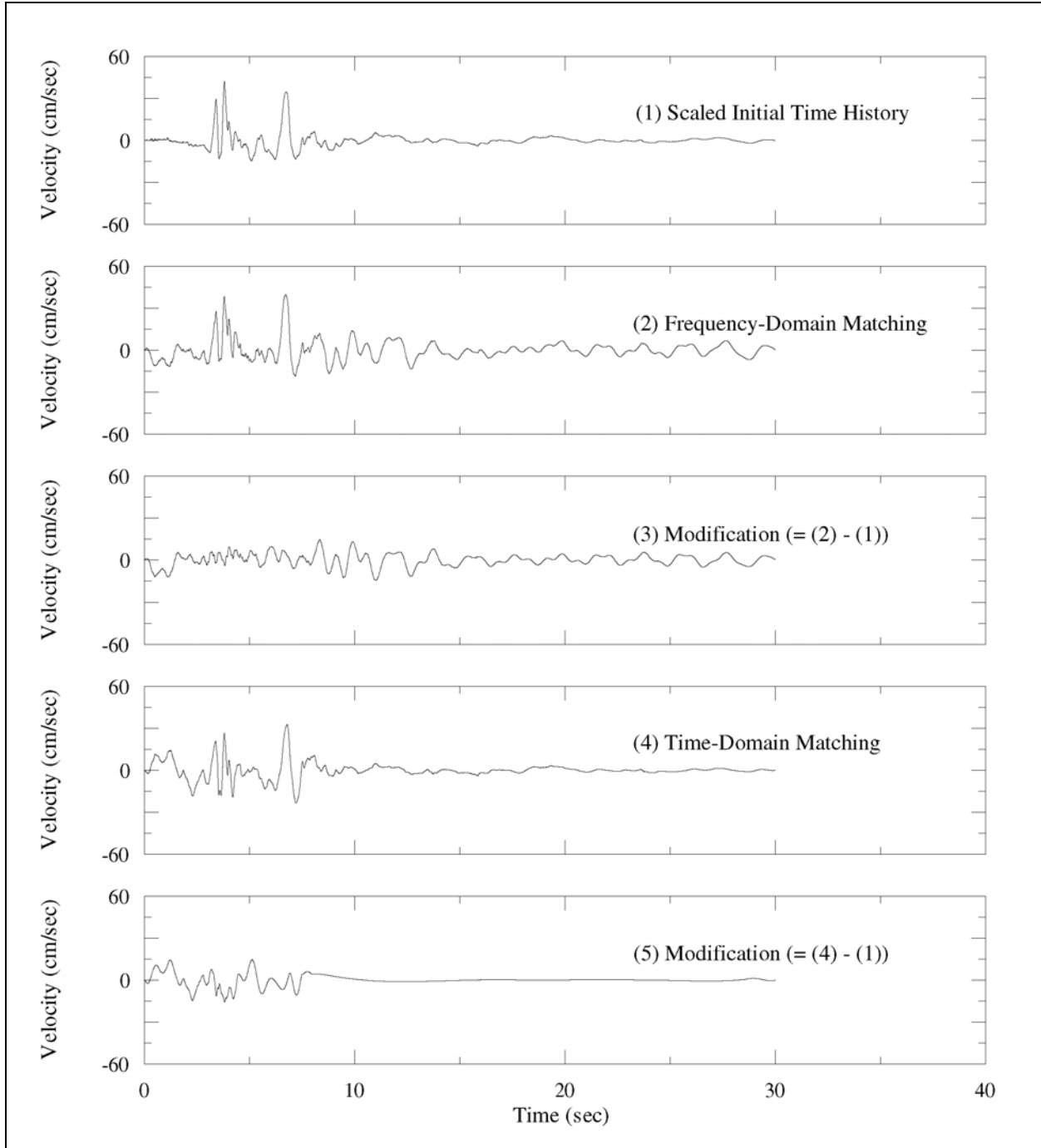
c. Comparison of displacement time-histories: (1) the scaled initial time-history; (2) frequency-domain-matched time-history; (3) modification to the time-history made by the frequency-domain method; (4) time-domain-matched time-history; (5) modification to the time-history made by time-domain method.

Figure C-5. (Sheet 3 of 3)



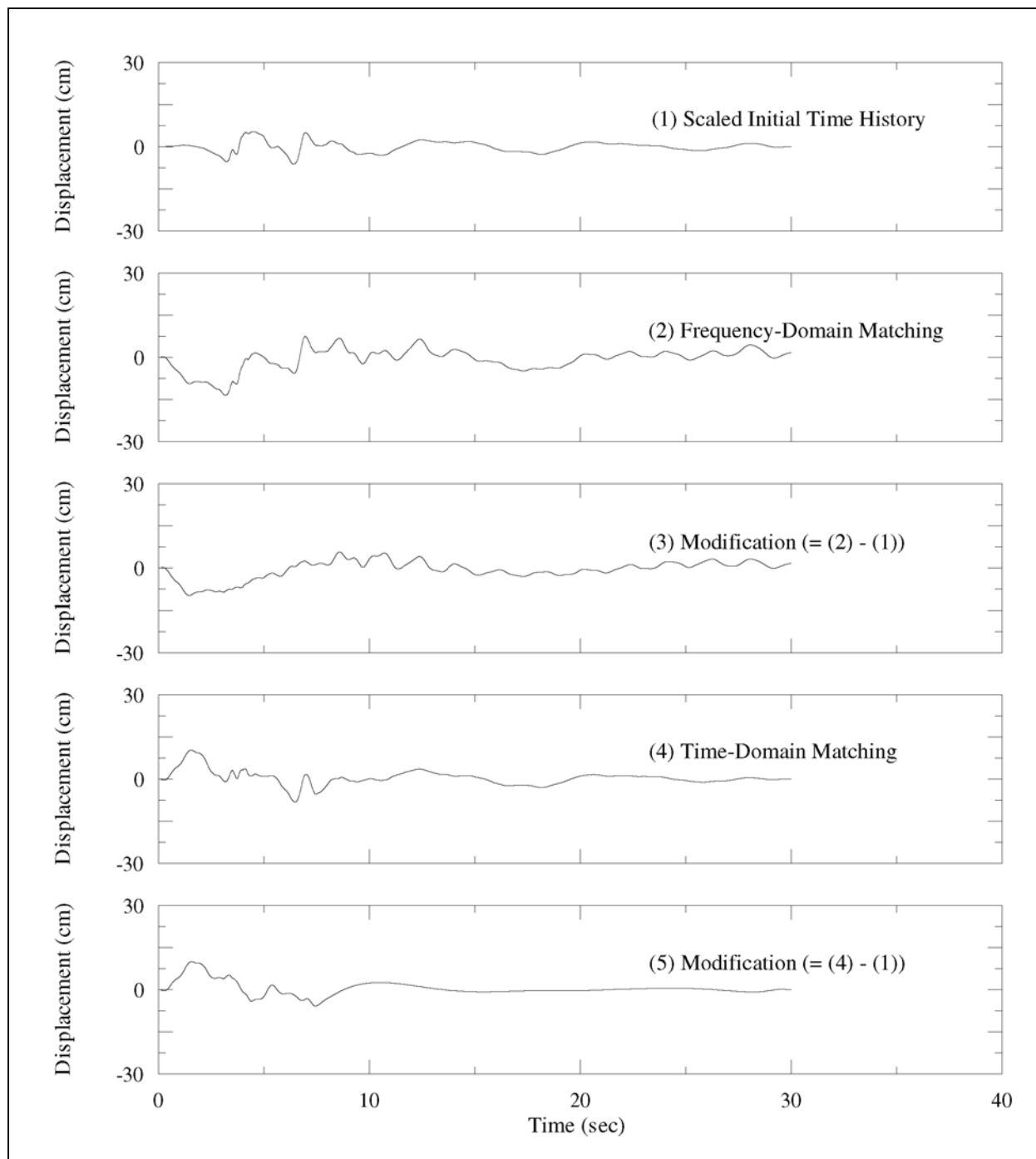
a. Comparison of acceleration time-histories: (1) the scaled initial recorded time-history; (2) frequency-domain-matched time-history; (3) modification to the time-history made by the frequency-domain method; (4) time-domain-matched time-history; (5) modification to the time-history made by time-domain method. Dashed lines indicate the time window used in the calculation of power spectral density function.

Figure C-6. Comparison of time-histories for Pacoima Dam recording (component 265E), 1994 Northridge earthquake (Sheet 1 of 3)



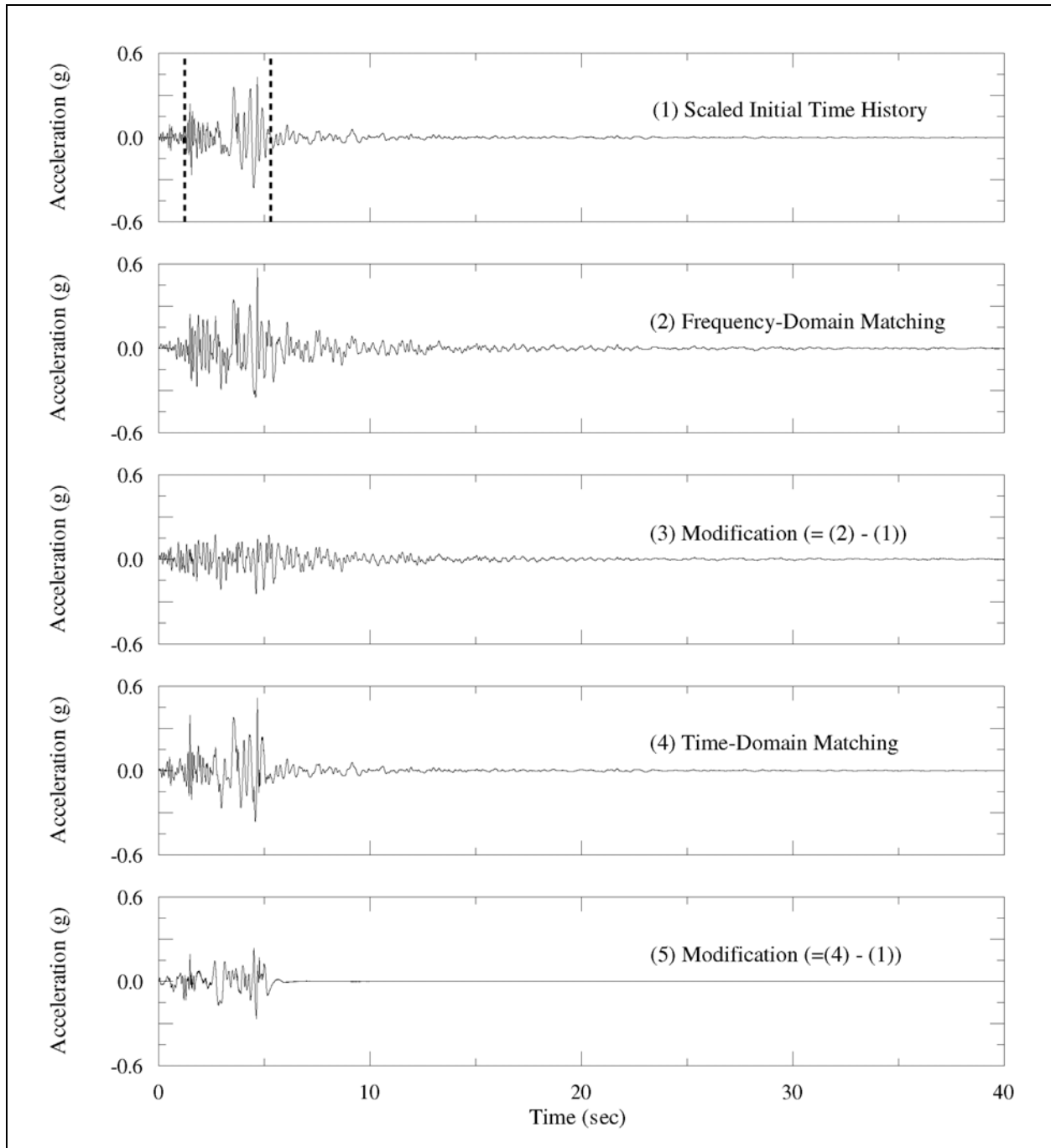
b. Comparison of velocity time-histories: (1) the scaled initial time-history; (2) frequency-domain-matched time-history; (3) modification to the time-history made by the frequency-domain method; (4) time-domain matched time-history; (5) modification to the time-history made by time-domain method.

Figure C-6. (Sheet 2 of 3)



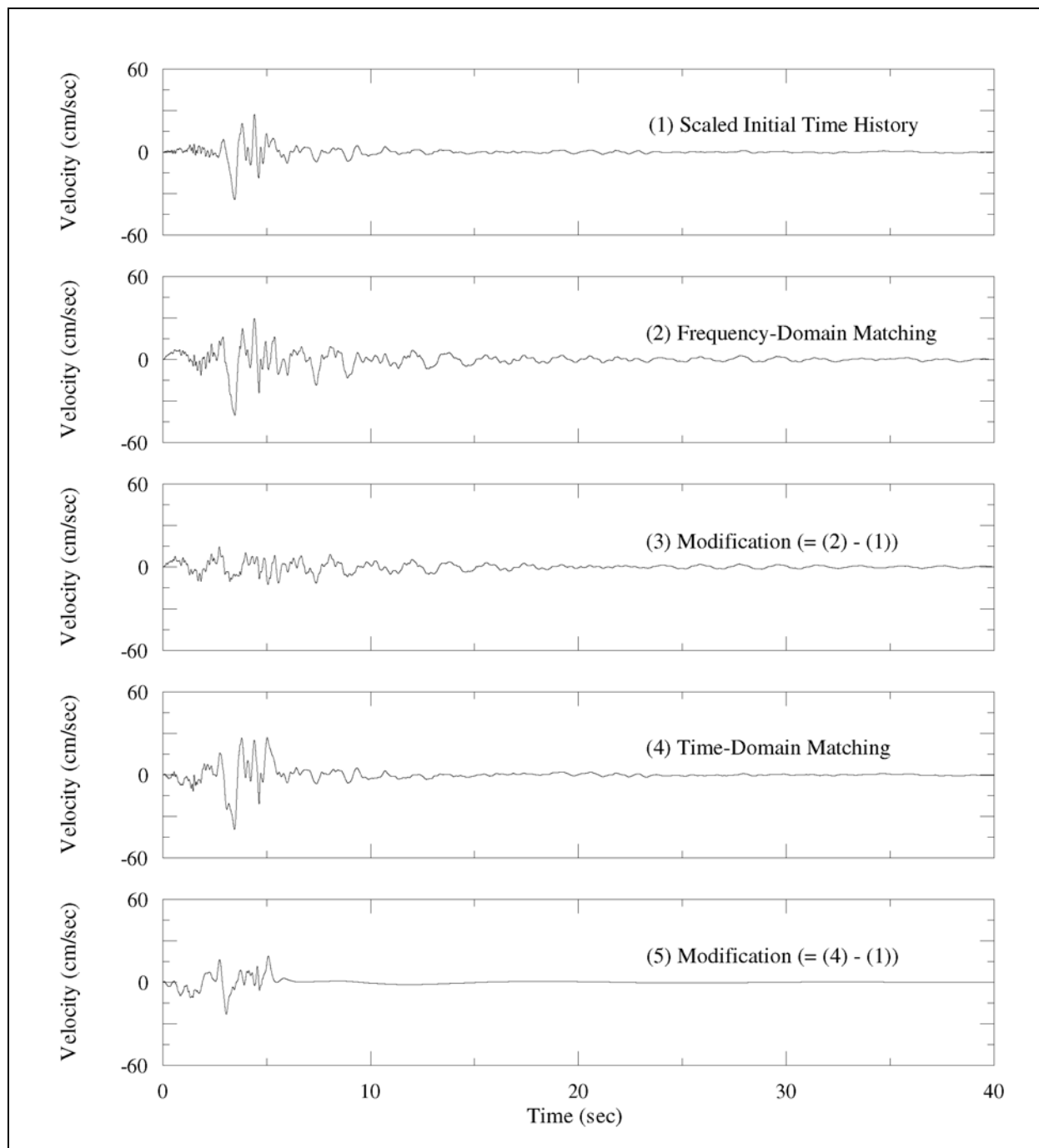
c. Comparison of displacement time-histories: (1) the scaled initial time-history; (2) frequency-domain-matched time-history; (3) modification to the time-history made by the frequency-domain method; (4) time-domain-matched time-history; (5) modification to the time-history made by time-domain method.

Figure C-6. (Sheet 3 of 3)



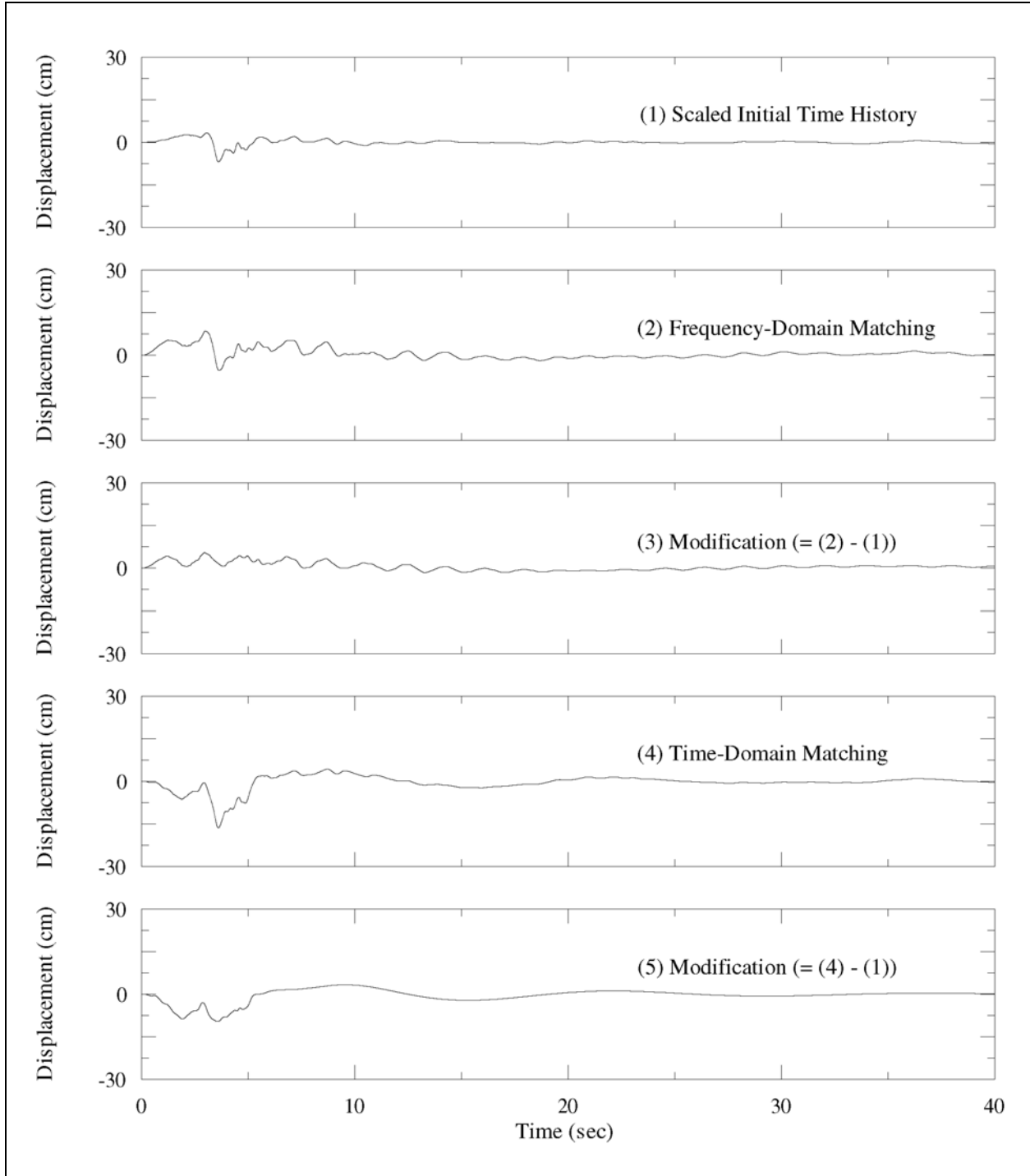
a. Comparison of acceleration time-histories: (1) the scaled initial recorded time-history; (2) frequency-domain-matched time-history; (3) modification to the time-history made by the frequency-domain method; (4) time-domain-matched time-history; (5) modification to the time-history made by time-domain method. Dashed lines indicate the time window used in the calculation of power spectral density function.

Figure C-7. Comparison of time-histories for Coyote Lake Dam recording (component 195E), 1984 Morgan Hill earthquake (Sheet 1 of 3)



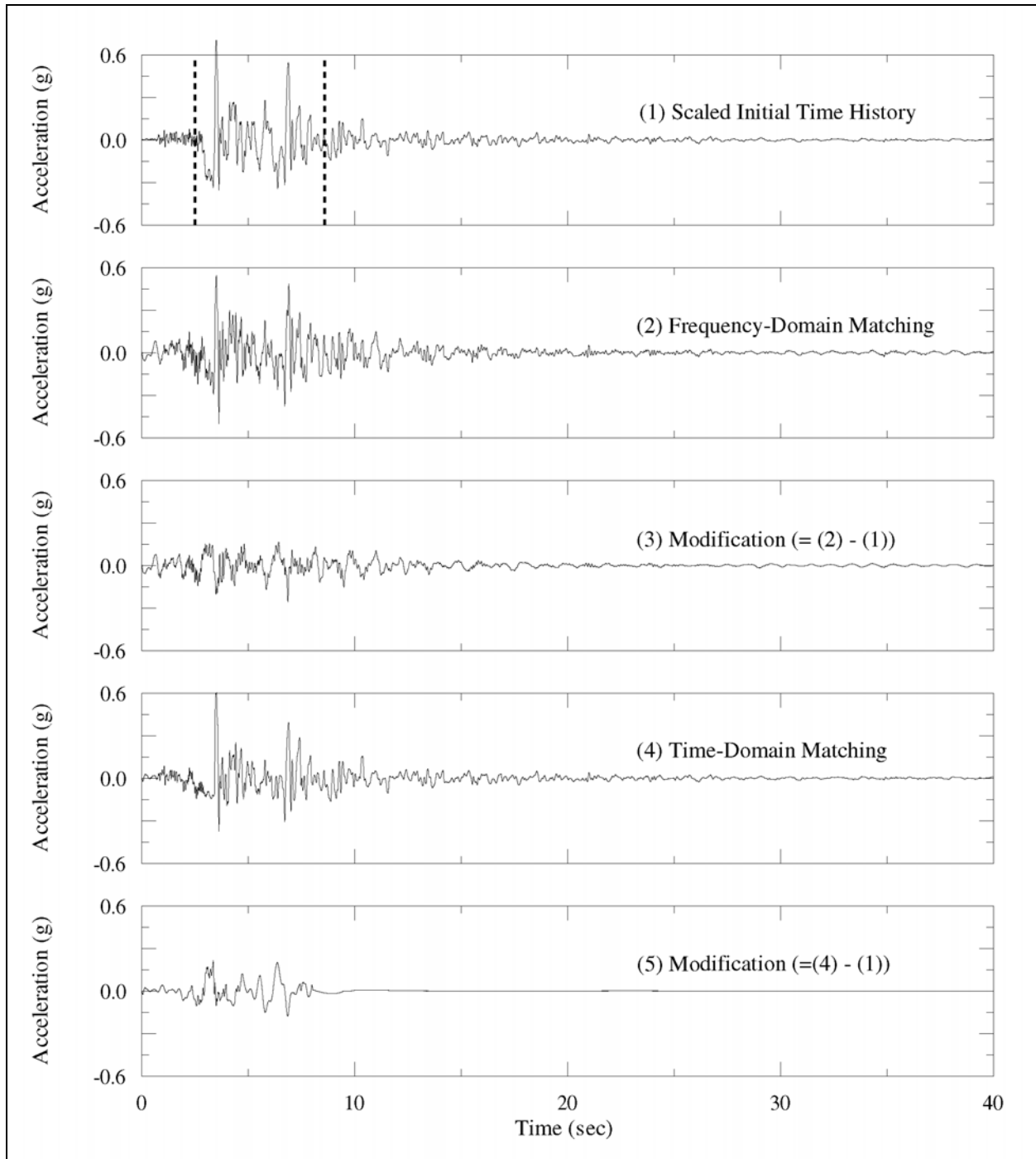
b. Comparison of velocity time-histories: (1) the scaled initial time-history; (2) frequency-domain-matched time-history; (3) modification to the time-history made by the frequency-domain method; (4) time-domain matched time-history; (5) modification to the time-history made by time-domain method.

Figure C-7. (Sheet 2 of 3)



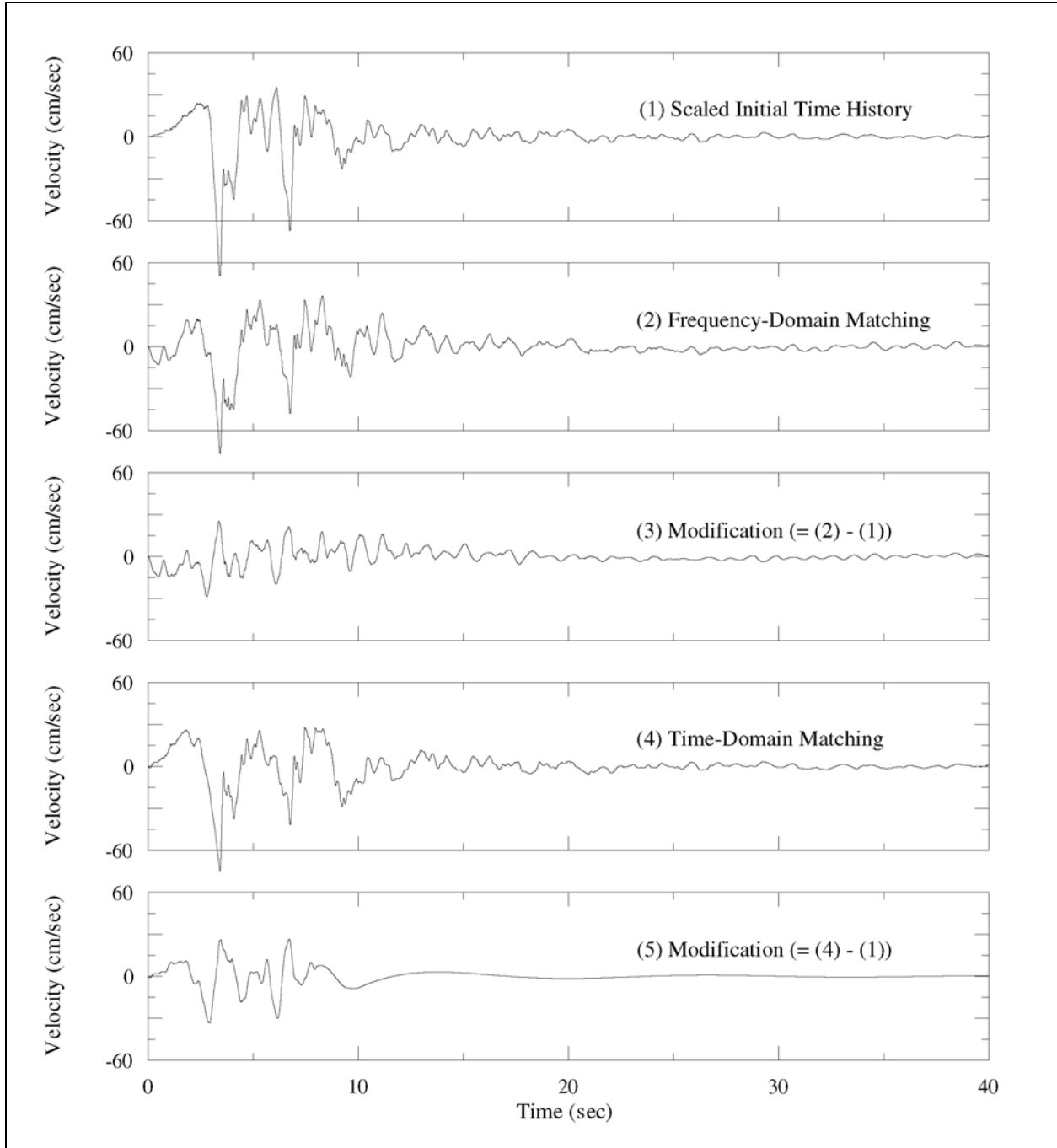
c. Comparison of displacement time-histories: (1) the scaled initial time-history; (2) frequency-domain-matched time-history; (3) modification to the time-history made by the frequency-domain method; (4) time-domain-matched time-history; (5) modification to the time-history made by time-domain method.

Figure C-7. (Sheet 3 of 3)



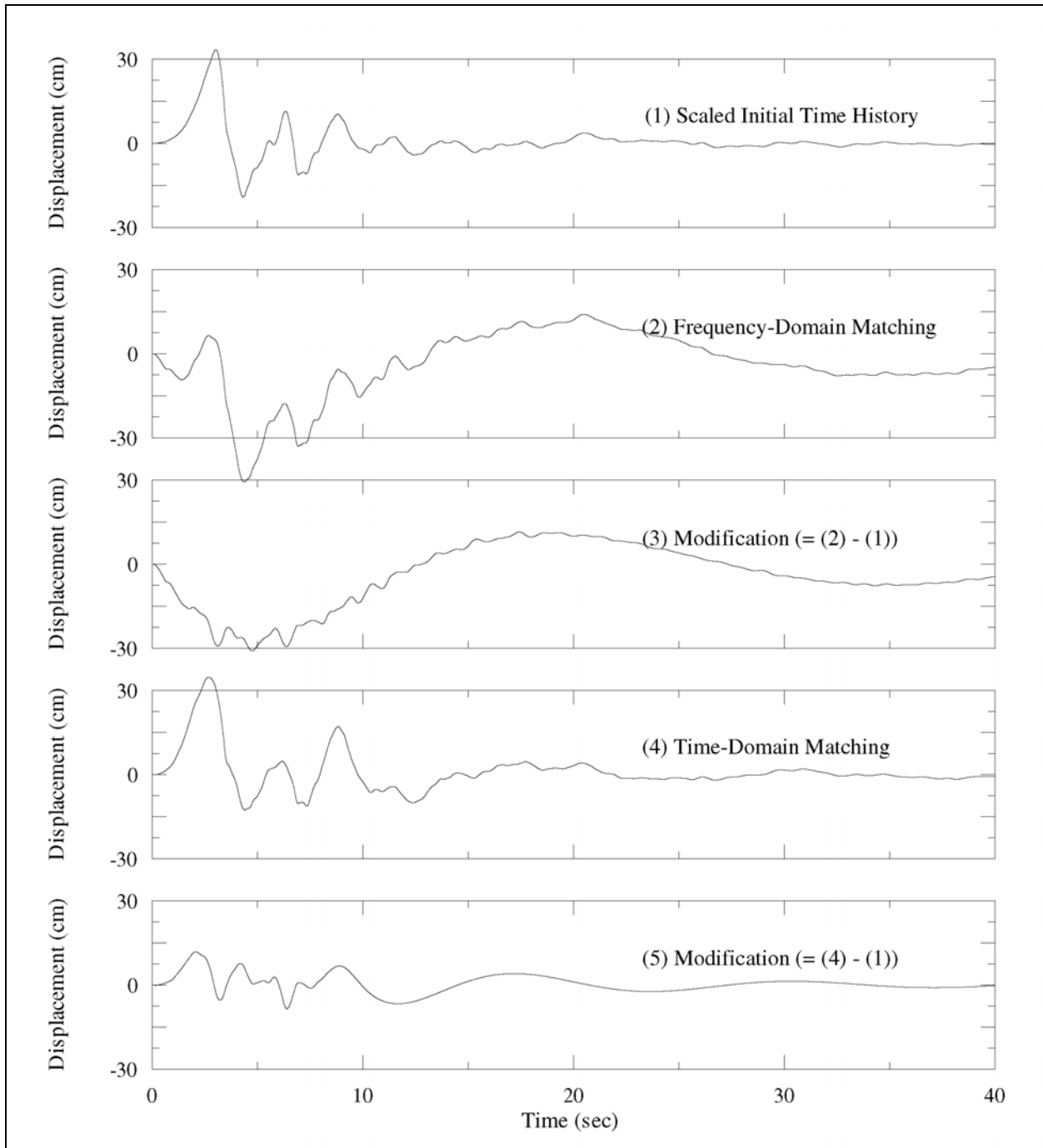
a. Comparison of acceleration time-histories: (1) the scaled initial recorded time-history; (2) frequency-domain-matched time-history; (3) modification to the time-history made by the frequency-domain method; (4) time-domain-matched time-history; (5) modification to the time-history made by time-domain method. Dashed lines indicate the time window used in the calculation of power spectral density function.

Figure C-8. Comparison of time-histories for SCSE recording (component 018E), 1994 Northridge earthquake (Sheet 1 of 3)



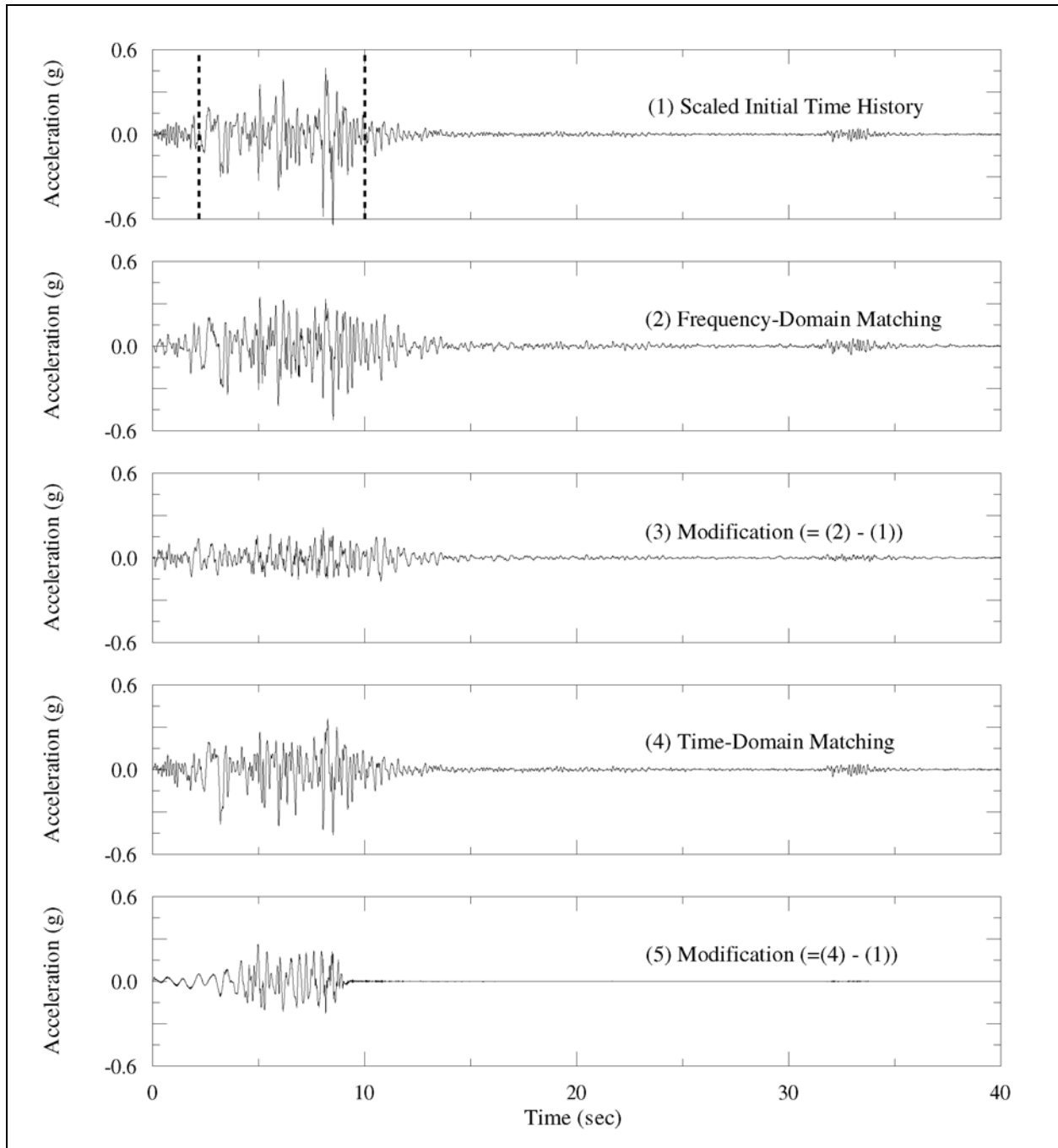
b. Comparison of velocity time-histories: (1) the scaled initial time-history; (2) frequency-domain-matched time-history; (3) modification to the time-history made by the frequency-domain method; (4) time-domain matched time-history; (5) modification to the time-history made by time-domain method.

Figure C-8. (Sheet 2 of 3)



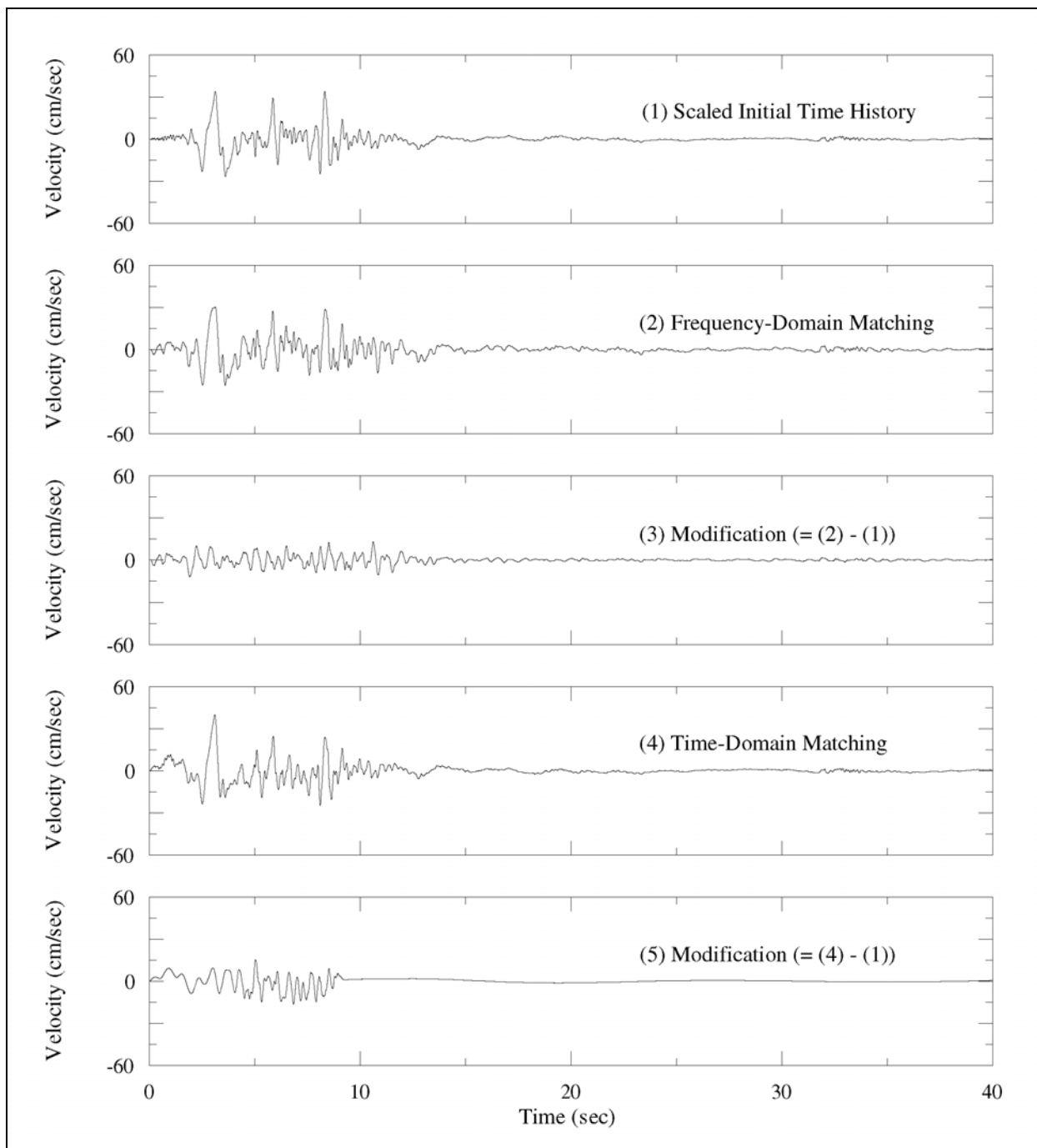
c. Comparison of displacement time-histories: (1) the scaled initial time-history; (2) frequency-domain-matched time-history; (3) modification to the time-history made by the frequency-domain method; (4) time-domain-matched time-history; (5) modification to the time-history made by time-domain method.

Figure C-8. (Sheet 3 of 3)



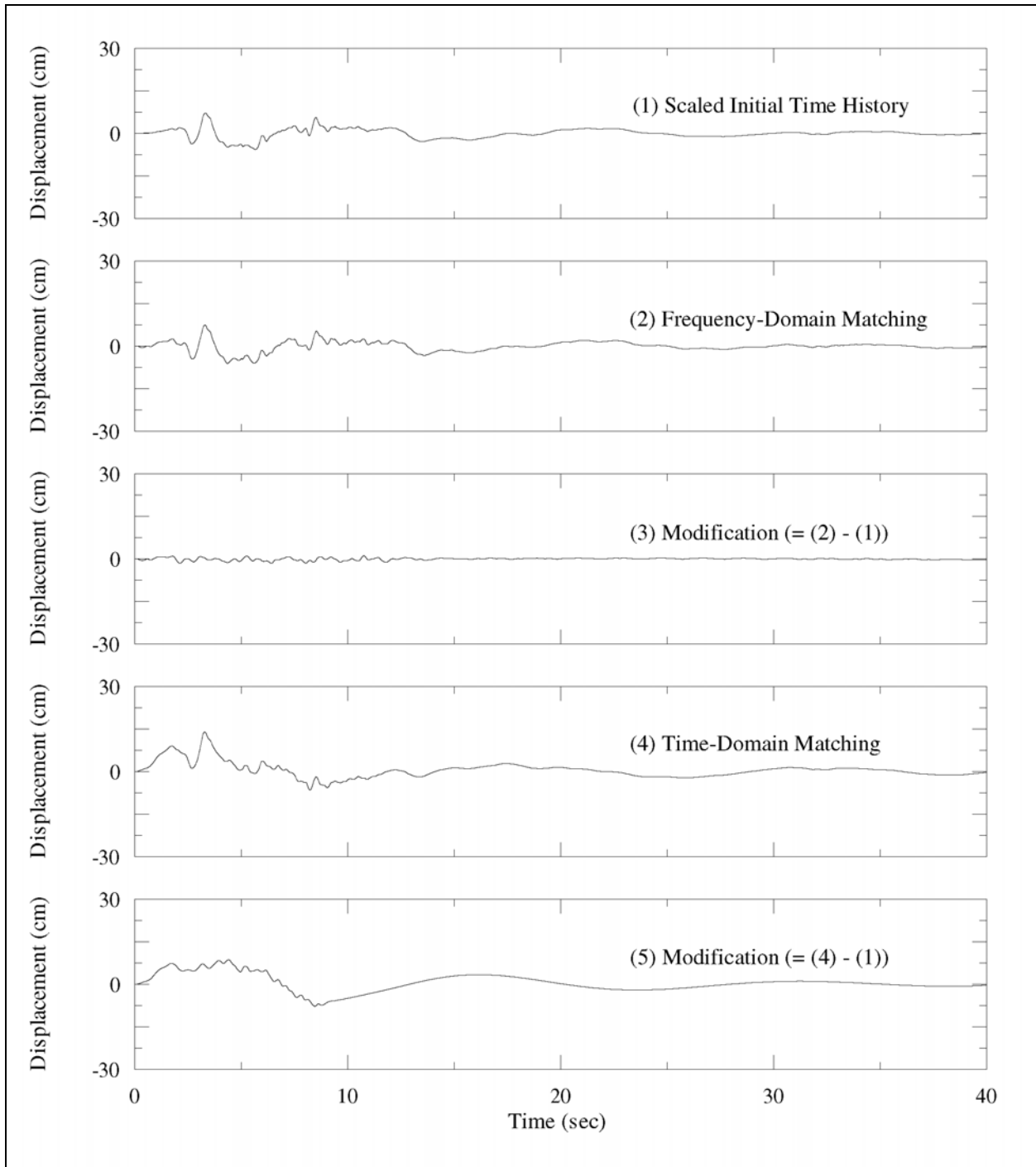
a. Comparison of acceleration time-histories: (1) the scaled initial recorded time-history; (2) frequency-domain-matched time-history; (3) modification to the time-history made by the frequency-domain method; (4) time-domain-matched time-history; (5) modification to the time-history made by time-domain method. Dashed lines indicate the time window used in the calculation of power spectral density function.

Figure C-9. Comparison of time-histories for Pacoima Dam recording (component 254E), 1971 San Fernando earthquake (Sheet 1 of 3)



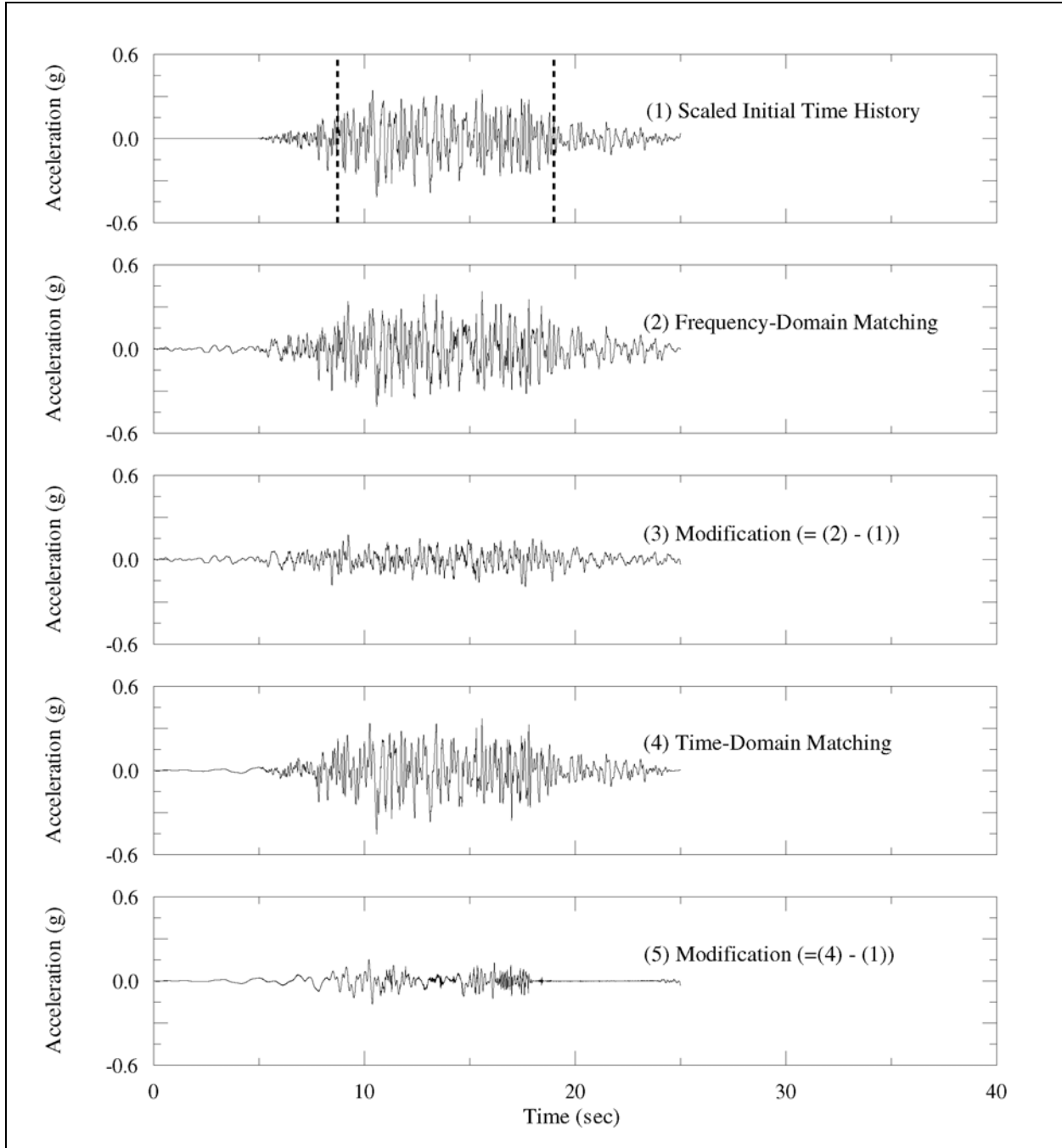
b. Comparison of velocity time-histories: (1) the scaled initial time-history; (2) frequency-domain-matched time-history; (3) modification to the time-history made by the frequency-domain method; (4) time-domain matched time-history; (5) modification to the time-history made by time-domain method.

Figure C-9. (Sheet 2 of 3)



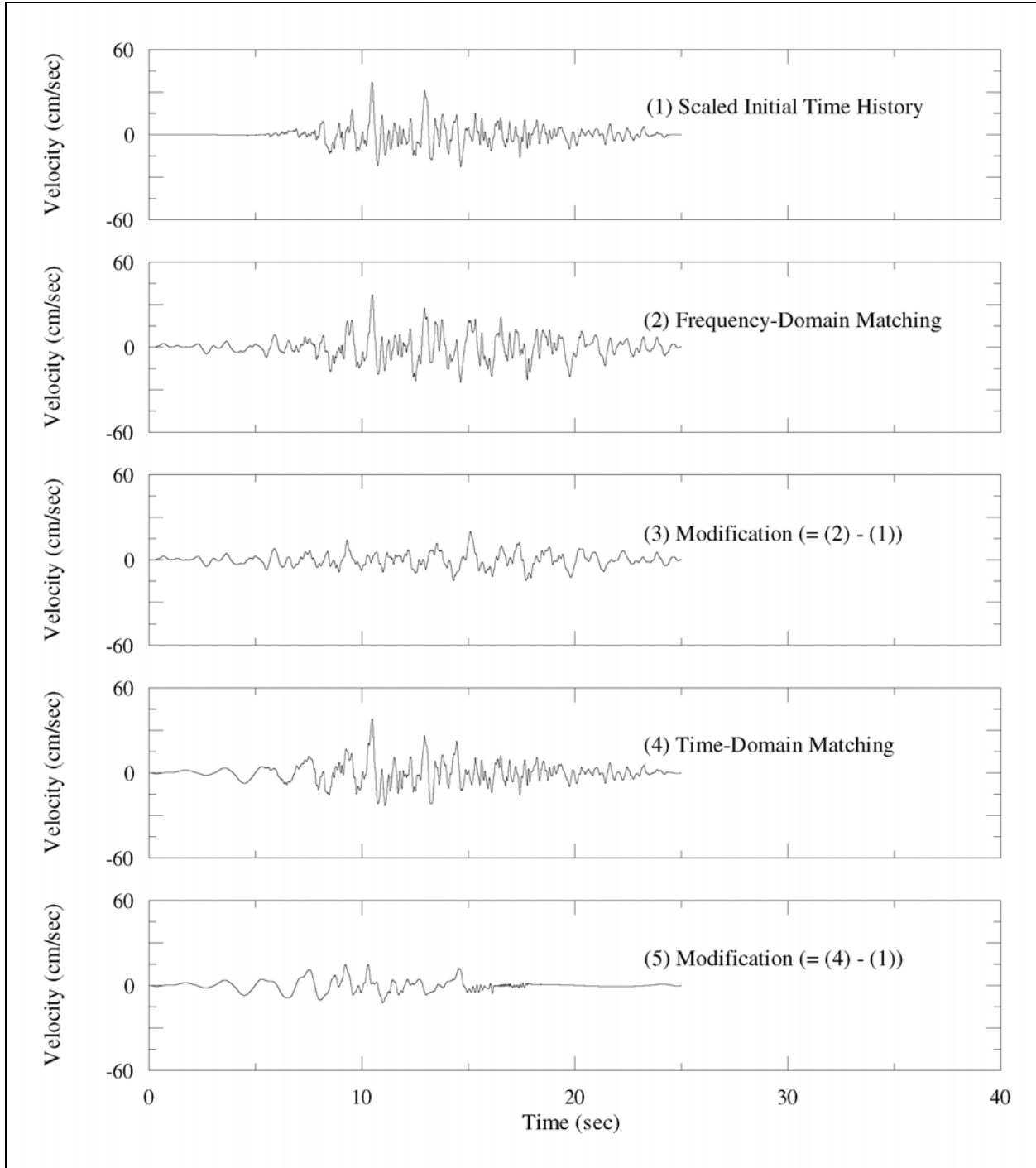
c. Comparison of displacement time-histories: (1) the scaled initial time-history; (2) frequency-domain-matched time-history; (3) modification to the time-history made by the frequency-domain method; (4) time-domain-matched time-history; (5) modification to the time-history made by time-domain method.

Figure C-9. (Sheet 3 of 3)



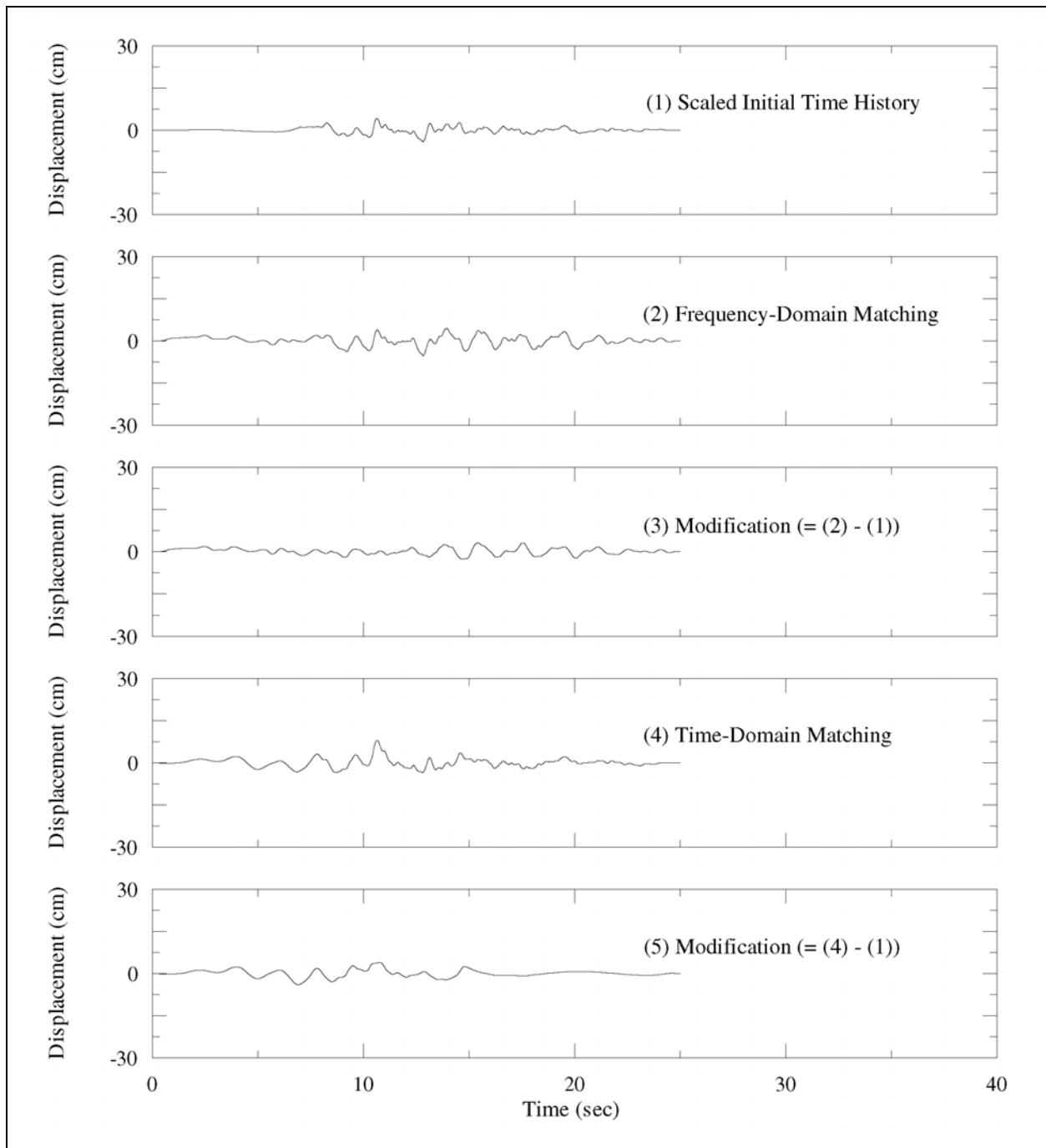
a. Comparison of acceleration time-histories: (1) the scaled initial recorded time-history; (2) frequency-domain-matched time-history; (3) modification to the time-history made by the frequency-domain method; (4) time-domain-matched time-history; (5) modification to the time-history made by time-domain method. Dashed lines indicate the time window used in the calculation of power spectral density function.

Figure C-10. Comparison of time-histories for UCSC BRAN recording (component 090E), 1989 Loma Prieta earthquake (Sheet 1 of 3)



b. Comparison of velocity time-histories: (1) the scaled initial time-history; (2) frequency-domain-matched time-history; (3) modification to the time-history made by the frequency-domain method; (4) time-domain matched time-history; (5) modification to the time-history made by time-domain method.

Figure C-10. (Sheet 2 of 3)



c. Comparison of displacement time-histories: (1) the scaled initial time-history; (2) frequency-domain-matched time-history; (3) modification to the time-history made by the frequency-domain method; (4) time-domain-matched time-history; (5) modification to the time-history made by time-domain method.

Figure C-10. (Sheet 3 of 3)

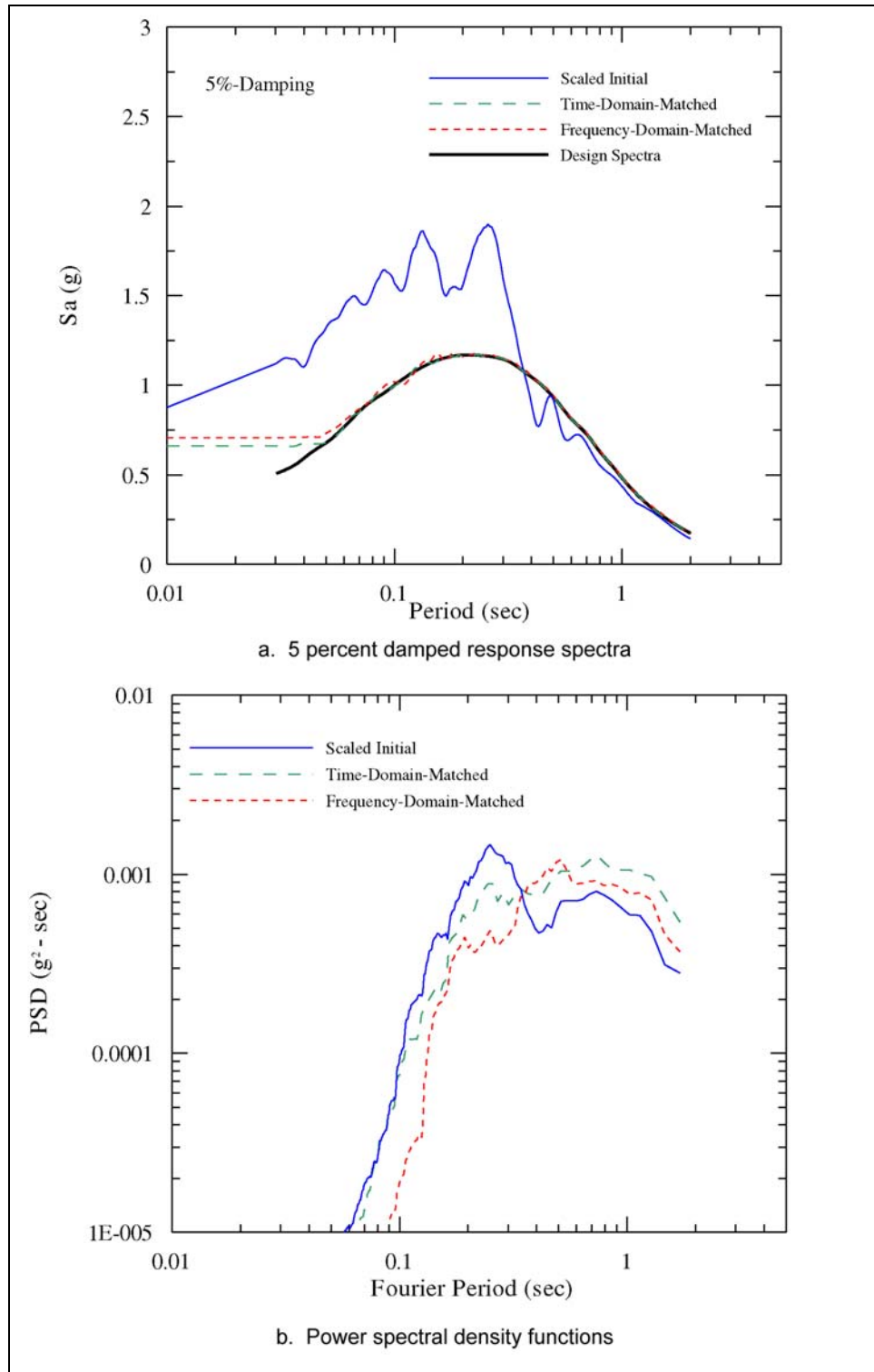


Figure C-11. Comparisons of response spectra and power spectral density functions for the scaled Petrolia recording (component 000E), 1992 Cape Mendocino earthquake, and the spectrum-compatible acceleration time-histories

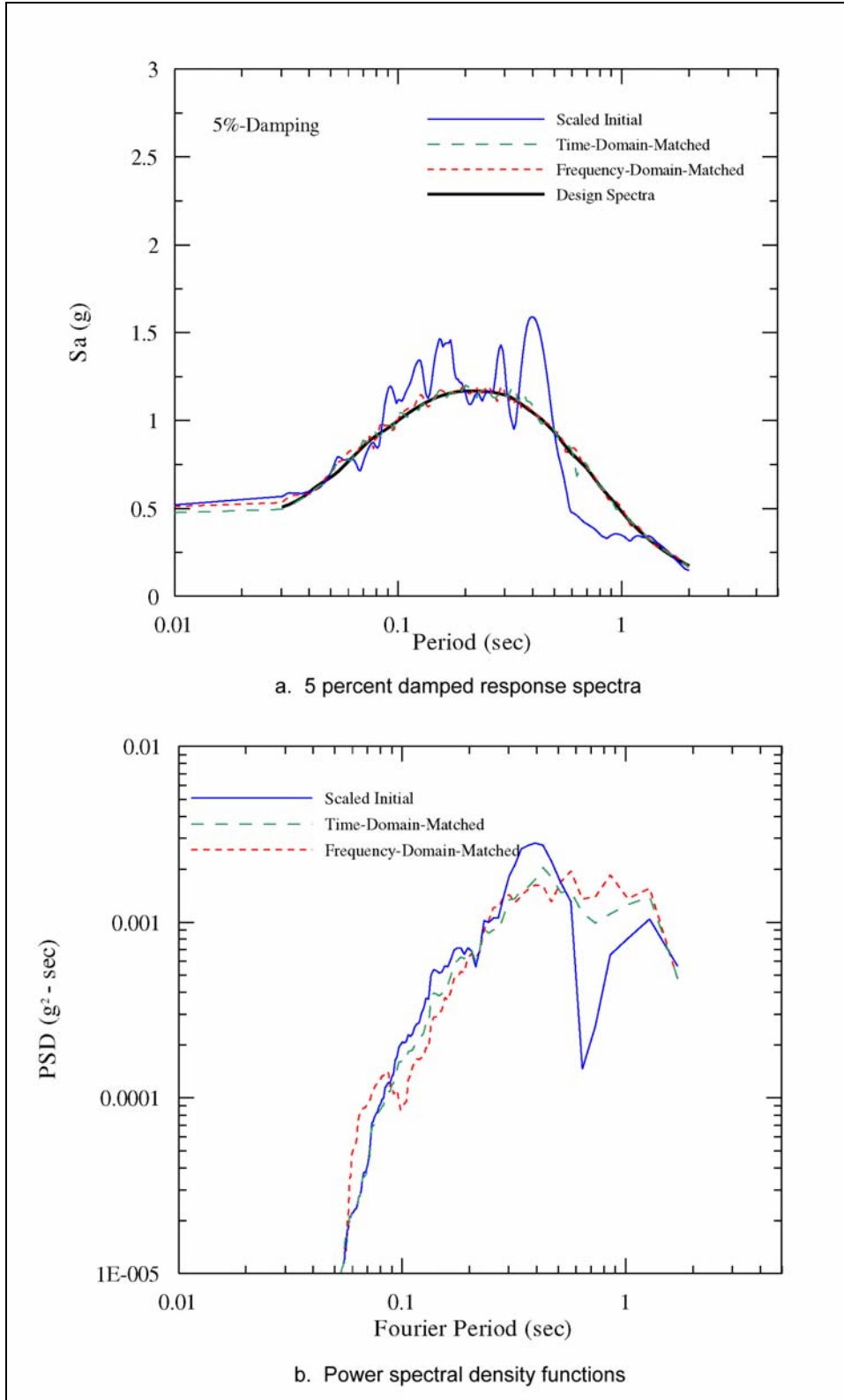


Figure C-12. Comparisons of response spectra and power spectral density functions for the scaled Gilroy recording (component 067E), 1989 Loma Prieta earthquake, and the spectrum-compatible acceleration time-histories

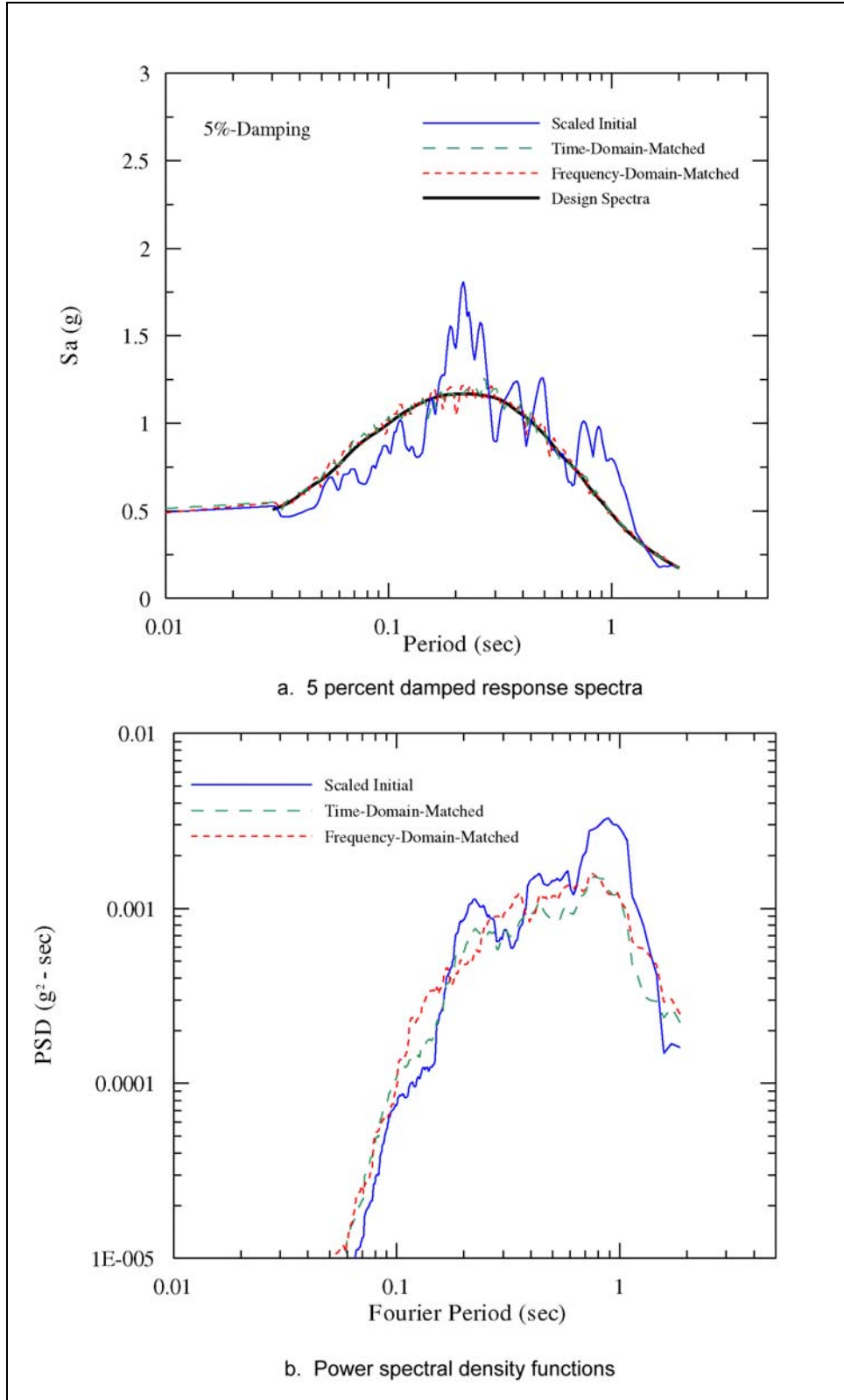


Figure C-13. Comparisons of response spectra and power spectral density functions for the scaled Griffith Park recording (component 270E), 1971 San Fernando earthquake, and the spectrum-compatible acceleration time-histories

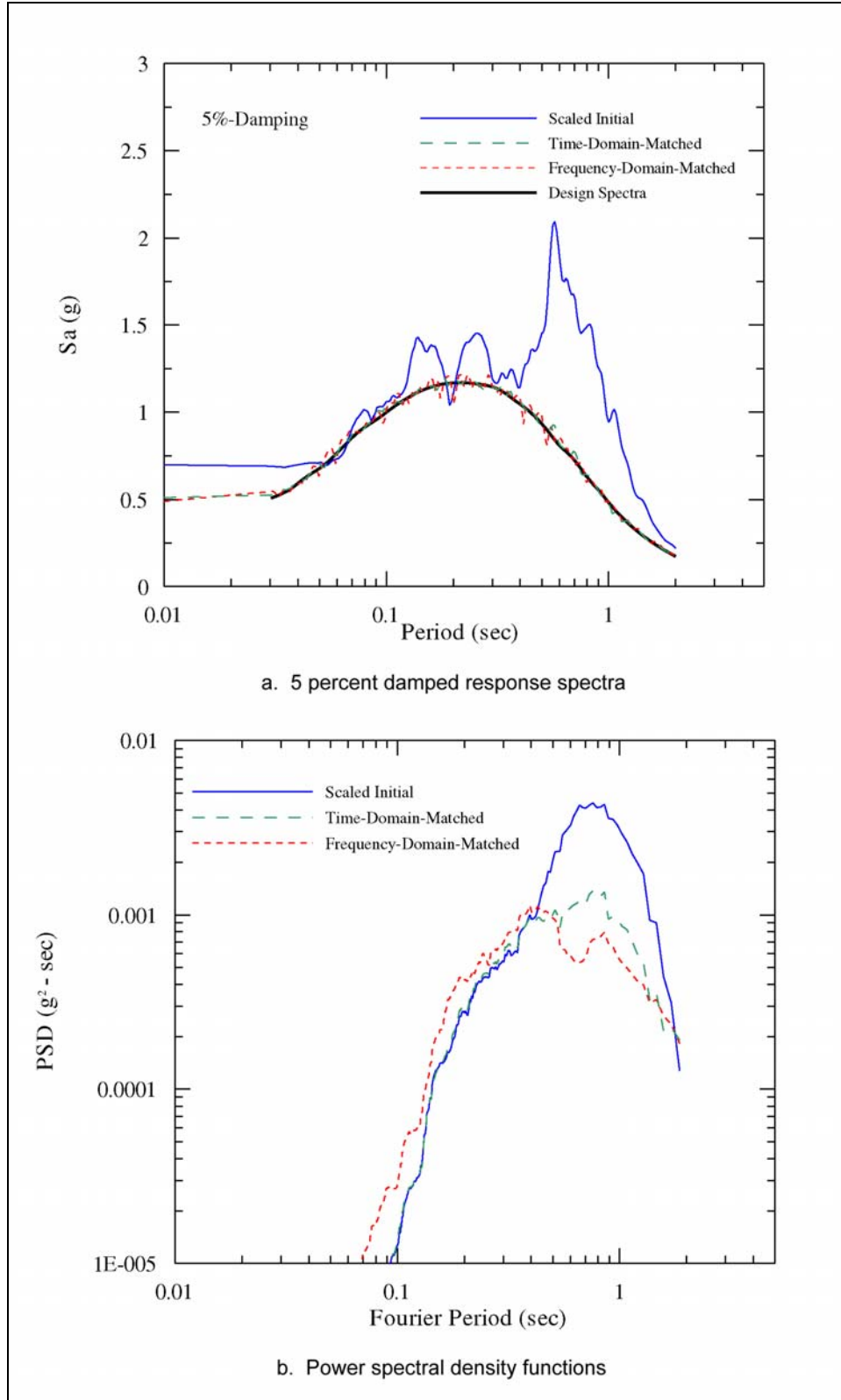


Figure C-14. Comparisons of response spectra and power spectral density functions for the scaled Halls Valley recording (component 240E), 1984 Morgan Hill earthquake, and the spectrum-compatible acceleration time-histories

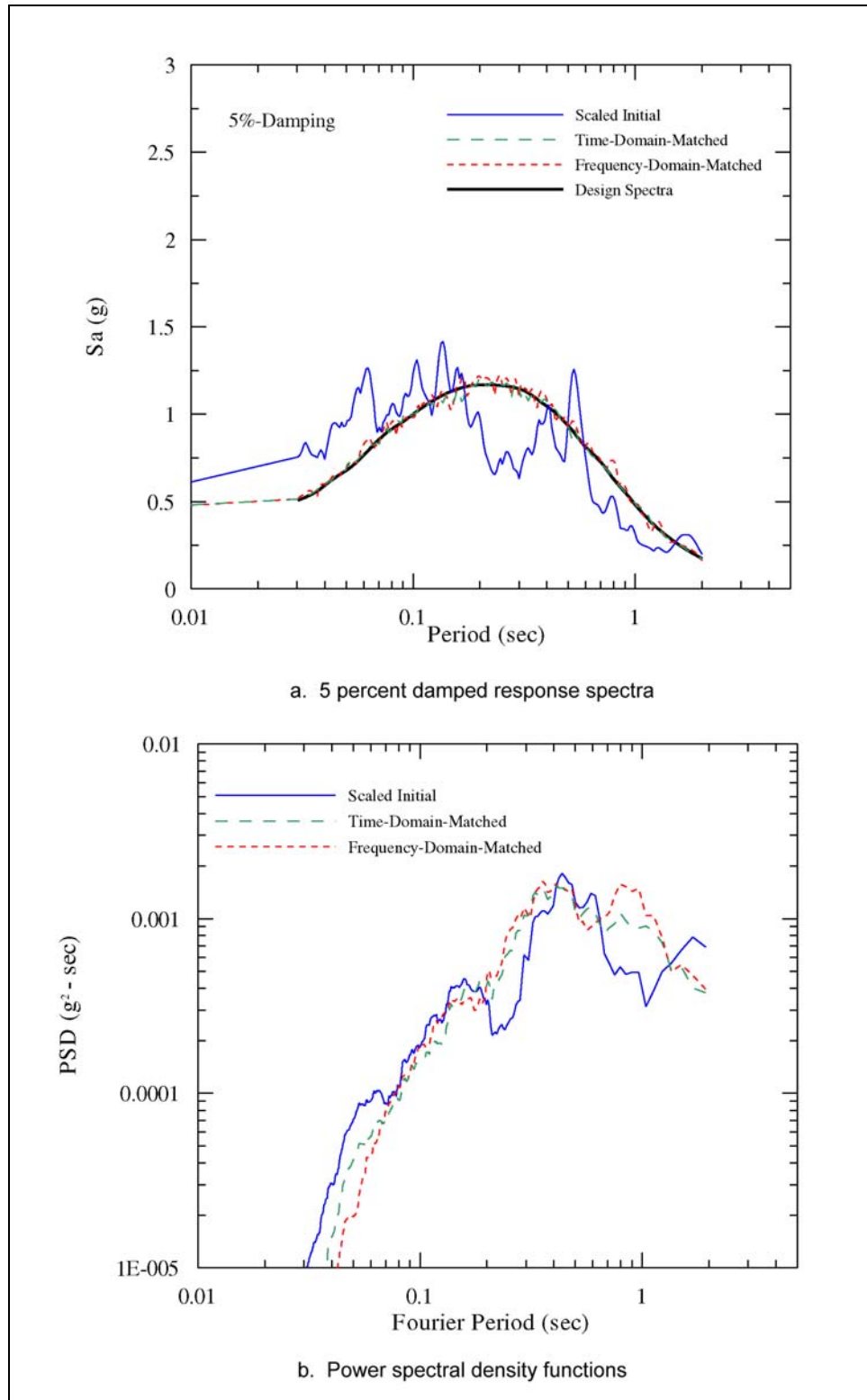


Figure C-15. Comparisons of response spectra and power spectral density functions for the scaled Gazli recording (component 090E), 1976 Gazli earthquake, and the spectrum-compatible acceleration time-histories

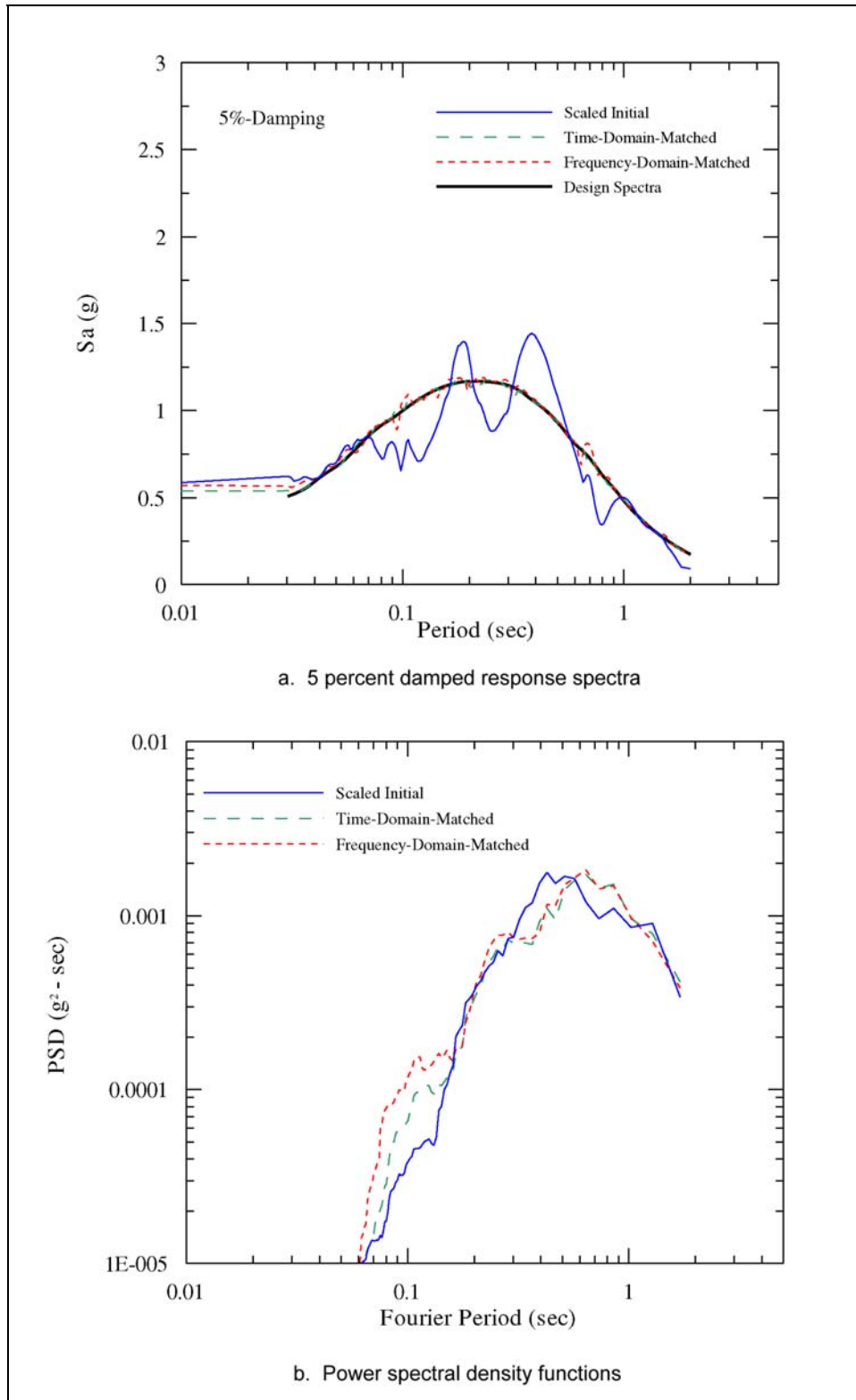


Figure C-16. Comparisons of response spectra and power spectral density functions for the scaled Pacoima Dam recording (component 265E), 1994 Northridge earthquake, and the spectrum-compatible acceleration time-histories

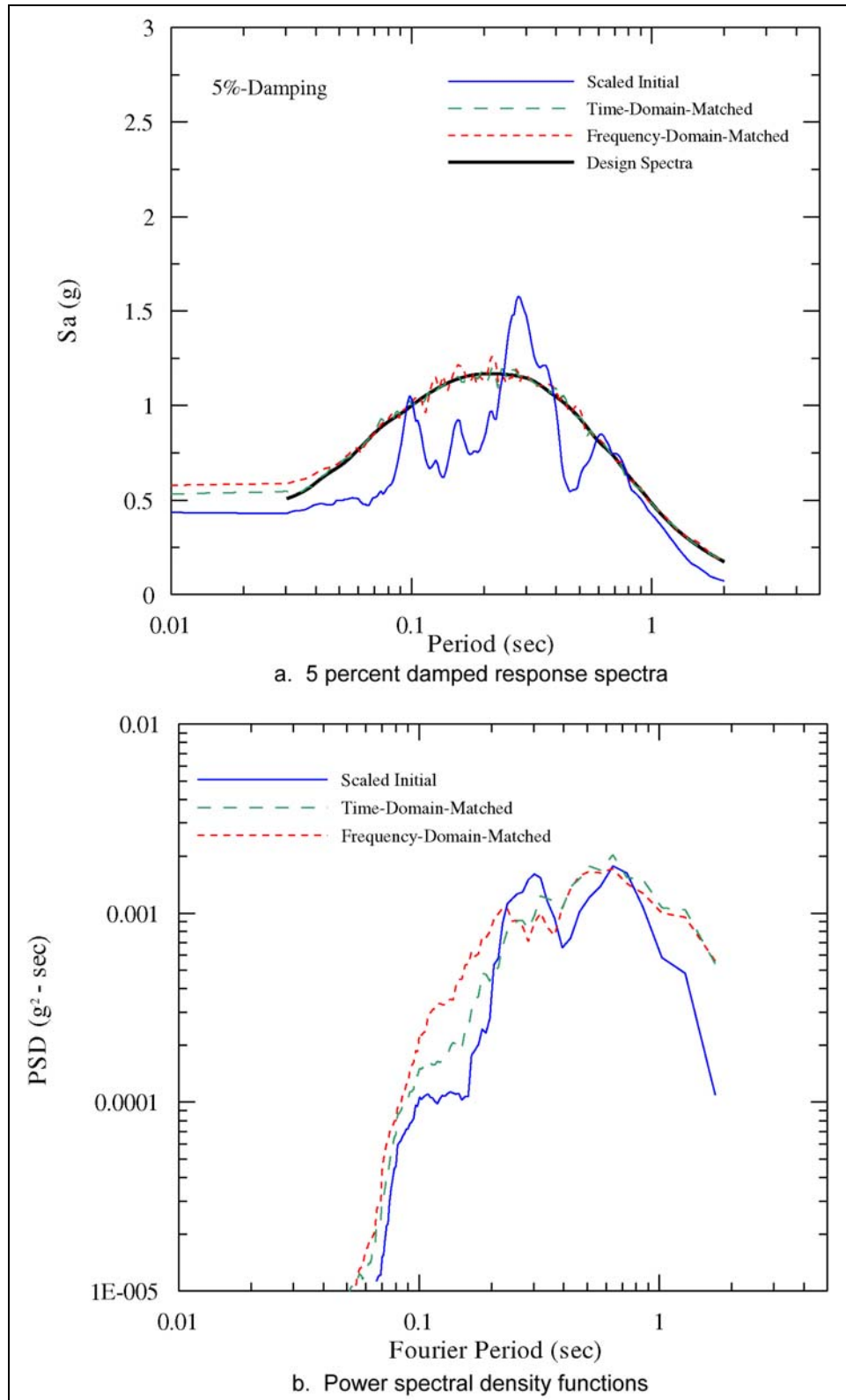


Figure C-17. Comparisons of response spectra and power spectral density functions for the scaled Coyote Lake Dam recording (component 195E), 1984 Morgan Hill earthquake, and the spectrum-compatible acceleration time-histories

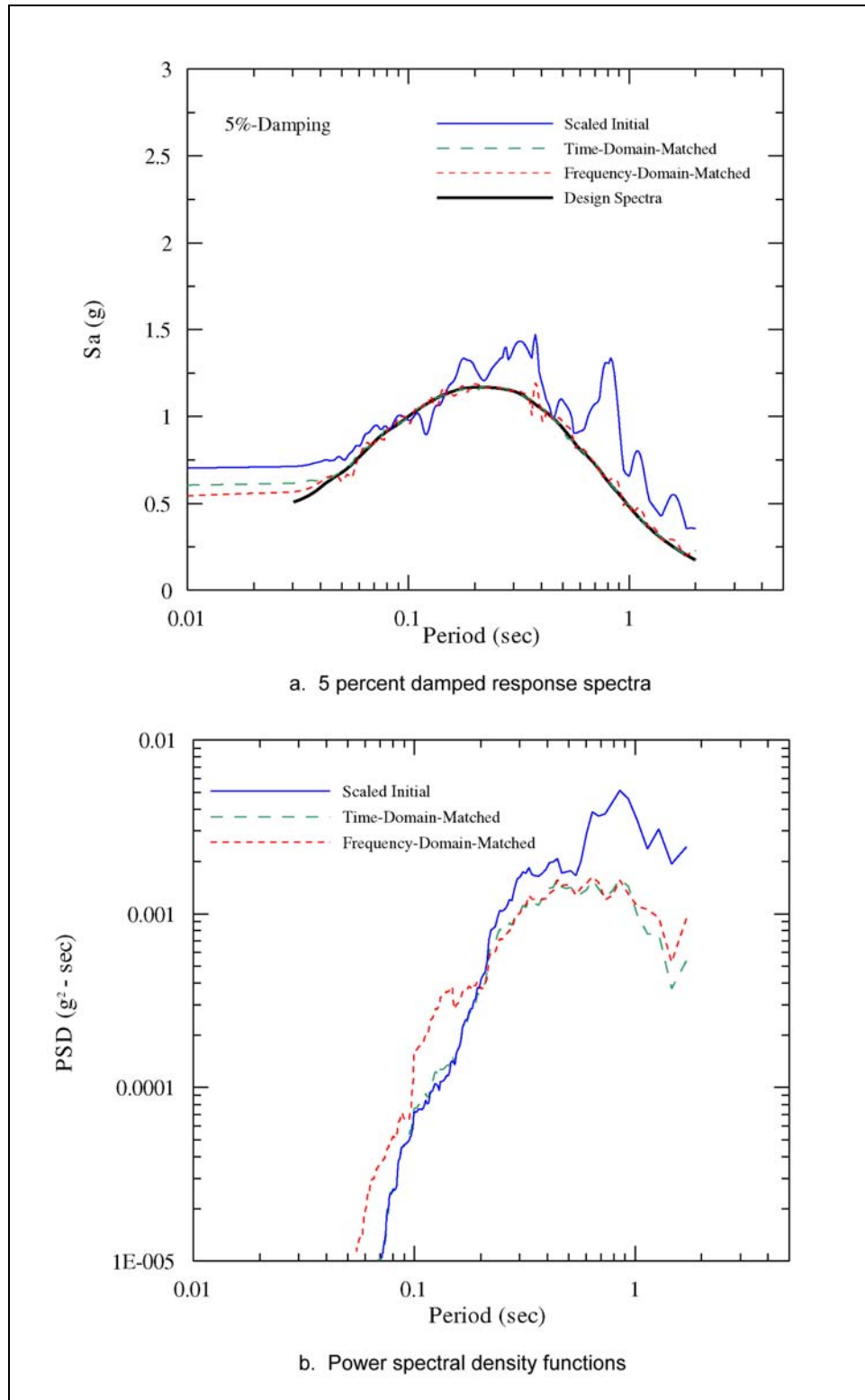


Figure C-18. Comparisons of response spectra and power spectral density functions for the scaled SCEC recording (component 018E), 1994 Northridge earthquake, and the spectrum-compatible acceleration time-histories

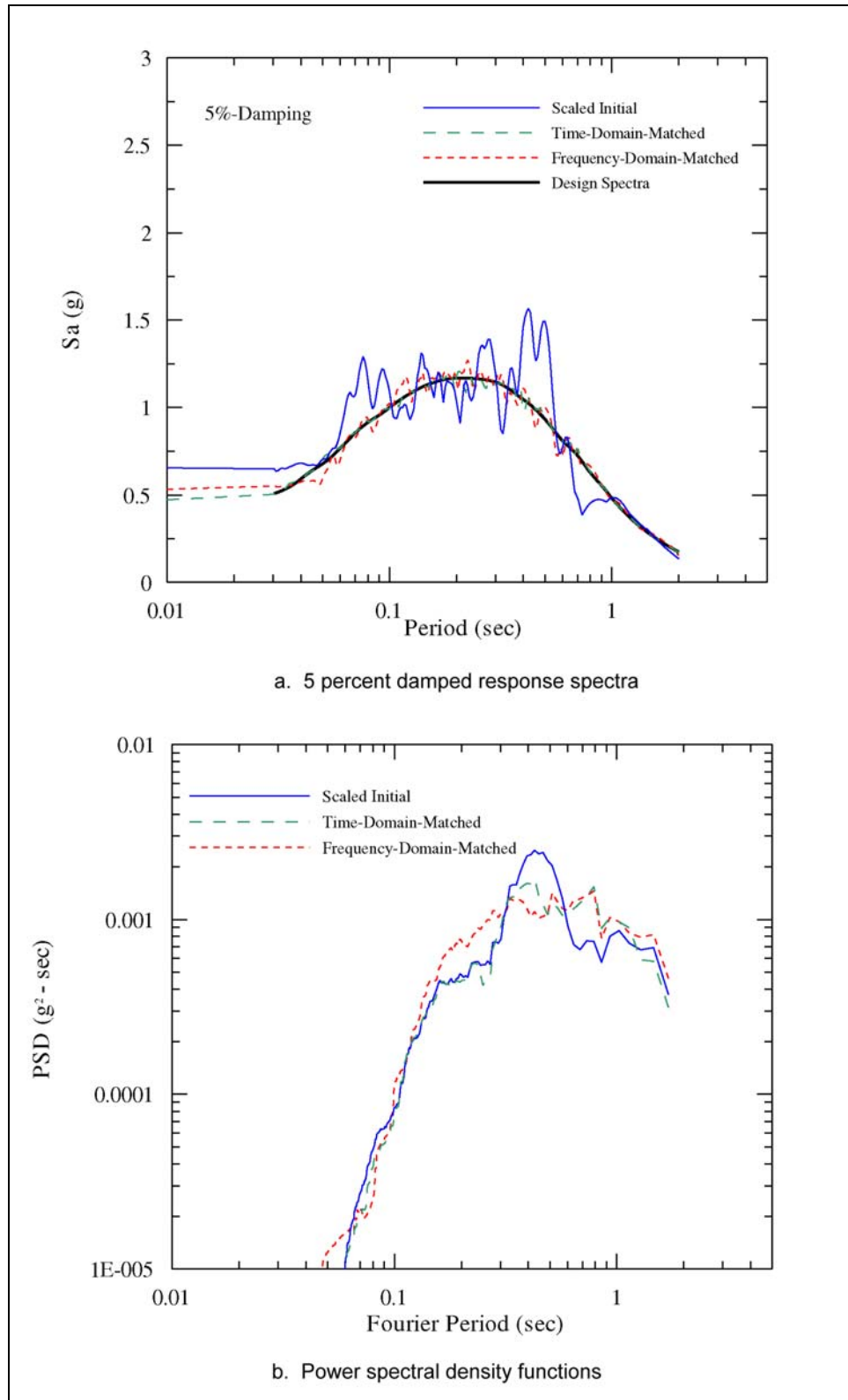


Figure C-19. Comparisons of response spectra and power spectral density functions for the scaled Pacoima Dam recording (component 254E), 1971 San Fernando earthquake, and the spectrum-compatible acceleration time-histories

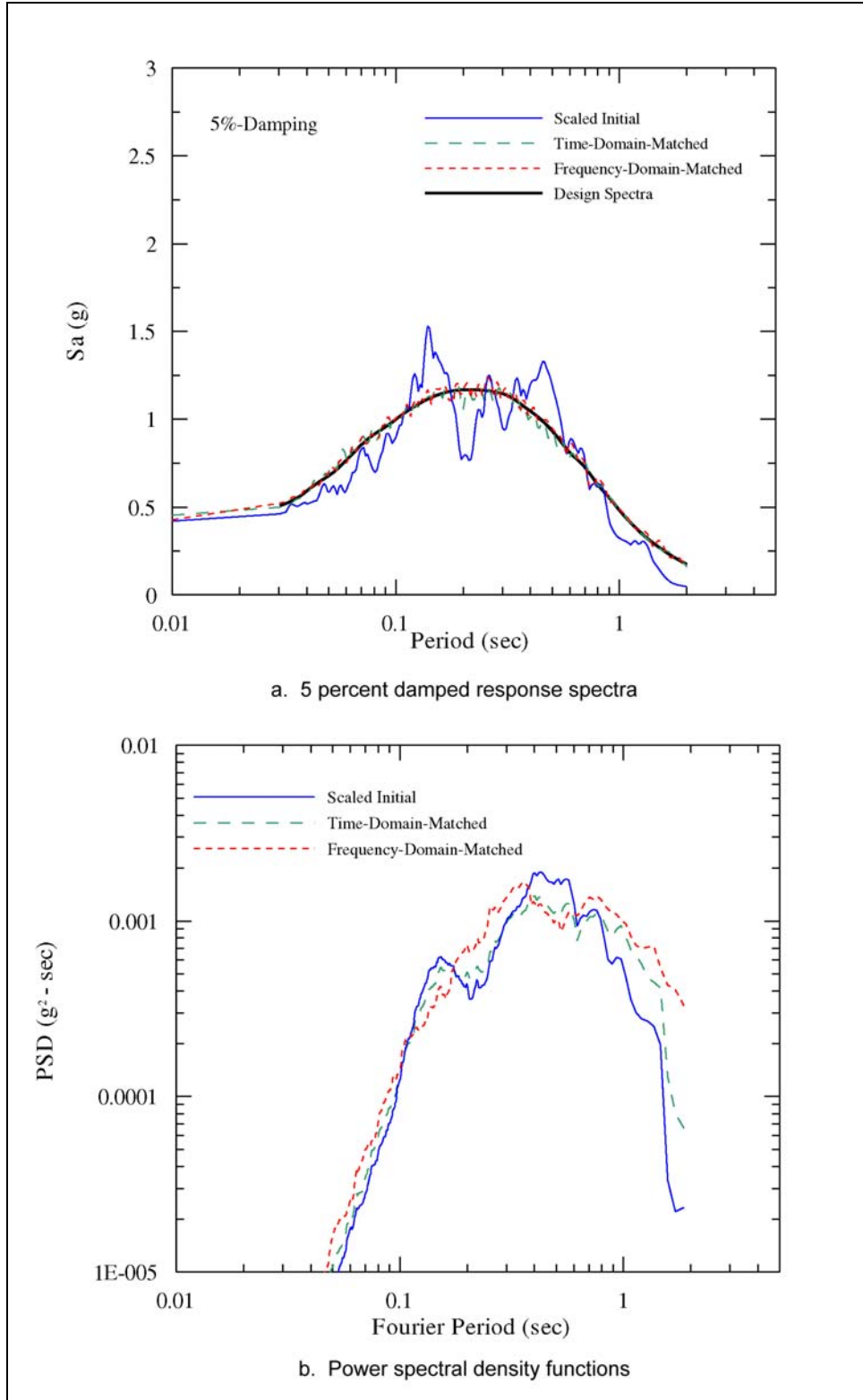


Figure C-20. Comparisons of response spectra and power spectral density functions for the scaled UCSC BRAN recording (component 090E), 1989 Loma Prieta earthquake, and the spectrum-compatible acceleration time-histories

Appendix D Effects of Spectrum Matching on Characteristics of Earthquake Ground Motion Time-Histories

D.1 Introduction

a. This appendix describes evaluations of the effects of spectrum matching on the characteristics of earthquake ground motion time-histories. The approach used in this examination was to select recorded natural earthquake strong motion time-histories; these selected time-histories were then scaled to provide a visual average fit and spectrally modified to provide a close fit to a target response spectrum. The effects of spectral matching were assessed by comparing the basic characteristics of the scaled time-histories with those of the spectrally matched time-histories.

b. The spectrum matching technique used in this study is based on the method originally developed by Lilhanand and Tseng (1988) for time-domain modifications of a time-history so that its response spectrum closely matches a prescribed smooth response spectrum. The technique is described in Appendix C.

D.2 Selection of Earthquake Ground Motion Time-Histories

a. The postulated design earthquake for these evaluations was a moment magnitude M_w 6.5 reverse faulting event located 5 km from the site of interest. For this design earthquake, a smooth design response spectrum (5 percent damping) of site ground motions was constructed for the period range of 0 to 0.6 sec. This period range was selected for spectrum matching in these evaluations because it encompasses the fundamental periods of most concrete hydraulic structures.

b. Ten earthquake strong ground motion time-histories were selected for matching to the smooth response spectrum. In selecting these time-histories, earthquake magnitude, source-to-site distance, and ground motion characteristics (amplitude and frequency content) were considered. Table D-1 lists the selected time-histories and their associated magnitudes and distances. The time-histories were recorded at sites underlain by rock, except for one record that was recorded on a stiff soil site, during earthquakes having moment magnitudes in the range of 6.2 to 7.0 at closest earthquake-source-to-site distances less than 12 km except for one record obtained at 17 km. To reduce the changes that occur to the characteristics of the original time-histories as a result of spectrum matching, time-histories were selected that have response spectral shapes that were generally somewhat similar to the smooth design site response spectrum in the period range of 0 to 0.6 sec.

D.3 Scaling and Spectrum Matching of Time-Histories

a. Each time-history was scaled to the approximate level of the design response spectrum. The scaling factors were obtained by visually “fitting” each response spectrum to the smooth response spectrum, such that spectral peaks would tend to exceed the smooth spectrum, and spectral valleys would tend to lie below it. The scaling factors for the selected time-histories are given in Table D-1. Baseline-corrected time-histories of acceleration, velocity, and displacement of these scaled records are shown in Figures D-1 through D-10. The response spectra of all the scaled time-histories are plotted in Figure D-11, along with the smooth response spectrum. The spectra of the individual scaled time-histories are plotted in Figures D-12 through D-21.

Table D-1
List of Selected Time-Histories

Earthquake	Year	Station	Site	Comp.	M_w	R , km	Scale Factor
San Fernando, CA	1971	279	Rock	254	6.6	2.8	0.60
Gazli, USSR	1976	9201	Rock	90	6.8	3.0	0.75
Morgan Hill, CA	1984	57217	Rock	195	6.2	0.1	0.86
Loma Prieta, CA	1989	UCSCB	Rock	90	7.0	10.3	1.00
		47006	Rock	67	7.0	11.6	1.50
Cape Mendocino, CA	1992	89005	Rock	0	7.0	8.5	0.44
Northridge, CA	1994	6273	Rock	18	6.7	7.8	0.83
		24207	Rock	265	6.7	9.8	1.68
		24436	Rock	90	6.7	16.8	0.33
		24279	Soil	90	6.7	7.6	0.89

Note: M_w = moment magnitude.

R = closest distance from recording station to ruptured fault.

b. After the time-histories were scaled, each time-history was then “matched” to the smooth target spectrum using the method of Lilhanand and Tseng (1988). Note that the spectral characteristics of the time-histories were modified only for periods less than 0.6 sec; at longer periods, the spectral characteristics of the original scaled time-histories were only slightly changed by specifying that the spectra of the original scaled time-histories were also the target spectra and baseline-correcting the spectrum-matched time-histories.

c. Figures D-12 to D-21 show the spectra of the individual scaled time-histories before and after spectrum matching, as well as the target spectrum. Figures D-22 through D-31 show the baseline-corrected time-histories for acceleration, velocity, and displacement for the spectrally matched time-histories.

d. Visual examination of the scaled time-histories (Figures D-1 through D-10) and spectrally matched time-histories (Figures D-22 through D-31) indicates that, in general, the spectrum matching process did not greatly change the time-domain character of the ground motions. The time series of accelerations and velocities are generally similar for the scaled and spectrally matched time-histories, especially for time-histories having scaled spectra that are more similar in shape to the target smooth spectrum. Examination of Figures D-12 through D-21 shows that the matching process achieved a close match to the target smooth spectrum except that a good match was sometimes not possible for very high frequency motions (frequencies equal to or greater than about 25 Hz (periods equal to or less than 0.04 sec).

D.4 Analysis of Characteristics of Time-Histories

a. To quantify the effects of spectrum matching, several characteristics of the scaled time-histories before and after spectrum matching were compared. These characteristics include peak ground acceleration (PGA), effective peak acceleration A_E , root-mean-square acceleration (RMS), peak ground velocity (PGV), peak ground displacement (PGD), strong motion duration T_D , energy E , rate of energy input (power) R , and absolute input energy (IE) to an elastic single-degree-of-freedom oscillator.

b. The definitions of effective peak acceleration, root-mean-square acceleration, strong motion duration, energy, and rate of energy input (power) follow those of Kennedy et al. (1984) and are given below.

(1) Strong motion duration T_D :

$$T_D = T_{0.75} - T_{0.05} \quad (D-1)$$

where $T_{0.75}$ and $T_{0.05}$ represent the times at which 75 percent and 5 percent, respectively, of the total energy (defined in (2) below) have been reached. This definition of strong motion duration is slightly different from that of Kennedy et al. (1984), in which the strong motion duration is defined by the larger of $T_{0.75}$ and the time associated with the first zero crossing following the peak acceleration. This definition of strong motion duration was proposed for stiff structures as an alternative to a more common definition of strong duration, which is:

$$T_D = T_{0.95} - T_{0.05} \quad (D-2)$$

where $T_{0.95}$ is the time associated with 95 percent of the total energy. The definition proposed by Kennedy et al. (1984) thus represents a shorter estimate for the strong motion duration; the shorter duration is based on observations that many ground motion records contain long tails of oscillation having significantly lower amplitudes.

(2) Energy E :

$$E = \int_0^{T_D} a^2(t) dt \quad (D-3)$$

where $a(t)$ is the ground motion acceleration as function of time t . In this analysis, E is calculated over the strong motion duration, $T_D = T_{0.75} - T_{0.05}$. Equation D-3 was proposed by Arias (1970) as a measure of the energy of a ground motion record.

(3) Rate of energy input or power R :

$$R = \frac{E}{T_D} \quad (D-4)$$

where T_D is taken equal to $T_{0.75} - T_{0.05}$.

(4) Root-mean-square acceleration RMS and effective acceleration A_E :

$$RMS = \sqrt{R} \quad (D-5)$$

The RMS acceleration is a statistical average of the absolute values of ground motion accelerations, taken over the strong motion duration T_D . The RMS acceleration can be used as a basis for selecting a design value of acceleration (effective acceleration). Assuming that ground motion can be modeled by a stationary random Gaussian motion, Vanmarcke and Lai (1980) have shown that the effective acceleration of a ground motion record can be expressed as:

$$A_E = K_P * RMS \quad (D-6)$$

$$K_P = \sqrt{2 \ln (2.8T_D / T_0)} \quad (D-7)$$

where T_0 is the predominant period of ground motion.

(5) Absolute input energy IE to an elastic single-degree-of-freedom oscillator is defined as (Mahin and Lin 1983):

$$IE = \int -[C\dot{u}(t) + Ku(t)]\dot{u}_g dt \quad (D-8)$$

where

C and K = damping and stiffness coefficients, respectively, for an elastic system

$u(t)$ = displacement of the system relative to the ground

$u_g(t)$ = displacement of the ground relative to a fixed reference axis

Input energy was calculated using the computer program NONSPEC (Mahin and Lin 1983). For this study, the input energy averaged over the period range of 0 to 0.6 sec was used. Part of the input energy is absorbed by the system (structure), and the rest is dissipated through viscous damping and inelastic (hysteretic) deformations.

c. Tables D-2 and D-3 summarize these characteristics for the scaled and spectrally matched time-histories, respectively. The ratios of ground motion characteristics between the spectrally matched and scaled time-histories are tabulated in Table D-4. The characteristics of the scaled and spectrally matched time-histories are compared in Figures D-32 through D-41.

d. The degree of alteration of the ground motion characteristics as a result of spectrum matching depends on sensitivity of a characteristic with respect to the changes in the amplitude and frequency content of the ground motions; numerical algorithm of the spectrum matching technique; and degree of initial spectral mismatch (before matching) of the scaled time-history and the target spectrum.

Table D-2
Summary of the Characteristics of the Scaled Time-Histories

Earthquake	Station	Comp	T_D^1 sec	T_D^2 sec	E g·g·sec	R g·g	PGA g	RMS g	A_E g	PGV cm/sec	PGD cm	IE (0-0.6 sec) cm/sec
San Fernando	279	254	5.84	7.22	0.13813	0.02364	0.65	0.15	0.46	33.9	7.09	45.78
Gazli	9201	90	5.37	6.74	0.12958	0.02412	0.52	0.16	0.49	35.4	7.3	38.24
Morgan Hill	57217	195	2.30	3.52	0.10018	0.04354	0.56	0.21	0.54	44.7	9.20	31.43
Loma Prieta	UCSCB	90	6.96	9.86	0.24087	0.03458	0.50	0.19	0.57	44.6	6.4	75.90
	47006	67	1.56	4.98	0.09248	0.05929	0.53	0.24	0.62	43.8	8.7	33.83
Cape Mendocino	89005	0	2.94	13.78	0.05122	0.01742	0.66	0.13	0.37	56.3	22.3	20.69
Northridge	6273	18	3.78	7.21	0.14157	0.03745	0.69	0.19	0.52	97.2	32.6	--
	24436	90	6.52	10.70	0.11238	0.01724	0.59	0.13	0.40	51.60	7.7	40.85
	24207	265	2.02	4.10	0.09230	0.04569	0.73	0.21	0.55	36.2	10.3	46.37
	24279	90	2.82	5.92	0.15517	0.05503	0.52	0.23	0.60	66.5	15.8	66.67
Average--	--	--	4.01	7.41	0.12530	0.03580	0.59	0.18	0.51	51.0	12.7	44.42

Note: Parameters are defined in text.

T_D^1 : Strong duration between 5 and 75 percent of total energy.

T_D^2 : Strong duration between 5 and 95 percent of total energy.

Table D-3
Summary of the Characteristics of the Spectrally Matched Time-Histories

Earthquake	Station	Comp	T_D^1 sec	T_D^2 sec	E g-g-sec	R g-g	PGA g	RMS g	A_E g	PGV cm/sec	PGD cm	IE (0-0.6 sec) cm/sec
San Fernando	279	254	5.44	7.02	0.14963	0.02751	0.59	0.17	0.49	32.8	8.3	53.78
Gazli	9201	90	5.13	6.73	0.15741	0.03067	0.58	0.18	0.54	34.7	6.9	52.03
Morgan Hill	57217	195	3.08	4.48	0.10283	0.03339	0.64	0.18	0.50	41.2	9.5	35.96
Loma Prieta	UCSCB	90	7.90	11.27	0.23827	0.03016	0.51	0.17	0.54	43.1	4.9	69.10
	47006	67	2.66	5.52	0.11499	0.04323	0.50	0.21	0.58	31.8	8.4	35.71
Cape Mendocino	89005	0	1.34	4.48	0.05889	0.04395	0.74	0.21	0.49	59.0	22.0	33.92
Northridge	6273	18	3.68	6.55	0.13219	0.03587	0.74	0.19	0.51	101.0	29.8	--
	24436	90	6.16	9.94	0.14255	0.02314	0.63	0.15	0.46	34.4	8.5	49.54
	24207	265	3.08	5.90	0.13988	0.04542	0.60	0.21	0.60	43.2	8.1	45.50
	24279	90	4.48	10.66	0.17222	0.03844	0.61	0.20	0.55	52.9	17.5	58.15
Average--	--	--	4.29	7.25	0.14100	0.03510	0.61	0.19	0.53	47.4	12.4	48.19

Note: Parameters are defined in text.

T_D^1 : Strong duration between 5 and 75 percent of total energy.

T_D^2 : Strong duration between 5 and 95 percent of total energy.

e. The results of the analyses for this examination generally indicate that the spectrum matching technique did not alter the ground motion characteristics greatly. Spectrum matching, however, increased on average the energy, power, and strong motion duration of the ground motions. From the analyzed time-histories, an average increase of about 10 to 20 percent in the strong motion duration, power, and energy content of a ground motion occurred as a result of spectrum matching (Table D-4).

f. For the 1992 Cape Mendocino record, spectrum matching produces much shorter strong motion duration. With only about 16 percent increase in the total energy of this record, the shorter duration results in much higher calculated power for the spectrally matched time-history (about 2.6 times higher). Spectrum matching also results in higher effective and RMS accelerations for the 1992 Cape Mendocino record. As shown in Figure D-6, the Cape Mendocino time-history is unusual in that it contains a single peak that is three times higher than any other peak of the accelerogram. The spectral shape of this record is much different from the smooth spectrum over the period range of matching (0 to 0.6 sec), being substantially lower in the period range 0.3 to 0.6 sec and substantially higher at periods less than 0.2 sec (Figure D-17).

g. Figures D-42 through D-51 present the correlations of initial spectral mismatch and the degree of alteration for the analyzed ground motion characteristics. Initial spectral mismatch $\delta(T)$ at a period T is defined as follows:

$$\delta(T) = \frac{|Sa(T) - Sa(T)_{Target}|}{Sa(T)_{Target}} \quad (D-9)$$

where $Sa(T)$ and $Sa(T)_{Target}$ are the response spectral ordinates of the scaled time-history (before matching) and the target spectrum, respectively, at the period T . Two measures of initial mismatch, over the period range of 0 to 0.6 sec, were used for this study:

Table D-4
Ratios of the Characteristics Between Spectrally Matched and Scaled Time-Histories

Earthquake	Station	Comp	T_D^1 sec	T_D^2 sec	E g·g·sec	R g·g	PGA g	RMS g	A_E g	PGV cm/sec	PGD cm	IE (0-0.6 sec) cm/sec
San Fernando	279	254	0.931	0.972	1.087	1.167	0.908	1.133	1.065	0.968	1.171	1.175
Gazli	9201	90	0.956	0.998	1.215	1.292	1.115	1.125	1.102	0.980	0.945	1.361
Morgan Hill	57217	195	1.339	1.273	1.030	0.750	1.143	0.857	0.926	0.922	1.033	1.144
Loma Prieta	UCSCB	90	1.134	1.142	0.988	0.857	1.020	0.895	0.947	0.996	0.766	0.910
	47006	67	1.705	1.108	1.250	0.729	0.943	0.875	0.935	0.726	0.966	1.056
Cape Mendocino	89005	0	0.456	0.325	1.157	2.588	1.121	1.165	1.324	1.048	0.987	1.639
Northridge	6273	18	0.975	0.908	0.930	0.973	1.072	1.000	0.981	1.039	0.914	--
	24436	90	0.945	0.927	1.277	1.353	1.068	1.154	1.150	0.667	1.104	1.213
	24207	265	1.525	1.439	1.522	0.978	0.822	1.000	1.091	1.193	0.786	0.981
	24279	90	1.589	1.800	1.110	0.691	1.173	0.870	0.917	0.795	1.108	0.872
Average	--	--	1.155	1.09	1.156	1.138	1.039	1.052	1.044	0.930	0.978	1.150

Note: Parameters are defined in text.
 T_D^1 : Strong duration between 5 and 75 percent of total energy.
 T_D^2 : Strong duration between 5 and 95 percent of total energy.

(1) Average mismatch $*_{ave}$:

$$\delta_{ave} = Average \{ \delta(T_1), \dots, \delta(T_N) \} \quad (D-10)$$

(2) Maximum mismatch $*_{max}$:

$$\delta_{max} = Maximum \{ \delta(T_1), \dots, \delta(T_N) \} \quad (D-11)$$

where T_1 and T_N are the N discrete periods over the period range of 0 to 0.6 sec.

h. Figures D-42 through D-51 show that there are no apparent correlations between the analyzed ground motion characteristics and average or maximum mismatch, with the exception that a positive correlation may be inferred for the peak ground acceleration (Figure D-42).

i. It should be noted that this study is based on a relatively limited number of records. These records were selected because their initial spectral shapes are generally similar to that of the target smooth design spectrum. The lack of correlation between the analyzed characteristics and initial spectral mismatch may be due to the fact that overall initial mismatch is relatively small.

j. Figure D-51 and Table D-4 indicate that, except for the Gazli and Cape Mendocino records, the input energy of the spectrally matched and scaled records are within a factor of about 1.2 of each other. The larger differences for the Gazli and Cape Mendocino records are likely due to the poor match at periods greater than 0.2 to 0.3 sec between the spectra of the scaled time-histories and the smooth spectrum, as shown in Figures D-13 and D-17.

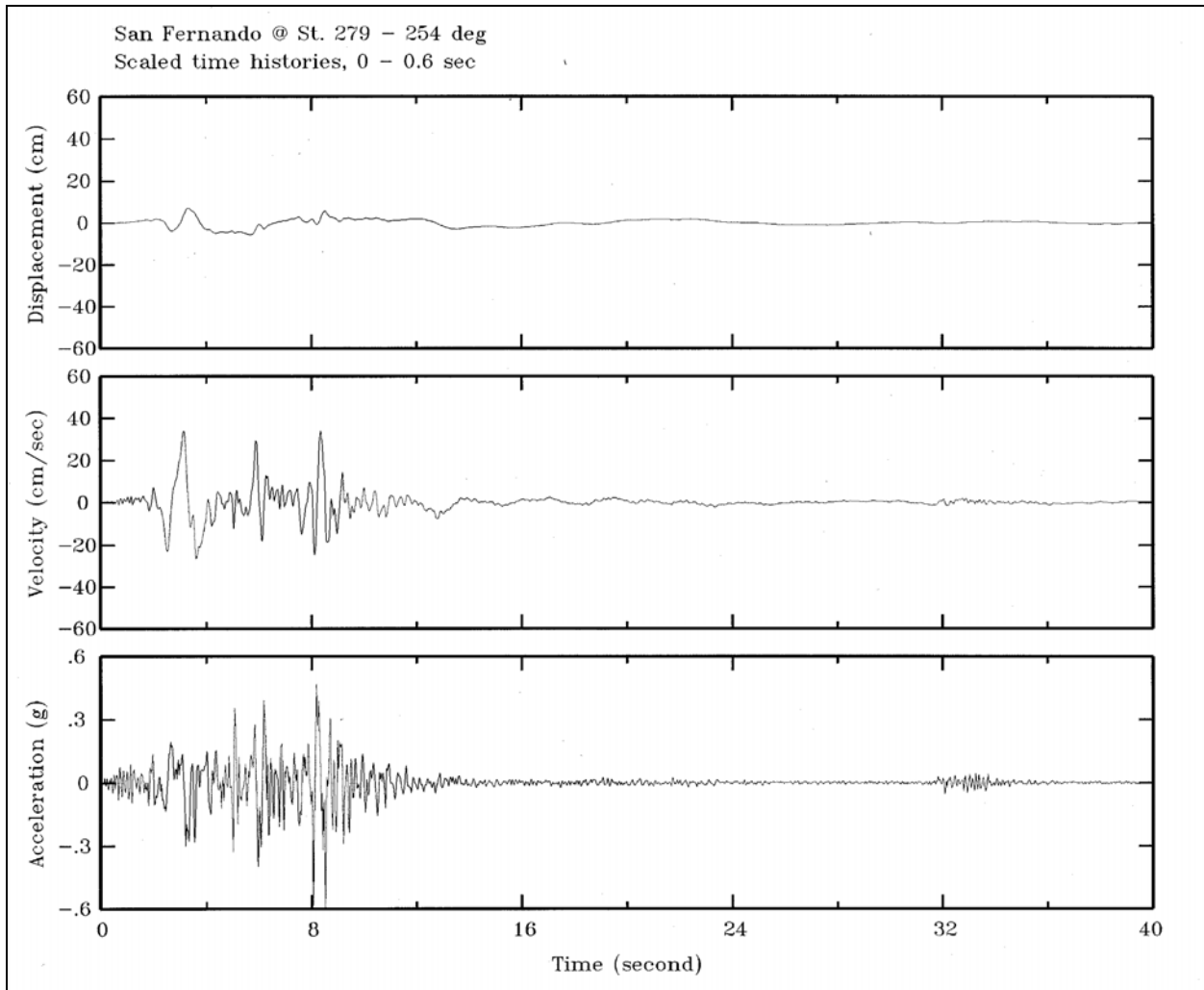


Figure D-1. Scaled time-histories of acceleration, velocity, and displacement for the 1971 San Fernando earthquake recorded at station 279

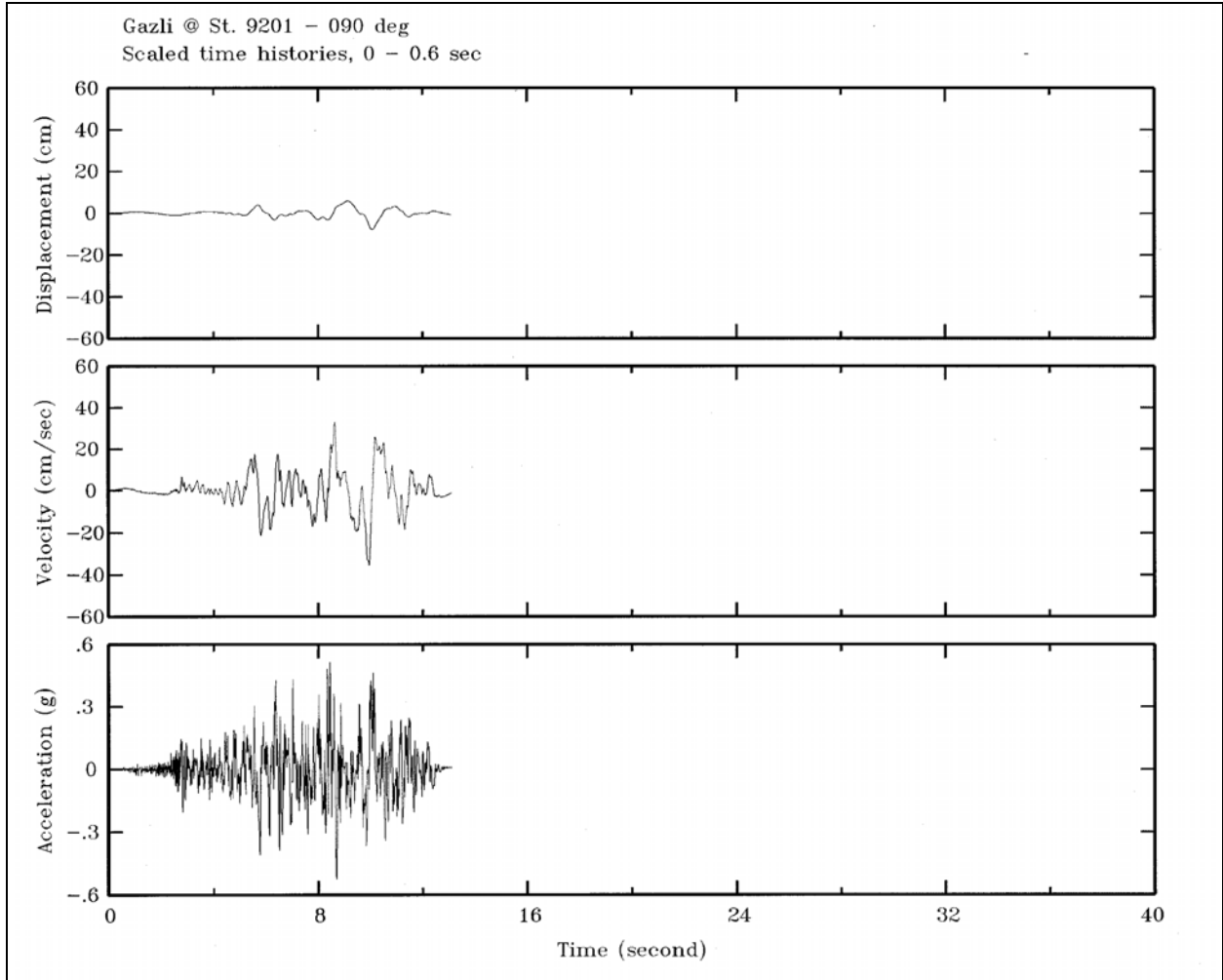


Figure D-2. Scaled time-histories of acceleration, velocity, and displacement for the 1976 Gazli earthquake recorded at Gazli

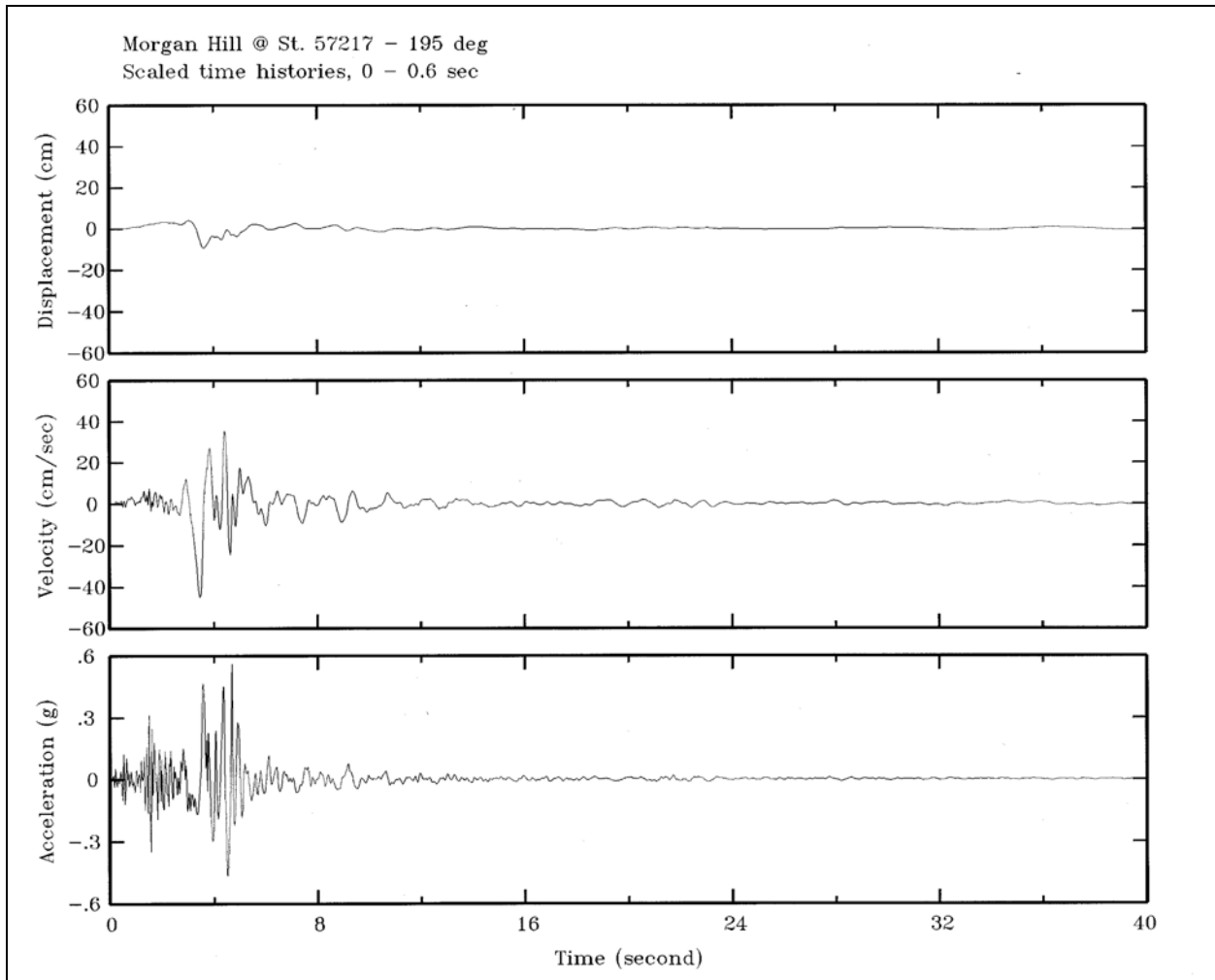


Figure D-3. Scaled time-histories of acceleration, velocity, and displacement for the 1984 Morgan Hill earthquake recorded at station 57217

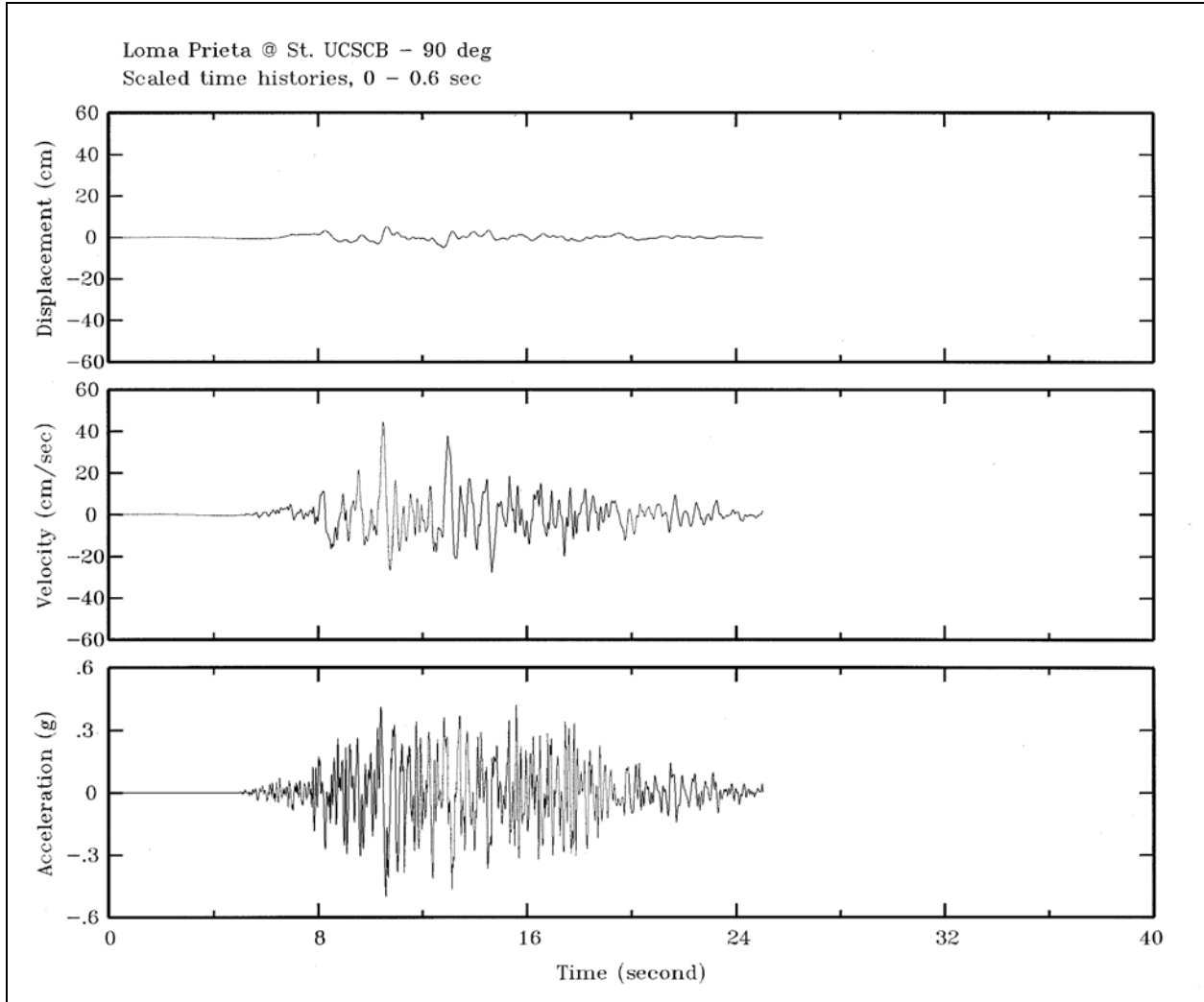


Figure D-4. Scaled time-histories of acceleration, velocity, and displacement for the 1989 Loma Prieta earthquake recorded at UCSC Brane building

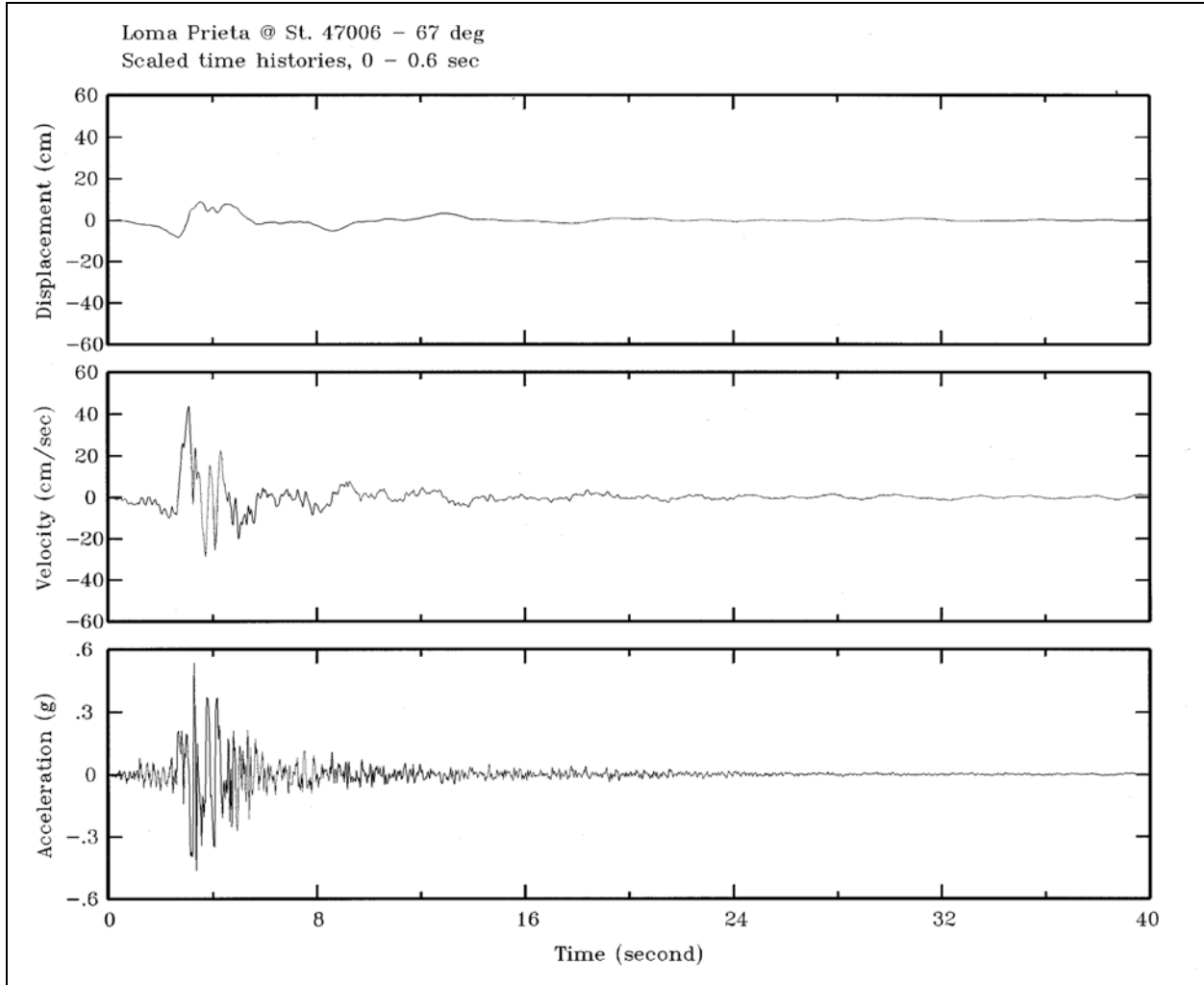


Figure D-5. Scaled time-histories of acceleration, velocity, and displacement for the 1989 Loma Prieta earthquake recorded at station 47006

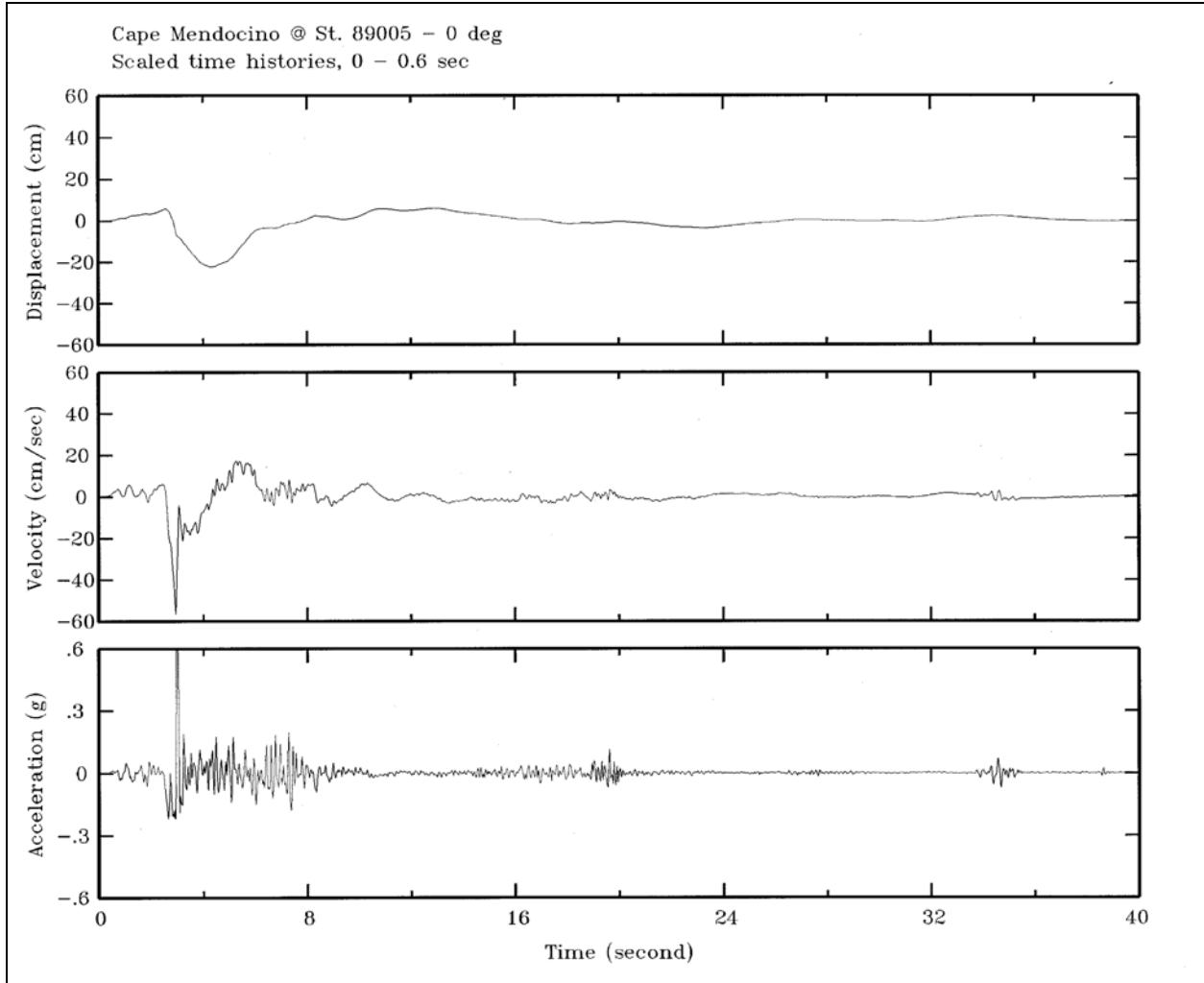


Figure D-6. Scaled time-histories of acceleration, velocity, and displacement for the 1992 Cape Mendocino earthquake recorded at station 89005

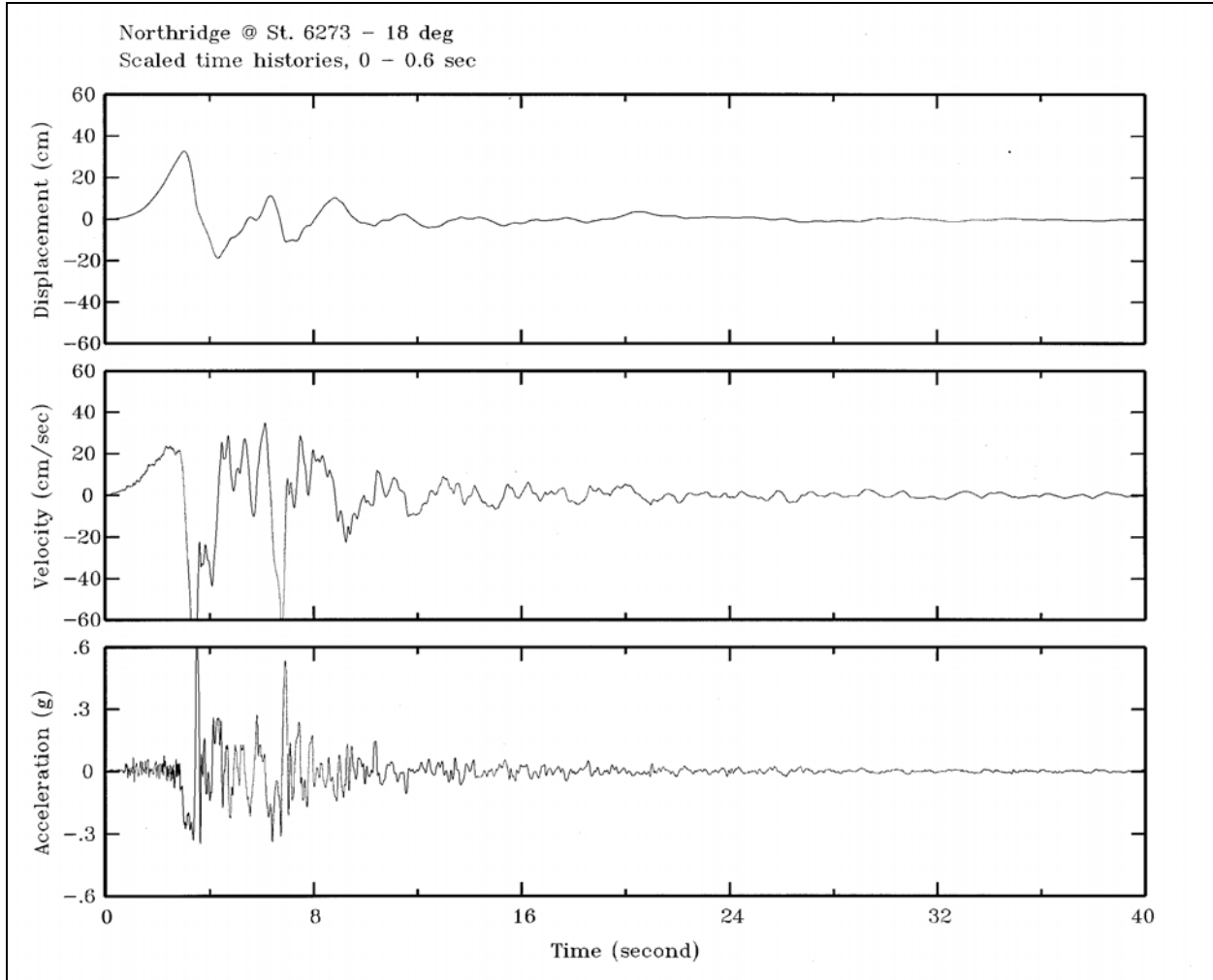


Figure D-7. Scaled time-histories of acceleration, velocity, and displacement for the 1994 Northridge earthquake recorded at station 6273

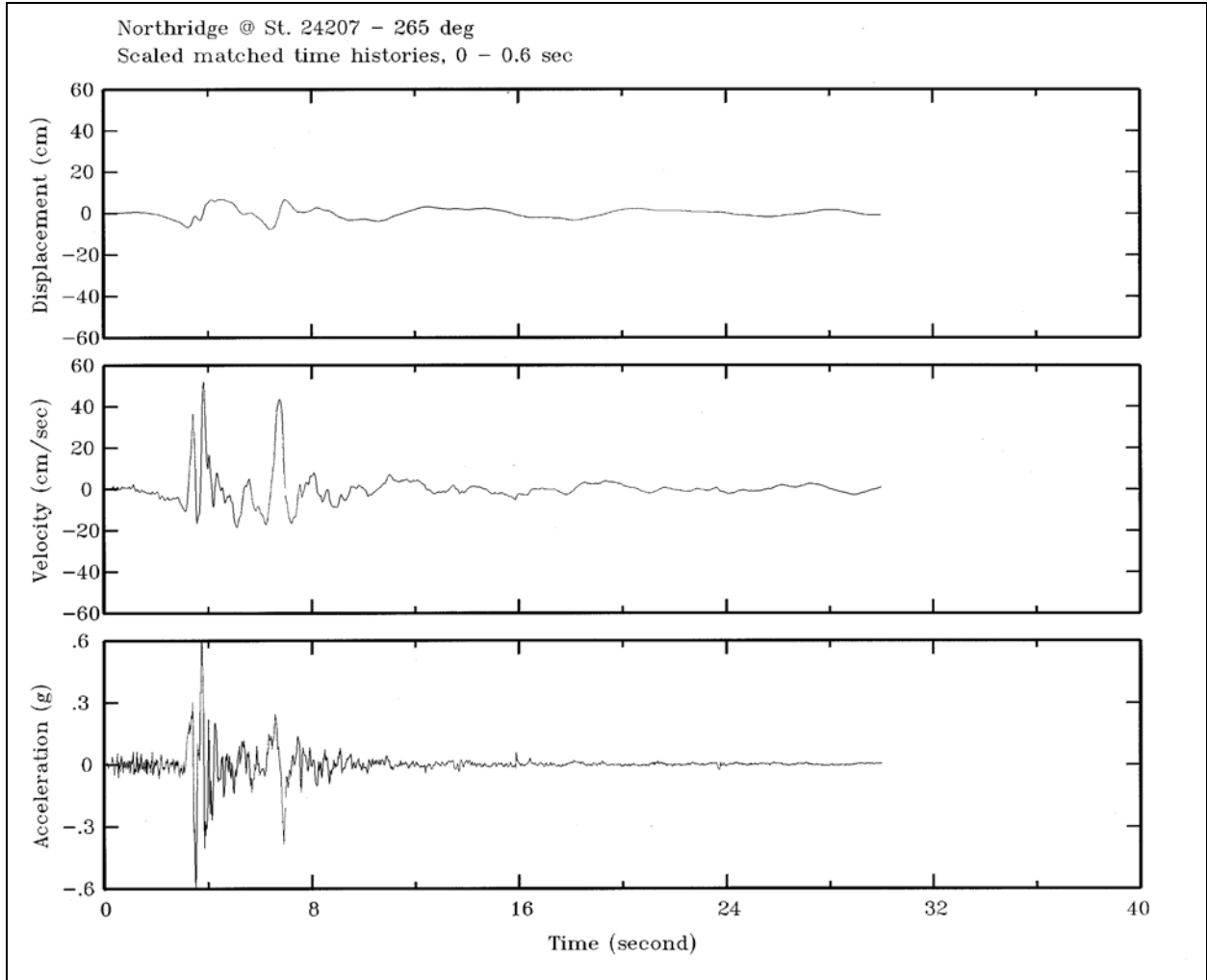


Figure D-8. Scaled time-histories of acceleration, velocity, and displacement for the 1994 Northridge earthquake recorded at station 24207

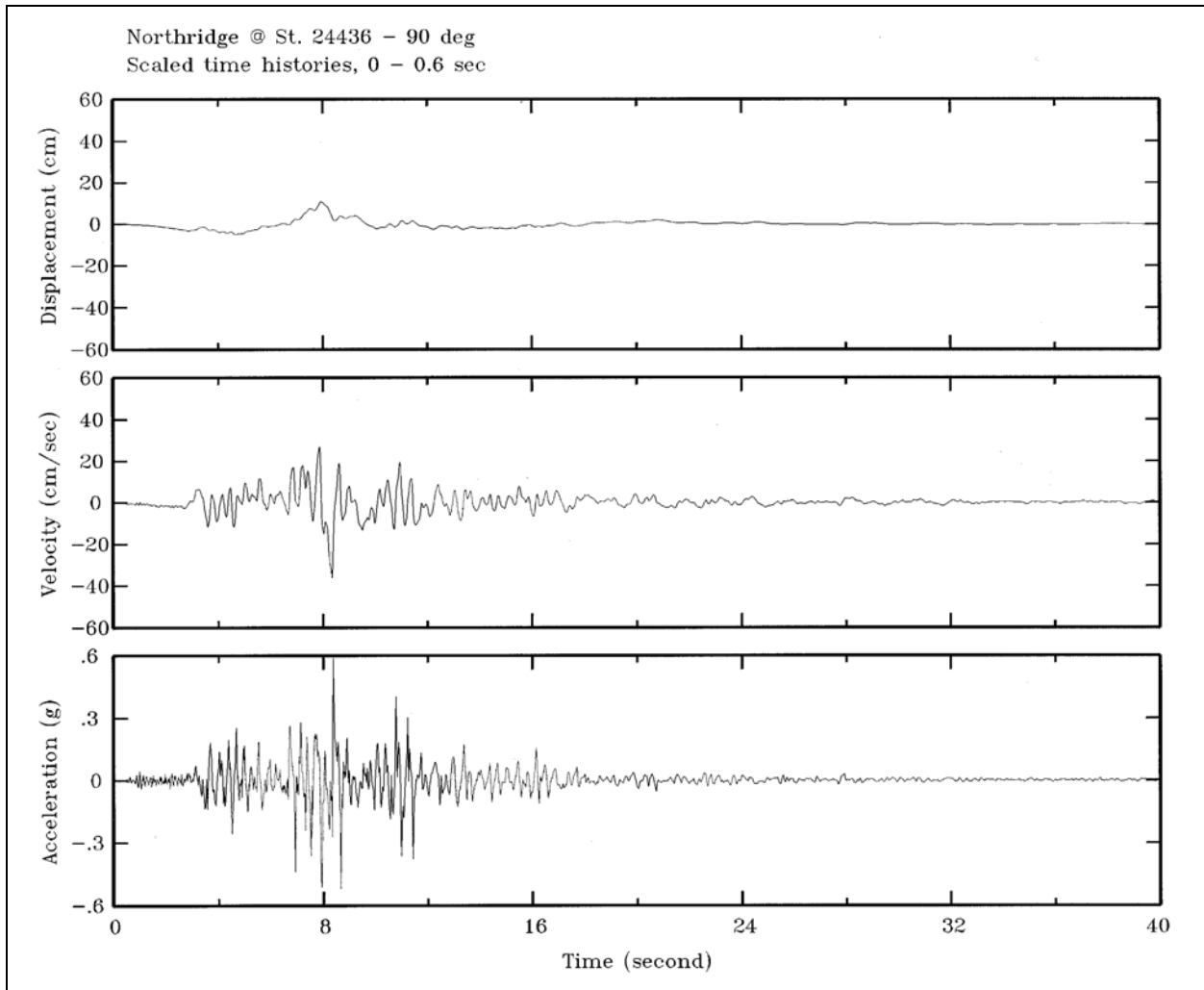


Figure D-9. Scaled time-histories of acceleration, velocity, and displacement for the 1994 Northridge earthquake recorded at station 24436

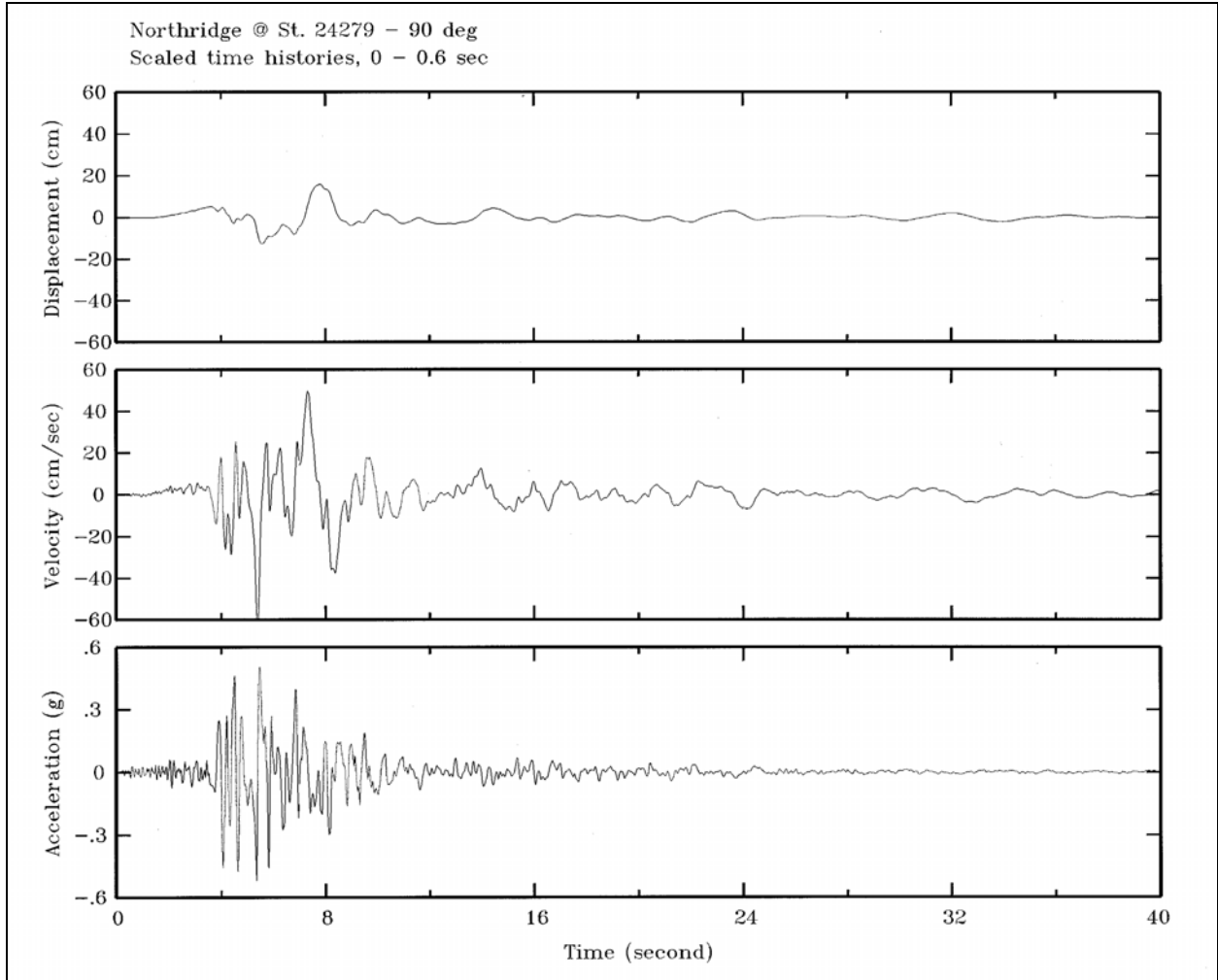


Figure D-10. Scaled time-histories of acceleration, velocity, and displacement for the 1994 Northridge earthquake recorded at station 24279

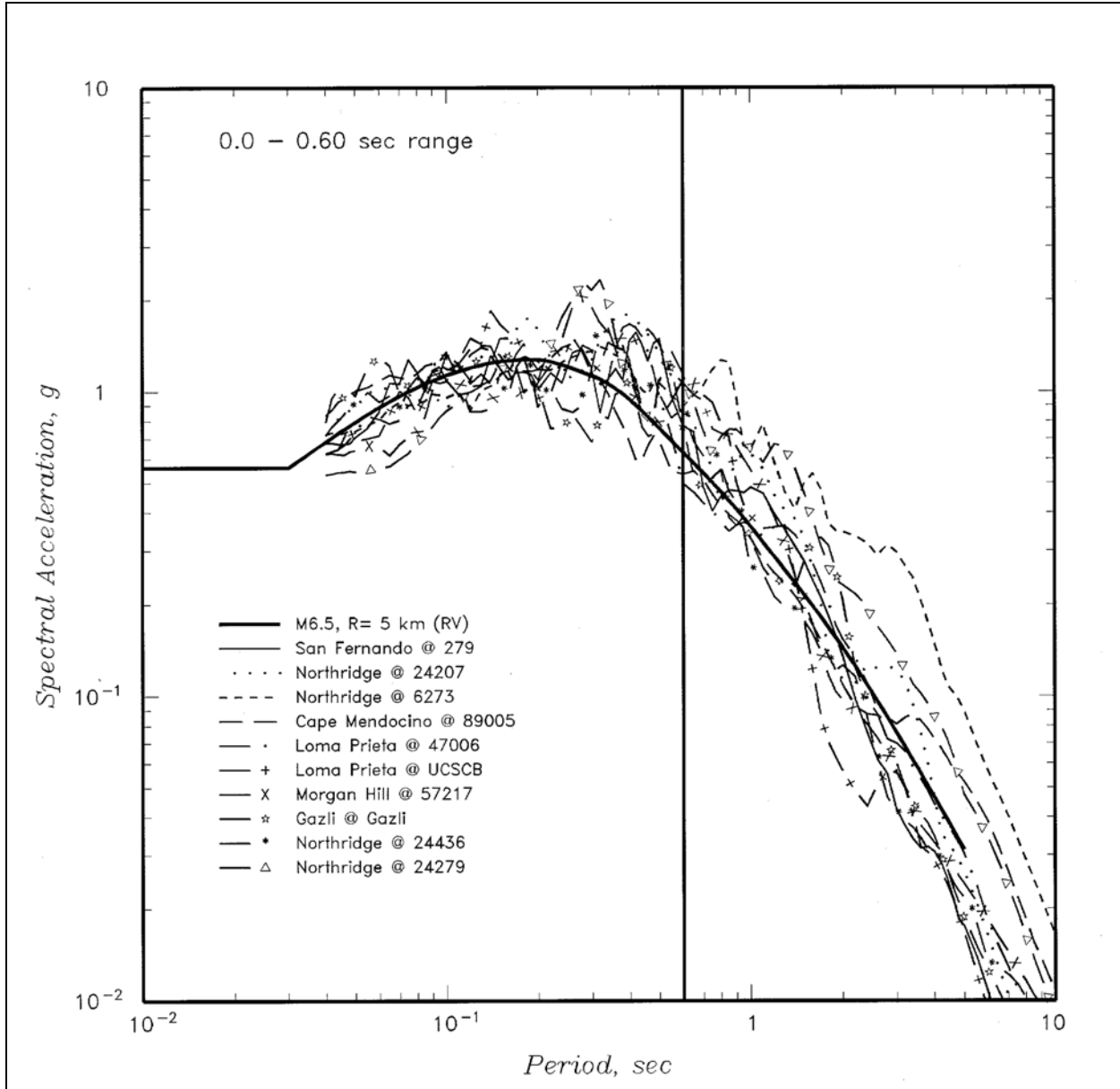


Figure D-11. Comparison of deterministic response spectrum and response spectra of scaled time-histories

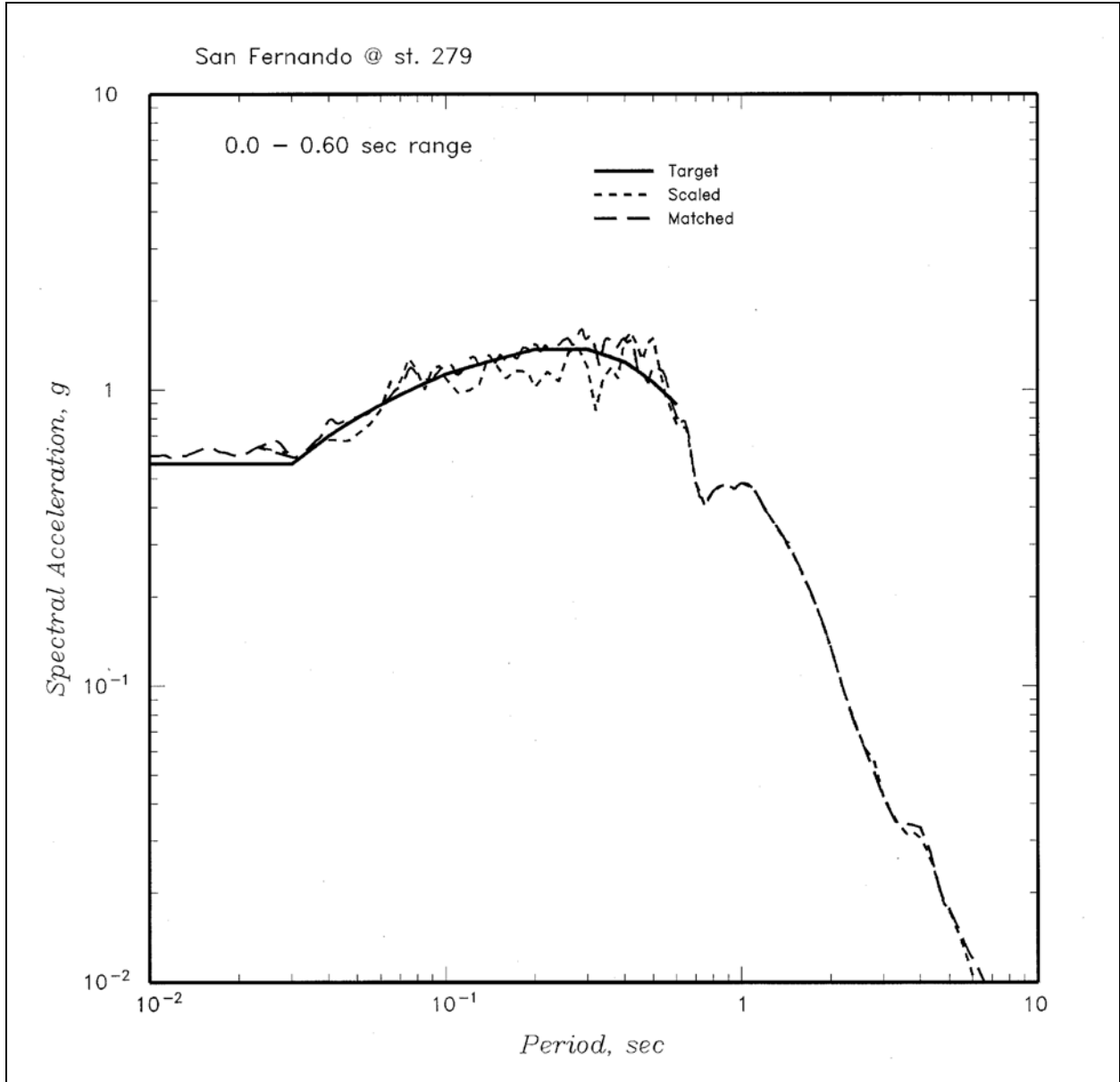


Figure D-12. Comparison of target spectrum and response spectra of time-history before and after spectral matching for the 1971 San Fernando earthquake recorded at station 279

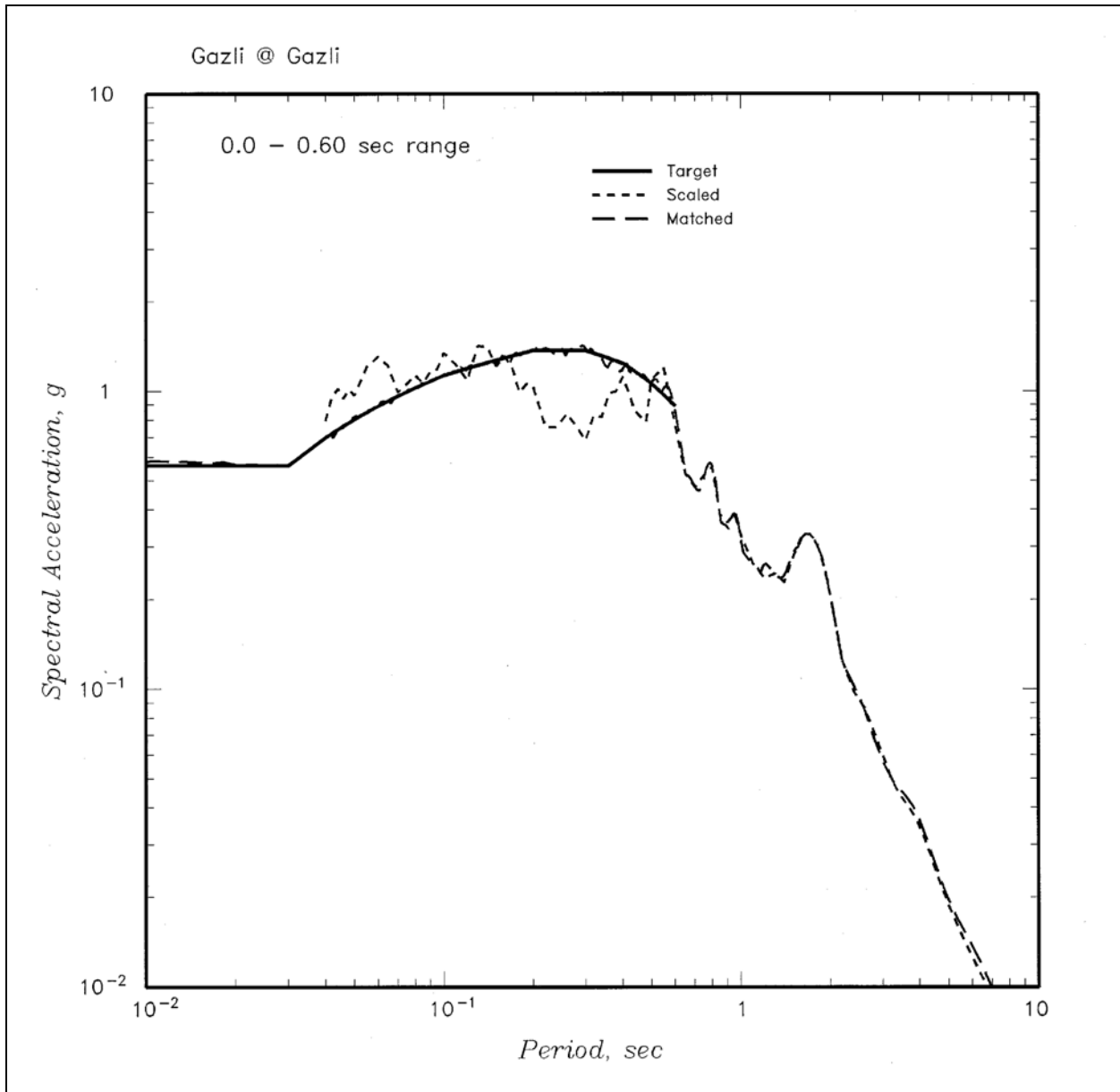


Figure D-13. Comparison of target spectrum and response spectra of time-history before and after spectral matching for the 1976 Gazli earthquake recorded at Gazli

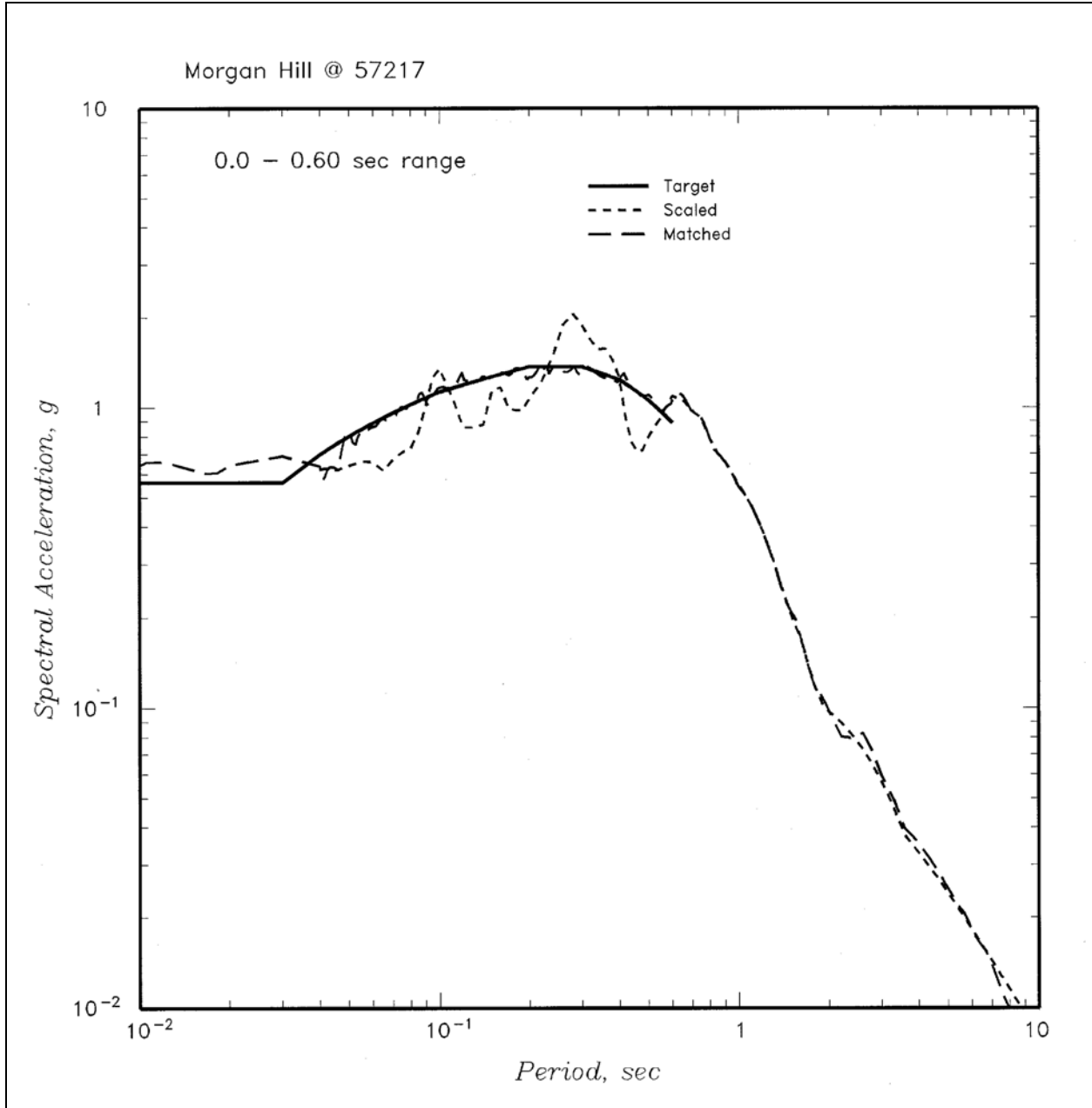


Figure D-14. Comparison of target spectrum and response spectra of time-history before and after spectral matching for the 1984 Morgan Hill earthquake recorded at station 57217

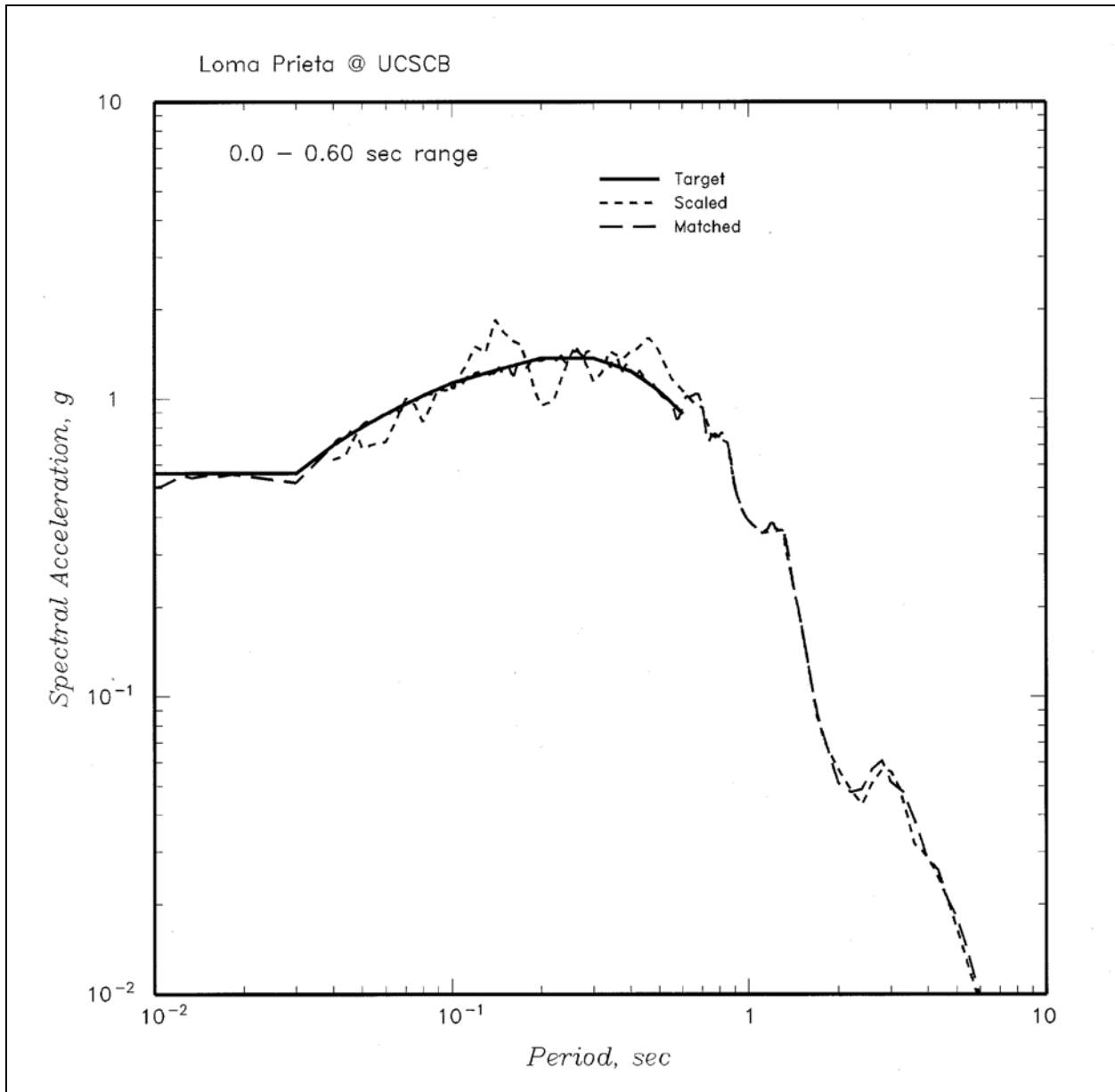


Figure D-15. Comparison of target spectrum and response spectra of time-history before and after spectral matching for the 1989 Loma Prieta earthquake recorded at UCSB Brane building

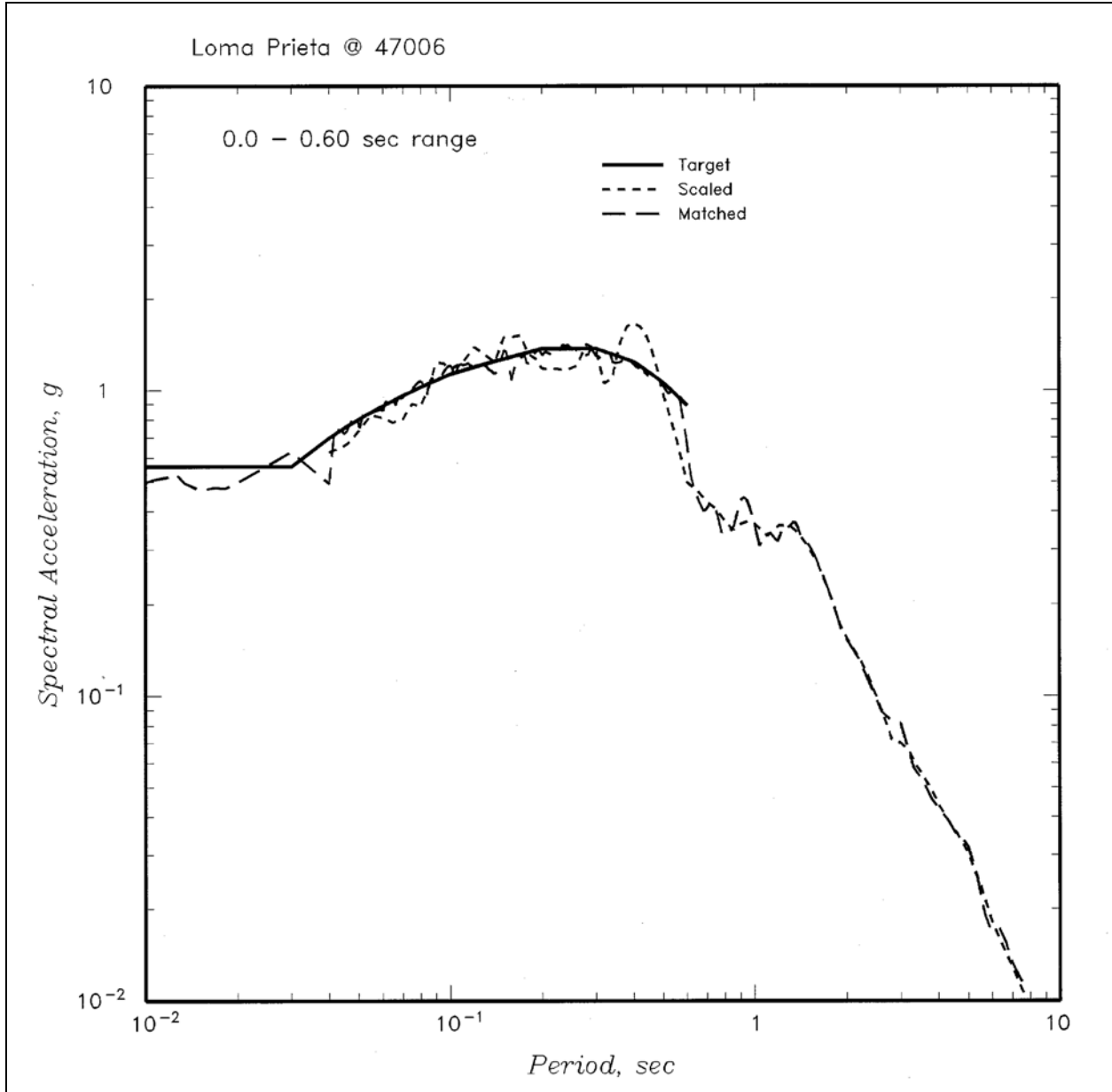


Figure D-16. Comparison of target spectrum and response spectra of time-history before and after spectral matching for the 1989 Loma Prieta earthquake recorded at station 47006

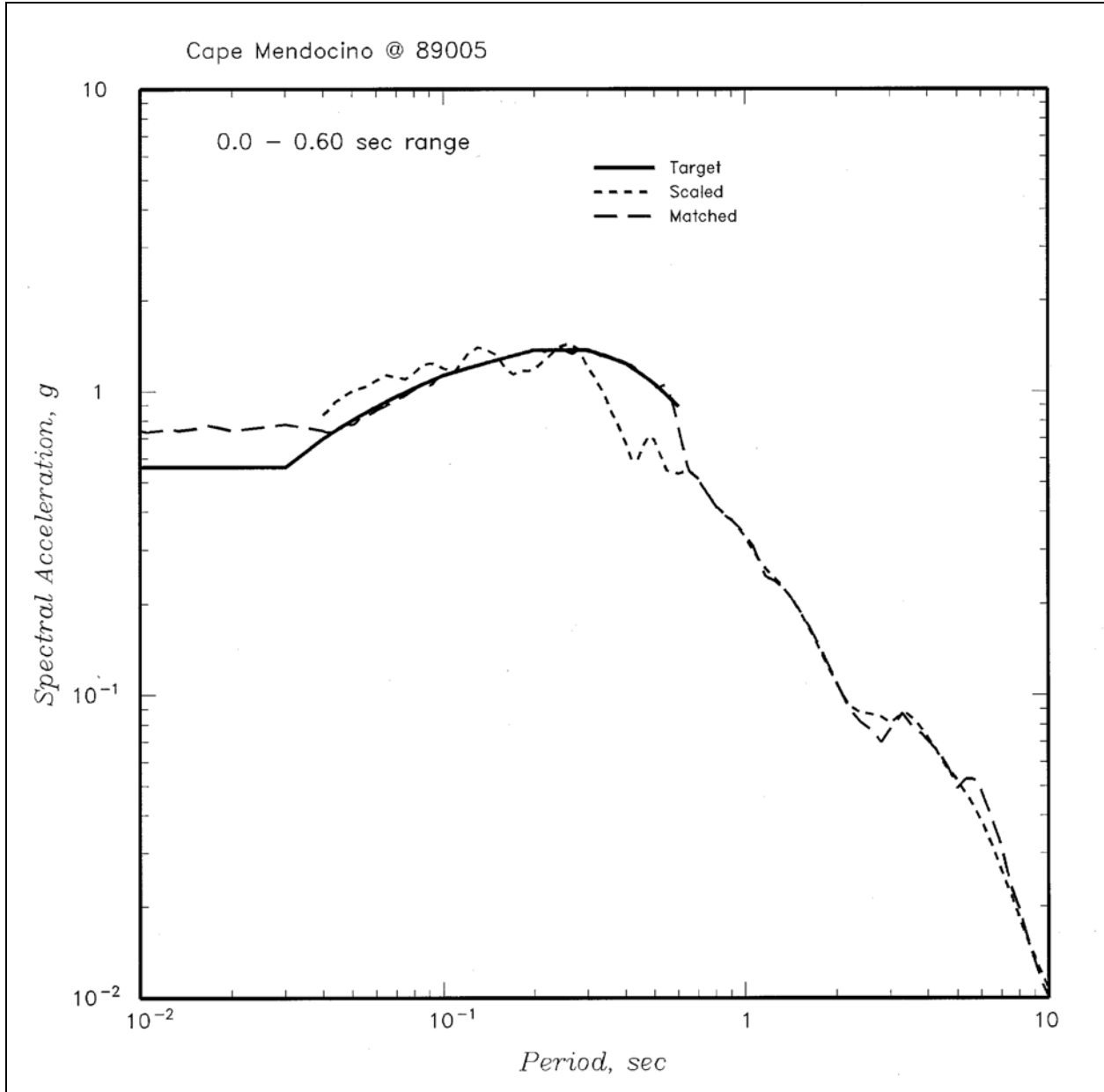


Figure D-17. Comparison of target spectrum and response spectra of time-history before and after spectral matching for the 1992 Cape Mendocino earthquake recorded at station 89005

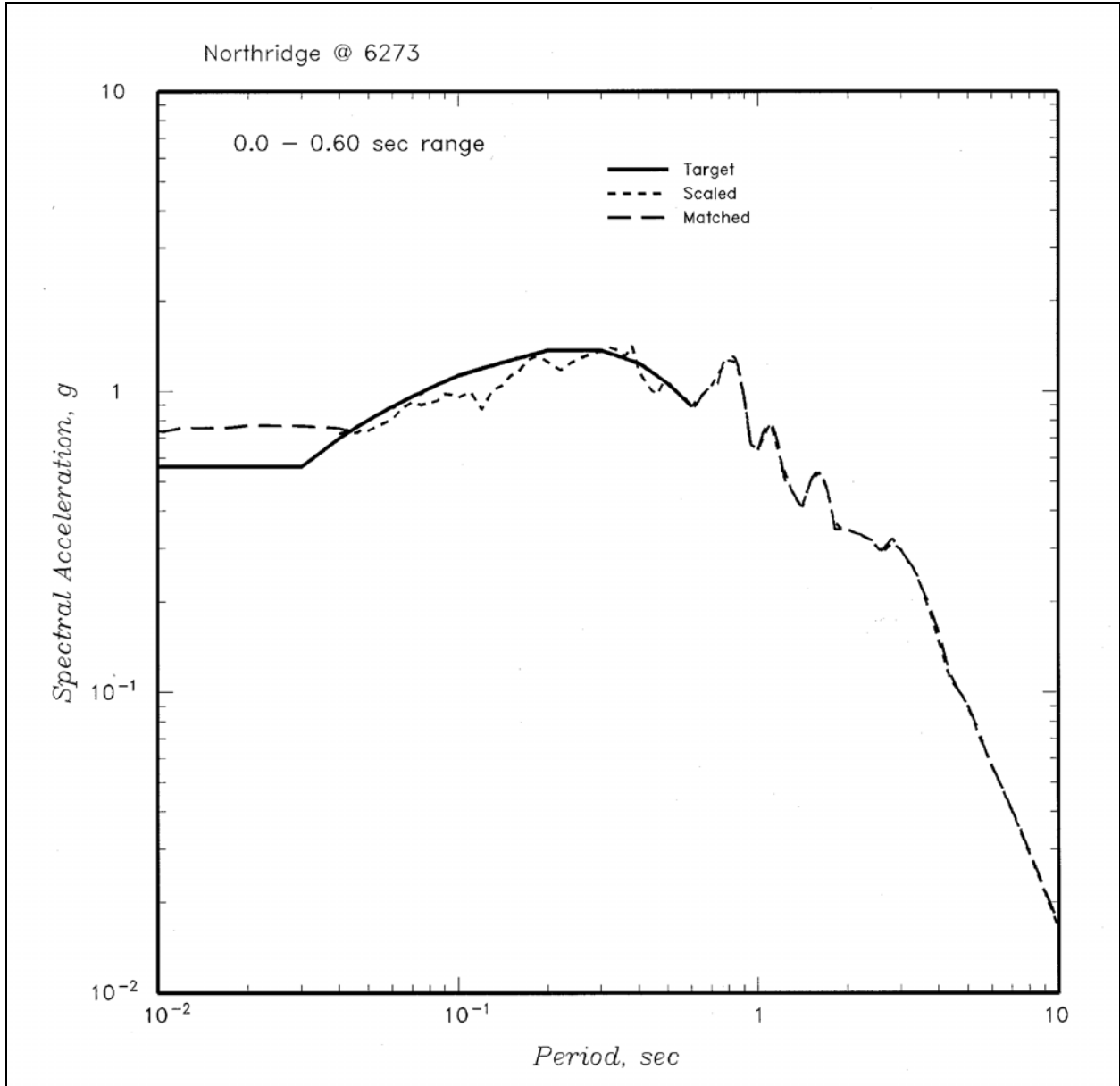


Figure D-18. Comparison of target spectrum and response spectra of time-history before and after spectral matching for the 1994 Northridge earthquake recorded at station 6273

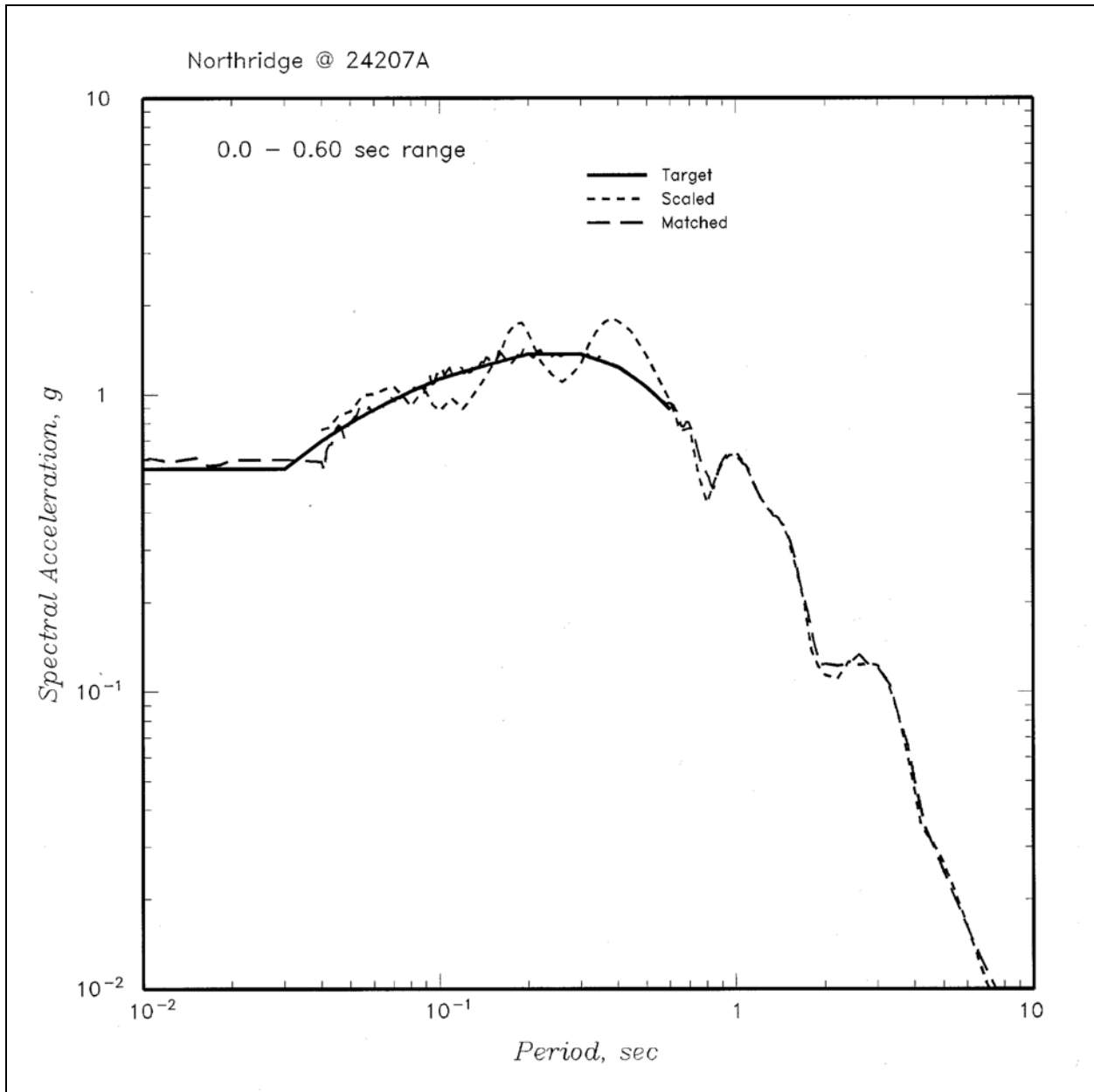


Figure D-19. Comparison of target spectrum and response spectra of time-history before and after spectral matching for the 1994 Northridge earthquake recorded at station 24207

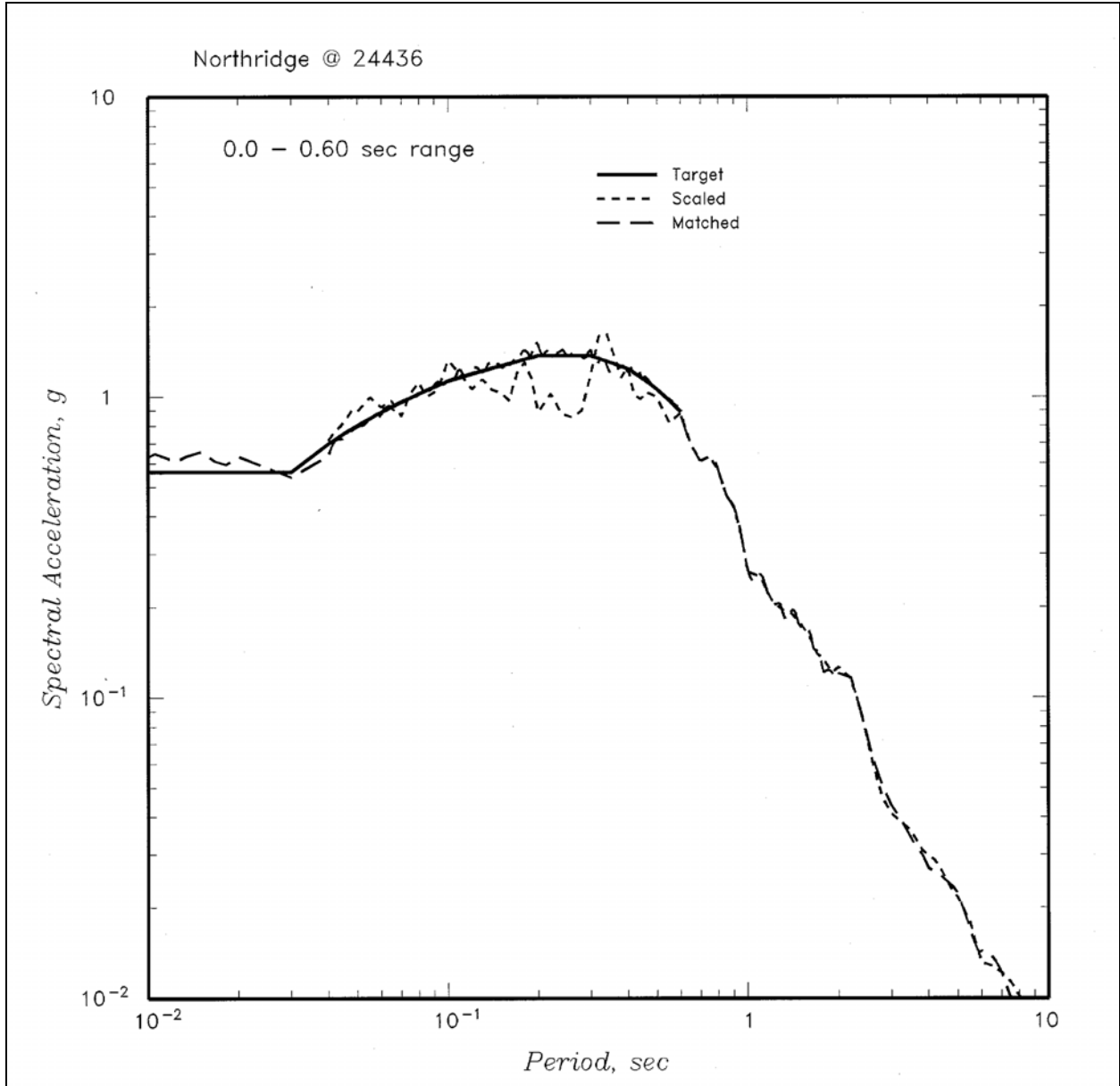


Figure D-20. Comparison of target spectrum and response spectra of time-history before and after spectral matching for the 1994 Northridge earthquake recorded at station 24436

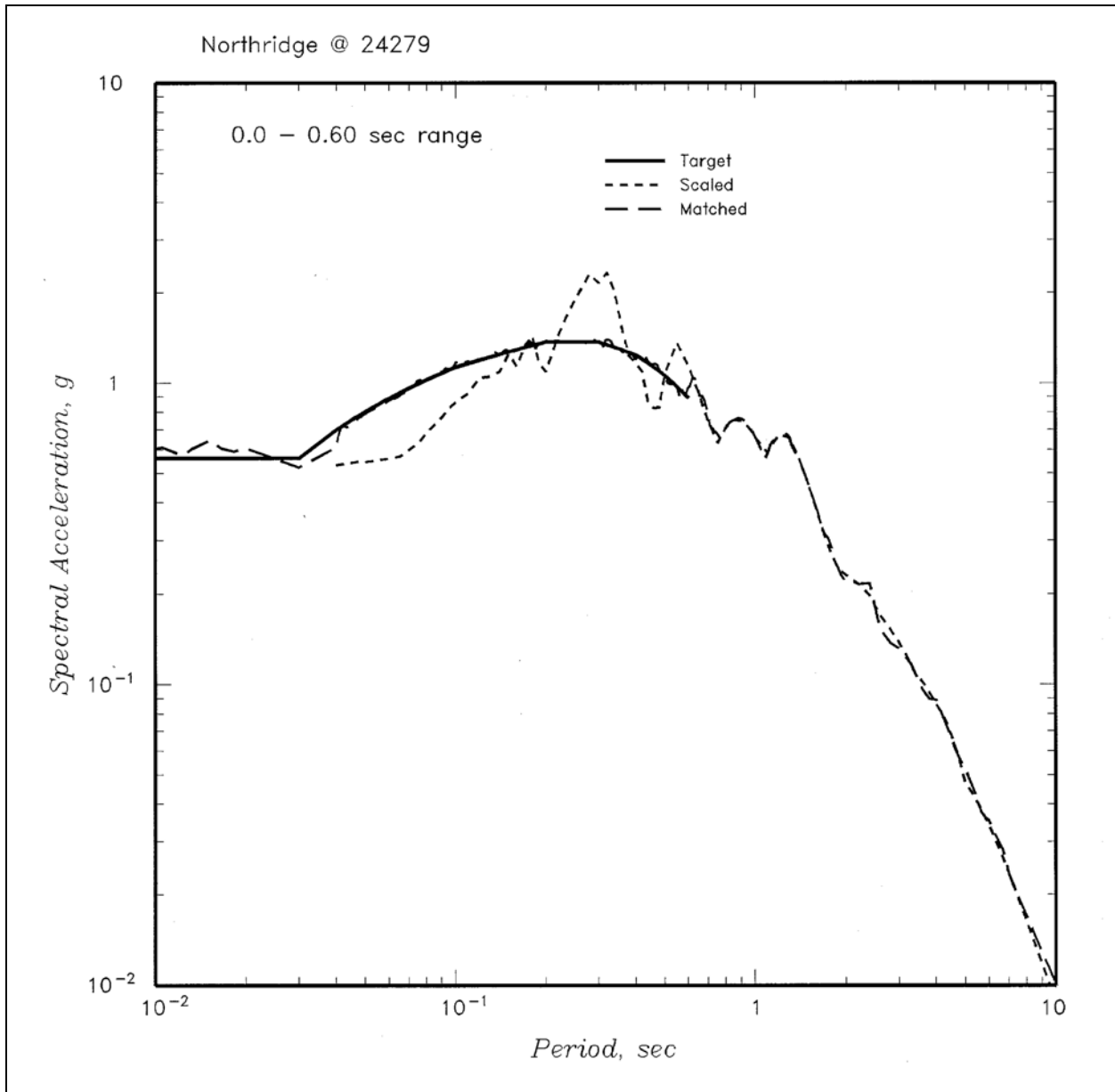


Figure D-21. Comparison of target spectrum and response spectra of time-history before and after spectral matching for the 1994 Northridge earthquake recorded at station 24279

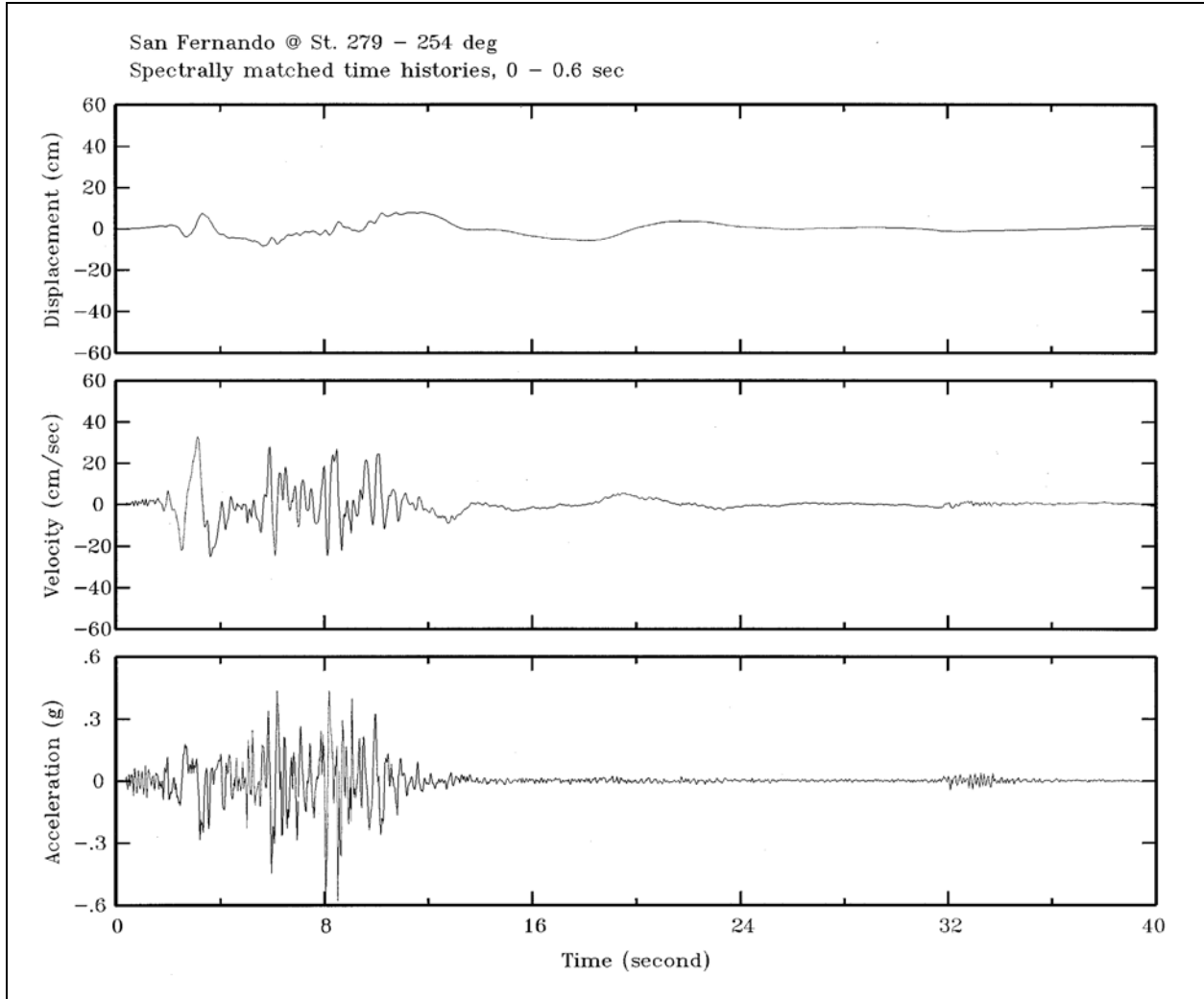


Figure D-22. Spectrally matched time-histories of acceleration, velocity, and displacement for the 1971 San Fernando earthquake recorded at station 279

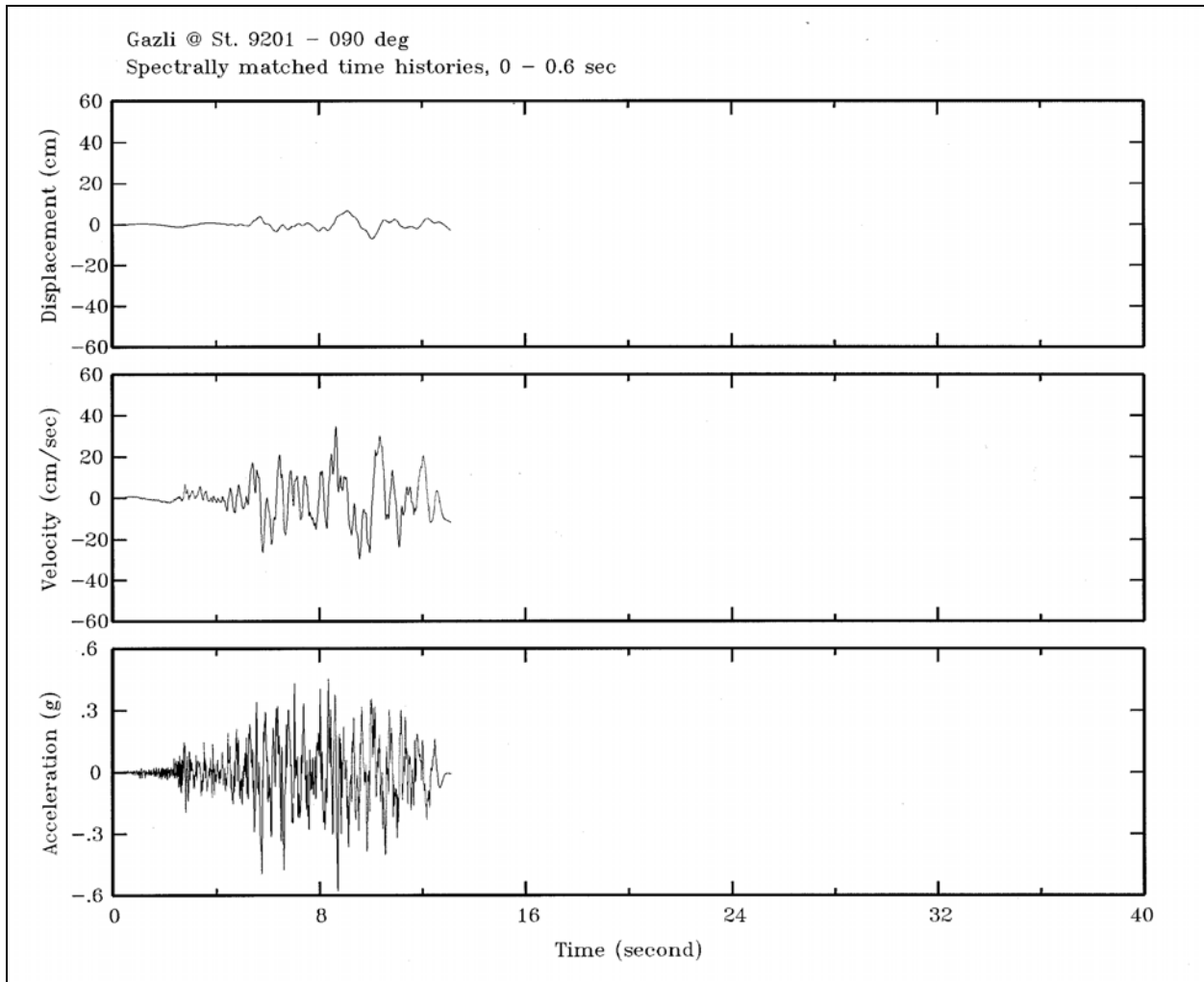


Figure D-23. Spectrally matched time-histories of acceleration, velocity, and displacement for the 1976 Gazli earthquake recorded at Gazli

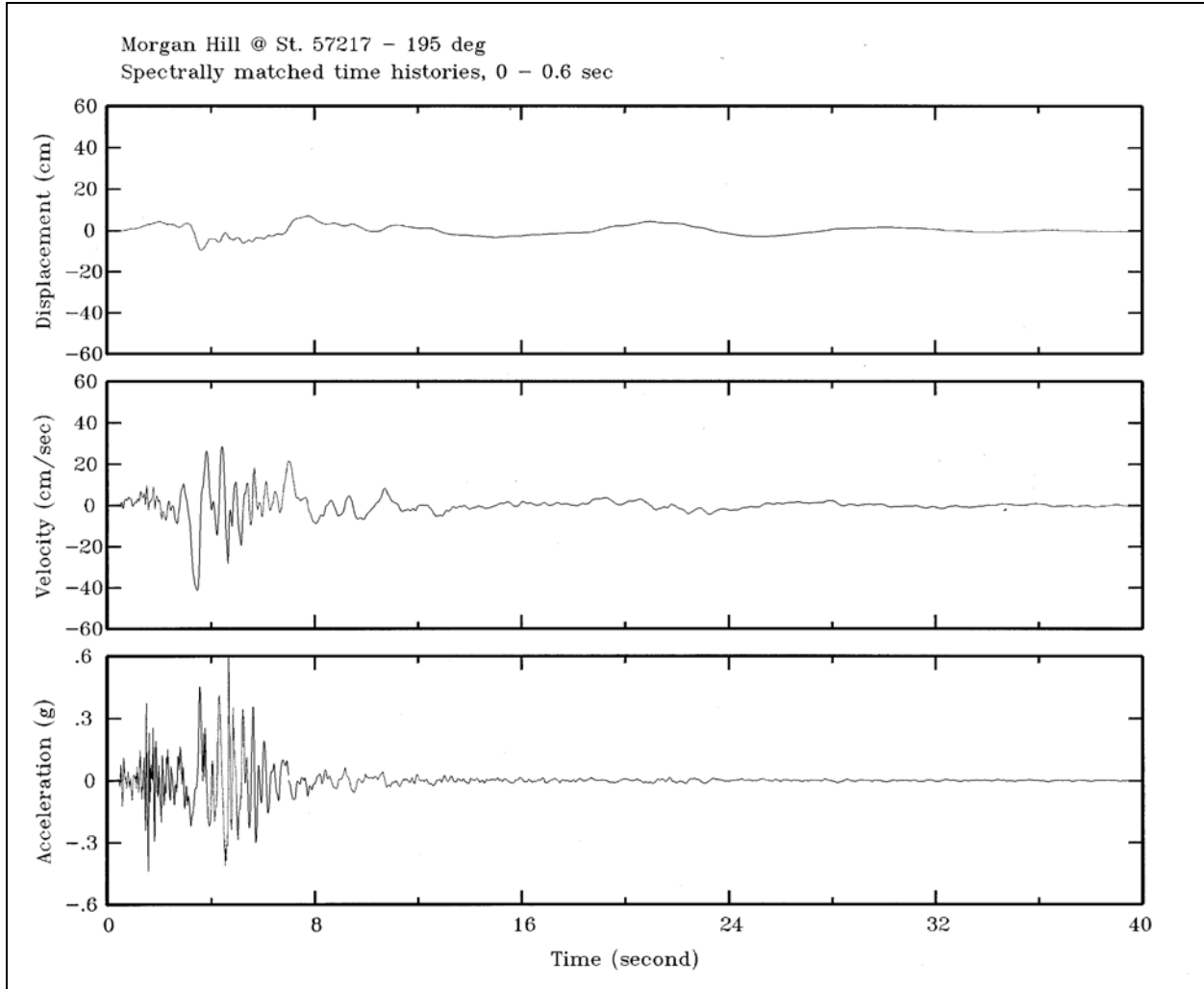


Figure D-24. Spectrally matched time-histories of acceleration, velocity, and displacement for the 1984 Morgan Hill earthquake recorded at station 57217

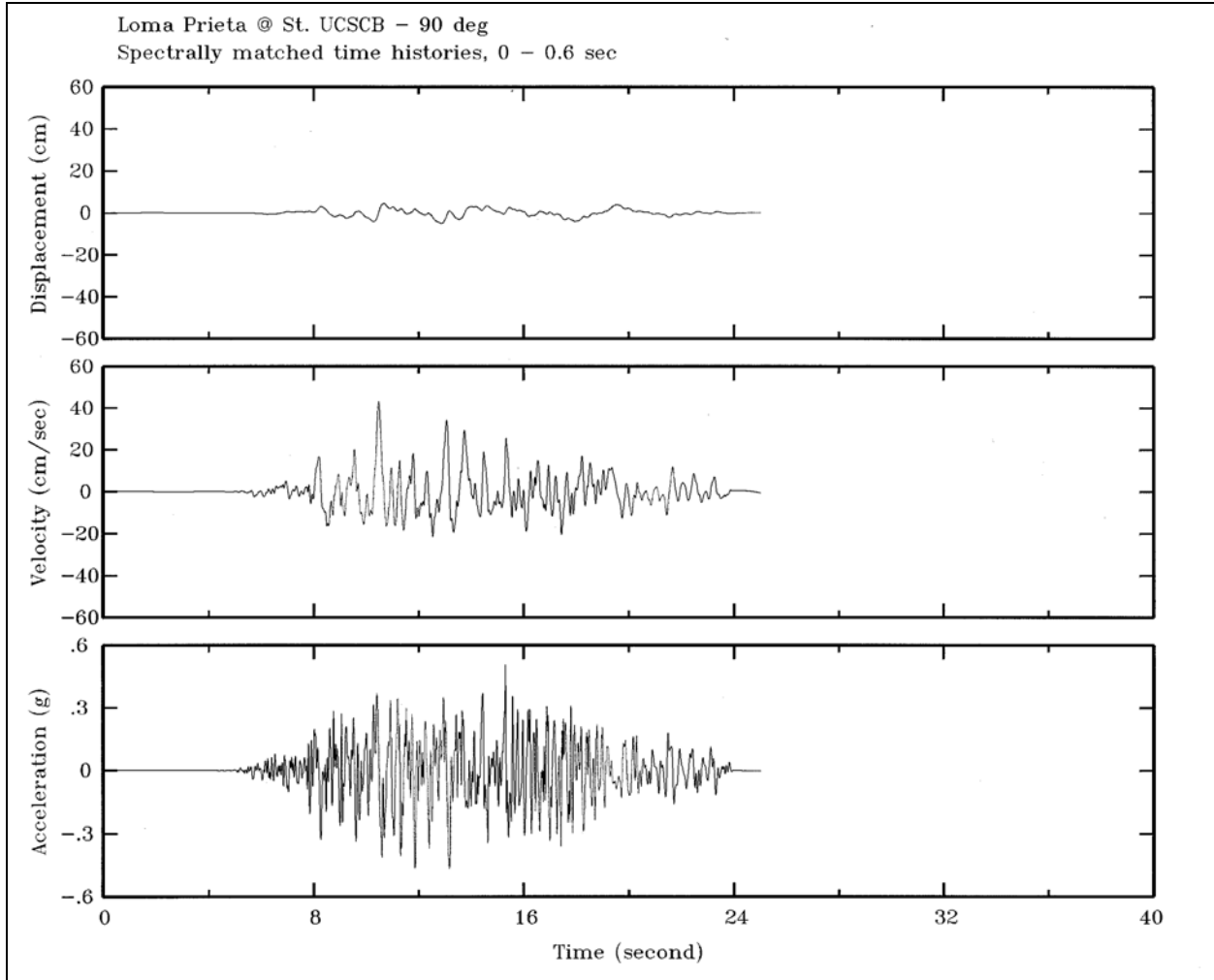


Figure D-25. Spectrally matched time-histories of acceleration, velocity, and displacement for the 1989 Loma Prieta earthquake recorded at UCSC Brane building

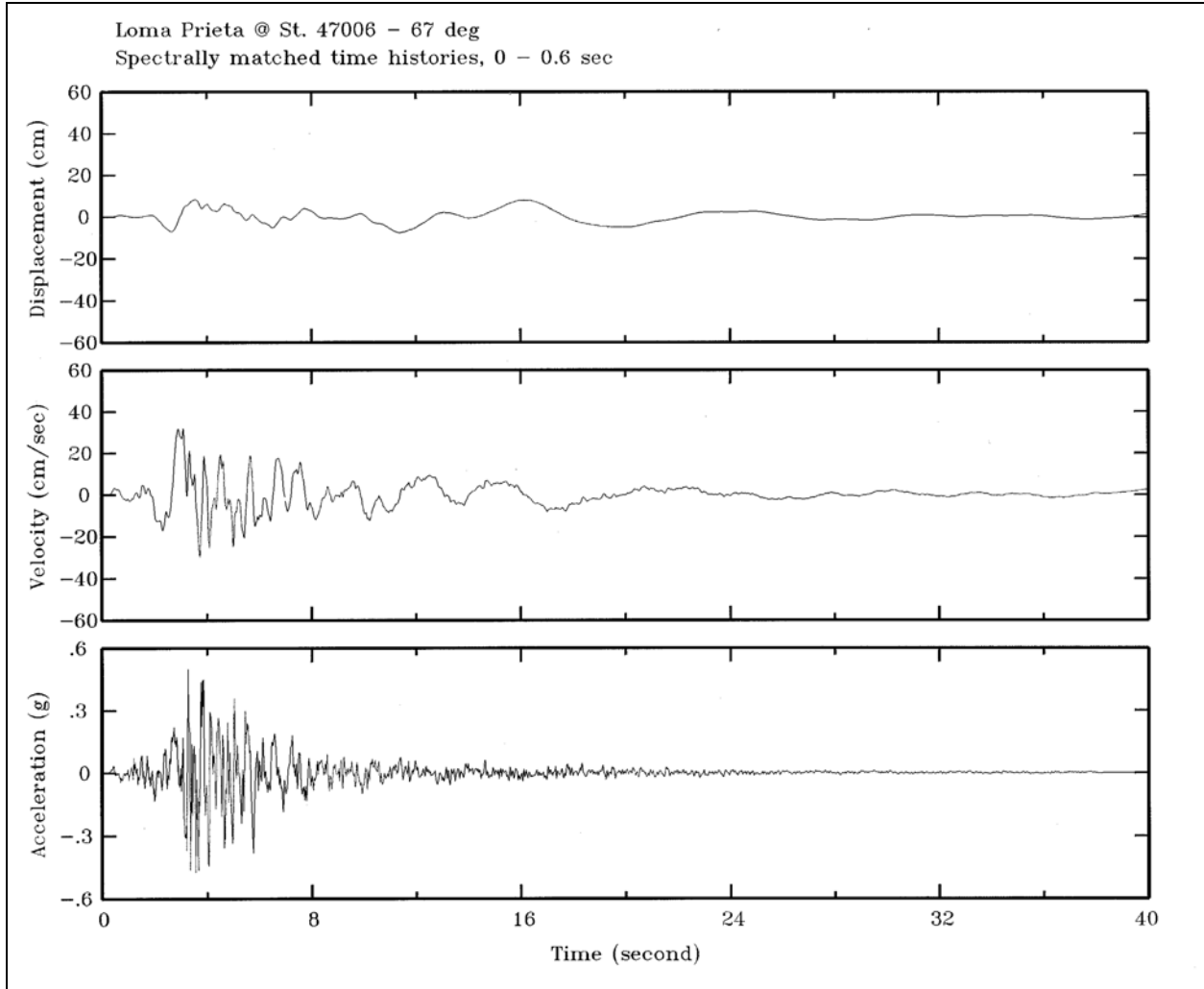


Figure D-26. Spectrally matched time-histories of acceleration, velocity, and displacement for the 1989 Loma Prieta earthquake recorded at station 47006

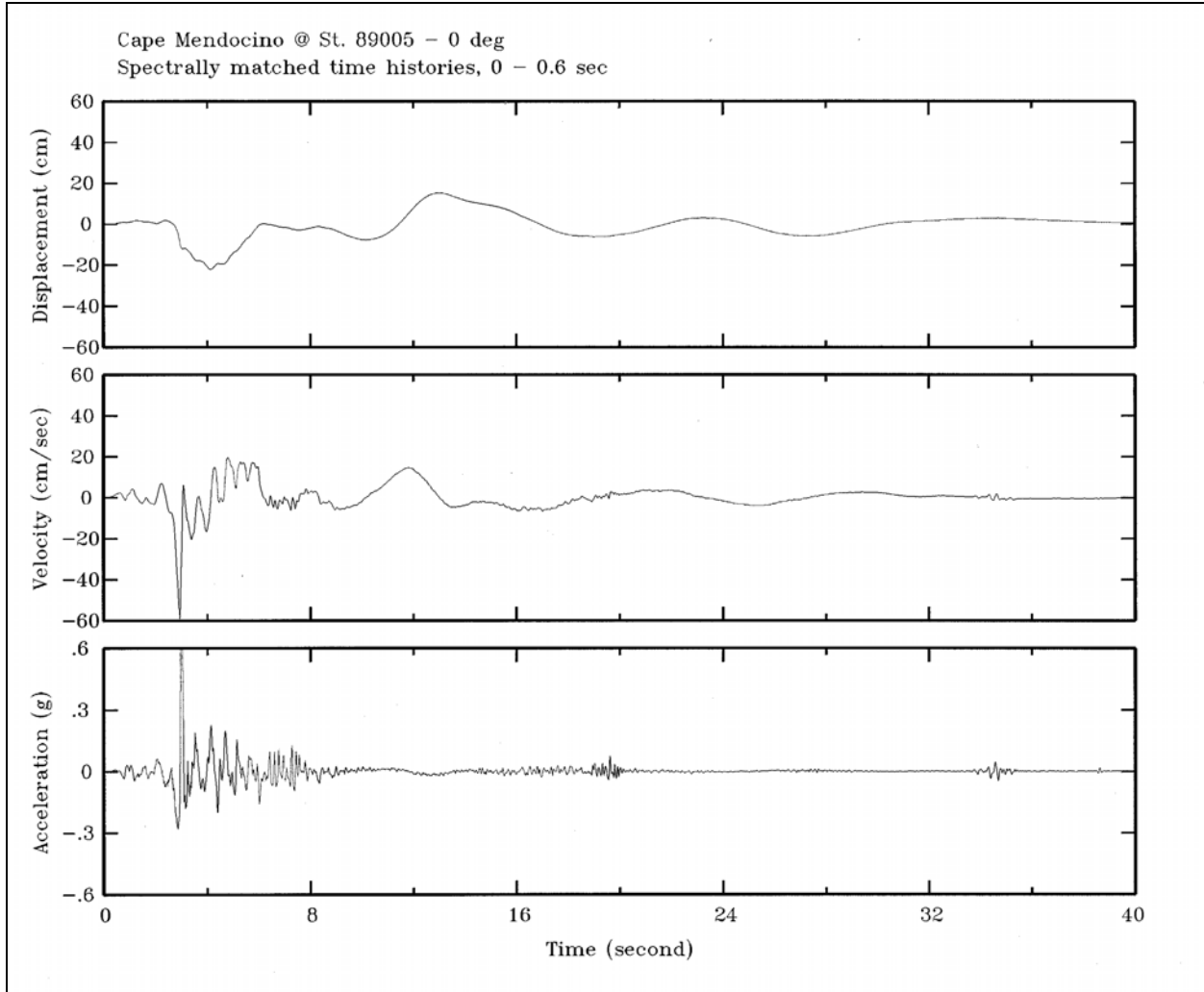


Figure D-27. Spectrally matched time-histories of acceleration, velocity, and displacement for the 1992 Cape Mendocino earthquake recorded at station 89005

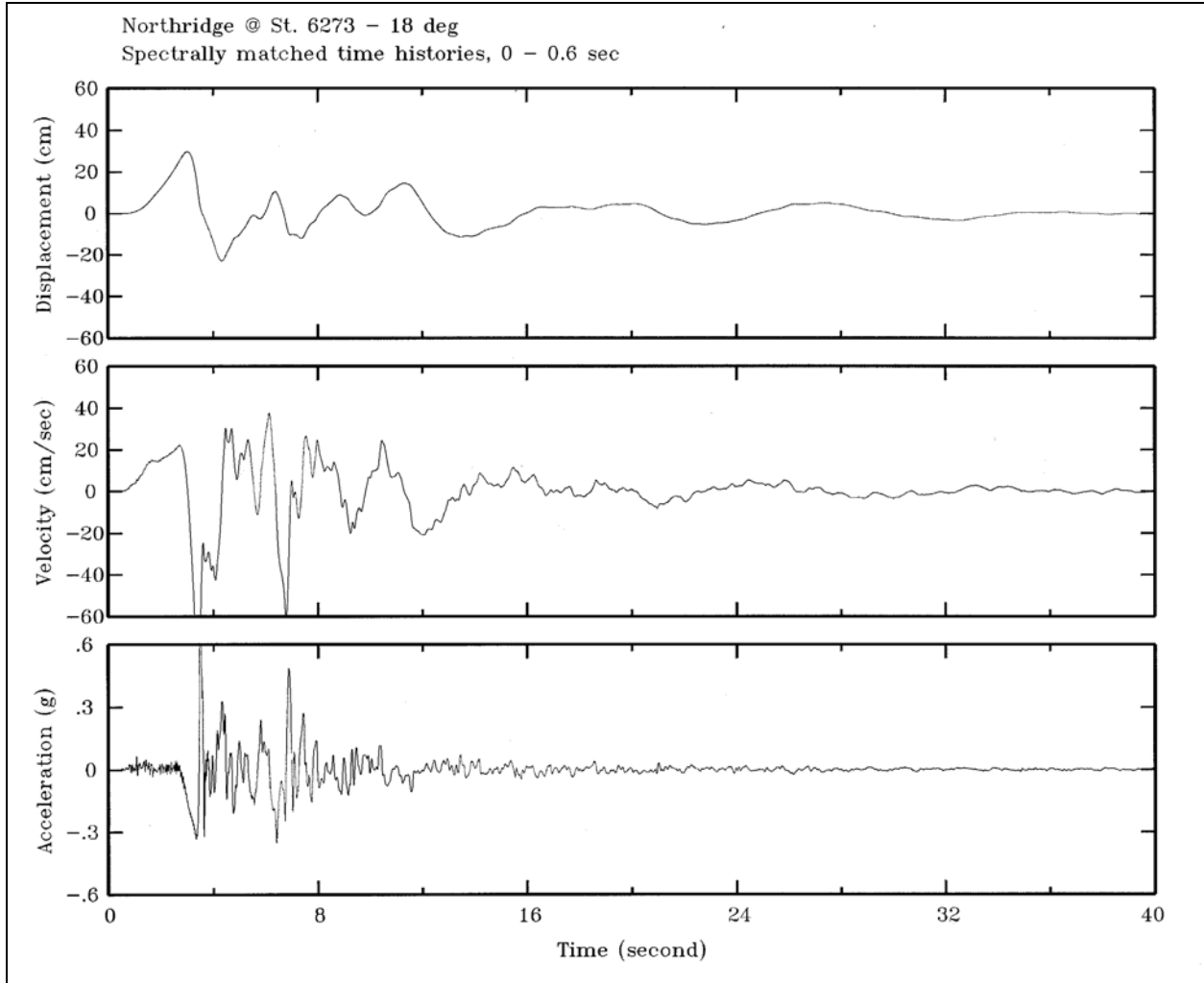


Figure D-28. Spectrally matched time-histories of acceleration, velocity, and displacement for the 1994 Northridge earthquake recorded at station 6273

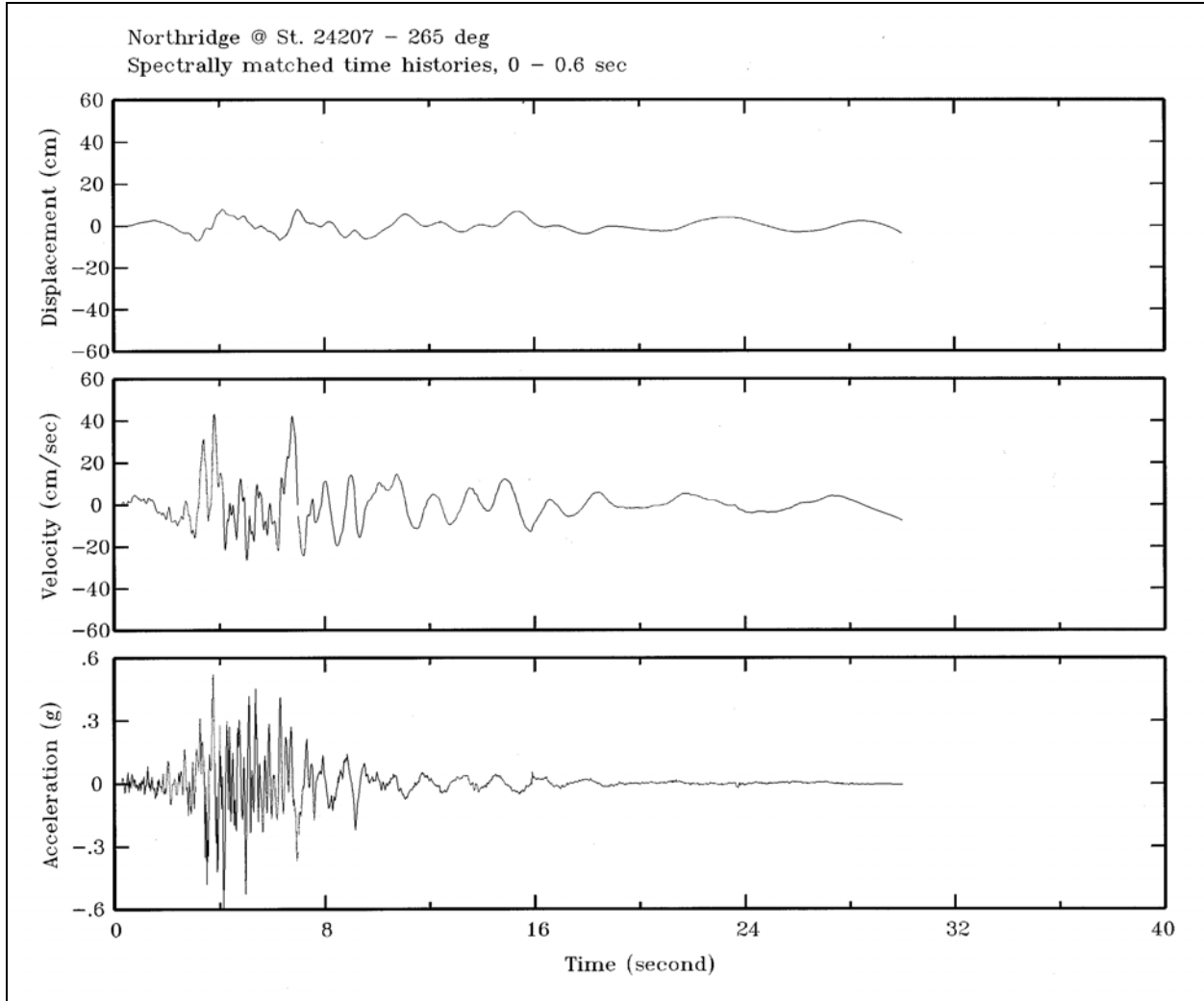


Figure D-29. Spectrally matched time-histories of acceleration, velocity, and displacement for the 1994 Northridge earthquake recorded at station 24207

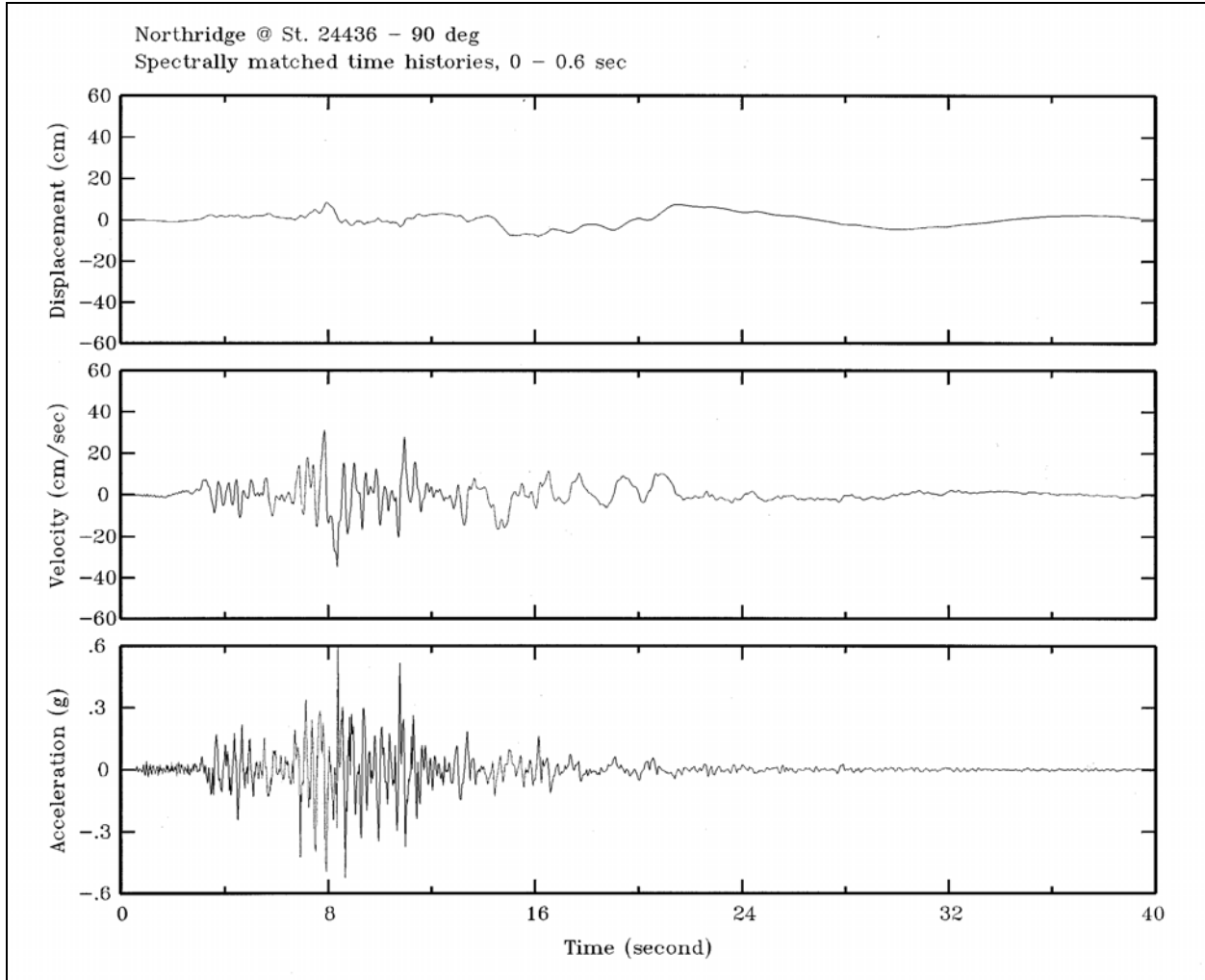


Figure D-30. Spectrally matched time-histories of acceleration, velocity, and displacement for the 1994 Northridge earthquake recorded at station 24436

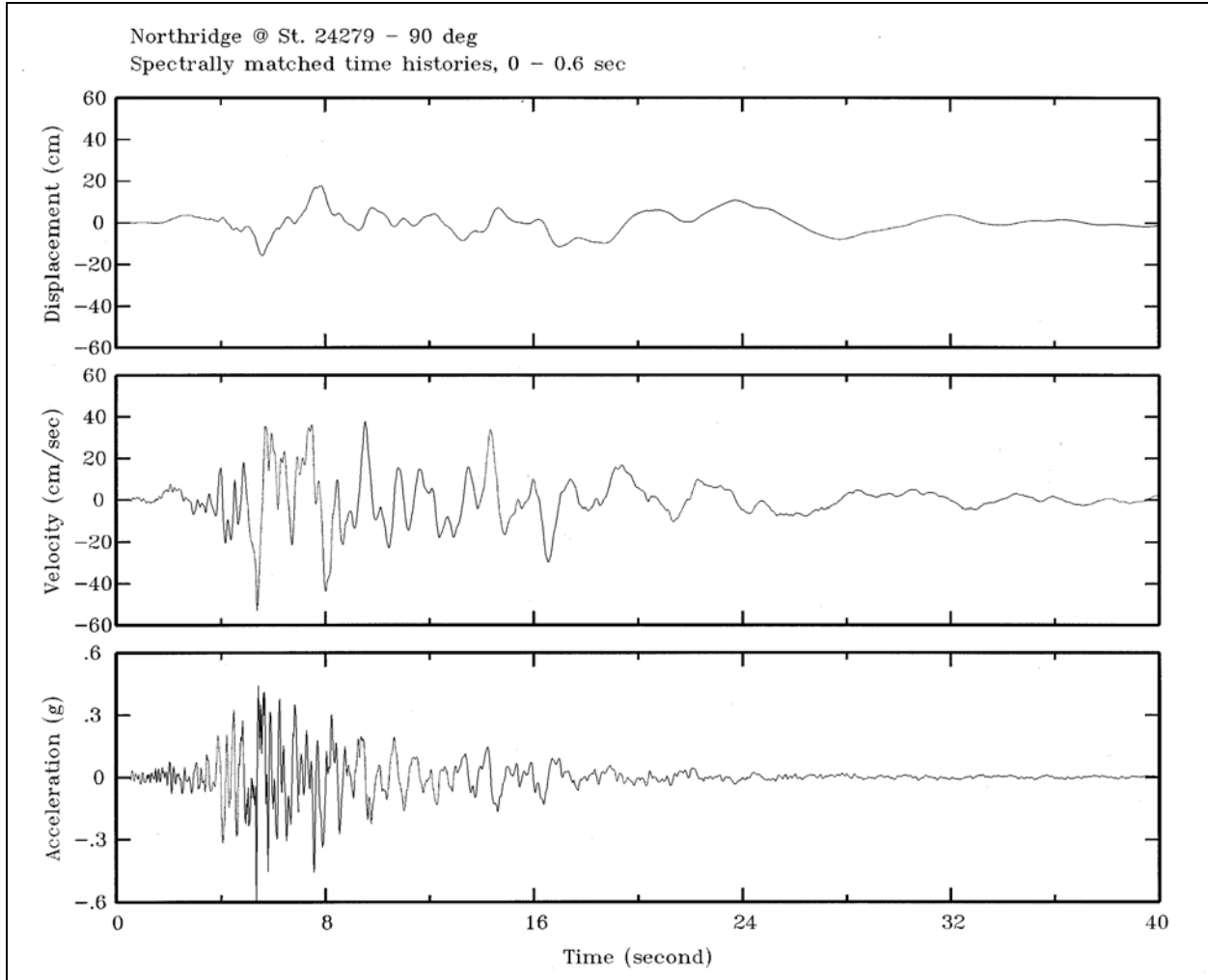


Figure D-31. Spectrally matched time-histories of acceleration, velocity, and displacement for the 1994 Northridge earthquake recorded at station 24279

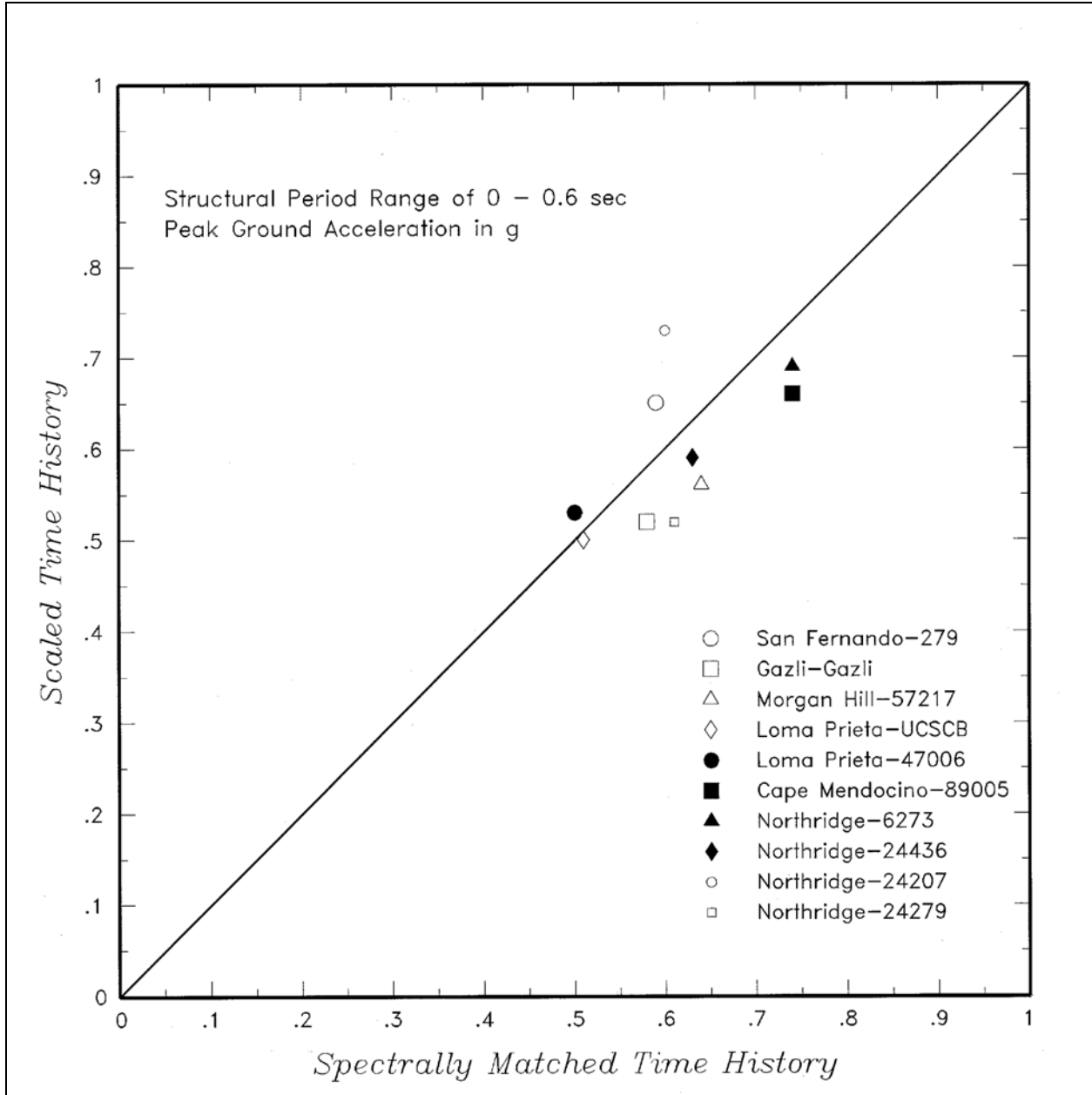


Figure D-32. Comparison for peak ground acceleration estimated from the scaled and spectrally matched time-histories

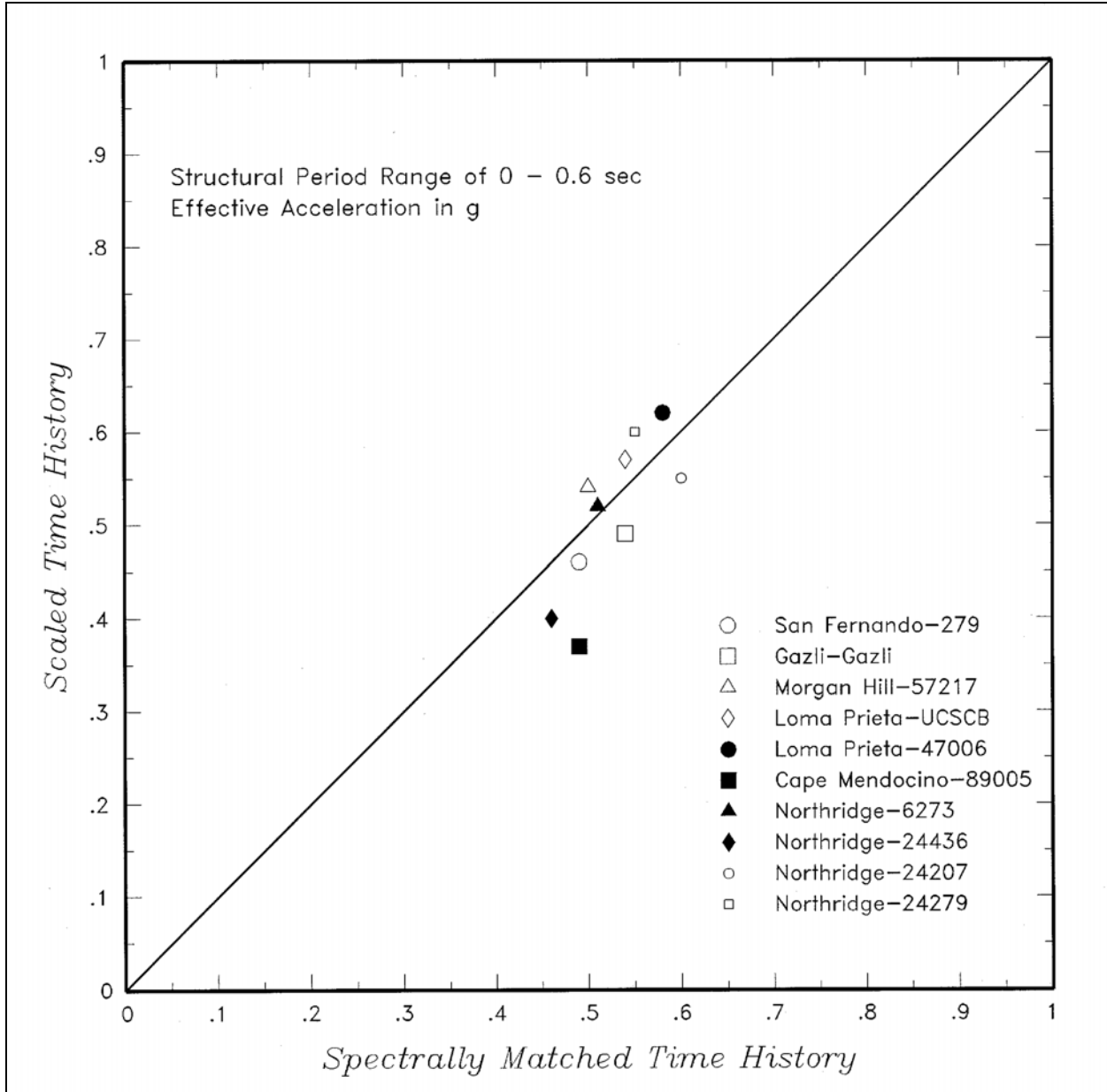


Figure D-33. Comparison for effective peak acceleration estimated from the scaled and spectrally matched time-histories

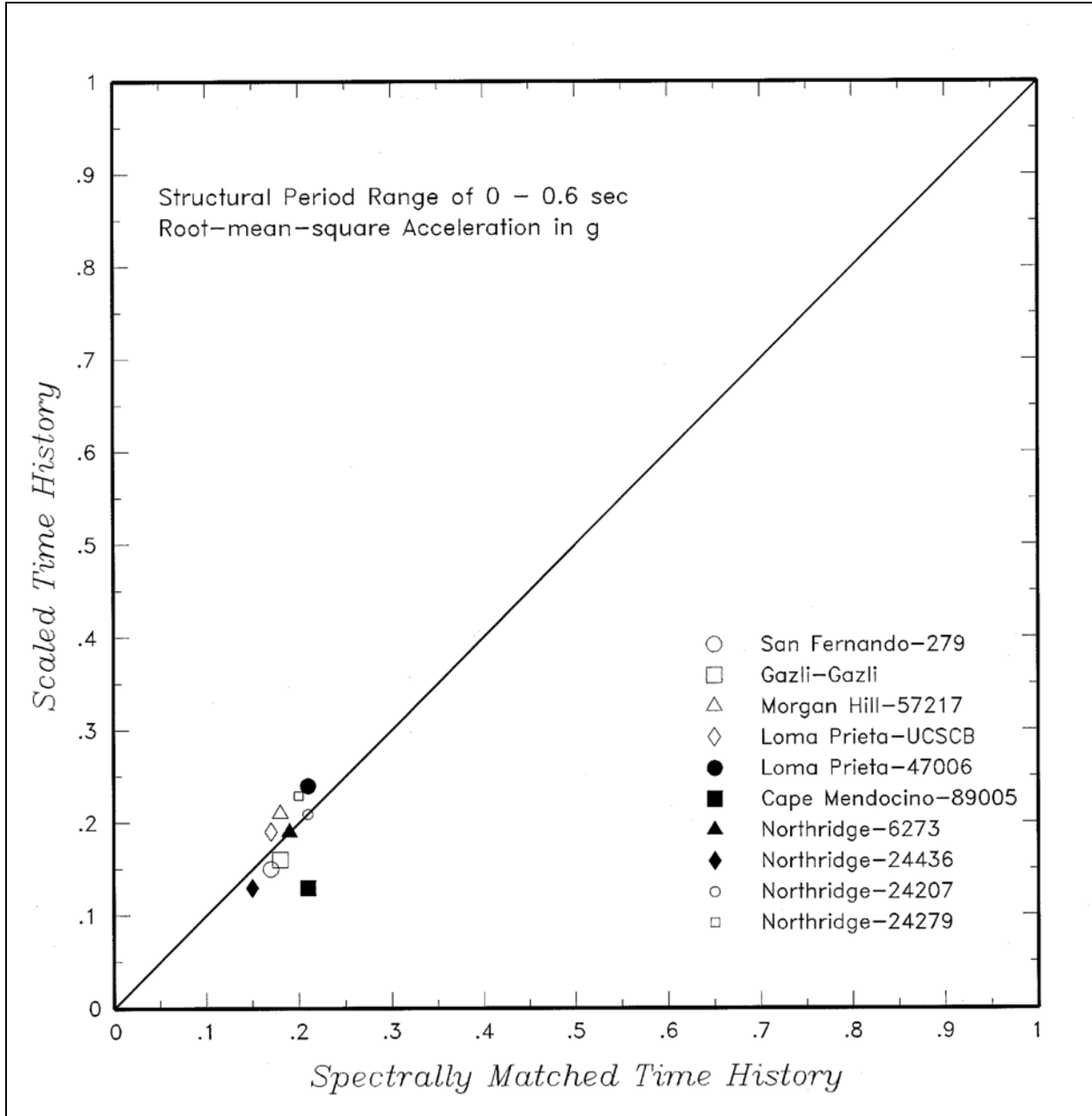


Figure D-34. Comparison for root-mean-square acceleration estimated from the scaled and spectrally matched time-histories

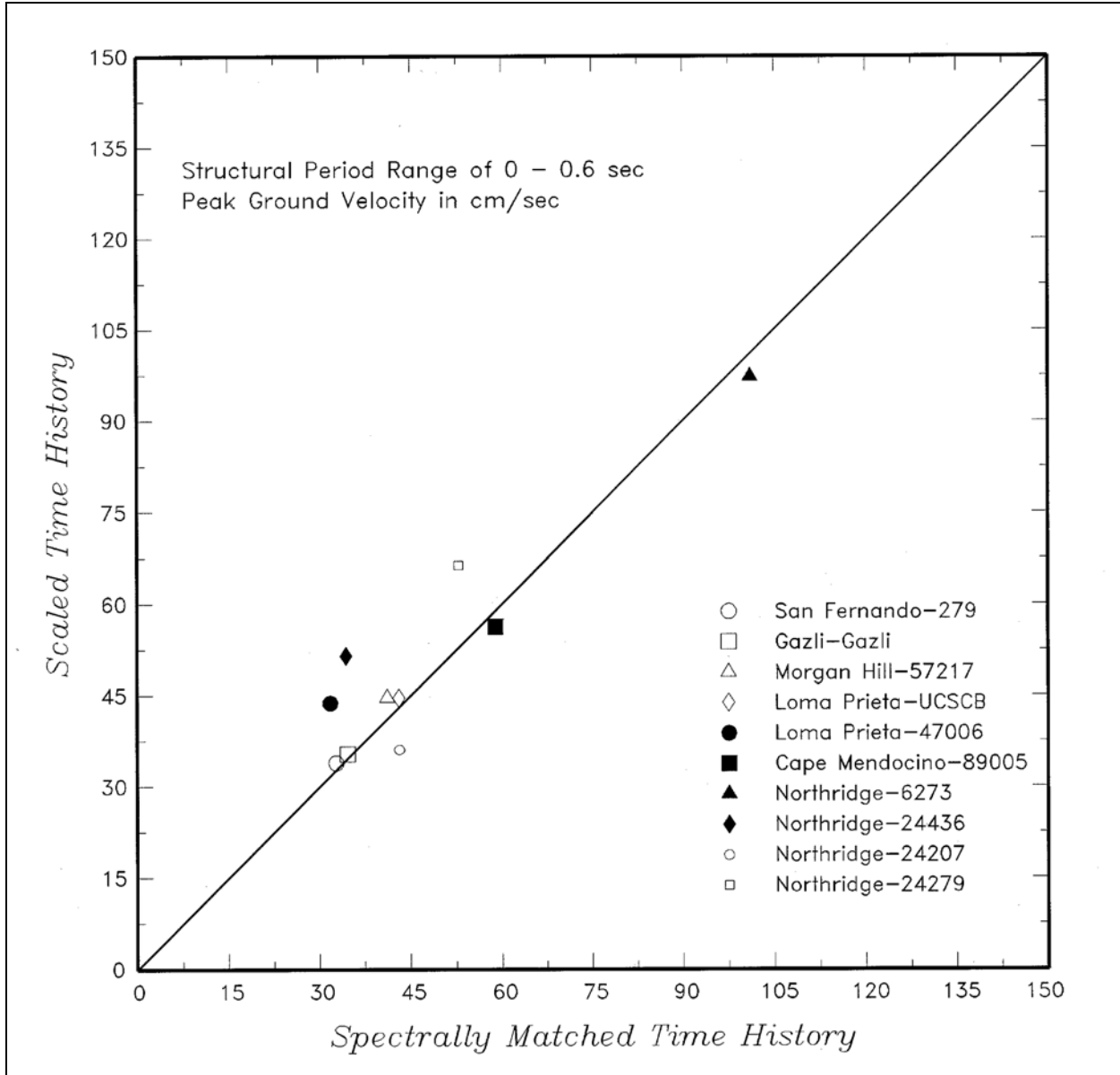


Figure D-35. Comparison for peak velocity estimated for the scaled and spectrally matched time-histories

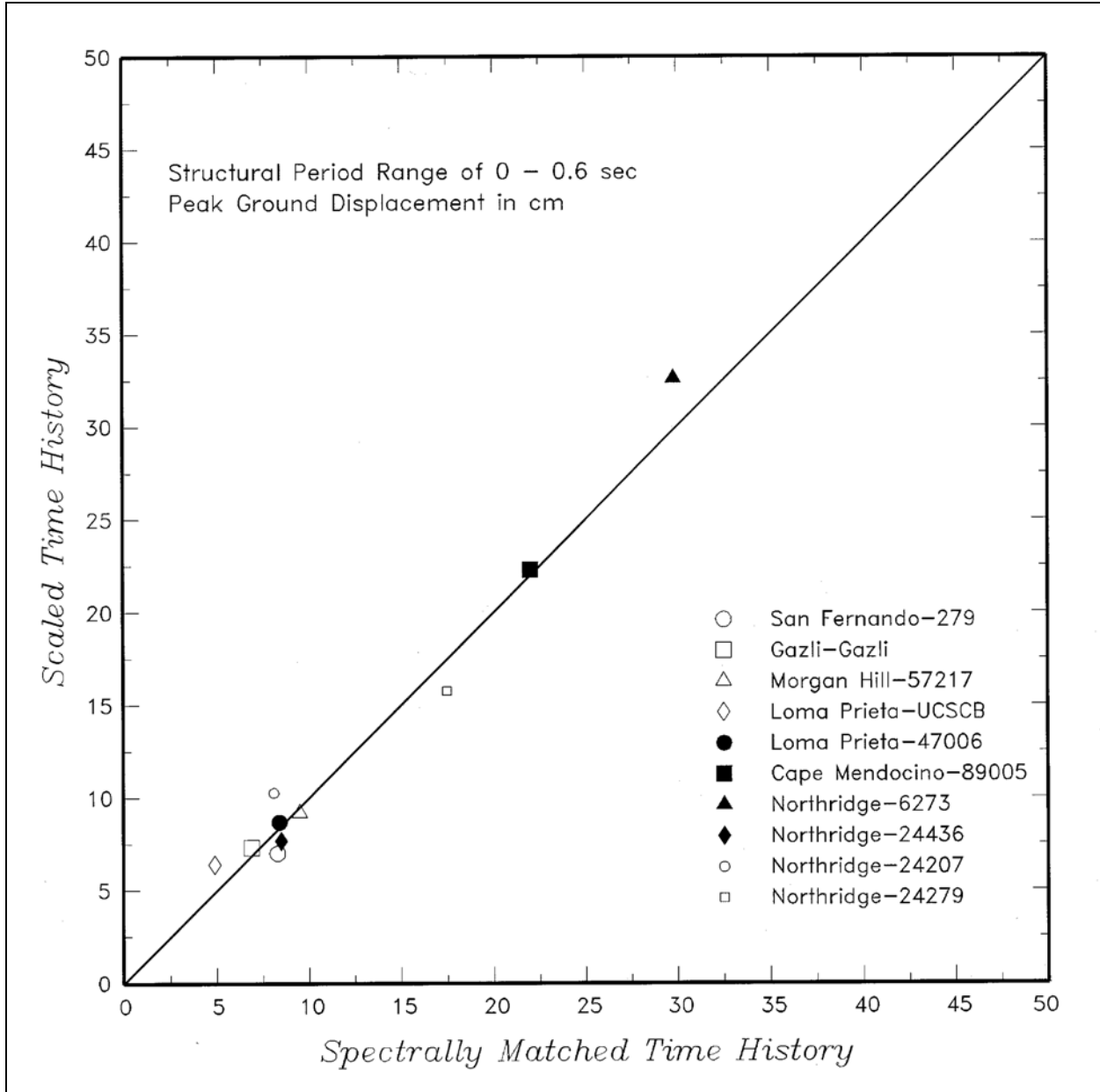


Figure D-36. Comparison for peak displacement estimated for the scaled and spectrally matched time-histories

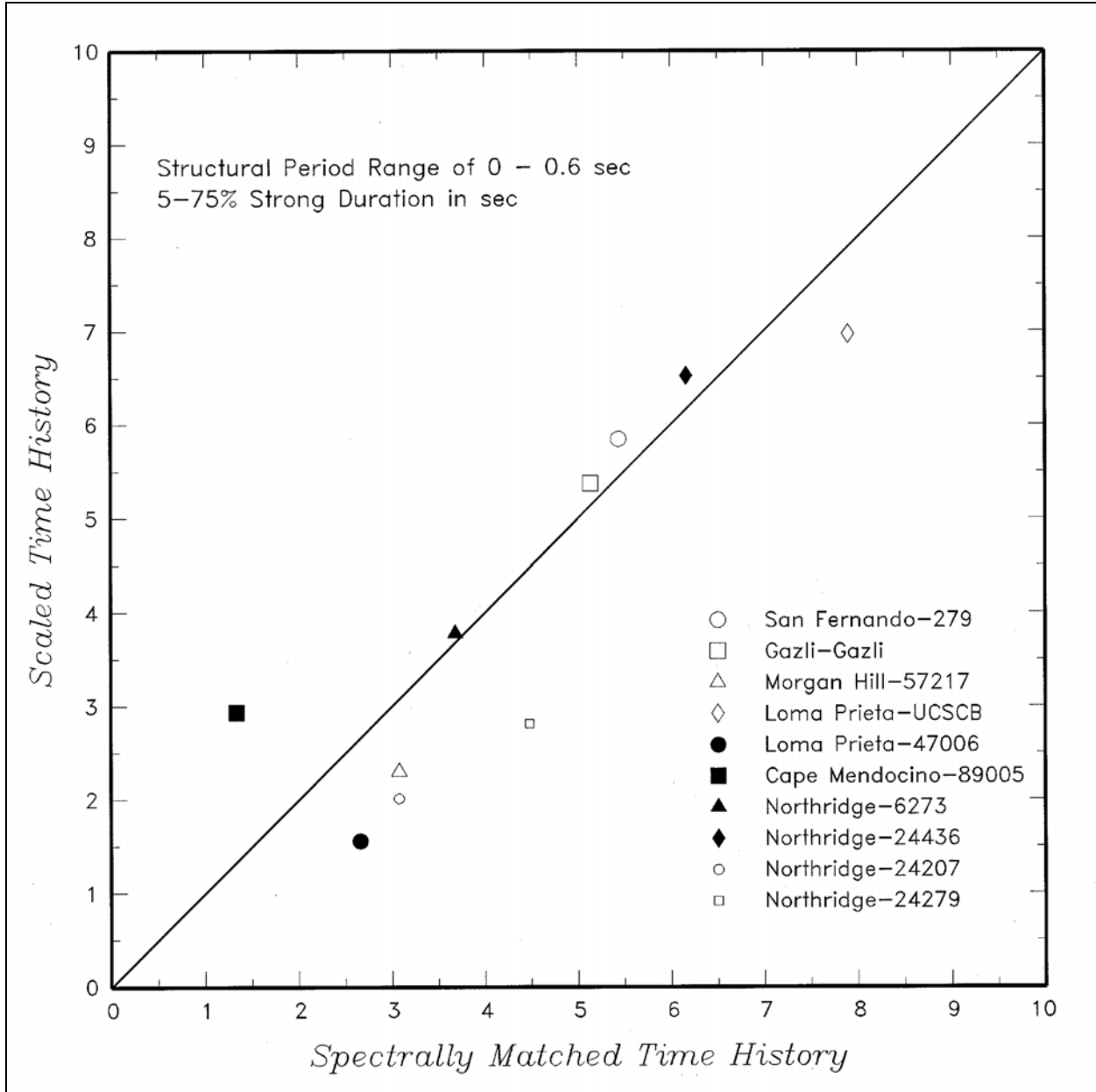


Figure D-37. Comparison for 5 to 75 percent strong duration estimated from the scaled and spectrally matched time-histories

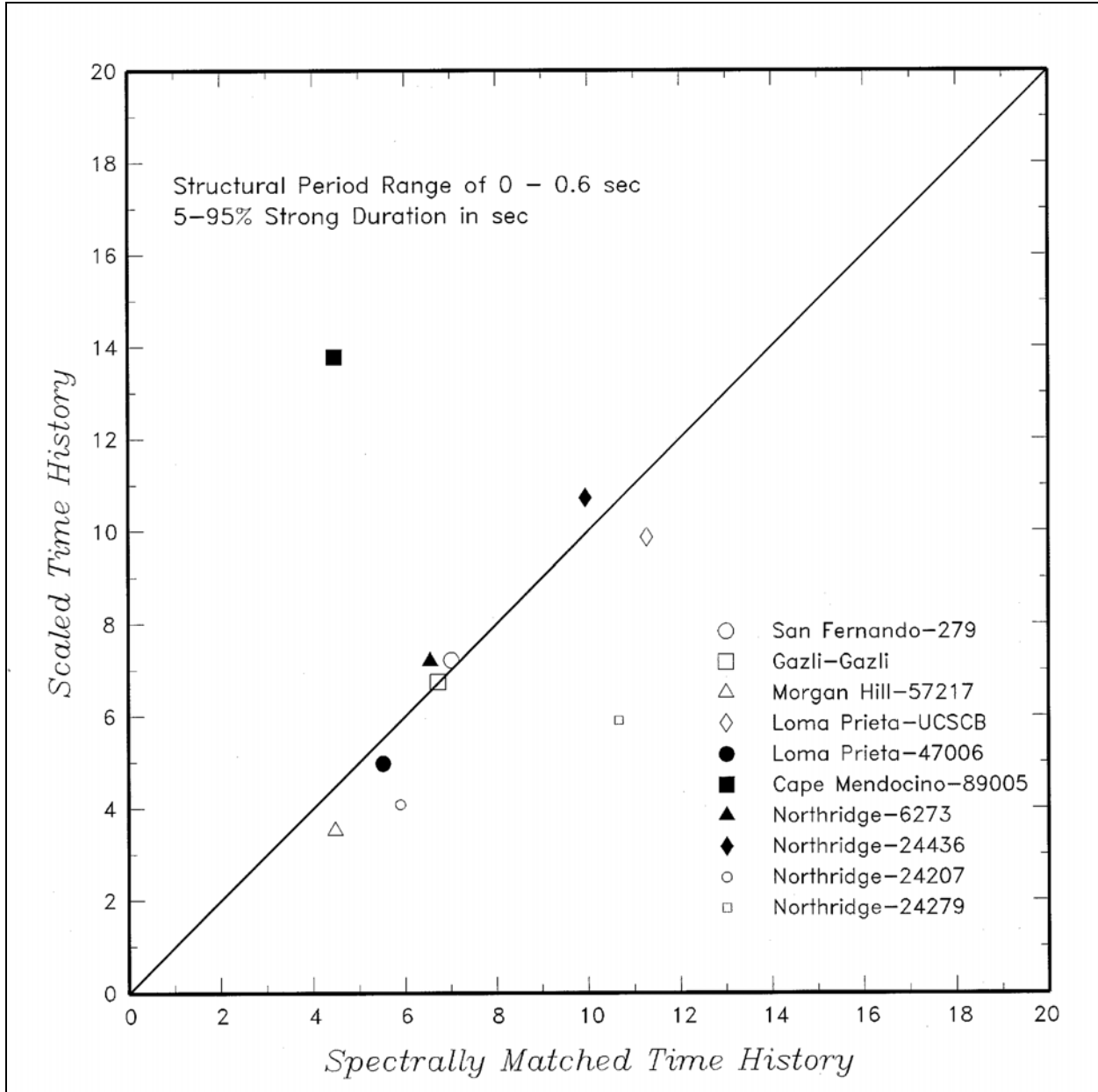


Figure D-38. Comparison for 5 to 95 percent strong duration estimated from the scaled and spectrally matched time-histories

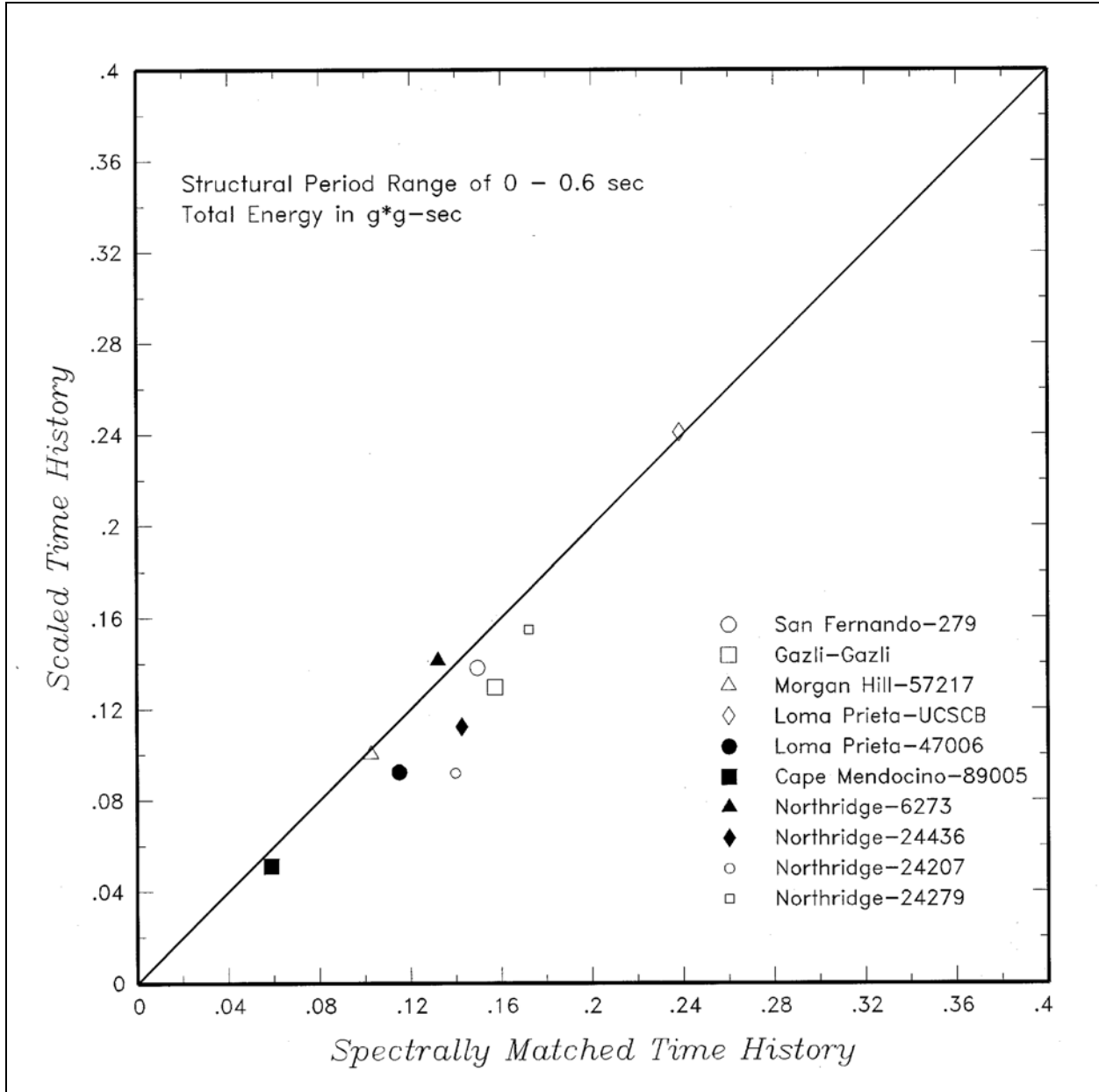


Figure D-39. Comparison for total energy estimated from the scaled and spectrally matched time-histories

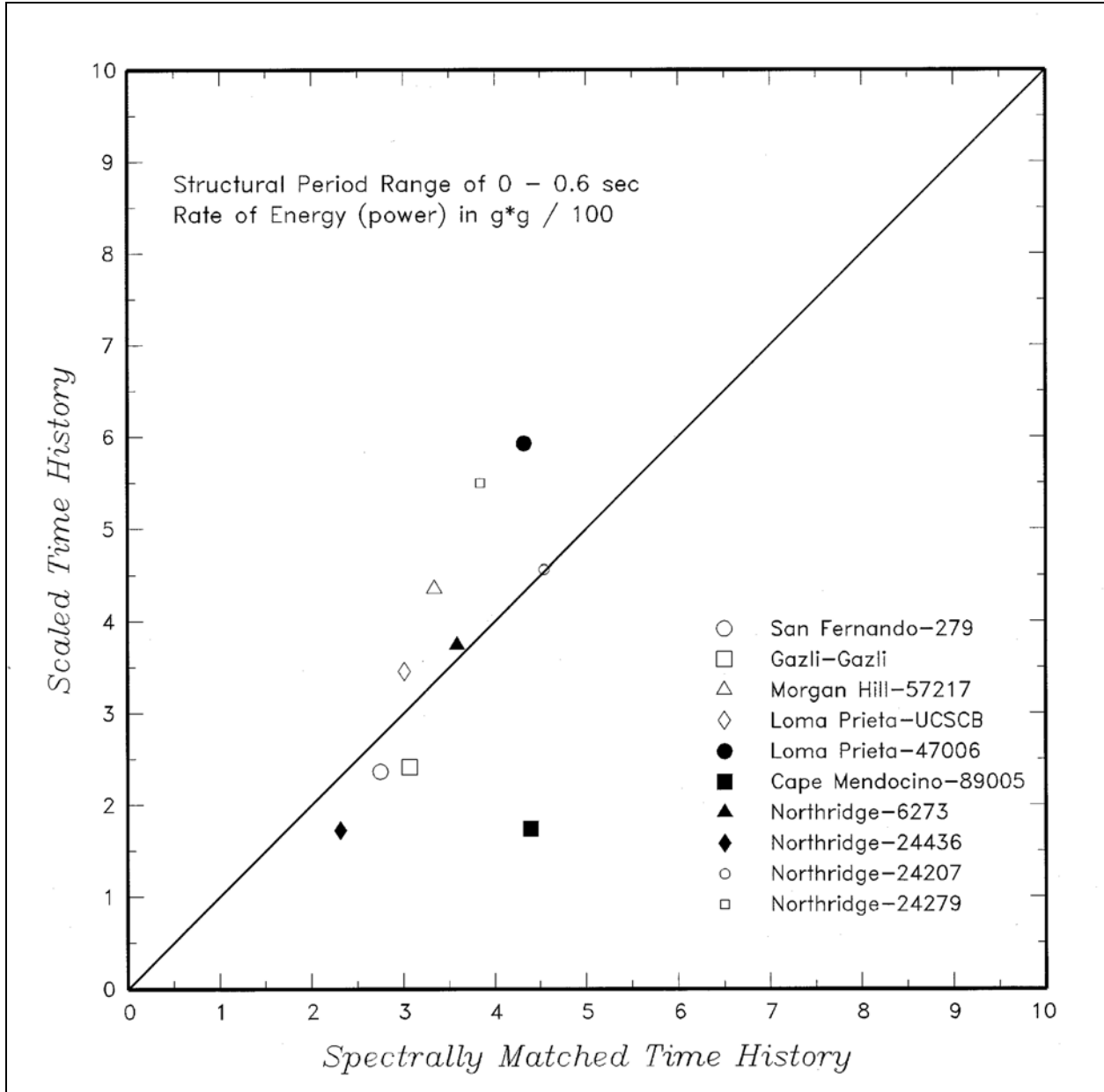


Figure D-40. Comparison for rate of energy (power) estimated from the scaled and spectrally matched time-histories

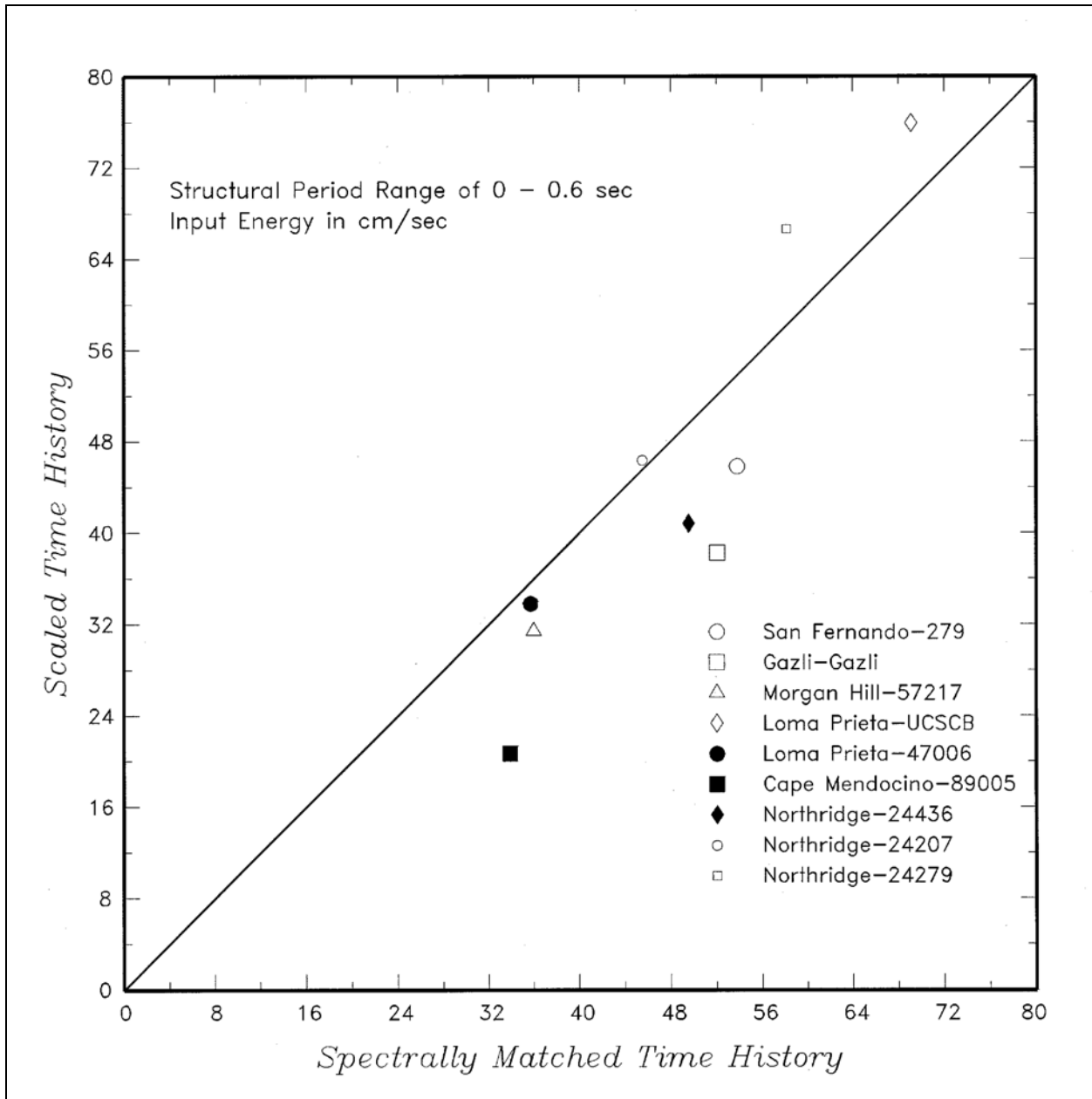


Figure D-41. Comparison for input energy estimated from the scaled and spectrally matched time-histories

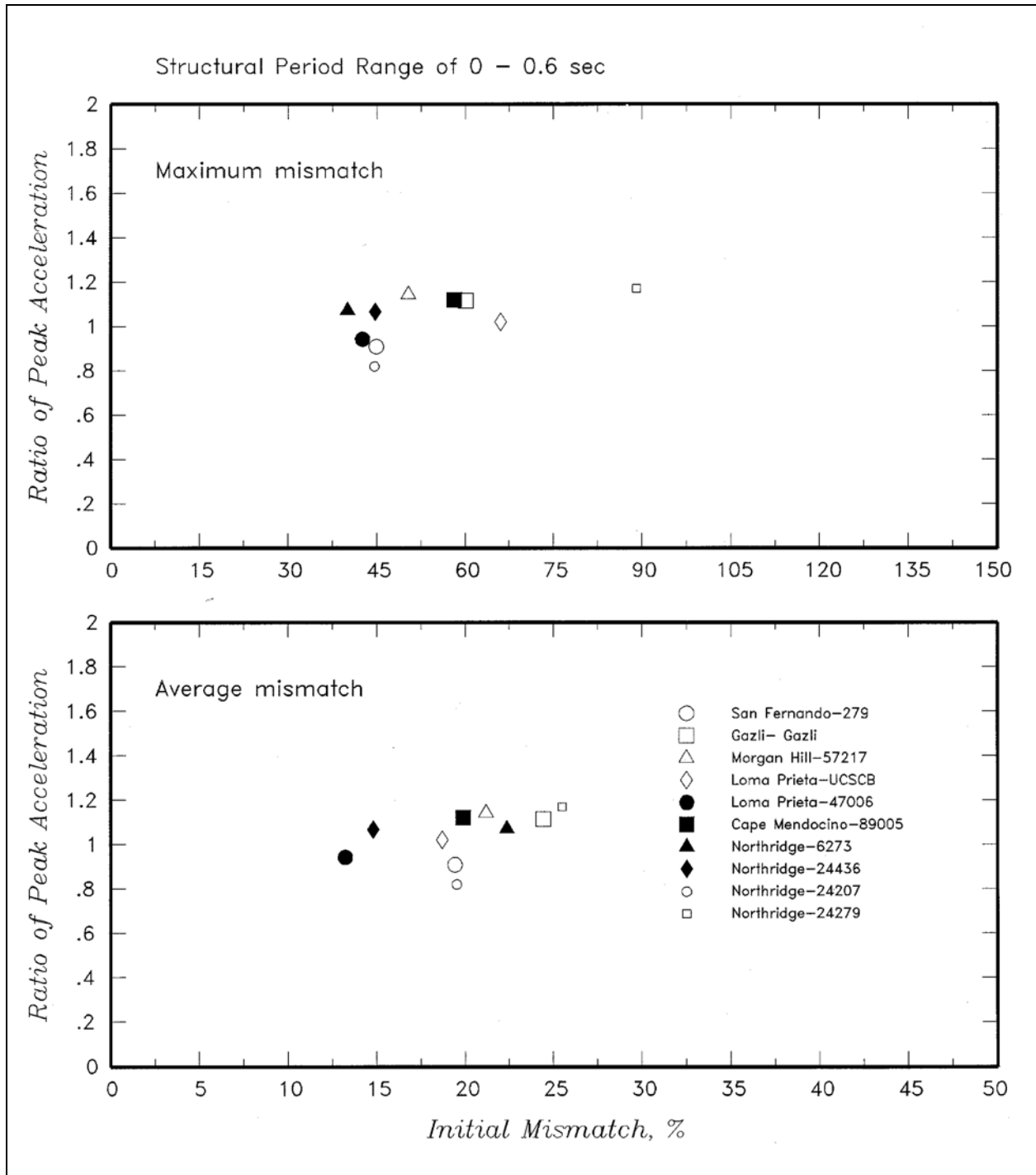


Figure D-42. Relationship between initial mismatch and peak acceleration ratio of spectrally matched and scaled time-histories

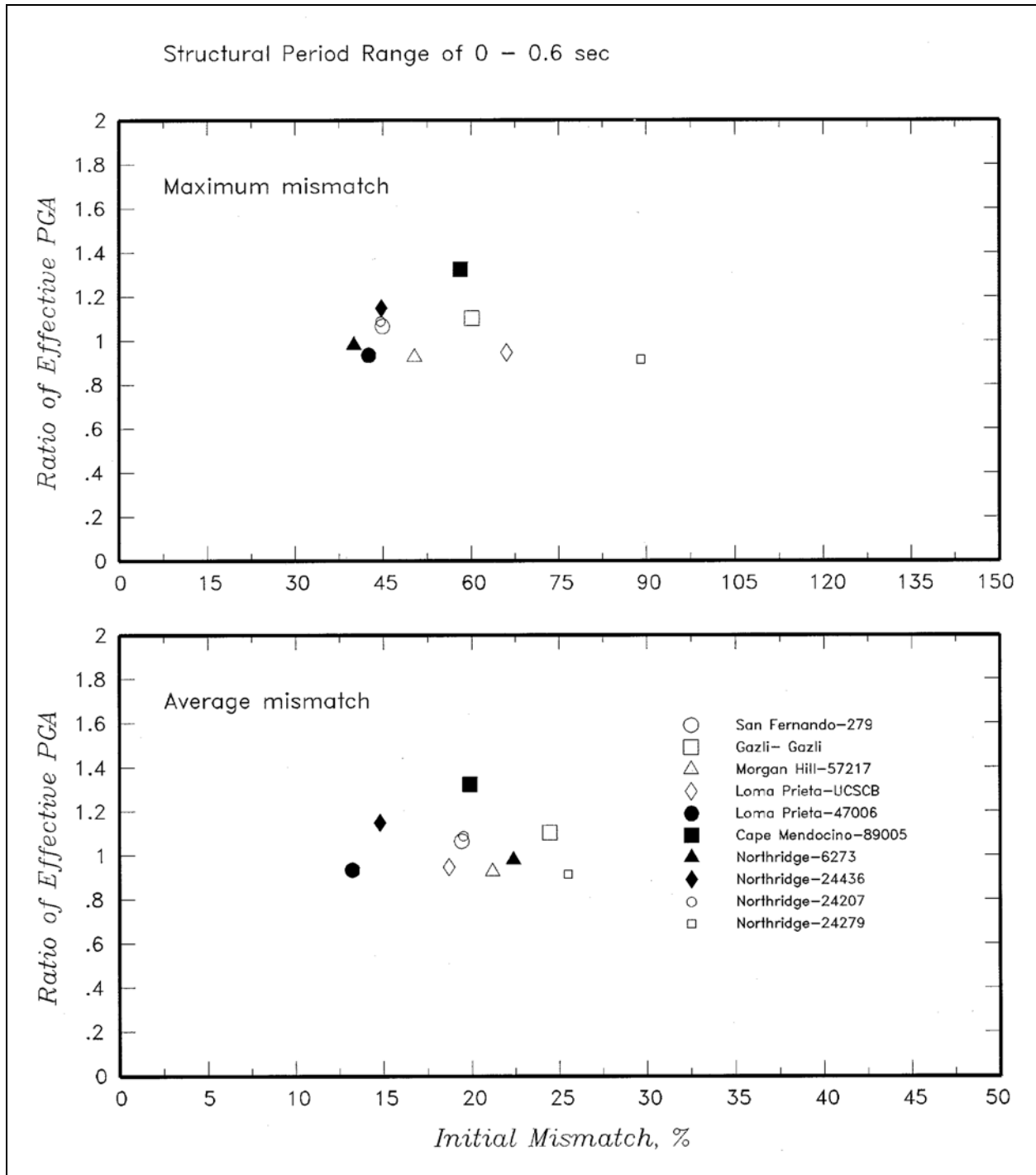


Figure D-43. Relationship between initial mismatch and effective peak acceleration ratio of spectrally matched and scaled time-histories

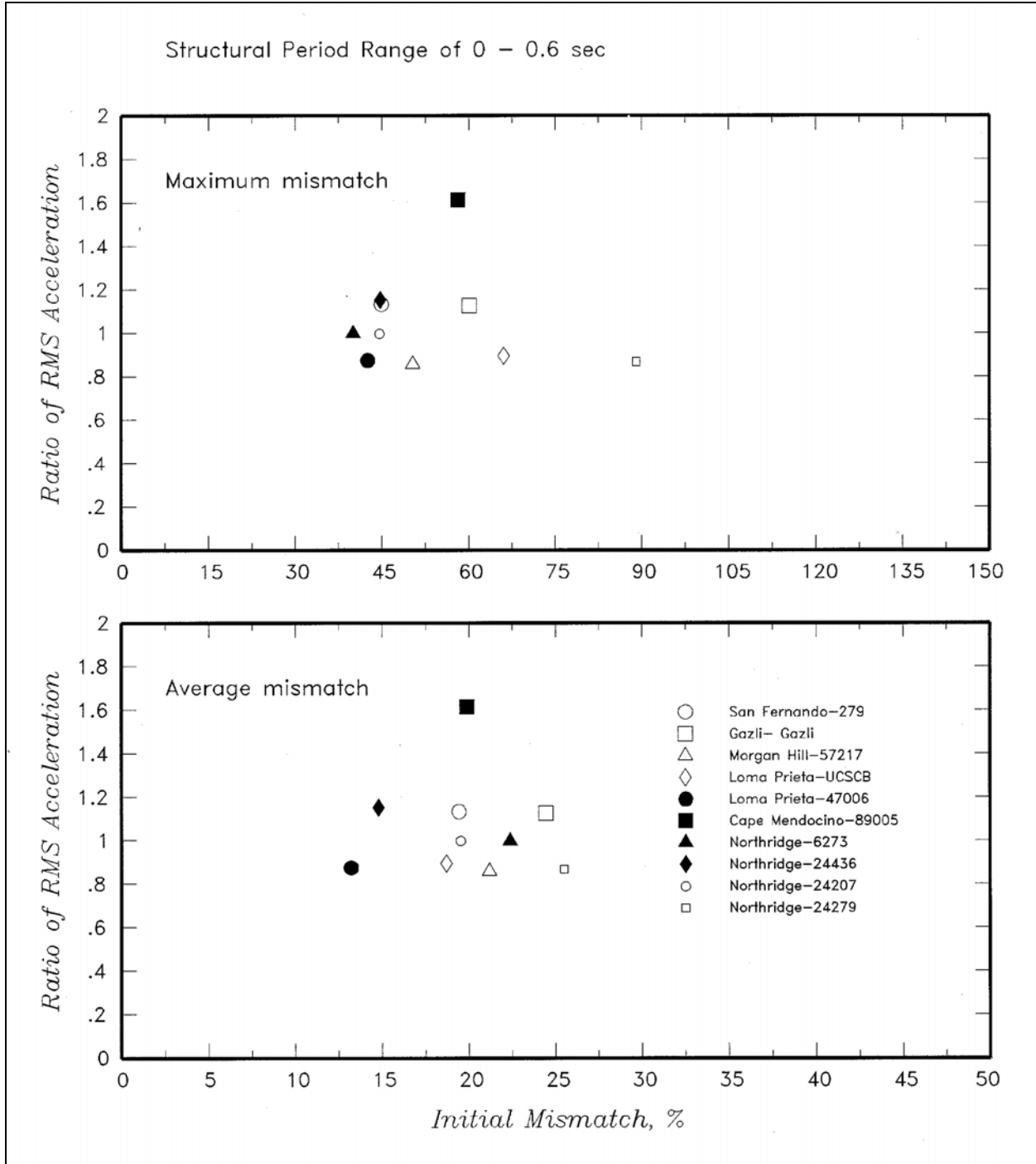


Figure D-44. Relationship between initial mismatch and root-mean-square acceleration ratio of spectrally matched and scaled time-histories

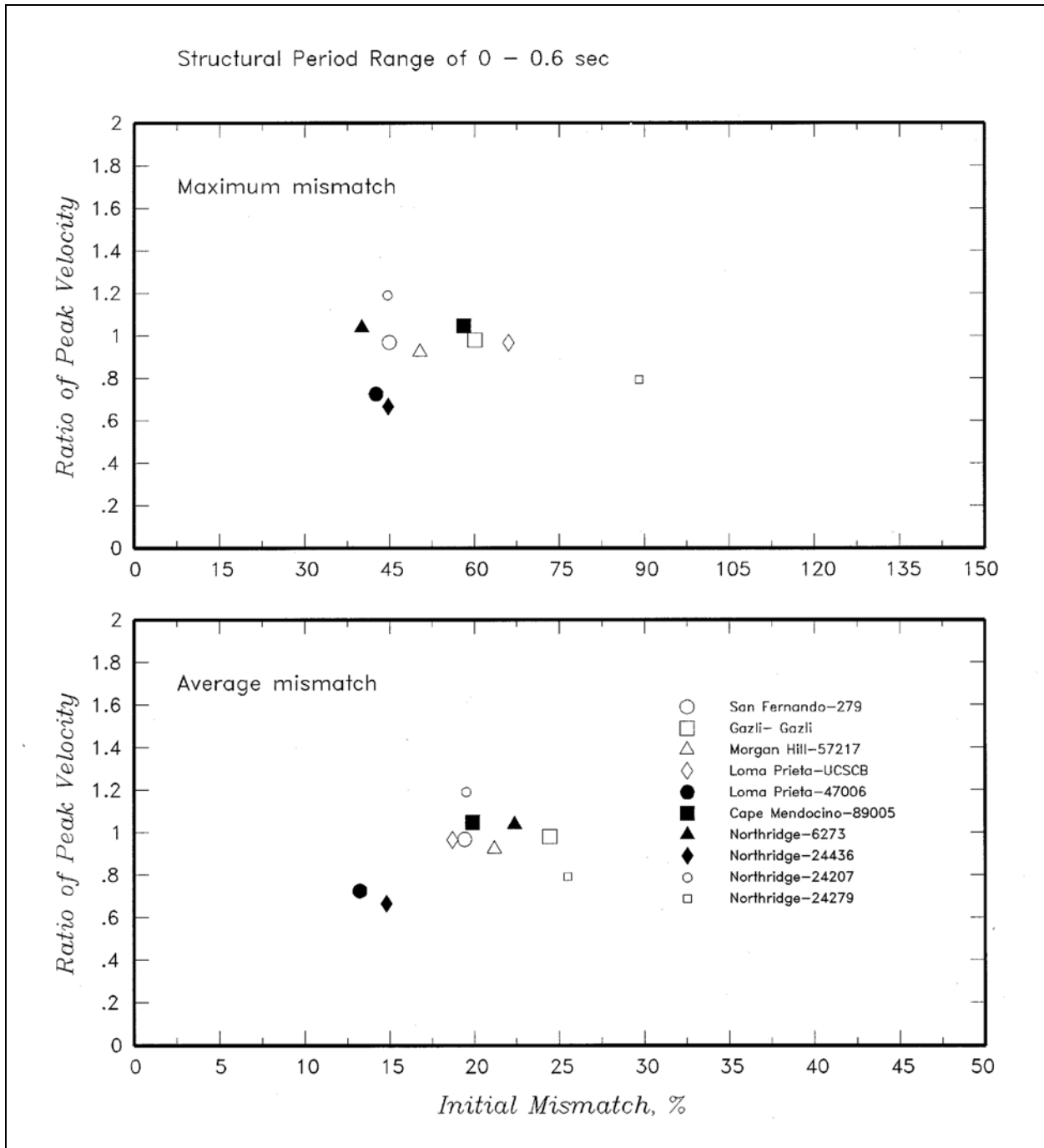


Figure D-45. Relationship between initial mismatch and peak velocity ratio of spectrally matched and scaled time-histories

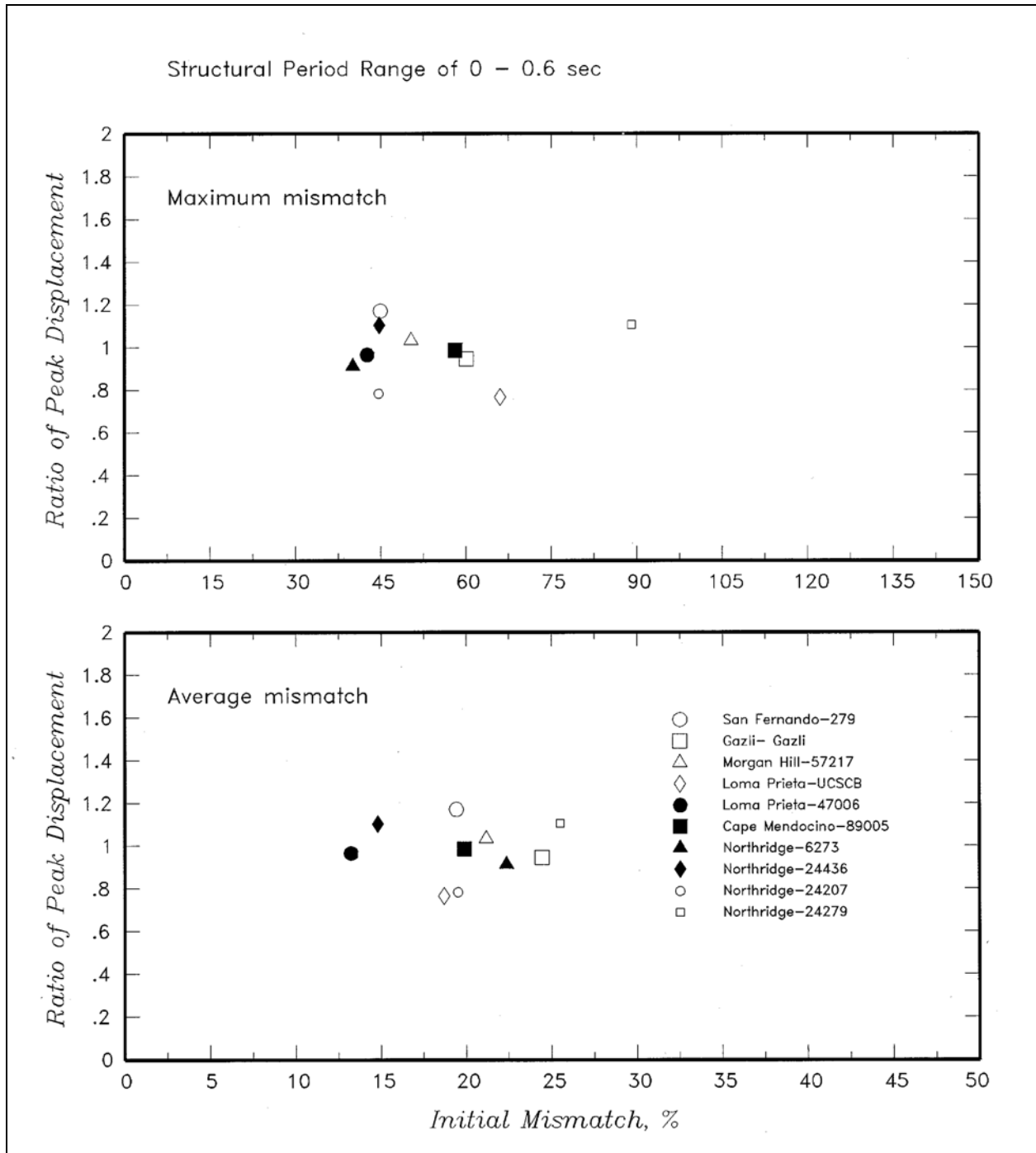


Figure D-46. Relationship between initial mismatch and peak displacement ratio of spectrally matched and scaled time-histories

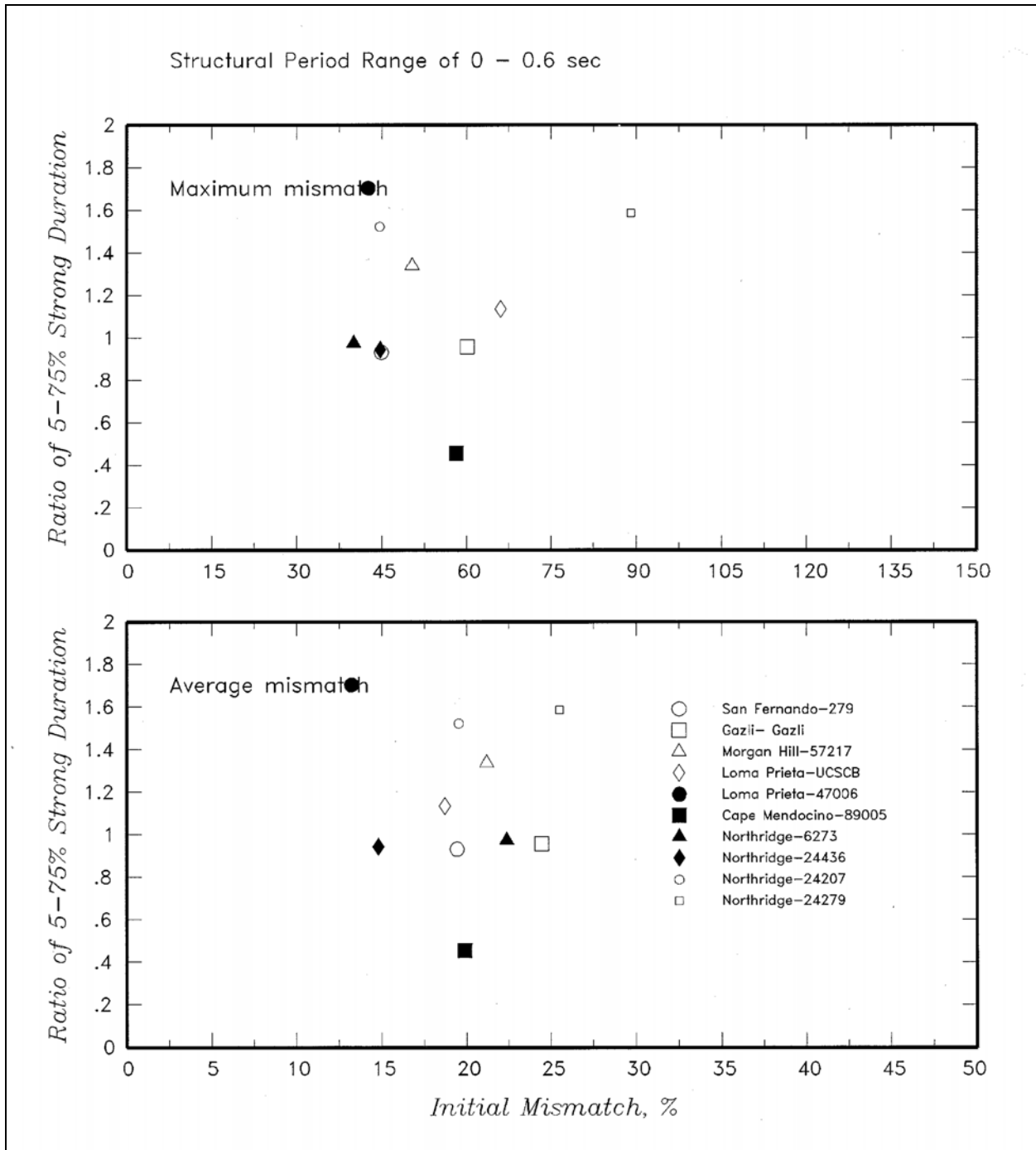


Figure D-47. Relationship between initial mismatch and 5 to 75 percent strong duration ratio of spectrally matched and scaled time-histories

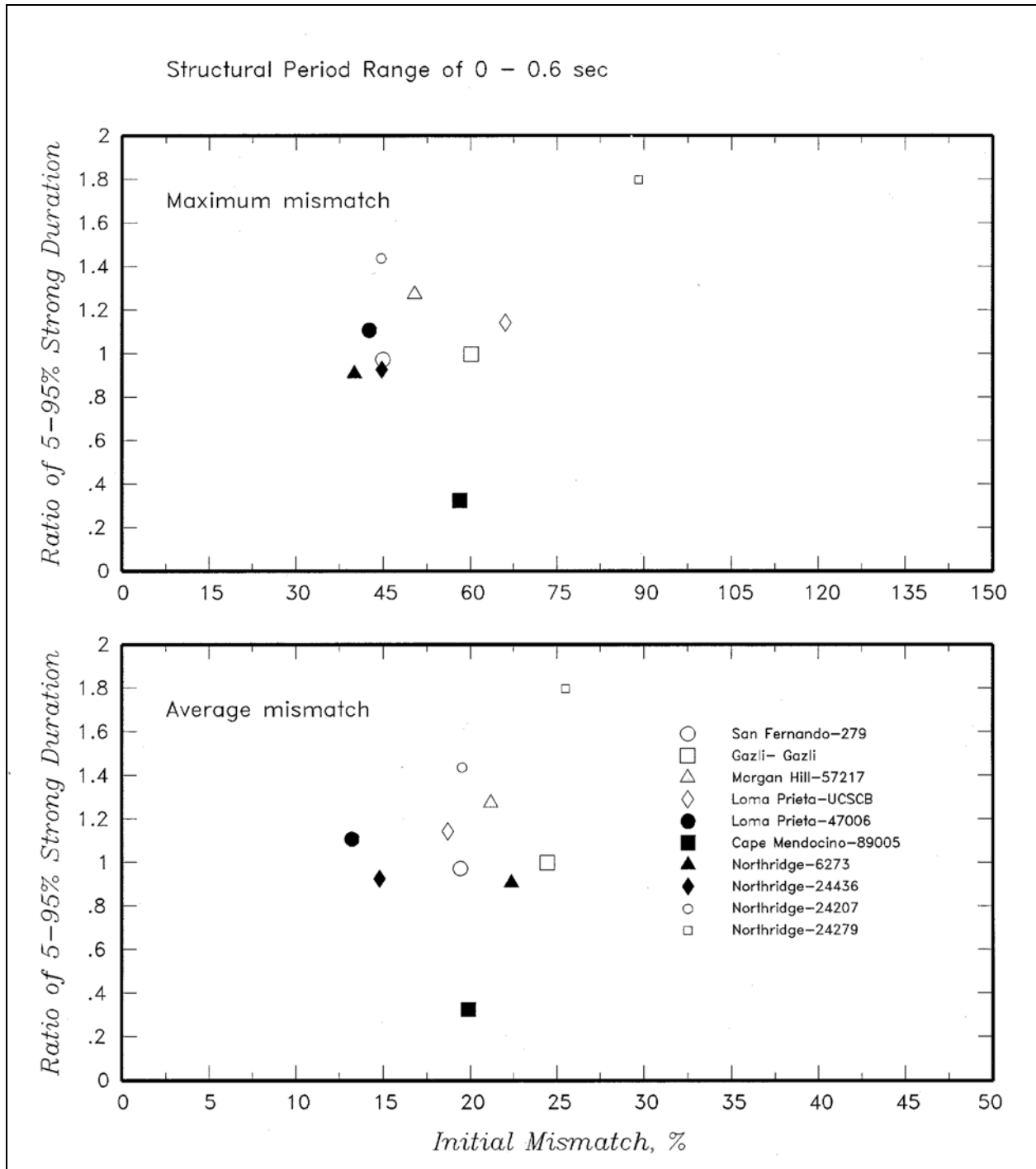


Figure D-48. Relationship between initial mismatch and 5 to 95 percent strong duration ratio of spectrally matched and scaled time-histories

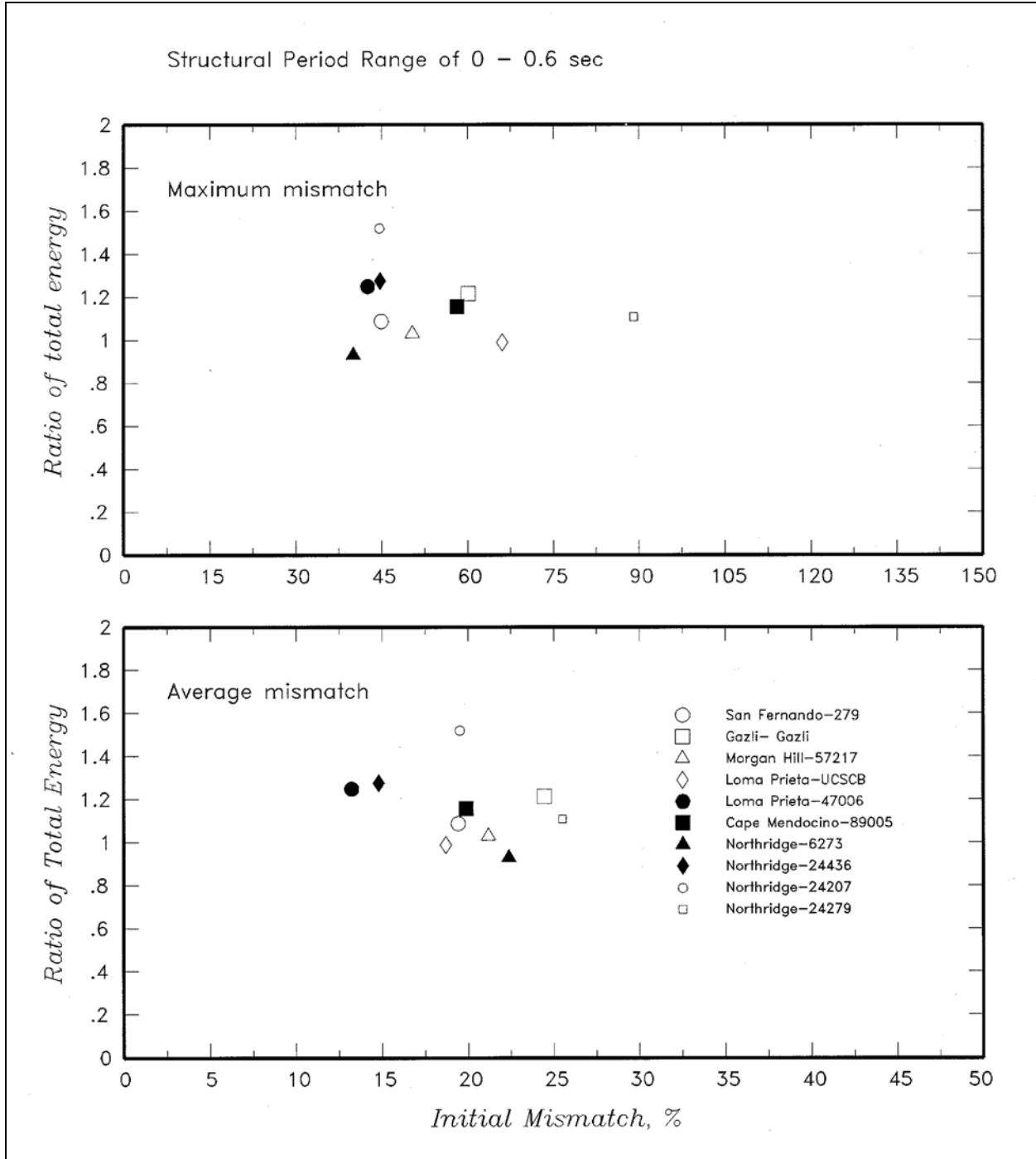


Figure D-49. Relationship between initial mismatch and total energy ratio of spectrally matched and scaled time-histories

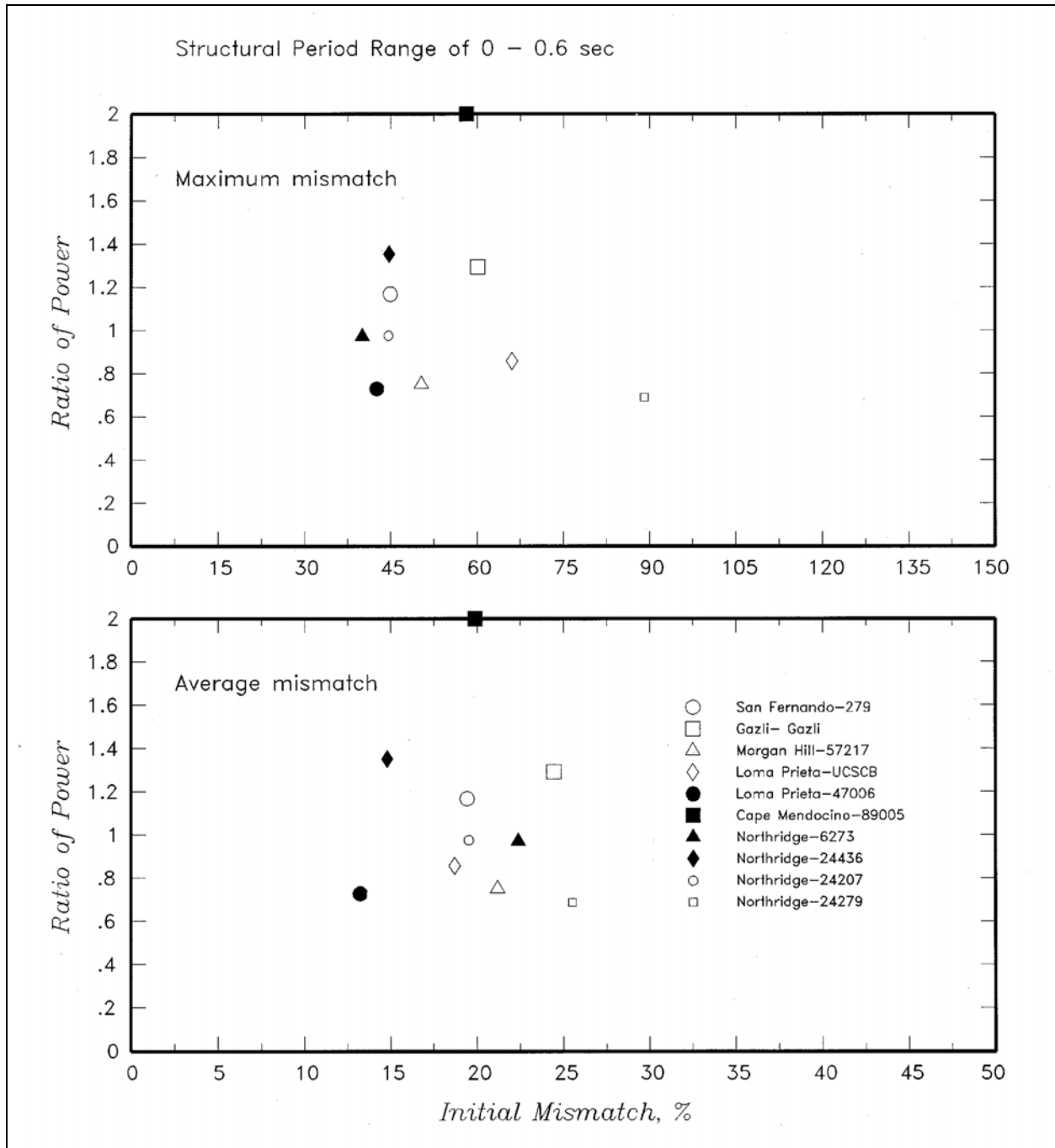


Figure D-50. Relationship between initial mismatch and power ratio of spectrally matched and scaled time-histories

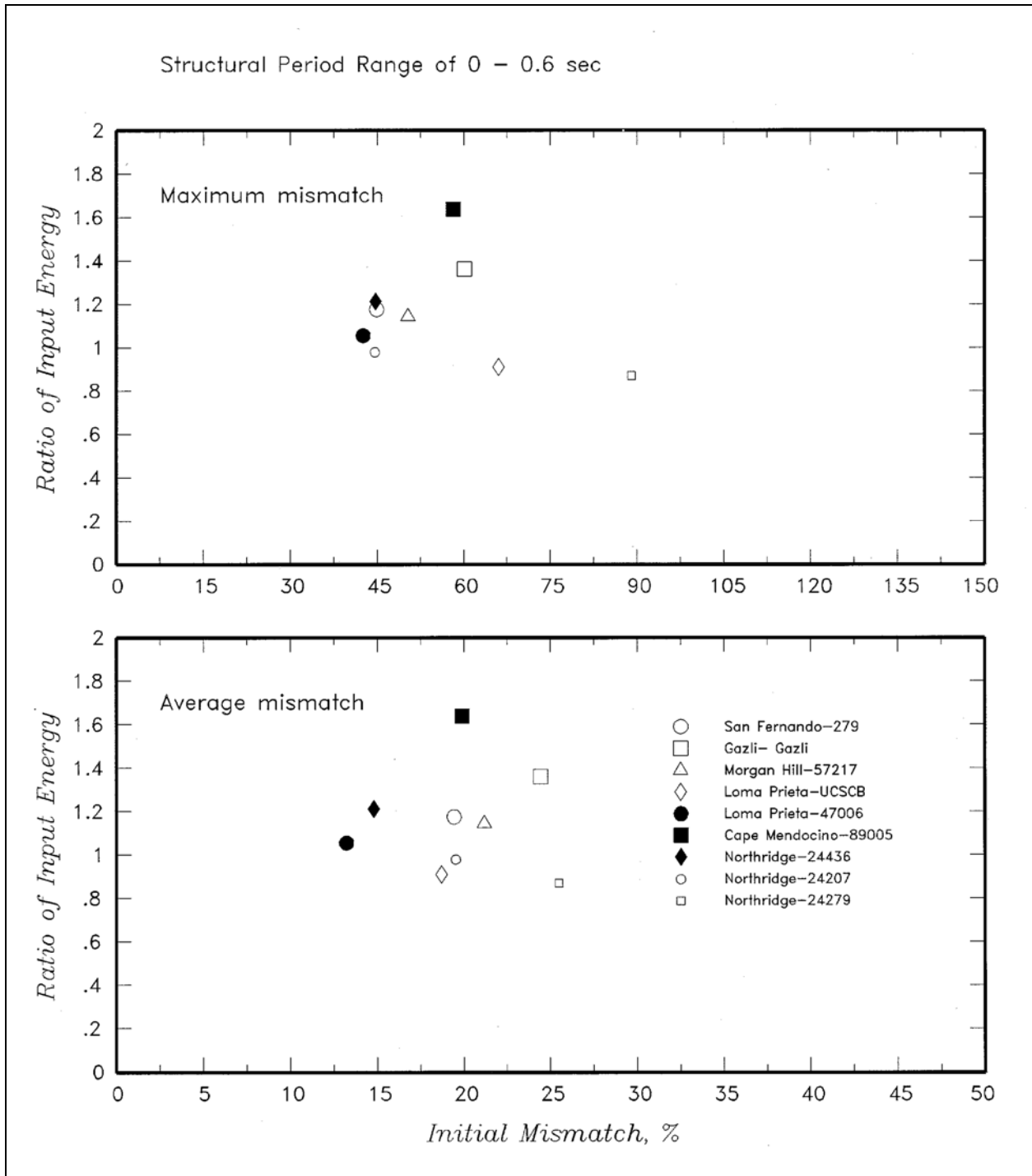


Figure D-51. Relationship between initial mismatch and input energy ratio of spectrally matched and scaled time-histories

Appendix E Discrete Soil Models

E-1. Introduction

This appendix provides a brief description of discrete soil models for a rigid disk on homogeneous half-space, an embedded cylinder, an embedded prism, and a strip supported on a homogeneous half-space. For a more detailed description and formulation refer to Wolf (1988).

E-2. Rigid Disk Supported on Half-Space

A rigid disk supported on a homogeneous half-space undergoes one horizontal and vertical translations and rocking and torsional rotations. A one-dimensional discrete model can approximate the soil medium for each of these four degrees of freedom. The sketch in Table E-1 shows one such model for the vertical component of ground motion. The model is made of mass M_0 attached to the rigid support by spring K and damper C_0 and mass M_I connected to Node 0 through damper C_I . Node 0, which connects the foundation to the structure, is defined at the center of the disk. The static stiffness K and dimensionless damper and mass coefficients needed to determine M_0 , M_I , C_0 , and C_I are given in Table E-1. Note that for some component of motion certain coefficients will be missing. For example only mass M_0 and spring K define the horizontal component of motion, while all coefficients are required to define the vertical component of motion.

E-3. Embedded Cylindrical Foundation

The static stiffness and dimensionless coefficient of a discrete model of massless rigid cylindrical foundation embedded in an elastic homogeneous half-space are summarized in Table E-2. Horizontal and vertical translations and rocking and rotational rotations define the motions of the rigid embedded cylinder, as shown in the sketch in Table E-2. For an embedded foundation, coupling between the horizontal and rocking motions is not negligible and should be considered by connecting the horizontal spring and damper at some distance above the base of the cylinder. These distances for the horizontal spring f_k and horizontal damper f_c are given by:

$$f_k = 0.25e \quad (\text{E-1})$$

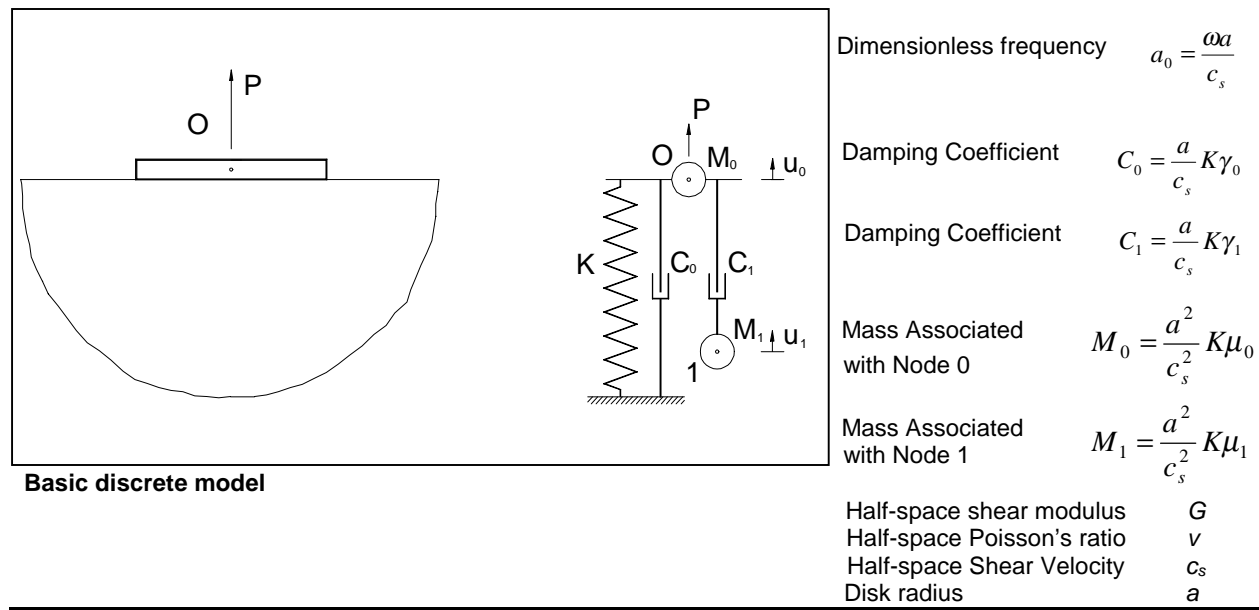
$$f_c = 0.32e + 0.03e \left(\frac{e}{a} \right)^2 \quad (\text{E-2})$$

Note that the coefficients given in Table E-2 are available only for $\nu = 0.25$. Also note that by setting $e = 0$, coefficients for the disk on the surface for $\nu = 0.25$ can be obtained from Table E-2.

E-4. Embedded Rectangular Foundation

The static and dimensionless coefficients for an embedded rigid rectangular foundation are given in Table E-3. The foundation is $2l$ long and $2b$ wide ($l \geq b$) and the embedment expressed as e (sketch in Table E-3). Defined with respect to the center of the basemat, motions of the foundation include vertical and two horizontal translations, two rocking rotations with respect to horizontal axes, and torsional rotation. The properties of the homogeneous half-space and motion notations are also summarized in this sketch. The coupling terms between rocking and horizontal motions are specified as:

Table E-1 Static Stiffness and Dimensionless Coefficients of Discrete Model for Disk Foundation		Dimensionless Coefficients			
Static Stiffness K		Dampers		Masses	
		γ_0	γ_1	μ_0	μ_1
Horizontal	$\frac{8Ga}{2-\nu}$	$0.78-0.4\nu$	—	—	—
Vertical	$\frac{4Ga}{1-\nu}$	0.8	$0.34-4.3\nu^4$	$\nu < 1/3$ $\nu > 1/3$	0 $0.9(\nu-1/3)$
Rocking	$\frac{8Ga^3}{3(1-\nu)}$	—	$0.42-0.3\nu^2$	$\nu < 1/3$ $\nu > 1/3$	0 $0.16(\nu-1/3)$
Torsion	$\frac{16Ga^3}{3}$	—	0.29	—	0.2



Basic discrete model

$$K_{hxry} = \frac{e}{3} K_{hx} \tag{E-3}$$

$$K_{hyrx} = \frac{e}{3} K_{hy} \tag{E-4}$$

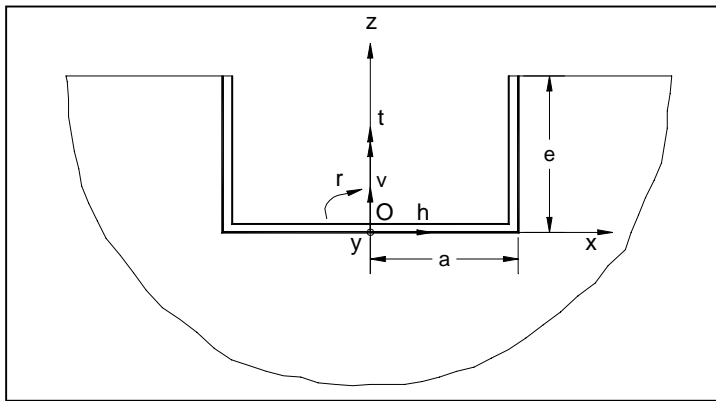
which indicate that the horizontal springs should be connected a distance of $f_{Kx} = f_{Ky} = e/3$ above the base basemat. For simplicity and lack of data, the spring eccentricity can also be used for the horizontal dampers. It should be noted that coefficients of the discrete model in Table E-3 are $\nu = 1/3$. Using these coefficients, masses M_0 and M_1 and dampers C_0 and C_1 are determined from expressions given in the sketch in Table E-1 with rectangular width b replacing the disk radius a . Note that by setting $e = 0$, a rectangular foundation at the ground surface can be treated as a special case of this problem.

E-5. Strip Foundation

The static and dimensionless coefficients of a discrete model of a rigid strip supported on a homogeneous half-plane are provided in Table E-4. The strip is $2b$ wide and the half-plane is characterized by G , ν , and ρ . The

Table E-2
Static Stiffness and Dimensionless Coefficients of Discrete Model for Embedded Cylindrical Foundation

Static Stiffness K	Dimensionless Coefficients for $\nu = 0.25$			
	Dampers		Masses	
	γ_0	γ_1	μ_0	μ_1
Horizontal $\frac{8Ga}{2-\nu} \left(1 + \frac{e}{a}\right)$	$0.68 + 0.57\sqrt{e/a}$	—	—	—
Vertical $\frac{4Ga}{1-\nu} \left(1 + 0.54\frac{e}{a}\right)$	$0.8 + 0.35\frac{e}{a}$	$0.32 - 0.01\left(\frac{e}{a}\right)^4$	—	0.38
Rocking $\frac{8Ga^3}{3(1-\nu)} \left[1 + 2.3\frac{e}{a} + 0.58\left(\frac{e}{a}\right)^3\right]$	$0.16\frac{e}{a}$	$0.40 + 0.03\left(\frac{e}{a}\right)^2$	—	$0.33 + 0.1\left(\frac{e}{a}\right)^2$
Torsion $\frac{16Ga^3}{3} \left(1 + 2.67\frac{e}{a}\right)$	—	$0.29 + 0.09\sqrt{e/a}$	—	$0.20 + 0.25\sqrt{e/a}$



h = horizontal
 ν = vertical
 r = rocking
 t = torsion
 a = radius

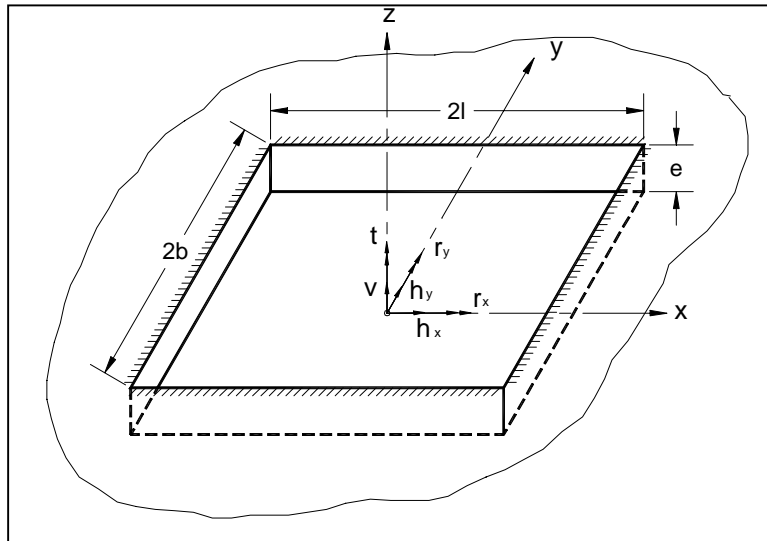
Embedded cylindrical foundation

Note: The lack of reliable data for other Poisson's ratios does not allow the dimensionless coefficients to be specified for as a function of ν .

three motions of the strip include one horizontal, vertical, and rocking. Knowing the coefficients given in Table E-4, masses M_0 and M_1 and dampers C_0 and C_1 are obtained from expressions in the sketch in Table E-1 by substituting b for the disk radius a .

Table E-3
Static Stiffness and Dimensionless Coefficients of Discrete Model for Rectangular Foundation

	Dimensionless Coefficients for $\nu = 1/3$			
	Dampers		Masses	
	γ_0	γ_1	μ_0	μ_1
Horizontal h_x h_y	$0.75 + 0.2 \left(\frac{l}{b} - 1 \right)$	—	—	—
Vertical	$0.9 + 0.4 \left(\frac{l}{b} - 1 \right)^{2/3}$	0.3	—	0.14
Rocking r_x	—	0.45	—	0.34
r_y	—	$0.45 + 0.23 \left(\frac{l}{b} - 1 \right)$	—	$0.34 + 0.55 \left(\frac{l}{b} - 1 \right)$
Torsion	—	$0.35 + 0.12 \left(\frac{l}{b} - 1 \right)$	—	$0.28 + 0.63 \left(\frac{l}{b} - 1 \right)$
Horizontal translation in x-direction	$K_{hx} = \frac{Gb}{2-\nu} \left[6.8 \left(\frac{l}{b} \right)^{0.65} + 2.4 \right] \left[1 + \left(0.33 + \frac{1.34}{1+\frac{1}{b}} \right) \left(\frac{e}{b} \right)^{0.8} \right]$			
Horizontal translation in y-direction	$K_{hy} = \frac{Gb}{2-\nu} \left[6.8 \left(\frac{l}{b} \right)^{0.65} + 0.8 \frac{l}{b} + 1.6 \right] \left[1 + \left(0.33 + \frac{1.34}{1+\frac{1}{b}} \right) \left(\frac{e}{b} \right)^{0.8} \right]$			
Vertical	$K_v = \frac{Gb}{1-\nu} \left[3.1 \left(\frac{l}{b} \right)^{0.75} + 1.6 \right] \left[1 + \left(0.25 + \frac{0.25b}{l} \right) \left(\frac{e}{b} \right)^{0.8} \right]$			
Rocking about x-axis	$K_{rx} = \frac{Gb^3}{1-\nu} \left(3.2 \frac{l}{b} + 0.8 \right) \left[1 + \frac{e}{b} + \frac{1.6}{0.35 + \frac{l}{b}} \left(\frac{e}{b} \right)^2 \right]$			
Rocking about y-axis	$K_{ry} = \frac{Gb^3}{1-\nu} \left(3.73 \frac{l}{b} + 0.27 \right) \left[1 + \frac{e}{b} + \frac{1.6}{0.35 + \frac{l}{b}} \left(\frac{e}{b} \right)^2 \right]$			
Torsion	$K_t = Gb^3 \left[4.25 \left(\frac{l}{b} \right)^{2.45} + 4.06 \right] \left[1 + \left(1.3 + \frac{1.32b}{l} \right) \left(\frac{e}{b} \right)^{0.9} \right]$			



Half-space shear modulus	G
Half-space Poisson's ratio	ν
Half-space mass density	ρ
Foundation length ($l \geq b$)	$2l$
Foundation width	$2b$
Foundation embedment	e
Horizontal translation in x-dir	h_x
Horizontal translation in y-dir	h_y
Vertical translation	v
Rocking about x-axis	r_x
Rocking about y-axis	r_y
Torsion about z-axis	t

Embedded rectangular foundation

Table E-4
Spring Coefficient and Dimensionless Coefficients of Discrete Model for Strip Foundation (width of strip is 2b)

	Spring Coefficient K	Dimensionless Coefficients				
		Dampers		Masses		
		γ_0	γ_1		μ_0	μ_1
Horizontal	$G(1+5\nu^2)$	$2-2.2\nu$	—		—	—
Vertical	$G(1+4\nu^2)$	$3.5-2\nu$	—	$\nu < 1/3$	0	—
				$\nu > 1/3$	$4.5(\nu - 1/3)$	—
Rocking	$Gb^2(1.8+5.2\nu^2)$	$0.14-0.24\nu^2$	0.4	$\nu < 1/3$	0	0.3
				$\nu > 1/3$	$0.25(\nu - 1/3)$	—

Appendix F Notations

F-1. Symbols

a	Reflection coefficient; acceleration
a_c	Critical acceleration
$a_g^x(t)$	Ground acceleration input in x-direction
A_i	Tributary surface area at point i
c	Overall damping matrix for the entire system; damping coefficient
C	Damping coefficient; velocity of sound in water
[C]	Damping matrix for the assemblage of elements
C_S	Sound velocity for bottom materials
E_f/E_c	Modulus ratio of the foundation to the concrete
EI	Flexural stiffness
f	Natural cyclic frequency of vibration, cycles/sec or Hz
f_c	Corner frequency; $1/f_c$ is a measure of duration of the earthquake source rupture
f_g	Ground motion frequency
f_1^r	Fundamental resonant frequency of impounded water
$\{F(t)\}$	Earthquake load vector
F_a	Allowable axial force (force capacity) for combining with allowable moment (moment capacity); axial force about the upstream-downstream axis computed either from the static or dynamic (excitation in the cross-stream direction) SSI analyses
g	Acceleration of gravity
h_m^*	Effective modal height
H	Depth of water
H_o	Prescribed elevation in a tower

i	$\sqrt{-1}$
I_p	Pile interaction factor
$I(\omega)$	Impedance function at frequency ω
Im	Imaginary part of the impedance function
k	Stiffness submatrix corresponding to nodal points above the base; linear spring of stiffness
k_b	Coupling stiffness submatrix relating nodal points above the base to nodal points at the base
k_b^T	Transpose of k_b
k_{bb}	Stiffness submatrix corresponding to nodal points at the base
K	Stiffness coefficient
[K]	Stiffness matrix for the assemblage of elements
f_a, m_x, m_y	Axial force and bending moments (force and moment demands) computed from either static or dynamic analysis
m	Mass matrix for the structure nodal points excluding the structure-foundation interface nodes; rigid mass in a damped single-degree-of-freedom system; mass submatrix corresponding to nodal points above the base
m_a points	Added hydrodynamic mass matrix having nonzero terms only at the structure-water nodal points
m_{ai}	Added mass of water at location i in Westergaard's method
m_b	Mass submatrix corresponding to nodal points at the base
m_d	Mass per unit height
m_s	Mass matrix of the structure
M	Mass coefficient; total mass of water for a unit width section of the tank or lock
[M]	Mass matrix for the assemblage of elements
M_a	Bending moment about the upstream-downstream axis computed either from the static or dynamic (excitation in the cross-stream direction) SSI analyses
M_w	Moment magnitude
M_x	Allowable moment about the strong axis

M_y	Allowable moment about the weak axis
M_n^*	Effective modal mass in mode n
$M_l S_a$	Maximum sloshing force
n	Direction normal to the surface
P_l	Sloshing force
$p(x,y,z)$	Hydrodynamic pressure in excess of the static pressure generated by acceleration of the structure-water contact surface and acceleration of the reservoir bottom
$P(t)$	Time-varying external forcing function
q	Damping coefficient
$\bar{Q}_h(\omega)$	Vector of frequency response functions for hydrodynamic forces corresponding to nodal points at the foundation surface beneath the water (see Figure 2-2)
\mathbf{r}	Vector of nodal point displacements for the complete system relative to the rigid base displacement
$\dot{\mathbf{r}}, \ddot{\mathbf{r}}$	Nodal point velocity and acceleration vectors, respectively
$\bar{\Gamma}^l(\omega)$	Frequency response functions for nodal displacements above the base ($l = x, y, \text{ or } z$) (see Figure 2-2)
$\bar{\Gamma}_b^l(\omega)$	Frequency response function for nodal displacements at the base (see Figure 2-2)
R	Distance
Re	The real part of the impedance function
$\bar{R}_n^l(\omega)$	Vector of frequency response functions for hydrodynamic forces corresponding to nodal points at the structure-water interface (see Figure 2-2)
S_a	Spectral acceleration at period T obtained from the response spectra of earthquake ground motion
$S_f(\omega)$	Dynamic stiffness matrix of the foundation region defined with respect to nodal points at the base
\underline{S}_{rq}	Coupling submatrix of dynamic stiffness of foundation region relating nodal points at the foundation surface under the structure base to nodal points at the foundation surface beneath the water

\underline{S}_{qq}	Submatrix of dynamic stiffness of foundation region defined with respect to nodal points at the foundation surface beneath the water
t	Time
t_f	Total duration of a time-history
T_g	Time interval required to complete each cycle of sinusoidal acceleration
T_N	Period of vibration of the highest mode associated with the system eigenproblem
T_o	Natural period of vibration, sec, of the undamped SDOF system
T_p	Period equal to total duration
T	Period of fundamental mode of sloshing; return period
\ddot{u}_g	Ground acceleration
\ddot{u}_x	Impulsive pressures due to a horizontal component of ground motion
\ddot{u}_{nb}	Normal component of ground acceleration at the reservoir boundary
\ddot{u}_{nd}	Normal acceleration
$u(t)$	Tower geometric displacement time-history
$\{u(t)\}$	Nodal displacements vector (double and single overdots represent the second and first derivative of displacement with respect to time)
$u_n(t)$	Geometric modal displacement time-history in each n mode
$x(t)$	Relative displacement
$x_{ground}(t)$	Displacement of the ground
$\ddot{x}_{ground}(t)$	Time-varying ground acceleration time-history
$x_{total}(t)$	Displacement of the mass from its at-rest position
$\ddot{x}_{total}(t)$	Acceleration of mass m
$y_n(t)$	Time-history of single-degree-of-freedom displacement for mode n
z_I	Height above the base of the dam
α	Ratio of reflected to incident wave amplitudes wave reflection coefficient

α_I	Westergaard pressure coefficient
β	Ratio of the excitation frequency to the natural free-vibration frequency; damping ratio
β, γ	Parameters defining the variation of response acceleration over the time-step and controlling the stability and accuracy of the method
ζ	Hysteretic damping factor
η_s	Constant hysteretic damping factor for the structure
$\lambda_i = \langle \lambda_x, \lambda_y, \lambda_z \rangle_i$	Normal direction cosines
ξ	Viscous damping ratio
ρ	Density of water
ρ_s	Density for bottom materials
ρ_w	Mass density of water
φ_n	Mode shape for node n
ω	Undamped circular frequency, rad/sec, of the single-degree-of-freedom system
ω_n	Natural circular frequency
ω	Harmonic excitation frequency
ω_s	Circular frequency of each of $(N/2 + 1)$ harmonic
$\underline{1}^l$	Subvector of 1's corresponding to nodal points above the base (see Figure 2-2)
$\underline{1}^b$	Subvector of 1's corresponding to nodal points at the base
$\underline{1}_s^x$	Vector of 1's corresponding to x-DOFs

F-2. Acronyms

CEUS	Central and eastern United States
CPGA	Critical peak ground acceleration
CQC	Complete quadratic combination method
FFT	Fast Fourier transform
FS	Factor of safety

IFFT	Inverse (or reverse) fast Fourier transform
MCE	Maximum credible earthquake
MDE	Maximum design earthquake
MDOF	Multi-degrees-of-freedom
OBE	Operating basis earthquake
PGA	Peak ground acceleration
PSHA	Probabilistic seismic hazard analysis
RCC	Roller-compacted concrete
RP	Return period
SDOF	Single-degree-of-freedom
SPSI	Soil-pile-structure interaction
SRSS	Square root of the sum of the squares method
SSI	Soil-structure interaction
WUS	Western United States